

ISSN: 2349-6495(P) | 2456-1908 (O)



International Journal of Advanced Engineering Research and Science

(IJAERS)

An Open Access International Journal



Journal DOI: [10.22161/ijaers](https://doi.org/10.22161/ijaers)

Issue DOI: [10.22161/ijaers.4.3](https://doi.org/10.22161/ijaers.4.3)

AI PUBLICATIONS

Vol.- 4 | Issue - 3 | March, 2017

editor@ijaers.com | <http://www.ijaers.com/>

Editorial Board

Dr. C.M. Singh

*BE., MS(USA), PhD(USA), Post-Doctoral fellow at NASA (USA)
Professor, Department of Electrical & Electronics Engineering, INDIA*

Dr. Ram Karan Singh

*BE.(Civil Engineering), M.Tech.(Hydraulics Engineering), PhD(Hydraulics & Water Resources Engineering),BITS- Pilani
Professor, Department of Civil Engineering, King Khalid University, Saudi Arabia.*

Dr.Asheesh Kumar Shah

*IIM Calcutta, Wharton School of Business, DAVV INDORE, SGSITS, Indore
Country Head at CraFSOL Technology Pvt.Ltd, Country Coordinator at French Embassy, Project Coordinator at IIT Delhi, INDIA*

Dr.Swapnesh Taterh

*Ph.d with Specialization in Information System Security
Associate Professor, Department of Computer Science Engineering
Amity University, INDIA*

Dr.Ebrahim Nohani

Ph.D.(hydraulic Structures), Department of hydraulic Structures, Islamic Azad University, Dezful, IRAN.

Dr.Dinh Tran Ngoc Huy

*Specialization Banking and Finance, Professor, Department Banking and Finance
Viet Nam*

Dr.Sameh El-Sayed Mohamed Yehia

*Assistant Professor, Civil Engineering(Structural), Higher Institute of Engineering -El-Shorouk Academy,
Cairo, Egypt*

Dr.Ahmadad Nabih Zaki Rashed

*Specialization Optical Communication System, Professor, Department of Electronic Engineering,
Menoufia University*

Dr. Alok Kumar Bharadwaj

BE(AMU), ME(IIT, Roorkee), Ph.D (AMU), Professor, Department of Electrical Engineering, INDIA

Dr. M. Kannan

*Specialization in Software Engineering and Data mining
Ph.D, Professor, Computer Science, SCSVMV University, Kanchipuram, India*

Dr.Sambit Kumar Mishra

*Specialization Database Management Systems
BE, ME, Ph.D, Professor, Computer Science Engineering
Gandhi Institute for Education and Technology, Baniatangi, Khordha, India*

Dr. M. VenkataRamana

*Specialization in Nano Crystal Technology
Ph.D, Professor, Physics, Andhara Pradesh, INDIA*

DR. C. M. Velu

Prof. & HOD, CSE, Datta Kala Group of Institutions, Pune, India

Dr. Rabindra Kayastha

*Associate Professor, Department of Natural Sciences
School of Science, Kathmandu University, Nepal*

Dr. P. Suresh

Specialization in Grid Computing and Networking, Associate Professor, Department of Information Technology, Engineering College, Erode, Tamil Nadu, INDIA

Dr. Uma Choudhary

Specialization in Software Engineering Associate Professor, Department of Computer Science Mody University, Lakshmanagarh, India

Dr. Varun Gupta

Network Engineer, National Informatics Center, Delhi, India

Dr. Hanuman Prasad Agrawal

Specialization in Power Systems Engineering Department of Electrical Engineering, JK Lakshmi Pat University, Jaipur, India

Dr. Hou, Cheng-I

Specialization in Software Engineering, Artificial Intelligence, Wisdom Tourism, Leisure Agriculture and Farm Planning, Associate Professor, Department of Tourism and MICE, Chung Hua University, Hsinchu Taiwan

Dr. Anil Trimbakrao Gaikwad

Associate Professor at Bharati Vidyapeeth University, Institute of Management, Kolhapur, India

Dr. Ahmed Kadhim Hussein

Department of Mechanical Engineering, College of Engineering, University of Babylon, Republic of Iraq

Dr. Gamal Abd El-Nasser Ahmed Mohamed Said

Computer Lecturer, Department of Computer and Information Technology, Port Training Institute (PTI), Arab Academy For Science, Technology and Maritime Transport, Egypt

Mr. T. Rajkiran Reddy








Specialization in Networking and Telecom

Research Database Specialist, Quantile Analytics, India










M. HadiAmini

Carnegie Mellon University, USA






Vol-4, Issue-3, March 2017





Sr No.	Details with DOI
1	<p><u>Gender Comparison in the Effectiveness of Guidance and Counselling Services in Enhancing Students' adjustment to School Environment in Boarding Secondary Schools in Kenya</u> Author: Dr. Benjamin Mugambi Kanga  DOI: 10.22161/ijaers.4.3.1 <i>Page No: 001-014</i></p>
2	<p><u>Reactive and Active Power Output Optimization in a Wind Farm Using the Particle Swarm Optimization Technique</u> Author: NazhaCherkaoui, AbdelazizBelfqih, Faissal El Mariami, Omar Sabri, Jamal Boukherouaa, Mohamed NouhDazahra, MeriemMajdoub  DOI: 10.22161/ijaers.4.3.2 <i>Page No: 015-019</i></p>
3	<p><u>Review of Research Papers Related to V4-cordial Labeling of Graphs</u> Author: N. B. Rathod  DOI: 10.22161/ijaers.4.3.3 <i>Page No: 020-021</i></p>
4	<p><u>Effect of Welding Speed on Mechanical Properties of Dissimilar Friction Stir Welded AA5083-H321 and AA6061-T6 Aluminum Alloys</u> Author: D. Devaiah, K. Kishore, P.Laxminarayana  DOI: 10.22161/ijaers.4.3.4 <i>Page No: 022-028</i></p>
5	<p><u>Rapid Manufacturing: Classification and Recent Development</u> Author: Lalit Kumar, AbidHaleem, QamarTanveer, Mohd. Javaid, MohdShuaib, Vineet Kumar  DOI: 10.22161/ijaers.4.3.5 <i>Page No: 029-040</i></p>
6	<p><u>Performance tests on Screw Feeder Conveyor for Nodule Transfer Deep Sea Applications</u> Author: Amudha.K, Ramesh N.R., Sundaramoorthi.V , Dineshkumar .D ,Muthuswamy.V, Rethnaraj.T , G.A.Ramadass  DOI: 10.22161/ijaers.4.3.6 <i>Page No: 041-045</i></p>
7	<p><u>Efficient Design of Error Recovery and Improve the Performance Using Mesh of Ring Topology Based NoC</u> Author: A. Kalimuthu, Dr. M. Karthikeyan  DOI: 10.22161/ijaers.4.3.7 <i>Page No: 046-050</i></p>

8	<p><u>An Improved Approach to Discover High Utility Item Set from Large Data Set</u> Author: Shilpa Shrivastava, Mr. Abhishek Tiwari  DOI: <u>10.22161/ijaers.4.3.8</u></p>	<i>Page No: 051-054</i>
9	<p><u>Modal Analysis of Engine Supporting Bracket using Finite Element Analysis</u> Author: A.S. Adkine, Prof.G.P.Overikar, Prof. S .S. Surwase  DOI: <u>10.22161/ijaers.4.3.9</u></p>	<i>Page No: 055-063</i>
10	<p><u>Plan and Implementation of Flexible D-Statcom for Mitigating Power Quality Problems and Improve the Distribution System Performance</u> Author: Ganji Vivekananda, Dr K. Chandra Sekhar  DOI: <u>10.22161/ijaers.4.3.10</u></p>	<i>Page No: 064-073</i>
11	<p><u>Laws of Heat Radiation from Spherical Gas Volumes. Part I. Laws Formulation</u> Author: Prof.Dr. A. N. Makarov  DOI: <u>10.22161/ijaers.4.3.11</u></p>	<i>Page No: 074-079</i>
12	<p><u>Laws of heat radiation from spherical gas volumes. Part II. Modeling of heat radiation from volume bodies by radiation from spherical and cylindrical gas volumes</u> Author: Prof.Dr. A. N. Makarov  DOI: <u>10.22161/ijaers.4.3.12</u></p>	<i>Page No: 080-087</i>
13	<p><u>Design of an Exponentially Weighted Moving Average (EWMA) and An Exponentially Weighted Root Mean Square (EWRMS) Control Chart</u> Author: Asst. Prof.Dr.Kawa M. Jamal Rashid  DOI: <u>10.22161/ijaers.4.3.13</u></p>	<i>Page No: 088-091</i>
14	<p><u>Flexural Strengthening of Reinforced Concrete Girders using Post-Tensioned Concrete Jackets</u> Author: Dina Zakaria, Hussein Okail, Amr Abdelrahman  DOI: <u>10.22161/ijaers.4.3.14</u></p>	<i>Page No: 092-104</i>
15	<p><u>Effect of Friction Stir Welding Parameters on the Mechanical & Microstructure Properties of Aluminium 6061 Alloys</u> Author: Ch.Mohana Rao, K.Mallikarjuna Rao  DOI: <u>10.22161/ijaers.4.3.15</u></p>	<i>Page No: 105-109</i>

16	<p><u>Determination of Dehydration Pattern and Sensory Properties variation of Blanched and Un-blanched, Cut and Whole Moringaolifera Leaves</u></p> <p>Author: Rathnayake A.R.M.H.A, Navarathna S.B.</p> <p> DOI: 10.22161/ijaers.4.3.16</p> <p style="text-align: right;"><i>Page No: 110-115</i></p>
17	<p><u>A Review on Simulation Optimization</u></p> <p>Author: Mobin Ahmad</p> <p> DOI: 10.22161/ijaers.4.3.17</p> <p style="text-align: right;"><i>Page No: 116-119</i></p>
18	<p><u>Simulation of Corner Skidding Control System</u></p> <p>Author: M. Arun Kumar, S. AshwinKannan, A. Sathish Kumar, S. Kumaravel</p> <p> DOI: 10.22161/ijaers.4.3.18</p> <p style="text-align: right;"><i>Page No: 120-125</i></p>
19	<p><u>Synthesis and Characterization of Hybrid Polymer Composites</u></p> <p>Author: AjaiAravind Nair, S. Prakash, Dr. R. Christu Paul</p> <p> DOI: 10.22161/ijaers.4.3.19</p> <p style="text-align: right;"><i>Page No: 126-131</i></p>
20	<p><u>Effective Implementation of Agile Software Development with a Framework, Metric Tool, and in Association with Cloud and Lean Kanban</u></p> <p>Author: V. Esther Jyothi, K. Nageswara Rao</p> <p> DOI: 10.22161/ijaers.4.3.20</p> <p style="text-align: right;"><i>Page No: 132-137</i></p>
21	<p><u>Self-Compacting Concrete - Robustness of SCC</u></p> <p>Author: NaliniThakre, DipakMangrulkar, Mahesh Janbandhu, Jaya Saxena</p> <p> DOI: 10.22161/ijaers.4.3.21</p> <p style="text-align: right;"><i>Page No: 138-141</i></p>
22	<p><u>A Framework for the analysis of 3-D Novel flange Microstrip Patch Antenna Design employing Flexible Teflon Substrate</u></p> <p>Author: Avneet Kaur, Ekambir Sidhu</p> <p> DOI: 10.22161/ijaers.4.3.22</p> <p style="text-align: right;"><i>Page No: 142-146</i></p>
23	<p><u>Design and analysis of composite Leaf Spring for light Weight Vehicle</u></p> <p>Author: D. Lydia Mahanthi, C. Venkata Siva Murali</p> <p> DOI: 10.22161/ijaers.4.3.23</p> <p style="text-align: right;"><i>Page No: 147-152</i></p>
24	<p><u>Automatic Solar Powered Fan for Regulation of Temperatures in a Green House</u></p> <p>Author: Harrison K. Tarus</p> <p> DOI: 10.22161/ijaers.4.3.24</p> <p style="text-align: right;"><i>Page No: 153-155</i></p>

25	<p><u>Implementation of CMOS Low Dropout Voltage Regulator with Frequency divider for Improved Stability</u> Author: Kamlesh Sharma, GajendraSujediya, Abdul Naim Khan  DOI: 10.22161/ijaers.4.3.25</p>	<i>Page No: 156-161</i>
26	<p><u>Develop a model to map client's people development requirements and the delivery of the service to achieve effective results</u> Author: S. K. Devanarayana, G. H. J. Lanel  DOI: 10.22161/ijaers.4.3.26</p>	<i>Page No: 162-165</i>
27	<p><u>An Improved AES Cryptosystem Based Genetic Method on S-Box, With, 256 Key Sizes and 14-Rounds</u> Author: Ashutosh Pandey, Umesh kumar Lilhore  DOI: 10.22161/ijaers.4.3.27</p>	<i>Page No: 166-171</i>
28	<p><u>Parametric Instability in Mathieu Equation for Interaction P-S Waves</u> Author: Hector Torres-Silva, Enrique Fuentes Heinrich  DOI: 10.22161/ijaers.4.3.28</p>	<i>Page No: 172-175</i>
29	<p><u>Impact Analysis of Soybean in Supply of Edible Oil in India</u> Author: Prem Narayan  DOI: 10.22161/ijaers.4.3.29</p>	<i>Page No: 176-190</i>
30	<p><u>A Study on Various Security Aspects in Cloud Policy Oriented Architecture</u> Author: Sonia, Kirti Bhatia  DOI: 10.22161/ijaers.4.3.30</p>	<i>Page No: 191-195</i>
31	<p><u>Secure and Efficient Data Transmission for Cluster Based Wireless Sensor Network Using Cryptography</u> Author: Sangamsh J. kalyane, Dr.Nagaraj B. Patil  DOI: 10.22161/ijaers.4.3.31</p>	<i>Page No: 196-204</i>
32	<p><u>Tourist Guide Information System using Google Map and GPS</u> Author: Honey Soe, MyintMyintSein  DOI: 10.22161/ijaers.4.3.32</p>	<i>Page No: 205-209</i>
33	<p><u>Optimizing the Size of A Multi-Layered Patch Antenna for K-Band Applications</u> Author: M.hamdaoui, J.Foshi, A. Roukhe  DOI: 10.22161/ijaers.4.3.33</p>	<i>Page No: 210-213</i>

34	<p><u>Analysis of High Temperature Monitoring Using Fiber Bragg Grating Sensor</u> Author: Shruthi S.V, S. Sundaravadivelu  DOI: <u>10.22161/ijaers.4.3.34</u></p>	<i>Page No: 214-218</i>
35	<p><u>Strain Measurement Using Fiber Bragg Granting Sensor for Crack Detection</u> Author: K. Vinnarasi, Dr. S. Sundaravadivelu  DOI: <u>10.22161/ijaers.4.3.35</u></p>	<i>Page No: 219-223</i>
36	<p><u>A Novel Study of Semiconductor Material as a Substrate Layer for Microstrip Patch Antenna</u> Author: Praveen Kumar E, Sundaravadivelu S  DOI: <u>10.22161/ijaers.4.3.36</u></p>	<i>Page No: 224-228</i>
37	<p><u>High Frequency Gas Tungsten Arc Welding Process for Dressing of Weldment</u> Author: Cibi Anthony J, K T Thilagham  DOI: <u>10.22161/ijaers.4.3.37</u></p>	<i>Page No: 229-235</i>
38	<p><u>A Slotted-sense Streaming MAC for Real-time Multimedia Data Transmission in Industrial Wireless Sensor Networks</u> Author: Md AbulKalam Azad, Amina Khatun, Md Abdur Rahman  DOI: <u>10.22161/ijaers.4.3.38</u></p>	<i>Page No: 236-244</i>
39	<p><u>Hybrid Model Based on User Tags and Textual Passwords and Pearsonian Type III Mixture Model</u> Author: PavanGujjarPanduranga Rao, Dr.P.Srinivasa Rao, Dr. G. Lavanya Devi  DOI: <u>10.22161/ijaers.4.3.39</u></p>	<i>Page No: 245-251</i>
40	<p><u>Enhancement of Natural Ventilation using Solar Chimney: A Numerical Investigation</u> Author: Jitendra Kumar, Abhishek Raj, Hari Mohan Sharma  DOI: <u>10.22161/ijaers.4.3.40</u></p>	<i>Page No: 252-257</i>
41	<p><u>Breast Cancer Diagnostic System Based on MR images Using KPCA-Wavelet Transform and Support Vector Machine</u> Author: Mustafa Zuhaer AL-Dabagh, Dr.Firas H. AL-Mukhtar  DOI: <u>10.22161/ijaers.4.3.41</u></p>	<i>Page No: 258-263</i>

42	<p><u>The impact of applying the Unified Banking Evaluation model (Camels) on enforcing the banking supervision of commercial banks (The case study of Bank Bemo Saudi French-BBSF)</u></p> <p>Author: Dr.Ghassan Farouk Ghandour</p> <p> DOI: 10.22161/ijaers.4.3.42</p> <p style="text-align: right;"><i>Page No: 264-274</i></p>
43	<p><u>Text Detection in Document Images: Highlight on using FAST algorithm</u></p> <p>Author: Geetika Mathur, Ms.SuneethaRikhari</p> <p> DOI: 10.22161/ijaers.4.3.43</p> <p style="text-align: right;"><i>Page No: 275-284</i></p>
44	<p><u>Analysis of Simply Supported Rectangular Kirchhoff Plates by the Finite Fourier Sine Transform Method</u></p> <p>Author: Mama B.O., Nwoji C.U., Ike C. C., Onah H.N.</p> <p> DOI: 10.22161/ijaers.4.3.44</p> <p style="text-align: right;"><i>Page No: 285-291</i></p>
45	<p><u>Flexural - Torsional Buckling Analysis of Thin Walled Columns Using the Fourier series Method</u></p> <p>Author: Onah H. N., Ike C.C., Nwoji C.U.</p> <p> DOI: 10.22161/ijaers.4.3.45</p> <p style="text-align: right;"><i>Page No: 292-298</i></p>

Gender Comparison in the Effectiveness of Guidance and Counselling Services in Enhancing Students' adjustment to School Environment in Boarding Secondary Schools in Kenya

Dr. Benjamin Mugambi Kanga

Department of Education, Chuka University, Kenya

Abstract— School adjustment is the process of coping in a new school environment in order to attain the individual and school's set goals and aspirations. The government, education managers and parents have expressed the need to strengthen school Guidance and Counselling services in order to enhance students' adjustment to the school environment. Public boarding secondary schools are expected to implement Guidance and Counselling policy of the Ministry of Education and help students adjust to secondary school environment. This study investigated the Gender comparison in the effectiveness of Guidance and Counselling services in enhancing students' adjustment to school environment in public boarding secondary schools in Kenya. The study adopted a descriptive research survey design. The study target population was 36,671 comprising of 35,659 form 3 students, 506 Form 3 class teachers and 506 teachers in charge of Guidance and Counselling from boarding secondary schools in Kitui, Nyeri and Nairobi counties in Kenya. Purposive and simple random sampling techniques were used to select 756 respondents comprising of 720 Form 3 students, 18 Form 3 class teachers and 18 teachers in charge of Guidance and Counselling from 18 secondary schools for the study. Questionnaires were used to collect data from Form 3 students and their class teachers while an interview schedule was used to collect data from teachers in charge of Guidance and Counseling. Using Spearman Brown Prophecy formula by split half technique reliability coefficient of 0.745, 0.746 and 0.736 were realized for students, class teachers and teachers In charge of Guidance and Counseling respectively. This was accepted because an alpha value of 0.7 and above is considered suitable for making group inferences that are accurate. The data was analyzed by use of inferential and descriptive statistics with the help of the Statistical Package for Social Sciences (SPSS) version 17.0 for

windows and presented in frequency distribution Tables and percentages. The findings of this study provide information to school administrators, policy makers, parents and other stakeholders on various issues that need to be addressed in Guidance and Counseling to enables students adjust to school environment. The study further suggest ways of ways of improving Guidance and Counselling services in order to make it more effective in public boarding secondary schools.

Keywords— *Guidance and Counselling, student adjustment, Gender and school adjustment, school environment.*

I. INTRODUCTION

Education improves the quality of people's lives and may also lead to broad social benefits to individual and society (Banathy, 1992). Hawkins (2002) observes that education aims at providing a forum where teachers and scholars are able to evaluate challenges facing the society from a balanced and a comparative social economic perspective. Education plays a crucial role in securing economic and social progress and improving income distribution (Bogonko, 1992). Education is expected to prepare and equip the youth of the country to play an effective role in a nation's life (Republic of Kenya, 1999). Education equips citizens with understanding and knowledge that enables them to make informed choices about their lives and those facing the society (Republic of Kenya, 2007). Education plays a very important role in the individual as well as society's life. That is why governments emphasize on children attending school in order to get formal education. School is an institution of learning where children go to be educated (Catterall, 1998). According to Clive et al (2003) schools aim at providing an all rounded programme of instruction using the educational practices that are

appropriate to the cultural, intellectual and social needs of the students. Schools aim at promoting social responsibility (Catterall, 1998). Midgley and Maehr (2000) observes that schools encourage acceptance and tolerance to the diversity of moral, traditional and religious values. According to Potter (2001) learning institutions aims at fostering a sense of individual responsibility, self-discipline, self-reliance, creative and active lifestyle and respect for self and others. Baills and Rossi (2001) state that school activities and programmes help in strengthening students bonds with the community. School therefore, plays a crucial role in inculcating traditional and religious values, self-respect, discipline, tolerance, morality and school culture to learners. However, Learners ability to tolerate the diversity of moral, traditional and religious values as well as develop to be all rounded personalities depends on their adjustment to the school environment.

Gonder and Hymes (1994) found that a school environment has physical, social and academic aspects. The physical environment includes school buildings, the noise levels, text books, recreational facilities and the neighborhood (Lapan, 2003). Adeyemo (2001) postulates that when students join secondary schools they find themselves in a more expansive school environment, larger classroom and an environment that has more noise than what they were used to in their relatively smaller primary schools. In Kenya the ministry of education policy expects secondary schools to organize orientation to induct new students to the school system (Republic of Kenya, 2001) this study sought to determine the extent to which schools implement this policy and evaluate its effectiveness in enhancing students' adjustment to school environment.

Armacost (1990) established that boys handle stress better than girls. Van Der Walt and Knoetze (2004) observe that Guidance and Counselling normally was more effective in socializing boys to be stronger and cope with their own problems than girls. Makesh and Kaji (2014) found that boys adjust to school social environment than girls. Other researches on gender differences in school adjustment has portrayed that girls are better adjusted as compared to boys. Alexitch and Page (1997) established that in Canada girls were more responsive to university and career information from their counselling teachers than boys. Bruce and Cockreham (2004) found that in America girls to be more tolerant towards rules, more willing to make exceptions and more easily reconciled than boys

Despite the emphasis given to Guidance and Counselling in schools in Kenya there are indicators that maladjustment still remains a challenge in public boarding secondary

schools. This has casted doubts on the role being played by Guidance and Counselling in helping students to adjust to the school environment. There was therefore, need to assess the effectiveness of Guidance and Counselling services in enhancing student adjustment to the school environment. This study investigated whether there is significance gender difference in the effectiveness of Guidance and Counselling services in enhancing students' adjustment to the school environment in public boarding secondary schools in Kenya.

Objective of the Study

This study was guided by the following objective:

- i) To determine whether there is gender difference in the effectiveness of Guidance and Counselling services in enhancing students' adjustment to school environment in boarding secondary schools in Kenya.

II. LITERATURE REVIEW

According to Mutie and Ndambuki (1999) Guidance is a process, developmental in nature, by which individuals are assisted to understand, accept and utilize their aptitude, interest and attitudinal patterns in relation to their aspirations. According to Nasibi (2002) guidance is a continuing process concerned with determining and providing for the developmental needs of Learners. Guidance is considered a lifelong process that involves helping individuals either as part of a group or at personal level. Guidance is meant to equip the client with knowledge and techniques that will enable them to identify and find ways of anticipating and solving problems (Mutie&Ndambuki, 1999). Guidance is a lifelong process that involves helping individuals either as part of a group or at personal level. It is on the basis of this that this study was carried out to determine the Guidance and Counselling services offered in public boarding secondary schools in Kenya. The study found that some of the services offered by school guidance and counselling include: peer counseling, career guidance, academic counselling, personalized counselling and mentorship. The study also sought to establish whether these services were effective in enabling students adjust to school environment.

The goal of Counselling is to reduce psychological disturbance (Egan, 2002). Counselling is a service designed to help individuals to analyze themselves by relating their capabilities, achievements, interest and mode of adjustment to their new decisions (Core, 1991). The goal of Counselling is to help the counselees learn how to deal effectively with self and the reality of the environment

(Regis, 2006). The guidance-counselor's role is to help the counsees to make their decisions or choice as intelligently and as wisely as possible (Mutie&Ndambuki, 1999). Guidance aims at promoting self-understanding, developing self-direction, self-guidance and self-improvement through an increased understanding of one's limitations, resources and problems (Okeyo, 2008). Okeyo (2008) further found that counselling aims at addressing and resolving problems, help in decision making, assists one to cope with crisis and work through feelings and inner conflicts so as to improve the relationship with oneself and others. According to Kinai (2006) counseling is a face to face human encounter whose outcome is greatly dependent on the quality of counseling relationship. The key element of counseling is provision of professional service by trained and competent persons to an individual or a group in need and it is the client determines the direction and the goals to be achieved (Kinai, 2006). Counseling is a dynamic relationship between the counselor and the counselee where the counselor establishes rapport but maintains a psychological distance to avoid an overlay emotional involvement; it is a teaching learning process where the client learns new behavior and attitudes through cognitive reasoning and behavior modification (Kinai, 2006). Teachers are required to identify and counsel students who are maladjusted with an objective of helping them adjust to school environment. Teachers in charge of Guidance and Counseling to coordinate student counseling and handle cases referred to them from peer counselors and other teachers.

Counseling emphasizes the aspects of increasing client's personal responsibility for their own lives (Regis, 2006). Kasomo (2009) observes that Guidance and Counseling is useful in helping individuals face the realities of life; identify talents, interests, needs and attitudes. Republic of Kenya (1999) suggests that learners in education and training institutions are in dire need of Guidance and Counseling. Guidance and Counseling is an integral part of education process and plays the role of supplementing and complementing all other educational programmes in the school system (Mutie&Ndambuki, 1999). The aim of Guidance and Counseling is to help learners understand themselves better, discover their personal needs, evaluate their own abilities and gradually develop life goals that are individually satisfying and socially acceptable (Kenya Institute of Education, 2003). The goal of counseling service is to change the learner's behavior, beliefs and values, coping skills, decision making and emotional distress (Republic of Kenya, 2009). The aim of helping learners to change their beliefs, evaluate their abilities,

develop decision making and coping skills is to enable them to adjust to school environment. The focus of this study was to assess whether Guidance and Counselling was effective in helping learners change their beliefs, develop decision making and coping skills and whether it enhanced their adjustment to the school environment.

School Guidance and Counselling Services

Guidance and Counselling help students to make decisions, solve problems, develop positive attitudes towards self and others, establish personal goals, develop educational plans as well as select the related courses based on individual interests and talents and be responsible for one's actions and choices (Charturvedi, 2007). Rgniyd (2008) observes that Guidance and Counselling aims at stopping wastage of human manpower and physical resources by helping the individuals to find their place in the society. Counseling is the process of helping individuals to accept and use information that can help them in their present problem or cope with it successfully (Nasibi, 2002). Guidance is meant for everybody, that is, students with problems and those without problems can benefit from guidance services (Mutie and Ndambuki, 1999). In a school set up teachers are expected to give guidance to students on various aspects of school and general social life as a way of helping them adjust to school and society in general. This study assessed the extent to which Guidance and Counselling is offered in public boarding secondary school and the effectiveness of these services in helping students' adjustment to school physical social and academic environment.

In Canada and America students are provided with occupational, educational, personal, social and other types of information needed by students for planning and self-adjustment (Hartman, 1999; Schmidt, 1993). The Counselling services can either be given to an individual student or to groups of students sharing common concerns (Hartman, 1999). During counselling services, individuals are offered an opportunity for self-knowledge and self-development through individual or group interventions (UNESCO, 2000). Understanding and knowledge of oneself and the environment gained through counselling leads to personal development and good decision making (UNESCO, 2000). According to Hartman (1999) in Canadian schools, effective school Guidance and Counselling services offer educational Counselling which gives information to students who need assistance in making decisions about aspects of their education, such as the choice of subjects, courses and choice of college. Educational Counselling increases students' awareness of educational opportunities (UNESCO, 2000). It provides

students with information on learning styles and study methods as well how their attitudes, interests and work habits affect their educational opportunities (UNESCO, 2000). Through educational Counselling, students are effectively helped to select subjects and career. They are guided on effective study skills. Students are also helped to balance between the co-curricular and curriculum activities as well as prepare for examination. The purpose of educational Counselling is to help students adjust to the school academic environment and consequently actualize their potential in academic performance. This study focused on the effectiveness of Guidance and Counselling in enhancing students' adjustment to school academic environment.

Personal social Counselling deals with emotional distress and behavioral difficulties that arise when individuals struggle to deal with developmental stages and tasks (UNESCO, 2000). It also aims at helping students develop and maintain a healthy and effective interpersonal relationship as well as to improve the students' self-understanding and self-esteem (Regis, 2006). Students are empowered and taught to develop positive attitudes towards themselves (UNESCO, 2000). As a result students acquire ability to acknowledge areas of expertise and develop freedom to make positive choices in life. This leads to adjustment.

Vocational Counselling involves school counsellors having individual contacts with students who they counsel in order to facilitate career development and this helps students to become aware of the many occupations to consider and decide what to do after school (UNESCO, 2000). Occupational information can also be obtained through occupational studies, vocational Counselling leaflets and career workshops (Hartman, 1999). This study intended to ascertain how the Counselling services offered in public boarding secondary school in Kenya help in enhancing students' adjustment to school environment.

Chivonivoni (2006) observes that despite government emphasis of Guidance and Counselling services in Zimbabwe some schools never offered the services. Gumbo (2002) observes that all secondary schools in Zimbabwe had circulars providing for personal social, educational, career, vocational and HIV/AIDS education Guidance and a draft of Guidance and Counselling services syllabus. According to Ngara (1998) schools timetable Guidance and Counselling, appoint school Guidance and Counselling coordinators and have separate Guidance and Counselling rooms. The Government of Zimbabwe requires that when secondary school reports are submitted annually, mention

must be made on progress of the implementation of guidance and counseling services (Murwira, 1998). Murwira (1998) further observes that each school in Zimbabwe is expected to have a team of male and female school counsellors. Mapfumo (2001) reports that courses were conducted throughout Zimbabwe for Education Officers, District Education Officers, school principals and new school counsellors on how best to institutionalize the Guidance and Counselling Services. Kasayira, Cherishe and Chipandambira (2004) found that it was the responsibility of the headmaster of the school to make sure that Guidance and Counselling Services are implemented and taken seriously in the school. The headmaster also appoints school Guidance and Counselling coordinators and is responsible for providing adequate space and time for Guidance and Counselling activities (Gumbo, 2002).

School Guidance is meant for every student, that is, guidance benefits students with problems and those without problems (Mutie and Ndambuki, 1999). In traditional context guidance involved educating the youth about the traditions and culture of the community. Guidance was done from generation to generation by elders who considered it their social responsibility (Mutie&Ndambuki, 1999). In a school set up teachers are expected to give guidance to students on various aspects of school and general social life as a way of helping them adjust and fit in the school and society in general. It was necessary to examine the effectiveness of guidance in helping students develop self-direction, self-guidance and how guidance enhances students' adjustment to school environment. Teachers are required to identify and counsel students who are maladjusted with the aim of helping them adjust to school environment. Teachers in charge of Guidance and Counselling are expected to coordinate student counselling and handle referral cases from peer counsellors and other teachers.

Guidance and Counselling is an integral part of education process and plays the role of supplementing and complementing all other educational programmes in the school system (Mutie&Ndambuki, 1999). The aim of Guidance and Counselling is to help learners understand themselves better, discover personal needs, evaluate own abilities and gradually develop life goals that are individually satisfying and socially acceptable (Kenya Institute of Education, 2003). The goal of Counselling service is to change the learner's behaviour, beliefs and values, coping skills, decision making and emotional distress (Republic of Kenya, 2009). The main aim of helping learners to change their beliefs, evaluate their

abilities, develop decision making and coping skills is to enable them to adjust to the school environment. To achieve this, school counsellors employ different counselling services. This study evaluated the nature of services offered in secondary schools and to what extent were these services effective in helping students' adjustment school.

School Orientation Service

Orientation is information or training given to students before they start new activities (Macmillan English Dictionary for Advanced Learners, 2002). Orientation in secondary school has to do with inducting or introducing students from primary school to secondary school life (Regis 2006). Orientation services are concerned with ensuring that the problems involved at those transition points where students move from familiar situation to an unfamiliar one are reduced (Hartman, 1999). That is, orientation services are given to new students to help them adjust to their new school environment. Students are introduced to schools physical facilities, social activities and academic programmes.

According to Maluwa–Banda (1998) secondary school years in Malawi are important in the adjustment of students because they represent the transition from the completely sheltered life in primary school to the freedom and responsibility of their tertiary education or employment. Regis (2006) indicates that almost everything the student encounters is new; new teachers, students, curricular programmes, physical facilities, rules, regulations and services. The student therefore, needs help in orienting to all these new factors. Rutondoki (2000) observes that the newly admitted students to secondary school feel socially and psychologically at a loss in the new environment. They no longer enjoy the psychological support of their parents and former teachers. Such students need orientation or adaptive services to help them adjust and familiarize themselves with new situation in the school they have joined (Rutondoki, 2000). The new situation always leads to a considerable period of stress and anxiety which rests in a decrease in school performance, school attendance and self-image (Akos&Galssi, 2004). To Rutondoki, (2000) developmental, social and other problems of adjustment at the beginning of the secondary school period may seriously divert a student energies and attention from academic pursuit. This transition presents students with problems of an educational, vocational, social and personal nature (Regis, 2006). Mwamwenda (1995) observes that effective school Counselling services play a crucial role in helping

students negotiate these challenges. For example, secondary school students are assisted with study methods, note taking, writing skills and research skills to enhance their academic success. Students may also be assisted in choosing subjects, careers and friends (Regis, 2006). Students receiving orientation services are better adjusted because they get an opportunity to acquire pertinent information about what lays ahead (Regis 2006). Better adjusted students are able to live productively, to overcome their challenges as they arise and to objectively face their strength and limitations (Regis 2006). Orientation of new students is a crucial Guidance and Counselling service because through it students are given information about the school mission, vision, motto, routine, value, culture, rules and regulations in order to help then adjust to the school environment. It was important to evaluate the effectiveness orientation Guidance and Counselling services in enhancing students' adjustment to the school and that is the focus of this study.

Peer Counselling

Peer counselling is where students offer Guidance and Counselling to their peers (Myrick, 2003). Peer Counselling is based on the understanding that people who share the same age and demographic conditions, experiences and challenges are more inclined to listen to one another and influence one another's behaviour (UNESCO, 2000). Students tend to relate more closely to those peers with whom they are comfortable (UNESCO, 2000).Robinson (1991) Indicates that school counsellor selects peer counsellors by asking students to give names of two students to whom they would go if they had a personal problem. Students with the highest number of votes receive peer Counselling training. Peer counsellors assist school counsellors in showing new students around the school, listening to peers who have concerns and providing outreach activities (Robinson, 1991). Effective school counsellors make maximum use of peer counsellors to offer needs assessment, orientation, information and Counselling services (Myrick, 2003). This is achieved through training and coaching peer counsellors in basic listening and helping skills as well as basic skills of problems solving and decision making (Robinson, 1991). Peer counsellors in a school assist in identifying students with adjustment challenges in order to helps them adjust to the school and refers those they are unable to handle to the teacher in charge of Guidance and Counselling.

Rutondoki (2000) argues that in Uganda, peer Counselling enables the students to discuss freely and express personal

problems about parents, the authority and themselves in a frank manner. Peer counsellors may help in defusing minor problems before they become crises and may provide support and information to their friends who might be experiencing normal developmental stress (De Rosenroll, 1990). Peer counsellors are first line helpers of students in a need for Counselling (Schmidt, 1993). They help students who have problems in their academic work and they befriend students who have been rejected by their peers (Schmidt, 1993). They are a bridge between a troubled student and the school counsellors and can help improve the learning climate in a school (Myrick, 2003). Presence of peer counsellors helps school counsellors have more time for the students with severe problems (Lapan, 2001) Peer counsellors can assist school counsellors in meeting the needs of a greater number of students (Schmidt, 1993). Peer counsellors play a big role of assisting new students know and adjust to the school environment by befriending them, showing them the compound, helping them understand the school rules, showing them how to use various school facilities and linking those with complicated adjustment challenges with the teachers. This study focused on the effectiveness of these Guidance and Counselling services in enhancing students' adjustment to the school environment in public day secondary schools.

School Environment

A secondary school environment has physical, social and academic aspects which students need to adjust to (Gonder&Hymes, 1994). The physical environment includes school buildings, the noise levels, text books, recreational facilities and the neighborhood (Lapan, 2003).when students join secondary school they find themselves in a more expansive school environment, larger size classroom and more noisy environment than what they were used to in their relatively smaller primary schools (Adeyemo, 2001). The expansive physical environment that new students in secondary schools find themselves in has library, laboratories, big dormitories, flush toilets, and many exercise and text books due to expanded curriculum, new games and facilities. Most of these facilities are new to some of these students and may need guidance on how to use them. This study was designed to establish how students' adjustment to school physical environment in public boarding secondary schools is addressed and the effectiveness of Guidance and Counselling services that school deployed.

School social environment includes constructs like peer relationship, making new acquaintances, school norms,

classroom culture and school culture (Johnston, 2004). Student who transits to secondary school find themselves in a new social environment that is, amidst new teachers, new students as well as new systems of relationship patterns (Bragget, Morris & Day, 1999). School social environment incorporates communication and interaction between teachers and students, parents and teachers as well as teachers and other stakeholders in the community (Richardson, 2002). Students also have Social concerns such as getting lost, bullying, and making friends (Schumacher, 1998). During this transition, students also imagine and experience structural problems (Kvaslund, 2000). Majority of students entering secondary schools have high expectations about the potential of their new school (Werner & Smith,1992). Graham and Hill (2001) observe that the most common response includes looking forward to the new school, new friend and learning new things. Students lack accurate information about the culture of the secondary school environment (Kirkpatrick, 2004). Students who are unable to adjust to school social environment are likely to become social misfits. Others end up engaging in self-defeating behavior like drug abuse, truancy, indiscipline, premarital sex, organizing school unrest and burning of school. This behavior coupled with peer pressure may further lead to education wastage. To mitigate for these repercussions this study encourages establishment improvement of Guidance and Counselling Services in secondary school.

A school academic environment refers to the systems that a school has put in place to promote learning by emphasizing on academics while respecting the various levels of students' intelligence and competence (Cotton, 1996). The expectation that the school management has for students and procedures used to encourage them to succeed are also part of school academic environment (Sara, 2009). A school academic environment further includes the designed teaching procedures and the programmes that the school has put in place to facilitate student adjustment (Richardson, 2002). Academic concerns such as homework, pressure to do well, and potential drops in achievement are paramount for both students and parents (Kvaslund, 2000). The most troubling aspect in relation to school work is the increase in homework (Graham & Hill, 2001). Students have increased levels of academic pressure and assignments, and shifts in pedagogy that is less child-centered and difficult to manage (Kvaslund, 2000). Students have the perception that teachers control their work (Kvaslund, 2000). These concerns hamper students' adjustment to the school environment and results to poor academic performance.

Guidance and Counselling services are meant to address these concerns and facilitate students' adjustment to the school academic environment. This made it necessary for a study to examine the effectiveness of these services in enabling students adjust to school academic environment in Kenya

Students' Adjustment to Secondary School Environment

Adjustment, in psychology, refers to the behavioral process by which humans and other animals maintain equilibrium among their various needs or between their needs and the obstacles of their environments. Human beings are able to adjust to the physical, social, academic and psychological demands that arise from having interpersonal dependability with other individuals (Raju & Rahamtulla, 2007). Adjustment refers to the psychological process through which people manage or cope with the demands and challenges of everyday life. It connotes conformity; it deals with the way an individual adapts to his environment and demand of life (Ogoemeka, 2012). This includes how he relates to others (interpersonal) and how he deals with his responsibilities and inner feelings. Psychologically, adjustment helps the organism to cope with the demands and pressures of the outside world as well as the needs, desires and conflicts experiences from within (Singh, 2006). Ogoemeka (2012) further asserts that adjustment, as a process describes and explains the ways and means of an individual's adaptation to his self and his environment without reference to the quality of such adjustment or its outcome in terms of success or failure. It is an organizational behavior in life situations at home, at school, at work in growing up and in ageing. It helps one to keep out basic impulses at tolerable levels, to believe in one's own abilities and to achieve desired goals. Thus, adjustment helps for self-initiated growth and development along intellectual, emotional, social, physical, and vocational dimensions.

Features of transition from primary to secondary school include moving from known to unknown, from a smaller primary school to a larger secondary school and from having one teacher for several subjects to a different teacher for each subject (Graham & Hill, 2001). Student's perceptions of the transition are both positive and negative (Akos, 2004). The transiting students are concerned about the size and layout of secondary schools, the time table, and complicated schedules, getting picked on, not knowing anyone, potentiality getting lost, having multiple teachers, and remembering where to go (Graham & Hill, 2001).

According to Hargreaves and Earl (1990) students experience anxiety on transfer to secondary school but this anxiety passes quickly leaving students the challenge of adjusting to the many uncomfortable realities of secondary school life. These challenges can restrict students' achievement by lowering their motivation and this may lead to one dropping out school in later years (Hargreaves & Earl, 1990). However, students have a perception of protective factors and attractive features of secondary school which include having more freedom, meeting new friends, and involvement in co-curricular activities (Akos, 2004). The transition to secondary school therefore inevitably includes a period of adjustment (Bates, 1998). Transition from primary to secondary interrupts friendship and other social network that a student had built in primary school (Hertzson & Morgan, 1998). Transition from primary to secondary school is accompanied by stress (Ward, 2001). The transiting students have particular expectations about the teachers and the process of teaching and learning in secondary school (Gorwood, 1994). Many students have anxiety on transition to secondary school mainly due to the size and complexity of their new school organization, the new form of discipline and authority, new demands of work, prospects for being bullied and the possibility of losing friends (Raju and Rahamtulla, 2007). Students at transition point are both excited and anxious, both doubtful and hopeful and their perceptions of transition are both positive and negative (Akos, 2004). Students adjustment to secondary school occurs as they are making other adjustments related to their onset of puberty (Kaur, 2012). Thus, it is essential for transition programme to provide social support activities that give students the opportunity to know and develop positive relationship between the older student and the incoming students (Akos, 2004). The adjustment period may last until students are able to show that they can cope by making appropriate responses to the demands of their new environment (Ward, 2001). Students' adjustment is therefore crucial for them to be able to achieve maximum benefit from the school. Student adjustment involves learning to cope with new teachers, student, subjects, facilities and challenges. This adjustment is facilitated by effective Guidance and Counselling services. This study assessed extent to which students in public boarding secondary schools are able to cope with the challenge of school environment.

Effectiveness of Guidance and Counselling in Enhancing Students' Adjustment to School

Environment

Zeedyk et al. (2003) observed that school Guidance and Counselling services have been successful in operating some type of transitional support services. School Guidance and Counselling services address developmental issues of students in three essential areas that is, educational development, career development and personal social development (Regis, 2006). Lonborg and Bowen (2004) argue that in America, effective school Guidance and Counselling services create a safe school environment. To Lapan, Gysbers and Petroski (2003) these services create greater students' feelings of safety in schools. In this kind of environment, students have a sense of belonging (Lapan, 2003). Lonborg and Bowen (2004) further found that in America students are able to make friends and hold their temper down as a result of school Guidance and Counselling service they received. Students who participated in school Guidance and Counselling services view themselves more positively and are confident of being successful in school and this enhances their adjustment to school environment.

Euvrard (1996) found that in South African high schools effective Guidance and Counselling equipped students with information, skills and attitudes which enabled them to successfully negotiate the challenges of adolescence and develop a social skill that enables them adjust to the school environment. Effective school Counselling result in fewer personality or school adjustment challenges (Euvrard, 1996). Effective school Guidance and Counselling services in America help students acquire developmental competencies such as establishing and maintaining peer relationship which in turn results to good adjustment to school environment (Euvrard (1996)). Borders and Drury (1992) cites studies in America that school increased academic achievement, academic persistence, school attendance and positive attitude towards school and others as a result of school Counselling. Maluwa-Banda (1998) observes that Malawian Secondary School Guidance and Counselling services help students understand their own interest, abilities and potentialities and develop them to their full. Students are also helped to identify educational and vocational opportunities and this motivates the students to adjust to the school as they work hard to achieve their educational and vocational goals (Jones, 1993). Lapan, Gysbers and Sun (1997) report that American schools with effective Guidance and Counselling services had student

reporting that they adjusted well to the school attained higher grades because they learnt that education was preparing them for their future because their school availed more career and college information to them and created a more positive climate. The school has physical, social and academic environment which students have to adjust to in order to actualize their potential. Guidance and Counselling is used to help students achieve this adjustment. There was therefore, a need to carry out a study to establish the effectiveness of Guidance and Counselling services in preparing students for new situations and enhancing their adjustment to school environment.

Gender Comparisons on Effectiveness of Guidance and Counseling Services

Parhar, et al. (2013) in his studies in India established that there was no much different in effectiveness of Guidance and Counselling between female and male secondary school students. Winga, et al. (2011) found that there were no significant differences between boys and girls in adjustment to school environment though in the Overall the boys had higher school adjustment when compared to the girls.

Some researchers have found that in some aspects boys adjusted better than girls. Armacost (1990) established that in America guidance and Counseling was more effective in enabling boys handle stress better than girls. Van Der Walt and Knoetze (2004) observe that Guidance and Counselling normally was more effective in socializing boys to be stronger and cope with their own problems than girls. Makesh and Kaji (2014) found that Guidance and Counselling was more effective in enabling boys adjust to school social environment than girls.

Other researches on gender differences in school adjustment have portrayed that girls are better adjusted compared to boys (Wang, et al., 2008). Another study by Kiuru, et al. (2009) looked at 1494 adolescents from Finland. They used questionnaires concerning peer relations and adjustment and maladjustment. 360 peer groups were identified and only peer group members were analyzed. Results showed that members of adolescents peer groups resembled each other in terms of school adjustment and maladjustment. Members of girls' cliques resembled each other more in satisfaction with their educational choice and school engagement when compared with boys. This shows that there are gender differences in school adjustment. The gap that the current study seeks to address concerning gender differences is based on the academic achievement of the gender. Alexitch and Page (1997) established that in Canada girls were more responsive to university and career information from their

counselling teachers than boys. Bruce and Cockreham (2004) found that in America Guidance and counseling enabled girls to be more tolerant towards rules, more willing to make exceptions and more easily reconciled than boys. Singh, et al. (2014) established that in India Guidance and Counselling was significantly effective in enabling girls adjust to the school emotional environment than boys.

III. METHODOLOGY

Research Design

The study adopted a descriptive survey research design to assess effectiveness of Guidance and Counselling in enhancing students' adjustment to school environment in public boarding secondary school in Kenya. Descriptive survey design is a method of collecting information by interviewing or administering questionnaires to a sample of individuals (Orodho, 2003). In this design, the researcher does not manipulate the variables under study but examines the variables in their natural state. The study was conducted within public boarding secondary schools. The aim of the study was to assess student utilization of services in Kenya. Descriptive survey design often results in the formulation of important principles of knowledge and solutions to significant problems since it produces statistical information about aspects of education that is used by policy makers, educators and other interested parties in different capacities (Kombo & Tromp, 2006). This design was therefore suitable because it enabled the study to assess the effectiveness of Guidance and Counselling in enhancing students' adjustment in secondary school environment in public secondary schools in Kenya.

Study Population

According to Kombo and Tromp (2006) population is a group of individuals, objects or items from which samples are taken for measurement. The target population for this study was 1,208,818 students in public boarding secondary schools in (Republic of Kenya, 2009). The accessible population is 151,944 students in the three counties that were sampled for the study that is Nairobi, Kitui and Nyeri. The population of form three students in these counties is 35,659.

Sampling Procedures and Sample Size

According to Gay (1992) a researcher selects a sample due to various limitations that may not allow researching the whole population. However, sampling ensures that subjects selected represent the characteristics of the entire population

in question and the findings may be generalized to them. Three counties were purposively sampled for this study, that is, Nairobi, Kitui and Nyeri to represent geographically urban, rural marginal and rural potential public secondary schools strata respectively.

Schools in each of the three counties were stratified into national, Extra County and county school strata. Each stratum (national, extra- county and county schools) was further stratified into boys and girls schools. A simple random sampling design was used to select one school from each stratum (boys and girls) So there were three girls' schools and three boys' schools representing national, extra-county and county schools. Purposive sampling design was used to select of Form 3 students because they had been in secondary school for a relatively longer period and so they were likely to have more information on effectiveness of Guidance and Counselling either out of their own experience or observation of other student experiences. Simple random sampling was also used in selecting one Form 3 stream from schools with more than one stream.

The three counties used in this study have a population of 35,659 form three students. The recommended sample size for a population of 35,659 is 379 according to Kathuri and Pals (1993). According to the Ministry of Education school enrolment is 40 students per class (Republic of Kenya, 2009). The expected number of schools was 379 respondents divided by 40 which give 9 schools. However, for this study, the sample was doubled so as to minimize errors associated with sampling and also to mitigate the observed heterogeneity of the counties. In each of the schools selected for the study data was also collected from for a three class teacher and the teacher in charge of Guidance and Counselling for triangulation. Therefore, the sample size of the study was 756 respondents comprising of 720 Form 3 students, 18 form 3 class teachers and 18 teachers in charge of Guidance and Counselling. Table 1 provides summary of the sample sizes that were taken for the study.

Table.1: Sample Size

County	Form 3 population	Students Sample	Sampled Class Teachers	Counselling teachers sample	Total
Nairobi	7,943	240	6	6	246
Kitui	14,320	240	6	6	246
Nyeri	13,394	240	6	6	246
Total	35,659	720	18	18	756

IV. RESULTS AND DISCUSSIONS

Mean of Gender Comparisons

Table 24 presents the mean comparisons on effectiveness of Guidance and Counseling in adjustment to school adjustment according to gender.

Table.24: Gender Comparison of Effectiveness Guidance and Counselling in Students' Adjustment to School Environment

	Gender	N	Mean	Sd
Effectiveness of G&C in enhancing student adjustment to the school physical environment	Boys	360	4.2781	.38407
	Girls	360	4.3072	.37854
Effectiveness of Guidance and Counselling on students' adjustment to school social environment	Boys	360	4.3008	.39541
	Girls	360	4.3208	.37355
Effectiveness of Guidance and Counselling on students adjustment to school academic environment	Boys	360	4.2308	.41754
	Girls	360	4.2369	.42753

The results in Table 24 show that some mean difference existed between girls (4.3072) boys (4.278).in effectiveness of Guidance and Counselling in enhancing students' adjustment to school physical environment. This shows that Guidance and Counselling was more effective in enhancing girls' adjustment to school physical environment than boy.

However to know whether the difference was significant a t-test had to be done.

t-test on Gender Comparison

To establish whether there was a significant gender difference in means a t-test was performed. The results of the test are as shown in Table 25

Table.25: t-Test of Gender Comparison

Levine's Test for Equality of Variances							
		F	Sig.	t	df	Sig. (2-tailed)	Mean Def.
Effectiveness of Guidance and Counseling on students adjustment to school environment	Equal variances assumed	.078	.780	-.790	718	.430	-.0184
	Equal variances not assumed			-.790	717.971	.430	-.0184

The information in Table 25 the t-test results indicate that the p value was greater than the critical p value that is, t value ($t=-0.790$, $P> 0.05$) in view of these findings there is no statistically significant gender difference in adjustment to the school environment in public boarding secondary schools. The null hypothesis (H_{01}) suggesting that there is no significant gender difference in the effectiveness of Guidance and Counselling in enhancing students' adjustment to school environment in public boarding schools in Kenya was therefore accepted.

V. DISCUSSIONS

These findings concurred with finding from related studies by Parhar, et al., (2013) whose study in India established that there was no significant difference in the effectiveness of Guidance and Counselling between female and male secondary school students. This differs with related studies by Armacost (1990) who established that in America guidance and Counseling was more effective in enabling boys to handle stress better than girls. Van Der Walt and Knoetze (2004) in a related study in South Africa observed that Guidance and Counselling was more effective in socializing boys to be stronger and cope with their own problems than girls. Alexitch and Page (1997) established that in Canada girls were more responsive to university and career information from their counselling teachers than boys. Bruce and Cockreham (2004) found that in America Guidance and counseling enabled girls to be more tolerant towards rules, more willing to make exceptions and more easily reconciled than boys. Singh et al (2014) established that in India Guidance and Counselling was significantly effective in enabling girls adjust to the school emotional environment than boys. On the contrary Makesh and Kaji (2014) found that Guidance and Counselling was more effective in enabling boys adjust to school social environment than girls. The differences in these studies could be attributed to the fact that each one of them was studying some aspects of students, adjustment while this study compare the overall student adjustment to school environment. From these finding it can be concluded that there are some unique differences in gender adjustment to the school environment. When these unique areas are identified and addressed effectively through Guidance and Counselling students are able to adjust better to the school environment.

VI. CONCLUSION

The study found that there was no significant gender difference in the effectiveness of Guidance and Counselling

in helping students' adjustment to school environment. The T-test of the hypothesis indicated that there was no significant difference between boys and girls adjustment to the school environment. The study further found that there was no gender sensitivity in the appointment of Guidance and Counselling personnel. Majority of teachers in charge of Guidance and Counselling were females even in boys' schools. Majority of the class teachers were not only females but were newly posted. This means they lacked experience in handling students' Counselling issues. The study also established that in some girls' schools male teachers were in charge of Guidance and Counselling. The Guidance and Counselling teachers had served for many years as teachers which mean they were experienced in student affairs.

The study further established that though girls adjusted better than boys, there was no significant gender difference in the effectiveness of guidance and Counseling in enhancing students' adjustment to the school environment.

VII. RECOMMENDATION

Although the study found that there was no gender difference in the effectiveness of Guidance and Counselling, it is necessary for schools to tailor their programs to address the Guidance and Counselling issues that are unique to each gender. Boys' schools should tailor their services to address issues that affect male gender and girls' school should do the same to address Counselling issues that are unique to female gender. To enhance this, school management should be gender sensitive in appointing guidance and counselling personnel so that a bigger percentage should be of the same gender with the students. This will ensure that issues that are unique are better handled by a counsellor of the

REFERENCES

- [1] Adeyemo, D. A. (2006). Parental Involvement, Interest in Schooling and School Environment as Predictors of Academic Self Efficacy among Fresh Secondary School Students in Oyo State University. *Electronic Journal of Research in Educational Psychology* 5, 3(1) 163-180.
- [2] Akos, P. &Galassi, J. P. (2004). Middle and High School Transition as Viewed by Students, Parents and Teachers. *ProfessionalSchool Counselling*. 7(2), 212 – 221.
- [3] Alexitch, L. R. & Page, (1992) Evaluation of Academic and Career Counselling Information and its Relation to Students Education Orientation. In

- Canadian Journal of Counselling*, 31 (3), p. 205 – 218.
- [4] Armacost, R. L. (1990). High School Stress and the Roles of counsellors. *In School Counsellor*, 38 (2), p. 105 – 112.
- [5] Baills, L. & Rossi, T. (2001). The Transition From Isolated, Rural Contexts to Boarding School: Can School Physical Education And Sport Play A Part? *Journal of Physical Education New Zealand*, 34(1), 40-52. Retrieved January 24, 2002, from ProQuest Education Complete.
- [6] Banathy, B. H. (1992). *A Systems View of Education Concepts and Principle for Effective Practice*. Englewood Cliffs, NJ, Education Technology.
- [7] Bogonko, S. N. (1992). *Reflections on Education in East Africa*. Nairobi. Oxford University Press.
- [8] Borders, L. D. & Drury, S. M (1992). Comprehensive School Counselling Programmes. A Review of Policy Makers and Practitioners. *Journal of Counselling and Development*. 70(4), 487 – 498.
- [9] Bragget, E., Morris, G. & Day, A. (1999). *Reforming Middle Years of Schooling*. Hawker Brown low Education.
- [10] Bruce, M. A. & Cockreham, D. (2004) Enhancing Spiritual Development of Adolescent Girls. *In Professional School Counselling*, 7(5), P. 334 – 342.
- [11] Catterall, J.S. (1998). Risk and Resilience in Student Transition to High School. *American Journal of Education*, 106(2), 302-333.
- [12] Chivonivoni, T. (2006). *The State of School Counseling in Chiredzi North Secondary Schools*. Bsc Counselling Dissertation. Zimbabwe open University.
- [13] Clive, M., Richard, W., Joan, G. & Ann, H. (2003). *Transition from Primary to Secondary School–Young People’s Experiences in the London Borough of Waltham Forest*. Retrieved August 14, 200 [http://www.ncb.org.uk/Resources/ Research Summary 188](http://www.ncb.org.uk/Resources/ResearchSummary188).
- [14] Cotton, K. (1996). School Size, School Climate, and Student Performance (School Improvement Research Series, Close-Up No. 20). Portland OR: Northwest Regional Educational Laboratory.
- [15] De Rosenroll, D. A. (1990). Centralised Approach to Training Peer Counsellors: 3 Years of Progress. *The School Counsellor*, 37, 304-313
- [16] Egan, G. (2002). *Implications for Time Limited Counselling and Treatment of Type A Behavior*. Unpublished Master’s Thesis. Ohio State University.
- [17] Euvrard, G. (1996). Career Needs of Eastern Cape Pupils in South Africa. *British Journal of Guidance and Counselling*, 24(1), 113 – 128.
- [18] Gay, L. R. (1992). *Educational Research: Competences for Analysts and Application: (4th Ed)*. London: Columbus Merrill.
- [19] Gonder, P. O., & Hymes, D. (1994). *Improving School Climate and Culture* (AASA Critical Issues Report No. 27). Arlington, VA: American Association of School Administrators. This Report Provides Extensive Information on School Climate and School Culture and Step-By-Step Suggestions for Improvement.
- [20] Gorwood, B. (1994). Curriculum Organization and Classroom Practice in Primary Schools-Can we learn from Middle Schools? *School Organization*, 14(2), 247 256.
- [21] Graham, C. & Hill, M. (2001). The SCRE Centre Website. *Negotiating the Transition to Secondary School*. Retrieved May 20, 2004 from [http://www.scre.ac.uk/spotlight/ spotlight89.html](http://www.scre.ac.uk/spotlight/spotlight89.html).
- [22] Gumbo, K. (2002). *Guidance and Counselling Activities and End of Year report*. Masvingo Region, Zimbabwe
- [23] Hargreaves, A., & Earl, L. (1990). *Rites of Passage: A Review of Selected Research about Schooling in the Transition Years*. Report to the Ontario Ministry of Education. Toronto: Queens Printer.
- [24] Hartman, J.B. (1999). *Secondary School Counselling Manual Canada*: University of Manitoba.
- [25] Hawkins, P. (2002). *Understanding Management and Examination Practices*. Nigeria: NERDC Press.
- [26] Hertzog, C.J. & Morgan, P. L. (1998). Breaking the Barriers between Middle School and High School: Developing a Transition Team for Student Success. *NASSP Bulletin*, 82(597), 94-98.
- [27] Johnstone, K. (2006). *The Transition to High School: A Journey to Uncertainty*. (retrieved)
- [28] www.aare.edu.au/02pap/jpohn020562.htm.
- [29] Kasayira, J. M; Chireshe, R. & Chipandambira, K. (2004) Educational Behaviour, BSC Hons Psychology, module HPSY 403, Harare, Zimbabwe Open University.
- [30] Kasomo, D. (2009). The position of African Traditional Religion in Conflict Prevention. *Journal of Sociology and Anthropology*, 2 (2), 023-028. Retrieve November 29, 2010. Retrieved November 29, 2010 from <http://www.academicjournals.com>.
- [31] Kenya Institute of Education (2003). *Guidance and Counselling: Teachers Handbook*. Nairobi KIE

- [32] Kinai, T. K. (2006). *Guidance Practice in Schools*. Unpublished Module, Kenyatta University.
- [33] Kirkpatrick, D. (2004). *Making the Change: Students' Experiences of the Transition to Primary School*. Retrieved May 20, 2004 from <http://edoz.com.au/education/Australia/archive/features/make.html>.
- [34] Kiuru, N., Nurmi J., Aunola K., Salmela –Aro, K. (2009). Peer group homogeneity in adolescents' school adjustment varies according to peer group type and gender. *International Journal of Behavioral Development* 33 (1) 65-76.
- [35] Kombo, D. K. & Tromp, D. L. (2006). *Proposal and Thesis Writing: An Introduction*. Nairobi: Paulines Publications Africa.
- [36] Kvalsund, R. (2000). The Transition from Primary to Secondary Level in Smaller and Larger Rural Schools in Norway: Comparing Differences in Context and Social Meaning *International Journal of Educational Research*, Vol. 33, Issue 4, p401-424.
- [37] Lapan, R. T. (2001). Results Based Comprehensive and Counselling Programmes, 4(4), 289 – 299.
- [38] Lapan, R. T.; Gysbers, N. C & Petroski, G.F. (2003). Helping Seventh Graders be Safe and Successful: Statewide Study of the Impact of Comprehensive Guidance and Counselling Programmes. *Professional School Counselling*, 6(3), 186 – 197.
- [39] Lapan, R. T., Gysbers, N. C., & Sun, Y. (1997). The Impact of More Fully Implemented Guidance Programmes on the School Experiences of High School Students: A Statewide Evaluation Study. *Journal of Counselling & Development*, 75(4), 292-302.
- [40] Lonborg, S. D. & Bowen, N. (2004). Counsellors, Communities and Spirituality: Ethical and Multicultural Consideration. *Professional School Counselling* 7 (5) 318 – 325.
- [41] Macmillan English Dictionary: Advanced to Learners. (2002). Macmillan Publishers.
- [42] Maluwa- Banda, W. (1998) Guidance and Counselling in Malawi. *British Journal of Guidance and Counselling*, 26 (2), 287 – 295.
- [43] Mapfumo, J. (2001). *Guidance and Counselling in Education*, Post Graduate Diploma in Education, Module PGDE 012. Harare. Zimbabwe.
- [44] Midgley, C. & Maehr, M.L. (2000). The Transition to High School Study: Report to Participating Schools and Districts. Ann Arbor, MI: University of Michigan.
- [45] Murirwa, O. (1998) *Guidance and Counselling: implementation procedures in the Mindland Regions*. Ministry of Education, Sports and Culture Zimbabwe. Unpublished Paper.
- [46] Mutie, E. K & Ndambuki, P. (1999). *Guidance and Counselling for Schools and Colleges*. Nairobi: Oxford University Press.
- [47] Mwamwenda, T. S. (1995). *Educational Psychology. An African Perspective*. Durban: Butter Worth's.
- [48] Myrick, R. D. (2003). Accountability: Counsellors Count. *Professional School Counselling*, 6(3) 174 – 179.
- [49] Nasibi, M. W. (2002). *Discipline Guidance and Counselling in Schools*. Nairobi. Strong Wall Africa.
- [50] Ngara, I. (1999). *Syllabus for Guidance and Counselling*. Mashonaland, Region. Unpublished paper.
- [51] Ogoemeka, O.H. (2012). A Study of The Emotional Intelligence and Life Adjustment of Senior Secondary School Students in Nigeria, *The 2012 Orlando International Academic Conference*, Orlando, Florida, USA 59.
- [52] Okeyo, A. T. O. (2008). *Peer Counselling Experience among Selected Secondary Schools*. Paper presented at KAPC Conference. Retrieved November 29, 2010 from <http://docs.google.com>
- [53] Orodho, J. A. (2003). *Techniques of Writing Research Proposals and Reports in Education and Social Sciences*. Nairobi: Masola Publishers.
- [54] Parhar, M. K., Khushwinder, K. & Pushpinder, K. (2013) Guidance Needs of Secondary School Students. *International Journal of Behavioral Social and Movement Sciences*. Vol.02(2) p 77-87.
- [55] Potter, N. (2001). *Looking Forward to Teaching: A Team Approach to Teaching in Years 9 And 10*. Wellington: New Zealand Council for Educational Research.
- [56] Raju, M.V.R. and Rahamtulla, T.K. (2007). Adjustment Problems among School Students, *Journal of the Indian Academy of Applied Psychology*, 33(1), 73-79.
- [57] Regis, C. (2006) An Assessment of the Effectiveness of School Guidance and Counselling service in Zimbabwean Secondary School. Unpublished PhD Thesis. University of South Africa.
- [58] Republic of Kenya. (1999). *Totally Integrated Quality Education and Training (TIQET)*. Report of the Commission of Inquiry into the Education System of Kenya. Nairobi. Government Printers.

- [60] Republic of Kenya. (2001). Report of the Taskforce on Student Discipline and Unrest in Secondary Schools. Nairobi. Jomo Kenyatta Foundation.
- [61] Republic of Kenya. (2007). *Kenya Vision 2030: A Globally Competitive and Prosperous Kenya*. Nairobi: Government Printers.
- [62] Republic of Kenya. (2009). *Careers Guide Book for Schools*. Nairobi. Government Printers.
- [63] Republic of Kenya. (2009). Training Module for Guidance and Counselling Heads of Department in Secondary Schools. Nairobi. Government Printers.
- [64] Rgniyd, Z. (2008). Adolescent Health and Development: Career beyond Horizon. Retrieved September, 28 2010 from, <http://www.rgniydadhp.gov.in/publication.htm>
- [65] Richardson, T. (2002). The Importance of Emotional Intelligence During Transition to Middle School: What Research Says. *Middle School Journal*, 33, 55 – 58.
- [66] Robinson, B. D. (1991). School Counsellors in England and Wales, 1965 – 1995. A Flawed Innovation? *Pastoral Care in Education*, 14 (3), 12 – 18.
- [67] Rutondoki, E. N. (2000). *Guindace and Conseling*. Kampala, Makelele University. Institute of Adult and Continuing Learning.
- [68] Sara, R. (2009). Using Concept of Mapping to Structure the School Environment's Contribution to School Violence: Proving Suggestions for School Environment Intervention. Unpublished PhD Thesis. John Hopkins University.
- [69] Schumacher, D. (1998). *The transition to middle school*. ERIC Educational Clearing House :no.ED 422119). www.ericfacility.net
- [70] Schmidt, J. J. (1993) *Counselling in Schools Essential Services and Comprehensive Programmes*. New York. Allyn and Bacon.
- [71] Singh, H. (2006). Effect of Socio Emotional Climate of the School on the Adjustment of Students. *Psychologia*, 36(2), 133- 143
- [72] Singh, T.K., Tripathi, S and Mahato, J. (2014). Health and Adjustment of High School Students, *The International Journal of Indian Psychology*, 1(4), 9-18.
- [73] UNESCO (2000). Module 8. Guidance and Counselling Programme Development Botswana.
- [74] Van Der Walt, J. L.; Grimbeck, M. & Marais, J. L. (2001) Guidance and Counselling in Multicultural Ex-model C Schools. *South African Journal of Education*, 21(3), 152 – 157.
- [75] Ward, R. (2001). *The Development of a Middle School*. Unpublished PhD Thesis. Hamilton: University of Waikato.
- [76] Werner, E., & Smith, R. (1992). *Overcoming the Odds: High-Risk Children from Birth to Adulthood*. New York: Cornell University Press. (ED 344 979)
- [77] Zeedyk, M.S.; Gallacher, J.; Henderson, M.; Hope, G, Husband, B & Lindsay, K. (2003). Negotiating the Transition from Primary to Secondary School: Perceptions of Pupils, Parents and Teachers. *School Psychology International* 24(1), 67 – 86.

Reactive and Active Power Output Optimization in a Wind Farm Using the Particle Swarm Optimization Technique

Nazha Cherkaoui, Abdelaziz Belfqih, Faissal El Mariami, Omar Sabri, Jamal Boukherouaa, Mohamed Nouh Dazahra, Meriem Majdoub

Laboratory of Electric Systems and Energy, ENSEM, Casablanca, Morocco

Abstract—In the recent years, the contribution of the wind power to energy supply has increased considerably; hence, the wind farms have to be able to participate to the grid power stability. In this paper, an optimization algorithm allows obtaining the reactive and active power dispatch in a wind power plant is presented. The aim of the proposed algorithm is to minimize the power losses and the difference between the reactive power obtained and required by the transmission system operator at the point of common coupling. The simulation results show the validity and the performance of the proposed algorithm.

Keywords—wind farms; grid stability; optimization algorithm; the reactive and active power dispatch; transmission system operator; point of common coupling.

I. INTRODUCTION

In the last years, the integration of wind energy into power grids has grown significantly. In order to ensure the power quality of the grid, transmission system operators (TSO) in different countries require from wind farms (WFs) to be able to contribute to ancillary services, especially in reactive power control.

Many works have been done in order to get an optimal reactive power dispatch using several methods such as particle swarm optimization (PSO) technique. In [1] a PSO technique for a reactive power wind farm function is presented. This technique allows obtaining the reactive power reference for each wind turbine with the aim to optimize the reactive power dispatch at a wind farm and minimize its power losses.

This paper is organized as follows: First, the doubly fed induction generator (DFIG) is presented. Second, the reactive power limitations of a wind turbine are determined using the method proposed in [2]. Then, a multi objective function that allows getting under several constraints both the reactive and active power set point for each wind turbine (WT) is presented. Finally, simulation results are reported.

II. DOUBLY FED INDUCTION GENERATOR (DFIG)

The doubly fed induction generator is coupled to the grid with the stator windings, while the rotor windings are connected to the grid via a back-to-back converter [3], as shown in figure 1. The DFIG exchanges the power with the grid through the stator windings as well as the rotor windings. The main part of the power passes from the generator through the stator into the grid, whereas only a fraction of the power is passed from the rotor windings through the power converter [2].

The DFIG technology is the most widely used generator in the wind farms for several reasons. First, it has the ability to control electrical torque (hence active power) and reactive power exchange with the grid. Besides, the DFIG is the cheapest solution to realize variable speed operation because the converters are sized only for 20%-35% of the stator power (not total turbine power) depending on the slip (or operating speed) range and reactive power requirements [4].

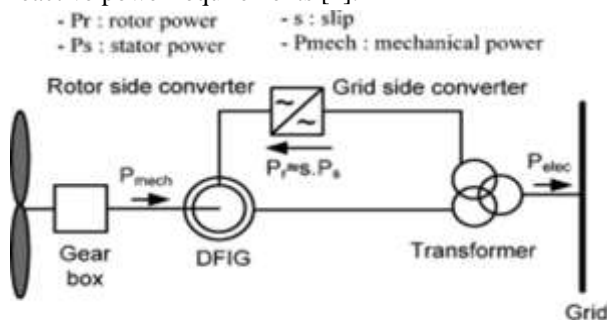


Fig. 1: The basic layout of a DFIG wind turbine [5]

III. DFIG CAPABILITY LIMITS CURVE

We use the method proposed in [2] in order to get the reactive power capability of a 2MW DFIG based wind turbine. In this method, we consider that the reactive power capability is limited by three parameters: stator current (I_s), rotor current (I_r), and rotor voltage (V_r). In order to obtain the PQ diagram, the stator voltage is considered to be equal to 1 p.u, and the steady state T-

equivalent circuit, as shown in figure 2, is used to derive the complex powers from the stator and the rotor windings.

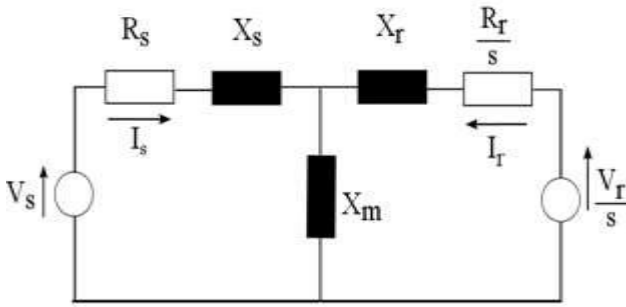


Fig. 2: Steady state T-equivalent circuit for the DFIG [2]

The reactive power capability of a DFIG is obtained by the most restrictive of the three limitations. Figure 3 shows the PQ curve of 2MW DFIG based wind turbine using the parameters illustrated in table I.

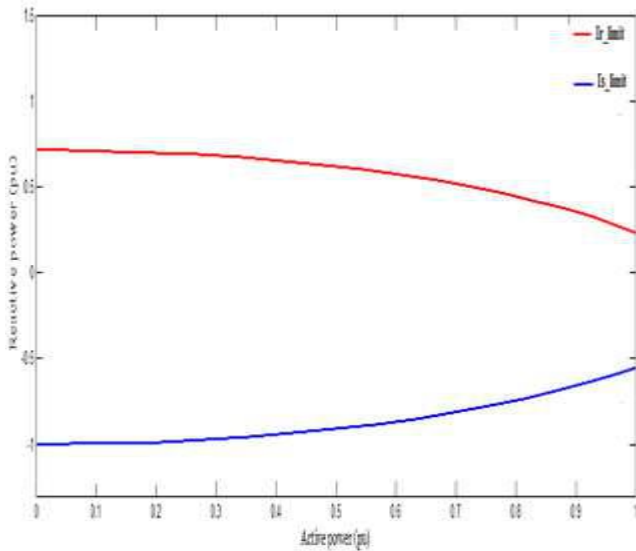


Fig. 3: Results reactive power capability used in this paper

Table I: REpower MM82 parameters [6]

Machine parameter	Value
Nominal active power	2MW
Nominal stator voltage	690 V
Stator resistance	0.00206 Ω
Stator inductance	0.032 Ω
Rotor resistance	0.0028 Ω
Rotor inductance	0.021 Ω
Magnetizing resistance	36.4 Ω
Magnetizing inductance	0.83 Ω
Turn ratio	2.43
slip	-0.2

IV. PARTICLE SWARM OPTIMIZATION METHOD

Particle swarm optimization is a heuristic global optimization method put forward originally by Doctor Kennedy and Eberhart in 1995 (Kennedy J, Eberhart R, 1995; Eberhart R, Kennedy J, 1995). It is developed from swarm intelligence and is based on the research of bird and fish flock movement behavior [7].

The particle swarm model consists of a group of particles that are randomly initialized in the d-dimensional search space. During an iterative process, particles explore this space effectively by exchanging information to find the optimal solution. Each i-th particle is described by its position x_i , velocity v_i , and best position $pbest_i$. Moreover, the particles have access to the best global position $gbest$ that has been found by any particle in the swarm [8].

Then, each particle updates its coordinates based on its own best search experience $pbest_i$ and $gbest$ according to the following velocity and position update equations: [9]

$$v_i^{k+1} = w v_i^k + c1 r1(pbest_i^k - x_i^k) + c2 r2(gbest^k - x_i^k) \quad (1)$$

$$x_i^{k+1} = x_i^k + v_i^{k+1} \quad (2)$$

Where:

w: Inertia weight

c1, c2: Acceleration coefficients

r1, r2: Two separately generated uniformly distributed random numbers in the range [0,1] added in the model to introduce stochastic nature.

The inertia weighting factor for the velocity of particle is defined by the inertial weight approach

$$w^k = w_{max} - \frac{w_{max} - w_{min}}{k_{max}} \times k \quad (3)$$

Where:

k_{max} is the maximum number of iterations, and k is the current number of iterations.

w_{max} and w_{min} are the upper and lower limits of the inertia weighting factor, respectively.

V. PROBLEM FORMULATION

We propose to use a multiobjective optimization function to calculate the reactive and active power set point for each wind turbine within the wind power plant. The multiobjective function is expressed as follows:

$$\min F(X) = |Q_{pcc}^{set} - Q_{pcc}| + \lambda P_{loss} \quad (4)$$

Where:

- $X = (Q1, Q2, Q3, Q4, Q5, P1, P2, P3, P4, P5)$

P_i is the WT active power generation.
 Q_i is the WT reactive power consumption/generation.

- Q_{pcc}^{set} is the reactive power required at the PCC by the TSO
- Q_{pcc} is the reactive power generated by the wind farm at the PCC ,and it is obtained as follows:

$$Q_{pcc} = \sum Q_{g_i} - Q_{Losses} \quad (5)$$

Where Q_{g_i} is the generated or absorbed reactive power of each iDFIG, and Q_{Losses} is the reactive power losses within the wind power plant.

- P_{loss} is the real power losses within the wind power plant.
- λ is the weight coefficient.

The minimization of the multiobjective function is subject to the following constraints:

1). The node power equation

$$P_i = U_i \sum_{j=1}^{Nb} U_j (G_{ij} \cos \theta_{ij} + B_{ij} \sin \theta_{ij}) \quad (6)$$

$$Q_i = U_i \sum_{j=1}^{Nb} U_j (G_{ij} \sin \theta_{ij} - B_{ij} \cos \theta_{ij}) \quad (7)$$

Where:

U_i and U_j are the voltage amplitude of nodes i and j respectively;

$\theta_{ij} = \theta_i - \theta_j$ is voltage phase angle difference of node i and j ;

G_{ij} and B_{ij} are mutual conductance and susceptance of admittance matrix respectively;

P_i and Q_i are injected active and reactive power of node i .

2). DFIG reactive capability limits

$$Q_i^{\min} \leq Q_i \leq Q_i^{\max} \quad (8)$$

3). DFIG active power limits

$$P_i^{\min} \leq P_i \leq P_i^{\max} \quad (9)$$

The PSO algorithm is initialized with the population of individuals being randomly placed between the space of possible values $[Q_{WT}^{\min}, Q_{WT}^{\max}]$ and $[P_{WT}^{\min}, P_{WT}^{\max}]$, and it looks for the optimal solution by updating individual generations. The velocity and the position of each particle are updating, at each iteration, according to its previous best position (P_{best}) and the best of the group g_{best} , as illustrated in figure 4.

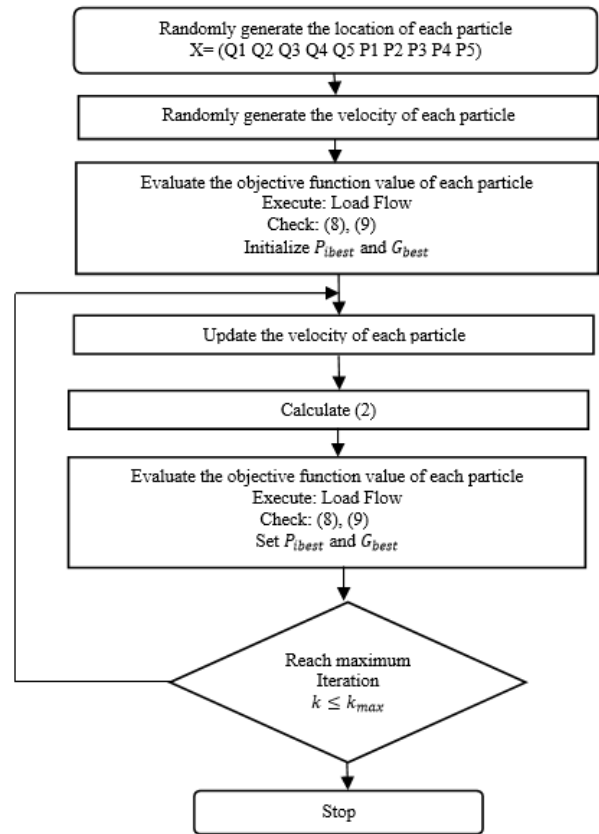


Fig.4: Flow chart of the proposed PSO algorithm

VI. SIMULATION RESULTS

An example system is used as shown in figure5 in order to verify the validity and performance of the proposed optimization algorithm. The wind farm consists of five 2 MW wind turbines, and it is connected to a 20 kV distribution system which exports power to 63 kV grid through a 10 km 20 kV feeder.

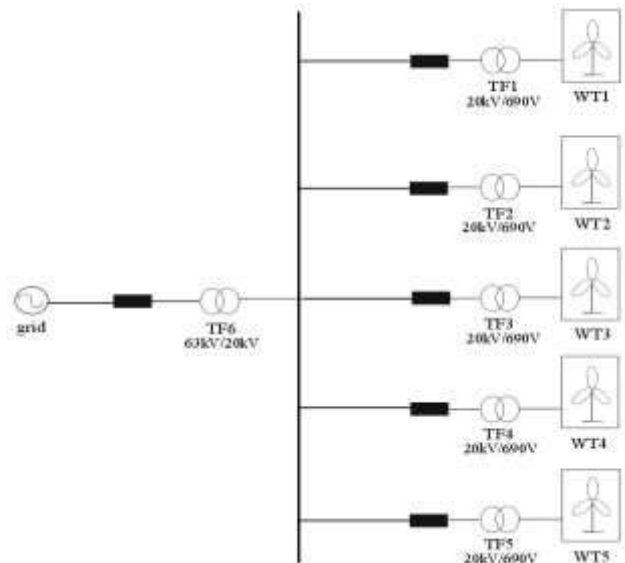


Fig. 5: An example system for simulation

Three different cases to do the reactive power dispatch are tested and compared. The WTs within the wind power plant are operating at full active power in both case 1 and 2; also, the reactive power Q_{pcc}^{set} required at the PCC by the TSO is equal to 0,7 Mvar in the all cases.

- Case1: the reactive power Q_{pcc}^{set} required at the PCC is proportionally distributed between the WTs within the wind power plant.
- Case2: The reactive power reference for each WT is obtained using the PSO optimization technique proposed in [1], where the OF is to minimize both the deviation between the reactive power Q_{pcc}^{set} required at the PCC and the reactive power generated by the WF and the losses along the branches of the WF, as shown in equation (4). In this case $X = (Q1, Q2, Q3, Q4, Q5)$.
Three values of the weight coefficient λ are tested: $\lambda = 0 ; \lambda = 0,5 ; \lambda = 0,9$
- Case3: the reactive and active power set point for each wind turbine within the wind power plant are obtained using the objective function as shown in equation (4). In this case $X = (Q1, Q2, Q3, Q4, Q5, P1, P2, P3, P4, P5)$.
The same values of λ used in the case 2 are tested in this case.

The results of the reactive and active power dispatching in the three cases are presented in table II:

Table II: Simulation results

Cas e1	Case2			Case3			
	$\lambda=0$	$\lambda=0,5$	$\lambda=0,9$	$\lambda=0$	$\lambda=0,5$	$\lambda=0,9$	
Q1	0,1	0,46	0,46	0,46	0,13	0,38	0,17
Q2	4	0,46	0,46	0,46	-	0,04	0,33
Q3	0,1	0,46	0,46	0,46	0,01	0,07	0,21
Q4	4	0,46	0,46	0,46	0,29	0,28	0,23
Q5	0,1	0,46	0,46	0,46	0,20	0,12	-
P1	4	2,00	2,00	2,00	0,28	1,00	0,04
P2	0,1	2,00	2,00	2,00	1,00	1,00	1,00
P3	4	2,00	2,00	2,00	1,00	1,00	1,00
P4	0,1	2,00	2,00	2,00	1,00	1,00	1,00
P5	4	2,00	2,00	2,00	1,00	1,00	1,00
	2,00				1,00		1,00
	0						
	2,00						
	0						
	2,00						
	0						
	2,00						
	0						
Object	-	0,01	0,09	0,16	0,00	0,00	0,01

ive functi on		82	82	23	44	98	77
$ Q_{pcc}^{set} - Q_{pcc} $	1,5	0,01	0,01	0,01	0,00	3,41 e-7	3,12 e-7
Line losses (MW)	0,161	0,1601	0,1601	0,1601	0,0196	0,0196	0,0196

The case 1 has the most important value of line losses, but it decreases significantly in the case 3 which represents a reduction of 87,83% in comparison with the case 1. We obtain the important value of the error in reactive power at the PCC in the case 1. This error decreases in the case 2 which represents a reduction of 98,85% in comparison with the case 1. However, the error is almost equal to 0 in the case 3 for all the values of λ .

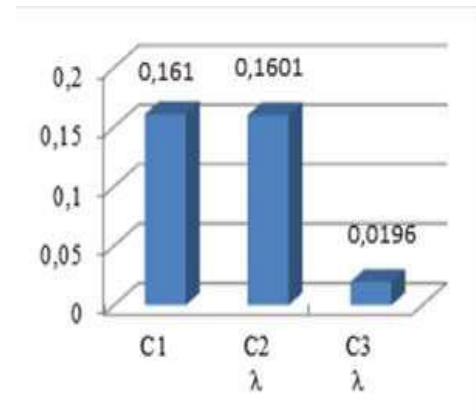


Fig. 6: Power losses in the WF in each case for $\lambda=0$

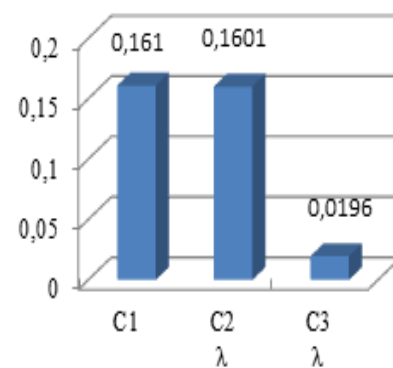


Fig. 7: Power losses in the WF in each case for $\lambda=0,5$

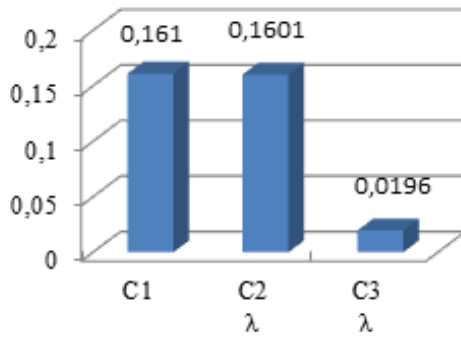


Fig. 8: Power losses in the WF in each case for $\lambda=0,9$

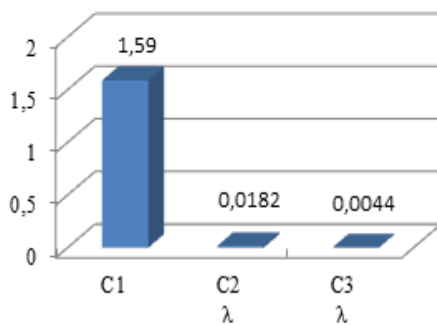


Fig. 9: Error in reactive power at the PCC in each case for $\lambda=0$

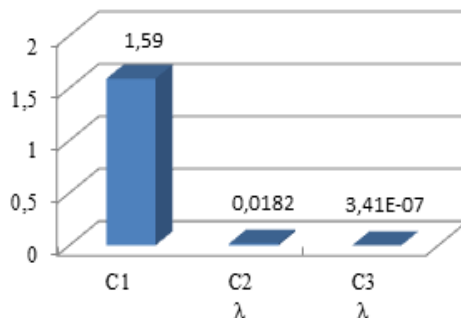


Fig. 10: Error in reactive power at the PCC in each case for $\lambda=0,5$

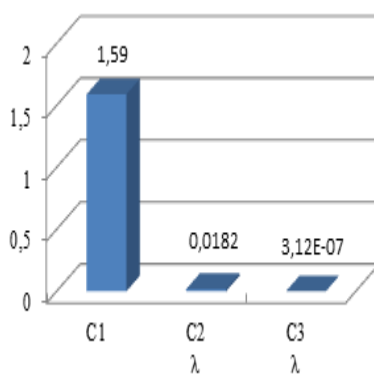


Fig. 11: Error in reactive power at the PCC in each case for $\lambda=0,9$

Comparing the results of the three cases, we can conclude that the case 3 is the most advantageous because it allows

reducing significantly the line losses in the WF, and obtaining an accurate value of the reactive power generated at the PCC that corresponds to Q_{PCC}^{set} required by the TSO, in comparison with all the other cases.

VII. CONCLUSION

In this work, we present an optimization algorithm of reactive and active power dispatch in a wind farm. The proposed algorithm allows minimizing both the power losses in the WF and the deviation between the reactive power reference Q_{PCC}^{set} and the reactive power generated by the wind power plant at the point of common coupling Q_{PCC} . By analyzing the obtained results, we can conclude that the proposed method is the most suitable to use in order to get an accurate value of the reactive power at the point of common coupling and minimize the power losses in the wind farm.

REFERENCES

- [1] M. Martinez-Rojas, A. Sumper, O. Gomis-Bellmunt "Reactive power management in Wind Farms using PSO technique". In: EPE J, 2010.
- [2] T. Lund, P. Sorensen, J. Eek "Reactive power capability of a wind turbine with doubly fed induction generator", Wind Energy, vol. 10, pp. 379-394, April. 2007.
- [3] J. Fortmann, M. Wilch, F. W. Koch, I. Erlich, "A novel centralised wind farm controller utilizing voltage capability of wind turbines", In Proceedings of the Power System Computation Conference, 2008.
- [4] M. Kayıkcı, J. Milanović, "Reactive power control strategies for DFIG-based plants", IEEE Transaction on energy conversion, vol. 22, no.2, June 2007.
- [5] A. Ahmidi, X. Guillaud, Y. Besanger, R. Blan, "A multilevel approach for optimal participating of wind farms at reactive power balancing in transmission power system", IEEE Systems journal, vol. 6, no.2, June 2012.
- [6] A. Ahmidi "Wind farms participation at voltage and reactive power regulation in the power system network", Phd dissertation, 2010.
- [7] Q. Bai "Analysis of Particle Swarm Optimization Algorithm", Computer and Information Science, vol. 3, no.1, February 2010.
- [8] T. Krzeszowski, K. Wiktorowicz "Evaluation of selected fuzzy particle swarm optimization algorithms", Proceedings of the Federated Conference on Computer Science and Information Systems pp. 571-575, vol. 8, 2016.
- [9] J. Zhu "Optimization of power system operation", John Wiley & Sons, Publication 2009

Review of Research Papers Related to V_4 -cordial Labeling of Graphs

N. B. Rathod

Research Scholar, R. K. University, Rajkot-360020, Gujarat, India.

Review of a Research Paper entitled, "Some V_4 -cordial graphs"

Concise Summary:

Authors: M. Seenivasan & A. Lourdusamy.

Published in: *Scientia Acta Xaveriana*, Vol. 1(1)(2009), 91-99.

In this research paper authors investigate a necessary condition for an Eulerian graph to be V_4 -cordial. They also proved that all trees except P_4 and P_5 are V_4 -cordial and the cycle C_n is V_4 -cordial, $n \neq 4$ or n does not congruent to $2 \pmod{4}$.

Evaluation of Paper:

1. Positive Aspects:

- (i) All the figures are very nicely drawn so any one can understand easily.
- (ii) The proof of Theorem 2.4 "Let f be a V_4 -cordial labeling of a graph G with P_4 and uv be an edge of G such that $f(u) = 0$ and $f(v) = f(u)$." is very useful to find some more graphs which admits V_4 -cordial labeling and also this proof can be used for finding V_4 -cordiality of generalized graph of any graph.

2. Negative Aspects:

- (i) The proof of Lemma 2.6 "If all trees on $4m$ vertices are V_4 -cordial then all trees on $4m+1$, $4m+2$, $4m+3$ vertices are also V_4 -cordial." contains very less explanation and not given any illustration so it's very difficult to understand.
- (ii) The proof of Theorem 2.7 "All trees except P_4 and P_5 are V_4 -cordial." is divided into two cases. In each case the explanation is difficult and authors are not given any illustrations so it is very difficult to understand the proof.

3. Discrepancy:

In Corollary 2.3 "The cycle C_n is not V_4 -cordial, where $n \equiv 2 \pmod{4}$, the generalized Peterson graph $P(n,k)$, where $n \equiv 2 \pmod{4}$ and $C_m \times C_n$, where m and n are odd are not V_4 -cordial." there is no given any proof about V_4 -cordiality of Peterson graph $P(n,k)$ and

$C_m \times C_n$.

Further comments:

- (i) The authors use V_4 -cordiality and this labeling is such a nice combination of group theory and graph theory. This labeling can be use in application of abstract algebra in graph theory.
- (ii) The authors give the proof of V_4 -cordial labeling of standard graphs Path and cycle. By using these graphs there may be found more graphs which may contain V_4 -cordiality.
- (iii) Authors should have to give some illustration so anyone can understand.

Review of a Research Paper entitled, "Generalized Graph Cordiality"

Concise Summary:

Authors: O. Pechenik & J. Wise.

Published in: *Discussiones Mathematicae Graph Theory*, Vol. 32 (3) (2012), 557-667.

In this paper authors investigate some A -cordial graphs, V_4 -cordial graphs and Q -cordial graphs. Authors proved the following results. All complete bipartite graphs are V_4 -cordial except $K_{m,n}$, where $m,n \equiv 2 \pmod{4}$. All Paths P_n are V_4 -cordial except P_4 and P_5 . All cycles C_n are V_4 -cordial except C_4 , C_5 and C_k , where $k \equiv 2 \pmod{4}$. All ladders $P_2 \times P_k$ are V_4 -cordial except C_4 . All prisms are V_4 -cordial except $P_2 \times C_k$, where $k \equiv 2 \pmod{4}$. All hypercube are V_4 -cordial, except C_4 .

Evaluation of Paper:

1. Positive Aspects:

In this paper authors proved all ladders $P_2 \times P_k$ and all prisms $P_2 \times C_k$ are V_4 -cordial. These graphs ladders and prisms are obtained by operation on standard graphs, which is very hard, but the authors make it very easy.

2. Negative Aspects:

- (i) In Theorem 3.4 authors proved that the path P_n is V_4 -cordial unless $n = 4, 5$. They proved this result by induction on n . But in 2009 Seenivasan and Lourdusamy[4] have been already proved that all trees except P_4 and P_5 are V_4 -cordial and path P_n is one type of tree.

- (ii) In theorem 3.5 authors proved that the cycle C_n is V_4 -cordial for n does not congruent to $2(mod 4)$ and $n \neq 4, 5$. But Seenivasan and Lourdusamy[4] have been already given a proof for V_4 -cordiality of cycle C_n .
- (iii) In this paper all symbols of graph operation do not appear properly.
- (iv) The authors prove that the d -dimensional hypercube Q_d is V_4 -cordial, but the authors have not been introduced the definition of d -dimensional hypercube Q_d .

Further comments:

- (i) This paper contains three types of labeling defined as A -cordial labeling, V_4 -cordial labeling and Q -cordial labeling. Using this combination of labeling authors can see the behavior of graphs in different labeling.
- (ii) Authors must have to give the definitions of new words.

Review of a Research Paper entitled, “ Z^2_2 -cordiality of K_n and $K_{m,n}$ ”

Concise Summary:

Authors: Adrian Riskin.

Published in: Cite: arXiv:0709.0290v1 [math.CO](2013).

In this paper author introduce new graph labeling known as Z^2_2 -cordial labeling (V_4 -cordial labeling). Author study the Z^2_2 -cordiality of K_n and $K_{m,n}$. Author proved few minor results and questions on the Z^2_2 -cordiality of trees.

Evaluation of Paper:

1. Positive Aspects:

- (i) The author has introduced the new labeling Z^2_2 -cordial labeling (V_4 -cordiality) obtained from A -cordial labeling.
- (ii) Author have been given a Z^2_2 -cordiality of two graphs K_n and $K_{m,n}$ and these two graphs have many applications in engineering.

2. Negative Aspects:

- (i) In this paper author introduce Z^2_2 -cordiality, but the author does not give an exact definition of Z^2_2 -cordiality.
- (ii) The author does not give any illustrations in all theorems.

Further comments:

- (i) The result $K_{m,n}$ complete bipartite graph is Z^2_2 -cordial can be extended to more generalize as complete k -partite graphs are Z^2_2 -cordial or not.
- (ii) Author must have to give enough illustration for better understanding.

REFERENCES

- [1] J. A. Gallian, A dynamic survey of graph labeling, *The Electronic Journal of Combinatorics*, 19(2016) #DS6.
- [2] O. Pechenik and J. Wise, Generalized graph cordiality, *Discussiones Mathematicae Graph Theory*, 2(3), 557-567(2012).
- [3] A. Riskin, Z^2_2 -cordiality of K_n and $K_{m,n}$, *arXiv:0709.0290* (2013).
- [4] M. Seenivasan and A. Lourdusamy, Some V_4 -cordial graphs, *Scientia Acta Xaveriana*, 1(1), 91-99(2009).

Effect of Welding Speed on Mechanical Properties of Dissimilar Friction Stir Welded AA5083-H321 and AA6061-T6 Aluminum Alloys

D. Devaiah¹, K. Kishore², P.Laxminarayana³

¹Research Scholar, Department of Mechanical Engineering, University College of Engineering, OU, Hyderabad, India.

²Professor, Department of Mechanical Engineering, Vasavi College of Engineering, Hyderabad, India.

³Professor, Department of Mechanical Engineering, University College of Engineering, OU, Hyderabad, India

Abstract— Fusion welding of aluminum and its alloys tends to degrade the mechanical strength at the weld joint area due to high thermal diffusivity and high melting point. Friction Stir Welding (FSW) is the best alternative for joining of these materials against fusion joining. FSW is an emerging solid state joining process in which the material that is being welded does not melt and recast. The main objective of this research is to use FSW for joining of 5 mm thick AA5083-H321 and AA6061 T6 aluminum alloys using taper cylindrical threaded tool pin profile and scrolling on shoulder surface. The microstructure and mechanical characterization of dissimilar friction stir welded AA5083-H321 and AA6061-T6 aluminum alloys were studied. Four different welding speeds (40, 63, 80 and 100 mm/min) were used to weld the dissimilar alloys at constant tool rotational speed of 1120 rpm, tilt angle 2.5°. The effect of welding speed on metallurgical and mechanical properties was analyzed. It is found that the welding speed of 80 mm/min produces good mechanical and metallurgical properties than other welding speeds. The observed results were correlated with the fracture features and microstructure. The fracture mode was observed to be a ductile fibrous fracture.

Keywords— AA5083-H321 and AA6061-T6 aluminum alloys, friction stir welding, welding speed, tensile strength, microstructure, Fractography.

I. INTRODUCTION

Dissimilar welding of aluminum alloys AA5xxx and AA6xxx is regularly faced in the manufacture of aircraft structures and other auxiliary applications [1]. Various welding defects happen in conventional fusion welding of aluminum alloys such as hot cracking, voids, distortion, loss of work hardening, lack of penetration, precipitate dissolution and hot cracking in the joints [2]. Therefore, Friction stir welding technique is preferred to solve those defects. Friction stir welding (FSW) is a suitable solid state welding procedure to successfully join any

combination of dissimilar aluminum alloys [3]. FSW was developed at The Welding Institute (TWI), UK in 1991. A non-consumable rotating tool harder than the parent material is plunged into the abutting edges of the plates to be joined under adequate axial force and progressed along the line of the joint. The tool consists of two parts, in particular pin and shoulder. The material around the tool pin is softened by the frictional heat produced by the tool rotation. Progression of the tool pushes plastically deformed material from front to back of the tool and forges to complete the joining process [4]. Since FSW is a solid state method, a solidification structure is not visible in the weld. In this way, all the defects related to the presence of the eutectic phases and brittle inter-dendritic are wiped out [5]. A few reviews on FSW of dissimilar AA6xxx and AA5xxx joints were recently described in Refs. [6-10]. LEAL et al [6] investigated the impact of tool shoulder geometry on material flow in 1 mm-thick AA6016-T4 and AA5182-H111 joints. A tool shoulder with a conical cavity was given to yield an onion ring structure. PARK et al [7] elaborated the influence of material locations on the properties of 2 mm-thick AA6061-T6 and AA5052-H32 joints and a proper mixing of dissimilar aluminum alloys was seen when AA5052-H32 was kept in the advancing side. PEEL et al [8] concentrated the impacts of tool rotational speed and traverse speed on the hardness, microstructure and precipitation distribution of 3 mm-thick AA6082 and AA5083 joints. STEUWER et al [9] measured the impact of traverse speed and tool rotational speed on the residual stresses of 3 mm-thick AA6082 and AA5083 joints. ELANGO VAN and BALASUBRAMANIAN [10] announced that the welding speed has a more prominent impact on the tensile strength. YAN et al [11] concentrated the dissimilar friction stir welding between AZ31 and AA5052 magnesium alloy and revealed that at the highest point of the mixing zone, AZ31 and AA5052 alloys are simply bonded, while onion ring structure which consisted of magnesium bands and aluminum

bands is formed at the bottom of the stir zone. The microstructural development of dissimilar welds as a function of processing parameters has been widely studied to discover the behavior of AA6061-AA2024 materials [12]. In this work, an attempt is made to join 5 mm-thick aluminum alloys AA5083-H321 and AA6061-T6 using FSW and investigate the effect of welding speed on the tensile strength and microstructure of the dissimilar joints.

II. EXPERIMENTAL

A FSW tool made of H13 steel having cylindrical taper threaded pin profile and with scrolled surface concave shoulder was used to weld the alloys. The tool had a shoulder diameter of 18 mm, pin diameter of 6 mm and pin length of 4.7 mm. The FSW tool was manufactured using CNC turning center and wire cut EDM machine to get a exact profile. The tool was oil hardened to 55HRC. Aluminum alloys AA5083-H321 and AA6061-T6 were used in this work. Their chemical composition is shown in Table 1. Plates with dimensions of 200 mm×75 mm × 5 mm were prepared from the rolled plates. AA5083-H321 and AA6061-T6 alloys were respectively kept on the advancing side and retreating side of the joint line. The FSW line was perpendicular to the rolling direction of AA5083-H321 and parallel to the rolling direction of AA6061-T6. The dissimilar butt welding was completed on a vertical milling machine. Four joints were fabricated at four different welding speeds of 40, 63,80 and 100 mm/min. The rotational speed and tool tilt angle were kept as 1120 r/min and 2.5°. Schematic draw of the weld joint and tool is as shown in Fig.2. A non-consumable H-13 tool steel with concave shoulder and scrolling on the shoulder surface is chosen as tool material to fabricate the joints, due to its high strength at elevated temperature, thermal fatigue resistance, and low wear. The diameter of the shoulder and pin used were 18mm, 6mm respectively and length of the pin is 4.7 mm with taper cylindrical threaded tool pin profile is used to weld. After the welding process, the joints were visually inspected for exterior defects and it was found that the joints were free from any external defects. The butted plates were clamped on a steel backing plate. The welding tool is tilted by 2.5 degrees of angle with reference to the welded plates and tool was rotated in the clockwise direction. A constant axial force is applied to all the joints. A specimen was cut from the welded plate perpendicular to the FSW line to carry out the microstructural characterization. The test sample was prepared according to the standard metallographic procedure and etched with modified Keller reagent. The computerized picture of the macrostructure of the etched specimen was captured utilizing a digital optical scanner.

The microstructure was seen utilizing an optical microscope and scanning electron microscope. The tensile samples were prepared according to ASTM E8 norms. Two such tensile specimens were prepared and the average ultimate tensile strength (UTS) was taken. The UTS was evaluated utilizing a computerized universal testing machine. The broken specimen of the maximum tensile strength was seen using a scanning electron microscope. Specimens for impact testing were taken in transverse to the weld direction and machined according to ASTM A370 norms. The charpy "V" notch impact test was carried out at room temperature utilizing pendulum type impact testing machine. The amount of energy absorbed in fracture was recorded and the absorbed energy is defined as the impact toughness of the material. The Schematic draw of impact and tensile specimens was shown in Fig.1. Specimens were cut at the center of the joints in the transverse direction to conduct microhardness study. Microhardness test was completed utilizing Vickers digital microhardness tester with a 500 g load for 10 s duration. The microhardness was measured at an interval of 3 mm over the WZ, Thermo-Mechanical Affected Zone (TMAZ), Heat-Affected Zone (HAZ) and (base metal) BM. The joints made with tool rotation speed at 1120rpm, tool tilt angle 2.5° and weld speed at 80 mm/min resulted in good mechanical properties as compared with other weld conditions due to adequate heat generation and proper mixing of the material in the weld zone.

Table.1: Chemical composition of parent materials (mass fraction, %)

Alloy	Mg	Mn	Cu	Cr	Si	Fe	Al
AA6061-T6	1.046	0.101	0.259	0.195	0.533	0.262	Bal
AA5083-H321	4.0	0.548	0.065	0.10	0.145	0.238	Bal

Table.2: Mechanical properties of parent materials.

Alloy	Yield strength Mpa	Ultimate tensile strength Mpa	% of Elongation mm	Average hardness at 0.5kg load (VHN)	Impact strength (J)
AA6061-T6	283	353	18	120	8
AA5083-H321	238	311	20	96	16

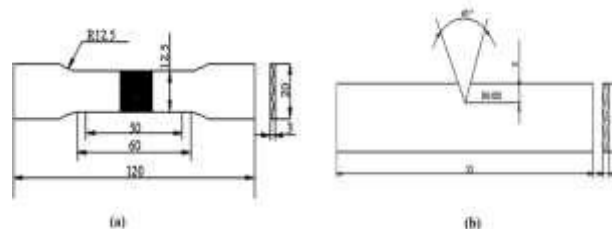


Fig.1: Schematic Sketch of (a) Tensile Specimen (b) Impact Specimen.

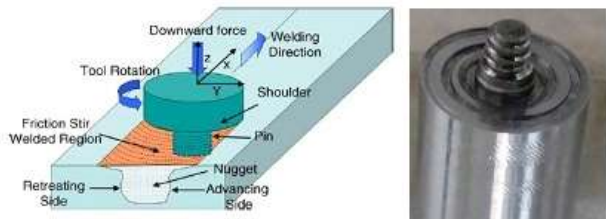


Fig.2: Schematic Sketch of Friction Stir welding showing the Various Characteristic Regions and tool

III. RESULTS AND DISCUSSION

FSW of 5 mm-thick aluminum alloys AA5083-H321 and AA6061-T6 were accomplished. The flow stresses of the two aluminum alloys are distinctive. Aluminum alloy AA5083 offers more resistance to plastic flow compared with AA6061 [13]. The rubbing of the FSW tool shoulder on the plates forms such features which are known as the wake effect [14]. It is clear that the joint has no defects such as piping or worm hole, tunnels. The macrostructure recommends that the sufficient frictional heat is formed at the chosen parameters to

1. Microstructure Studies

In conventional welding of aluminum alloys, the defects like slag inclusion, porosity, solidification on crack, and so on decreases the weld joint properties and weld quality. Notwithstanding, utilizing FSW the joints are free from these imperfections since there is no melting occurs during the welding and metals are bonded in the solid state itself because of the heat produced by the friction and flow of the metal affected by the stirring activity. The samples for metallographic examination were cut to the required size from the FSW joints transverse to the welding direction, polished and then etched with a solution of **Keller's reagent** - 2ml HF (48%) + 3ml HCl + 5ml HNO₃ + 190ml H₂O. This etchant gives the possibility to reveal grain boundary complexity and precipitates in several wrought alloys. The etchant reveals that AA5083 is lighter and AA6061 is darker in colour. The microstructural changes from the weld zone to the unaffected base metal were examined with optical microscopy. The microstructure of the friction stir welded aluminum alloys joint consists of different zones such as (a) stir zone (b) thermo mechanical affected zone (c) heat affected zone. The development of above zones is influenced by the material flow behaviour under the affected by welding speeds with rotating nonconsumable tool. The optical microstructure of the weld zone at various weld speeds with constant tool rotation speed and tool tilt angle are displayed in Fig.3. From the observed microstructure, the joints fabricated at the condition with the tool rotation speed of 1120rpm, weld speed of 80 mm/min and tool tilt angle of 2.5° observed to be having finer grains contrasted to other conditions which yielded

defect free weld. This refinement is because of the dynamic recrystallization caused by simultaneously received plastic shear deformation and frictional heat [15]. The plasticized dissimilar alloys are mechanically coupled to each other. The infiltration of one aluminum alloy into the other is not fully accomplished. Yet, dynamic recrystallization of grains is clear. The stirring action of the tool causes intense plastic deformation and in situ extrusion of aluminum alloys AA6061 and AA5083. The plasticized material is moved layer by layer, which structures such a lamellae structure. The penetration and mixing of both the aluminum alloys in this area is extreme. Figures 3(a) and (b) show the microstructures of the base material of AA5083 and AA6061 respectively. Different grain sizes of the stir zones are also observed in Figs.3(c)-(f). Figure 3(e) shows the stir zone composed of fine-equiaxed recrystallized grains and precipitates scattered in a finer matrix. The fine recrystallized structure at the stir zone is a high plastic deformation followed by dynamic recrystallization happening amid thermo-mechanical processing. TMAZ neighbouring the weld nugget is plastically deformed and thermally affected.

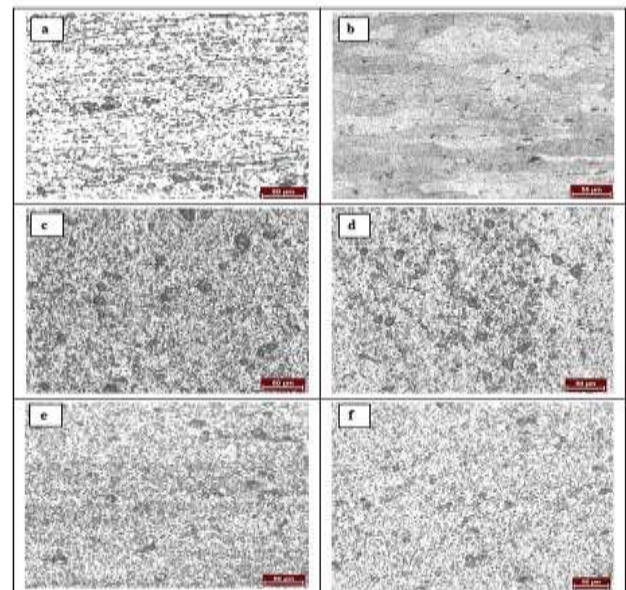


Fig.3: Microstructure of Weld Zones of FSW Joints at Various Conditions: (a) Base Metal AA5083, (b) Base Metal AA6061, (c) F1=1120 rpm, 40mm/min, 2.5°, (d) F2= 1120 rpm, 63 mm/min, 2.5° and (e) F3= 1120 rpm, 80 mm/min, 2° (f) F4= 1120 rpm, 80 mm/min, 2.5°

The hardness profiles assessed over the stir zone at various conditions is shown in Fig.7. The hardness of the base metal is 96HV and 120 HV. The hardness of the nugget zone is influenced by annealing softening and grain refinement in pure metals [16]. The average hardness of weld zone is found to be significantly lower than that of the hardness of the base metal. In Harries and

Norman's work, it is recommended that the variation of the microhardness values in the welded zone and base metal is because of the difference between the microstructure of the parent metal and weld zone [17]. In any case, in the present review, the hardness of the weld zones fabricated by tool rotation speed at 1120 rpm, tool tilt angle 2.5° and weld speed at 80 mm/min observed to be 84Hv which is higher than that of other conditions. This is because of the presence of very finer grains at the stir zone. The weld center has bring down hardness than that of the base metal regardless of smaller grain size.

2. Mechanical Properties

Mechanical properties for example, yield strength, tensile strength and percentage of elongation have been assessed. At each condition, two samples were tested and the average of the results of two samples is presented. Table 2 shows the tensile properties of base metal and Table 3 indicates mechanical properties of the aluminum alloys weldments. From the experimental outcome, at the tool rotation speed of 1120 rpm, tool tilt angle 2.5° and weld speed of 80 mm/min exhibited better tensile and impact properties and the joint efficiency (58.8%) is also higher as compared to other conditions.

Table.3: Mechanical properties of weld materials.

EXP NO	UTS (MPa)	YS (MPa)	%EL (mm)	MH (VH)	IE (J)	joint efficiency %
F1(1120 rpm - 40 mm/m- 2.5°),	175	140	6.6	75	30	56.3
F2 (1120 rpm - 63 mm/m- 2.5°),	178	143	6.9	78	32	57.2
F3 (1120 rpm - 80 mm/m- 2.5°),	183	150	8.2	84	34	58.8
F4 (1120 rpm - 100 mm/m- 2.5°),	178	120	7.4	75	24	57.2

2.1. Effect of Welding Speed

The translation of tool moves the mixed material from the front to the back of the tool pin. The rate of heating of thermal cycle in FSW is a function of the welding speed. A huge increment in welding speed is accomplished with high weld quality and fabulous weld joint properties. The softened region is smaller for the higher welding speed than that for the lower welding speed. In this way, the tensile strength of aluminum alloys weldments has a proportional relationship with welding speed. The joints fabricated by tool rotation speed at 1120 rpm, tool tilt angle 2.5° and weld speed at 80 mm/min obtained higher tensile strength than other conditions. This is because of the intense plastic deformation and adequate frictional heat generation in the weld zone. At lower welding speed (i.e. 40 and 63mm/min) brought about higher temperature and slower cooling rate in the prepared zone causes grain development which brings about the decline in quality and hardness. The welding speed has a strong affect on productivity in streamlined generation of FSW of

aluminum alloy sections. A huge increment in welding speed is achieved with high weld quality and superb joint properties. The impacts of welding speed on mechanical properties of the dissimilar joints are shown in Fig. 4-8. At the lowest (i.e. 40 and 63mm/min) and the highest (100mm/min) welding speeds, a lower tensile strength was noticed. The increment of welding speed prompts to the increment of the tensile strength up to the highest value, while additionally increase in welding speed effects in the decrease in the tensile strength of friction stir welded joints. The welding speed prompts the translation of tool, which thusly pushes the stirred material from front to the back of the tool pin and finishes the welding. The rubbing of tool shoulder and pin with the workpiece generates frictional heat. The welding speed determines the exposure time of this frictional heat per unit length of the weld and in this way influences the grain growth and precipitates. Optimum presentation time and translation of stirred material will lead to great consolidation of material with finer grains. Since joint which encounters such condition at the welding speed of 80 mm/min during welding displayed the highest UTS. The reduction in frictional heat production with an increase in welding speed was observed. Higher heat conditions prevail at lower welding speeds with slower cooling rate, which leads to coarsening of grains and dissolution of precipitates [10,18] Lower welding speeds cause uncalled for solidification of material, which leads to the reduction in UTS attributable to the defect. The mixing gets to be distinctly lacking at higher welding speeds. The material present on the advancing side of the tool does not travel enough to the retreating side, which causes a defect. Lower heat production with rapid cooling rate happens at higher welding speeds. The inclination of the tool to drag at higher welding speeds furthermore adds to the lower UTS. The welding speed impacts the plastic stream of material, change in grain size and precipitates and development of defects. The components that find the tensile strength of dissimilar aluminum alloy joints are the existence of macroscopic defects in weld zone and the level of plastic flow and amount of stirring of both the materials.

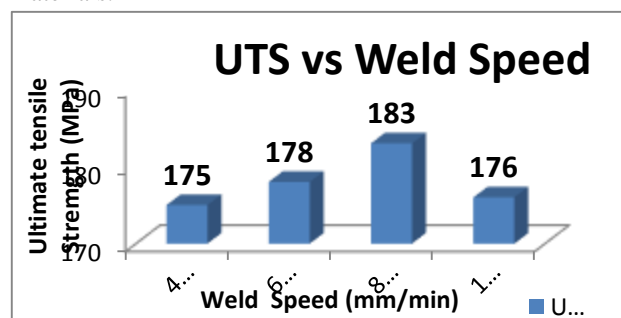


Fig.4: The effects of welding speed on ultimate tensile strength of the dissimilar joints

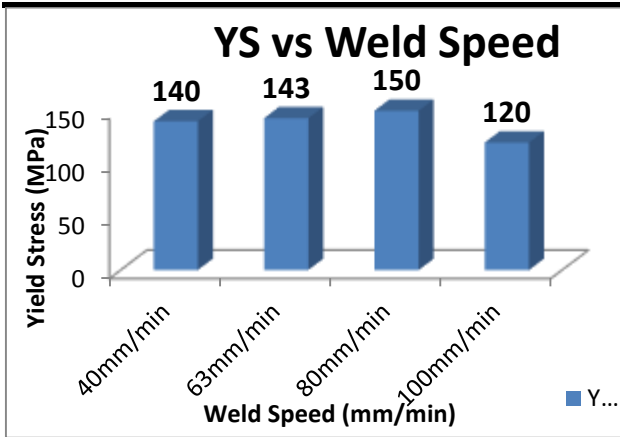


Fig.5: The effects of welding speed on the yield strength of the dissimilar joints.

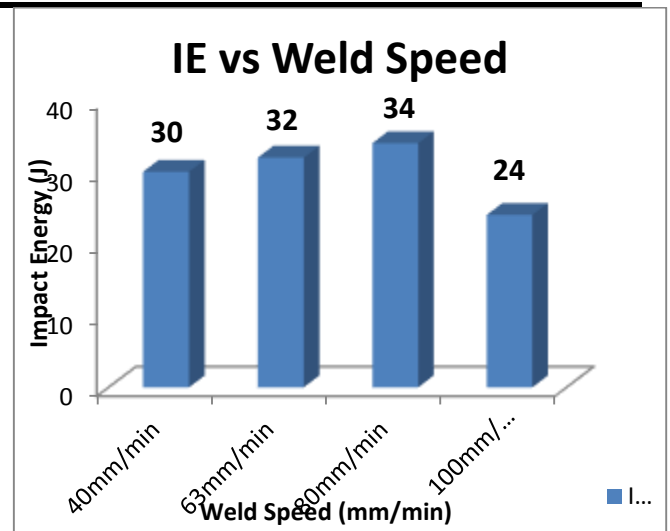


Fig.8: The effects of welding speed on impact energy of the dissimilar joints.

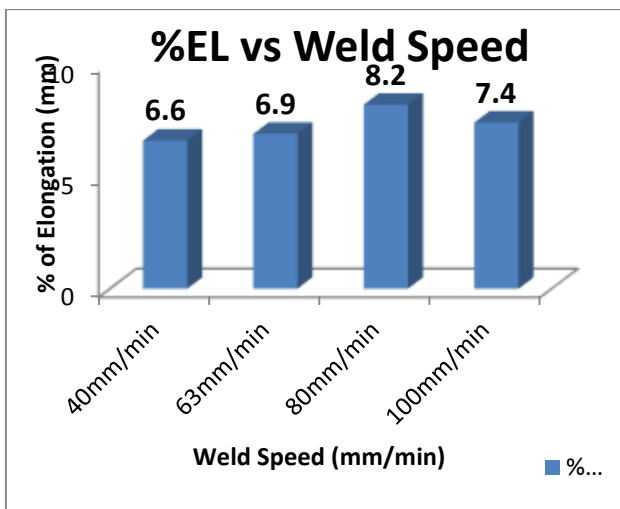


FIG 6: The effects of welding speed on % of elongation of the dissimilar joints.

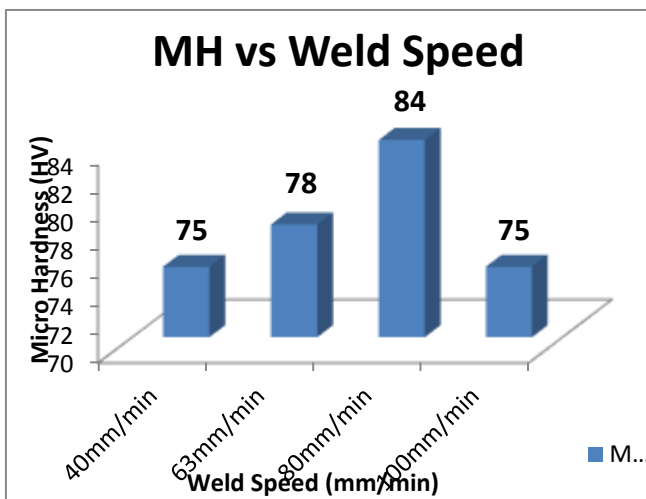


Fig.7: The effects of welding speed on microhardness of the dissimilar joints.

3. Fractography

The fractural morphology of the tensile and impact specimens of the fracture surface of the weld joints was studied utilizing the scanning electron microscopy (SEM) to understand the mode of failure. Fractured specimens of the weld joints are shown in Fig.6 and Fig.7. The dimple pattern is seen in the whole width of the specimen. All joints were failed on the retreating side during tensile testing where hardness value is least. The joints fabricated at the condition of tool rotation speed at 1120rpm, tool tilt angle 2.5° and weld speed at 80 mm/min exhibited higher ductility as compared with other conditions. This is due to a presence of tiny shallow dimples and also some large dimples resulted from micro dimples coalescence. It could be credited to the high plastic deformation which shows the more intense ductile fracture.

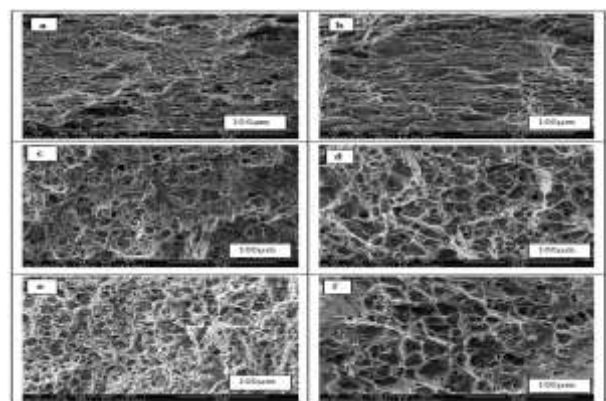


Fig.6: Tensile fracture images (a) Base AA5083, (b) Base AA6061, (c) F1, (d) F2, (e) F3, (f) F4.

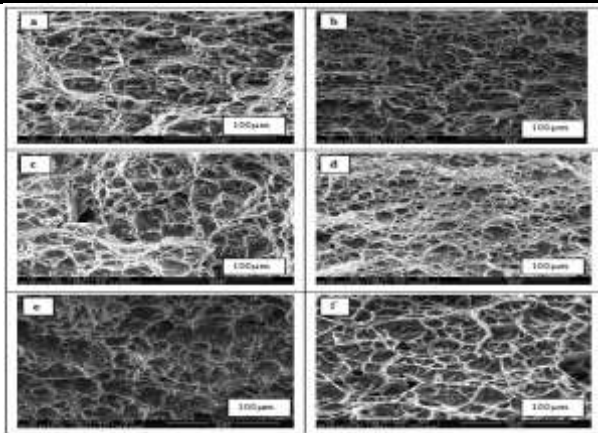


Fig.7: IMPACT fracture images (a) Base AA5083 , (b) Base AA6061, (c) F1, (d) F2, (e) F3, (f) F4.

IV. CONCLUSIONS

The mechanical properties of AA5083 to AA6061 weldments made by FSW were investigated. The following conclusions can be drawn. The weldments made by FSW at the tool rotation speed of 1120rpm, weld speed of 80mm/min and tool tilt angle 2.5° displayed better mechanical properties. This is because of adequate heat generation and proper mixing of the material in the weld zone. Further, it is additionally watched that finer grains were shaped in the weld zone which is because of dynamic recrystallization. The fracture surface of both tensile and impact specimens shows a ductile fibrous fracture at weld zone of AA5083 to AA6061 weldments. The dissimilar joint shows the presence of different zones such as heat affected zone (HAZ), thermomechanically affected zone (TMAZ) and stir zone (SZ). The welding speed affects the formation of plastic flow region. The joints fabricated at the lowest or highest welding speeds show the absence of mixed flow region.

ACKNOWLEDGEMENTS

The authors would like to thank the authorities of Vasavi College of Engineering, Hyderabad. Defence Research Metallurgical Laboratories (DMRL), Hyderabad, India for providing the facilities to carry out this work.

REFERENCES

[1] HEINZ A, HASZLER A, KEIDEL C, MOLDENHAUER S, BENEDICTUS R, MILLER W S. Recent development in aluminium alloys for aerospace applications [J]. Materials Science and Engineering A, 2000, 280(1): 102_107.
[2] LUIJENDIJK T. Welding of dissimilar aluminium alloys [J]. Journal of Material Processing Technology, 2000, 103: 29_35.
[3] MURR L E. A review of FSW research on dissimilar metal and alloy systems [J]. Journal of

Material Engineering Performance, 2010, 19(8): 1071_1089.
[4] MISHRA R S, MA Z Y. Friction stir welding and processing [J]. Materials Science and Engineering R, 2005, 50(1_2): 1_78.
[5] THREADGILL P L, LEONARD A J, SHERCLIFF H R, WITHERS P J. Friction stir welding of aluminium alloys [J]. International Journal of Material Review, 2009, 54(2): 49_93.
[6] LEAL R M, LEITAO C, LOUREIRO A, RODRIGUES D M, VILACA P. Material flow in heterogeneous friction stir welding of thin aluminium sheets: Effect of shoulder geometry [J]. Materials Science and Engineering A, 2008, 498(1_2): 384_391.
[7] PARK S K, HONG S T, PARK J H, PARK K Y, KWON Y J, SON H J. Effect of material locations on properties of friction stir welding joints of dissimilar aluminium alloys [J]. Science and Technology of Welding and Joining, 2010, 15(4): 331_336.
[8] PEEL M J, STEUWER A, WITHERS P J, DICKERSON T, SHI Q, SHERCLIFF H. Dissimilar friction stir welds in AA5083-AA6082. Part I: Process parameter effects on thermal history and weld properties [J]. Metallurgical and Materials Transactions A, 2006, 37(7): 2183_2193.
[9] STEUWER A, PEEL M J, WITHERS P J. Dissimilar friction stir welds in AA5083-AA6082: The effect of process parameters on residual stress [J]. Materials Science and Engineering A, 2006, 441(1_2): 187_196.
[10] ELANGO VAN K, BALASUBRAMANIAN V. Influences of tool pin profile and welding speed on the formation of friction stir processing zone in AA2219 aluminium alloy [J]. Journal of Material Processing Technology, 2008, 200(1_3): 163_175.
[11] YAN Yong, ZHANG Da-tong, QIU Cheng, ZHANG Wen. Dissimilar friction stir welding between 5052 aluminum alloy and AZ31 magnesium alloy [J]. Transaction of Nonferrous Material Society China, 2010, 20(S2): s619_s623.
[12] OUYANG J H, KOVACEVIC R. Material flow and microstructure in the friction stir butt welds of the same and dissimilar aluminum alloys [J]. Journal of Material Engineering Performance, 2002, 11(1): 51_63.
[13] LEITAO C, EMILIO B, CHAPARRO B M, RODRIGUES D M. Formability of similar and dissimilar friction stir welded AA5182-H111 and AA 6016-T4 tailored blanks [J]. Material and Design, 2009, 30(8): 3235_3242.

-
- [14] CESCHINI L, BOROMEI I, MINAK G, MORRI A, TARTERINI F. Effect of friction stir welding on microstructure, tensile and fatigue properties of the AA7005/10vol.%Al₂O₃p composite [J]. *Composite Science and Technology* 2007, 67(4): 605_615.
- [15] Y.S. Sato, S.H.C. Park, H. Kokawa. "Microstructural Factors Governing Hardness in Friction-Stir-Welds of Solid-Solution-Hardened Al Alloys". *Metall. Mater. Trans. A*, Vol.32A-12, Pp.3032-3042, 2001.
- [16] W. B.Lee and S.B.Jung. "The joint properties of copper by friction stir welding" *Mater.Lett.* Vol 58, Pp.1041-1046, 2004.
- [17] D Harris, A F Norman, "Properties of Friction Stir Welded joints: A review of the literature, E U POSTIR", program report presented at the 6th PSG meeting, 17-18 June 2003.
- [18] PALANIVEL R, KOSHYMATHEWS P. Prediction and optimization of process parameter of friction stir welded AA5083-H111 aluminum alloy using response surface methodology [J]. *Journal of Central South University of Technology*, 2012, 19(1): 1_8.

Rapid Manufacturing: Classification and Recent Development

Lalit Kumar¹, Abid Haleem², Qamar Tanveer³, Mohd. Javaid⁴, Mohd Shuaib⁵, Vineet Kumar⁶

^{1,3,5,6}Research Scholar, Department of Mechanical Engineering, Jamia Millia Islamia, New Delhi, INDIA

²Professor, Department of Mechanical Engineering, Jamia Millia Islamia, New Delhi, INDIA

⁴Assistant Professor, Department of Mechanical Engineering, Jamia Millia Islamia, New Delhi, INDIA

Abstract—Rapid Prototyping is an emerging technology in the field of advance manufacturing process/technique in which components/parts/models are rapidly created from the visual world (CAD model) to real world with minimum human interaction. Since the manufacturing starts with the creation of geometric data, either as a 3D solid using a CAD model, or 2D layers using a 3D scanning device therefore it is also referred as Layer Manufacturing, Material Deposition Manufacturing, Additive Manufacturing, Solid Freeform Manufacturing and Three-Dimensional Printing. This is one of the best techniques to manufacture prototypes which may be used for physical visualization, making some typical and intrinsic geometry. For the same requirement, in most of the cases it is very cost effective, flexible and time saving than any other available manufacturing technique. Therefore it is the most appropriate technique to manufacture or to recreate components/parts/model in different engineering viz. aerospace, product and tool development. A lot of new developments are occurring in the field of Rapid Prototyping Techniques in recent years.

This paper also provides the development, trends and applications of the Rapid Prototyping Techniques. The authors cover various available literatures to prepare concise and progressive review. There are various components which are associated with RP technique and some of them are listed in this paper.

Keywords— Classification of Rapid Prototyping, 3 Dimensional Printing, Poly-jet Printing, Rapid Prototyping; Sustainable Product Development.

I. INTRODUCTION

As the manufacturing field is one which converts raw material into finished/useful goods. The advancement in the field of science and technology make it versatile as new emerging technologies are coming into existence. These changes force the manufacturing industries to develop better quality of products in shorter period of time to have better market share in the competitive environment. Therefore it is required to evaluate all the feasible design alternatives which have least manufacturing cost and time

constraints in order to obtain sustainable product development in the current era. The research shows that computer aided design; manufacturing tools and analysis technologies provides a very powerful resource tool for the futuristic designs. Further recent development in technologies like reverse engineering, rapid prototyping and rapid tooling etc. shows that these technologies provide very fast and less expensive ways to create parts directly from computer aided designed models (L. Kumar, Kumar, & Haleem, 2016).

In Rapid Prototyping (RP) technique, the physical model/prototype is quickly built directly from 3D CAD data. In totality, all the fabrication processes can be classified into three categories mainly, subtractive, additive, and compressive (Onuh & Yusuf, 1999). Every manufacturing process either falls completely into one of these categories, or combination of any of the mentioned process. In the subtractive process, the desired shape of material is carved out from a block of material with the help of tool whereas in additive process the desired shape/product is built up by adding particles/layers of the raw material, and in the compressive process the forces are applied on semi-solid/liquid material to produce the desired shape and it is hardened/solidified if required. In RP processes the product is produced by addition of material layer-by-layer whereas in conventional methods this was done by removal of materials only.

In manufacturing field the productivity can be achieved by transforming product/object from raw material, as fast as possible with least cost and resource. Rapid prototyping can achieve this target effectively. RP techniques are capable of producing any complex geometries or internal cavities easily and efficiently. Also the cost, time, wastage etc. associated with RP is less as compared to conventional methods.

By using these technologies instead of conventional methods, the manufacturing time for producing parts with any complex geometry can be reduced to few hours as compared to days/weeks/months or we can say in other words, it is rapid. RP is an automatic manufacturing process and the basic concept of all RP process can be summarized into following steps:

Step1. Firstly create a computer design (CAD) of the required model/design/prototype.

Step2. Then convert this CAD file into machine file format (.STL file format).

Step3. Slicing the STL (Stereolithography) file format into the required 2-D cross sectional layers.

Step4. Then growing 2-D design to produce required model/prototype

Step5. Post processing the model if required.

The RP cycle begins with the requirement of the desired product/model and end with the manufacturing of desired model/prototype however the whole cycle is repeated again and again till the required specifications are achieved and pictorial representation of the RP cycle/steps is shown in the Fig.1 below.

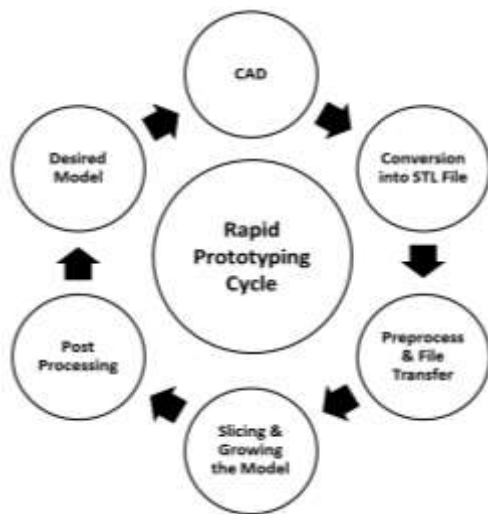


Fig.1: The RP Cycle from CAD design, repeated several times until desired characteristics are achieved. (Cooper, 2001)

II. HISTORY OF RAPID PROTOTYPING DEVELOPMENT

The history of RP techniques (Chee Kai Chua & Leong, 1997) is around two decades old as first RP system was developed in 1988. The development has gone through a number of changes which initially begins from the introduction of mechanization in 1770. The one of the biggest milestones in the history was the introduction of first computer which was in 1946. The introduction of computers eventually speed up the growth process by reducing the process time. The manufacturing industry starts growing and developing when the computer was used along with numerical control in machine tool in 1952. The RP techniques can't be developed without the introduction of laser (1960) and robots (1961) for the manufacturing industries. The introduction of graphic system (CAD) in 1963 changes the whole approach of the manufacturing sector. The first RP system was introduced in 1988 by integrating all these systems to build model/prototype

directly from CAD model without human interaction. The introduction of first RP machine initiated different RP systems along with it which are still under advancement by introduction of new and sophisticated control systems. The history of RP development (Chee Kai Chua & Leong, 1997) is given in the Table.1 below:

Table.1: History of RP Development

1770	Mechanization
1946	Development of 1 st computer
1952	Introduction of 1 st NC (Numerical Control) machine tool
1960	Introduction of first commercial LASER
1961	Developed first commercial Robot
1963	First interactive graphics system (early version of Computer Aided Design)
1988	Development of 1 st RP system (Stereolithography).

III. DIFFERENT TECHNIQUES OF RAPID PROTOTYPING

There are different RP processes developed in last few decades and some of them are discussed in this literature which are as follows:

1. SLA (Stereolithography)
2. Photo Masking or Solid Ground Curing technique
3. SLS (Selective Laser Sintering)
4. FDM (Fused Deposition Modeling)
5. LOM (Laminated Object Manufacturing)
6. 3DP (Three Dimensional Printing)

3.1 Stereolithography:

Patented in 1986 and this technique was invented by Charles Hull. A LASER is used in this technique to generate ultraviolet (UV) beam which solidifies the uppermost layer of the photopolymer as per STL file. The process continues layer by layer until the finished product is completed. The input to the machine/system is fed in the form of 3 dimensional CAD model. The support structure is designed along with the final product in CAD model so that the structure is stable. The dimension of CAD model is such that the removal of bur is minimum. A translator is used to convert the drawing into .STL file. After successful loading, the control unit of the system, slice the drawing/model into numbers of layers with very small thickness. The automatic system (optical scanning system) is used to control and focuses the UV beam on the surface of liquid (photopolymer) as per the program file to solidify the polymer. The platform moves/drops downward which is equivalent to layer thickness after one layer gets solidified by UV rays and then second surface of the liquid gets deposited on the previous solidified layer. This process repeats layer by layer to build complete part/product. Then the product is

moved out from the machine tray and all the extra material/polymer is removed. Finally the post process curing is done to improve the physical properties like strength if required.

3.2 Solid Ground Curing

The Cubital Ltd. (Israel) proposed and commercially developed Solid Ground Curing method which is similar to SLA. The input data is generated by slicing three dimensional drawing (CAD model) according to the layer thickness. The production machine uses this processed data file (.STL file) to produce entire product by curing a photopolymer layer by layer in controlled environment. The ultraviolet (UV) light is used to cure the material through a photo mask. In this technique post curing is not required.

From CAD file in the form of image of the layers are sent to the mask plotter. The mask plotter produces image (basically a negative image) of the same layer with the help of a glass plate (which is charged with cations) and an electrostatic toner. During this time, the resin is spread on the work piece carriage. The resin loaded the work carriage and the mask plotter are kept together in sandwich manner at the exposure area, where the shutter opens for small time interval (2-3 seconds) and expose the resin under UV light from transparent areas of mask plotter. After the exposure through transparent mask plotter, the exposed resin is completely cured and mask plotter returns back to its original position (plotting station). The wiper wipes out the uncured resin from the work piece. The mask plotter is then electrostatically erased and prepared for next layer. Simultaneously in the same time, the part is kept under the UV light but without the plotter which solidifies the remaining resin that was not wiped out by the wiper. The whole carriage assembly is taken to the polymer/wax station, where a layer of wax is sprayed (which is very thin say 0.2 mm) on the work piece which fills all cavities and voids if present. The wax layer is then solidified with the help of a cooling plates present at the cold station.

The work piece assembly is taken to next station where the required thickness is cut down with the help of milling operation & the chips produced during this process are collected with the help of vacuum. The carriage is lower down as per the layer thickness and resin is spread for the next layer. The process continues in repetitive manner until the complete component is manufactured. The final prepared model is cured by dipping in hot water. In SGC process support structures are not required. Chips which are produced in this method are wastage and cannot be reused. This process can be used for geometric complex shapes with ease.

3.3 Selective Laser Sintering

Carl Deckard developed SLS in 1986 at Texas University (Austin). Selective layer sintering is a process that employs the use of powdered material approach to rapid prototyping. In this process a very thin layer (approximate 0.2mm depending on machine configuration) of hot powder (temperature just below melting point) is sprayed on the work table. A laser beam then moves on the surface area of hot powder in a specific pattern which is controlled by the source file (CAD file or .STL file). The heat generated by the lasers inters the powder together. This process continued layer by layer till the final component/product is produced. The unused/ un-sintered powder can be recycled/reused. The unused powder also acts like support for the work piece, so this process also removes the requirement of support structure. The materials which are used in this process include plastics, wax, metals, and coated ceramics.

However this method is different from the SLA. In SLA there is only one phase transition (from liquid to solid); whereas in the SLS there are two phase transition (first from solid to fluid & second from fluid to solid again).

3.4 Fused Deposition Modeling

FDM is also a RP technique which begins with software processing of CAD file (.STL file). Before starting the process, the selection of layer thickness and orientation of the component/prototype are mathematically done. The support structures are to be designed as per the requirements before starting the process. This machine can use a wide range of materials and colors to process components so that different goals are achieved, say one color/material layer is used to manufacture one part of the prototype/model, another color/material for another part and another color/material for supporting the component/structure (L. Kumar, Tanveer, Kumar, Javaid, & Haleem, 2016).

In the beginning, of this process desired materials/thermoplastics are warmed up to a certain temperature (to glass transition temp.). This heated material is driven out in molten state with the help of an extrusion head. The extrusion head is been controlled by the tool-path defined by CAM software as per the instruction in the CAD file (.STL file). The part is manufactured from down to up, layer by layer. The raw material is provided in wire form, from the roller. The machine connected to the nozzle control the flow of the hot material (V. Kumar, Kumar, Haleem, & Rajesh, 2016).

3.5 Laminated Object Manufacturing

This process was invented by Helixsys, Inc., Torrance; CA in 1989. The laminated object manufacturing is different from other systems. As in SLA, FDM & SLS the parts are building up by additive approach i.e. by stacking one layer over other through a forming process, but in LOM we use

subtractive approach, i.e. the materials is fed in form of continuous sheet which eventually make stake by cutting the desired shape through laser.

In LOM firstly, the sheets which are in winding bundles/ribbons are unwinds and then these ribbons are fed up to the machine with the help of motors through rollers. The rollers move the sheet over the work table and properly orient the material as per the machine platform. Sheet is placed on the work table of the machine. The sheet is cut according to the required shape with the help of a strong laser (CO₂ laser) beam. The unused sheet is wind on the other roller, in this process the new sheet comes over the cut section. A hot roller moves on the surface of the new sheet which binds the sheets together. The laser again cut the new sheet according to the new dimensions as per the .STL file. The process continues in repetitive manner. The laser beam is guided on the x-y positioning table with the help of sensors, mirrors and optics reflectors. Sometimes the unused sheet is not removed so that it can acts like support structure. After the completion of the process the stack of unused material is removed.

This technique/process is faster as compared to other techniques/process because the laser beam cuts the material on the periphery, which can produces a thick cross sectional layer in place of thin layers. Another advantage of LOM is that its part manufacturing ability is not limited by the complexity of the product/model which eventually leads to no internal stresses. The dimension accuracy is a problem.

The 3 dimensional printing is a process in which the three dimensional models/prototypes are manufactured directly from a computer drawing (CAD file). The 3DP process is very much same as that of a common laser/inkjet printer used in houses/offices. It works on the material addition approach in which different layers of material are buildup to produce the desired model. This technique used here is different from old manufacturing techniques in which products were produced mostly by removing the material. In this method the printing process begins with loading of required design file into .STL file format (from CAD file) in machine software. The machine deposits a layer of powder/liquid (as per machine specification) on the work table as per the instructions in .STL file. When the powder is used then the binder layer or laser (as per the machine specification) is used to join different layers. After the deposition of binder layer again a new layer of powder is spread on the work table. Since the binder is sprayed on the required area according to the dimensions, the new layer binds with the previous layer. If laser is used, the laser melts the powder on specified location which eventually binds with the previous layer.

Although there are numerous RP technologies available, they have some advantages and limitations. The selection of best technique depends upon many factors and however comparing all the available RP techniques one can easily find out the suitable process as per the requirement (V. Kumar, Kumar, & Haleem, 2016).

3.6 Three Dimension Printing

IV. COMPARISONS OF DIFFERENT RAPID PROTOTYPING TECHNIQUES

Table 2: Comparison of different RP techniques based on material used, energy required and wastage (V. Kumar, Kumar, & Haleem, 2016)

Technique	Short Name	Materials Used	Energy Required	Fixture & Tool	Laser Used	Solid Waste	Liquid Waste	Aerosol Waste	Disposal/ Handling of Residues
Conventional Machining	CM	Iron, HSS, Al, metals & Alloys	Mechanical Energy	Required	Not Used	Tool scrap, Chips	Fluid mixture (Cutting cooling)	Tool particulate fluid vapors	By Landfill, recycling
Stereo lithography	SLA	Photosensitive Liquid (Photopolymer)	Energy of Laser (UV) beam	Not Required	Used	Resin & Supports	Non	Not Produced	By Burning, landfilling
Selective Laser Sintering	SLS	Polymer, Metals, Wax & Ceramics	Energy of laser beam (High power)	Not Required	Used	Chips of waste material	Non	Not Produced	By Burning, landfilling, recycling

Fused Deposition Modeling	FDM	Polymer, Ceramic, Wax & Alloy	Only Heat Energy	Not Required	Not Used	Chips & Supports	Non	Not Produced	By Burning, landfilling, recycling
Laser Engineered Net Shape	LENS	Metals & binders	Energy of laser beam (High Power)	Not Required	Used	Material Chips	Non	Not Produced	By Burning, landfilling, recycling
Laminated Object Manufacturing	LOM	Paper, Polymers, Metals & Ceramic	Energy of laser beam (High Power) & Heat	Not Required	Used	Material Chips	Non	Not Produced	By Burning, landfilling, recycling
Inkjet printing	IJP	Liquid Material Inks	Energy of Piezoelectric nozzle	Not Required	Not Used	Microchip & Supports	Non	Not Produced	By Burning, landfilling, recycling
Three Dimensional Printing	3DP	Metals, Ceramics & Binders	Energy of Piezoelectric nozzle & Heat	Not Required	Not Used	Supports & Chips	Non	Not Produced	By Burning, landfilling, recycling

V. RECENT DEVELOPMENTS IN THE FIELD OF RAPID PROTOTYPING

The RP is a very new and emerging technique which is developing day by day. However there is lots of work which required to be done in this field and as per the available literature the development of RP can be summarized into six basic categories namely (1) Basic fundamental about RP Technique (2) Selection from different RP techniques (3) Product development/design using RP (4) Optimization of RP machine (5) New material development in RP (6) Impact of RP. The development about RP is discussed in these sections and these are discussed one by one in the coming sections described below:

5.1 Basic fundamental about RP Technique:

Poly Jet 3Dimensional printing is a technique which is similar to laser/inkjet printing of documents. The difference between two is that in place of printing/ink jetting the liquid drop on the paper as in conventional printing, here we build the liquid layer of photopolymers/powder on build tray which can move and cure the printed material under ultra violet or laser light (Javaid, Kumar, Haleem, & Kumar, 2015). And then after curing is done for one layer we move the tray by layer thickness and whole process repeats and goes on increasing to produce final 3D mode/prototype. Finally curing of model is done if required. The basic idea of almost all the RP techniques is similar and a brief overview about RP can be addressed from the following papers/authors.

(Tu, Xie, & Kam, 2006) presents main objectives of rapid OKP development for the global manufacturing industries environment and also reviewed the background for rapid development of products. The issues such as continual customer influence, product data complications, flaws related to information, complications of logistics management, very high customization, fatter/looser production planning and control etc. are discussed. And the

requirement (Enterprise integration, Support cooperation and collaboration, Stability and easiness in use and maintain etc.) needed for developing of a new production system (new generation) which can produce product rapidly was purposed. A reference system was also developed for easy comparison and understanding. The suggested reference system was open structure and it is internet based on the process of development of the products rapidly.

(Onuh & Yusuf, 1999) provides an overview about the growths and trend of the technology, areas of applications and significant benefits of RP technology to manufacturing industries. The study covers process fundamental and also deal with the issues related to (1) the stair-stepping phenomenon (2) Selection of layer thickness (3) Deviation of actual geometry from CAD model (4) Issue related to orientation of parts (5) The use of support structures. Process flow chart and application of RP technology is also discussed in brief.

(C K Chua, Hong, & Ho, 1999) discussed various popular rapid tooling techniques and classified them as hard or soft tooling (also direct or indirect tooling). The comparison of different techniques was also addressed based on the factors as tool life, development time of tool and the cost related to the development of tool.

5.2 Benchmarking/Selection of RP techniques

Different RP technologies have different advantages and limitations and the selection between these techniques depends upon the need of manufacturer. Depending upon the requirements and benefits of the manufacturer can compare all the RP techniques and select best among them. However for most suitable technique the comparison should be done carefully by considering all the factors/points. For selection among different techniques available on RP one can go through these papers which present very good comparison based on different requirements/questionnaires to choose best machines which suit as per requirement.

(Way, Zu Hazmin, Zainal, & Zahir, 2009) presents a QFD based benchmarking technique to compare and to select the best RP machine for different purpose (academic as well as educational) in Malaysia. Their research consider 17 aspects as customer requirements (Demanded Quality) and 17 aspects of functional requirements (technical measures of quality) and competitive analysis them for 5 different RP techniques. Among these five techniques (FDM, 3DP, LOM, SLS, SLA) the result shows that 3DP machine is best for educational purpose based on fact of machine cost, machine maintenance cost, reliable to produce complex design, raw material cost and another important aspects. However one of the limitations of their QFD approach is that it cannot take into account the uncertainty and ambiguity inherent in the assessment of customer requirements.

(Brown & Stier, 2002) presents different questionnaire for selecting RP system for first time purchaser. Their work covers different questionnaire based upon (1) Hardware, software and contractual questions (2) Faculty related questions (3) Industry type questions (4) Prototype related questions (5) Facilities and machine supervision questions and also suggested comparison chart for different machines. These questionnaires help in selecting the current type of RP technology or in purchasing the RP technology for the 1st time. The question of purchasing and selection is very hard to answer accurately as it depends upon many factors but yet they provided many details and included many issues which tries in providing optimum solution to the problem.

5.3 Product development/design using RP

The RP has the ability to quickly produce real working prototypes. These models can be used in many ways such as to understand how a design looks, feels and operates. It also gives us better and fast result to develop new product/component or to modify existing model. For development of new design or product RP is best techniques. (Ilmars & Natalija, 2011) discusses the new product development stages (development phase to production phase), and the innovative development result in functional prototype RP method. They analyze the benefits of using RP in new product development and make a comparison (based on different raw materials) between different RP systems which are available and can be used for innovative product development. The suggested stages consists of, development of product from its idea, making the 3 dimensional drawing/model of the idea, analyzing different parts of the model, rapid prototyping the model, and then post treatment if required.

(Xie & Tu, 2006) presented a computer based RP system which can work on internet or intra net based systems. The suggested system consists of many computers which are interlink through intra/internet and every computer function like a subsystem for the main system for

fast working. The system works on product development method/strategy which is known as “prototype based incremental product development strategy.” The system has product production data structure for database management which is actually a management software tool used for rapid development of intra/internet based product development systems. The industrial implementation is also listed in the paper with database management structure and product development method/strategy. The proposed work decreases the product development time in companies switched in New Zealand (SMOKP companies).

(Ilyas, 2013) provides an aspect that how to combine the machine vision (3Dimensional MV) with rapid prototyping. The proposed system based on reverse engineering which simplify and groups the main system into 3 main sub system/phases. First is the scanning phase, second the processing and modeling phase, and third is verifying the model. The suggested process was integrated with Fused Deposition Modeling (FDM) for rapidly development of prototyping for design. Implementation procedures at POLMAN Bandung, was also overviewed by the authors and for better understanding the problem the also provides some examples.

5.4 Optimization of RP machine

The optimization of different techniques is very much necessary as to remove unwanted time and resource which are of no use. The optimization work done by different authors can be summarized in the Table.3 described below.

Table.3: Optimization of RP machines

S r. N o.	Year	Authors	Area of Work/Research	Finding
1.	2000	(Allen & Sachs, 2000).	<ul style="list-style-type: none"> Worked on the fabrication of metal tooling parts for molding plastic tools. Worked on tool steel powder and bronze infiltrates Infiltrates are used which contain depressant (fast diffusers) to reduce meltingpoint. 	<ul style="list-style-type: none"> Obtained improved mechanical properties Improved the macro hardness Surface finish was improved with accuratedim ensions also wear resistivity and product complexity improved.

2.	2008	(Kumbhar, Pandey, & Rao, 2008)	<ul style="list-style-type: none"> Presented a curve model which was based on Intermediate point curve method(IPC M). The reverse engineering was combined with rapid prototype technique. Improve the process by removing the process of validation/repair of .STL file. 	<ul style="list-style-type: none"> As the .STL file was improved it removes the errors arising due to best fitting of surface and its triangulations. Proposed system was verified/ tested on both simple and complex objects. Its limitation is that this approach cannot handle the objects itself. 					<p>disciplinary Technical Development .</p> <ul style="list-style-type: none"> They optimized the data input software. Compared the surface quality (surface roughness) for inkjet printing and polymer jetting printing Work was focused on fitting of different parts on the building tray with considering all previous points. 	<p>n of time of building and support structures with the criteria of better surface quality.</p> <ul style="list-style-type: none"> The result shows that the quality of components /parts manufactured with poly jet printing technology was very good and also they did not required any post processing Whereas the components /parts manufactured by Z Printer have lowest precision and were very fragile (require post processing).
3.	2010	(Ollison & Berisso, 2010)	<ul style="list-style-type: none"> Determine the effects of building orientation, printing head & its life along with the diameter of the 3D printed part on their cylinder city An analysis of variance (ANOVA) study was conducted 	<ul style="list-style-type: none"> The results of this study suggest that the building orientation was the only one parameter which had a significant effect on the cylinder city of 3D printed parts 						
4.	2011	(Udroiu & Nedelcu, 2011)	<ul style="list-style-type: none"> This research was performed under the innovative platform developed for inter 	<ul style="list-style-type: none"> The part orientation was optimized on the build tray based on minimization 						

5.5 New material development in RP

The RP is one of the philosophies which can use almost all the materials (Polymers, wax, cement, wood, metals, ceramics, nylon, glass, alloys etc.) to convert them into finished goods. For the development of new material that can be used in RP machine various observations or findings are discussed in Table.4 below.

Table.4: New material development in RP

S r. N o.	Year	Authors	Material (Study/Used) / Outcome
1	2006	(Prashant, Senthilkumar, Pandey, & Rao, 2006).	<ul style="list-style-type: none"> Polymers, ceramics/cermet, wax, composites nylon/glass composite, alloys, metal-polymer powders and metals. Research covers the issues related to processing of bio-materials and functionally graded material (FGM) for bio –medical applications.
2	2006	(Makoto et al., 2006).	<ul style="list-style-type: none"> Works on the formulation of novel hot melt inks. Inks have been modified with particular chemical substances, blowing agents, in order to obtain raised images on a substrate. The novel hot melt ink consists of different waxes(Carnauba/PE wax alloy), tackifier (Hydrogenated rosin ester) and plasticizer resins (Polyamide), rheology modifiers, and gas releasing agents. The blowing agents (sodium bicarbonate; p-toluene sulfonylhydrazide; azodicarbonamide (ADC); and p, p-oxy-bis(benzenesulfonylhydrazide)) present in the ink decompose right after the ink deposition and form gas bubbles, which are entrapped in the solidifying ink droplets.
3	2008	(Utela, Storti, Anderson, & Ganter, 2008)	<ul style="list-style-type: none"> Presented the steps involved in process development for new material system in 3 DP which makes the material flexibility in 3DP. The numbers of steps involved are 1stFormulation of the new powder,
			<ul style="list-style-type: none"> 2ndSelection of the necessary binding method, 3rdFormulation of the new liquid binder and testing its suitability and interaction with printed powder, 4thSpecification for the print process's parameters, and 5thSpecification for the post-processing techniques/procedures
4	2011	(Williams, Cochran, & Rosen, 2011)	<ul style="list-style-type: none"> Additive manufacturing process based on layer printing for metallic cellular materials. Cellular ceramic green components/parts are fabricated by selectively printing the metal oxide which is very fine powders (the powder is spraydried along with a binder to increase granules formation for the processing) with a 3 Dimensional Printing machine. The part is then sintered (3 stage sintering) in a reducing atmosphere (10% H₂) to convert it into metal chemically. The resultant metal is maraging steel (Fe, 18.5Ni, 8.5Co, 5Mo) obtained by converting metal oxide. It creates cellular artifacts and can also be used to produce walls (thickness up to 270µm), channels (up to 1.1mm diameter), and angled trusses (up to 1mm diameter). The process can produce final/finished parts which have relative density on 63% and shrinkage (linear) of 45 %.
5	2011	(Gill & Kaplas, 2011).	<ul style="list-style-type: none"> Compared the efficiency of two 3 Dimensional powder based technologies (Z Cast process and investment casting) for casting of light

			<p>aluminum alloys (A356) and zinc alloy (ZA-12)</p> <ul style="list-style-type: none"> • In Z casting process, Z Cast 501 powder was used to print split pattern with sand support for aluminum alloy. • Investment casting of starchbased zinc alloy (ZP14) powder and plaster based (ZP100) powder were infiltrated (acrylate and wax) to make pattern.
6	2011	(Castilho, Pires, Gouveia, & Rodrigues, 2011).	<ul style="list-style-type: none"> • Worked on 3 Dimensional printing for bone repair. • Prepared tissueengineered scaffold for bone repairing which have very tight distribution of pore size and good controlled geometries.
7	2013	(Maleksaeedi et al., 2013).	<ul style="list-style-type: none"> • Use of Inkjet 3D printer to print titanium scaffolds bone parts with customized pores and part geometry. • To make titanium printable, its power (titanium powder) with spherical shaped particles with suitable size was prepared • The ball mill/mixer or vibratory mill/mixer is used for powder making and then the powder is dried mixed with a polymer (PVA) which is water soluble. • Titanium it is a biocompatible metal as it is biologically inactive and also it does not produce any undesirable effect on growing cells in the implant. • With suitable/optimum process selection we can produce porous titanium body parts which have similar mechanical properties as that of bone.

performance evaluation of RP based on its impact on environment, human, economy, society is been discussed here and the impact of various factors can be summarized as:

5.6.1 Environmental Performance

(Luo, Leu, & Ji, 1999) present a method based on environment friendliness which compares different rapid prototyping (RP) and rapid tooling (RT) process. Their work was based on the assessment of environmental performance for RP and RT process and the result was based upon the environmental indexes which utilize the eco indicators to measure the performance. Each of these processes was divided into four numbers of life stages namely, 1st material preparation 2nd part build 3rd part use and 4th part disposal. And then the impact/performance based on environment friendliness of each stage was evaluated firstly by identifying stage wise environmental impact factors and then summing all these values to calculate total impact. The assessment method considers material use, energy consumption, process waste and disposal of part after normal life at different stages for evaluation also their work covers an example to illustrate this assessment method applied on one stereo lithography process and two rapid tooling processes.

5.6.2 Economic Analysis

(Wittbrodt et al., 2013) presented a study to evaluate the economic selection between rapid prototyping technique and conventional method. This research was based on the printing of 20 designs which are used in common household. These design are freely available on the open internet source and these are the common household items which can be printed through Rep Rap technology in United States of America. The economic analysis was based on the cost and time taken to produce these items through RP and then result was compared with other methods (low/high market price, internet sources) to have these products. The analysis includes the printing time taken, filament consumed rate and other costs in printing. The result of the analysis shows that by using RP there is saving in cost range from \$300 to \$2000/year and it provides a payback time of 0.3 to 2 years with rate of return 40% to 200%. However the analysis do not covers all the variables which can also affect the result financial like energy cost, primary capital cost, discounts, inflations, loan charges etc.

5.6.3 Mechanical Noise

(Cohen et al., 2011) presented a study to measure/calculate the mechanical noise produced in tissue printing. The mechanical noise/temporal variation produced during tissue printing using hydrogel as printing material was measured and the effect of mixing different homogeneity of alginate hydrogels was studied. The result suggest that for reduction

5.6 Impact of RP

Without considering the impact of any technique we cannot conclude whether the technique is useful or not. So the

of mechanical noise up to 82% can be achieved using proper mixing (up to 128 cycles) between alginate and cross linkers. The smoothness in surface texture shows the improvement in geometrical fidelity with better target matching and very less point defects. The mixing also shows positive effect on cell viability which was improved by 34 % with curing time of 45 min. The result also shows a rise in modulus strength by 110 % that was 4 kPa before and 8.4 kPa after increasing the mixing cycle to 200 cycles from 8 cycles.

5.6.4 Societal Impact

(Huang, Liu, Mokasdar, & Hou, 2013) compares the additive manufacturing (AM) processes with conventional manufacturing based on their societal impact. This study covers the impact of additive manufacturing on human health, along with its impact on manufacturing supply chain. The environmental effects of chemicals which are used in AM processes is studied, & their potential health and occupational hazards, energy consumption and environmental impact is also considered. However the limitations of this study shows that the health factor of all the AM materials used, was not established and also it required more research to accurately evaluate various AM processes.

5.6.5 Structural Strength

(Le et al., 2012) studied the hardened properties of printed concrete. The concrete was printed through extrusion with a 9 mm diameter nozzle. The concrete was a fiber reinforced to improve its performance and made up of fine aggregate through layer by layer process printing process (3 D Printing). Different mix proportions were made and their effect on different properties of concrete (strength compressive, tensile and flexural, % shrinkage when dry, and density) was studied with different printing layers orientations. The result obtained shows that a well printed concrete can have a density of 2350 kg/m³, compressive strength of 75–102 MPa, flexural strength of 6–17 MPa. However these results depend on the testing process and direction. The voids (porosity) depends upon the printing process can vary from 4.8% (poor printing) to 1% (good printing) whereas it was 3.8% for mold casting process. However further research is needed to verify/assess the behavior of the printed concrete under actual working/service conditions also to find the effect of different layers on durability of the structure.

VI. APPLICATIONS, ADVANTAGES AND DISADVANTAGES

6.1 Applications of RP:

The RP technique is an optimum method to produce any product and it has wide range of applications. Even if this technique is still under development it can be effectively

applied almost everywhere and for any shape and any material. Some of the typical applications of RP include reverse engineering, rapid tooling, casting, modelling, and product development. It finds its immense applications in the medical field like custom fit mask, new organ development, operation practice etc. It is also used in fine art and jewelry design for fast and custom fitted designs. It is also used in forensic science and ancient monument redesign and study. Most recent development and study shows that RP is also being used for making houses, automobile parts, aircraft parts etc. Thus this technique has lots of potential which have to be utilized.

6.2 Advantages of RP:

This technique offers a number of advantages. Studies show that application of RP in the industries drastically reduces both cost and time. It saves lots of resource, time and money in the process of new product development. Burns M (Burns, 1993) suggest that companies are trying to utilize this technique in more innovative ways than others. The use of RP increases the complexity in shape and size of the product. An added advantage of this technique is that, unlike subtractive manufacturing, it does not leave unused cut-off stock or chippings. Since the corrections in the product are made early in the process stage so it saves time during product development stage.

6.3 Disadvantages of RP

The RP technology is an emerging technology which is still in its development phase and requires a lot of thought and development. Despite of recent the advancements in this field, there are numerous limitations associated with it. One of the biggest limitations is the cost factor which limits its application in small scale. Traditional manufacturing process is usually much faster and less costly when mass producing identical parts. Another limitation is the lack of flexibility in the materials which can be used in the RP machine. Since it lacks sophisticated control and laser systems, controlling the surface finish and precise dimensional accuracy is somewhat challenging which requires lots of work to eliminate the gap. However with the incorporation of new and better techniques these limitations will cease to exist. Further for its rapid growth, awareness about this technique and concurrent research is needed. However a complete shift of the paradigm from conventional techniques to RP technique is not an easy task and requires time to gain the confidence and to overcome the fear among the people about the shift. Some of the main disadvantages of rapid prototyping are as follow:

- Traditional manufacturing process is usually much faster when mass producing identical parts.
- Per piece cost can be high, base material expensive, no economy of scale.
- Most have poor surface quality.

- No quite as strong, often more brittle.
- Material options are limited.

VII. CONCLUSION

This paper covers an overview about the different rapid prototyping techniques (Fused deposition modelling, Stereo lithography, 3D printing, Selective laser sintering, Laminated object manufacturing). The RP is a new and emergent technology in which models/prototypes are produced directly from CAD into desired shape by additive process (in layer by layer). In this paper the classification and comparison of these different techniques/processes based on different factors is been done. Also the advantages, limitations, performance, and applications of RP techniques/processes are addressed in this paper. It covers the history and development of different RP technique based on various available literatures. It tries to address how to select best technique from different RP techniques based on manufacturers requirements/questionnaires and the problem of benchmarking product development and new material development has been addressed and then the optimization with performance evaluation of RP techniques/processes is also been done.

REFERENCES

- [1] Allen, S. M., & Sachs, E. M. (2000). Three-dimensional printing of metal parts for tooling and other applications. *Metals and Materials*, 6(6), 589–594. <http://doi.org/10.1007/BF03028104>
- [2] Brown, B. R., & Stier, K. W. (2002). Selecting Rapid Prototyping Systems. *Journal of Industrial Technology*, 18(1), 1–8. Retrieved from www.nait.org
- [3] Burns, M. (1993). *Automated fabrication: improving productivity in manufacturing*. Englewood Cliffs, N.J.: PTR Prentice Hall. Retrieved from <http://trove.nla.gov.au/version/45461950>
- [4] Castilho, M., Pires, I., Gouveia, B., & Rodrigues, J. (2011). Structural evaluation of scaffolds prototypes produced by three-dimensional printing. *The International Journal of Advanced Manufacturing Technology*, 56(5), 561–569. <http://doi.org/10.1007/s00170-011-3219-4>
- [5] Chua, C. K., Hong, K. H., & Ho, S. L. (1999). Rapid tooling technology. Part 1. A comparative study. *The International Journal of Advanced Manufacturing Technology*, 15(8), 604–608. <http://doi.org/10.1007/s001700050108>
- [6] Chua, C. K., & Leong, K. F. (1997). *Rapid prototyping: principles and applications in manufacturing* (1st ed.). New York: John Wiley.
- [7] Cohen, D. L., Lo, W., Tsavaris, A., Peng, D., Lipson, H., & Bonassar, L. J. (2011). Increased Mixing Improves Hydrogel Homogeneity and Quality of Three-Dimensional Printed Constructs. *Tissue Engineering*, 17(2), 239–248. <http://doi.org/10.1089/ten.tec.2010.0093>
- [8] Cooper, K. G. (2001). *Rapid Prototyping Technology: Selection and Application*. (L. L. Faulkner, Ed.). Madison Avenue, New York: Marcel Dekker CRC Press. Retrieved from www.dekker.com
- [9] Gill, S. S., & Kaplas, M. (2011). Efficacy of powder-based three-dimensional printing (3DP) technologies for rapid casting of light alloys. *The International Journal of Advanced Manufacturing Technology*, 52(1), 53–64. <http://doi.org/10.1007/s00170-010-2716-1>
- [10] Huang, S. H., Liu, P., Mokasdar, A., & Hou, L. (2013). Additive manufacturing and its societal impact: a literature review. *The International Journal of Advanced Manufacturing Technology*, 67(5), 1191–1203. <http://doi.org/10.1007/s00170-012-4558-5>
- [11] Ilmars, B., & Natalija, M. (2011). Research on rapid prototyping influence in manufacturing technology. In D. S. Ekinovic, D. J. V. Calvet, & D. E. Tacer (Eds.), *15th International Research/Expert Conference "Trends in the Development of Machinery and Associated Technology"* (pp. 729–732). Prague, Czech Republic. Retrieved from <http://tmt.unze.ba/proceedings.php>
- [12] Ilyas, I. P. (2013). 3D Machine Vision and Additive Manufacturing: Concurrent Product and Process Development. *IOP Conference Series: Materials Science and Engineering*, 46(1), 12029. <http://doi.org/10.1088/1757-899X/46/1/012029>
- [13] Javaid, M., Kumar, L., Haleem, A., & Kumar, V. (2015). Product Design and Development using Polyjet Rapid Prototyping Technology. *Control Theory and Informatics*, 5(3), 12–20. Retrieved from <http://iiste.org/Journals/index.php/CTI/article/view/23079>
- [14] Kumar, L., Kumar, V., & Haleem, A. (2016). Rapid Prototyping Technology for New Product Development. *IJISSET - International Journal of Innovative Science, Engineering & Technology*, 3(1), 287–292. Retrieved from http://ijiset.com/vol3/v3s1/IJISSET_V3_I1_39.pdf
- [15] Kumar, L., Tanveer, Q., Kumar, V., Javaid, M., & Haleem, A. (2016). Developing low cost 3 D printer. *Int. Journal of Applied Sciences and Engineering Research*, 5(6), 433–447. <http://doi.org/10.6088/ijaser.05042>
- [16] Kumar, V., Kumar, L., & Haleem, A. (2016). Rapid prototyping technology ranking using an ANP approach and its sensitivity analysis. *International Journal of Engineering Sciences & Research*

- Technology, 5(9), 93–103.
<http://doi.org/10.5281/zenodo.61471>
- [17] Kumar, V., Kumar, L., & Haleem, A. (2016). Selection of Rapid Prototyping Technology Using an ANP Based Approach. *IOSR Journal of Mechanical and Civil Engineering (IOSR-JMCE)*, 13(4), 71–78.
<http://doi.org/10.9790/1684-13040647178>
- [18] Kumar, V., Kumar, L., Haleem, A., & Rajesh. (2016). Design and Development of Thermal Rapid Prototyping Machine and Its Application. *International Journal of Emerging Technologies in Engineering Research (IJETER)*, 4(2), 101–106. Retrieved from <http://www.ijeter.everscience.org/Manuscripts/Volume-4/Issue-2/Vol-4-issue-2-M-12.pdf>
- [19] Kumbhar, V. K., Pandey, P. M., & Rao, P. V. M. (2008). Improved intermediate point curve model for integrating reverse engineering and rapid prototyping. *The International Journal of Advanced Manufacturing Technology*, 37(5), 553–562.
<http://doi.org/10.1007/s00170-007-0995-y>
- [20] Le, T. T., Austin, S. A., Lim, S., Buswell, R. A., Law, R., Gibb, A. G. F., & Thorpe, T. (2012). Hardened properties of high-performance printing concrete. *Cement and Concrete Research*, 42(3), 558–566.
<http://doi.org/10.1016/j.cemconres.2011.12.003>
- [21] Luo, Y., Leu, M. C., & Ji, Z. (1999). Assessment of environmental performance of rapid prototyping and rapid tooling processes. *Solid Freeform Fabrication Symposium*, 783–792.
- [22] Makoto, N., Nishiyama, Y., Henmi, C., Iwanaga, S., Nakagawa, H., Yamaguchi, K., ... Takiura, K. (2006). Novel Phase Change Inks for Printing Three-Dimensional Structures. *Journal of Imaging Science and Technology*, 50(6), 550–555.
[http://doi.org/10.2352/J.ImagingSci.Technol.\(2006\)50:6\(550\)](http://doi.org/10.2352/J.ImagingSci.Technol.(2006)50:6(550))
- [23] Maleksaeedi, S., Wang, J. K., El-Hajje, A., Harb, L., Guneta, V., He, Z., ... Ruys, A. J. (2013). Toward 3D Printed Bioactive Titanium Scaffolds with Bimodal Pore Size Distribution for Bone Ingrowth. *Procedia CIRP*, 5, 158–163.
<http://doi.org/http://dx.doi.org/10.1016/j.procir.2013.01.032>
- [24] Ollison, T., & Berisso, K. (2010). Three-Dimensional Printing Build Variables That Impact Cylindricity. *Journal of Industrial Technology*, 26(1), 1–10. Retrieved from www.atmae.org
- [25] Onuh, S. O., & Yusuf, Y. Y. (1999). No Title. *Journal of Intelligent Manufacturing*, 10(3/4), 301–311.
<http://doi.org/10.1023/A:1008956126775>
- [26] Prashant, K. J., Senthilkumaran, K., Pandey, P. M., & Rao, P. V. M. (2006). Advances in Materials for Powder Based Rapid Prototyping. In *In Proceeding of International Conference on Recent Advances in Materials and Processing* (pp. 1–8). Coimbatore, INDIA. Retrieved from http://web.iitd.ac.in/~pmpandey/RP_html_pdf/ADVANCES_IN_MATERIALS_FOR_POWDER_BASED_RAPID_PROTOTYPING_with_date.pdf
- [27] Tu, Y. L., Xie, S. Q., & Kam, J. J. (2006). Rapid one-of-a-kind production. *The International Journal of Advanced Manufacturing Technology*, 29(5), 499–510.
<http://doi.org/10.1007/s00170-005-2534-z>
- [28] Udriou, R., & Nedelcu, A. (2011). *Optimization of Additive Manufacturing Processes Focused on 3D Printing. ... Prototyping Technology-Principles and Functional ...*. INTECH Open Access Publisher.
<http://doi.org/10.5772/21433>
- [29] Utela, B., Storti, D., Anderson, R., & Ganter, M. (2008). A review of process development steps for new material systems in three dimensional printing (3DP). *Journal of Manufacturing Processes*, 10(2), 96–104.
<http://doi.org/http://dx.doi.org/10.1016/j.jmapro.2009.03.002>
- [30] Way, Y., Zu Hazmin, B., Zainal, M., & Zahir, H. (2009). Benchmarking the rapid prototyping machines (RPM) for education purpose using quality function deployment (QFD). In *International Conference on Advances in Materials & Processing Technology (AMPT 2009)* (pp. 1–17). Kuala Lumpur. Retrieved from <http://irep.iium.edu.my/id/eprint/5957>
- [31] Williams, C. B., Cochran, J. K., & Rosen, D. W. (2011). Additive manufacturing of metallic cellular materials via three-dimensional printing. *The International Journal of Advanced Manufacturing Technology*, 53(1), 231–239.
<http://doi.org/10.1007/s00170-010-2812-2>
- [32] Wittbrodt, B. T., Glover, A. G., Laureto, J., Anzalone, G. C., Oppliger, D., Irwin, J. L., & Pearce, J. M. (2013). Life-cycle economic analysis of distributed manufacturing with open-source 3-D printers. *Mechatronics*, 23(6), 713–726.
<http://doi.org/10.1016/j.mechatronics.2013.06.002>
- [33] Xie, S. Q., & Tu, Y. L. (2006). Rapid one-of-a-kind product development. *The International Journal of Advanced Manufacturing Technology*, 27(5), 421–430.
<http://doi.org/10.1007/s00170-004-2225-1>

Performance tests on Screw Feeder Conveyor for Nodule Transfer Deep Sea Applications

Amudha.K, Ramesh N.R., Sundaramoorthi.V , Dineshkumar .D ,Muthuswamy.V,
Rethnaraj.T , G.A.Ramadass

National Institute of Ocean Technology, Chennai, India

Abstract—A screw conveyor is a versatile conveyor used in many process plants for the transfer of bulk solids and powders. The following article has written to understand screw conveyor design and selection of the right screw conveyor for underwater applications to convey crushed manganese nodules to the pump system for nodule transfer.

The nodules from the sea bed will be collected by a pickup device and crushed into less than 30mm pieces by using a crusher and pumped by a positive displacement pump to the mother vessel. Screw feeder is used to transfer crushed Polymetallic Nodules from hopper to pump system with controlled feed rate. A land based screw feeder is modified to suit the under water applications.

Studies on screw conveyors were conducted to examine performance in land as well as underwater. Most of these studies were experimental in nature. This paper presents a critical review on the design and validation of a screw conveyor.

Keywords— Mining, Manganese nodules, Polymetallic nodules, Screw conveyor.

I. INTRODUCTION

Deep sea mining of polymetallic nodules is of increasing importance to many countries, due to the potential of abundant supply of manganese, nickel, copper and cobalt. The nodules are available in all sizes up to 100mm in diameter; but usually range from 20 to 70mm. The nodules occur in ocean depths up to 6000m; hence various countries have been developing technologies for mining them from such depths. Schematic of deep subsea technology for mining these resources as shown in Fig.1. It is a major challenge considering the ultra-high pressure environment of 550 bar (about 250 times the pressure in automobile tyres), very soft soils of shear strength 2.5 kPa (similar to heavy grease) and other factors.

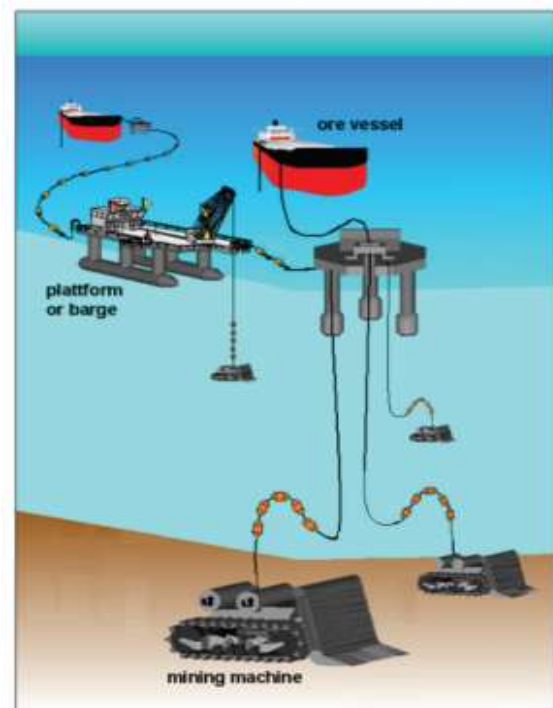


Fig. 1: Integrated deep-sea mining system using Flexible Riser configuration.

A study was taken in developing a deep sea mining system using flexible riser concept (Grebe, 1997). The concept has been realized and tested upto 512 m depth in the Indian seas. Initially, the system was tested for sand and silt mining operations-short term operations at 451m depth in 2001 and long term operations at 521m depth in 2006. The developed mining machine was augmented with polymetallic nodule collector and crusher, large solids handling pump and tested for operations at 512 m depth using artificial nodules. For laying artificial nodules, initially a remotely operable artificial nodule laying system was developed and tested at 518 m depth in 2007. Now the effort is towards the development of mining systems for 6000 m depth.

The traction force required to manoeuvre the mining machine along with reciprocating pump is a difficult task and the pump system from the miner is being separated and positioned in a the pump frame system.

In the proposed integrated mining system configuration the Pump frame is proposed to be vertically hanging from the mother vessel and the crawler based mining system would be with a pump, collector, pickup and crusher systems on the seabed.

The objective of paper is to study the screw feeder performance to feed the crushed manganese nodules to the pump which will pump to the mother ship. The crushed manganese nodules stored in the hopper system has to be transferred for the corresponding flow rates.

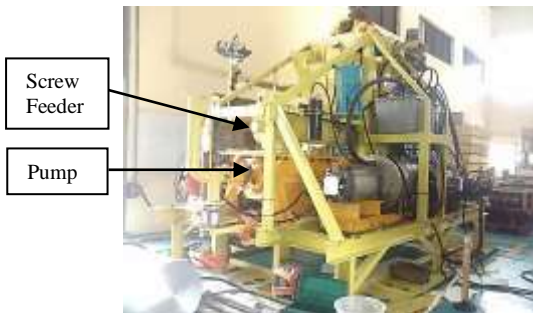


Fig. 2: Assembled view of pump system

As a first phase it was planned to conduct a sea trial at lower depth. The above Fig.2 shows the assembled view of the screw feeder with pump system.

II. DESIGN REQUIREMENT

For the applications as shown in the Fig.3 the horizontal screw feeder has been chosen to transport nodules as per Conveyor Equipment Manufacturers' Association (CEMA) standards. The screw feeder should be suitable for working in sub-sea high pressure low temperature environment & operating conditions. A land based screw feeder system was designed to suit underwater requirement by incorporating suitable sealing, bearing etc.,for the required feed rate and loading conditions, and it was tested in a test set up for evaluating its performance.

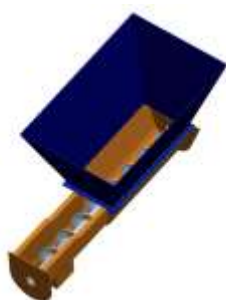


Fig. 3: Screw Feeder with Hopper

The conveyor screw imparts a smooth positive motion to the material as it within the trough. The Fig.4 shows that it consists of a tube (shaft) containing a spiral blade coiled around a shaft, driven at one end and held

at the other. As per table 1,the rate of volume transfer is proportional to the rotation rate of the shaft. Advantages of the horizontal screw feeder are: reduced risk of environment pollution, the transported material is protected from exterior contamination, flexibility of use, functional reliability, can control the flow of material very well.

Table.1

Bulk Density of material	2000 kg/m ³		
Required Capacity (m ³ /hr)	2	3	4
Revolutions of Screw per minute	8	12	16

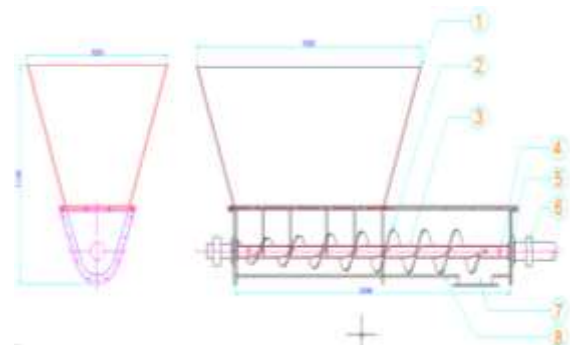


Fig.4: View of Screw Feeder With Hopper

1. Hopper
2. Tapered Screw
3. Pipe
4. Shaft
5. Seals
6. Plummer Block
7. Discharge Outlet
8. Trough

III. SELECTION OF PARAMETERS

The capacity of the screw conveyor in cubic feet per hour per revolution per minute is:

$$C = \frac{0.7854 \times (Ds^2 - Dp^2) \times P \times K \times 60}{1728 \times \text{rpm}}$$

The diameter of conveyor would be selected from corresponding percentage loading to achieve the equivalent capacity within the recommended rpm range. From the theoretical calculation the trough loading was calculated as 45%.Based on the experiments conducted the trough loading arrived was 53% .

The diameter of screw and pitch of the screw was chosen was 228.6 mm and diameter of pipe 63.5 mm. For the present case the ball bearing was chosen and hence hanger bearing factor considered was 31.

V. TEST AT LAND

The test set up at land as shown in Fig.5 consists of 44 cc hydraulic motor which provides a torque 0.63 Nm/bar was utilized for the present study. The Gear box was coupled to the drive motor and the screw

feeder shaft. A 8 station servo valve pack was utilized to control the flow of hydraulic motor. The results are tabulated in the table 3 confirms that nodule output rate was 8.6 kg per rotation.



Fig. 5: Test set up at Land

Flow (m ³ /hr)	Speed (rpm)	Output (kg)	Time (Mins)
40	1.9	16.4	1
90	4.9	41.6	1
90	4.9	41.1	1

VI. TEST AT UNDERWATER

Preliminary trials were conducted on land with the system kept inside a water tank of size 8m x 4m x2 m as shown in Fig 6.



Fig.6: Test set up at in Tank

The inner diameter of the transport hose used for the present study is 102 mm. For the hydraulic transport of grain type solids, the particle diameter should be one-third of the hose diameter to avoid clogging. Therefore, the maximum allowed particle size should be less than 30 mm. The nodule was pumped using reciprocating pump through a hose of Ø102 mm, vertically to a height of 30 meters.

Flow(m ³ /hr)	Speed (rpm)	Output (kg)	Time (Mins)
30	17.8	223	1.5
30	18.3	150	1
40	8.4	142	2
40	8.4	149	2
40	15.5	141	1

From the above table 4 it confirms for different flow rates and feed rate the nodule output rate found to be 8.6 kg per rotation which was measured in the load cell.

VII. TEST AT SEA

The Fig.7 shows the system was tested at a depth of 150 m at sea and the screw feeder was operated to provide feed at 4 Tn/hr and 8 Tn/hr. The slurry was collected at ship and nodules were drained and the output weight was calculated.



Fig. 7: Test at sea

It was observed the collected quantity was 14 % less than the calculated value as shown in the table 5. From the operation it was observed that while collection of nodules in the hopper placed at mother ship finer particles got washed away. It was observed feeder continued supplying for some more time in the 2 minutes of operation which was collected 149 kg/min

Flow(m ³ /hr)	Speed (rpm)	Output (kg)	Time (Mins)
30	8	59.4	1
30	8	149.5	2

VII. DATA ACQUISITION AND CONTROL SYSTEM

The Data Acquisition and Control System (DACs) for the this test was formulated using stand alone real time controller namely compact Reconfigurable Input Output (cRIO) along with associated input and output modules, signal conditioning circuits, video and data telemetry system. The configuration details for each I/O modules along with main cRIO-9025 controller for various final control elements / sensors are listed in the below Fig.8.

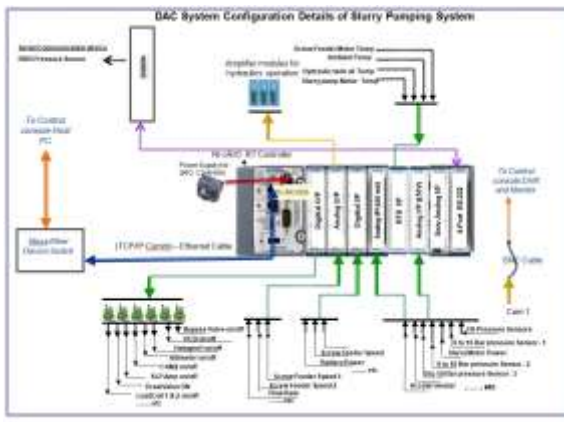


Fig.8: Data Acquisition and Control System (DACs)

VIII. SENSORS AND AMPLIFIERS

The speed of the screw feeder has been measured by using an inductive type proximity sensor with an accuracy of 0.1% Full scale. An inductance pick up device fixed on the shaft of the screw feeder, senses the rotation of switching distance of 1 mm and provides a pulse sequence proportional to the number of rotations. The speed of the screw feeder is controlled hydraulically by two proportional control valves. The proportional control valves can be controlled by a voltage controlled amplifier module, which is commanded from the analog output module of the DAC system. Hydraulic coils are connected to the amplifier module and input to the amplifier module is a differential output voltage (+/-10 V DC) from the analog output module. By varying the differential voltages to the amplifier, proportional control valve can be operated in the forward and reverse direction of the screw feeder. The screw feeder pump pressure also

been measured by using 900 bar rated pressure sensor, the accuracy of this sensor is about $< \pm 0.25 \%$ Full scale range.

IX. UNDERWATER VISION SYSTEM

One set of Underwater camera and lamps were used for monitoring the operation of screw feeder. The camera and lamp was mounted on the Pan& Tilt unit to enhance the view angle of the camera. The screw feeder operation videos have been recorded by using a Digital Video Recorder (DVR) at ship side as shown in Fig 9.



Fig. 9: Real Time Acquired Screw feeder Snap

X. GRAPHICAL USER INTERFACE

The user interface software as shown in Fig10 (Graphical User Interface (GUI)) is developed using LabVIEW. The following parameters were acquired through DAC system @ 10 Hz sampling rate and displayed in the front panel in the host PC with appropriate engineering units and also logged these parameters with date and time stamp. The data telemetry between DAC System and Host PC has been formulated by using TCP/IP (Transmission Control Protocol / Internet Protocol)communication.

Real-time measured parameters for screw feeder operations are,

- Screw Feeder Pump Pressure (bar)
- Screw Feeder Motor Temperature (°C)
- Screw Feeder speed(rpm)



Fig. 10: Graphical User Interface of Operator Screen

XI. ELECTRICAL UNIT

The screw feeder is driven by a hydraulic motor and is powered from a separate sub-sea Hydraulic power unit (HPU) . Since the screw feeder is designed for subsea operation a sub sea HPU unit is used. The speed of the screw feeder is variable through the control of proportional flow control valves.

The HPU is powered by a 55kW 3 phase sub-sea electric motor operating at 3000V AC. Higher operating voltage is chosen to overcome the voltage drop in the subsea cable through which the electric power is transmitted. The electric motor (HPU) is oil filled and pressure sensor compensated type and is started through a Medium voltage soft starter system to avoid high inrush current during motor starting.

XII. CONCLUSION

From the experiments it is evident that there is no loss in mass flow rate with different flow rates and feed rate. The nodule output rate found to be 8.6 kg per rotation. The screw feeder operated at 150 m depth there was mass loss of 14 % due to wash away of finer particles and feeder continued to supply some more time which has to be studied further. The above design will be validated in the sea trials for higher depth and the input would be useful for 6000m design of screw feeder systems.

ACKNOWLEDGEMENTS

We sincerely thank Ministry of Earth and Science and Deep sea Technology and Ocean Mining group, NIOT for its support and development of the system.

REFERENCES

- [1] Classification and definition of Bulk materials CEMA standard 550-2003
- [2] Screw conveyor dimensional standards CEMA standard 300-2003
- [3] S.Rajesh, A.A. Gnanaraj, A. Velmurugan, R. Ramesh, P. Muthuvel, M.K. Babu, N.R. Ramesh, C.R. Deepak, M.A. Atmanand (2011) Qualification tests on Underwater Mining System with Manganese Nodule Collection and Crushing Devices Proceedings of the Ninth (2011) ISOPE Ocean Mining Symposium, Maui, Hawaii, USA, June 19-24
- [4] Amudha, K, Rajesh, S, Ramesh, N R, Muthukrishna Babu, Raju Abraham, Deepak.C R, Atmanand, M.A (2009). "Development and Testing of Remotely Operated Artificial Nodule Laying System at 500 m water depth" Proc. 8th ISOPE Ocean Mining Symposium, Chennai, India, ISOPE, pp 233-238.

- [5] Uematsu, T., Nakamura, S., Hino, Y. and Suyama, H. "A study of the screw conveyor." Trans. JSME, 26(162), 180-186. (1960).
- [6] Don McGlinchey "Bulk Solids Handling: Equipment Selection and Operation" Page No. 197-219 Blackwell Publishing Ltd. ISBN: 978-1-405-15825-1, 2008
- [7] Chris Rorres "THE TURN OF THE SCREW: OPTIMAL DESIGN OF AN ARCHIMEDES SCREW", Page : 72-80, JOURNAL OF HYDRAULIC ENGINEERING / JANUARY 2000
- [8] Alma Kurjak, "The vertical screw conveyor-powder properties and Screw conveyor design", SE-221 00 Lund, Sweden, January 2005
- [9] Atmanand, MA, Shajahan, MA, Deepak CR, Jeyamani, R, Ravindran, M, Schulte, E, Panthel, J, Grebe, H and Schwarz, W (2000). "Instrumentation for underwater crawler for mining in shallow waters," Proc. International symposium of Autonomous Robots and Agents, Singapore, May 26, 2000.
- [10] Atmanand, MA, Deepak CR, Jeyamani, R, Ravindran, M, Schulte, E, Panthel, J, Grebe, H and Schwarz, W (2000). "Instrumentation and Control System of a Sand Mining System for Shallow Water", Proc. International symposium The Fourth (2001) Ocean Mining Symposium Szczecin, Poland, September 23-27, 2001.

Efficient Design of Error Recovery and Improve the Performance Using Mesh of Ring Topology Based NoC

A.Kalimuthu¹, Dr.M.Karthikeyan²

¹Department of ECE, JCT College of Engineering and Technology, Coimbatore, India

²Principal, Tamilnadu College of Engineering, Coimbatore, India

Abstract— generally, the System-on-chips (SoCs) is usually an Integrated Circuit in which integrates new elements in a single chip. Because of rise in number of transistors on a single chip gives complex system. To reduce the system complexity integrated SoC within a system, it forms a Network on Chip (NoC). Designed for NoC architectures, high performance efficient router design having minimal power consumption are necessary for real-time applications. NoCs having mesh and Ring structured interconnection topologies now are popular for their simple structures. In this paper, we designed the energy-efficient however high performance approach to conventional Hybrid mesh based-Ring using deflection on-chip networks. Most of us try to achieve the scalability associated with meshes by the router simplicity as well as effectiveness of rings. Our design can be a hierarchical ring interconnect that will keep all the simplicity of conventional ring patterns while reaching high scalability as more complex buffered hierarchical ring designs. We propose a router design and also show these types of routers will be significantly simpler, additional area and power efficient compared mesh based routers. In this work, we all establish the conventional error rates of the on-chip and also designed suitable Error Correction Code (ECC) mechanisms to improve their reliability. We show that using the planned specific ECC method it is easy to achieve significantly reduced power dissipation and high performance in the NoC.

Keywords— NoC, mesh of ring topology, error correction code (ECC)

I. INTRODUCTION

Although, network-on-chip is really important allow for scalable multi-core processors. A NoC is necessary in selecting over-all process performance because it affects latency moreover bandwidth with overall cost, including power and area. While devices reduce in size towards the nanometer scale, on-chip interconnects have been an important bottleneck in achieving performance and power consumption needs in the chip design. Industry and

academia recognize the interconnect difficulties due to the fact involving an important design constrains, as a result, mesh-based Network on Chips (NoCs) are proposed to handle challenges with rising interconnect complexity [5-14]. The Hierarchical Rings structured network-on-chip, consists important features that will allow us to mostly maintain the simplicity of conventional simple ring topologies while supplying larger power effectiveness and also scalability [1-4]. In this paper, we deal with reliability problems inside of a hybrid mesh of ring topology in NoC [4] through proposing a specific Error Correction Code (ECC) structure with various schemes for interconnect links. In the hybrid NoC experience larger error rates compared to regular wires thereby more robust ECC technique need to restore the reliability on this kind of links. During this perform many of us determine the conventional error rates from the on-chip interconnect links and propose appropriate ECC methods to improve their reliability. We show that using the proposed specific ECC scheme it is possible to attain significantly low power dissipation and high performance in a NoC.

II. RELATED WORK

Hierarchical ring based interconnect has been developed in an earlier types of work [14, 15]. We now have by now as compared to previous hierarchical ring scheme performance. The important huge difference between our proposal and this earlier work is we propose deflection-based routers with minimal buffering and also node routers with no buffering; alternatively, most of these previous performs implement routers with in-ring buffering, along with apply wormhole switching and flow control. This really is comparable the difference between buffered mesh routers [16] and bufferless deflection mesh routers [17].

Bufferless Mesh-based Interconnects, while we focus on ring based interconnects to achieve simpler router design and less significant power, further more perform for modifies traditional buffered mesh routers by reducing

the buffers and also applying deflection [17]. Even as we present within evaluations, although such types effectively minimize power and area, they support the essential complexity of mesh based routers, and hierarchical ring designs really are a improved overall performance and power.

Other Ring based Topologies, Spidergon [18] proposes a bidirectional ring improved with links in which directly connect nodes opposite one another on the ring. These types of extra links minimize the typical hop range for traffic. But, the cross-ring links develop into extended while the ring develops, avoiding scaling previous particular point, while our design doesn't have such scaling bottleneck. Octagon [21] types a network through combination Spidergon models of 8 nodes each. Designs are joined by dealing with a connection node in common. This kind of design scales linearly. But, it is utilize hierarchy, while our design employs global rings to join local rings. Other Minimal Cost Router Designs, Finally, Kim [20] proposes a low-cost router design that's superficially related to the proposed node router design routers present traffic along rows and columns in a mesh without using crossbars, only pipeline registers and multiplexer. After traffic enters a row or column, it remain till it reaches their location, as in a ring. Traffic also moves from a row to a column analogously to a ring |move within our design, employing a turn buffer. But, since a turn is possible at any node in a mesh, every router needs this kind of buffer on the other hand, we involve these move buffers just at bridge routers, and their cost is amortized |overall nodes. Mullinset al. [19] proposes a buffered mesh router with single cycle arbitration. We reveal the target of developing a simpler, faster.

1 Evaluation to four standard models

- 1.1 Buffered mesh,
- 1.2 Bufferless mesh,
- 1.3 Single ring,
- 1.4 Buffered hierarchical ring.
- 1.5 Mesh of Rings Topology

1.1 Buffered Mesh

A mesh interconnects routes obviously to a 2-D tiled CMP design. Meshes are therefore a typical selection for multi-core CMPs. A mesh topology has excellent performance scalability relative to ring-based types, since their bisection bandwidth develops obviously with the network. On the other hand, single- and hierarchical-ring topologies should expand a ring to maintain sufficient bisection bandwidth. But, a mesh topology allows cross-chip traffic to go to every node along a path. In comparison, a hierarchical topology such as for instance hierarchical ring with deflection (HiRD) enables traffic to corner the chip with fewer hops by utilizing the global

ring. A buffered mesh router includes a large complexity and cost compared to the node router at each cache node in the HiRD NoC. In a buffered mesh, each router includes buffers at every router input, and must add a crossbar to move flits from any input to any output. In HiRD, a node router just connects to the ring nodes on each side of the present node, and doesn't have any in-ring buffers. Bridge routers have buffering, but the necessary buffer space is significantly less than in a buffered mesh, and there are fewer bridge routers than nodes in total.

1.2 Bufferless Mesh

Bufferless mesh networks get rid of the buffers from traditional mesh routers, and provide significant energy performance improvements at low-to-medium load. The exact same topology tradeoffs must like the buffered mesh also apply in this case; the improvements produced by a bufferless mesh NoC apply only to the router design itself. A bufferless mesh router is conceptually much like a bridge router in HiRD for the reasons that equally use deflection, since neither router can use backpressure and booth traffic on a router input. In case of HiRD, rings don't have any in-ring buffers, and therefore traffic on rings remains to flow. In case of a bufferless mesh with deflection routing, no router includes in-network buffers, therefore all traffic moves continuously. On the other hand to a bufferless mesh router, a HiRD bridge router includes buffers for traffic that moves between rings. Equally routers include a crossbar. The routing logic in a bufferless mesh router is more complex, as it should consider flit priorities and two dimensional mesh routing. However, despite these tradeoffs, a HiRD system includes fewer bridge routers than nodes, although a bufferless mesh includes this type of router at every node.

1.3 Single Ring

A single ring network has an easier topology when compared to a hierarchical ring. At reduced load, and in small networks, a single ring performs well since each hop includes a reduced latency. But, even as we also show, a ring scales defectively relative to different topologies as load raises or as network size increases. At large load, the lower bandwidth of a ring develops into the main bottleneck, and ring usage rises rapidly. While the network scales up, bisection bandwidth continues to a bottleneck, but the typical number of hops also develops faster than in different topologies: traffic that crosses single-ring network visits half of the nodes throughout their journey, and this will cause high latencies and high power. Developing a network with hierarchy allows show transportation on a global ring, and retains decrease ring use by segmenting the network into multiple local rings.

1.4 Buffered Hierarchical Rings

A buffered hierarchical ring network area local buffering at each node router in a ring. In-ring buffers let the usage

of flow control, and bridge routers utilize this flow control to booth inward traffic on a ring whenever move buffer becomes full. On the other hand, HiRD doesn't have flow control in any ring, and must utilize deflections whenever a move buffer fills. Putting buffers in the ring prevents deflections but provides significant buffer area and power to every node router, and also involves flow-control logic at every router in the ring.

1.5 Mesh of Rings Topology

Another method to develop ring topology scalable is always to position local rings in a mesh design as shown in Figure-1. this kind of topology provides the same scalability for a mesh topology, each having complexity proportional to the total number of nodes in the network. The mesh of rings topology also offers the main benefit of easy router design because the essential block node router and bridge router have the same design as these in a hierarchical ring network. As the deadlock and livelock avoidance in mesh of rings topology and we evaluate the performance and power consumption of mesh of rings [4].

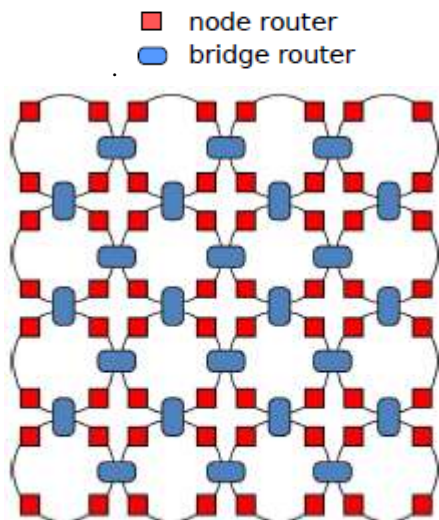


Figure-1 Mesh of Rings Topology

III. ROUTER DESIGN

We propose hierarchical mesh of ring Network on chip design based on very simple router architectures to obtain single cycle latencies. Using this method, HiRD, places a typical ring router at most network node, connects local rings with global rings implementing bridge routers, which may have minimal buffering and use deflection instead of flow control for inter ring transfers. We developed with added for Error Correction code (ECC) of traffic ensuring that inter ring moves do not cause livelock or deadlock, even yet in the worst case.

1. Node Router Operation

At each node on a local ring, we position an individual node router, shown in Figure 2. A node router is simple: it moves through circulating traffic, enables new traffic to enter the ring through a multiplexer (MUX), and allows

traffic to go the ring when it occurs at their destination. Each one router includes one pipeline register for the router point, and one pipeline register for link traversal, therefore the router latency is exactly one cycle and the per-hop latency is two cycles[1].

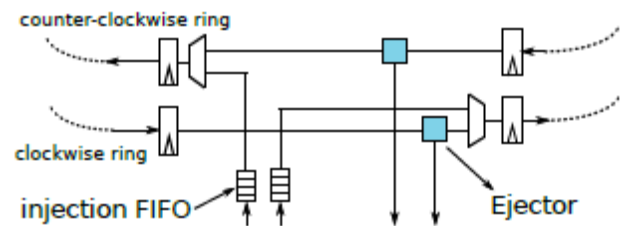


Figure 2: Node router.

2. Bridge Router Operation

The bridge routers link a local ring and a global ring. The high-level block diagram of a bridge router is shown in Figure 3. A bridge router appears like two node routers, one for every one of two rings, linked through FIFO-buffers both in directions. Every time a flit comes on one ring which will requires a move for the ring, it can retain their present ring and also wait in a FIFO provided that there is space available. These types of move FIFOs appear, therefore the moving flit's arrival do not need be completely arranged with a free position on the destination ring. But, this transfer FIFO will often fill. because, if any flit occurs that will requires a move, the bridge router only does not eliminate the flit from their current ring; the flit can continue to travel across the ring, and will ultimately come back to the bridge router, at which stage there may be an open slot available in the transfer FIFO.

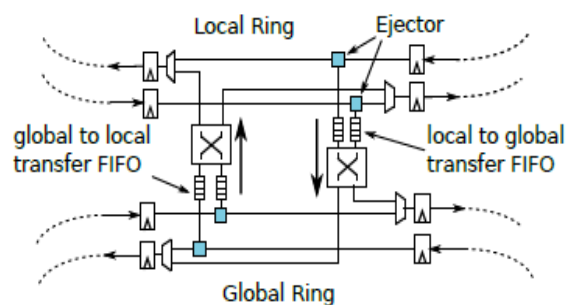


Figure 3: Bridge router.

3. Error detection and correction

The register includes position, data and parity registers needed by router. All the registers in this module are latched on increasing edge of the clock. Data registers latches the data from data input predicated on state and position control signals, and this latched data is delivered to the FIFO for storage. Besides it, data can be latched into the parity registers for parity computation and it is contrast to the parity byte of the packet. Errors indicate is produced if packet parity is not equal to the determined parity. Inner parity register stores the parity determined

for packet data, when packet is sent completely, the internal calculated parity is compared with parity byte of the packet.

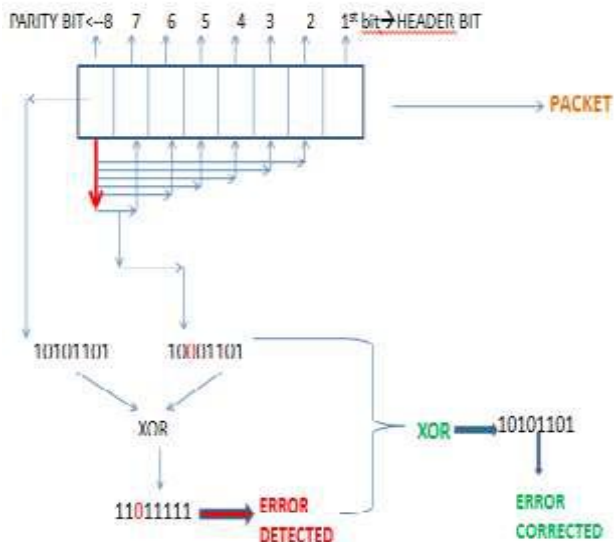


Fig.4: error detection and correction method

IV. RESULT

The NoC router architecture is simulated. In that mesh of ring based NoC the concepts requires a change path to achieve the location even though there is errors in the propagating route. So the message achieves the location even though the router in the transmitting route is faulty. The data sent is free of error as a result of effective exploitation of with error correction code (ECC), by simulation of the ECC module output.

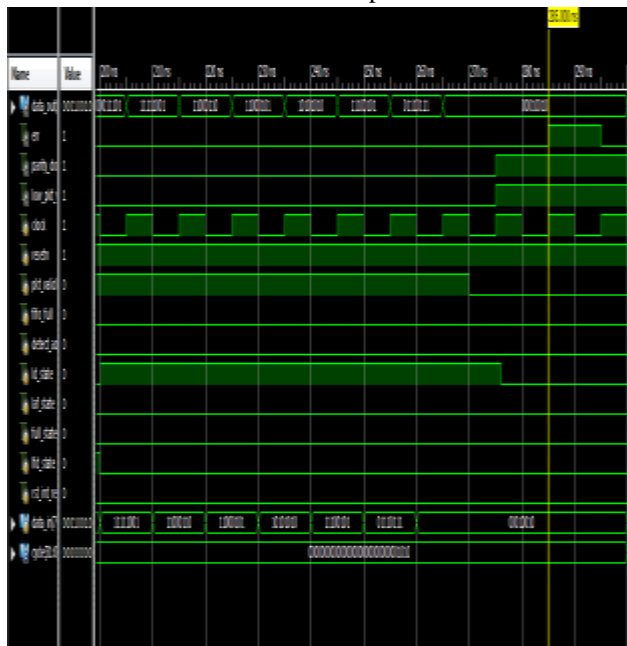


Fig.4: Error detected in the register block of transmitted data.

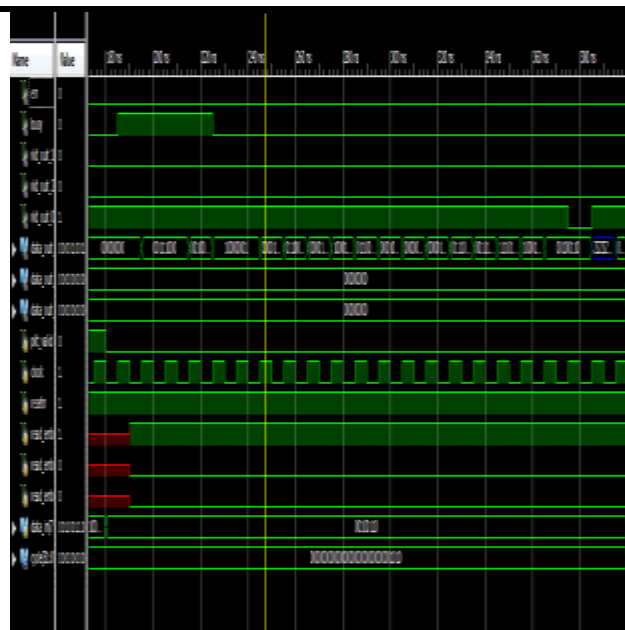


Fig.5: Error corrected in the register block of Received data.

V. CONCLUSION

Our design is a hierarchical ring interconnect that will keep all the simplicity of conventional ring patterns while reaching high scalability as more complex buffered hierarchical ring designs. We propose, a router architectures and show that these routers are significantly simpler, more area and power effective than mesh based routers. In this work we establish the conventional error rates of the on-chip and propose appropriate Error Correction Code (ECC) mechanisms to improve their reliability.

REFERENCES

- [1] R. Ausavarungnirun et al. Achieving both High Energy Efficiency and High Performance in On-Chip Communication using Hierarchical Rings with Deflection Routing. In SBAC-PAD, 2016.
- [2] C. Fallin, C. Craik, and O. Mutlu. CHIPPER: A low-complexity bufferless deflection router. HPCA-17, 2011
- [3] R. Ausavarungnirun et al. Staged Memory Scheduling: Achieving High Performance and Scalability in Heterogeneous Systems. In ISCA, 2012.
- [4] Chris Fallin, Xiangyao Yu, Gregory Nazario, Onur Mutlu A High-Performance Hierarchical Ring On-Chip Interconnect with Low-Cost Routers, SAFARI Technical Report No. 2011-007 (September 6, 2011)
- [5] D. Bertozzi, L. Benini, G. De Micheli, "Error control schemes for on-chip communication links: the energy- reliability tradeoff," Computer-Aided

- Design of Integrated Circuits and Systems, IEEE Transactions on , vol.24, no.6, pp.818,831, June 2005
- [6] Ganguly, A; Pande, P.P.; Belzer, B., "Crosstalk-Aware Channel Coding Schemes for Energy Efficient and Reliable NOC Interconnects," Very Large Scale Integration (VLSI) Systems, IEEE Transactions on, vol.17, no.11, pp.1626,1639, Nov. 2009.
- [7] Cédric Killian, Camel Tanougast, Fabrice Monteiro, and Abbas Dandache, "Smart Reliable Network-on-Chip", IEEE Transactions on Very Large Scale Integration (VLSI) Systems, Vol. 22, No. 2, February 2014
- [8] S. Jovanovic, C. Tanougast, S. Weber, and C. Bobda, "A new deadlock-free fault-tolerant routing algorithm for NoC interconnections," in Proc. Int. Conf. Field Program. Logic Appl., Aug.–Sep. 2009, pp. 326–331.
- [9] M. Valadbeigi and F. Safaei, "PDR: A Protocol for Dynamic Network Reconfiguration Based on Deadlock Recovery Scheme," in Elsevier Journal of Simulation Modeling Practice and Theory, vol. 24, no.1, 59-70, 2012
- [10] D. Park, et al, "Exploring Fault-Tolerant Network-on-Chip Architectures", In Proc. of International Conference on Dependable Systems and Networks, June 2006.
- [11] M. Majer, C. Bobda, A. Ahmadiania, and J. Teich, "Packet routing in dynamically changing networks on chip," in Proc. 19th IEEE Int. Parallel Distrib. Process. Symp., Apr. 2005, p. 154b.
- [12] Y. Kang, T. Kwon, J. Draper, "Fault-Tolerant Flow Control in On-Chip Networks," in Proc. NoCs, pp.79-86, 2010.
- [13] Q. Yu and P. Ampadu, Transient and Permanent Error Control for Networks-on-Chip. Springer, 2012.
- [14] X. Zhang and Y. Yan. Comparative modeling and evaluation of CC-NUMA and COMA on hierarchical ring architectures. Parallel and Distributed Systems, IEEE Transactions on, 6(12):1316 –1331, Dec 1995.
- [15] V. C. Harmacher and H. Jiang. Hierarchical ring network configuration and performance modeling. IEEE Transaction on Computers, 50(1):1–12, 2001.
- [16] W. Dally and B. Towles. Principles and Practices of Interconnection Networks. Morgan Kaufmann, 2004.
- [17] T. Moscibroda and O. Mutlu. A case for bufferless routing in on-chip networks. ISCA-36, 2009.
- [18] M. Coppola et al. Spidergon: a novel on-chip communication network. Proc. Int'l Symposium on System on Chip, Nov 2004.
- [19] R. Mullins et al. Low-latency virtual-channel routers for on-chip networks. ISCA-31, 2004.
- [20] J. Kim. Low-cost router microarchitecture for on-chip networks. MICRO-42, 2009
- [21] F. Karim et al. On-chip communication architecture for oc-768 network processors. DAC-38, 2001.

An Improved Approach to Discover High Utility Item Set from Large Data Set

Shilpa Shrivastava¹, Mr. Abhishek Tiwari²

¹Research Scholar, Information Technology Department, MIT, Ujjain, MP India

²Reader, Information Technology Department, MIT, Ujjain, MP, India

Abstract— The term data mining is often used to apply to the two separate processes of knowledge discovery and prediction. Knowledge discovery provides explicit information that has a readable form and can be understood by a user. Forecasting, or predictive modeling provides predictions of future events and may be transparent and readable in some approaches (e.g. rule based systems) and opaque in others such as neural networks. Moreover, some data mining systems such as neural networks are inherently geared towards prediction and pattern recognition, rather than knowledge discovery. Utility item set mining is addition to the frequent pattern mining. The goal of high utility item set mining is to find all item sets that give utility greater or equal to the user specified threshold. The deficiency of this approach is that it does not consider the statistical aspect of item sets. Utility-based measures should incorporate user-defined utility as well as raw statistical aspects of data. Consequently, it is meaningful to define a specialized form of high utility item sets, utility-frequent item sets which are a subset of high utility item sets as well as frequent item sets. In this paper we proposed an efficient approach to mine high utility items form transactional records.

Keywords— Utility, Candidates, Transactions, Thresholds, Item set.

I. INTRODUCTION

Mining high utility item sets is upgrades the standard frequent item set mining framework as it employs subjectively defined utility instead of statistics-based support measure. User-defined utility is based on information not available in the transaction dataset. It often reflects user preference and can be represented by an external utility table or utility function. Utility table (or function) defines utilities of all items in a given database (we can also treat them as weights). Besides subjective external utility we also need transaction dependent internal utilities (e.g. quantities of items in transactions). Utility function we use to compute utility of an item set takes into account both internal and external utility of all items in a item set. The most usual form

that is also used in products of internal and external utilities of present items.

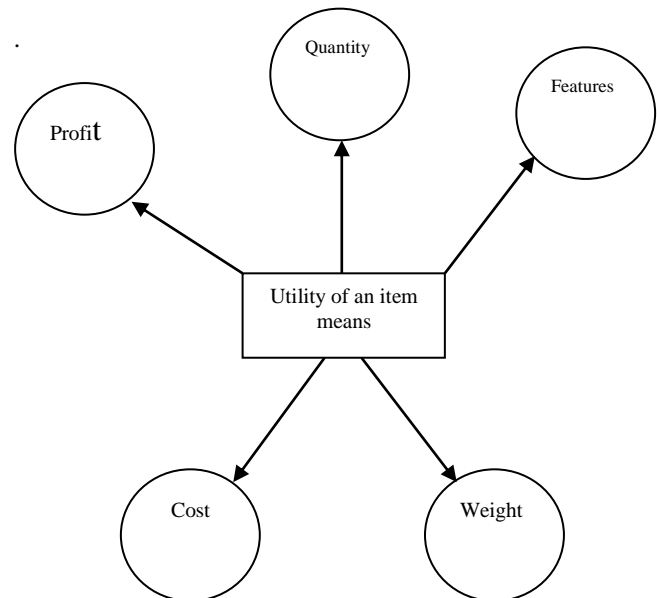


Fig.1.1: Utility means many things

II. ARCHITECTURE

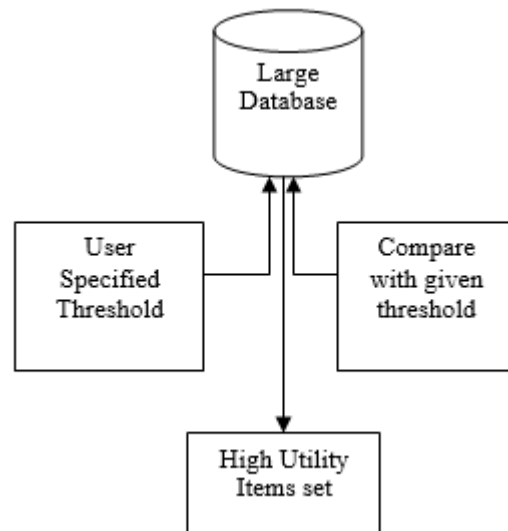


Fig.2: Architecture

User gives a minimum threshold value. We calculate total utility value entire database and compare with given threshold value. The item set which satisfy the given condition known as high utility.

III. BACKGROUND

Consider a simple example of transactional database

Table.1: Transactional data set

TID & ITEM	I1	I2	I3	I4	I5
T1	0	0	18	0	1
T2	0	6	0	1	1
T3	2	0	1	0	1
T4	1	0	0	1	1
T5	0	0	4	0	2
T6	1	1	0	0	0
T7	0	10	0	1	1
T8	3	0	25	3	1
T9	1	1	0	0	0
T10	0	6	2	0	2

The utility table, the right column displays the profit of each item per unit in dollars

Table.2: Profit table

ITEM	PROFIT\$(Per Unit)
I1	3
I2	10
I3	1
I4	6
I5	5

External Utility: - The external utility of an item i_p is a numerical value y_p defined by the user. It is transaction independent and reflects importance (usually profit) of the item. External utilities are stored in a utility table. For example, external utility of item I2 in Table 2 is 10.

Internal Utility:-The internal utility of an item i_p is a numerical value x_p which is transaction dependent. In most cases it is defined as the quantity of an item in transaction. For example, internal utility of item I5 in transaction T5 is 2 in table 1.

The utility of item: - The utility of item i_p in transaction T is the quantitative measure computed with utility function from above definition $u(i_p, T) = f(x_p, y_p)$, $i_p \in T$. For example: utility of item I5 in transaction T5 is $2 * 5 = 10$.

The utility of item set S in transaction T: - The utility of item set S in transaction T is defined as

$$u(S, T) = \sum_{i_p \in S} u(i_p, T), S \subseteq T$$

For example utility of itemset {I2, I5} in transaction T2 is $u(\{I2, I5\}, T2) = u(\{I2\}, T2) + u(\{I5\}, T2) = 6 * 10 + 1 * 5 = 65$.

The utility of item i_p in item set S: - The utility of item i_p in item set S is defined as

$$u(i_p, S) = \sum_{T \in DB, S \subseteq T} u(i_p, T)$$

For example, utility of item E in item set {I2, I5} is $u(I5, \{I2, I5\}) = u(I5, T2) + u(I5, T7) + u(I5, T10) = 20$.

The utility of item set S in database DB: - The utility of item set S in database DB is defined as

$$u(S) = \sum_{T \in DB, S \subseteq T} u(S, T) = \sum_{T \in DB, S \subseteq T} \sum_{i_p \in S} f(x_p, y_p)$$

For example, utility of item set {I1, I5} in database from Table 1 is

$u(\{I1, I5\}) = u(\{I1, I5\}, T3) + u(\{I1, I5\}, T4) + u(\{I1, I5\}, T8) = 33$.

The utility of transaction T:- The utility of transaction T is defined as

$$u(T) = \sum_{i_p \in T} u(i_p, T)$$

For example: utility of transaction T10 is $u(T10) = u(\{I2\}, T10) + u(\{I3\}, T10) + u(\{I5\}, T10) = 72$.

The utility of database DB :- The utility of database DB is defined as

$$u(DB) = \sum_{T \in DB} u(T)$$

For example, utility of database DB from table 1 and table 2 is $u(DB) = u(T1) + \dots + u(T10) = 23 + \dots + 72 = 400$.

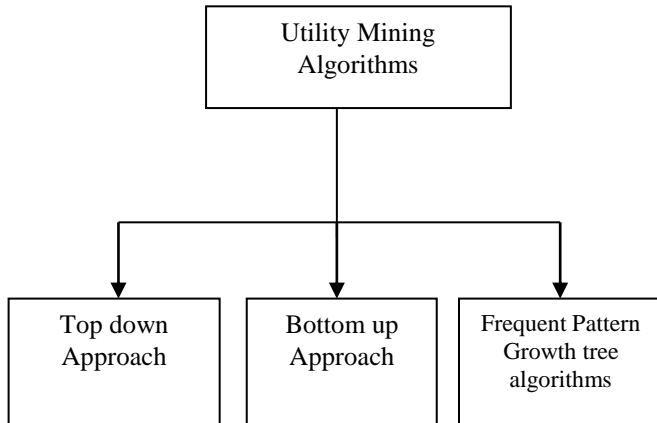
The utility share of item set S in database:- The utility share of item set S in database DB is

For example, utility share of item set {I1, I4, I5} in database from Table 1 is $U(\{I1, I4, I5\}) = 46/400 = 0.115 = 11.5\%$.

IV. CATEGORIES OF UTILITY MINING ALGORITHMS

Utility mining algorithm is mainly classified into three categories. First categories include top down approach, second categories include bottom up approach and third

approach based on Frequent Pattern Growth tree. Top down approach based algorithm are those algorithm which is based on up word words closer properties mean generate candidates set and then use pruning strategy to remove useless candidates. In seconds categories algorithms us utility pattern growth tree based concepts for generating use full pattern . These algorithms use tree like structure which contain main root node and other sub tree.



V. LITERATURE REVIEW

In (1994) Agarwal proposed the mining of association rules for finding the relationships between data items in large databases.

In 2003 Chan observes that the candidate set pruning strategy exploring the ant monotone property used in classical algorithm does not hold for utility mining.

In 2004 Yao defines the problem of utility mining formally. The work defines the terms transaction utility and external utility of an itemset. The mathematical model of utility mining was then defined based on the two properties of utility bound and support bound.

In 2006, 2007 Yao defines the utility mining problem as one of the cases of constraint mining. This work shows that the downward closure property used in the standard Classical algorithm and the convertible constraint property are not directly applicable to the utility mining problem.

In 2008 Li proposed two efficient one pass algorithms MHUI-BIT and MHUI-TID for mining high utility item sets from data streams within a transaction sensitive sliding window. Liu et al in proposes a Two-phase algorithm for finding high utility item sets.

In 2009 Shankar presents a novel algorithm Fast Utility Mining (FUM) which finds all high utility item sets within the given utility constraint threshold.

In 2010 Vincent S. Tseng, et. al. Proposed a data structure, named UP-Tree, and then describe a new algorithm, called UP-Growth, The framework of the UP-Growth.

In 2012 Mengchi Liu et al. proposed “Mining High Utility Item sets without Candidate Generation”].

In 2013 Arumugam P et al. proposed “Advance Mining Of High Utility Item sets In Transactional Data”.

In 2014 More Rani N. and Anbhule Reshma V “Mining High Utility Item sets From Transaction Database”[13,14].

VI. PROBLEM STATEMENT

In utility mining process very large number of candidates is generated. These useless candidates make execution process slow because we have to prune these items and consider only that item which satisfies the threshold value. So improving pruning strategies is a difficult task.

In previous algorithms the function used for calculating utility is also in efficient because some algorithm are based on expected utility mining model and some are based on transaction weighted utility model. Improving accuracy is also a challenge.

VII. PROPOSED ALGORITHM

We proposed an efficient method which combined reducing the cost of database scans by transaction merging and pruning search space by using utility and local utility.

Calculate Transaction-weighted utility value for one item by using $twu(X)$ formula.

Generate high utility one item set by comparing Transaction-weighted utility value of each one item set with give utility threshold value ϵ .

Update the transaction weighted utilization table by subtracting the utility value of deleted one item set.

While ($|C_k| > 0$ and $k = K$) (more candidate)

Generate candidate set for next level and Transaction-weighted utility value for item set using $twu(X)$ formula.

Generate high utility one item set by comparing Transaction-weighted utility value of each one item set with give utility threshold value ϵ .

Generate all high utility item set .

VIII. EXPERIMENTAL ANALYSIS

We evaluate the performance of proposed algorithm and compare it with iFUM and TP (Two Phase) algorithms. The experiments were performed on i3 processor (2.5GHz Intel Processor with 4M cache memory), 2GB main memory and 400 GB secondary memory , and running on Windows XP. The algorithms are implemented in using C# Dot Net Framework language version 4.0.1. Both synthetic datasets are used to evaluate the performance of the algorithms.

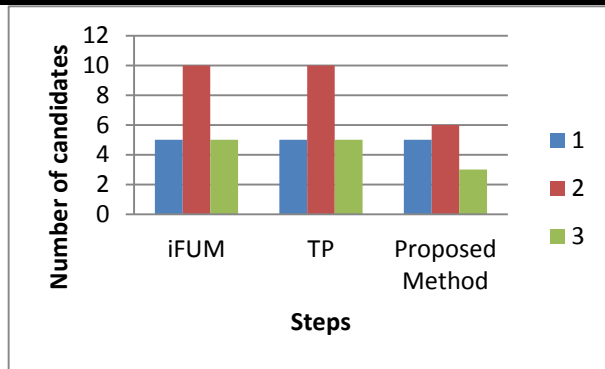


Fig.2: Comparison graph

IX. CONCLUSION

Mining Expected Utility Two Phase and several other algorithms have mine high utility item set very efficiently. But there is need to enhance this algorithm so that it can be applied to large sized dataset. The complexity factor for frequent pattern mining algorithm includes several factors like Execution time and I/O cost. The proposed method reduce candidates generations at different stages

REFERENCES

- [1] R. Agrawal and R. Srikant. Fast algorithms for mining association rules. In Proc. of the 20th Int'l Conf. on Very Large Data Bases, pp. 487-499, 1994.
- [2] C. F. Ahmed, S. K. Tanbeer, B.-S. Jeong and Y.-K. Lee. Efficient Tree Structures for High-utility Pattern Mining in Incremental Databases. In IEEE Transactions on Knowledge and Data Engineering, Vol. 21, Issue 12, pp. 1708-1721, 2009.
- [3] R. Chan, Q. Yang and Y. Shen. Mining high-utility item sets. In Proc. of Third IEEE Int'l Conf. on Data Mining, pp. 19-26, Nov., 2003.
- [4] Y. L. Cheung, A. W. Fu, Mining frequent item sets without support threshold: with and without item constraints. IEEE Transactions on Knowledge and Data Engineering, Vol. 16, No. 6, pp. 1052-1069, 2004.
- [5] K. Chuang, J. Huang, M. Chen, Mining Top-K Frequent Patterns in the Presence of the Memory Constraint, The VLDB Journal, Vol. 17, pp. 1321-1344, 2008.
- [6] A. Erwin, R. P. Gopalan and N. R. Achuthan. Efficient Mining of High-utility Item sets from Large Datasets. In PAKDD 2008, LNAI 5012, pp. 554-561, 2008.
- [7] A. W. Fu, R. W. Kwong and J. Tang, Mining N-Most Interesting Item sets, In Proc. of ISMIS'00, 2000.
- [8] J. Han, J. Pei and Y. Yin. Mining frequent patterns without candidate generation. In Proc. of the ACM-SIGMOD Int'l Conf. on Management of Data, pp. 1-12, 2000.
- [9] J. Han, J. Wang, Y. Lu and P. Tzvetkov, "Mining Top-k Frequent Closed Patterns without Minimum Support," In Proc. of ICDM, 2002.
- [10] Y. Hirate, E. Iwahashi and H. Yamana, TF2P-Growth: An Efficient Algorithm for Mining Frequent patterns without any Thresholds, In Proc. of ICDM 2004.
- [11] H.-F. Li, H.-Y. Huang, Y.-C. Chen, Y.-J. Liu, S.-Y. Lee. Fast and Memory Efficient Mining of High Utility Item sets in Data Streams. In Proc. of the 8th IEEE Int'l Conf. on Data Mining, pp. 881-886, 2008.
- [12] Y. Liu, W. Liao, and A. Choudhary. A fast high-utility item sets mining algorithm. In Proc. of the Utility-Based Data Mining Workshop, 2005.
- [13] Y.-C. Li, J.-S. Yeh and C.-C. Chang. Isolated Items Discarding Strategy for Discovering High-utility Item sets. In Data & Knowledge Engineering, Vol. 64, Issue 1, pp. 198-217, 2008.
- [14] S. Ngan, T. Lam, R. C. Wong and A. W. Fu, Mining N-most Interesting Item sets without Support Threshold by the COFI-Tree, Int. J. Business Intelligence & Data Mining, Vol. 1, No. 1, pp. 88-106, 2005.
- [15] J. Pisharath, Y. Liu, B. Ozisikyilmaz, R. Narayanan, W. K. Liao, A. Choudhary and G. Memik, NU-Mine Bench version 2.0 dataset and technical report, <http://cucis.ece.northwestern.edu/projects/DMS/MineBench.html>.
- [16] T. M. Quang, S. Oyanagi, and K. Yamazaki, Ex Miner: An Efficient Algorithm for Mining Top-K Frequent Patterns, ADMA 2006, LNAI 4093, pp. 436 – 447, 2006.

Modal Analysis of Engine Supporting Bracket using Finite Element Analysis

A.S. Adkine¹, Prof.G.P.Overikar², Prof. S .S. Surwase³

¹PG Student Department of Mechanical Engineering, Shree Tuljabhavani College of Engineering, Tuljapur, India

²Assistant Prof. Department of Mechanical Engineering, Shree Tuljabhavani College of Engineering, Tuljapur, India

³Associate Prof. Department of Mechanical Engineering, Shree Tuljabhavani College of Engineering, Tuljapur, India

Abstract— *The Engine supporting bracket plays a vital role by reducing noise, vibration and harshness. The current work describes the finite element approach for modal and static structural analysis of engine supporting bracket. CAD model of engine supporting bracket was created in CATIA software and same was analyzed for stress and vibration analysis using ANSYS workbench 15.0. Both initial design and modified design was compared for output responses in terms of equivalent Von-Mises stress, deformation and strain energy absorbed. In modal analysis, bracket was considered for vibration studies. The sole aim of modal analysis was to check whether the self excitation frequency of engine supporting bracket was less than natural frequency. Four alternative materials (Gray C.I., Aluminum alloy, Magnesium alloy and ERW-1) were analyzed. Stress analysis results suggest that deformation and Von-Mises stresses observed in ERW-1 materials was less (0.495 mm and 164.87 MPa). Further natural frequency of modified design was found to be 257.83 Hz which was well within the range below self-excitation frequency and less than the natural frequency (268.59 Hz) of initial design. It was found that aluminum bracket limit its use for the said application due to greater deformation and less stiffness. Magnesium bracket can be the option to ERW-1 steel for the Engine supporting bracket application but it cannot be deployed as it is highly susceptible to corrosion. From the results, it can be concluded that ERW-1 material best suit the requirement of the desired application and can be deployed with some safety standards.*

Keywords— *Engine Supporting bracket, Finite element analysis, Modal Analysis.*

I. INTRODUCTION

Engine supporting assembly includes support members which are attached to a main frame vehicle body. A good mounting system separates engine generating vibration from vehicle body and suppresses the effect uneven road surface inputs to the vehicle driver. Noise, vibration and harshness are important vehicles characteristics and decrement in these characteristics motivates manufacturer for achieving customer satisfaction. The automotive engine bracket is very important due to different aspect of vehicle

performance. The finite element model of engine mount is created using CAD & Hypermesh and simulation of the engine mount is carried out using LS-Dyna. Based on the finite element model created, the mountings frequency response function curves are determined and multi-dimensional effects in the mounts responses are observed. Engine mounts in which the design of four arm symmetry engine mount curve is obtained from LS-Dyna approach follows exactly the experimental test curve and also this design has the highest natural frequency amongst all of design iterations. The engine mounts time dependent response study is compared to the ones obtained using a damping material model suggested by the automotive constructors. The results indicated that the rubber used in the engine mount had increased the frequency from 1.2Hz (Basic design) to 1.8Hz (four arm symmetry) ^[1].

Model of Engine Mount bracket assembly was performed using FEA and modal analysis techniques. Mg alloy bracket has highest natural frequency followed by Al alloy & Cast Iron gives less frequency so it is rejected. The results are compared with experimental results and it was found that the bracket manufactured with Mg alloy gives optimized frequency. In addition, Al can be used in few applications but CI alloy gives minimum frequency. Mg and Al are preferred ^[2]. 3-D modeling of the engine mount has been designed using CATIA V5 software. The computational testing on the component is done at isotropic state through the application of Thermo-mechanical Vibration Analysis using the Comsol Multiphysics 4.2 version software. The main objective of the research is to reduce weight without changing impact of the component. The Engine mounting bracket is been used to reduction of the vibration created by the engine. The results obtained states that 60% of the weight reduction is done to the component. The weight is reduced 60% through the usage of the optimized AlSiC MMC composite material made component. The future work focuses on the cost reduction of the material without varying the weight of the component ^[3].

Alternative materials for Static Structural Analysis of Bracket Using Materials are Cast Iron, Aluminum & Magnesium & Equivalent (von misses) stresses of

Aluminum, Magnesium. Modal analysis of bracket using materials Cast Iron, Aluminum and Magnesium was done in earlier stages. Experimental Analysis for Natural Frequency Analysis & Static analysis of modified Bracket with Aluminum material. After reducing the thickness of the Bracket the von-misses stresses coming on the bracket are well within the yield strength (280 MPa) of the Aluminum. So, after selecting the light weight material Aluminum & reducing its thickness by 2 mm the reduction in the mass up to 0.43 Kg ^[4]. It has been developed durability test on vehicles in the end- user environment to reduce failure and warranty cost in the end- user hands. The failure analysis of muffler mounting brackets of three-wheeler vehicles was done for durability test. Cracks at the weld location between the engine cradle and bracket were observed in all the vehicles at an observed in all the vehicles at an average distance of 10,000 km. Many possible causes of the failure are identified using fishbone diagram.

Further investigations were carried out on the design using finite element method (FEM). FEM model developed for the engine cradle assembly in which assembly in which engine and muffler were modeled as point mass. Results show high magnitude of stresses and strain energy at the weld location. Results show high magnitude of stresses and strain energy at the weld location. Analysis of the design suggested that bracket was acting as a cantilever beam with one plane welding mounting on the engine cradle modified design through eliminated the above failure shifted the failure mode to the bush –bracket region^[7].

II. METHODOLOGY

Firstly, the theoretical study of engine supporting bracket is done. The main purpose of the bracket is to supports the engine. To modify the existing design of engine supporting bracket and to carry out static structural analysis for various materials Gray C.I., Aluminum alloy, Magnesium alloy and ERW-1. Modal Analysis of engine mounting bracket for determines the modified design has a natural frequency of component lower than the self-excitation frequency. Best material is selected for engine supporting bracket.

2.1 Position and Design of Engine Supporting Bracket



Fig.1: Position of ESB

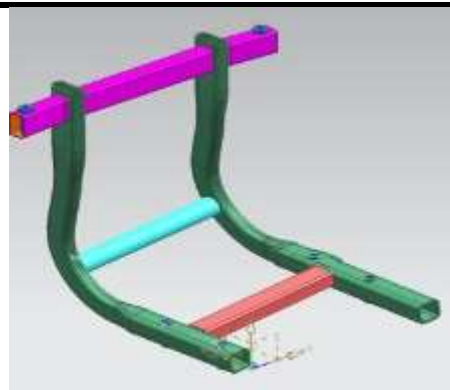


Fig.2: 3-D CAD model of ESB Initial design

Engine is most essential or an important component of automotive vehicle and which is rest on this structural L-shaped frame is known as Engine supporting bracket and these are connected to the skeleton of vehicle. Hence, during its operation engine is produced undesirable vibration and road roughness can directly transmit through the frame to bracket. Due to that reason discomforts ride as well as passenger or might even damage the bracket. Engine supporting bracket is to resist the vibration response to engine vehicle. Vehicle is running on the road dynamic response of the bracket to calculate the Static structural characteristics of engine supporting bracket.

2.2 Finite Element Analysis

Finite element analysis is most important software tool that can solve many kinds of engineering problem with high degree of precision as necessary. FEM is computational technique ANSYS 15.0 is used to analyses a wide range of engineering problem.in this analysis a complicated shapes or complex region define a continuum is discretized into simple geometrical shape called as finite element.

Modern mechanical design involves Complex or complicated shapes, sometimes made of different materials that as a whole cannot be solved by existing mathematical tools. Engineers need the FEA to evaluate their designs. The process of dividing the complicated shapes model into small pieces is called **meshing**. The behavior of each element is well-known under all possible support and load scenarios. Unknown value of element is called as **nodes**.

2.2 General Procedure of FEA

Any Analysis Involved main three Step

Pre processing

- Create or import model geometry
- Mesh the Geometry

Solution

- Apply the load
- Solve

Post processing

- Review Results
- Check the Solution.

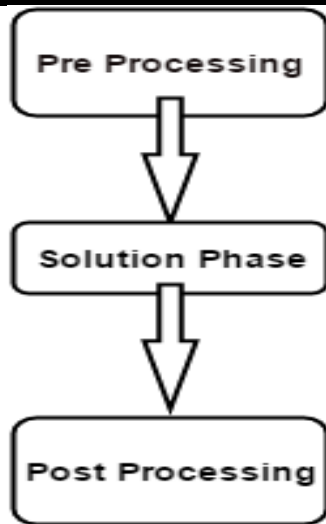


Fig.3: Typical FEA Procedure

2.3 Alternative Materials

Designed will test for different Materials. They are gray cast iron; Aluminum Alloy, Magnesium Alloy & ERW-1 best suited material are found out.

Gray cast iron: These are alloys of iron, carbon and silicon, containing more than 2% carbon (as flake graphite), up to 3% silicon and less than total 1% of alloying elements (mainly chromium, copper, magnesium, molybdenum, nickel, phosphorous, silicon, sulphur, titanium and vanadium). They are used to make heavy machine beds, camshafts, cranks, elevator buckets, and railway wheels

Al Alloy: It is a soft silvery white metal with about one third of density of ferrous metals and low tensile strength in its pure form. It is an excellent conductor of heat and electricity and has corrosion resistance in most environments including seawater, oils and many chemicals. To improve its strength, hardness and fluidity, silicon, copper, magnesium and zinc are added. Aluminum has only about one third the density of steel and the most commercial aluminum alloys posses substantially higher specific strength than steel. A vehicle weight reduction would not only result in higher oil savings, but also gives a significant reduction in emission. For these reasons there is preference to use more aluminum and replace steel in automotive applications.

Magnesium Alloy: Magnesium is the lightest of all metals used as the basis for constructional alloys. It is this property due to which automobile manufactures has to replace denser materials, not only steels, cast irons and copper base alloys but even aluminum alloys by magnesium base alloys. The advantages of magnesium alloys are listed as follows, lowest density of all metallic constructional materials. It posses high specific strength, good cast ability, which suitable for high pressure die casting good welding properties, higher corrosion resistance. Also compared with polymeric materials it posses better mechanical properties, better electrical and thermal conductivity and it is recyclable.

ERW-1: Electrical resistance welded steel tube & seamless tube are often used in application with automobiles ERW to their convention properties should also innovation which reduces cost, weight & to their high strength. Mechanical Properties of ERW-1are

Table.1: Mechanical Properties of ERW-1

IS 3074 ERW-1	
Young's modulus N/m ²	2.1 e+10 N/m ²
Poisson's ratio	0.29
Density Kg/m ³	7800 Kg/m ³
Yield strength N/m ²	2.4e+8 N/m ²

2.4 Fishbone Diagram

The study and analysis of the problem present here would be easy to visualize by adopting the cause effect method for fault finding. The Fishbone diagram provides a visualization of a problem with respect to factors affecting it. Such as, Measurement, Methods, Man, materials, design, etc. Arranging all such factors in the form of the fishbone diagram, provides a reasonable and logical guideline for analysis and fault finding. The diagram present here is the fishbone diagram constructed for the component being studied. Following points are considered:

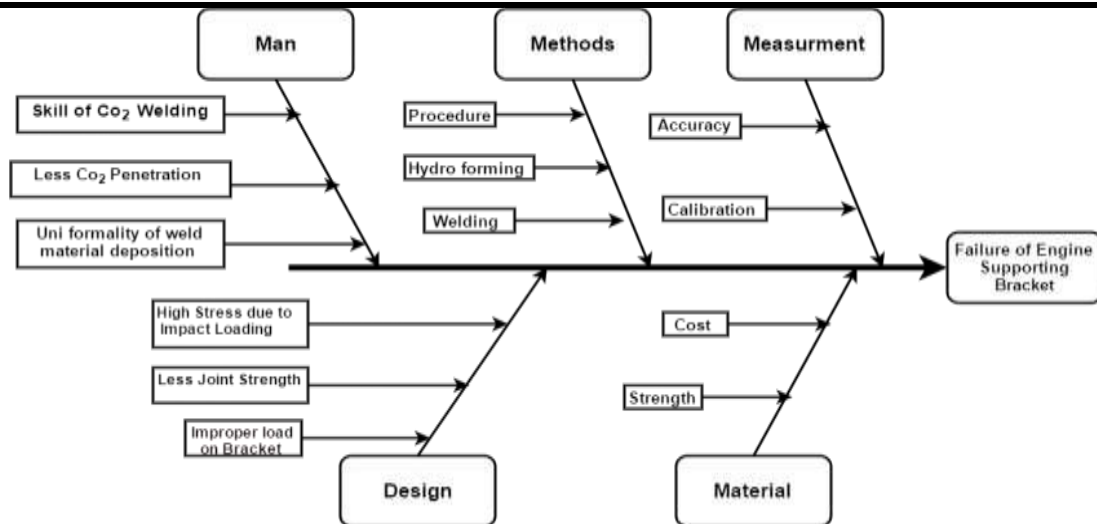


Fig.4: Fishbone diagram

Many possible causes are identified of failure system using fishbone diagram.

Man: Human being is the factor which would results in welds related defects like incomplete penetration between joints, incomplete fusion, less CO₂ penetration undercutting and bad weld design.

Material: Here materials being used for production of component are decided. The criterion for selection of material is the yield strength .In that sense low yield strength of material will lead to insufficient strength and poor weldability.

Methods: This factor summarizes the setup and different production processes used for manufacturing the component. Process like hydroforming & welding are performed to contribute for manufacturing. Any wrong sequence in Procedure can lead to defects described above.

Measurement: this factor deal with various measuring system used for calibration of instrument. Tolerances and allowances are to be studied. Any misfortune in inspection would definitely affect the accuracy and ultimately the final quality of the component.

Design: The major problems associated with factor design are bracket acting as cantilever beam, high thermal stress due to radiation effect, ergonomic consideration; improper load on bracket has strong influences on weld failure. Meanwhile the above factors will govern the range of dimensions of component.

III. RESULTS AND DISCUSSION

3.1 Static Structural and Modal Analysis of Initial Model

The analysis of engine supporting bracket is done with the help of FEA commercial software ANSYS workbench. First stage prepares the CAD model of Engine supporting bracket using CATIA Software & model importing into the geometry in ANSYS workbench. Further that the material

selection is done from in engineering data sheet of FEA package software. Meshing or discretization done as hex mesh a solid element is generated is to required small pieces. Static structural analysis engine supporting bracket weight of the engine is distributed in equilibrium condition. Stress analysis of engine mounting bracket upper end is connected to main frame of the vehicle and then the engine weight load is applied on bracket is 800N & silencer weight is act at silencer rest is 20N as a point load. Process flow of ANSYS Workbench.

- Preparation of CAD model.
- Import in ANSYS Workbench 15.0.
- Define Material Properties (young's modulus, poisson ratio, density, yield strength) Discretization (Mesh generation).
- Apply Loading Condition (Define Boundary Condition).
- Solution (Static Structural & to find deformation, stress, strain energy Results)
- Modal Analysis (Find out Frequency Hz with mode results)

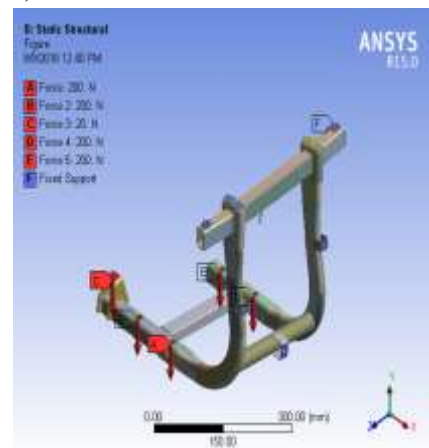


Fig.5: Boundary condition of initial design

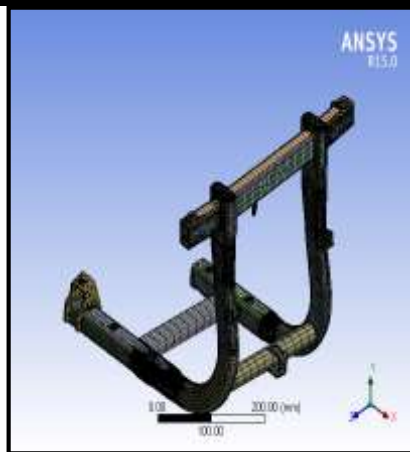
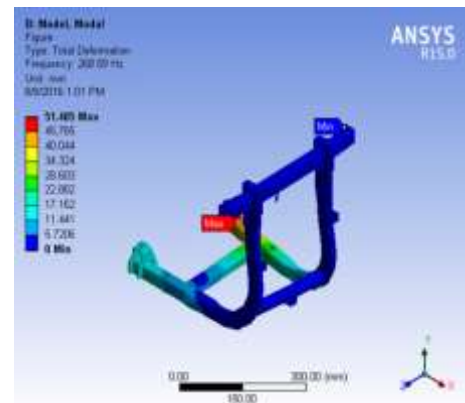
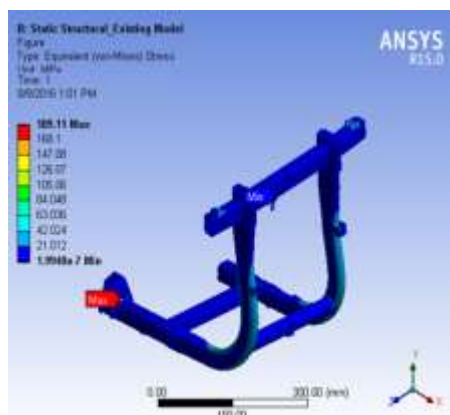
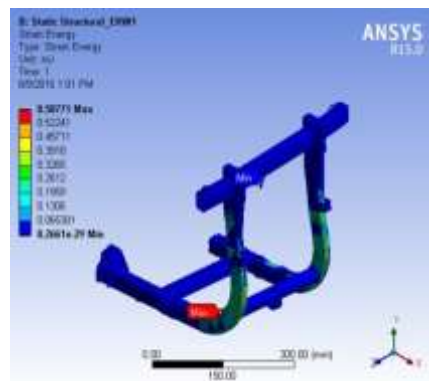
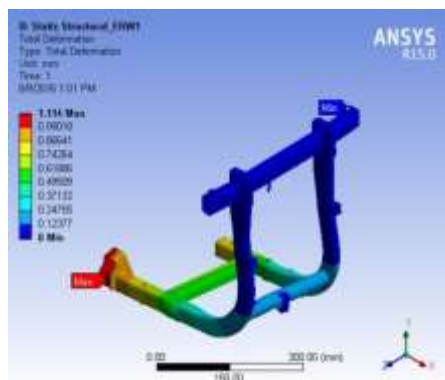


Fig.6: Meshed Model of ESB

Static structural Analysis of Engine Supporting Bracket ERW-1. (Initial Design)	
Total Deformation mm	1.114
Von-Mises Stress Mpa	189.11
Strain Energy mJ	0.58771

Fig 7 Total deformation, Equivalent (Von- Mises) Stress & Strain Energy for Initial design of ESB of Initial Model



Mode	Frequency [Hz]
1	148.12
2	167.32
3	268.59
4	500.92
5	630.92
6	700.3

Fig.8: Modal Analysis of Initial Engine supporting Bracket.

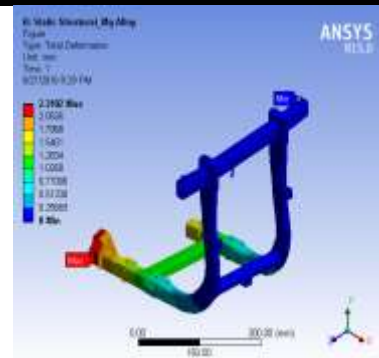
Static structural of Engine supporting frame using ERW-1 material for initial design analysis by ANSYS Workbench R15.0 and getting results of total deformation is 1.114 mm, Equivalent (Von- Mises) Stress is 189.11 MPa & Strain Energy is 0.58771 mJ.

3.2 Static Structural and Modal Analysis of Modified Design

Static Analysis deals with the conditions of the equilibrium of the bodies acted upon by forces .A Static analysis is used to determine the total deformation in mm with alternative materials Gray cast Iron, Al Alloy, Mg Alloy & ERW-1.



Fig.9: Modified design of engine supporting bracket for 3-D Model



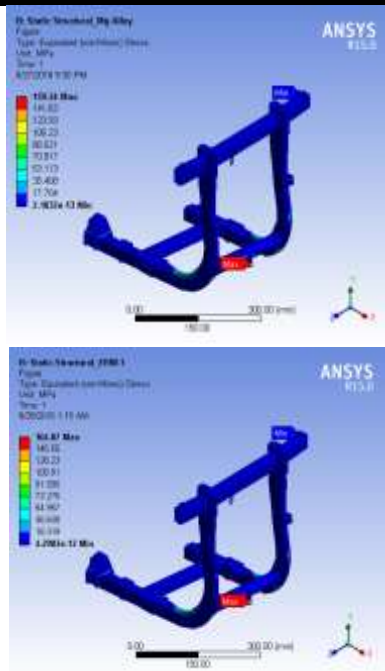


Fig.11: Equivalent Von-Mises Stress observed during stress analysis in Cast iron, Aluminum, Magnesium and ERW-1 Engine Supporting bracket respectively

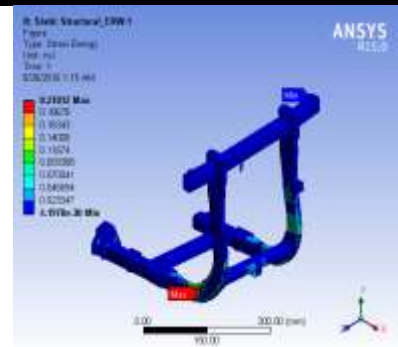
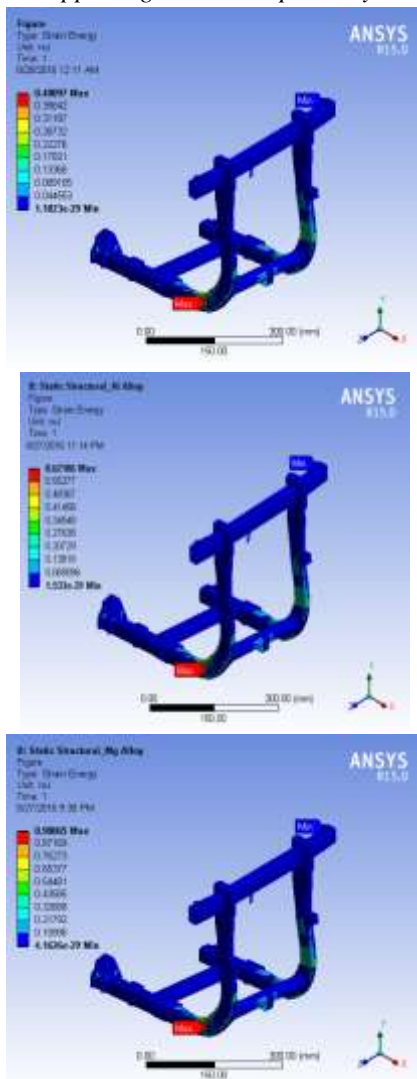


Fig.12: Strain Energy observed during stress analysis in Cast iron, Aluminum, Magnesium and ERW-1 Engine supporting bracket respectively.

The figure above shows the comparative study of Strain Energy observed during stress analysis in Cast iron, Aluminum, Magnesium and ERW-1 Engine. This Cast iron, Aluminum, Magnesium and ERW-1 materials were tested for alternative materials for suitable application and results were summarized. Stress induced in magnesium material was found out to be lower than ERW-1 and aluminum. It was probably due to high specific strength of magnesium and its ability to get denser. It can be anticipated that ERW-1 is the best for the desired application (figure 12).

Table.2: Static Structural of Engine Supporting bracket Modified Design

Materials	Gray C.I	Al Alloy	Mg Alloy	ERW-1
Total Deformation mm	0.9448	1.4646	2.3102	0.495
Equivalent (Von-Mises) Stress MPa	165.77	161.22	159.34	164.87
Strain Energy mJ	0.40097	0.62186	0.98065	0.21012

3.3 Modal Analysis of Modified Model

The Stress analysis of Engine Supporting bracket was carried out using ANSYS. Modal analysis was done for obtaining the different frequencies for Cast Iron, Aluminum Magnesium, ERW-1, and Table-1 Frequency Cast Iron vs. Aluminum vs. Magnesium vs. ERW-1.

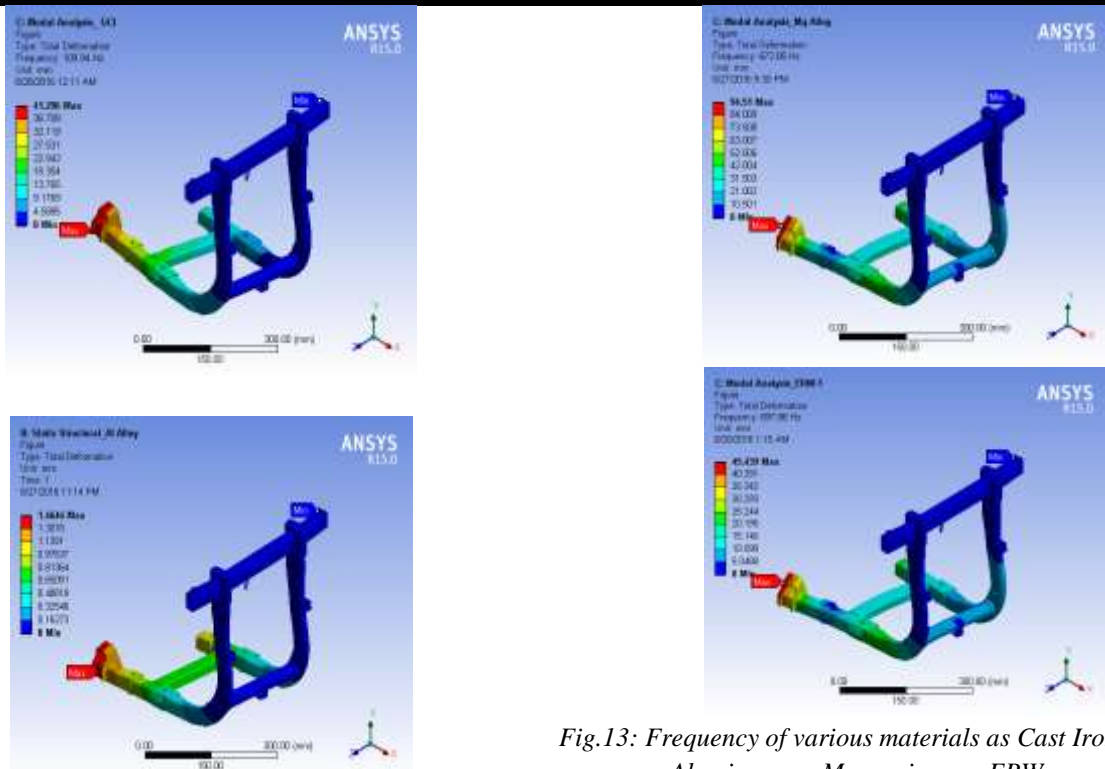


Fig.13: Frequency of various materials as Cast Iron vs. Aluminum vs. Magnesium vs. ERW

Table.3: Modal Analysis of Engine Supporting bracket Modified Design

Mode	GCI in Hz	Al Alloy in Hz	Mg Alloy in Hz	ERW-1 in Hz
1.	109.94	142.06	140.06	145.86
2.	124.09	160.38	158.32	164.62
3.	194.25	251.63	248.62	257.83
4.	368.96	477.6	471.68	489.68
5.	457.39	592.33	585.14	607.07
6.	525.71	681.05	672.85	697.86

As the mode of frequency was changed, initially no change was observed in ERW-1 and Magnesium material. This is probably due to the varying composition and superior mechanical properties of ERW-1 material.

Table.4: Static Structural Analysis of engine supporting bracket

Parameter	Initial Design	Modified Design
Total deformation mm	1.114	0.495
Von Mises stress Mpa	189.11	164.87
Strain energy mJ	0.58771	0.21012

Results are in tabulated form of Comparative study of initial and modified design for ERW-1. Initial model having less % of carbon was having more von-mises stress may fail in design criteria. But the design was fabricated and analyzed for new existing alternative materials aluminum, magnesium and ERW-1. It was found that the stress generated in ERW-1 material was less than initial design. Again the frequency and vibration studies through Fast

Fourier Transform show good little convergence of frequency well within stipulated permissible limit. So, it reveals in natural frequency of Engine Supporting bracket of modified design matches is less than self-excitation frequency. It can be anticipated from the above analysis that the modified Engine Supporting bracket is safe and suitable for further operation.

Table.5: Comparative Study of Initial and Modified Design

Mode	Initial Design		Modified Design	
	Deformation mm	Frequency Hz	Deformation mm	Frequency Hz
1.	31.974	148.12	39.651	145.86
2.	34.628	167.32	32.521	164.62
3.	51.485	268.59	47.839	257.83
4.	35.781	500.92	34.254	489.68
5.	34.976	630.92	32.792	607.07
6.	45.02	700.3	45.439	697.86

Mode shape is obtained were similar to that initial design of bracket. Thus change only the values of natural frequencies and amplitudes. First six frequencies are shown are called as Natural frequencies. Since applied load and damping effect are ignored in this analysis. A static structural analysis is required pre stressed modal analysis. This modal analysis was done to find out the vibration characteristic of the structure or particular component in the form of the natural frequency and mode shape of the bracket. Results are shown in tabulated from with comparison of all frequencies values and it is observed that third mode of vibration and here bracket to subject to maximum deformation at the end section of bracket.

IV. CONCLUSIONS

- Evaluation of modified engine mounting bracket was done using static structural analysis and modal analysis.
- It was found that, for the modified design deformation was 0.4950 mm with equivalent von-Mises stress 164.87 MPa which was very less than initial design with 1.14 mm deformation and equivalent von-Mises stress 189.11 MPa.
- Further natural frequency of modified design was found to be 257.83 Hz which was well within the range below self-excitation frequency and less than the natural frequency (268.59 Hz) of initial design.
- It was found that aluminum bracket limit its use for the said application due to greater deformation and less stiffness.
- Magnesium bracket can be the option to ERW-1 steel for the Engine supporting bracket application but it cannot be deployed as it is highly susceptible to corrosion.
- From the results obtained for initial design and modified design, it can be concluded that ERW-1 material best suit the requirement of the desired application and can be deployed with some safety standards.

REFERENCES

- [1] Dr. Yadavalli Basavaraj, Manjunatha.T.H, "Design Optimization of Automotive Engine Mount System" IJESI, (2013), vol.2 Issue 3 pp 48-53.
- [2] Pavan B. Chaudhari, Dr.D. R. Panchagad "Comparison of Magnesium, Aluminium and Cast Iron to obtain Optimum Frequency for Engine Bracket using Finite Element Analysis" IJERA, ISSN: 2248-9622 Vol. 2, Issue 5, September- October 2012, pp.1016-1020.
- [3] M.V. Aditya Nag "Material Selection and Computational Analysis on DOHC V16 Engine's Mounting Bracket Using COMSOL Multiphysics Software" Excerpt from The Proceedings of Comsol Conference in Bangalore 2012.
- [4] Mr. Pramod Walunje and Prof. V.K. Kurkute, "Optimization of Engine Mounting Bracket Using FEA" (2013), Indian Journal of Research, Volume 2, pp 72
- [5] Umesh S. Ghorpade, D. S. Chavan, Vinaay Patil and Mahendra Gaikwad, "Finite Element Analysis and Natural Frequency Optimization of Engine Bracket" (2012) IJMIE, ISSN No. 2231 -6477, Vol-2 pp 1-6.
- [6] Jasvir Singh Dhillon, Priyanka Rao, V.P. Sawant, "Design of Engine Mount Bracket for a FSAE Car Using Finite Element Analysis" Int. Journal of Engineering Research and Applications, (2014), vol. 4, Issue 9, pp 74-81.
- [7] Senthilnathan Subbian, O.P. Singh, Srikanth K. Mohan, Arockia P, Jeyaraj, "Effect of muffler mounting bracket design on durability" Engineering Failure Analysis 18 (2011) 1094-1107.

Plan and Implementation of Flexible D-Statcom for Mitigating Power Quality Problems and Improve the Distribution System Performance

Ganji Vivekananda¹, Dr K. Chandra Sekhar²

¹Research scholar in Department of EEE, Acharya Nagarjuna University, Guntur, AP, India

²Professor & Head, Department EEE, RVR & JC College of Engg, Guntur, AP, India

Abstract— This paper gives point by point data about adaptable D-STATCOM, which is utilized to decrease a wide range of deficiencies and enhance control quality and work as a Distributed Generation. It gives proceeds with power supply to the heaps even the primary source is separated and doesn't intrude. In this manner D-STATCOM works same as an adaptable D-STATCOM and consequently is known as Flexible D-STATCOM. The execution of Flexible D-STATCOM framework is to enhance the power quality by decreasing flaws in circulation framework execution under a wide range of framework related unsettling influences and framework lopsided deficiencies, for example, Line-to-Line and DLG blames under islanding condition. 12-bit D-STATCOM setup is used with IGBT which is planned and is utilized as a part of deciding the graphical portrayal of the D-STATCOM utilizing the product PSCAD/EMTDC electromagnetic transient recreation program. The unwavering quality and heartiness of the control conspires in the framework is dictated by the voltage aggravations happened by Line to line and twofold line to ground issues and islanded working condition are along these lines confirmed in the outcomes acquired in reproduction.

Keywords— D-STATCOM Voltage Sags, Distribution System, Faults, Energy Storage Systems, Islanding Condition.

I. INTRODUCTION

The electrical utilities systems for transmitting and distributing Powers are entering a sudden period of change. Their operation is due to be fine-tuned, to an unprecedented degree, by the application of power electronics, microprocessors and microelectronics in general and communications. Between these technologies will make the transmission and distribution of electricity more reliable, more controllable and more efficient.

At present numerous transmission offices go up against at least one constraining system parameters in addition to the powerlessness to direct power stream freely. The

dispersion static synchronous compensator (DSTATCOM) is a certainties controller, can be utilized different strategies have been connected to alleviate voltage droops. The ordinary techniques utilize capacitor banks, new parallel feeders, and uninterruptible power supplies (UPS). Be that as it may, the power quality issues are not totally comprehended because of wild responsive power remuneration and high expenses of new feeders and UPS. The D-STATCOM has developed as a promising gadget to give to voltage hang relief as well as for a large group of other power quality arrangements, for example, voltage adjustment, gleam concealment, control consider redress, and symphonious control. D-STATCOM is a shunt gadget that produces an adjusted three-stage voltage or current with capacity to control the greatness and the stage point. DG gives many advantages, for example, top shaving, fuel exchanging, enhanced power quality and unwavering quality, expanded productivity, and enhanced ecological execution. There is an appeal for utility DG establishments because of their favorable circumstances updating the circulation foundation. Most DG units are associated with the appropriation framework through a shunt nonlinear connection, for example, a VSI or a Current Source Inverter (CSI).

There are many sorts of Distributed Generation. Among them are wind, biogas, energy units and sun based cells. For the most part, these sources are associated with matrix through inverters and their principle capacity is to convey dynamic power into the framework. The to control the genuine power and receptive power. Freely. There are numerous techniques for lessening the issues, yet because of misfortunes in the framework they are not reasonable for working. Because of less productivity and misfortunes happening in the framework different strategies are not ideal. An adaptable D-STATCOM framework intended to work in two unique modes. At first, it can moderate voltage lists created by LL and DLG issues. Also, it can alleviate voltage droops created by three-stage open-circuit blame by opening the three

periods of an electrical switch and separating the principle control source (islanding condition). Receptive power pay is a critical issue in the control of dispersion frameworks. Responsive current builds the dispersion framework misfortunes, decreases the framework influence calculate, shrivel the dynamic influence ability and can bring about extensive plentifulness varieties in the heap side voltage. DGs are intended to supply dynamic power or both dynamic and responsive power.

The new patterns in power gadgets converters make the execution of such numerous capacities achievable. A DG is islanded when it supplies energy to a few burdens while the principle utility source is separated. Islanding recognition of DGs is considered as a standout amongst the most vital perspectives while interconnecting DGs to the dispersion framework. With the expanding entrance and dependence of the dissemination frameworks on DGs, the new interface control systems are being proposed.

This paper proposes an adaptable D-STATCOM framework intended to work in two distinct modes. At first, it can moderate voltage droops created by LL and DLG shortcomings. Also, it can relieve voltage hangs created by three-stage open-circuit blame by opening the three periods of an electrical switch and disengaging the principle control source (islanding condition). Receptive power remuneration is an essential issue in the control of circulation frameworks. Receptive current expands the dissemination framework misfortunes, diminishes the framework influence figure, shrivel the dynamic influence ability and can bring about vast adequacy varieties in the heap side voltage. Different techniques have been connected to alleviate voltage lists.

The customary techniques utilize capacitor banks, new parallel feeders, and uninterruptible power supplies (UPS).

The power quality issues are not totally illuminated because of wild receptive power pay and high expenses of new feeders and UPS. The D-STATCOM has developed as a promising gadget to give to voltage hang alleviation as well as for a large group of other power quality arrangements, for example, voltage adjustment, glimmer concealment, control calculate rectification, and consonant control. D-STATCOM is a shunt gadget that creates an adjusted three-stage voltage or current with capacity to control the extent and the stage edge.

By and large, the D-STATCOM design comprises of a normal 12-beat inverter course of action, a dc vitality stockpiling gadget; a coupling transformer associated in shunt with air conditioning framework, and related control circuits. The designs that are more advanced utilize multi-beat as well as multilevel setups. The VSC changes over the dc voltage over the capacity gadget into

an arrangement of three-stage air conditioning yield voltages. These voltages are in stage and combined with the air conditioner arrangement of system through the reactance of the coupling transformer. In this strategy, Clark and Park changes are not required. They have been examined voltage droop/swell relief because of simply load variety while no adjusted and unequal issues have been researched. In this paper, another control strategy for relieving the heap voltage hangs brought about by a wide range of blame is proposed. To identify the relative pick up of PI controller is construct just with respect to Trial and Error Method. In this paper, the relative pick up of the PI controller is settled at a same esteem, for a wide range of issues, by tuning the transformer reactance in an appropriate sum. At that point the power and unwavering quality of the proposed strategy is more than the said strategies.

In this technique, the dc side topology of the D-STATCOM is changed for moderating voltage mutilations and the impacts of framework blames on the delicate burdens are explored and the control of voltage lists are dissected and recreated.

II. PROBLEM DESCRIPTION

Control quality is absolutely a noteworthy worry in the present time; it turns out to be particularly critical with the presentation of modern gadgets. Numerous issues are happening in power quality, for example, Power Factor, Voltage gleaming, Harmonic Distortions, Voltage Transients, Voltage Sags or Dips, Voltage Swells These are power quality issues in the dissemination framework. To enhance the power quality these might be connected: Power figure revision, Transient voltage surge concealment, Special line score sifting, appropriate earthing frameworks, Uninterruptible power supplies, Harmonic separating and control Power quality is unquestionably a noteworthy worry in the present time, it turns out to be particularly imperative with the presentation of complex gadgets, whose execution is exceptionally delicate to the nature of force supply The electronic gadgets are extremely touchy to unsettling influences and in this manner modern burdens turn out to be less tolerant to power quality issues, for example, voltage plunges, voltage swells, and sounds.

The fundamental reason for the coupling inductors is to sift through the present symphonious parts that are produced predominantly by the throbbing yield voltage of the power converters. The STATCOM is associated with the power systems at a PCC, where the voltage-quality issue is a worry. Every single required voltage and streams are measured and are encouraged into the controller to be contrasted and the summons. As a rule, the VSC is spoken to by a perfect voltage source related

with interior misfortune associated with the AC influence by means of coupling reactors. On a basic level, the trading of genuine power and responsive power between the STATCOM and the power framework can be controlled by altering the adequacy and period of the converter yield voltage. On account of a perfect lossless power converter, the yield voltage of the converter is controlled to be in stage with that of the power framework. For this situation, there is no genuine power flowed in the STATCOM; in this manner, a genuine power source is not required. To work the STATCOM in capacitive mode or var era, $+Q$, the extent of the converter yield voltage is controlled to be more prominent than the voltage at the PCC. Conversely, the size of the yield voltage of the converter is controlled to be not as much as that of the power framework at the PCC on request to retain receptive power or to work the STATCOM in inductive mode, $-Q$. To direct the capacitor voltage, a little stage move d is presented between the converter voltage and the power framework voltage. A little slack of the converter voltage regarding the voltage at the PCC makes genuine energy to spill out of the power framework the STATCOM, while the genuine power is exchanged from the STATCOM to the power framework by controlling the converter voltage so it drives the voltage at the PCC.

Voltage plunges are viewed as a standout amongst the most extreme aggravations to the modern hardware Electronic supplies are exceptionally touchy burdens against sounds in light of the fact that their control relies on upon either the pinnacle esteem or the zero intersection of the provided voltage, which are altogether impacted by the consonant twisting. As one of the unmistakable power quality issues, the starting point, outcomes and relief methods of voltage list/swells and intrusions issue. The methods of rectifying the issues in a dissemination framework by solid power hardware based gadgets called Dynamic Voltage Restorer (DVR) and the Distribution Static Compensator (D-STATCOM). Voltage from both gadgets is associated into the framework to redress the issues. The execution of the DVR and the D-STATCOM is considered for the power quality issues to be seen.

For the most part two sorts of VSC-based compensators have been normally utilized for alleviation of the voltage droops and swells and directing the heap transport voltage. Those are shunt and arrangement gadgets which are DSTATCOM and DVR individually. The execution of the DSTATCOM and the DVR utilized for the heap transport voltage control have been broke down and looked at when a nonlinear load is associated over the heap transport. Both of these compensators are utilized under shut circle voltage-control mode. The DSTATCOM

and the DVR has been acquired for the frail and solid air conditioning supply frameworks.

In this manner the execution of FD-STATCOM framework is to alleviate control quality issues and enhance circulation framework execution under a wide range of framework related aggravations and framework uneven flaws, for example, Line-to-Line (LL) and Double Line to Ground (DLG) blames and supplies energy to delicate loads under islanding condition. The 12-beat D-STATCOM arrangement with IGBT is outlined and the realistic based models of the D-STATCOM are created utilizing the PSCAD/EMTDC electromagnetic transient reproduction program. The unwavering quality and strength of the control conspires in the framework reaction to the voltage unsettling influences brought on by LL and DLG shortcomings and islanded working condition are clearly demonstrated in the reproduction comes about.

III. STRUCTURE OF FD-STATCOM:

The STATCOM is the strong state-based power converter form of the SVC. The idea of the STATCOM was proposed by Gyugyi in 1976. Working as a shunt-associated SVC, its capacitive or inductive yield streams can be controlled freely from its associated AC transport voltage.

There are distinctive strategies utilized for executing and for moderating deficiencies are: FD-STATCOM is worked by utilizing Unified Power Flow Controller (UPFC), Insulated Gate bipolar transistor (IGBT), Super capacitor vitality stockpiling framework (SCESS) Step up and venture down transformer associated in Y-Y and Y- Δ association.

Unified Power Flow Controller

Bound together Power Flow Controller (UPFC) comprise from two sections, arrangement and shunt, to deal with the stream of dynamic power from one section to the next, however FDG comprise of one section just, in light of the fact that it has a supply of the dynamic power from DG framework.. The essential electronic piece of the FD-STATCOM is the voltage source inverter that changes over an info dc voltage into a three-stage yield voltage at major recurrence. These voltages are in stage and combined with the air conditioner framework through the reactance of the coupling transformer. Appropriate modification of the stage and extent of the FD-STATCOM yield voltages permits successful control of dynamic and receptive power trades between the FD-STATCOM and the air conditioner framework.

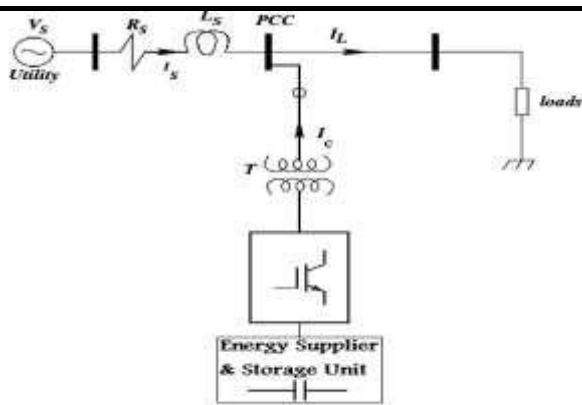


Fig.1: schematic representation of the FD-STATCOM

A run of the mill 12-beat inverter course of action using two transformers with their primaries associated in arrangement. The principal transformer is in Y-Y association and the second transformer is in Y-Δ association. Every inverter works as a 6-beat inverter, with the Y-Δ inverter being postponed by 30 degrees as for the Y-Y inverter. The IGBTs of the proposed 12-beat FD-STATCOM are associated hostile to parallel with diodes for compensation purposes and charging of the DC capacitor. This is to give a 30 degrees stage move between the beats and to diminish music created from the FD-STATCOM. The FDSTATCOM is associated in shunt to the framework.

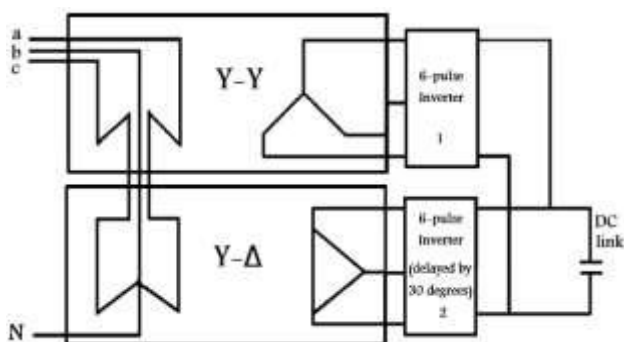


Fig.2: The 12-pulse FD-STATCOM arrangement

The square outline of the control plot intended for the FD-STATCOM is construct just with respect to estimations of the voltage VRMS at the heap point.

The piece graph of the control plot intended for the FD-STATCOM. It is construct just in light of estimations of the voltage VRMS at the heap point. The voltage blunder flag is acquired by contrasting the deliberate VRMS voltage and a reference voltage, VRMS Ref. A PI controller forms the contrast between these two flags keeping in mind the end goal to get the stage point δ that is required to drive the mistake to zero. The edge δ is utilized as a part of the PWM generator as the stage edge of the sinusoidal control flag. The exchanging recurrence

utilized as a part of the sinusoidal PWM generator is fsw=1450 Hz and the balance file is $Ma \approx 1$. The balancing edge δ is connected to the PWM generators in stage A. The points of stages B and C are moved 120 and 240 degrees, individually.

IV. OPERATION OF FD-STATCOM

Keeping in mind the end goal to relieve voltage hangs brought about by LL and DLG blames and to supply energy to delicate load, another strategy is proposed in which the FD-STATCOM and Super Capacitor Energy Storage framework (SCESS) are incorporated. Diverse sorts of deficiencies may happen in appropriation framework, controller framework must have the capacity to alleviate any sorts of voltage hangs. The incorporation and control of SCESS into a FD-STATCOM is produced to alleviate such issues, upgrade control quality and enhance circulation framework unwavering quality. The new technique builds up the control ideas of charging and releasing the SCESS by DSTATCOM, and approves the execution of an incorporated DSTATCOM SCESS for enhancing dissemination framework execution under a wide range of framework related unsettling influences and framework issues, for example, LL and DLG shortcomings and under islanded working condition. The SCESS is clarified as taking after:

SCESS:

Super capacitor is another vitality gadget developed lately. It is otherwise called twofold layer capacitor. The electrical twofold layer capacitor is a novel vitality stockpiling segment. the super capacitor does not have electrochemical response and just have electric charges adsorption and desorption when it is charged and released. It has many merits, for example, high charge/release present, less upkeep, long life and some other immaculate execution. In the meantime, its little spillage current empowers it has long time of vitality stockpiling and the productivity could surpass 95%.

The structure of SCESS, Its circuit is essentially made out of three sections:

- (a) Rectifier Unit
- (b) Energy Storage Unit
- (c) Inverter Unit.

Rectifier unit embraces three stage full extension rectifiers to charge super capacitor and supply dc control vitality to inverter unit.

Inverter unit embraces three stage voltage inverter made out of IGBTs, it interfaces with power network by means of transformer.

At the point when SCESS works typically, voltage at dc side is changed over into airconditioning voltage with an indistinguishable recurrence from power matrix through IGBT inverter. At the point when just considering crucial

recurrence, SCESS can be identical to air conditioning synchronizing voltage source with controllable greatness and stage. Vitality stockpiling unit i.e. super capacitor vitality stockpiling exhibits are made out of numerous solid super capacitors. In the event that an expansive number of super capacitors are set in parallel, in the meantime it enhances limit of force hardware gadgets in power transformation framework in this manner it can be effectively made out of more vast limit SCESS, Thus the operational unwavering quality and control adaptability won't be influenced. Super capacitor is effectively modularized, when required, and it is extremely advantageous in limit extension.

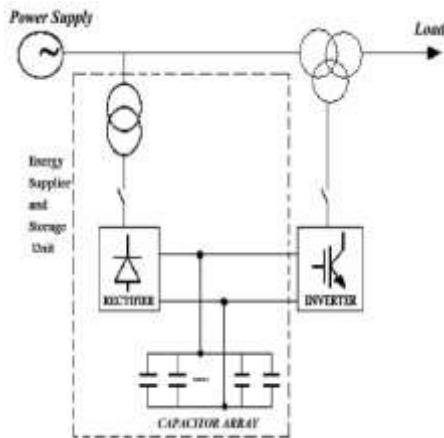


Fig.3: Structure of SCESS

SCESS in view of DG associated with power lattice can be separated into three capacity squares: super capacitor exhibits parts put away vitality, control vitality change framework in vitality change and transmission, and a coordinated control framework. SCESS stores vitality as electric field vitality utilizing super capacitor exhibits. At the absence of vitality crisis or when vitality required, the put away vitality is discharged through control framework, quickly and precisely repaying framework dynamic and receptive power, to accomplish the adjust of force vitality and security control. Deciding the quantity of vitality stockpiling module can spare super capacitors, and further lessening volume, quality and cost of the vitality stockpiling unit. the FD-STATCOM supplies responsive energy to the framework.

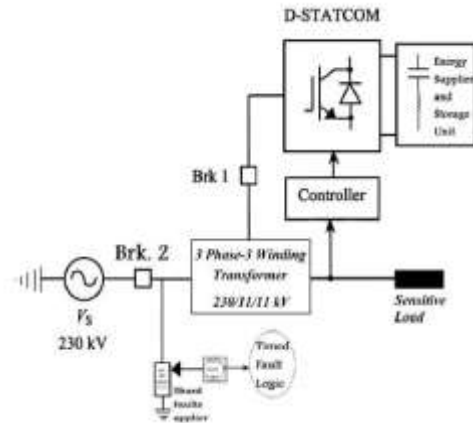


Fig.4: Distribution system with FD-STATCOM integrated with SCESS and controller

Inverter based solutions:

Inverter based arrangements all have in like manner that they depend on power electronic rectifiers, converters or inverters to help the gear to withstand a voltage plunge. The majority of the arrangements utilize some sort of vitality stockpiling.

Uninterruptible Power Supply:

The most widely recognized alleviation gadget is the UPS. The reason is the low venture, basic operation and control. It is typically associated between the system and the hardware to secure, however different designs exist. The UPS is typically made of a diode rectifier, a battery and a converter. Different setups with other vitality sources than batteries exist, however are not as normal. The UPS is utilized for rather restricted power necessities since the cost brought about by the misfortunes in the two converters and the upkeep of the batteries are generally high. In mechanical situations UPS are ordinarily used to ensure control hardware and PCs.

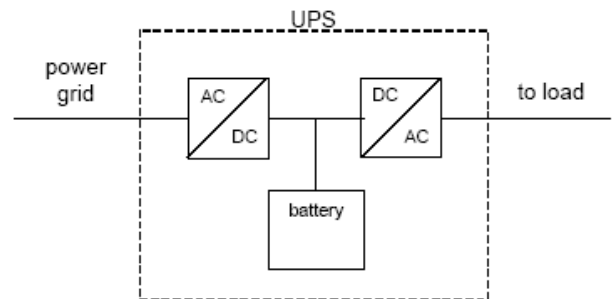


Fig.5: Example of a standard UPS

A change of the UPS is the disconnected UPS. These units are frequently littler and intended for shorter interferences. The UPS is ordinarily not associated with the heap. Rather a power electronic switch controls the association between the matrix and the heap. The aggregate time from detecting a voltage plunges and change to the battery source is 2-4ms in normal. When the

utility voltage gives back, the UPS switches stack back and the batteries energize.

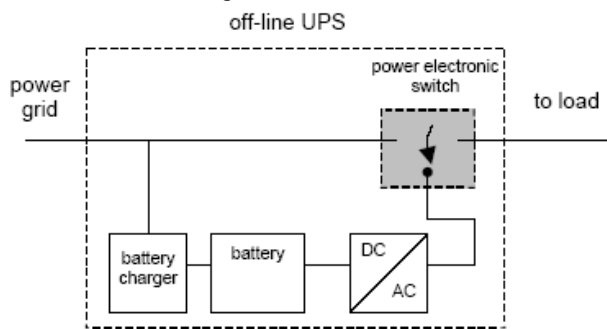


Fig.6: Example of an off-line UPS.

Voltage source converters (VSC):

A voltage-source converter is a power electronic gadget, which can create a sinusoidal voltage with any required size, recurrence and stage point. Voltage source converters are broadly utilized as a part of customizable speed drives yet can likewise be utilized to alleviate voltage plunges. The VSC is utilized to either totally supplant the voltage or to infuse the „missing voltage“. The „missing voltage“ is the distinction between the ostensible voltage and the genuine. The converter is ordinarily in light or some likeness thereof of vitality stockpiling, which will supply the converter with a DC voltage. The strong state gadgets in the converter is then changed to get the craved yield voltage. Typically the VSC is utilized for voltage plunge relief, as well as for other power quality issues, e.g. gleam and music.

Series Voltage Controller [Dynamic Voltage Restorer (DVR)]:

The arrangement voltage controller is associated in arrangement with the secured stack. Generally the association is made by means of a transformer, yet setups with direct association by means of force gadgets likewise exist. The subsequent voltage at the heap transport bar measures up to the aggregate of the matrix voltage and the infused voltage from the DVR. The converter creates the receptive power required while the dynamic power is taken from the vitality stockpiling. The vitality stockpiling can be diverse relying upon the necessities of adjusting. The DVR regularly has constraints on the profundity and length of the voltage plunge that it can adjust. In this manner right measured must be utilized as a part of request to accomplish the craved protection. Batteries for more yet less extreme extent drops and super capacitors in the middle. There are likewise different blends and designs conceivable.

There are designs, which can work with no vitality stockpiling, and they infuse a slacking voltage with the heap current. There are likewise extraordinary methodologies on what to infuse to acquire the most

intense arrangement. The principle advantage with this strategy is that a solitary DVR can be introduced to secure the entire plant (a couple MVA) and also single burdens. In view of the quick switches, normally IGBT's, voltage remuneration can be accomplished in under a large portion of a cycle. Weaknesses are that it is moderately costly and it just mitigates voltage plunges from outside the site. The cost of a DVR primarily relies on upon the power rating and the vitality stockpiling limit.

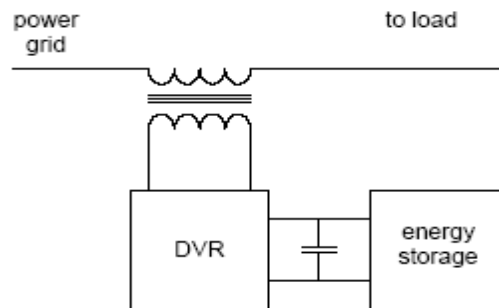


Fig.7: Example of a standard configuration for a DVR.

Shunt Voltage Controller [Distribution Static Compensator (DSTATCOM)]:

The shunt voltage controller is a voltage source converter associated in parallel with the heap transport bar through a transformer or a reactor. The distinction between the DVR and the SVC is that as opposed to infusing a voltage, the current through the reactance is controlled. The shunt voltage controller is ordinarily utilized for power calculate rectification, voltage gleam, dynamic sifting, and so on., instead of voltage moderation. For issues started near the SVC, on a similar voltage level or near the heap, the impedance seen by the SVC will be low. Since the commitment to the transport bar voltage measures up to the infused current increased by the impedance, a high responsive current will be drawn amid such ablame. Regardless of the possibility that the SVC can be utilized for voltage plunge relief reason, it is not the better option contrasted with DVR.

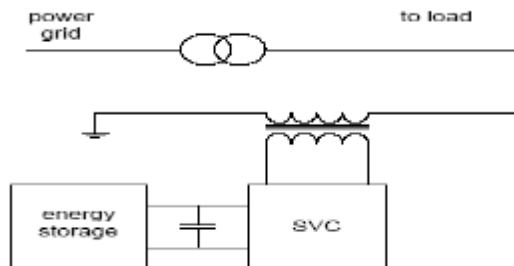


Fig.8: Example of a standard configuration for a shunt voltage controller

Combination of a DVR and a SVC:

An improvement of the voltage source converters is a mix of the DVR and the SVC. By utilizing them together, the SVC will amid a voltage plunge utilize the rest of the

voltage to get the obliged vitality to the DVR by taking a current from the power framework. The DVR will then infuse the missing voltage as portrayed before along these lines repaying the voltage plunge. Utilizing this setup appeared in figure18, no vitality stockpiling is required with the exception of a little capacitance to settle the DC-interface. The primary impediment with the SVC and vast streams amid deficiencies still remains.

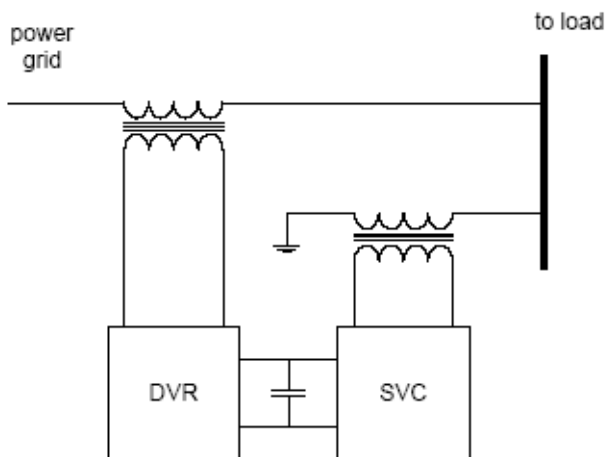


Fig.9: Combination of a DVR and SVC without energy storage.

Energy storage:

The vitality required amid an aggravation through voltage source converters; rectifiers, inverters, UPS, can be put away electrically, actively, synthetically, or attractively. These can be actualized by capacitors, flywheels, batteries or superconducting attractive curls (SMES).The improvement of new stockpiling medium outcomes in expanded ability of those gadgets.

Capacitors:

Capacitors can be utilized as vitality stockpiling to deliver dynamic power. The measure of vitality put away on the capacitor is relative to the square of the voltage. To supply a steady dc-voltage there must be a dc-dc converter to direct the voltage, since the capacitor voltage diminishes when the capacitor is released. Capacitors can regularly be utilized something like a few moments ride-through, contingent upon the heap.

Batteries:

Batteries have a higher vitality thickness than capacitors and supply control for a more extended time than capacitors, however at a slower rate. Batteries have a couple detriments contrasted with capacitors; they may contain substances, which are not ecologically inviting, a constrained lifetime, and they oblige upkeep to work as planned.

V. SIMULATIONS AND RESULTS

This area portrays the PWM-based control conspire with reference to the D-STATCOM. The point of the control plan is to keep up consistent voltage size at the point where a delicate load is associated, under framework unsettling influences. The control framework just measures the r.m.s voltage at the heap point, i.e., no receptive power estimations are required. The VSC exchanging procedure depends on a sinusoidal PWM method which offers straightforwardness and great reaction. Since custom power is a moderately low-control application. PWM strategies offer a more adaptable choice than the key recurrence exchanging (FFS) techniques supported in FACTS applications. Additionally, high exchanging frequencies can be utilized to enhance the productivity of the converter, without bringing about critical exchanging misfortunes.

A three-stage alternator of 42.5 kVA, 50 Hz, 400V (L-L) rating sustains energy to disconnected dissemination framework. The alternator is coupled to the diesel motor with senator as prime mover. The heap considered on the framework speaks to an acceptance engine stack. The synchronous machine yield voltage and recurrence are utilized as criticism contributions to a control framework, which comprises of the diesel motor with senator and also an excitation framework. The fundamental graph of DSTATCOM associated as shunt compensator. It comprises of a three-stage, current controlled voltage source converter (CC-VSC) and an electrolytic DC capacitor. The DC transport capacitor is utilized to give a self-supporting DC transport. The test framework includes a 230 kV transmission framework. An adjusted load is associated with the 11 kV, optional side of the transformer. Brk. 1 is utilized to control the operation time of the FD-STATCOM. A 12-beat FD-STATCOM is associated with the tertiary twisting by shutting Brk. 1 at 0.2 s, for keeping up load RMS voltage at 1pu. A SCESS on the dc side give the FD STATCOM vitality stockpiling capacities. The reproductions are done for both situations where the FDSTATCOM is associated with or disengaged from the framework.

The recreations of the FD-STATCOM in blame condition are done utilizing LL and DLG deficiencies and under islanded working condition. In LL and DLG deficiencies the blamed stages are stages An and B while in islanded working condition, three conductors open by Brk. 2 in 0.4 – 0.5 s. The length of the islanding condition are considered for around 0.1 s and the LL and DLG shortcomings are considered for around 0.3 s. The shortcomings are applied at 0.4 s. The aggregate reenactment time is 1.6 s. In this paper, the FD-STATCOM utilizes the proposed control strategy to alleviate the heap voltage droops because of a wide range

of flaws. The reenactments are accomplished for a wide range of issues presented in the 11kV appropriation frameworks as takes after:

Simulation results for Line-to-Line fault:

At the point when the framework works without FD-STATCOM and under LL blame. For this situation, the voltage drops by just about 20% regarding the reference esteem. Int = 0.2 s, the FD-STATCOM is associated with the dissemination framework. The voltage drop of the touchy load point is moderated utilizing the proposed control strategy. The moderated RMS voltage utilizing this new strategy an exceptionally powerful voltage control is given the RMS voltage and Vab (line voltage) at the heap point in interim 0.4 - 0.7 s, individually, for the situation when the framework works without FD-STATCOM and under LL blame. The Vab recurrence ranges amid alleviation of voltage droop that is displayed in percent. The THD in percent for Vab in amid moderation of LL blame event is 0.034%. In light of a 12-beat FD STATCOM is utilized as a part of this paper, and after that the THD for Vab is little.



Fig.10: Current waveforms at PCC without FD-STATCOM

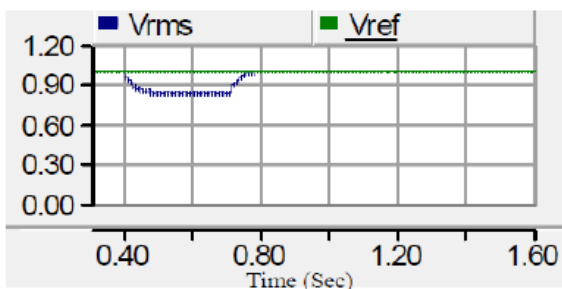


Fig.11: The RMS Voltage (VRMS) at PCC without FD-STATCOM

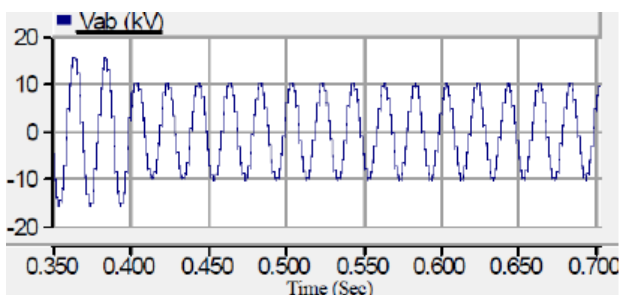


Fig.12: Vab at PCC Without FD-STATCOM

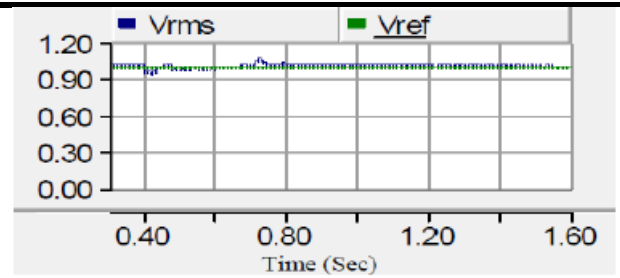


Fig.13: Compensated RMS Voltage under LL fault

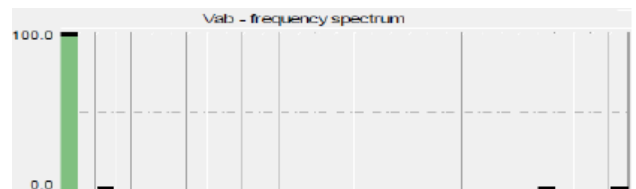


Fig.14: Frequency Spectrum for Vab during mitigation of L-L fault

Simulation results for Double Line to Ground fault:

At the point when the framework works without FD-STATCOM and uneven DLG blame is happened. The RMS voltage faces with 20% abatement as for the reference voltage. It is watched that the proposed technique has accurately relieved voltage droop. The RMS voltage and line voltage Vab at the heap point, individually, for the situation when the framework works without FD-STATCOM and unequal DLG blame is happened. The RMS voltage faces with 20% lessening as for the reference voltage. The Vab recurrence ranges amid relief of voltage droop. The THD of Vab in amid alleviation of DLG blame event is exceptionally reasonable and 0.036%.The RMS Voltage (VRMS) at PCC without FD-STATCOM.

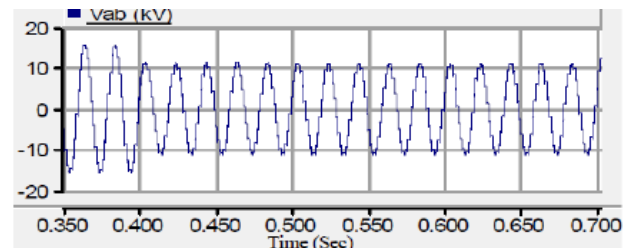


Fig.15: Vab Line Voltage at PCC without FD-STATCOM

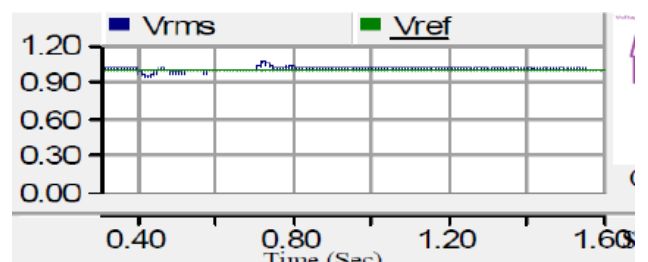


Fig.16: Compensated RMS Voltage

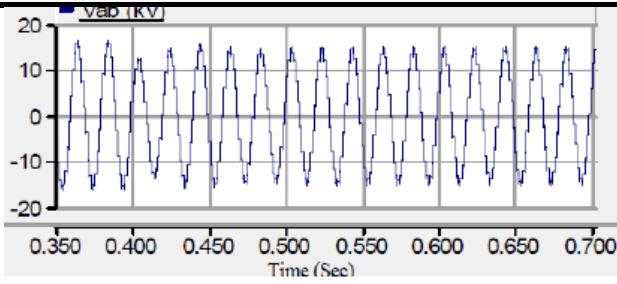


Fig.17: Mitigated Line Voltage V_{ab} at the Load Point

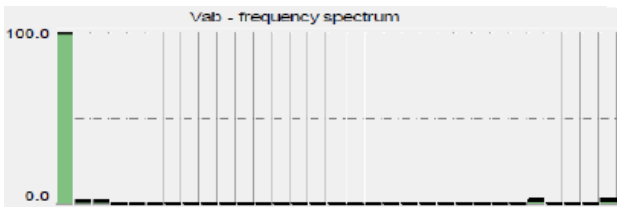


Fig.18: Frequency spectrum for V_{ab} during mitigation of DLG fault

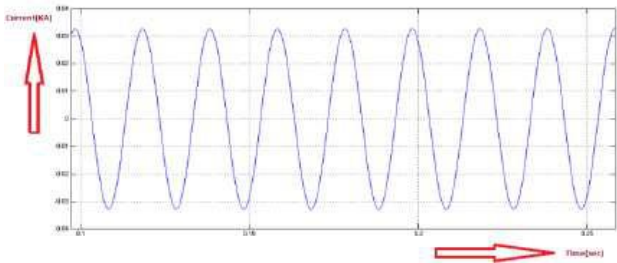


Fig.19: Compensated line Current (KA) at the load point

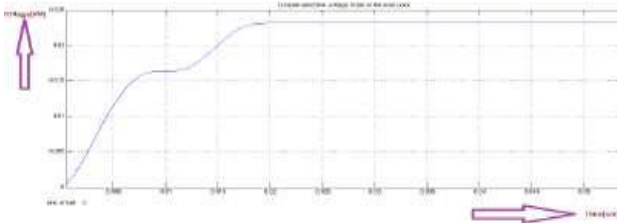


Fig.20: RMS voltage without using D-STATCOM

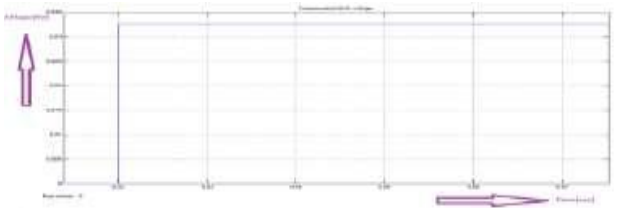


Fig.21: Compensated RMS Voltage by using D-STATCOM

Simulation results under islanded operating condition:

The RMS voltage, line voltages and load streams (versus kA) at the PCC, separately, for the situation when the framework works without FD-STATCOM and under islanded working condition.

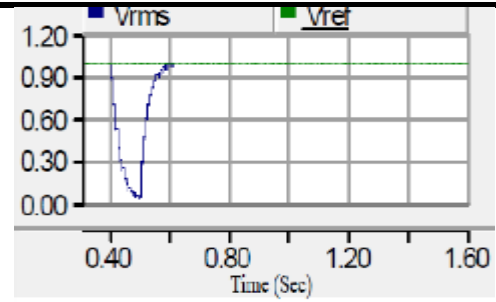


Fig.22: VRMS at PCC without FD-STATCOM under islanding condition.

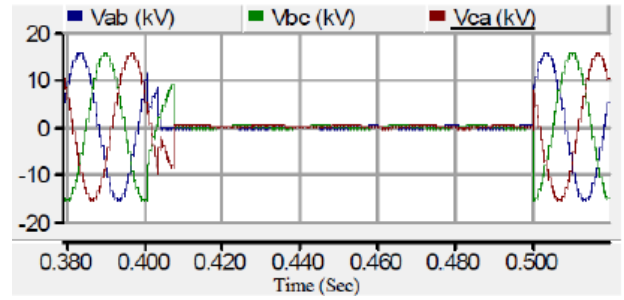


Fig.23: Line Voltages at PCC without FD-STATCOM

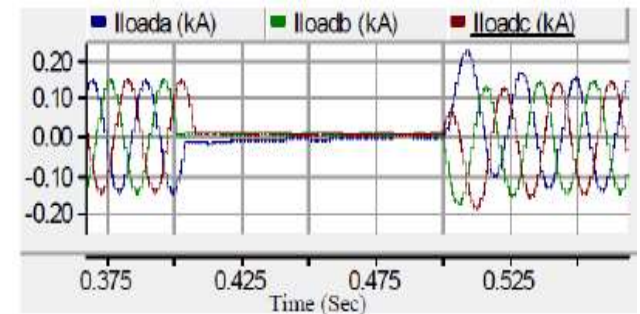


Fig. 24: Load Currents without FD-STATCOM in islanding condition

The relieved RMS voltage, line voltages at the heap point and remunerated load streams, separately, utilizing the proposed strategy. It is watched that the RMS stack voltage is near the reference esteem, i.e., 1pu and FD-STATCOM can supply energy to delicate burdens, effectively. The V_{ab} recurrence ranges amid alleviation of voltage hang brought about by islanding condition.

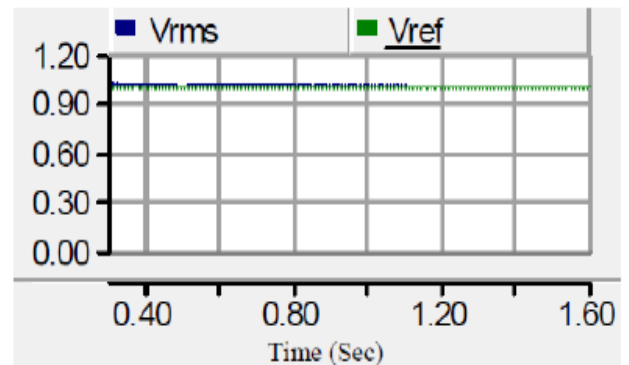


Fig.25: Compensated RMS voltage

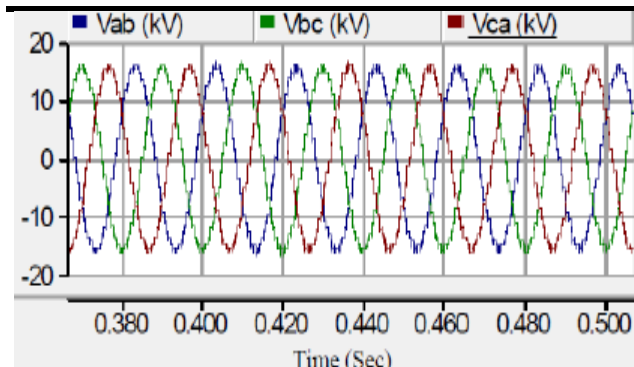


Fig.26: Compensated line voltages at the load point

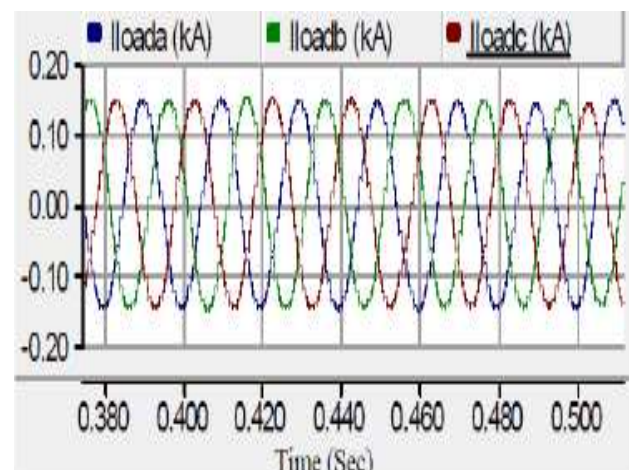


Fig.27: The mitigated load currents (in KA)

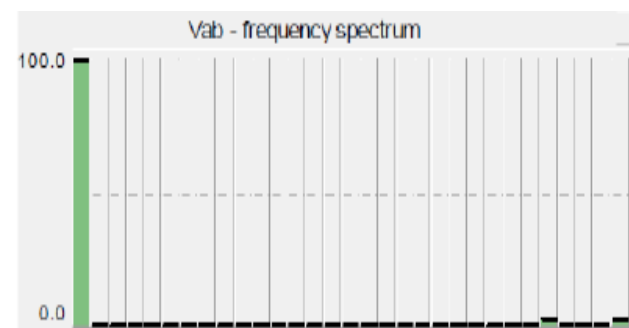


Fig.28: Frequency spectrum for Vab under islanding operating condition

VI. CONCLUSION AND FUTURE WORK

In System configuration record I have recognized the distinctive kind of modules in my venture, and delineated diverse sort of circuit outlines for the modules to depict about the Statcom gadgets. An adaptable D-STATCOM is suggested that could both alleviate uneven blames and work as a DG, when it supplies energy to delicate burdens while the principle utility source is detached. Subsequently, D-STATCOM works same as a FDG and thusly, it is called FD-STATCOM. Likewise, this venture has proposed another control strategy for relieving the voltage lists, brought on by uneven shortcomings and islanding condition, at the PCC. The proposed technique

depends on incorporating FD-STATCOM and SCESS. This proposed control plan was tried under an extensive variety of working and it was watched that the proposed strategy is exceptionally hearty for each situation. Furthermore, the controlled VRMS voltage demonstrated a sensibly smooth profile. It was watched that the heap voltage is near the reference esteem, i.e., 1pu and the voltage hangs are totally limited.

REFERENCES

- [1] Elements of power system analysis by William D. Stevenson.
- [2] C. J. Gajanayake, D. M. Vilathgamuwa, P. C. Loh, F. Blaabjerg, and R. Teodorescu, "A z-source inverter based flexible DG."
- [3] M. I. Marei, E. F. El-Saadany, and M. M. A. Salama, "A novel control algorithm for the DG interface to mitigate power quality problems," IEEE Trans. Power Del., vol. 19, no. 3, pp. 1384-1392, July 2004
- [4] L. S. Patil and Ms. A. G. Thosar, "Application of D-STATCOM to mitigate voltage sag due to DOL starting of three phase induction motor," in Proc. IEEE International Conference on Control, Automation, Communication and Energy Conservation, 2009, pp. 1-4.
- [5] E. Babaei, A. Nazarloo, and S. H. Hosseini, "Application of flexible control methods for D-STATCOM in mitigating voltage sags and swells," in Proc. IEEE International Power and Energy Conference (IPEC), Singapore, 2010, pp. 590-595.
- [6] H. Hatami, F. Shahnia, A. Pashaei, and S.H. Hosseini, "Investigation on D-STATCOM and DVR operation for voltage"
- [7] Understanding FACTS: Concepts and Technology of Flexible AC Transmission Systems Narain G. Hingorani, Laszlo Gyugyi.
- [8] M. I. Marei, E. F. El-Saadany, and M. M. A. Salama, "Flexible distributed generation: (FDG)," in Proc. IEEE Power Engineering Soc. Summer Meeting, 2002, vol. 1, pp. 49- 53
- [9] H. H. Zeineldin, E. F. El-Saadany, and M. M. A. Salama, "Impact of DG interface control on islanding detection and no detection zones," IEEE Trans. Power Del., vol. 21, no. 3, pp. 1515-1523, July 2006
- [10] High voltage direct current transmission by J. Arrillaga.

Laws of Heat Radiation from Spherical Gas Volumes.

Part I. Laws Formulation

Prof. Dr. A. N. Makarov

Department of Electrical Supply And Electrical Engineering, Tver State Technical University, nab. Afanasiya Nikitina 22, Tver, 170026 Russia

Abstract— In 2014-16 the author of this article disclosed the laws of heat radiation from isothermal isochoric concentric spherical gas volumes, that the article presents. Radiating gas volumes of any complex form can be entirely filled by concentric spherical together with coaxial cylinder gas volumes and calculate heat radiation from gas volumes, furnace torches, fire boxes, combustion chambers on the heating surfaces with high accuracy.

Keywords—Scientific Disclosure, Laws, Heat radiation, Torch, Furnaces. Fire Boxes.

I. INTRODUCTION

This monograph is the continuation of the research work, which results are presented in [1,2]. Flaring of gaseous, liquid, pulverized fuel in furnaces, fire boxes combustion chambers is characterized by volume heat radiation. Quadrillions of particles, atoms radiate in torch. We need to consider radiation from every particle, atom to the calculated area.

To calculate the heat radiation from all the atoms that make up the torch to the calculated area it is necessary to solve triple integral equations. The solution for triple integral equations to determine the average beam path length from the radiating particles, the angular radiation coefficients of gas volumes to the calculated area was not found in the 20th century [1,2].

It is considered, that the problem of calculation heat radiation in torch furnaces, fire boxes, combustion chambers was solved with the appearance of computers and use of numerically modeled heat transfer integral equations. However, long-term analytical and experimental studies of heat transfer showed, that the results from numerical solution of integral heat transfer equations on computers are not entirely correct.

This method uses the laws of heat radiation from solid bodies, Stefan-Boltzmann law, large mass of approximate temperatures and optical coefficients of surface and volume zones and error made in calculations accounts for 20-40% [3,4].

At the end of the 20th century, in 1996-2001 the laws of heat radiation from isothermal isochoric coaxial cylinder gas volumes were disclosed [5].

The laws are called Makarov's laws with the goal of adherence to the age-old scientific traditions and copyright [4,5]. Based on the scientific discovery the new heat transfer calculation concept in torch furnaces, fire boxes, combustion chambers is developed [4-6].

In accordance with the new concept and method for calculation, cylindrical gas volumes, from which the calculation of radiation fluxes on the calculated areas and the heating surfaces, inscribe in the torches.

In accordance with the new concept and the method for calculation, cylinder gas volumes, from which the calculation of radiation fluxes on the calculated areas and heating surfaces is performed, inscribe in torches.

Radiation fluxes from the torch, heated surfaces, combustion products are determined for every calculated area including the multiple reflection and absorption of radiations. The new concept and method of calculation stood the test of time, the calculation results are confirmed by experimental studies on the operating furnaces, fire boxes, combustion chambers, calculation error does not exceed 10%.

In 2001-16 the author continued investigation of heat radiation from torches of furnaces, fire boxes, combustion chambers, symmetrical radiating gas volumes. In 2014-16 the author of this article disclosed the laws of heat radiation from isochoric isothermal concentric spherical gas volumes.

This article informs the scientific community of the scientific discovery and its practical use of heat transfer calculations in furnaces, fire boxes, combustion chambers.

II. LAWS OF HEAT RADIATION FROM SYMMETRICAL GAS VOLUMES

2.1. Laws of heat radiation from cylindrical gas volumes

Symmetrical radiating gas volumes include cylindrical and spherical radiating gas volumes, which possess a number of unique properties.

To calculate heat radiation incident on the calculated area from gas volumes of any arbitrary form, it is necessary to solve two problems.

The first problem is to calculate elementary angular coefficient of radiation from gas volume on the calculated area. The second problem is to calculate the average path length of beams from quadrillions of radiating particles of gas volume to the calculated area [1].

Elementary angular radiation coefficient from gas volume to the calculated area shows heat radiation ratio from gas volume to the calculated area of all heat radiation from gas volume in the surroundings.

To solve the first and the second problems, it is necessary to solve two triple integral equations with limits of integration by the gas volume.

In the 20th century the solution for triple integral equations was not found, the problem has reached a deadlock. The formulas for calculating the elementary angular radiation coefficients of gas volumes and the average beam path length were not developed.

In the 20th century, the double integral equations were solved, formulas for calculating the average beam path length and elementary angular coefficients of radiation from flat and convex surfaces on the calculated areas at their any spatial collocation were obtained and referenced [3].

Formulas for calculating the average beam path length and elementary angular coefficients of radiation from surfaces were used for calculating heat radiation from gas volumes, the radiation from volumes were replaced by the gas volume bounding surface and calculations were performed by the laws for radiation from solid bodies.

The error made in calculations was 20-40%.

The study of heat radiation from symmetrical radiating gas volumes, isochoric isothermal coaxial cylinder gas volumes allowed to disclose their unique properties, the laws of Makarov, and derive formulas for calculating local angular radiation coefficients of gas volume and determining the average beam path length from all of the radiating particles of gas volume to the calculated area [1,2].

In exercise the copyright, the author has combined four laws of heat radiation from isochoric isothermal coaxial cylinder gas volumes into one law read as follows.

«The average path length of beams from quadrillions of radiating particles of each isochoric isothermal coaxial gas volume to the calculated area is equal to the arithmetic mean distance from the symmetry axis of volumes to the calculated area and angular coefficients of radiation,

densities of radiation fluxes of gas volumes to the calculated area are equal.

The flux density of heat radiation from the central coaxial cylinder volume of a small diameter on the calculated area is equal to the sum of the densities of radiation fluxes from all gas volumes in radiation power released in a small diameter volume equal to the sum of radiation power released in all isochoric isothermal coaxial cylinder gas volumes radiating on the calculated area".

Naturally occurring harmony, consistency of heat radiation from quadrillions of radiating particles of isothermal symmetrical radiating volumes is discovered.

The uniqueness, harmony, consistency of heat radiation from quadrillions of radiating particles is that the average beam path length from these particles is equal to the arithmetic mean distance from the calculated area to the symmetry axis of the particles.

Complex triple integration within the gas volume to determine the average beam path length [1], that doesn't have the solution is reasonably replaced by simple arithmetic operations of addition and division, the result, which would have received in triple integration is obtained.

As a result of harmonious coherent heat radiation of quadrillions of particles radiating isochoric isothermal coaxial cylinder gas volumes, radiation flux densities, angular radiation coefficients of gas volumes are equal and for their definition it is sufficient to carry out a single integration of trigonometric functions within the height of the cylindrical volume along the axis of their symmetry.

On the basis of the scientific discovery a new concept and method for calculating heat transfer in furnaces, fire boxes, combustion chambers is developed [4-6]. The new concept and method for calculation included in the textbook [7], which was approved by Educational Association of Ministry of Education and Science of the Russian Federation for training university students in metallurgical and energy specialties. The tutorial [7], as well as a monograph of 1992 [8] are used in metallurgical and energy companies for selection the rational heat conditions of the operating and constructed electric arc and torch furnaces, fire boxes, combustion chambers.

The new concept and method for calculating heat transfer in furnaces, fire boxes, combustion chambers allow thousands of researchers and engineers in dozens of countries worldwide to save millions of tons of gaseous, liquid, pulverized fuel.

Fuel saving is achieved by selection of rational sizes and location of the burner torches, optimization of heat conditions in the operating constructed furnaces, fire boxes, combustion chambers.

This statement is confirmed by the following facts. Currently, about 40% of the steel in the world is melted in arc steel melting furnaces (ASFs). Until 1978, arc steel melting furnace (ASF) represented a "black box", uninvestigated phenomenon, qualitative method for calculating heat transfer in ASFs was not available.

In 1978-82 years the author developed geometric, physical, mathematical model of the electric arc, the main source of energy in the ASF as ionized gas radiating cylinder gas volume [9, 10].

Electric arc model as a radiant heat source was defended by the author of this article in 1982 at Moscow Power Institute in the form of a master's thesis.

In 1983-92's, the author of this article developed experimental investigations in metallurgical plants of Russia: Severstal, Chelyabinsk, Orsk-Khalilov, Oskol Electric and others.

The theory of heat transfer and the results from experimental researches are defended by him in the form of a doctoral thesis at St. Petersburg Electrotechnical University in 1995.

The results from theoretical and practical studies of heat transfer in ASFs are published in 1992 in Moscow publishing house "Energoatomisdat" in the form of a monograph "The optimal thermal conditions of ASFs" [8]. Since 1992 the monograph has been a major reference book on heat transfer in ASF within Russian metallurgists, as well as teachers and students of metallurgical faculties of universities.

Over 60-hundred-ton electric arc furnaces with a capacity of 90 MW are installed at Russian metallurgical plants with a productivity rate of 1 million ton of steel each.

At the end of the 1980s the specific energy consumption in these furnaces was 450-460 kWh, the total consumption of a furnace was 450-460 million kWh per year.

By 2015, due to technological factors and the proper organization of heat transfer, the specific energy consumption in these furnaces has decreased to 350-360 kWh, total energy consumption has decreased to 350-360 million kWh per year by a furnace.

Energy saving is 100 million kWh per year for a furnace.

Some of the credit for energy savings at metallurgical plants, reduction fuel consumption for the production of this energy belongs to the author of this article, the developer of rational methods of calculating heat transfer in electric arc furnaces. The developer of the new concepts and techniques with students continue to develop new cost-effective ways for smelting steel in ASFs [11].

In 2001-16 the author continued investigation of heat radiation from torches of furnaces, burners, combustion chambers, symmetrical radiating gas volumes. In the years 2014-16 the author of this article discovered the laws of

heat radiation from isochoric isothermal concentric spherical gas volumes.

This article informs the scientific community about scientific discovery and practical use of it in heat transfer calculations in furnaces, fire boxes, combustion chambers.

2.2. Laws of Heat Radiation from Spherical Gas Volumes.

In accordance with the new concept and the method for calculation radiating cylinder gas volumes, from which the calculation of radiation fluxes on the calculated areas and heating surfaces is performed, inscribe in torches.

However, torches, gas radiating volumes may have a complex three-dimensional form, which cylindrical gas volumes cannot fulfill. The parts of the gas torch volume, which radiation are not included in the calculations, remain unfilled.

To increase the accuracy of calculations and further filling of gas radiating volumes, the author studied heat radiation of spherical gas volumes in 2010-16.

During the study of heat radiation from spherical gas volumes, the scientific laws for heat radiation was discovered. The essence of scientific discovery is in the following.

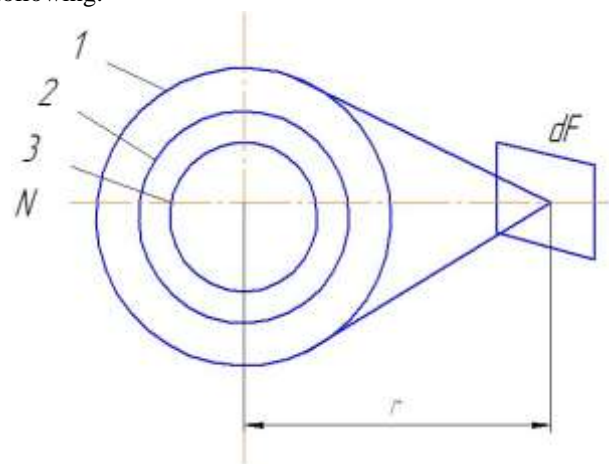


Fig.1: The radiation from spherical gas volume on the calculated area dF .

Consider the radiation from isothermal spherical gas volume of diameter $D_1 = 3\text{m}$ on the calculated area dF , sizes $0,5 \times 0,5\text{m}$ located on a vertical surface at a distance $r = 3\text{m}$ from the spherical gas volume (Fig. 1).

Perpendicular N to the area dF passes through the center of spherical gas volume. For example, $15 \cdot 10^{15}$ atoms, uniformly filling the volume, radiate in spherical gas volume at the same time. The power, radiated by the gas volume is $P = 42\text{ MW}$ [2], the volume of gas confined in the sphere is $V = \pi D^3 / 6 = 14,13\text{ m}^3$.

Divide isothermal spherical gas volume into three equal volume spherical volumes with a common center. The diameter of the first spherical volume is $D_1 = 3\text{m}$, the second is $D_2 = 2,62\text{m}$, the third is $D_3 = 2,08\text{m}$.

The volume of radiating isothermal gas in each space between 1 and 2, 2 and 3, and also within the third sphere is $V_1 = V_2 = V_3 = V / 3 = 4,71\text{m}^3$. We got three isochoric isothermal concentric spherical gas volumes that radiate on the calculated area dF .

Assume, that the radiation from inner layers of concentric spherical gas volumes is absorbed by neighbor layers and radiation from only external surface layer of spheres of gas spaces goes outward.

In this case, the isochoric isothermal radiation from three concentric spherical gas volumes can be represented by radiation from three spheres F_1 - F_3 .

Formulas for calculating angular radiation coefficients from one surface to another were obtained in the 20th century [3, 12].

Angular radiation coefficient φ_{dFF} of dF area on the sphere F is determined by the expression [12]:

$$\varphi_{dFF} = \frac{\cos\alpha}{H^2}, \quad (1)$$

where α is the angle between the perpendicular N to the center area dF and the ray connecting the center of the area and sphere; $H = r / (D / 2)$.

Elementary angular radiation coefficients of concentric spheres to the area dF 1-3 are defined as follows:

$$\begin{aligned} \varphi_{F_1dF} &= \frac{\varphi_{dFF_1} F_{dF}}{F_1} = \frac{0,25 \cdot 0,25}{3,14 \cdot 3^2} = 0,0022; \\ \varphi_{F_2dF} &= \frac{\varphi_{dFF_2} F_{dF}}{F_2} = \frac{0,189 \cdot 0,25}{3,14 \cdot 2,62^2} = 0,0022; \quad (2) \\ \varphi_{F_3dF} &= \frac{\varphi_{dFF_3} F_{dF}}{F_3} = \frac{0,121 \cdot 0,25}{3,14 \cdot 2,08^2} = 0,0022, \end{aligned}$$

where φ_{dFF1} , φ_{dFF2} , φ_{dFF3} – angular radiation coefficients of dF area on the spheres 1-3, respectively; F_{dF} - the area of dF platform; F_1 - F_3 – the area of spheres 1-3.

From the calculation results (2) follows the first law of heat radiation from isochoric isothermal concentric spherical gas volumes: "Elementary angular radiation coefficients of isochoric isothermal concentric spherical gas spaces, layers are equal."

Angular coefficients of radiation are the main design quantities of radiative heat transfer in furnaces, fire boxes, combustion chambers.

When modeling the radiation from hundreds and thousands of concentric spheres, including in the volume of the first sphere, we would get the same result: elementary angular radiation coefficients of concentric gas layers are equal.

From the first law follows, that when calculating angular radiation coefficients φ_{vdF} of isochoric isothermal concentric gas spaces we need not solve triple integral, similar to that described in [1]:

$$\varphi_{vdF} = \iiint_V \frac{\cos\alpha_i \cos\beta_i}{2\pi^2 l_i^2} d\alpha d\beta dl \quad (3)$$

From the first law follows, that for the calculation of the angular radiation coefficients of isochoric isothermal concentric gas volumes it is sufficient to determine the angular radiation coefficient of concentric spherical gas volume of infinitesimal diameter that is, perform a single integration.

Let us calculate the heat radiation flux density incident on the calculated area dF from isochoric isothermal concentric spherical gas layers, which emits radiation power $P_1 = P_2 = P_3 = 42/3 = 14\text{MW}$. We accept the parameters of gaseous medium inherent to steam boiler box, coefficient of absorption of the gas medium $k = 0.162$ [2.7]. The results from calculation of radiation flux densities of concentric spherical gas layers to the calculated area dF :

$$\begin{aligned} q_{F_1dF} &= q_{F_2dF} = q_{F_3dF} = \frac{\varphi_{F_1dF} P_1}{F_{dF}} e^{-kl_1} = \\ &= \frac{\varphi_{F_2dF} P_2}{F_{dF}} e^{-kl_2} = \frac{\varphi_{F_3dF} P_3}{F_{dF}} e^{-kl_3} = \\ &= \frac{0,0022 \cdot 14 \cdot 10^3}{0,25} e^{-0,162 \cdot 3} = \\ &= \frac{0,0022 \cdot 14 \cdot 10^3}{0,25} e^{-0,162 \cdot 3} = \\ &= \frac{0,0022 \cdot 14 \cdot 10^3}{0,25} e^{-0,162 \cdot 3} = \\ &= 76,1 \text{ kW} / \text{m}^2 \end{aligned} \quad (4)$$

where $l_1 = l_2 = l_3 = l$ – average beam path length of 1 – 3 spherical layers to the calculated area.

Average beam path length l_{av} is determined as arithmetic mean distance from elementary particles, atoms, which

surfaces of spheres consisted of to the calculated area dF [1].

Average beam path length of any spherical gas layer equals to arithmetic mean distance from the center of symmetry of concentric spheres to the calculated area. From the calculation results (4) follow another two laws of radiation from isochoric isothermal concentric spherical gas layers, spaces.

The second law:

«Average beam path length from isochoric isothermal concentric spherical gas volumes, layers to the calculated area equals the distance from ball centers to the calculated area»:

$$l = l_1 = l_2 = l_3 = r \quad (5)$$

The third law: «Radiation flux densities, incident on the calculated area from isochoric isothermal concentric spherical gas coaxial volumes, layers, which arc and torch consisted of are equal».

Total radiation flux densities incident from three isochoric isothermal concentric spherical gas volumes, layers on dF area is determined according

to the principle of superposition, summation of radiation fluxes incident:

on the calculated area from individual sources of heat radiation [12]:

$$q_{FdF} = \sum_{i=1}^3 q_{F_i dF} = 228,3 kW / m^2 \quad (6)$$

Assume, that radiating power $P=42$ MW is generated in the third spherical gas space. Let find the heat radiation flux density of the third spherical gas volume on dF area:

$$q_{F_3 dF} = \frac{\varphi_{F_3 dF} P}{F_{dF}} e^{-k_3} = \frac{0,0022 \cdot 42 \cdot 10^3}{0,25} e^{-0,162 \cdot 3} \quad (7)$$
$$= 228,3 kW / m^2$$

The fourth law of heat radiation from isochoric isothermal concentric spherical gas spaces, layers is evident from the calculated data by equations (6) and (7):

«Total heat radiation fluxes density incident on calculated area from several radiative and absorbing isochoric isothermal concentric spherical gas spaces equals radiation flux density of concentric spherical gas space of small diameter on calculated area at radiating power, released in it that equals total radiated power, released in all concentric spherical gas spaces radiating on the calculated area»:

$$q_{F_3 dF} = q_{FdF} = \sum_{i=1}^3 q_{F_i dF} \quad (8)$$

The disclosed laws of heat radiation from isochoric isothermal concentric spherical gas spaces allow researchers, designers, calculate the heat fluxes, the average beam path length, the angular radiation coefficients of the gas spaces of any complex volume form, inscribing spherical volumes in them. An example of such a calculation is given in the second part of the article.

III. CONCLUSION

The laws of heat radiation from isochoric isothermal concentric spherical gas volumes are disclosed. Dozens, hundreds spheres of large, medium, small or infinitely small diameter can be inscribed in gas volumes depending on the complexity. Concentric spherical with coaxial cylindrical gas volumes can entirely fill radiating gas volumes of any complex volume form and calculate heat radiation from gas volumes to the heating surfaces with high accuracy.

REFERENCES

- [1] A.N. Makarov “Modeling of a Torch and Calculation of Heat Transfer in Furnaces, Fire Boxes, Combustion Chambers. Part I. Calculation of Radiation from Solids and Gas Volumes by the Laws of Radiation from”, International Journal of Advanced Engineering Research and Science, Vol. 3, №12, pp. 44-48, 2016, DOI: 10.22161/ijaers/3.12.9
- [2] A.N. Makarov “Modeling of a Torch and Calculation of Heat Transfer in Furnaces, Fire Boxes, Combustion Chambers. Part II. Calculation of Radiation from Gas Volumes by the Laws of Radiation from Cylinder Gas Volumes”, International Journal of Advanced Engineering Research and Science, Vol. 3, №12, pp. 49-54, 2016, DOI: 10.22161/ijaers/3.12.10
- [3] R.Siegel, Y.Howell “Thermal Radiation Heat Transfer”, Mir, Moscow, 934p., 1975.
- [4] A.N. Makarov “Calculation of Heat Transfer in Torch Furnaces by Gas Volume Radiation Laws”, World Journal of Engineering and Technology, №4, pp. 488-503, 2016. DOI: 10.4236/wjet.2016.43049
- [5] A.N. Makarov “Theory of radiative heat exchange in furnaces, fire boxes, combustion chambers is replenished by four new laws”, Science Discovery, №2, pp. 34-42, 2014. DOI: 10.11648/j.sd.20140202.12
- [6] A.N. Makarov “Flare Temperature and Nitrogen Oxide Emission Reduction in the TGMP-314I Steam Boiler Firebox”, Power Technology and Engineering,

- Vol. 50, №2, pp. 200-203, 2016. DOI: 10.1007/S10749-016-0683-x
- [7] A.N. Makarov “Heat transfer in electric arc and torch metallurgy furnaces and energy plants: textbook”, Lan’, St-Petersburg, 384p., 2014.
- [8] A.N. Makarov, A.D. Svenchanskii “Optimal Operating Conditions of Arc Steel Melting Furnaces”, Energoatomizdat, Moscow, 96p. 1992
- [9] A. N. Makarov, A. D. Svenchanskii, (1992) “Determining heat fluxes of arcs in Arc Steel Melting Furnaces”, Electrotermiya, №6, pp. 6-8, 1982.
- [10] A.N. Makarov, A.D. Svenchanskii « The calculation of the reflected component of the irradiation lining from arcs in ASFs», Electrotermiya, №5, pp. 1-2, 1983.
- [11] A.N. Makarov, V.V. Rybakova, M.K. Galicheva “Electromagnetism and the Arc Efficiency of Electric Arc Steel Melting Furnaces”, Journal of Electromagnetic Analysis and Applications, №9, pp. 184-192, 2014. DOI: 10.4236/jemaa.2014.67018
- [12] A.G. Blokh, Yu.A. Zhuravlev, L.N. Pyzhkov “Radiant Heat Transfer: A Handbook”, Energoatomizdat, Moscow, 432p., 1991.

Laws of heat radiation from spherical gas volumes.

Part II. Modeling of heat radiation from volume bodies by radiation from spherical and cylindrical gas volumes

Prof. Dr. A. N. Makarov

Department of Electrical Supply and Electrical Engineering, Tver State Technical University, nab. Afanasiya Nikitina 22, Tver, 170026 Russia

Abstract—The results stemming from mathematical modeling of radiation from gas volumes of torches of furnaces, fire boxes, combustion chambers by spherical and cylindrical gas volumes are presented. The calculation results in the simulation of torches by cylindrical and spherical gas volumes differ by 0,4-2,3%. The calculation of radiation fluxes from torch on a heated product and burner throat in changing the length of the torch is performed, the results from the calculation are given.

The density of radiation flux from torch on the burner throat and the burner increases with decreasing the torch length. The calculation results are confirmed by experimental data. Using the laws of radiation from cylindrical and spherical gas volumes, the laws of Makarov and method for calculation heat transfer in furnaces, fire boxes, combustion chambers, developed on their basis, allow to improve exploited and projected flares, improve capacity utilization of fuel in furnaces from 20-45% to 55 -65%, reduce fuel consumption in many countries, development pressure on the environment.

Keywords— *Scientific Disclosure, Laws, Heat radiation, Torch, Fuel Use Efficiency.*

I. INTRODUCTION

The laws of heat radiation from isochoric isothermal concentric spherical gas volumes, which are called Makarov's laws for the purpose of adhering to centuries-old traditions of science and copyright. According to these laws: "The average beams from quadrillions of radiating particles of each isochoric isothermal concentric spherical gas volume to the calculated area equal to the distance from the center of the sphere to the calculated area and angular radiation coefficients, radiation flux densities from are equal.

Heat radiation flux density of the central spherical gas volume of a small diameter equal to the total power, radiated in all concentric spherical gas volumes to the calculated area. "

The volume model of the atom presents the nucleus in the form of spherical volume and electrons, which orbit in a concentric with nucleus spherical paths. Therefore, gas volumes, the torches of any complex shape can be filled with the spherical gas volumes of small and infinitely small diameter and their heat radiation can be calculated with high precision. Let us model the radiation from the part of torch that represents isothermal volume of rectangular parallelepiped [1.2], spherical and cylindrical gas volumes.

II. MATHEMATICAL MODELING OF HEAT RADIATION FROM GAS VOLUME

2.1. Mathematical modeling of heat radiation from gas volume by the radiation from cylindrical and spherical gas volumes.

Consider the radiation from the part of torch volume, that represents isothermal gas volume 1 in the form of rectangular parallelepiped of $a \times b \times h = 3 \times 3 \times 3$ meter [1.2] on the calculated area dF of the area $F = 0,5 \times 0,5 = 0,25$ m² (Fig. 1).

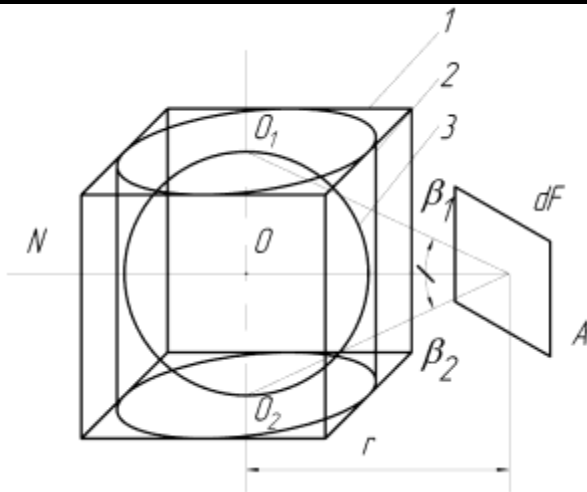


Fig.1: Modeling of heat radiation from gas volume in the form of rectangular parallelepiped by the radiation from cylindrical and spherical volumes.

Inscribe cylinder gas volume 2 of diameter 3 m, height $l_2 = 3$ m and spherical gas volume 3, 3 m in diameter in the rectangular parallelepiped 1.

Each of 1-3 gas emits $15 \cdot 10^{15}$ atoms at the same time, uniformly filling the volumes.

Perpendicular N, dropped to the center A of the area dF passes through the center of the symmetry O of the sphere 3 and the symmetry axis of cylinder gas volume 2 and bisects the symmetry axis O_1O_2 of the rectangular parallelepiped 1 and the cylinder 2 between their upper and lower bases.

The distance between the point O and the center of area symmetry dF is $r = 3$ m. Fig. 1 shows the following notation of angles: $\angle O_1AO = \beta_1$, $\angle O_2AO = \beta_2$, $\beta_1 + \beta_2 = \beta$. Each of the radiating gas volume releases equal radiation power $P_1 = P_2 = P_3 = 42$ MW, the absorption coefficient of the gas medium $k = 0.162$ [2].

The density of heat radiation flux incident on the calculated area dF from radiating cylindrical gas volume 2 is determined by the expression [2]:

$$q_{2dF} = \varphi_{2dF} P_2 F^{-1} e^{-kl_2} = \frac{FP_2 e^{-kl_2}}{F^2 \pi^2 l_y} \left[\beta + \sin \beta \cos(\beta_1 - \beta_2) \right] = \dots (1)$$

$$= \frac{0,2542 \cdot 10^3 \cdot e^{-0,1623 \cdot 11}}{0,252 \cdot 3,14^2 \cdot 3 \cdot 3} \left[\frac{52}{57} + \sin 52^\circ \cos 0^\circ \right] = 217,1 \text{ kW/m}^2$$

The first part of this article addresses the calculation of heat radiation flux density incident on the calculated area dF from spherical gas volume:

$$q_{3dF} = \varphi_{3dF} P_3 F^{-1} e^{-kl_3} = \frac{0,0022 \cdot 42 \cdot 10^3 \cdot e^{-0,162 \cdot 3}}{0,25} = 228,3 \text{ kW/m}^2 \quad (2)$$

In the process of calculation of heat radiation fluxes incident on the calculated area dF from cylindrical and spherical gas volumes, we obtained the results, that differ by no more than 5%. The difference Δ in the results of the calculations we determine by the expression:

$$\Delta = \left(1 - \frac{q_{2dF}}{q_{3dF}} \right) \cdot 100 = \left(1 - \frac{217,1}{228,3} \right) \cdot 100 = 4,9\% \quad (3)$$

Calculation accuracy of heat radiation flux density incident on the calculated area dF from gas volume in the form of a rectangular parallelepiped can be improved, provided that several tens of spherical gas volumes would be inscribed in it.

2.2. Mathematical modeling of heat radiation from gas volume by radiation of 216 spherical gas volumes.

Inscribe uniformly spherical gas volumes of 0.5 m diameter into the gas volume in the form of a rectangular parallelepiped (Fig. 2).

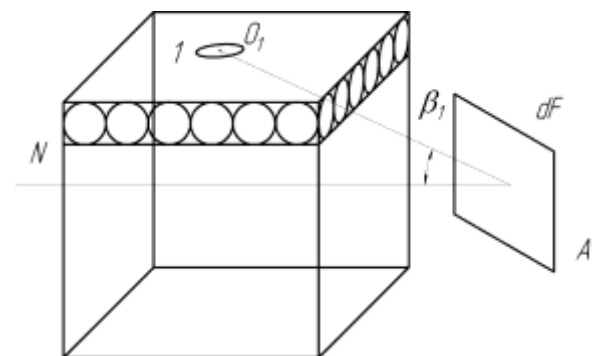


Fig. 2. Modeling of heat radiation from gas volume by 216 spherical gas volumes.

$$P_1 = P_2 = P_3 = \dots = P_{216} = 42 \cdot 10^3 / 216 = 194,4 \text{ kW}$$

Inscribe 6 rows of spheres along the height of parallelepiped, 36 spheres in each row, 216 spheres in total (Fig. 2). Each of 216 spherical releases the radiation power equal to $P_1 = P_2 = P_3 = \dots = P_{216} = 42 \cdot 10^3 / 216 = 194,4 \text{ kW}$.

In [3] it is derived a generalized analytical expression for calculating elementary angular coefficient of radiation from sphere of a small diameter to any calculated area, arbitrarily located in space.

For example, the formula for calculating the elementary angular coefficient of radiation from spherical gas volume 1, located in the center of the top row of the spheres

inscribed in parallelepiped on the area (Figure 2) has the form [3]:

$$\varphi_{1dF} = \frac{F \cos \beta_1}{4\pi l^2}, \quad (4)$$

where $\angle OAN = \beta_1$ is the angle between the perpendicular to the area dF and the ray OA , connecting the center of the area and the sphere 1; $AO = l$ is the distance between the center of the area dF and the sphere 1; F is the area of the platform dF .

Since, according to the law of Makarov, the elementary angular coefficients of radiation from isochoric isothermal concentric spherical gas volumes are equal, then using the expression (4), we can calculate the angular radiation coefficients of spherical radiation sources of infinitely small diameter on the calculated area as well as spherical giant radiation sources, such as heavenly stars, stars.

In the future, during long space flights, it will be important to know how far a spacecraft can move closer to the star without the risk of thermal destruction. The disclosed laws allow to calculate the heat fluxes incident on the hulk from the star at any distance to it, and the spatial position of the ship.

We determine the elementary angular coefficient of radiation from spherical gas volume of 1 on the calculated area dF (Figure 2.)

$$\varphi_{1dF} = \frac{F \cos \beta_1}{4\pi l_1^2} = \frac{0,25 \cdot \cos 18^\circ}{4 \cdot 3,14 \cdot 3,2^2} = 0,0018 \quad (5)$$

The density of heat radiation flux incident on the calculated area dF from the spherical gas volume 1 we determine by the expression:

$$q_{1dF} = \varphi_{3dF} P_1 F^{-1} e^{-kl_1} = \frac{0,0018 \cdot 194,4}{0,25 \cdot e^{0,1623,2}} = 0,833 \text{ kW/m}^2 \quad (6)$$

Similarl

y, we define the densities of heat radiation fluxes incident on the calculated area dF from each of the 216 spherical gas volumes that fill a rectangular parallelepiped.

To automate the calculations, we used the program for calculating the angular coefficients of radiation and the radiation flux densities on a computer.

The total density of radiation fluxes $q_{\Sigma 216}$, incident on the area dF from 216 spherical gas volumes is determined by summing the radiation flux densities from 216 spherical gas volumes.

$$q_{\Sigma 216} = \sum_{i=1}^{216} q_{idF} = 212,2 \text{ kW/m}^2 \quad (7)$$

Compare

the results from (1), (2), (7) of modeling heat radiation from gas volume in the form of rectangular

parallelepiped by cylinder (1), spherical (2) gas volumes and 216 spherical gas volumes (7).

The most accurate results is presented in (7), as 216 inscribed spherical gas volumes fulfill the volume of a rectangular parallelepiped.

Calculation results from modeling heat radiation of gas volume in the form of rectangular parallelepiped by cylindrical gas volume have an error $\Delta_{cy1} = (1-212,2 / 217,1) \cdot 100 = 2,3\%$, a spherical gas volume $\Delta_1 = (1-212,2 / 228,3) \cdot 100 = 7,1\%$.

Thus, the heat radiation from gas volume in the form of rectangular parallelepiped can be modeled by the radiation from cylindrical gas volume inscribed in it, as the calculation error does not exceed 3%.

Heat radiation from gas volume in the form of a rectangular parallelepiped is not recommended to model by spherical gas volume inscribed in it since calculation errors exceed 7%.

The smallest error in the results of calculations from the true value of heat radiation density from gas volume in the form of a rectangular parallelepiped on the calculated area is achieved in modeling the radiation of parallelepiped by a few dozen spherical gas volumes inscribed in it.

To increase the number of inscribed in rectangular parallelepiped spherical gas volumes up to several hundreds or thousands of spheres is inappropriate, as this increases the number of computing operations, and the accuracy of calculations increases by tenths of a percent, namely (0,1- 0,8)% in comparison with the actual value of the radiation flux.

The preceding is confirmed by the following calculations confirm.

2.3. Mathematical modeling of heat radiation from gas volume by radiation of 15, 108, 432 spherical gas volumes.

Inscribe 15 spherical gas volumes 1 m in diameter each in a rectangular-parallelepiped gas volume in three rows I-III along the height and of 5 spherical gas volumes each (Fig. 3).

$$q_{2dF} = \frac{P_2 \cos \beta_2}{4\pi l_2^2} e^{-kl_2} = \frac{2,8 \cdot 10^3 \cdot \cos 40^\circ}{4 \cdot 3,14 \cdot 3,8^2} e^{-0,1623,8} \dots (8) \\ = 6,4 \text{ kW/m}^2$$

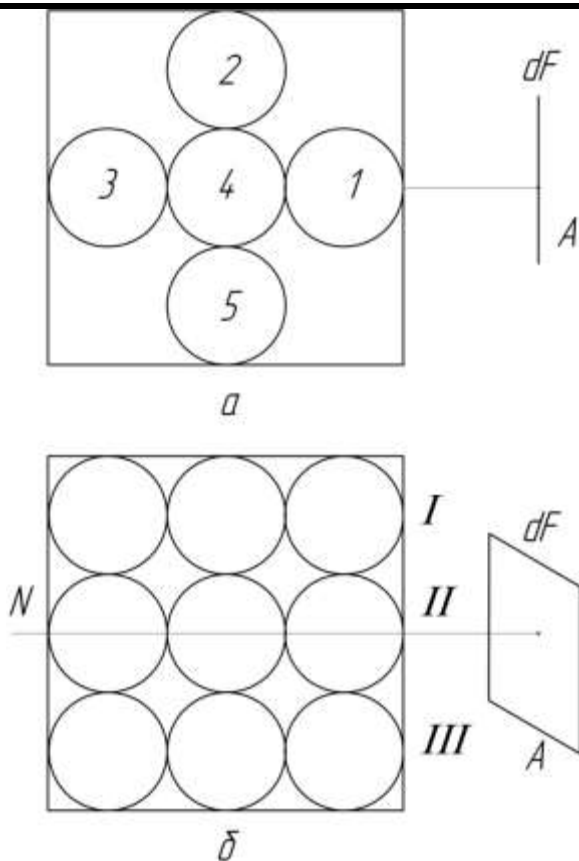


Fig.3: Modeling of heat radiation from gas volume by 15 spheres of gas volume, a - top view; b - front view. Each of the 15 spherical gas volumes radiate an equal radiation power $P1=P2=P3=...=P15=42 \cdot 103/15=2.8$ MW.

We denote by 1-5 spherical gas volumes of the first row. Substituting (4) into (6), we will calculate heat radiation flux densities incident on the calculated area dF from spherical gas volumes 1-3 (Fig. 3):

$$q_{1dF} = \frac{P_1 \cos \beta_1}{4\pi_1^2} e^{-k_1} = \frac{2,8 \cdot 10^3 \cdot \cos 27^\circ}{4 \cdot 3,14 \cdot 2,2^2} e^{-0,162 \cdot 2,2} = 28,7 \text{ kW/m}^2 \quad \dots(9)$$

Similarly, we determine heat radiation flux densities incident on the calculated area dF from 4-15 spherical gas volumes.

By eq. (7) we determine the total radiation flux density from 1-15 spherical gas volumes on the calculated area dF:

Calculated area dF:

$$q_{3dF} = \frac{P_3 \cos \beta_3}{4\pi_3^2} e^{-k_3} = \frac{2,8 \cdot 10^3 \cdot \cos 14^\circ}{4 \cdot 3,14 \cdot 4,2^2} e^{-0,162 \cdot 4,2} = 6,22 \text{ kW/m}^2$$

...(10)

$$q_{\Sigma 15} = \sum_{i=1}^{15} q_{idF} = 207,5 \text{ kW/m}^2 \quad \dots (8)$$

Calculate the error of calculation in modeling of heat radiation from gas volume in the form of rectangular parallelepiped by 15 spherical gas volumes: $\Delta 15 = (1 - 207,5 / 212,2) \cdot 100 = 2.2\%$.

Similarly, we modeled heat radiation from rectangular parallelepiped by 108 and 432 spherical gas volumes. As a result of calculations, we obtained the following values of total radiation flux densities incident on the calculated area dF from spherical gas volumes:

$$q_{\Sigma 432} = \sum_{i=1}^{432} q_{idF} = 213,1 \text{ kW/m}^2 \quad (12)$$

$$q_{\Sigma 108} = \sum_{i=1}^{108} q_{idF} = 210,3 \text{ kW/m}^2 \quad (13)$$

Miscalculation in modeling heat radiation from gas volumes in the form of parallelepiped by 108 and 432 spherical gas volumes equal to, respectively: $\Delta 108 = (1 - 210,3 / 212,2) \cdot 100 = 0,9\%$, $\Delta 432 = (1 - 212,2 / 213,1) \cdot 100 = 0,4\%$.

Miscalculation in modeling heat radiation from gas volume in the form of parallelepiped by one cylindrical gas volume is 2.3%, one spherical gas volume is 7.1%, 15 spherical gas volumes is 2.2%, 108 spherical gas volumes is 0.9%, 432 spherical gas volumes is 0.4%.

Thus, gas volume in the form of parallelepiped can be modeled by cylindrical gas volume, one-two hundred spherical gas volumes and obtain the results from calculations with high accuracy.

III. CALCULATIONS OF HEAT RADIATION FROM THE TORCH ON THE HEATING SURFACES

3.1. Calculation of heat radiation from torch on the surface of products and burner throat.

The torch is used in heating furnaces, fire boxes, steam boiler boxes and combustion chambers of gas-turbine power plants[1-4].

Torch, created by a single burner, is an ellipsoid of revolution, which burns the fuel, supplied to the burner [1-4]. Torch length is the distance from the burner, at which at least 98% of the fuel is burnt. To calculate heat radiation from torch on the heating surfaces, it is necessary to solve triple integral equations, describing volume radiation from torch. In the 20th century the

solution for triple integral equations in the form of analytical expressions, formulas was not found [1]. However, the disclosure in the late 20th century of the laws for heat radiation from cylindrical and spherical gas volumes, laws of Makarov and the methods for calculation, developed on their basis, allow to simulate the torch by a set of cylindrical and spherical gas volumes and calculate the fluxes of the heat radiation incident on the heating surface from the torch [1- 4].

The developed method of heat transfer in torch furnaces allows to calculate the rational fuel consumption, the location of the burners and the rational parameters of the torch: length, power and its distribution over the length, the spatial position in the furnace, the angle of torch. We use the results from analytical studies to calculate the torch radiation fluxes incident on the heating surfaces in the torch furnace.

Investigate the effect of torch length on the distribution of heat radiation fluxes along the heating surface.

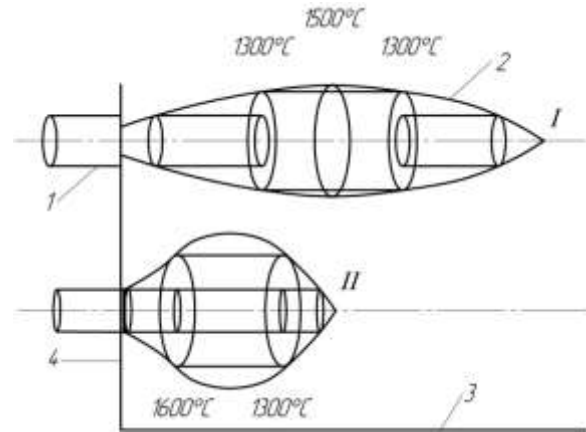


Fig. 4: Location of the torch in the furnace.

Fig. 4 shows a portion of the working space of the heating furnace and we used the following notations: 1 - burner; 2 - torches I and II; 3 - the horizontal surface of the heated product; 4 – the vertical lined wall of furnace with burner throat.

Burners are located in the wall embrasures. Torch length I $l_{I1} = 8\text{m}$, torch length II $l_{I2} = 3\text{m}$, torches power is the same and equal to 5 MW.

The axes of the torches I and II are in the same vertical plane with the axis of symmetry of the product and parallel to the horizontal surface of the product 3 and removed from it at a distance of 0.8m.

In order for torches I and II to not combine torches into one, Fig. 4 uses a different scale of their location on the vertical wall 4.

In accordance with the location of isotherm of 1300, 1500 °C, the torch I is modeled by four cylinder gas volumes, the torch II is simulated by three cylindrical gas volumes in calculations.

According to the method, described in [2-4], as well as in the first part of the monograph, we calculated heat radiation flux densities of torches I and II incident on the horizontal surface along the length of the product l_p and vertical surface along the height of embrasures H_e . The calculation results are shown in Fig. 5.

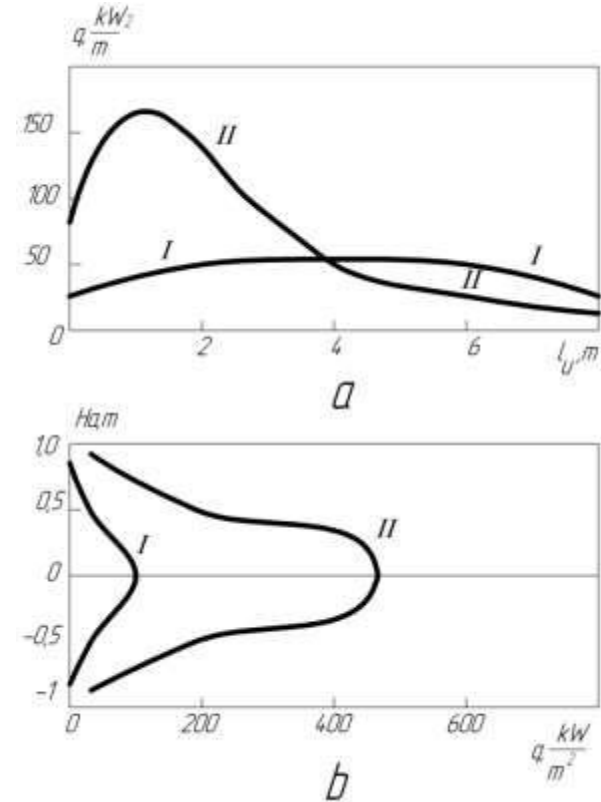


Fig.5: The distribution of the heat fluxes from the torch along the horizontal surface (a) and embrasure surface (b).

As can be seen from the results of calculations, the distribution of the heat radiation flux densities from the torches depends heavily on their geometric dimensions: length and expansion angle.

The distribution of heat radiation fluxes incident on the surface of the product from the torch I 8 m in length is uniform: 28 kW/m² is on the periphery, 57 kW/m² is in the center.

With the decrease of the torch length at its constant capacity, the densities of radiation fluxes on the product regions, located near the walls and burner throat increase 2-3 times, and decrease 3-5 times on the regions distant from the burner throat.

With the length of the torch 3m, the torch radiation flux densities on the product is 165 kW/m² at a distance of 1m from the vertical wall, at a distance of 8 meters from a vertical wall is 5 kW/m².

Radiation flux densities incident on the burner throat and the burner increase with the changes in the torch length. With the torch length of 8m and 3m, the flux density

incident on the burner throat and the burner along its is 78 kW / m² and 520 kW / m² ,respectively and decreases sharply along the height of the burner throat.

The calculation results are confirmed by experimental data [5,6]. The long experience of operation of steam boilers TGMP-314TS with cyclone burners of 50-60MW at power plants CHP-21, Mosenergo CHP-23, Konakovo DWP and other power plants with short torches deepened in the burner throat showed frequent burnout of burners, refractories destruction of burner throat, that is connected with large fluxes of heat radiation from the torch on the burner throats and burners.

After the reconstruction of boilers, installation of gas-oil burners and increase the torch length 2 times, the service life of the burners was increased from 1 year up to 5-10 years and more [5,6], that is connected with a decrease in heat fluxes from the torch on the burner, a decrease in the temperature of metal of the burners, refractories of the burner throat.

Similar results were obtained by the calculation . Thus, the results from the calculations are confirmed by the results of experimental studies of the effect of the torch length on the heating fluxes, thermo destruction and burners life [5,6].

3.2. Using the laws of heat radiation from cylindrical and spherical gas volumes in the practice of the operation and design of torch furnaces, combustion chambers.

Using the laws of heat radiation from cylindrical and spherical gas volumes, laws of Makarov and method for calculating heat transfer in torch furnaces, combustion chambers, developed on their basis, allow to improve the exploited and designed flares.

Torch furnaces is widely used in metallurgy and in all branches of industry: heavy, chemical, nuclear, energy, transport and other industries, as well as in glass, ceramic, porcelain industry, autoindustry.

Flare furnaces are used in these industries for heating products before plastic deformation (forging, stamping, pressing), heat treatment of products (hardening, annealing, tempering, carburizing, nitriding, normalizing, austenitizing) and drying products.

Flame box furnaces, single-stack furnaces, rotary-hearth furnaces, roller-hearth furnaces, tunnel-type furnaces, continuous furnaces, pusher-type furnaces with product-loading mass of 100kg to 120 tons with a burners capacity of 10kW to 50MW are used for heating and heating treatment of products.

In the 20th century due to the lack of triple solutions of integral equations, describing the volume radiation from the torch, parameters of torches and their location in the furnaces were determined largely experimentally on test

stands and operating furnaces, fire boxes, combustion chambers.

The operating and designed heating furnaces have short torches, often placed irrationally, far from the heated products. Torches are placed away from the heated products to cause no melting of products surface. Torches are placed so as to heat fire-resistant surfaces of walls, arch, hearth, and heated fire-resistant surfaces radiate heat flux on the products, heating them [4], however, such organization of heat transfer causes conductive heat losses through the walls, arch, hearth of the furnace.

It is assumed, that the products are heated by combustion products, gases leaving the torch and filling the working space of the furnace.

However, the calculations showed, that the proportion of the heat flow incident on the heating surface [4] from the combustion products is 5-7% of the total heat flux. As a result of such organization of heat transfer, fuel efficiency in torch furnaces is 25-45% at this time [7].

The use of scientific discovery and calculation methods, developed on its basis, allow to determine the following rational parameters of the torch, burners, and products. Rational position of products in the furnaces, the location of the burners, power, expansion angle, the length of the torches, the rational distribution of the torch fluxes densities on the heating surface wherein limit heat fluxes, causing melting of the surfaces of products are not exceeded.

In rational arrangement of the products and burners, the torches, the parameters of torches, fuel efficiency ratio in furnaces can be increased to 55-65%.

Torch of gas turbine combustion chambers has a complicated shape, which depends on the number of burners, swirlers, traffic organization of air, fuel, combustion products [3,8]. The camera has several active zones of fuel combustion, the torches of complex geometric form. Calculation of heat radiation fluxes of the torches on the flame tube, burner, swirlers is a complex scientific task.

Typically, the information of heat radiation fluxes on the heating surfaces of the combustion chamber is obtained by expensive testing of the combustion chamber on the test stands. Scientific discovery of laws of radiation from gas volumes allows to simulate the heat radiation from torches of combustion chambers by cylindrical and spherical gas volumes.

Mathematical modeling allows to calculate the heating and cooling flows of the combustion chamber at the design stage, to organize a rational heat transfer in the chamber, to decrease the testing time and the costs for camera testing on the stands [3].

Modeling steam boiler boxes by cylindrical gas volumes allows to calculate the distribution of radiation fluxes

density along the perimeter of furnace walls, distribute water-cooled surfaces of the torches burners by provided heat quantity and identify the most tense areas to determine the schedule of repairs, to reconstruct the furnaces in order to increase their efficiency [9,10].

Over the last century the use of the laws of radiation from solid bodies, the laws of Stefan-Boltzmann, Planck, Wien in the design of solid furnaces, fire boxes allow to increase fuel efficiency ratio in these plants from 25-30% at the beginning to 70-90% at the end of the 20th century. Similar processes are expected in the 21st century with the design of torch furnaces using the laws of radiation from gas volumes, Makarov's laws. Currently, fuel efficiency in torch furnaces is 25-45%. The use of the laws of radiation from gas volumes in design and calculation of laws of radiation from gas volumes allow to increase the fuel efficiency in torch furnaces from 25-45% to 55-65% in the coming decades.

IV. CONCLUSION

The new concept and method for calculating heat transfer in furnaces, fire boxes, and combustion chambers is developed. In accordance with them cylindrical and spherical radiating gas volumes from which the calculation of heat radiation fluxes on the heating surface is performed, inscribe in the torch.

Heating fluxes of the torch, heated surfaces, combustion products are calculated for heated surfaces, taking into account the reflection and absorption. The calculation error does not exceed 10%.

The new concept and method for calculation allow thousands of researchers and engineers in dozens of countries around the world to create new design of the heating and melting furnaces and power plants.

New constructions of torch furnaces, fire boxes, combustion chambers is expected to increase productivity, fuel efficiency, prolong the time between overhauls, reduce fuel rate, environmental impact.

The author together with his students developed three dozens of new designs of electric arc steel melting furnaces and the ways for steel melting in them [11], torch heating furnaces and the ways for product heating in them [12].

New designs of arc steel melting furnaces and torch furnaces are characterized by a decrease in electricity and fuel consumption, a raise in the productivity.

New designs of steam boiler boxes [9,10] and combustion chambers [13] are developed and characterized by the alignment of the heat flows on the heating surfaces, decrease in fuel consumption, increase in the time between overhauls [14].

REFERENCES

- [1] A.N. Makarov "Modeling of a Torch and Calculation of Heat Transfer in Furnaces, Fire Boxes, Combustion Chambers. Part I. Calculation of Radiation from Solids and Gas Volumes by the Laws of Radiation from", International Journal of Advanced Engineering Research and Science, Vol. 3, No 12, PP. 44-48, 2016, DOI: 10.22161/ijaers/3.12.9
- [2] A.N. Makarov "Modeling of a Torch and Calculation of Heat Transfer in Furnaces, Fire Boxes, Combustion Chambers. Part II. Calculation of Radiation from Gas Volumes by the Laws of Radiation from Cylinder Gas Volumes", International Journal of Advanced Engineering Research and Science, Vol. 3, No 12, PP. 49-54, 2016, DOI: 10.22161/ijaers/3.12.10
- [3] A.N. Makarov "Heat transfer in electric arc and torch metallurgy furnaces and energy plants: textbook", Lan', St-Petersburg, 384p., 2014
- [4] A.N. Makarov "Calculation of Heat Transfer in Torch Furnaces by Gas Volume Radiation Laws", World Journal of Engineering and Technology, No 4, pp. 488-503, 2016. DOI: 10.4236/wjet. 2016. 43049
- [5] A.N. Zroichikov, Yu.P. Enykin B.N. Glusker, I.V. Galas, V.V. Zypkin, N.A.Chuprov, V.A. Vereshagin «Modernization of boilers TGMP-314Z, equipped with cyclone predoplaty to reduce harmful emissions and improve the reliability of operation of burners and heating surfaces», Teploenergetika, No 12, pp.17-21, 2002.
- [6] K.V. Osintsev, "Method of reducing heat flow to the burner throats", Electrichekieskie stancii No 11, pp.13-17, 2009.
- [7] A. M. Vohmykov, M. D. Kazyaev, B. N. Arseev, D. M. Kazyaev, A. I. Ryaposoov "Integrated modification of heating furnaces", Proceedings of the universities. Chernaya Metallurgiya, No 12, pp. 56-59, 2009.
- [8] G. G. Olkhovskiy, "Thermal testing of stationary gas turbine plants", Energiya, Moscow, 406 p., 1971.
- [9] A.N. Makarov, M.N. Shevchenko. Furnace for reducing gas and fuel-oil / Patent for the invention No 2400668, Inventions, №27, 2010.
- [10] A.N. Makarov, F.N. Neverov, A.V. Kyznetsov. Furnace for oil-gas fuel burning / Patent for invention No 2547675. Inventions, №10, 2015.
- [11] A. N. Makarov, E. V. Kruglov, V. V. Rybakov. DC ASF // Patent for the invention №2516896, Inventions, No. 15, 2014
- [12] A.N. Makarov, E.V. Kruglov, V.V. Rybakova. Heating furnace with ring bottom/ Patent for invention №2517079. Inventions, No 15, 2014.
- [13] A.N. Makarov, A.V. Kuznetsov Combustion chambers of turbogas unit / Patent for the useful model No 157527, Inventions, No 34, 2015.

- [14] A.N. Makarov “Flare Temperature and NTitrogen Oxide Emission Reduction in the TGMP-314 I Steam Boiler Firebox”, Power Technology and Engineering, Vol. 50, №2, pp. 200-203, 2016. DOI: 10.1007/S10749-016-0683-x

Design of an Exponentially Weighted Moving Average (EWMA) and An Exponentially Weighted Root Mean Square (EWRMS) Control Chart

Asst. Prof. Dr. Kawa M. Jamal Rashid

College Administration and Economics, University Of Sulaimani, Kurdistan Region, Iraq

Abstract— Some of the most widely-used form of control charts Walter Shewhart charts are sensitive to detecting relatively large shifts in the process.

On Shewhart charts every observation is plotted independently of previous observations. The quantity plotted on Cusum charts include all previous observations;

All of which are given equal weight in calculating the plotted value.

Exponentially Weighted Moving Average (EWMA) charts are a kind of compromise between these two extremes.

The plotted quantity is a weighted average of all the observations to date, but the weights decrease very quickly backwards in time, so that the most recent observations are the main determinants of the current plotting point.[3][4]

A cumulative sums (CUSUM) charts plot the of the deviations of each sample value from a target value. It has been used in various industries (especially the chemical industry)

and the form of the CUSUM has been refined over the years to further increase its sensitivity. Two types of charts are primarily used to detect smaller shifts, namely Cumulative Sum (CUSUM) charts and Exponentially Weighted Moving Average (EWMA) charts. E.S. Page2 (1954) originally developed the CUSUM chart. [2][3]

Geometric moving-average control chart is effective alternatives to the Shewhart control chart may be used when small process shifts are of interest primarily used to detect smaller shifts, namely CUSUM and EWMA charts are excellent alternatives to the Shewhart control chart.

EWMA methodology - developed by S.W. Robert in 1959, he chose the weights to decrease geometrically with the age of the observations, he referred to the control chart based on such a weighting system as a geometric moving – average control chart.

Mac Gregor and Harris (1993) recommend that the square root of EWMS, $SQR(EWMS)$, be plotted. Accordingly, they call the corresponding control chart an exponentially weighted root mean square (EWRMS) chart, The EWRMS statistic will react not only to shifts in the process variance but also shifts in the process mean[4] [8]

Keywords— Exponentially Weighted Moving Average (EWMA)-Chart, exponentially weighted root mean square (EWRMS)-Chart.

I. INTRODUCTION

The control charts namely, Shewart chart (Shewhart, 1924), EWMA chart (Roberts, 1959) and CUSUM chart (Page, 1954) are often used for detecting shifts in a sequence of independent normal observations with common variance coming from a particular process. [1][2][6]

Statistical Quality control methods have a large area of study. In its own right is. Central to success in modern industry with its emphasis on reducing costs while at the same time improving quality, Statistical quality control came from Dr. Walter Shewhart in 1924. He recognized that in a manufacturing process, there will always be variation in the resulting products.

Shewhart developed a simple graphical technique - the control chart - for determining if the product variable is within acceptable limits or not.

The control charts namely, Shewart chart (Shewhart,1924),EWMA chart (Roberts,1959) and CUSUM chart (Page, 1954) are often used for detecting shifts in a sequence of independent normal observations with common variance coming from a particular process. [1][3][5]

1-Exponentially Weighted Moving Average(EWMA)

The Exponentially Weighted Moving Average (EWMA) control charts and other sequential approaches, like Cumulative Sum (CUSUM) charts, are an alternative to

Shewhart control charts and are especially effective in detecting small process shifts EWMA control chart was introduced by Roberts (1959). [4][5]. And defined as:

$$Z_i = \lambda x_i + (1 - \lambda)z_{i-1} \dots 1$$

Where $0 < \lambda \leq 1$ is a constant and the starting value required with the first sample at $i=1$ is the process target value, so that $Z_0 = u_0$

Sometimes the average of the data is used to start value then it become $Z_0 = \bar{x}$

If the observations X_i are independent random variables with σ^2 then the variance is:

$$\sigma_{xi}^2 = \sigma^2 \frac{\lambda}{2-\lambda} [1 - (1-\lambda)^{2i}] \dots 2$$

Then the EWMA control chart would be constructed by plotting Z_i versus the sample number I . The center line and control limits for the EWMA control chart are as follows [7][11]:

$$UCL = \mu_0 + L\sigma \sqrt{\frac{\lambda}{2-\lambda} [1 - (1-\lambda)^{2i}]} \dots 3$$

Ceterline = μ_0

$$LCL = \mu_0 - L\sigma \sqrt{\frac{\lambda}{2-\lambda} [1 - (1-\lambda)^{2i}]} \dots 4$$

From the UCL, and LCL that the term $[1 - (1-\lambda)^{2i}]$ Approaches unity as I get larger, than the ULC and LCL it become as:

$$UCL = \mu_0 + L\sigma \sqrt{\frac{\lambda}{2-\lambda}} \dots 5$$

Ceterline = μ_0

$$LCL = \mu_0 - L\sigma \sqrt{\frac{\lambda}{2-\lambda}} \dots 6$$

2-Monitoring Variability of Individual:[3][6][11]

MC Gregore and Harris (1993) discuss the use of EWMA-based statistics for monitoring the process slandered deviation, Let X_i be a normally distribution with mean and standard deviation then the exponentially weighted mean square error (EWMS) is:

$$S_i^2 = \lambda(X_i - \mu)^2 + (1 - \lambda)S_{i-1}^2 \text{ Shown that } E(S_i^2) = \sigma^2$$

Has been an approximate to Chi-Square distribution with degrees of freedom $v = (2 - \lambda) / \lambda$ the exponentially weighted root mean square (EWRMS) control limits given by:

$$UCL = \sigma_0 \sqrt{\frac{\chi_{v,\alpha/2}^2}{v}} \dots 7$$

$$LCL = \sigma_0 \sqrt{\frac{\chi_{v,1-(\alpha/2)}^2}{v}} \dots 8$$

And the Exponentially weighted moving variance (EWMV_{zi}) as:

$$S_i^2 = \lambda(X_i - Z_i)^2 + (1 - \lambda)S_{i-1}^2 \dots 9$$

It is possible to construct Cusum control charts for monitoring process variability.

Consider a process with its quality characteristic X_i distributed as normal with mean μ and variance σ^2 . Then the standardized random variable The standardized random variable is :

$$Z_i = (X_i - \mu_0) / \sigma,$$

Hawkins (1981-1993) showed that the random variable $\sqrt{|Z_i|}$ is approximately distributed as normal with mean 0.822 and standard deviation 0.349; that is, the random variable As show us:

$$V_i = \frac{\sqrt{|Z_i|} - 0.822}{0.349} \dots 10$$

Is distributed as standard normal. Furthermore, when the variance of X_i increases, the mean of V_i will increase. However, any change in the mean of V_i can be detected by designing a two- sided CUSUM - Chart, Where V_i is approximately $N(0,1)$. The exponentially weighted moving variance (EWMV) and the exponentially weighted root mean square (EWRMS) charts to monitor the variation of the process that generates an individual autocorrelated observation. The (EWRMS) statistic uses the squared deviation of observation from the known process mean or from the target value. The (EWMV) statistic uses the squared deviations of the observations from an estimate of the process mean. [3][8][9][10]

The degree of freedom is related to exponential weighing constant λ as follows;

$$f = \frac{2-\lambda}{\lambda} \dots 11$$

II. NUMERICAL ILLUSTRATION:

In this paper highlight the positive measurement features of above proposed EWMA and EWRMS control limit. Then drawing charts of both control limits to compare the numerical result analysis and charts. For that In this case use the data of chemical analysis on (Loss on ignition L.O.I) from cement. The data are forty sample with a sample size of (4) the total measurement number is (160). As shows in table (1).

Table.1: Data of L.O.I and EWMA

#	X1	X2	X3	X4	Mean	Rang	EWMA
1	3.66	3.11	3.66	3.04	3.3675	0.62	2.5
2	3.65	3.44	3.65	2.63	3.3425	1.02	2.67
3	3.71	3.53	3.71	2.6	3.3875	1.11	2.81
4	3.54	3.69	3.62	2.54	3.3475	1.15	2.92
5	3.63	3.87	3.55	2.67	3.43	1.2	3.01
6	3.69	3.48	3.14	2.86	3.2925	0.83	3.09
7	3.62	3.47	3.58	2.78	3.3625	0.84	3.13

8	3.55	3.83	3.53	2.8	3.4275	1.03	3.18
9	3.14	3.84	3.57	2.87	3.355	0.97	3.23
10	3.58	3.81	3.62	2.61	3.405	1.2	3.25
.
.
.
35	3.01	2.05	2.13	2.63	2.455	0.96	2.59
36	2.97	1.83	2.37	2.58	2.4375	1.14	2.56
37	2.71	2.26	2.68	2.61	2.565	0.45	2.56
38	2.91	2.11	2.74	2.96	2.68	0.85	2.58
39	3.12	2.1	2.63	2.85	2.675	1.02	2.60
40	3.13	2.53	2.8	2.46	2.73	0.67	2.63

9	1.392	1.233	0.687	0.829
10	1.500	1.286	0.714	0.845
.
.
.
35	-1.496	-1.024	0.069	0.262
36	-1.342	-1.088	0.056	0.236
37	-1.322	-1.135	0.045	0.213
38	-0.636	-1.035	0.043	0.207
39	-0.660	-0.960	0.040	0.201
40	-0.412	-0.850	0.043	0.207

Determining the EWMA value of data in a table (1) by using Eq. (5 and 6). The value of upper limits is (3.464), the lower limit is (2.54), and central limit is (3), where the target value is (2.5). Fig (1) shows the EWMA control chart. From the control chart it shows that the first (17) point between central and upper limits. The c value is (3.605), and the first value is (3.3675), after that point the value of EWMA falling down to the lower limits as shown in the fig(1)

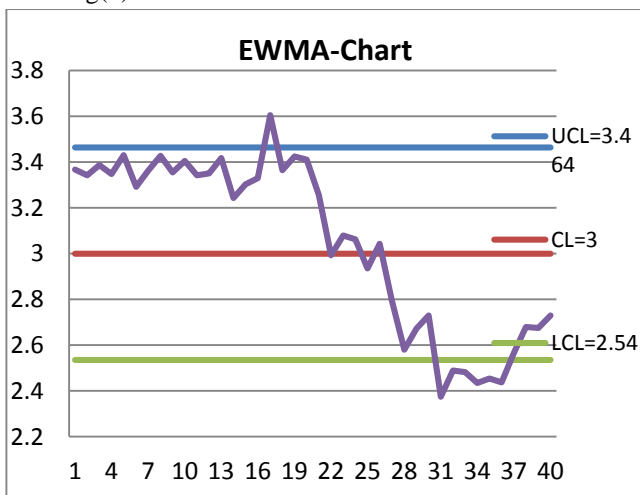


Fig.1: EWMA-Chart

Table.2: Value of EWMA_{vi} and EWRMS

	Vi	EWMA Vi	EWMA s	EWRMS
1	1.419	0.284	0.327	0.571
2	1.364	0.500	0.403	0.635
3	1.462	0.692	0.480	0.693
4	1.375	0.829	0.528	0.726
5	1.552	0.974	0.595	0.771
6	1.252	1.029	0.602	0.776
7	1.408	1.105	0.630	0.794
8	1.547	1.193	0.676	0.822

Also By using the data incoming in table (1) and Eq (7, 8 and 10) it is a Possible to calculate the value of Vi, EWMA_s and EWRMS as shows in table (2). Then determine upper and lower control limit value of the EWRMS as shows in fig (2), Upper control limits are (0.73) and Lower Limit is (0.2). This chart quite definitively indicates the output of control from the point (5) up to (25), Chart changed direction towards lower of the points 25, this exponentially chart is weighted by the mean square error.

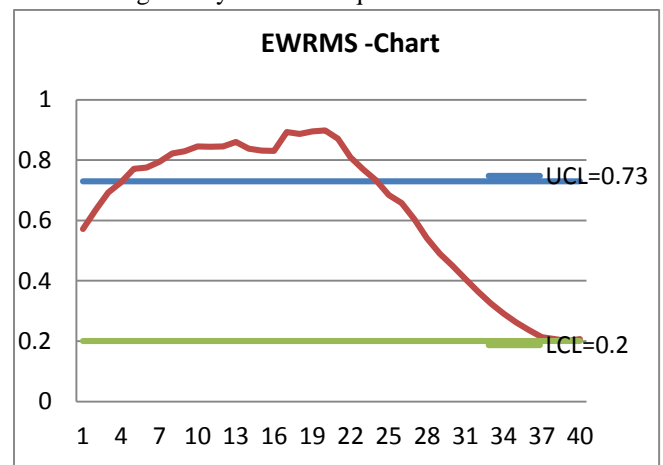


Fig.2: EWRMS-Chart

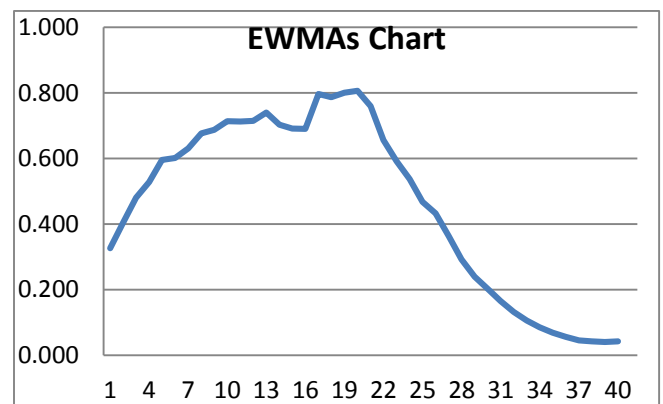


Fig.3: EWMA's-Chart

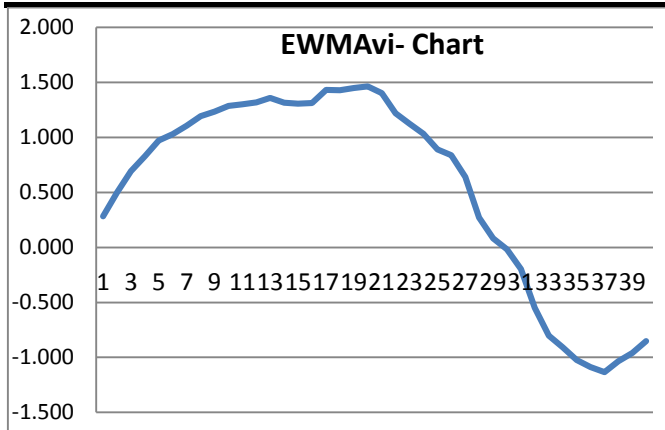


Fig.4: EWMAvi-Chart

Fig (3) is EWMA_s-Chart and Fig (4) is EWMA_v - Chart, from the both chart shows that the first (20) points located towards upper within the of control limits, after the point(20) change the direction of the chart towards to the lower, the maximum Value of EWMA_v is (1.462) and the minimum value is (- 0.850) less than zero. During the comparison between two Cusum charts it shows that the fig.(4) more clear than fig. (3).

III. SUMMARY AND CONCLUSIONS

In this paper achieves limitations of the traditional concept of Cusum, EWMA and EWRMS clear that the planned EWRMS is a good technique between the note in contrast transition process in the process means.

Leaning in a similar way to respond both mean and variance changes, The EWRMS statistic is a good sensitive to shifts the process variance and also shifts in the process mean.

And EWMV-Chart which allows for changing mean it is clear in the event of a control signal, if the signal each of the graphs, we suspect that the change in the average minimum happened with the possibility of both mean and variance having changed.

REFERENCE

- [1] Alpaben K. Patel and Jyoti Divecha, 2010 Modified exponentially weighted moving average (EWMA) control chart for an analytical process data . Journal of Chemical Engineering and Materials Science Vol. 2(1), pp. 12-20, January 2011 Available online at <http://www.academicjournals.org/jcems> ISSN-2141-6605 ©2011 Academic Journals
- [2] Arthur B. Yeh , Dennis K. J. Lin (2004) , Quality Technology & Quantitative Management Vol.1, No.1 pp. 65-86, 2004 Unified CUSUM Charts for Monitoring Process Mean and Variability

- [3] Bhasham C. Gupta, H. Fred Walker ,2007 “ Statistical Quality Control for the Six Sigma Green Belt”
- [4] Dan Trietsch 1999 (Statistical Quality Control)
- [5] Douglas C. Montgomery 2009, Introduction to Statistical Quality Control 6th edition.
- [6] Eamonn Mullins Trinity College, Dublin, Ireland, 2003, Statistics for the Quality Control Chemistry Laboratory
- [7] James R. Thompson, Jacek Koronacki , 2008 Statistical Process Control, Second Edition.
- [8] John Oakland 2008 Statistical Process Control, Sixth Edition.
- [9] Layth C. Alwan 2000 “Statistical Process Analysis
- [10] Ryan T.P (2000) : (Statistical Methods For Quality Improvement), 2nd Edition-

Flexural Strengthening of Reinforced Concrete Girders using Post-Tensioned Concrete Jackets

Dina Zakaria^{1*}, Hussein Okail², Amr Abdelrahman³

¹ Graduate Researcher, Structural Engineering Department, Faculty of Engineering, Ain Shams University, Egypt

² Associate Professor of Structural Engineering, Structural Engineering Department, Faculty of Engineering, Ain Shams University, Egypt

³ Professor of Concrete Structures, Structural Engineering Department, Faculty of Engineering, Ain Shams University, Egypt

Abstract— This study discusses the flexural behavior of reinforced concrete girders strengthened using post-tensioning embedded in concrete jackets. The concept benefits from the external jacket to help increasing the cross-section inertia as well as to host the post-tensioning tendons without the need of external deviators. This results in a significant enhancement to the strength and stiffness of the original girder. The experimental phase of the study was conducted on two stages the first deals with girders loaded on their original section firstly and then strengthened with the jacket and loaded to failure, while the second had the girders that were strengthened before being subjected to loads. In addition to the stage of jacket introduction, the difference between the original girder and the jacket's concrete compressive strength was also studied. In the analytical phase of the study, a numerical model was built using the finite element method to simulate the response of the tested girders in the two experimental stages. This paper presents findings of the experimental program as well as the comparison with the analytical results of the model which showed a close correlation. This model may then be used with confidence to conduct an extensive analytical study for untested parameters.

Keywords— Flexural strengthening, reinforced concrete, post-tensioned concrete, jackets, finite element model, ABAQUS.

I. INTRODUCTION

Rehabilitation of existing structures has always been an important sector of structural engineering. Sometimes, repair of deteriorated concrete structures is more economical than building new one, if by repairing a safe and serviceable structure can be achieved. Strengthening for load capacity increase is also a crucial aspect of the rehabilitation industry. The success of a repair or a rehabilitation project will depend on the degree to which the work is executed in conformance with plans and specifications [1]. Strengthening of girders in flexure can be

achieved by adding a new structural element to the section, either steel or reinforced concrete [2] or most recently, Fiber Reinforced Polymers. The necessity to rehabilitate a Reinforced Concrete (RC) structure emerges from several reasons such as new safety requirements, change of structure occupancy, incorrect design calculations and/or degradation of materials with time. One of the most commonly used mitigation practices to strengthen and repair RC girders is the application of RC jackets to the girders sides [3].

Strengthening of concrete structures using external prestressing tendons has now been used for some time. External prestressing was initially developed for retrofitting of bridges, but now it is used for both retrofitting and in building new structures. Due to their simplicity and cost effectiveness, pre-stressed concrete bridges with external prestressing are becoming popular [4]. It has been found to provide an efficient and economical solution for a wide range of bridge types and conditions. The technique is growing in popularity because of the speed of installation and the minimal disruption to traffic flow. It increases the flexural and shear strength of strengthened girders as well as increasing stiffness which will reduce deflection. This technique is more economic compared to other methods [5].

II. PREVIOUS STUDIES ON STRENGTHENING RC GIRDERS

2.1 Previous Studies using the External Prestressing Technique

Jafar Sadak Ali et al, [6] introduced a method for the calculation of cable strain, which is based on the deformation compatibility of girder and friction at the deviators, was proposed to predict entire response of externally pre-stressed concrete girders up to elastic limit. Application of the developed method in numerical analysis on a rectangular girder with different profiles of prestressing cable was then performed. An algorithm has been developed to determine the structural behavior at the

deviator points in an externally pre-stressed girder. The predicted results showed that the structural behavior of externally pre-stressed concrete girders could be satisfactorily predicted from zero loading stage up to the proportional limit loading stage for different cable profiles.

Ali Hussein et al, [7], presented a nonlinear finite-element analysis to investigate the behavior up to failure of continuous composite steel-concrete girder with external prestressing tendons, in which a concrete slab is connected with steel I-girder by means of headed stud shear connectors, subjected to symmetrically static loading. ANSYS computer program (version 12.1) has been used to analyze the three-dimensional model. This covers: load deflection behavior, strain in concrete, and strain in steel girder and failure modes. The results obtained by finite element solutions have shown good agreement with experimental result.

M. A. Algorafi et al, [8], worked in an experimental investigation of the structural behavior of externally pre-stressed segmented (EPS) bridged under combined bending, shear, normal, and torsion stresses. A parametric study was carried out to investigate the effect of different external tendon layouts and different levels of torsion. The many advantages of this type of structure include offering fast and versatile construction, no disruption at ground level, high controlled quality and cost savings that have made them the preferred solution for many long-elevated highways.

Swoo-Heon Lee et al, [9], conducted a full-scale experimental study assessed the behavior of continuous concrete girders retrofitted with external pre-stressed bars. Three three-span girders were tested in two-point loading of the interior span. The results indicate that the external prestressing increased the load-carrying capacity by about 25% and the flexural stiffness by about 15%.

Mohamed H. Harajli, [10], tested sixteen girders, in which they were firstly subjected to cyclic fatigue loading at a constant load range to induce fatigue deformations. Then, they were externally pre-stressed and subjected to monotonically increasing load to failure. The nominal flexural strengths of the girders were increased by up to 146 percent and the induced fatigue deflections were reduced by up to 75 percent.

2.2 Previous Studies on Concrete Jackets

Concrete jacketing enhances both the strength and stiffness of the original member which is beneficial in case of seismic retrofitting and upgrading of the structural durability. El-Ebweini and Ziara [11] repaired six girders after corrosion by removing concrete cover and adding to the corroded part two longitudinal bars fixed with shear

dowels. The main differences in the specimens were in the type of the repairing material. The results conducted from this study were that the flexural capacity of the repaired girders was increased by 47% compared with the control girders.

Constantin E. Chalioris et al. [12] repaired five girders after shear failure by using self-compacting reinforced jacket. The results indicated that this rehabilitation method was a reliable one since the capacity of the repaired girders was fully restored according to the initial specimens.

Qasem Khalaf et al. [13] studied the flexural behavior of 26 reinforced concrete girders repaired using two techniques, concrete jackets and steel plates. The test variables were the aim of strengthening (shear or flexure), the technique used in strengthening (concrete jackets or steel plates) and the type of bond between the old concrete and the strengthening element (mechanical or chemical). The conducted results show that the specimens that strengthened by concrete jackets bonded either mechanically or chemically was more effective than that strengthen by steel plates.

Raval and Dave [14] tested the strengthening of reinforced concrete girders using concrete jackets. Ten girders were tested; four girders were prepared with smooth surface and other four with chipped surface while the remaining two girders were considered as control test girders. Four different techniques of bonding were used in this study. The results show that the girders with smooth surface and using jacket with combined shear dowels and bonding agent with micro-concrete was the most effective technique and for the girders with chipped surface, the most effective technique was using only micro-concrete and without use of shear dowels and bonding agent.

In this paper, an innovative technique is proposed to use the external prestressing method in a more easy-to-apply way for flexural strengthening of girders. This is done by means of embedding the draped profile tendons in a concrete jacket, externally bonded to the original girder. In the following sections, the experimental and analytical phases of the research are presented to verify the adequacy of the proposed technique.

III. EXPERIMENTAL WORK

The experimental phase of this research program consisted of two main stages, in the first stage two girders were cast with the cross-section shown in figure (1) and were loaded up to 80% of their ultimate moment capacity which was calculated by first principles.

In the second stage, the two tested girders of the first stage were strengthened and re-tested up to failure. In addition two girders untested girders were jacketed and then loaded

to failure. Figure (2) shows the cross-section and the cable profile of strengthened girders. The strengthened girders of stage two differs in the compressive strength of jacket and

the damage level in the original section of each girder. The properties of the girders in each stage are summarized in Table (1).

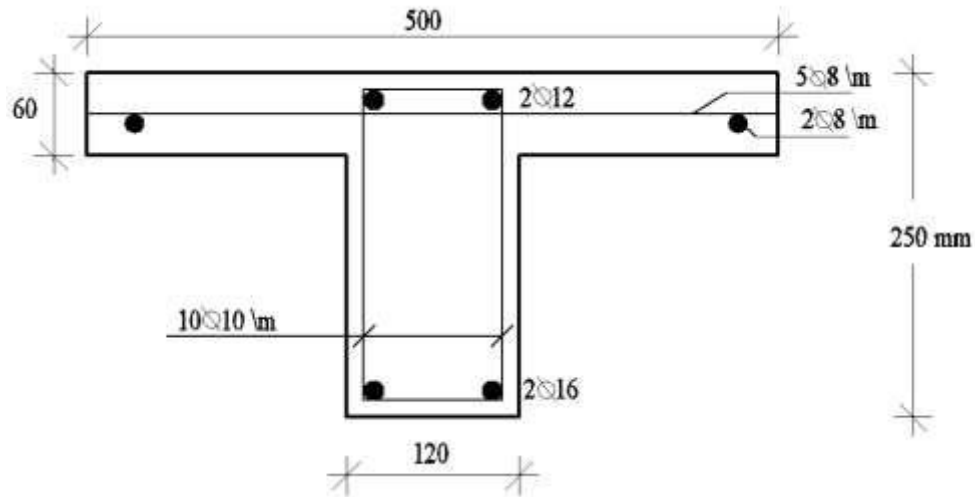
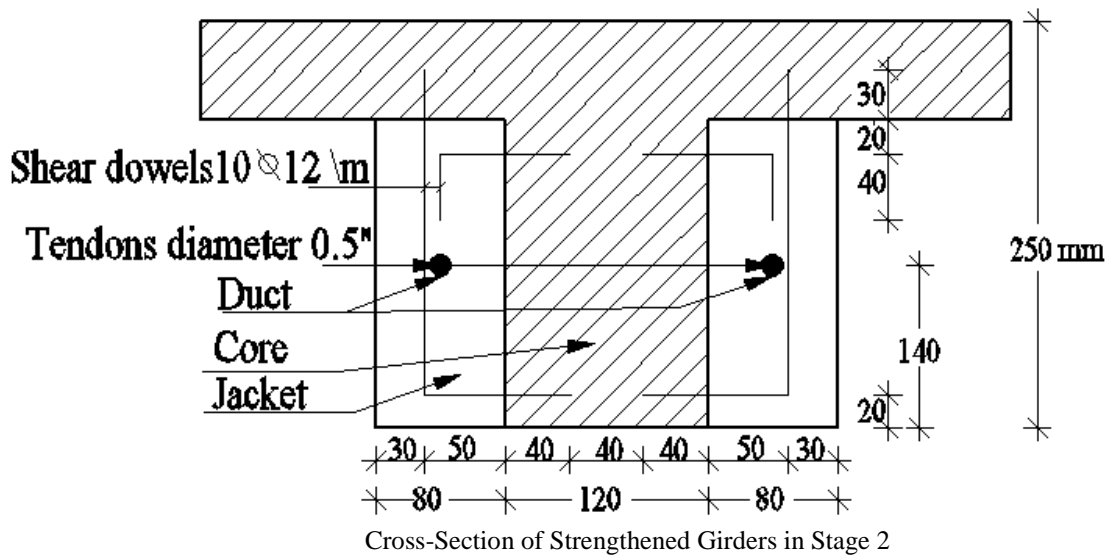


Fig.1: Cross-Section of all Girders in Stage 1



Cross-Section of Strengthened Girders in Stage 2

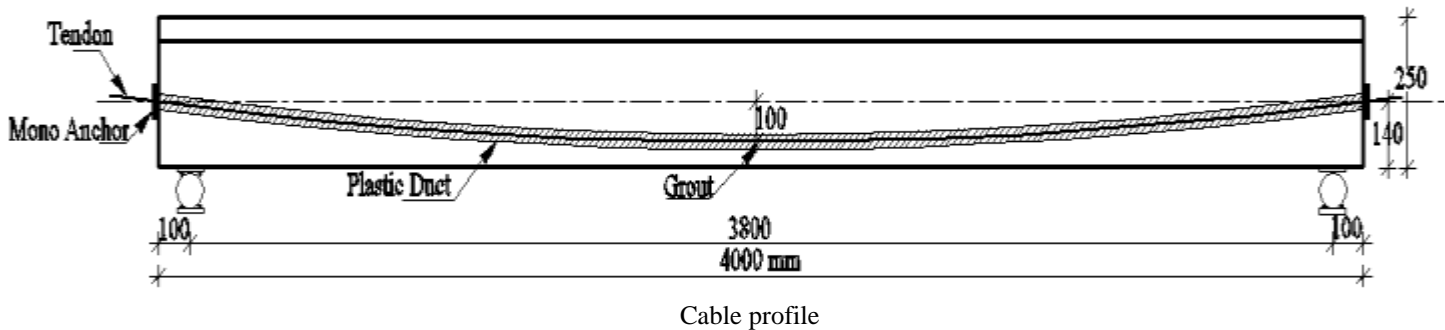


Fig.2: Cross-Section and Cable Profile of the Girders in Stage 2

Table.1: The main variables of girders in each stage

Stage No.	Specimen Label	Core f_{cu} (MPa)	Jacket f_{cu} (Mpa)	Damage level for core
1	RC 1-1	30	--	Loaded before strengthening up to 80 % of its loading capacity.
	RC 1-2			Loaded before strengthening up to 80 % of its loading capacity.
	RC 1-3			No loading for this girder in this phase.
	RC 1-4			No loading for this girder in this phase.
2	PC 2-1	30	30	80% before strengthening.
	PC 2-2		60	80% before strengthening.
	PC 2-3		30	0% before strengthening.
	PC 2-4		60	0% before strengthening.

3.1 Material Properties

The girders core for phase 1 was cast with a concrete having a 28-days cube compressive strength of 30 MPa. For phase 2 there are two different concrete mixes for the concrete jacket which as shown in table (1), the girder jackets' were cast with a concrete having a 28-days cube compressive strength of 30 and 60 MPa. Ordinary Portland cement and local natural sand and the coarse aggregate "crushed limestone" (Dolomite) with 10-mm maximum size were used. All the used materials were matched with the Egyptian Code of Practice (ECP 203) [15].

Silica fume was used to achieve concrete compressive strength 60 Mpa. The workability of the mix was improved by using a high-range water reduction admixture under a commercial name of Sika Viscocrete. The compressive strength of concrete was evaluated after 28-days of casting based on the cube (15.8 x 15.8 cm²), and was found to be as 30.94 and 61.63 MPa respectively.

Steel bars of grade 240/350 and grade 360/520 were used. The mild steel smooth bars of grade 240/350 which have minimum yield strength of 240 MPa and ultimate tensile strength of 350 MPa were used for bar size of 8mm. The high tensile steel deformed bars of grade 360/520 that have minimum proof strength of 360 MPa and ultimate tensile strength of 520 MPa were used for bar sizes of 12 and 16 mm. All the previous types of steel had constant modulus of elasticity of 210 GPa. High tensile, low relaxation PT tendons (ASTM A416, grade 270) [16] were used with a diameter 0.5" (12.7 mm).

3.2 Test Setup:

The experimental work was conducted in the reinforced concrete laboratory of the faculty of engineering at Ain Shams University, Figure (3) shows the test setup used in this study. All girders were tested as a simple span with a clear span of 3800 mm using two points loading system spaced 1200 mm.



Fig.3: Test Setup for all Girders in the Two Stages

3.3 Loading Protocol

Girders RC1-1 and RC1-2 were aligned before strengthening in test rig with the required effective spans and were subjected to an incremental loading till 80% (45 KN) and then strengthened with the jacket and retested till failure. While girders PC 2-3 and PC 2-4 were strengthened firstly and then tested to failure.

3.4 Instrumentation

The accuracy of the measurement devices determines the reliability of the experimental program results. In this

respect, a powerful combination of measurement devices was used to monitor and record the test outputs. Figure (4) indicates three 0.01mm accuracy Linear Variable Displacement Transducers (LVDTs) were used to measure the deflections at different points. The strain on the ordinary steel was measured by four electrical strain gauges (ES), mounted on the mid span for the top and bottom steel bars. All the LVDTs and electrical strain gauges of stage one and two were connected to the appropriate number of channel boxes (4 channels each). Finally, all the data were recorded by the data acquisition device.

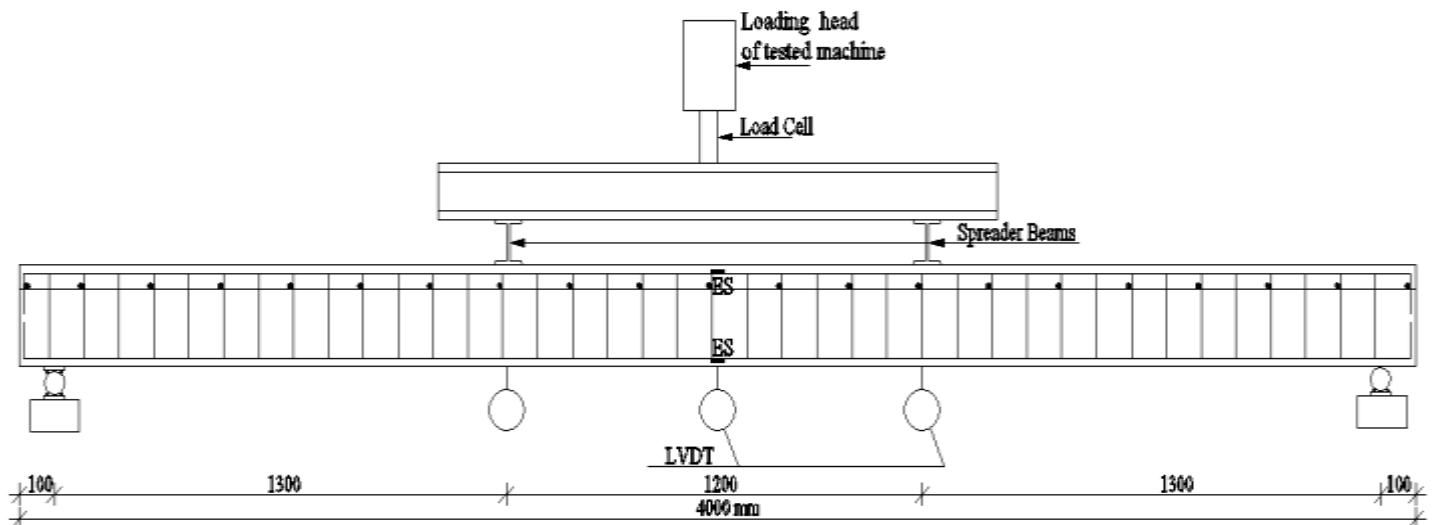


Fig.4: Deflection and Steel Strain Measurements for all Girders

3.5 Results and Discussion

3.5.1 Crack Pattern

In the first stage, the crack pattern of the two tested girders (RC 1-1, RC 1-2) was similar as shown in figure (5). First crack appeared in the constant moment zone at a load 15 and 15 kN for girders RC (1-1) and RC (1-2) respectively. With increasing loads till 45 kN, the number and width of the flexural cracks increased and propagated vertically towards the girders' flange and gradually covering longer portions of the girders' spans. About 25 cracks were observed in these two girders and the average spacing between cracks was about 8 cm.

In the second stage, the crack pattern of all the girders was similar as shown in figure (6). At the early stages of loading, first crack appeared in the constant moment zone at a load 60, 50, 50 and 50kN for girders PC 2-1, PC 2-2, PC 2-3 and PC 2-4 respectively. With increasing loads, flexural cracks increased in number and width while propagating

vertically towards the girders' flange axis and gradually covering longer portions of the girders. About 15 cracks were observed in these four girders, which is less than the number of cracks in the girders before strengthening, and the average spacing between cracks was about 12 cm. During this phase the vertical load increased to 126.45, 138.83, 142.00 and 150.00 KN for girders PC 2-1, PC 2-2, PC 2-3 and PC 2-4 respectively, which represent the failure load for each girder.

In summary, all girders failed in flexure through ductile failure as monitored for girders PC 2-1, PC 2-2, PC 2-3 and PC 2-4. All tested girders behaved the same mode of failure as crushing in the upper surface of concrete under one of the loading girders. Figure (7) shows mode of failure of each girder. It is noted that this crushing appeared after several flexural cracks have developed in the girders, hence the ductile nature of the failure.

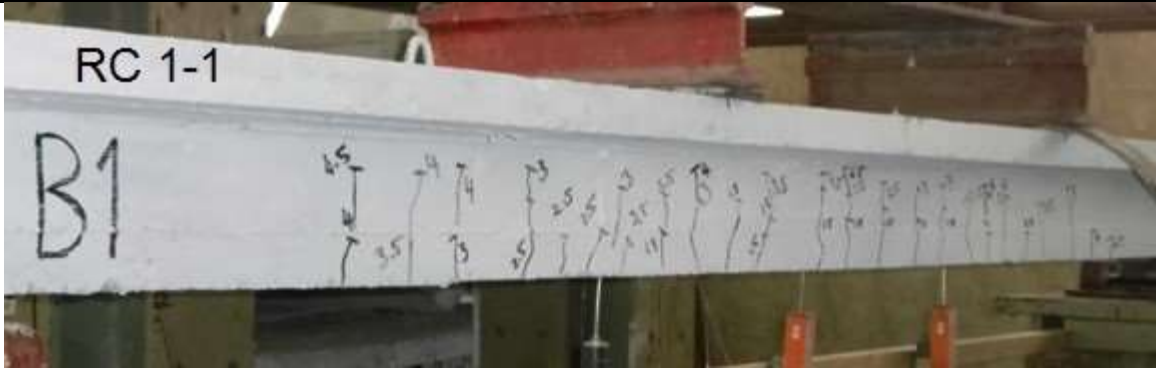


Fig.5: Crack pattern of girders RC (1-1) and RC (1-2) respectively



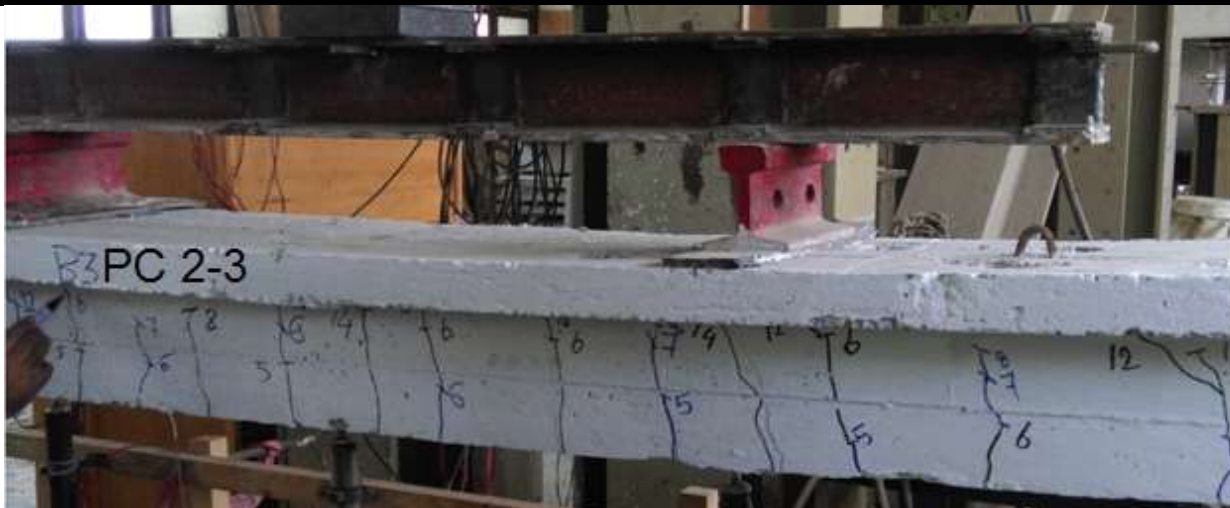


Fig.6: Crack pattern of girders (PC 2-1, PC 2-2, and PC 2-3 and PC 2-4 respectively)





Fig.7: Mode of failure of the girders (PC 2-1, PC 2-2, PC 2-3and PC 2-4)

3.5.2 Load-Deflection Response

The vertical load and the mid-span deflection were measured for all girders in each stage. Figure (8) shows a comparison between the girders that were loaded on their original section firstly and then strengthened with the jacket and reloaded to failure. It was observed that the strengthened girders (PC 2-1 and PC 2-2) were stiffer than the girders (RC 1-1 and RC 1-2). At load 45 KN, the mid-span deflection [as shown in table (3)] of the girders PC 2-1

and PC 2-2 were less than the girders RC 1-1 and RC 1-2 by 47% and 63% respectively.

The flexural behavior for girders PC 2-1 and PC 2-2 were similar, but the load-carrying capacity of girder PC 2-2 was higher than girder PC 2-1 by 9.8% as shown in figure (9) which may be attributed to the difference between the jacket’s concrete compressive strength for girders PC 2-1 and PC 2-2 as illustrated in the previous table (1).

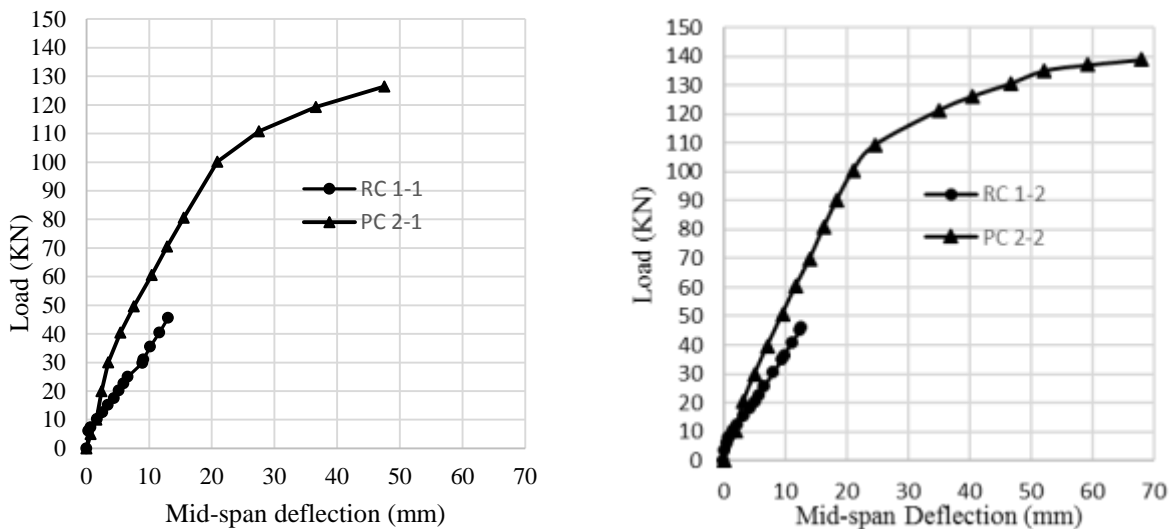


Fig.8: Load vs. Mid-Span Deflection

Table.3: Mid-Span Deflection at Load 40 KN

Girder Label	Mid-span Deflection (mm) at Load = 45 KN
RC 1-1	11.66
RC 1-2	11.13
PC 2-1	5.41
PC 2-2	7.01

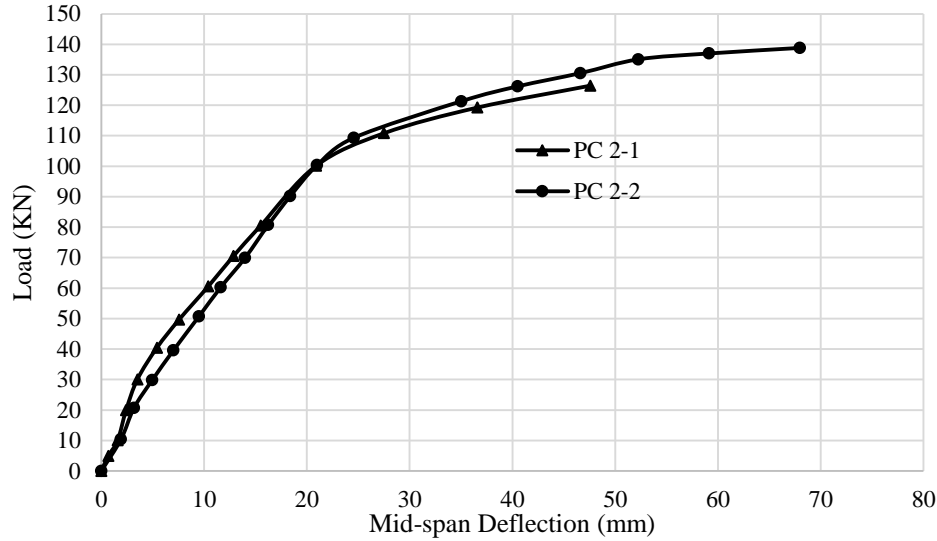
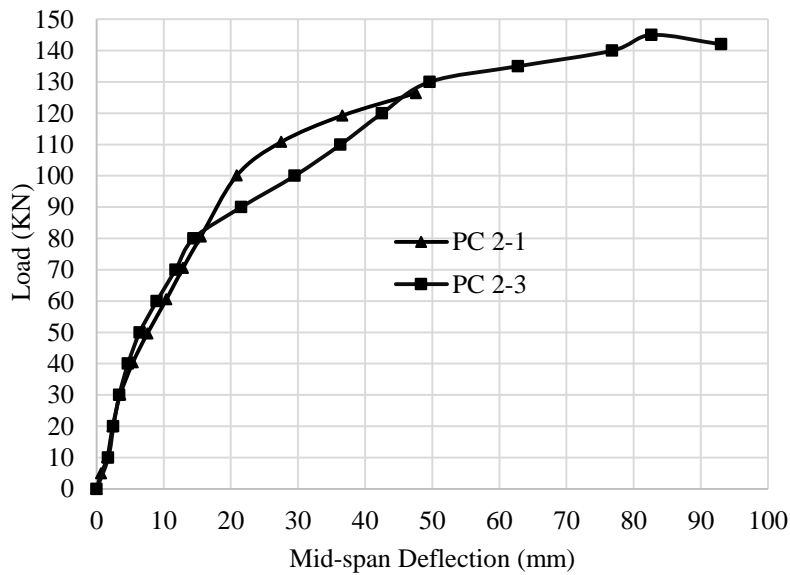


Fig.9: Load versus Mid-Span Deflection

Figure (10) shows a comparison between the strengthened girders (PC 2-1 and PC 2-3) and (PC 2-2 and PC 2-4), where the main difference between each two girders were the damage level of the original girder before strengthening as illustrated in the previous table (1). It was observed that the load-carrying capacity of the girder PC 2-3 and PC 2-4 were more than the girder PC 2-1 and PC 2-2 by 11% and 7.5% respectively.



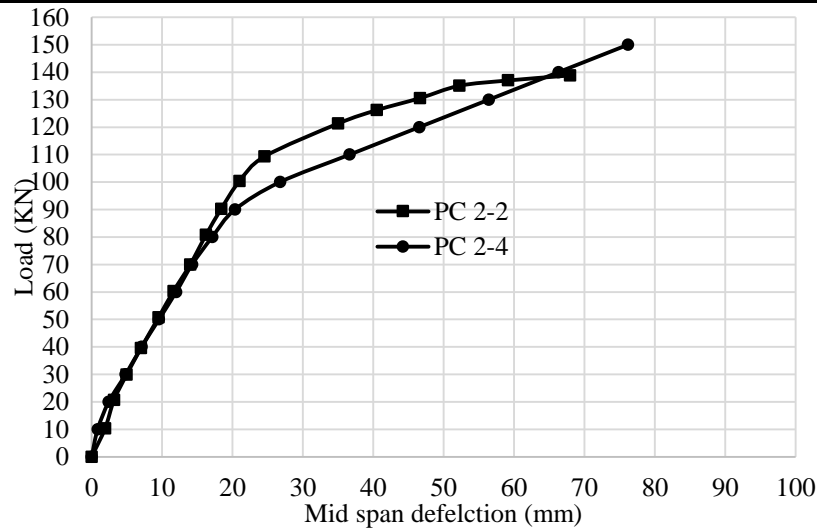


Fig.10: Load versus Mid-Span Deflection

The experimental results for the girders before and after strengthening were summarized in Table (2). Results were expressed in terms of their first-crack load, ultimate load-carrying capacity and ultimate displacement.

Table.2: Summary of the experimental test results

Phase no.	Girder Label	P _{cr} (KN)	Δ _{cr} (mm)	P _u (KN)	Δ _u (mm)
1	RC 1-1	15	3.43	--	--
	RC 1-2	15	3.23	--	--
2	PC 2-1	60	10.41	126.45	47.57
	PC 2-2	50	9.50	138.83	67.69
	PC 2-3	50	6.42	142.00	93.03
	PC 2-4	50	9.56	150.00	76.20

P_{cr} = first crack load, P_u = ultimate Load, Δ_{cr} = mid-span deflection at first crack, Δ_u = mid-span deflection at failure load

IV. FINITE ELEMENT ANALYSIS

Modelling using finite element approach for reinforced concrete is a delicate task. Both elastic and plastic behavior of concrete in tension and compression is to be incorporated while creating a proper model. The behavior of reinforced concrete under tension can be incorporated using tension stiffening. In this study, the ABAQUS software package which uses the finite element method was used to model the flexural behavior of the girders in stages one and two. Concrete damaged plasticity material model was implemented for the concrete continuum.

4.1 Material Properties for the Numerical Simulation

4.1.1 Concrete

The concrete damaged plasticity (Cdp) model depends on assuming that the failure mechanism will be as the compressive crushing and tensile cracking. The uniaxial compressive strength of concrete core in stage one was 30 MPa and for stage two the compressive strength of post-

tensioned concrete jacket was 30 and 60 MPa. The plastic strain of concrete is considered as 0.035 and which was used in the analysis. The Poisson’s ratio of concrete is suggested as $\nu = 0.2$.

4.1.2 Steel Reinforcement

The steel rebars were modeled as truss elements with yield stress 360 MPa and 240 MPa for the main steel reinforcement and for the stirrups respectively. The tendons used in phase two for post-tensioned concrete jackets were modeled as truss elements with yield stress 1674 MPa. The young’s modulus of steel reinforcement and tendons was 200 GPa and poisson’s ratio 0.3. The rebars and tendons can be defined as a one- dimensional strain element and is embedded in the concrete. This can be achieved by using embedded constraint criteria in ABAQUS.

4.2 The Finite Element Mesh

In order to get accuracy in results, all the elements of FE model were assigned the same mesh size so that each two

different materials can share the same node among them. The mesh type selected in the model is given below. The mesh elements for concrete core and post-tensioned concrete jackets were taken as 3D solid element which is called C3D8 and for steel reinforcement and tendons 2D truss element is assigned which is called T3D2.

V. DISCUSSION OF ANALYTICAL RESULTS

5.1 Load–Displacement Response

The mid-span deflection was calculated for the bottom face of the girders from the numerical model. Figures (13) and (14) show the load-deflection curves of the girders before and after strengthening for both the tested beams and the numerical simulation results. The results from the finite element correlate well with those from the experimental

data at both stages. From these figures, it can be concluded that the variation between the experimental and analytical results ranged from 6% to 10% in terms of maximum load and peak deflection response. The overall shape of the load-deflection relationship matches to an acceptable degree.

It can be clearly noted from the figures that the model is quite capable of capturing the variations in the stiffness along the elastic and inelastic domains of the response. Initial stiffer response is observed for the analytical simulation results which may be attributed to two reasons, firstly the nature of the finite element simulation which mathematically should yield a stiffer response and secondly the minor sliding between the jacket and the base concrete which is not represented in the analytical model.

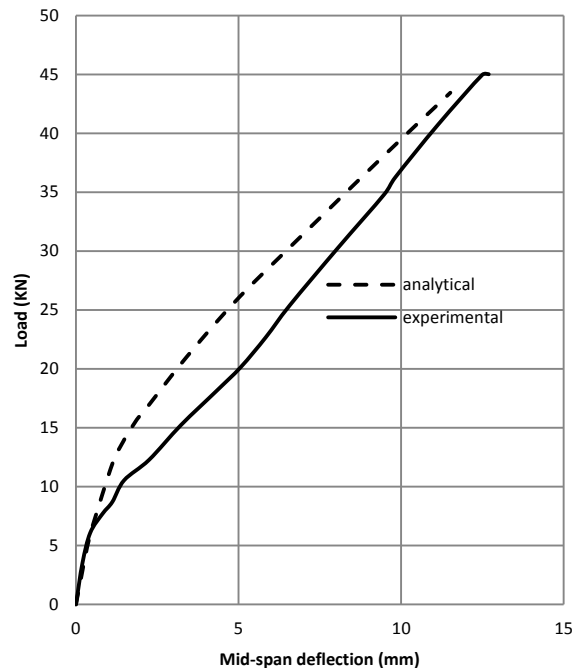
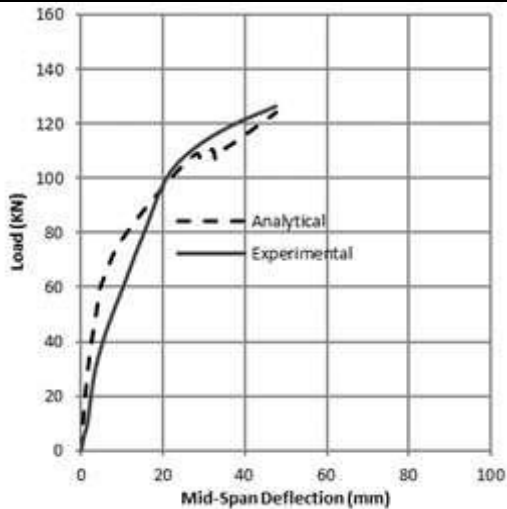
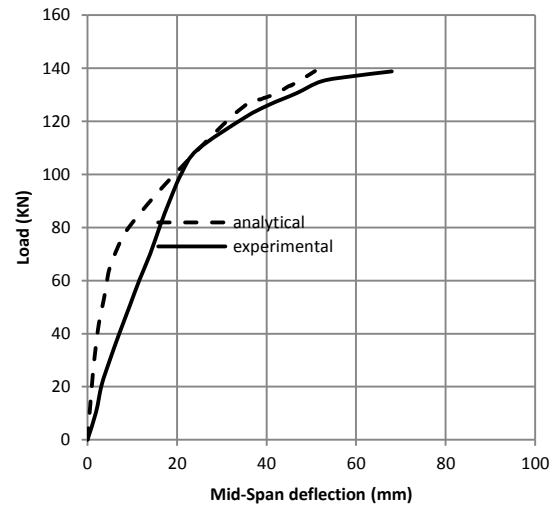


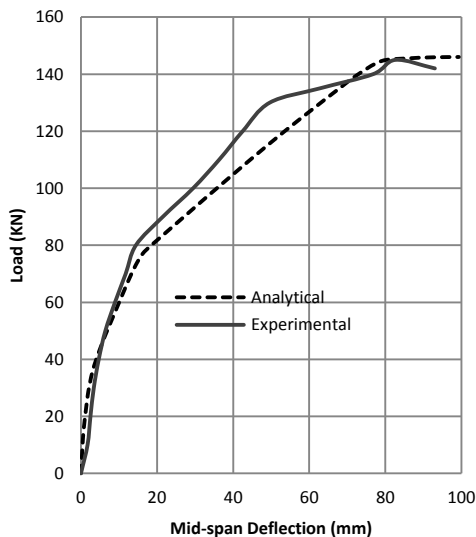
Fig.13: Load-Mid span deflection before strengthening



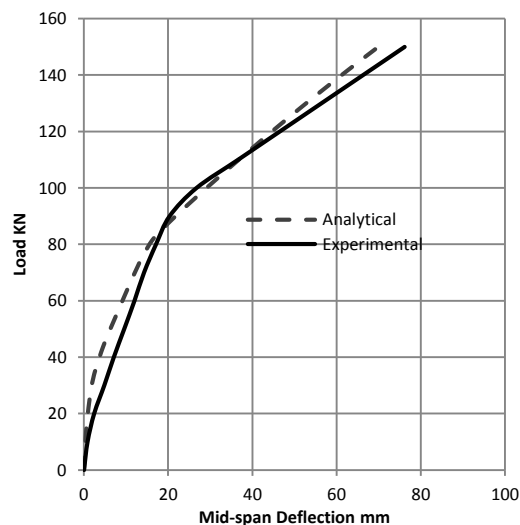
a: Load-Mid span deflection for (PC 2-1)



b: Load-Mid span deflection for (PC 2-2)



c: Load-Mid span deflection for (PC 2-3)



d: Load-Mid span deflection for (PC 2-4)

Fig.14: Load-Mid span deflection for analytical and experimental results of girders PC (2-1), PC (2-2), PC (2-3) and PC (2-4) after strengthening

VI. CONCLUSIONS

This paper presented an experimental and analytical investigation in the flexural response of flanged RC girders strengthened with post-tensioned concrete jackets. The results of the experimental and analytical investigation yielded the following conclusions.

Post-tensioned concrete jackets can be used as an effective strengthening method for damaged and undamaged girders. Both the strength and the stiffness of the girders were enhanced significantly. This means that this technique can be used for mitigating the effect of increase deflections as well as loss of strength.

The stage at which the jacket is introduced slightly affects the strength and stiffness of the girders. The difference is

not large enough to be considerable. This clearly demonstrates one of the merits of this system which is that it can be used on damage substrate without initial repair.

Increasing the jacket concrete compressive strength may result in a slight increase in the strength by about 10% of the original girder capacity.

A numerical model based on the finite element method was developed and compared to the experimental results. The results show a very good match and correlation between the two results. This model will be used in the future to develop a design methodology for the post-tensioned jacketing technique.

REFERENCES

- [1] Adnan Sadiq Al-Kuaity, "Strengthening of cracked reinforced concrete T-beam by jacketing", Journal of Engineering Vol. 16 No. 3, September (2010),
- [2] Ibrahim Abd El Malik Shehata, Lidia da Conceicao ~o Domingues Shehata, Euler Wagner Freitas Santos and Maria Luisa de Faria Simoes, "Strengthening of reinforced concrete beams in flexure by partial jacketing", Materials and Structures (2009)
- [3] M. Monir Ajan Alhadid and Maged A. Youssef, "Strengthening and Repair of Reinforced Concrete Beams Using Concrete Jackets", PROTECT2015 Conference on Response of Structures under Extreme Loading, June (2015)
- [4] Soliman Khudeira, "Strengthening of Deteriorated Concrete Bridge Girders Using an External Posttensioning System", Practice Periodical on Structural Design and Construction Vol. 15, Issue 4, November (2010)
- [5] Jafar Sadak Ali, Soumendu Bagchi and Sumit Gupta "A Numerical Model of Externally Prestressed Concrete Beam" International Journal of Scientific & Engineering Research Vol. 4, Issue 5, May (2013)
- [6] Ali Hussein Qader, V.C. Agarwal and Amer M. Ibrahim "Nonlinear Behavior of Continuous Composite Steel Concrete Beam with External Prestress", International Journal of Innovative Technology and Exploring Engineering (IJITEE) ISSN: 2278-3075, Volume-3, Issue-7, December (2013)
- [7] M. A. Algorafi, A. A. A. Ali, I. Othman, M. S. Jaafar, and R. A. Almansob), "Evaluation of Structural Behavior of Externally Prestressed Segmented Bridge with Shear Key under Torsion", Journal of Engineering, Project, and Production Management, June (2011)
- [8] Swoo-Heon Lee, Kyung-Jae Shin, and Thomas H.-K. Kang, "Flexural strengthening of continuous concrete beams using external Prestressed steel bars", PCI Journal Vol. 60, Issue 1, January - February (2015)
- [9] Mohamed H. Harajli, "Strengthening of Concrete Beams by External Prestressing", PCI Journal Vol. 38, Issue 6, Dec. (1993)
- [10] Mohamed El-Ebweini, "Structural Performance of Repaired Corroded Reinforced Concrete Beams", The 3rd International Conference on Engineering & Gaza Reconstruction (IEC3), October (2010)
- [11] Constantin E. Chalioris and Constantin N. Pourzitidis, "Rehabilitation of Shear-Damaged Reinforced Concrete Beams Using Self-Compacting Concrete Jacketing", ISRN Civil Engineering Volume 2012, Oct. (2012)
- [12] Qasem Khalaf, "Comparative Study for Strengthening Techniques of RC Beams Using Concrete Jackets and Steel Plates", Feb. (2015)
- [13] Sachin S. Ravala , Urmil V. Dave, "Effectiveness of Various Methods of Jacketing for RC Beams", Chemical, Civil and Mechanical Engineering Tracks of 3rd Nirma University International Conference on Engineering Vol. 51, April (2013)
- [14] ECP 203 "Egyptian Code of Practice: ECP 203; 2007"
- [15] American Society for Testing and Materials, ASTM A 416/ A 416M-02 (2002) "Standard Specification for Steel Strand, Uncoated Seven-Wire for Prestressed Concrete".

Effect of Friction Stir Welding Parameters on the Mechanical & Microstructure Properties of Aluminium 6061 Alloys

Ch.Mohana Rao¹, K.Mallikarjuna Rao²

¹Asst.Professor, Dept. of Mechanical Engineering, G.Narayanamma Institute of Technology &Science(for Women),Shaikpet, Hyderabad,500104,India

²Professor, Dept. of Mechanical Engineering, JNTUK College of Engineering , Kakinada,E.G Dt., 533003,India

Abstract— Objective: Friction stir welding (FSW) is a relatively new solid state welding technique for similar and dissimilar materials, especially on current interest with Aluminium 6061 to Aluminim 6061.

Method/Analysis: The present paper discusses the process parameters followed by mechanical properties and microstructures which affect the weld strength.

Findings: Mechanical properties-Tensile strength attained with different process parameters and Microstructures are obtained by Optical Metallurgical Microscopy (MET SCOPE-1) and a Scanning Electron Microscopy equipped with an X-radiation detector EDS

Conclusion/Application: In this study Similar FSW between Al 6061 to Al 6061 plates with thickness 6mm were performed. The future research will contain creep tests and microstructural investigations using aluminium 6061 alloy using TEM microscopy (Transmission Electron Microscopy).It is demonstrated that FSW of aluminium to aluminium alloys is becoming an emerging technology with numerous commercial applications.

Keywords— FSW; Aluminium alloy, Mechanical properties, Microstructures, SEM.

I. INTRODUCTION

A rotating High Speed Steel pin advances into the workpiece, creating a highly deformed, plastic zone which flows around to its trailing side. No melt occurs, and the weld forms by solid-state plastic flow at elevated temperature. There is no porosity and other fusion weld-type defects associated with the weld zone if the rotational speed (R) and travel speed (T) are optimized.

In this study, we have used light metallography (microscopy) (LM) and Scanning electron microscopy (SEM) to characterize the microstructures in the friction stir weld zone and compare them with the original 6061

aluminium alloy work-piece microstructures. We have also measured the associated micro harness profile extending from the work-piece and through the weld zone. The aim of this paper to present a very brief but comprehensive microstructural overview of this process and illustrate corresponding hardness profiles associated with these microstructures.

II. EXPERIMENTAL DETAILS

6061 aluminium alloy plate (nominally 6mm thick) was used in friction-stir welding experiments to be reported. A series of simulated weld in solid plate sections were conducted, as illustrated schematically in fig 1, at rotational speeds (R) ranging from 500-1000 Rpm , and travel speed of 100 mm/min. The high speed steel welding pin fig.2 was used. Welded cross-sections were ground, polished, and etched with Keller's reagent (150ml distilled water, 3ml nitric acid, 6ml hydrochloric acid at room temperature) for optical metallography. Instrumental (digital) Vickers micro hardness measurements were also made throughout the weld zone and into the initial aluminium alloy plate using a 100gf load.

Material Selection &Material Composition:

Aluminium alloys have steadily increased in aerospace applications because of their Excellent strength to weight ratio, Good ductility, Corrosion resistance and cracking resistance in adverse environments.

Chemical Composition of AA6061

Si 0.80 Mg 1.2
Cr 0.35 Fe 0.70
Zn 0.25 Ti 0.15
Al balance Cu 0.40
Mn 0.15

Table.1: Mechanical Properties of AA6061

Yield Strength (Mpa)	Ultimate strength (Mpa)	Elongation (%)	Reduction in cross-sectional area(%)	Hardness(HN)
302	334	18	12.24	105

Table.2: Physical Properties of AA6061

Density (g/cm ³)	Melting Point(°c)	Modulus of Elasticity (Gpa)	Poison ratio
2.7	580	70-80	0.33

Welding Parameters

In this study, downward force and welding speed are kept constant, only the tool rotation speed is varied. The welding parameters are given in Table 1.

Table.3: Welding parameters

Downward force (Tones)	40
Tilt angle (Degrees)	2°
Plunge Depth (mm)	3
Travel speed (mm/min)	100
Tool Rotation speed (Rpm)	500, 700, 900, 1000

Tool Parameters:

Straight Cylindrical tool was used as shown in figure. The tool is made up of M2 high speed steel and which was tempered and hardened to 60 HRC. The tool material composition is given in Table 2.

Table.4: Tool Parameters

Material	C	Cr	W	Mo	V	Fe
M2	0.85	4.0	6.0	5.0	2.0	Remaining

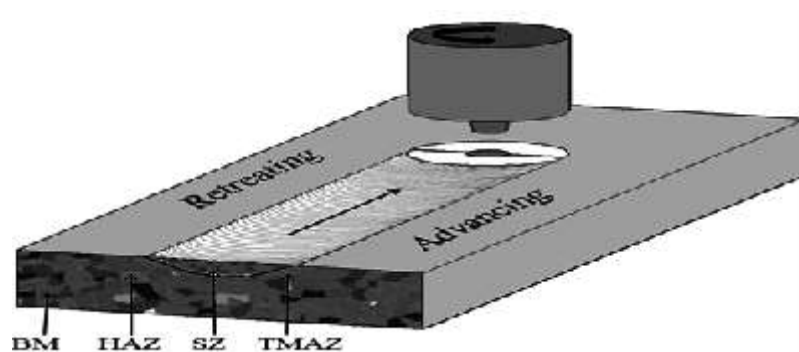


Fig.1: Schematic Drawing of Friction stir Welding



Fig.2(a): FSW Tool

Tapered tool made up of HSS, its
 Tool probe or pin length = 4.8mm
 Pin diameter = 4mm
 Shoulder diameter = 25mm
 Shoulder length = 26mm

Weld trails

Four sets of welding trails were made at the base material AA6061, only by varying the tool rotation speed and keeping downward force, travel speed, plunge depth and tilt angle as constant, the values of the parameters are given in Table 3.

Table.5: Weld trails

Specimen Code No.	S500	S700	S900	S1000
Downward force (Tones)	40	40	40	40
Tilt angle (Degrees)	2°	2°	2°	2°
Plunge Depth (mm)	3	3	3	3
Welding Speed (mm/min)	100	100	100	100
Tool Rotation speed (Rpm)	500	700	900	1000



Fig.3: Schematic drawing of FSW



Fig 4: Macrograph of the welded part under 700rpm

III. RESULTS AND DISCUSSIONS

3.1 Tensile test

Tensile tests were performed to determine the tensile properties of the weld material such as tensile strength and percentage of elongation. One specimen of each was tested at S500 and S700 condition were measured and reported. The tensile tests specimens were cut as per the ASTM 8 standard size on the 6mm thick plate. Tensile tests were conducted on FIE/UTN-40 machine.

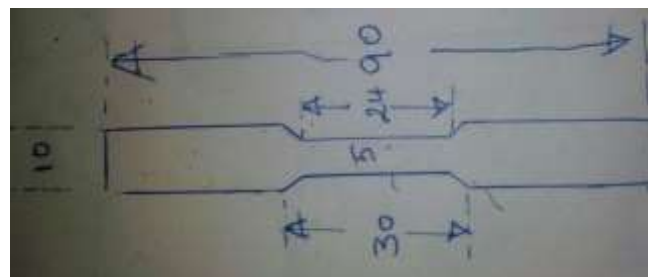


Fig.5: Dimension of the tensile specimen

Table.6: Tested specimen results

S.NO	Specimen Code	Breaking load KN	Tensile Strength Mpa	Elongation %	Fracture position
1	S500	16.200	136.778	2.740	Weld nugget
2	S700	25.42	180.92	2.90	Weld nugget
3	Base Metal (ASTM Hand ook, Vol.9)	----	330	18	-----

3.2 Microstructure:

The microstructure of the different regions of the welded similar material is shown in fig 6&7. Though the weld undergoes considerable amount of the thermal cycle, there is no significant changes in the microstructure of the base metals. The conclusion of the given sample had grain size number as per ASTM E 112 has 5.5 at nugget zone and 5.5 at heat affected zone.



Fig.6: Optical Metallography of Aluminium-Aluminium at Nugget zone



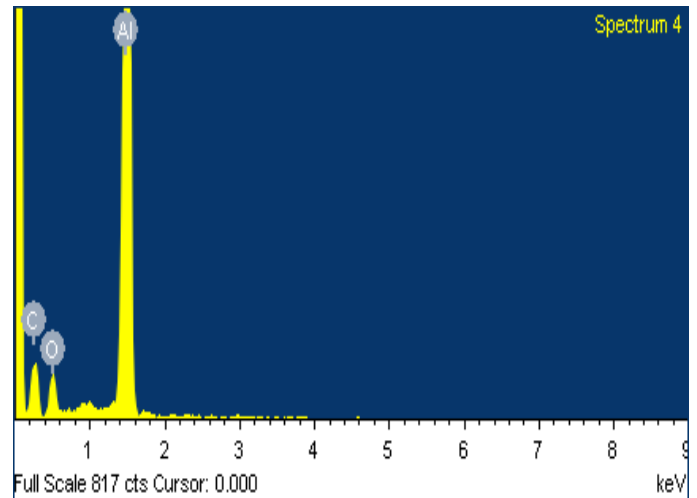
Fig.7: Optical Metallography of Aluminium- Aluminium at HAZ

Grain Size analysis: Results summary

Fields measured : 1
 Analyzed Area : 5005 sq. mm
 Standard used : ASTM E 112

At NZ	Grain size#
Grain size	5.5
Intercepts	139
Mean Int.length (um)	50.9
Std dev.	.
95% CI	.

At HAZ	Grain size #
Grain size	5.5
Intercepts	157
Mean Int.length (um)	45.1
Std dev.	.
95% CI	.



3.3 SEM and EDX analysis:

Elemental analysis of the macro regions in weld zone was performed using a scanning electron microscope (SEM) equipped with an EDX system. This analysis was conducted to gauge the distribution of alloying elements in the FSW zone. SEM image was analyzed at a magnification of 50X. EDAX was taken at the center of the weld zone as shown in the fig.8 Presence of Al (57.58%), C (33.76%) and O (8.66%) were prominent in that region.

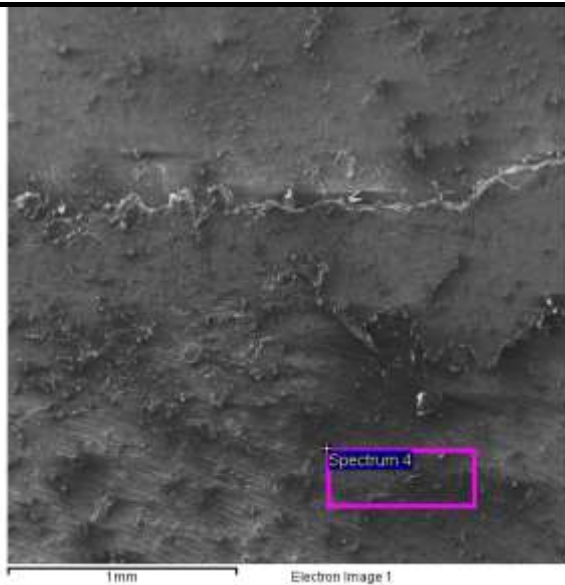


Fig.8: SEM and EDAX analysis

- [6] K. Tsuzaki, H. Xiaoxu, and T.Maki,Acta Mater., 44(11), 4491 (1996).
- [7] Q. Liu, M. Huang, m. yao, and J.Yang, Acta Metall. Mater., 40, 1753 (1992).
- [8] E.Nes, Metal Sci., 13, 211 (1979).
- [9] T.Chandra (Ed.), Recrystallization '90, TMS, Warrendale, PA, 1990.
- [10] L.E. Murr, H.K. Shih, C-S. Niou, Mater. Characterization, 33,65 (1994).

3.4 Hardness:

Vickers hardness tests were conducted across the regions of the weld spacing of (0.25mm) Average hardness value of 420 HV was obtained across the weldment for tapered pin.

IV. CONCLUSION

The FSW process parameters were optimized with respect to mechanical and metallurgical properties of the weldments. Tensile strength for S700 has more value than S500 also at nugget zone and HAZ the grain size is 5.5 the future research will contain creep tests and microstructural investigations using aluminium 6061 alloy using TEM microscopy (Transmission Electron Microscopy).

REFERENCES

- [1] Jata, K.V.: Semiatin, S.L. Continousdynamic Recrystallization during Friction Stir Welding of High Strength Aluminium Alloys. Scr. Mater. 200, 43,743-749. [CrossRef]
- [2] Ahmed Khalid Hussain, Evaluation of Parameters of Friction Stir Welding, 20 september 2012,2012 h.
- [3] M. Sivashanmugam, S. Ravikumar, T. Kumar, V. SeshagiriRao, D. Muruganandam, "A Review on Friction Stir Welding for Aluminium Alloys", 978-1-4244-9082- 0/10/\$26.00 ©2010 IEEE, pp. 216 – 221
- [4] Z.Y. MA "Friction Stir Processing Technology: A Review" Metallurgical and Materials Transactions A, 2008, vol.39A, pp.642-658.
- [5] Mandeep Singh Sidhu,Sukhpal Singh Chatha "Friction Stir Welding – Process and its Variables: A Review" IJETAE Volume 2, issue 12, 2012.

Determination of Dehydration Pattern and Sensory Properties variation of Blanched and Un-blanched, Cut and Whole *Moringa olifera* Leaves

Rathnayake A.R.M.H.A, Navarathna S.B.

Department of Food Science and Technology, Faculty of Applied Sciences, University of Sri Jayewardenepura, Gangodawila, Nugegoda, Sri Lanka

Abstract—Present dietary scenario necessitates exploring the possibility of incorporating novel ingredients that can improve quality in commonly consumed foods. *Moringa olifera* is abundant in sub-tropical regions that is an excellent source of beta carotene and other vitamins, minerals and amino acids. This study was conducted to determine effect of cutting and steam blanching before dehydration on organoleptic properties and dehydration pattern of *Moringa olifera* leaves. Fresh leaves were harvested from same location and dehydrated under four conditions according to two factor factorial design. Organoleptic properties of dehydrated leaves were compared for four sensory attributes as colour, aroma, taste and overall acceptability using five point hedonic scale. $L^*a^*b^*$ values were determined and drying curves were plotted for each treatment combination. Results revealed that, blanching and cutting can darker the colour and alter the flavour of dehydrated products. Further the surface area of the leaves have a significant effect in dehydrating time while blanching can accelerate the rate of moisture removal.

Keywords— *Blanching, Cutting, Dehydration, Moringa, Sensory properties.*

I. INTRODUCTION

Moringa oleifera plant is the most widely cultivated species among the 13 known species [1] of *Moringaceae* family [2],[3]. While native to the Indian sub-continent, *Moringa* has spread throughout the tropical and sub-tropical regions of the world such as Africa, tropical America, Sri Lanka, Mexico, Malaysia, Phillipine Islands etc. [2], [3].

Moringa is known in different regional names throughout the world such as Benzolive tree (Haiti), Horseradish tree (Florida), Nébéday (Senegal), Drumstick tree (India), Kelor, Marango, Mlonge, Mulangay, Saijihan, Sajna etc. [4]. In Sinhala it is called “Murunga” and in Tamil it is

called “Murungakai” [5]. *Moringa* grows mostly in dry zone in Sri Lanka such as Jaffna, Kalpitiya, Mannar, Puttalam and Hambantota [6].

Several varieties of *Moringa* such as *Rann murunga* (local variety), *Jaffna* and *Chavakachcheri murunga* are widely grown in Sri Lanka. In addition several hybrid types such as Kalpitiya, V 19 and V 16 have also been introduced [5] for local farmers.

Various studies have proved that *Moringa olifera* leaves have numerous nutritional values including vitamins, minerals and amino acids making it a virtually ideal dietary supplement [7],[8], [9]. As such, the leaves have been used to combat malnutrition, especially among infants and nursing mothers [7], [10], [11].

Since there are antioxidant and phytochemical properties have been found in *Moringa olifera* leaves, it is capable of being identified for having lots of medicinal uses, which have been recognized in the Ayurvedic and Unani systems of medicine [12]. Considering as a natural anticancer, antihypertensive, diuretic, antispasmodic, antiulcer, antihelminthic, antibiotic, detoxifying and immune building agent and also possess some cholesterol lowering activities [11].

Drying can be considered as the most commonly used method for preservation, packaging, transportation and distribution of leafy vegetables. The principle of preservation by dehydration process can be considered as to remove the moisture content of a material to a level where microorganism may not be able to grow and spoil it [8].

During the drying process there can be lots of losses in the sphere of nutritional, physical and chemical composition of leaves [13]. Therefore, to minimize drying losses various pretreatments such as blanching can be used.

Blanching is important mainly for the purpose of inactivating enzymes that can cause undesirable changes to reduce the quality of the final product; modifying

texture; preserving color, flavour, and nutritional value of the product (retain certain nutrients such as vitamins; and removing trapped air[8]). According to a research done by TitiMutiara K et al., [19] steam blanching had been able to show the highest amino acid content than un-blanching, hot water blanching and hot water blanch with sodium bicarbonate.

Thus, the current study was carried out to determine the effect of cutting and steam blanching before dehydration on the organoleptic properties and dehydration pattern of *Moringa olifera* leaves.

II. MATERIALS AND METHOD

2.1 Sample preparation

Fresh plant materials (leaves with the stalks) were taken from the same plant for the whole study.

Thereafter, fresh, undamaged, leaves were selected while discarding the bruised, discolored, decayed and wilted leaves. Fresh leaves were cut from the main branches and wash with distilled water. The washed leaves were then spread over a stainless steel mesh racks for 15 min to drain out the water. Thereafter, the leaves were dehydrated in a hot air oven at $48 \pm 2^\circ\text{C}$ for 150 minutes considering two major variables as, Cutting (a) and blanching (b) under two factor factorial design as,

a_0b_0 (Oven dry whole leaves without steam blanching), treatment No 127

a_0b_1 (Oven dry whole leaves with steam blanching for 4 minutes), treatment No 327

a_1b_0 (cut (about $1 \times 0.4\text{cm}$) & oven dry leaves without steam blanching), treatment No 227

a_1b_1 Cut & oven dry (about $1 \times 0.4\text{cm}$) with steam blanching for 4 minutes), treatment No 427.

2.2 Sensory evaluation

The sensory evaluation was performed by evaluating four major sensory attributes namely colour, Intensity of *Moringa* aroma, Intensity of *Moringa* taste and Overall acceptability using a five point hedonic scale. A semi trained sensory panel with thirty members was participated for this study.

2.3 Analysis of the colour variation in each treatment combination

Each sample was loaded tightly into the Granular-Materials Attachment (CR-A50) and the colour was measured using the Chromameter (Konica Minolta, CR-400 Head) as L^* , a^* , b^* colour values. Test was carried out three times per each sample.

2.4 Plotting the drying curve

Initially moisture content and weight of the four leaves samples were determined and those samples were kept in the hot air oven at $48 \pm 2^\circ\text{C}$ for 180 minutes while replicating each sample thrice. The weights of the each

sample were recorded at every 15 minute intervals. Finally, drying curves were plotted "Moisture content (%) versus Time (minutes)". The calculations were based on the equations (1) and (2).

$$\text{Weight loss \% after t time} = \frac{M_i - M_x}{M_i} * 100 \quad (1)$$

Where, Initial weight of dish with sample (M_i) and Weight after t time period (M_x).

If the answer of the equation (1) is w, equation (2) can be applied to calculate the moisture content at each 30 minutes interval.

$$\text{Moisture \% after t time period} = \text{Initial moisture content} - w(2)$$

2.5 Statistical analysis

The collected data pertaining to the non-parametric were analyzed according to Kruskal-Wallis and Mann Whitney U test and parametric data according to two sample t test using Minitab 17 Statistical Software package and graphical representation was done using Microsoft Office Excel 2010.

III. RESULTS AND DISCUSSION

3.1 Organoleptic properties of the four dehydrated leaves samples.

Organoleptic properties pertaining to colour, Intensity of *Moringa* aroma, Intensity of *Moringa* taste and Overall acceptability of for dehydrated *Moringa* leaves samples are given in table 1.

Table.1: The mean rank of the four dehydrated *Moringa* leaves samples with respect to the four sensory attributes.

Sample number	Colour	Intensity of <i>Moringa</i> aroma	Intensity of <i>Moringa</i> taste	Overall Acceptability
127	49.4 ^a	73.1 ^a	74.5 ^a	38.1 ^a
227	71.8 ^b	95.5 ^b	91.4 ^b	59.5 ^b
327	89.6 ^c	49.9 ^c	48.9 ^c	94.5 ^c
427	31.3 ^d	23.6 ^d	27.2 ^d	49.9 ^{ab}

^{a,b,c,d} Values in the same row with different superscripts are significantly different at 0.05 significant level.

According to sensory evaluation (table 1), all four samples are significantly different in colour, intensity of *Moringa* aroma and intensity of *Moringa* taste ($P \leq 0.05$). When considering the overall acceptability, sample number 127 and 427 had shown no significant different ($P \geq 0.05$) and also sample number 227 and 427 had shown no significant different ($P \geq 0.05$).

3.2 Chromameter values of the four dehydrated *Moringa* leaves samples

Mean Chromameter colour values of the dehydrated *Moringa* leaves samples are given in table 2.

Table.2: Mean Chromameter colour values of the dehydrated *Moringa* leaves samples

Sample	Average colour values from Chromameter		
	L*	a*	b*
a ₀ b ₀	44.82 ± 0.06	-6.79 ± 0.12	10.71 ± 0.11
a ₁ b ₀	44.74 ± 0.10	-6.29 ± 0.07	10.79 ± 0.06
a ₀ b ₁	38.54 ± 0.03	-3.46 ± 0.02	5.58 ± 0.05
a ₁ b ₁	37.96 ± 0.16	-2.74 ± 0.11	4.93 ± 0.08

As given in table 2, the lightness of the four samples are declining proving that the samples become darker. Whereas, all a* values are negative representing the green colour of the samples and the values are more closer to the center representing the reduction of the purity of the green colour (Chromacity). All b* values are positive representing the yellow colour and the values are closer to the center representing the reduction of the purity. According to the results, the un-blanching samples having lighter green colour than the blanching samples which imparts a dull green colour.

The natural green colour of leaves is due to presence of chlorophyll which directly relates to magnesium. During drying, the chlorophyll molecules are converted to pyropheophytin and pheophytin. Therefore, at high temperatures greenness is reduced. Thus, visually, dark green colour of the leaves convert into dull green-yellow due to degradation of chlorophyll. Same observation has been reported by Ali et al., [14].

According to both sensory evaluation and chromameter colour values, colour of the samples after dehydrating had variations. Likewise, sample "a₁b₀" had darker colour than "a₀b₀", while "a₁b₁" had darker colour than "a₁b₀" and also when comparing blanching samples with un-blanching samples, blanching samples had shown darker and thermally damaged colour than un-blanching samples. The colour values from the Chromameter also proved that observation. When considering the *Moringa* aroma and taste, "a₁b₀" had more intense *Moringa* aroma and taste (raw leafy taste with a little pungency but highlighting the characteristic flavors of *Moringa* more) than "a₀b₀" and also when comparing the blanching samples with un-blanching, blanching samples had less raw *Moringa* flavour than the un-blanching samples and had developed a flavour like in tea leaves (specially the aroma).

3.3 Plotting the drying curve

Fig 1 to 4 represents the drying curves for the four dehydrated *Moringa* leaves samples. And table 3

represents the moisture contents of the four samples initially and after dehydrating at 48±2°C for 180 minutes.

Table.3: Initial and final moisture content of the four dehydrated *Moringa* leaves samples.

Sample	Initial moisture % (w/b)	Moisture % after 180 minutes (w/b)
a ₀ b ₀	76.16 ± 0.20	3.26 ± 0.72
a ₁ b ₀	77.66 ± 0.24	2.50 ± 0.47
a ₀ b ₁	81.47 ± 0.36	1.07 ± 0.08
a ₁ b ₁	80.13 ± 0.33	2.39 ± 1.13

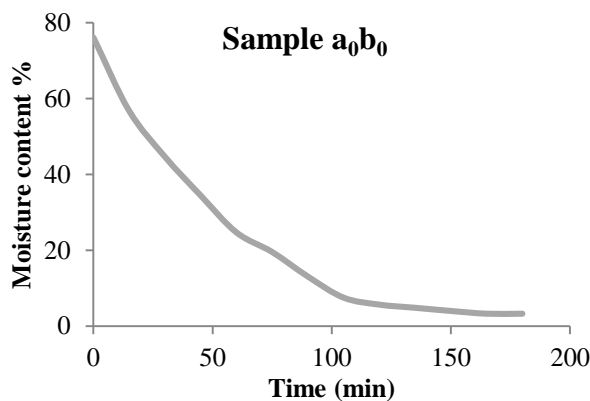


Fig.1: Drying curve for sample a₀b₀

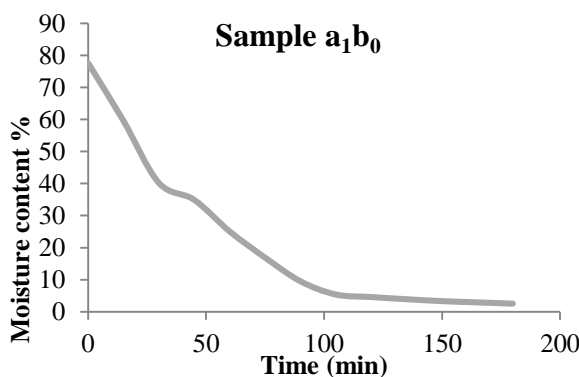


Fig. 2: Drying curve for sample a₁b₀

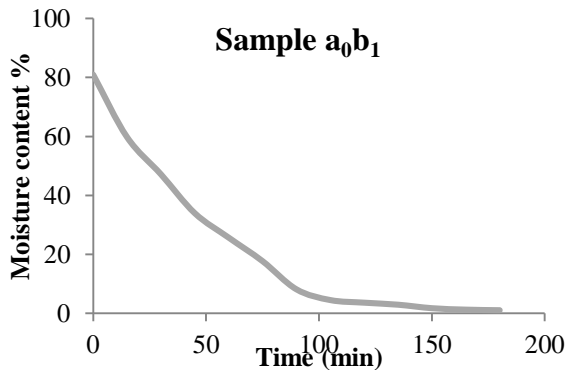


Fig.3: Drying curve for sample a₀b₁

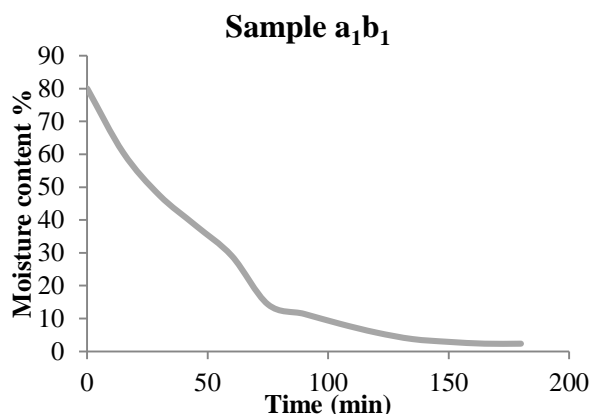


Fig.4: Drying curve for sample a₁b₁

The graphs in fig. 1, 2, 3, and 4 clearly indicate that initially only a minor change in moisture content occurs representing the preheat period. This can be happened because all the heat provided in the drying air is used to heat up the material to the drying temperature. Then after a certain period, it could be observed that water evaporated from the product at rather a constant rate which can be named as the constant heat period. During this period, the mass of water start to evaporate from the surface in equal intervals of time [15]. Then the drying rate began to reduce (Falling rate period) which can identify clearly in all the four graphs. This can be happened because it takes more time for internal moisture to move to the surface [15]. The point at which the drying rate starts to reduce can be declared as the Critical moisture content of the particular product.

Leaves in all four samples were dehydrated at same time under the same conditions such as drying temperature, air velocity, humidity of the air surrounding the food item etc.making the only variations between the four samples are blanching step and surface area.

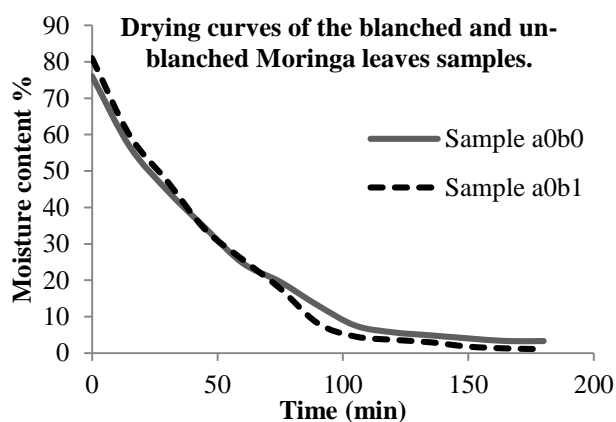


Fig.5: Comparison of the drying curves of the blanched and un-blanched Moringa leaves samples.

Fig 5 and 6 declares the variation of the dehydrating pattern with respect to the two treatment variables of cutting (a) and blanching (b).

According to the fig 5, moisture content of the blanched sample reducesto the critical moisture content within a short time span than the un-blanched sample. And the weight loss is higher in blanched samples compared to the un-blanched. According to Greve et al. [16] and Waldron et al. [17], cells lose their wall integrity during blanching process and thus the water removal is higher. Apart from that, certain volatile compounds and water soluble nutrients such as certain vitamins like vitamin C and minerals can be loss during blanching process which can also reduce the dry matter content of the samples up to some extent. Hence weight loss in blanched samples is higher than that of un-blanched samples.

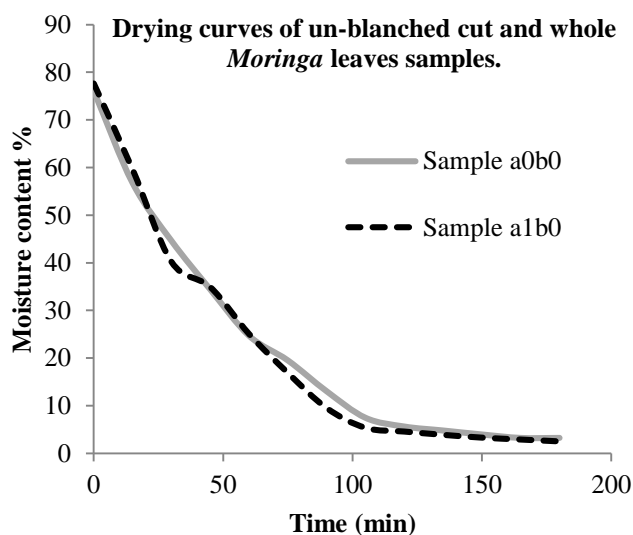


Fig.6: Comparison of the drying curves of the un-blanched cut and whole Moringa leaves samples.

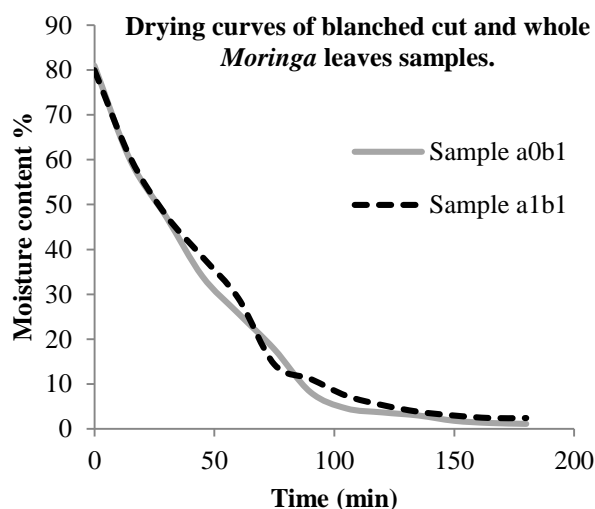


Fig.7: Comparison of the drying curves of the blanched cut and whole Moringa leaves samples.

When considering the particle size, if the particle size is smaller, larger the surface area which may lead to increase the speed of heat and mass transfer rate reducing the time required to reach the critical moisture content that can be identified clearly in both fig 6 and 7.

The reason for this can be described as the larger surface area provides more surface in contact with the heat medium and more surface from which moisture can be escaped. And also smaller the particles it can reduce the distance that heat can transfer to the center and reduce the distance that the moisture have to travel to reach the surface [18].

IV. CONCLUSION

When considering the four treatment combinations, the colour and aroma can be affected from cutting the *Moringa* leaves before dehydration by improving characteristic *Moringa* flavour. And further, blanching process can also darken the colour and alter the flavour of the leaves.

According to the drying curve, it can be concluded that the surface area of the samples and blanching can have a significant effect in dehydrating time while increasing the rate of moisture removal.

ACKNOWLEDGEMENT

The authors wish to offer their gratitude towards all the academic and non-academic staff of the Department of Food Science and Technology, University of Sri Jayewardenepura, Sri Lanka.

REFERENCES

- [1] Khawaja T.M, Tahira M and Ikram U.H, (2010), "Moringa oleifera : A natural gift- A review", Journal of Pharmaceutical Science and Research, vol. 2: pp. 775- 781
- [2] Ramachandran C., Peter K. V. and Gopalakrishnan P. K., (1980), Drumstick (*Moringa oleifera*): A Multipurpose Indian Vegetable, Economic Botany, 34(3), 1980, pp. 276-283
- [3] Adeyemi, S.B., Ogundele, K.O. and Animasaun, M.A., (2014), Influence of drying methods on the proximate and phytochemical composition of *Moringa oleifera* lam, Global journal of medicinal plant research, 2(2), pp. 11-15
- [4] Price, M.L.,(1985), The Moringa Tree, ECHO Technical note, USA, [ONLINE] available at: www.echonet.org
- [5] Liyanage R., Jayathilaka C., Perera O.S., Kulasooriya S.A., Jayawardana B.C., Wimalasiri S., (2014), Protein and Micronutrient Contents of *Moringaoleifera* (*Murunga*) Leaves Collected from Different Localities in Sri Lanka, Asian Journal of Agriculture and Food Science, Volume 02 – Issue 04, pp. 264-269
- [6] Tilakaratne B.M.K.S, Arachchi M.K.U, Wimalasiri K.M.S and Wijesinghe D.G.N.G, (2015), Development of Nutri Mix Fortified with Dehydrated *Murunga* Leaves and Pumpkin Powder, Proceedings of 8th International Research Conference, KDU, Published November 2015, pp. 81-84
- [7] Mishra S.P., Singh P and Singh S., (2012), Processing of *Moringaoleifera* Leaves for Human Consumption, Bulletin of Environment, Pharmacology and Life Sciences, Volume 2 [1] December 2012: pp. 28- 31
- [8] TitiMutiar K, Harijono, Teti Estiasih and EndangSriwahyuni., (2012), Nutrient Content of Kelor (*Moringa Oleifera*Lamk) Leaves Powder under Different Blanching Methods, Food and Public Health 2012, 2(6): pp. 296-300
- [9] Mouminah H.H.S, (2015), Effect of Dried *Moringa oleifera* Leaves on the Nutritional and Organoleptic Characteristics of Cookies, Alexandria science exchange journal, vol.36, No.4
- [10] Moyo B, Masika P.J., Hugo A. and Muchenje V., (2011), Nutritional characterization of *Moringa* (*Moringaoleifera* Lam.) leaves, African Journal of Biotechnology Vol. 10(60): pp. 12925-12933
- [11] Okiki P.A. Osibote I.A., Balogun O, Oyinloye B.E., Idris O., Olufunke A, Asoso S.O. and Olagbemide P.T., (2015), Evaluation of Proximate, Minerals, Vitamins and Phytochemical Composition of *Moringaoleifera* Lam. Cultivated in Ado Ekiti, Nigeria, Advances in Biological Research 9 (6): pp. 436-443
- [12] Mughal MH, Ali G, Srivastava PS, Iqbal M. 1999. Improvement of drumstick (*Moringa pterygosperma*Gaertn.) – a unique source of food and medicine through tissue culture. Hamdard Med 42: pp. 37–42.
- [13] Satwase A.N, Pandhre G. R, Sirsat P.G and Wade Y.R., (2013), Studies on Drying Characteristic and Nutritional Composition of Drumstick Leaves by Using Sun, Shadow, Cabinet and Oven Drying Methods. 2:584 doi:10.4172/scientificreports.584, Open Access Scientific Reports, Volume 2, Issue 1
- [14] Ali M.A., Yusof Y.A., Chin N.L., Ibrahim M.N. and Basra S.M.A., (2014), Drying Kinetics and Colour Analysis of *Moringa Oleifera* Leaves, Agriculture and Agricultural Science Procedia 2 (2014): pp. 394 – 400
- [15] Sinha N.K., Hui Y.H., Evranuz E.O., SiddiqM.,Ahmed J., (2011), Handbook of vegetable

- and vegetable processing, First edition, Wiley-blackwell.
- [16] Greve, L.C., Shackel, K.A., Ahmadi H., McArdle R.N., Gohlke., J.R. and Labavitch J.M., (1994). Impact of heating on carrot firmness: contribution of cellular turgor. *J Agric Food Chem*: pp.45:2896-9
- [17] Waldron K.W, Parker M.L and Smith A.C. (2003). Plant Cell Wall and Food Quality. *Areview.J.Sc.Food Technol. 2*: pp. 109-110
- [18] Potter N.N, Hotchkiss J.H., (1996), *Food Science*, Fifth edition, Chapman and Hall, New York: pp. 200-243
- [19] Titi Mutiara K, Harijono, Teti Estiasih and EndangSriwahyuni., (2012), Effect of Blanching Treatments against Protein Content and Amino Acid Drumstick Leaves (*Moringa oleifera*), *Journal of Food Research*; Vol. 2, No. 1, pp. 101-108

A Review on Simulation Optimization

Mobin Ahmad

Department of Mathematics, Faculty of Science, Jazan University, Saudi Arabia

Abstract— One of the primary and most important employments of simulations is for optimization. Simulation optimization can be characterized as the way toward finding the best info variable qualities from among all potential outcomes without unequivocally evaluating each possibility. The goal of simulation optimization is to minimize the assets spent while boosting the data acquired in a simulation experiment. The purpose of this paper is to review the zone of simulation optimization. A critical review of the methods employed and applications developed in this generally new range are introduced and striking victories are highlighted. Simulation optimization software tools are discussed. The target group is simulation practitioners and theoreticians and additionally fledglings in the field of simulation.

Keywords— Simulation, Optimization, important, process, resources, information, methods, develop, successes, software tools.

I. INTRODUCTION

The mathematical model of a system is concentrated on using simulation; it is known as a simulation model. System behavior at particular estimations of info factors is assessed by running the simulation model for a settled timeframe. A simulation experiment can be characterized as a test or a progression of tests in which significant changes are made to the information factors of a simulation model so that we may observe and recognize the purposes behind changes in the output variable(s). At the point when the quantity of information factors is huge and the simulation model is perplexing, the simulation experiment may turn out to be computationally restrictive. Other than the high computational cost, a much higher expense is brought about when imperfect info variable qualities are chosen. The way toward finding the best info variable qualities from among all potential outcomes without unequivocally evaluating each plausibility is simulation optimization. The goal of simulation optimization is minimizing the assets spent while amplifying the information acquired in a simulation experiment.

A general simulation model comprises n input variables (x_1, x_2, \dots, x_n) and m output variables

$(f_1(x), f_2(x), \dots, f_m(x))$ or (y_1, y_2, \dots, y_m) (Figure 1). Simulation optimization entails finding optimal settings of the input variables, i.e. values of x_1, x_2, \dots, x_n , which optimize the output variable(s).

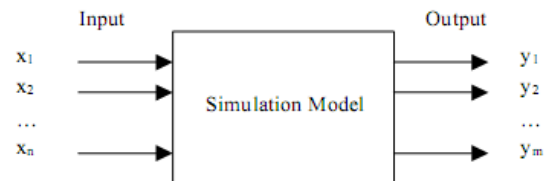


Fig.1: A Simulation Model

Such problems emerge habitually in engineering, for example, in process design, in mechanical experimentation, in design optimization, and in reliability optimization. This is the issue we will address in this paper. A simulation optimization model is shown in Figure 2. The yield of a simulation model is utilized by an optimization strategy to give criticism on advancement of the quest for the optimal solution. This thus manages further contribution to the simulation model.

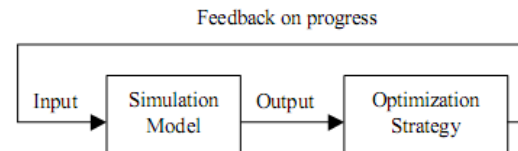


Fig.2: A Simulation Optimization Model

II. REVIEW OF LITERATURE

Simulations Optimization of true occasions can permit a complex problem to be dismembered and examined in a productive, safe, and financially savvy way. A simulation becomes a much more valuable instrument when optimizing an arrangement of parameters, especially in circumstance where experiments on this present reality framework are troublesome or impractical. Simulation optimization, as a rule, tries to minimize an objective function:

$$\min_{x \in \Theta} f(x)$$

Where $x \in \Theta$ represents an input vector of parameters, $f(x)$ is the scalar objective function and Θ is the constraint set [1, 2]. The info parameters are frequently alluded to as

variables, while the yield exhibitions are known as the reactions [3]. Simulations can be subdivided into two classifications of element variable sorts: consistent or discrete. In continuous simulations, the limitations are normally the set or every single genuine number, $n \in \mathbb{R}$. In discrete event simulations, the response function is not specifically accessible, may not be nonstop, or may not be in shut structure, and subsequently standard mathematical extremism solutions cannot be utilized. In this manner, a hunt must be performed over the discrete factor set [1, 2, 3, and 4]. This comprises of picking a worth for all parameters, running the simulation until the appropriate stopping criteria are met, and after that measuring the yield of the simulation that is to be optimized. In simulations with numerous parameters, a comprehensive inquiry turns into a period expending errand. Propels in computational power, consolidated with more current strategies for decreasing the pursuit space, have permitted discrete optimization techniques to be deployed with more success.



Fig.3: Six Domains of Simulation Optimization

Simulation Optimization has also become an integral part of many commercially available software simulation packages. Bowden and Hall [5] have described six domains which should be addressed when designing automatic simulation optimization tools (figure 3).

III. GRADIENT AND STOCHASTIC METHODS

Stochastic approximation methods (SAM) endeavor to discover minima by moving toward the steepest slope of the function. This is an iterative process, where every cycle comprises of evaluating the angle of the simulation model at the current decision point, and after that moving this decision point along the slope with a specific stride size. This development of the decision point can be expressed as

$$x^{n+1} = \Pi(x^n - \alpha_n \hat{\nabla}f(x^n))$$

Where x^n the current decision point solution is $\hat{\nabla}f(x^n)$ is the estimate of the gradient, α_n is the step size, and Π is a mapping onto the set Θ [2, 4, 11]. This method has received much attention, mainly because it has been proven to

converge to the minima as the step size gets sufficiently smaller [2, 4]. The difficulty in using this approach is estimating the gradient, which will not be continuous for discrete simulations. The most common gradient approximation method is the method of finite differences, where a small number of output values are taken for small changes in the simulation parameters. The two-sided, central difference gradient operator, for example, is:

$$\hat{\nabla}f(x_i) = \frac{f(x_i + \Delta x_i p_i) - f(x_i - \Delta x_i p_i)}{2\Delta x_i}$$

Where Δx_i is the perturbation of input parameter i and p_i is a vector with a one in the i th place and zeros elsewhere. This is essentially taking the discrete derivative, or “slope” of the function for each separate dimensional input parameter, denoted by i [2, 4, 8]. However, if the simulation output is noisy, then the gradient estimation could also be noisy, possibly making the decision point move in an inappropriate direction [4, 7].

It is clear that simulations with a higher number of variable input parameters will require more calculations to appraise the slope. In particular, utilizing the focal distinction inclination, it will take $2q$ simulation measurements, where q is the dimensionality, or number of variable input parameters [2, 8]. Another method has been proposed to lessen the quantity of simulation measurement required. This technique is known as Infinitesimal Perturbation Analysis (IPA), and is summarized in [5] by the formula:

$$\hat{\nabla}f(x) = \frac{f(x + \Delta x) - f(x - \Delta x)}{2\Delta x_i}$$

Now, the vector Δx becomes a random perturbation vector, and the gradient estimation requires only two simulation measurements, regardless of the input vector dimensionality. Thus, the speedup using this gradient estimator is potentially q . However, this potential is realized only if the number of iterations required for convergence is not increased. It is also been shown that the Δx vector should be independently and symmetrically distributed about zero with finite inverse moments. This can be achieved by using the Bernoulli ± 1 distribution.

IV. SIMULATION OPTIMIZATION APPLICATIONS

Simulation optimization methods have been connected to applications with a solitary target, applications that require the optimization of multiple criteria, and applications with non-parametric objectives.

Azadivar et al. (2010) connected a simulation optimization algorithm based on Box's perplexing hunt strategy to

optimize the locations and stock levels of semi-completed items in a force sort production system.

Corridor et al. (2009) utilized ES with a simulation model for streamlining a kabana sizing problem. Dad technique to stock models where the interest has a related restoration arrival process.

Tompkins and Azadivar (2011) proposed an approach to join a GA and an article oriented simulation model generator to locate the ideal shop floor design. an approach to consolidate the process plant production operations into the design of an office by joining simulation and GA. a calculation that joined SA and simulation to locate a suitable dispatching need of operations to minimize the aggregate lateness for a business flexible manufacturing system (FMS).

V. SIMULATION OPTIMIZATION SOFTWARE

A longstanding goal among a portion of the simulation practitioners and theoreticians was having the capacity to direct a progression of simulations in the most effective way as opposed to performing "blind" analyses and accepting that no less than one of the tests will yield the best contrasting option to execute (Glover et al., 2012). Numerous simulation software developers today have turned out to be more mindful of the importance of finding optimal and close optimal solutions for applications in minutes, instead of playing out a comprehensive examination of pertinent options in days or months. Simulation software that incorporates extraordinary hunt techniques to control a progression of simulations to uncover optimal or close ideal scenarios includes: Pro-Model, Auto-Mod, Micro Saint, Lay-OPT, and Factory OPT. A brief portrayal of every software’s optimization and/or statistical module follows.

The extra optimization module for Pro-Model is called Sim Runner Optimization. This module consists of two elements for investigating and optimizing existing Pro-Model simulation models. The primary component is a factorial configuration of tests that uncovers the impact of an adjustment in info element on the objective function. The second feature is a multi-variable optimization that tries different combinations of input components to land at the combination that yields the best objective function value.

VI. GENETIC ALGORITHMS

Genetic Algorithms (GA) are a subset of Evolutionary Algorithms, which are main stream in optimization literature on account of their generality. In particular, they just require the Monte-Carlo simulation output, with no

learning of capacity or information imperatives [9]. Genetic Algorithms endeavor to iteratively discover an all inclusive optimum solution by investigating the reaction surface of the simulation, and developing the best solutions in a comparable way to Darwin's hypothesis of evolution. A conceivable solution is encoded as a chromosome, with every quality in a chromosome speaking to a variety of a solitary input parameter. The wellness of a chromosome speaks to how close the chromosome's qualities will convey the simulation to its optimum value. A chromosome with low wellness will have a higher likelihood of being expelled from the population. A population is a gathering of chromosomes in one algorithm iteration. GA requires two operations, cross over and mutation, to change over one population of chromosomes to the following [3, 4]. The essential stream of hereditary calculations is demonstrated in figure 4.

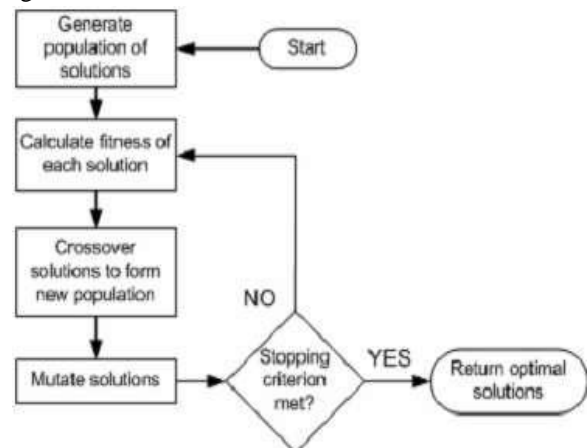


Fig.4: Genetic Algorithm flow chart

Some of the issues when implementing GA’s include gene representation, crossover operator selection, and mutation operator selection. Binary strings are a very common choice for gene representation, because they are very general, can be used for any size data type, and require minimal storage. An example of a binary string chromosome with genes representing byte sized parameters X, Y, and Z is given in figure 5.

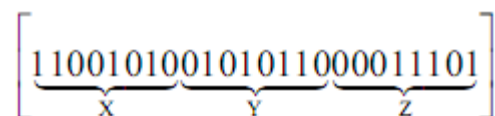


Fig.5: Chromosome of 3 bytes

The crossover operator is in charge of making new chromosomes from two existing ones. A famous way to deal with this is to choose a little number of bits from every quality and essentially swap them between the two

chromosomes [3, 4]. The mutation operator is basic since it permits the changing of qualities to keep a solution from being caught in a local optimum. This can be expert by arbitrarily selecting a bit from every chromosome, and upsetting it with a predefined probability distribution [3, 4]. As the iterations of the calculation increase, chromosomes (solutions) with lower wellness will be evacuated in the hybrid stage, so populaces will comprise of more chromosomes with higher wellness. The calculation can end when a sought number of cycles has been come to, or the standard deviation of a population's fitness has been minimized.

VII. CONCLUSION

We have provided an introduction to simulation optimization, with emphasis on gradient-based techniques for continuous parameter simulation optimization and on random search methods for discrete parameter simulation optimization. Although simulation optimization has received a fair amount of attention from the research community in recent years, the current methods generally require a considerable amount of technical sophistication on the part of the user, and they often require a substantial amount of computer time as well. Therefore, additional research aimed at increasing the efficiency and ease of application of simulation optimization techniques would be valuable.

REFERENCES

- [1] M.C. Fu, F. W. Glover, and J. April., Simulation Optimization: A Review, New Developments, and Applications, Proc. Of the 2010 Winter Simulation Conference, Orlando, FL, 83-95.
- [2] S. Olafsson, and J. Kim, Simulation Optimization, Proc. Of the Winter Simulation Conference, San Diego, CA, 2011, 79-84.
- [3] J. April, et al, Practical Introduction to Simulation Optimization, Proc. of the Winter Simulation Conference, New Orleans, LA, 2008, 71-78.
- [4] T. M. Alkahmis, and M. A. Ahmed, Simulation- Based Optimization Using Simulated Annealing With Confidence Interval, Proc of the 2007 Winter Simulation Conference, 514-519.
- [5] A. A. Prudius, and S. Andradottir, Two Simulated Annealing Algorithms for Noisy Objective Functions, Proc of the 2010 Winter Simulation Conference, Orlando, FL, 797-802.
- [6] J. A. B. Montevechi, R. G. A. Filho, and A. L. Medeiros, Application of Factorial Designs for Reducing Factors in Optimization via Discrete-Event Simulation, Proc. of the Winter Simulation Conference, Monterey, CA, 2008.
- [7] A. Persson, H. Grimm, A. Ng, T. Lezama, J. Ekberg, S. Falk, and P. Stablum, Simulation-Based Multi-Objective Optimization of Real-World Scheduling Problem, Proc of the Winter Simulation Conference, Monterey, CA, 2012.
- [8] A. Persson, H. Grimm, and A. Ng, On-Line Instrumentation for Simulation-Based Optimization, Proc. of the Winter Simulation Conference, Monterey, CA, 2011, 304-311.
- [9] Azadivar, F., J. Shu, and M. Ahmad. 2010. Simulation Optimization in Strategic Location of Semi-Finished Products in a Pull-Type Production System, Proceedings of the Winter Simulation Conference, 1123-1128.
- [10] Hall, J. D., and R. O. Bowden. 2011. Simulation Optimization for a Manufacturing Problem, Proceedings of the Southeastern Simulation Conference Huntsville, AL, Society for Computer Simulation, 135-140.
- [11] Tompkins, G. and F. Azadivar. 2011. Genetic Algorithms in Optimizing Simulated Systems, Proceedings of the Winter Simulation Conference, 757-762.
- [12] Glover, F., J. P. Kelly, and M. Laguna. 2012. New Advances and Applications of Combining Simulation and Optimization, Proceedings of the Winter Simulation Conference, 144-152.

Simulation of Corner Skidding Control System

M. Arun Kumar¹, S. Ashwin Kannan², A. Sathish Kumar³, S. Kumaravel⁴

^{1,2,3} Assistant Professor, Department of Mechanical Engineering, St. Joseph's Institute of Technology, TN, India

⁴ Assistant Professor, Department of Mechanical Engineering, Kongunadu College of Engg&Tech, TN, India

Abstract—Traction control system in automotive applications increases the stability and safety of vehicles. There are various types of vehicle control systems employed in internal combustion engine vehicles. The application of control system to motorcycles (two wheelers) is not so widely used as that of four wheelers, because of high cost of the control system. If one moves at high speed in motorcycles at the corners, the centripetal force exceeds the frictional force. At that time lower amount of traction effort occurs in between the tire and road and hence high amount of skidding will occur in the motorcycles. The proposed control system design helps the rider in maintaining a secure of the motorcycle in bend. Geometry parameters such as rolling angle and steering angle of the bike are taken into consideration. The centripetal force and frictional force can be measured using the sensors by interfacing it with the Lab VIEW software. The simulation of the control system design has been carried out and the values for the skidding condition are obtained.

Keywords— Traction control system, frictional force, centripetal force, Rolling angle, Steering angle, Simulation.

I. INTRODUCTION

Traction control is a widely used in automotive applications in order to increase stability and safety of vehicles. Well known vehicle control systems such as Anti Slip Regulation (ASR), Electronic Stability Program (ESP) and Antilock Brake System (ABS) are used in IC engine vehicles. This type of Traction control prevents the vehicle from skidding occurrence when accelerating over a wet or loose surface, by reducing engine output, so that the vehicle can move without skidding, and produces the maximum stability while cornering especially in wet roads. Critical conditions in riding a motorcycle is the rearing up in bend. The corner skidding control system design should be measuring the centripetal force and frictional force by using the sensors. Then those values should be compared with the theoretical values. The simulation of the control system design has been carried out using Lab VIEW software and the values for the skidding condition are obtained. **Faruk Kececi et al (2009)** developed an adaptive vehicle skid control concept (control algorithms). Dynamic

equations of an electric vehicle are formulated and the effect of the road friction coefficient has been studied. The study has been carried out by two cases.

i) When the information of road condition is not available, the roundedness of the velocity and position error are proved.

ii) The controller performance is examined when the road condition is measured (but the friction coefficients of road are assumed not to be known).

The simulation of adaptive vehicle skid control has been done. The Simulation results has shown the effectiveness of the controller schemes.

II. LITERATURE SURVEY

Jae - Bok Song et al (1999) studied over the improvement in acceleration performance, stability and steerability on slippery roads using slip control systems has been carried out. This paper mainly deals with the engine control algorithm via adjustment of the engine throttle angle. The vehicle tests have been carried out on low friction roads to verify the control algorithm. From the test results, it is found that the controlled vehicle has more performance in acceleration and stability than the non-controlled vehicle.

Jose Mayora et al (2009) investigated about the 'Pavement-tire friction' provides the grip which is required for maintaining vehicle control and for stopping in an emergency situations. Crash frequencies on dry and wet pavement were analysed using two methods. They are

1. Cross-sectional analysis and
2. Before-after analysis.

From the above analysis it is found that both wet- and dry-pavement crash rates present a decreasing trend as skid resistance values increase. Also the Wet-pavement crash rates were found to be significantly higher in curves than in tangents. Pavement friction improvement schemes were found to result in significant reductions in wet-pavement crash rates. This research confirmed the importance of maintaining adequate levels of pavement friction to safeguard traffic safety and the potential of pavement friction improvement schemes to achieve significant reductions in wet-pavement crash rates .

Pascal Cardinale et al (2009) adapted a new algorithm and its hardware implementation of traction control for supermotard or motocross has been implemented. In this

study the torque applied to the rear wheel can be controlled by reducing the gasoline injected closing through the butterfly valve or reducing the electrical current to the sparking plug. The proposed system modifies the sparking scheme inserting an switch in addition, parallel to the manual turn off switch. This switch simply bypasses to ground the electrical current flows in the sparking coil. This switch is controlled by a microcontroller on the basis of the output of some additional sensors.

Patrick Seiniger et al (2012) studied over corner braking and brake steer torque problems during real corner braking. This study describes the potential of stability control systems to help save motorcyclists lives. It summarizes safety research conducted and commissioned by the Federal Highway Research Institute (Bundesanstalt fur Strassenwesen, BASt) during the last twenty years, with particular focus on the state of the art in motorcycle control systems. In order to eliminate the problems arising from the BST effect, four different approaches are presented.

1. Reducing the brake force
2. Reducing the offset between steering axis and tire contact patch
3. Adapting the steering damper characteristics
4. Providing an active counter steer torque.

III. METHODOLOGY

The control system architecture has been designed based on the various results obtained through the theories related for skidding condition. The Conditions for Skidding are derived as follows

$$\text{Frictional force} = \mu (mg)$$

For skidding,

$$\begin{aligned} \text{Centripetal force} &> \text{frictional force} \\ (mv^2/r) &> \mu \end{aligned}$$

$$[\mu = mg]$$

$$(v^2/rg) > \mu$$

But $(v^2/rg) = \tan \theta$

$$\tan \theta > \mu$$

When the tangent of the angle of banking is greater than co-efficient of friction, skidding occurs.

Overall condition for skidding,

$$(v^2/rg) > \tan \theta$$

Where,

V - velocity of vehicle in m/s

r - radius of the track in m

θ -angle of inclination of vehicle with reference from vertical

Based on the above conditions, the design has been made using various sensors and microcontrollers. If the skidding condition occurs, then the fuel flow rate will reduced so that the torque can be reduced to avoid

skidding. The working procedure of the proposed model and the overall design of the system is shown in "Fig. 1".

The microcontroller is interfaced with various sensors and it is programmed based on skidding conditions. The various valves to control the fuel flow rate are interface with microcontroller. The controller architecture of the proposed system is shown in "Fig. 2".

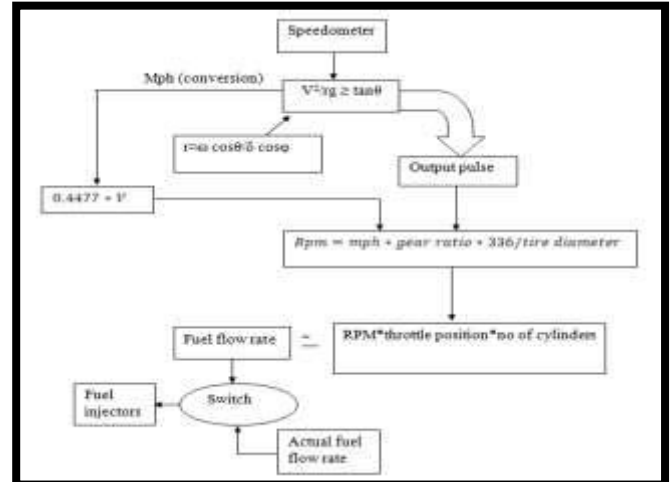


Fig. 1: Working procedure of the proposed model

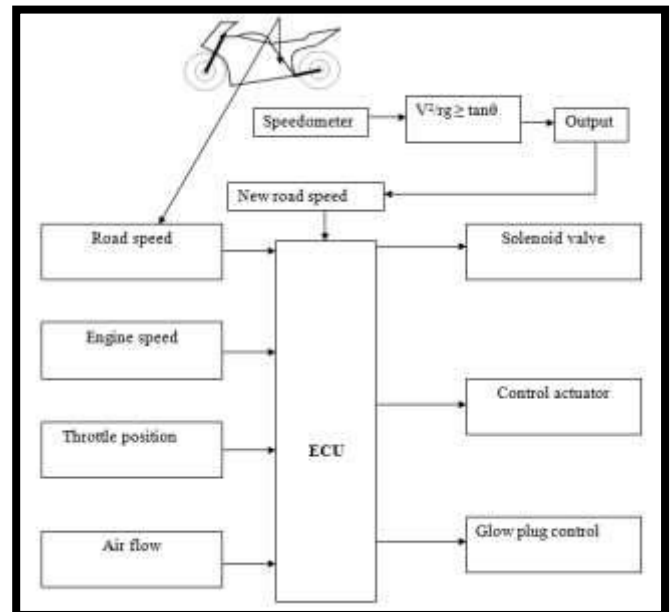


Fig. 2: Controller Architecture

The various sensors to measure speed, steering angle and bend angle are interfaced with microcontroller to get input values. The microcontroller will be programmed based on skidding conditions. The architecture of the sensor-microcontroller interfacing is shown in "Fig.3".

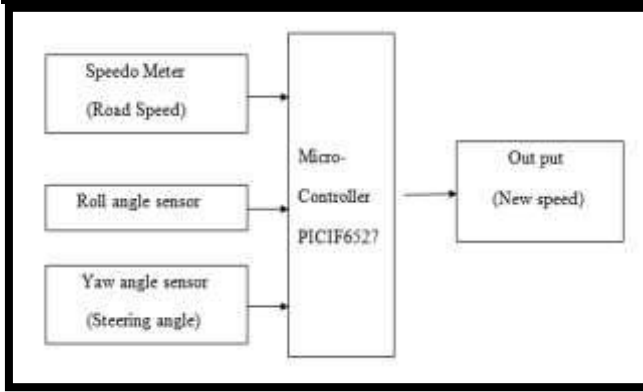


Fig. 3: Architecture of the sensor- microcontroller interfacing



Fig.5: Rotary Potentiometer

IV. SELECTION OF SENSORS

The sensors are used for measuring the various input values. The roll angle sensors are used for measuring the rolling angle of the two wheeler, the rotary potentiometer is used for measuring the steering angle of the two wheeler and reflective infrared sensor (RPM sensor) are used for measuring the speed of the rollers. These sensors will give the input voltages to the microcontroller.

4.1. Roll Angle Sensor

This sensor is used for measuring the inclination angle of the bike. When the bike is inclined or bends, this sensor should be generating the voltages for the corresponding angles of bend. The Roll angle sensor is shown in "Fig 4".

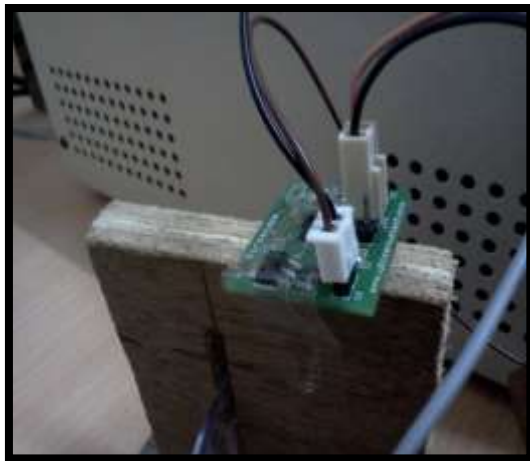


Fig.4: Roll Angle Sensor

4.2. Rotary Potentiometer

A Potentiometer is a device that can be used to convert a linear or angular displacement into a voltage. The potentiometer has an input shaft to which a wiper is attached. It is shown in "Fig 5". The displacement is applied to the input shaft when the shaft moves, the wiper contact slides over the resistance material. Hence the voltage is generated.

4.3. Reflective Infrared Sensor (Rpm Sensor)

The behaviour of sensor shown in Fig. can be used to generate a pulse train that can then be converted into a measurement of RPM by counting the number of pulses that occur during a known time interval.



Fig.6: Reflective Infrared Sensors

V. SENSORS ANALYSIS

Laboratory Virtual Instrumentation Engineering Workbench (Lab VIEW) is a platform from National Instruments. It contains comprehensive set of tools for acquiring, displaying, analyzing and storing data.

5.1. Lab VIEW - Sensor Interfacing

Here the sensors are interfaced with Lab VIEW as shown in "Fig 7" to find the response of the roll angle sensor.

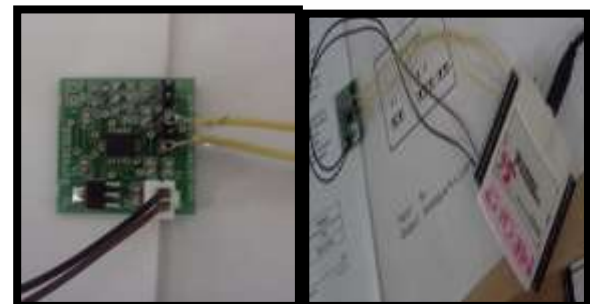


Fig.7: Sensors Interfacing with the DAQ Card

5.2. Procedure of Lab VIEW Program

1. Open Lab VIEW.
2. The 'Front Panel' and 'Block Diagram Panel' appear.
3. Create DAQ assistant from the function palette.
4. Configure DAQ. Select input > DAQ assistant.
5. Select the appropriate channel through which you have connected the wires (ai0, ai1) and click 'Next'.
6. In the next dialog box, select voltage range as 0 – 5 V, Terminal configurations > RSE and acquisition mode > N samples.
7. Create the program starting from DAQ assistant and create while loop.
8. Select the graph indicators and chart from the control palette.
9. Create another chart in a similar fashion to display the displacement waveform. Name one chart in a similar fashion to display the displacement waveform.
10. Also Click control palette > Numerical indicators > numerical indicator to display voltage or displacement as digital indicator.

Execute the program by clicking run button and get the output. The developed program and the results obtained in the display are shown in “Fig. 8”

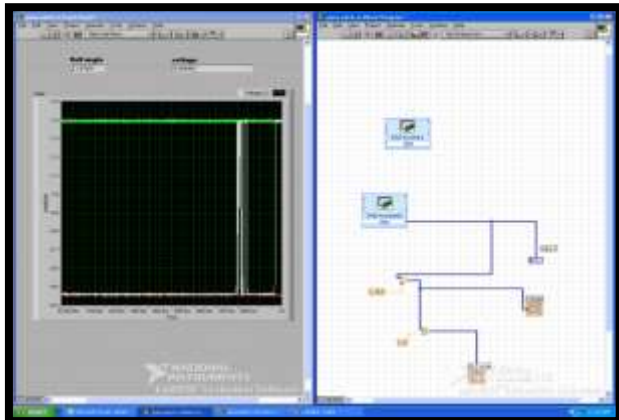


Fig. 8: Lab VIEW Diagram

5.3. Angle Calibration of Rotary Potentiometer

On interfacing with Lab VIEW, the result of Rotary Potentiometer can be obtained as

Turning of 1 degree = output voltage is 0.67 mV/sec



Fig. 9: Rotary Potentiometer



Fig. 9.1: Rotary Potentiometer connected with multimeter

Rotary potentiometer shown in “Fig .9.1” gives the following voltages for the particular angles. We have taken those values by using the multimeter. The Potentiometer calibration has been shown in Table.1

Table.1: Potentiometer Angle Calibration

S. No	Angle (degree)	Voltage (volts)
1	1	0.018
2	10	0.18
3	45	0.81
4	60	1.08
5	90	1.66
S. No	Angle (degree)	Voltage (volts)
6	135	2.43
7	180	3.33
8	225	4.16
9	270	5

VI. MODEL INTERFACING WITH Lab VIEW

6.1. Basic Idea of Model Interfacing With Lab VIEW

The model with three input values is interfaced and the condition for skidding has been manipulated. The block diagram for the Lab VIEW simulation is shown in “Fig. 10”.

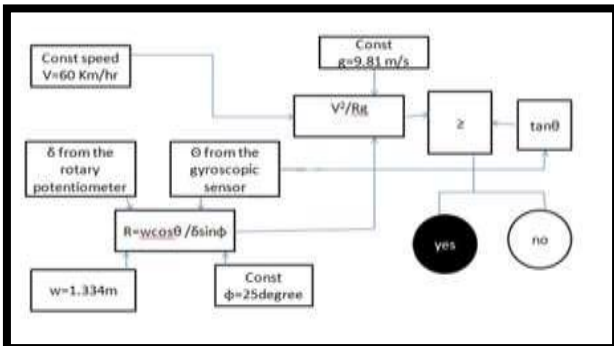


Fig. 10: Block diagram of Model Simulation

6.2. Lab VIEW - Model Interfacing

The model is interfaced with Lab VIEW to achieve the skidding condition of the model. The experimental setup for the Simulation is shown in “Fig. 11”.



Fig.11: Lab VIEW - Model Interfacing

6.3. Lab VIEW Program

The Program has been developed in the Lab VIEW software to find out the skidding condition. The developed program with sensors interfacing is shown in “Fig 12”.

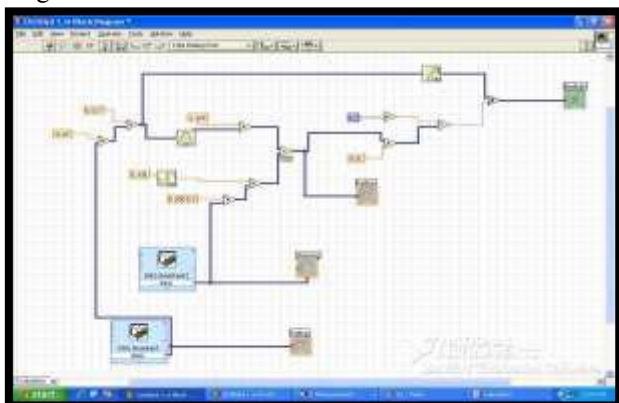


Fig.12: Lab VIEW Program

VII. RESULTS & DISCUSSIONS

7.1. THEORETICAL SKIDDING CONDITION VALUES

The theoretical values are compared with the simulation results. Three parameters such as velocity, radius and inclination angle are independent to each other. The theoretical condition for simulation model is taken as follows.

$V = 60 \text{ km/hr}$

$R = 50 \text{ m}$

Condition $V^2/Rg \geq \tan\theta$

So, $\theta = 30.4 \text{ degree}$

The skidding condition values of the two wheelers for corresponding angles and velocity are tabulated.

Table.2: Skidding Condition Parameter Values (Theoretical)

S. No	Velocity (km/hr)	Radius (m)	Angle (degree)
1	54	35	33.22
2	80	50	45.18
3	85	60	43.07
4	90	50	51.87
5	60	50	30.04
6	36	10	45.54
7	45	30	29.96

In this simulation model the speed of the vehicle should be constant. The radius of the curvature has been attained by four parameters. Those parameters are Wheel base, caster angle, steering angle, inclination angle. The skidding condition has been attained at the following values.

Speed (V) = 60 km/hr

Caster angle (φ) = 25 degree

Wheel base (w) = 1.334m

Inclination angle (θ) = 29.92 degree

Steering angle (δ) = 97.4 degree

VIII. CONCLUSION

The control system architecture has been developed with sensors of low cost and the Lab VIEW simulation has been carried on the model. The values for the skidding condition are obtained. Results were compared with the theoretical values and it is found that the simulation results coexist with the theoretical results. This work can be further developed by conducting an experiment using proposed model in a two wheeler.

REFERENCES

- [1] Farukkececi, Gang Tao (2006) “*Adaptive Vehicle Skid Control*” *Mechatronics*, Vol. 16, pp. 291–301.
- [2] Jae-Bok Song, Byong- Cheolkim, Dong- Chul Shin (1999) “*Development of traction control system slip control logic based on engine throttle control*” *KSME International Journal*, Vol. 13, pp.74-81.
- [3] Jose M.PardilloMayora, Rafael Jurado Pi (2009) “*An assessment of the skid resistance effect on traffic safety under wet pavement conditions*” *Accident Analysis and Prevention*, Vol. 41, pp. 881–886.
- [4] Pascal Carotinale, CamilloD’Angello and Massimoconti (2009) “*The traction control system for motor cycles*” *EURASIP Journal on Embedded Systems*, Article ID 161373.
- [5] Patrick Seiniger, A.KaiSchroter (2012) “*Perspectives for motor cycle stability control systems*” *Accident Analysis and Prevention*, Vol. 44, pp. 74– 81.
- [6] S S Rattan (2005), “*Theory of Machines*” The McGraw Hill Corporation, second edition, pp. 699-710.

Synthesis and Characterization of Hybrid Polymer Composites

Ajai Aravind Nair¹, S. Prakash², Dr. R. Christu Paul³

¹P.G Scholar, Mechanical Engineering, C.S.I Institute of Technology, Thovalai, India

²Mechanical Engineering, Immanuel Arasar JJ College of Engineering, Nattalam, India

³Mechanical Engineering, C.S.I Institute of Technology, Thovalai, India

Abstract—The replacement of synthetic fibers by natural fibers paves the way for awareness about environmental degradation and stresses on the need for a constant and reliable development for the betterment of the environment.. Therefore this study is based on fabrication and an investigation on the mechanical properties of animal fiber - plant fiber hybrid bio composites. Out of varied plant and animal fibers, the fibers chosen for this research work are coir and human hair. One of the reasons for selecting hair as the reinforcement material is due to the fact that, human hair is unceasingly produced in large quantity and which becomes a waste in large quantity too. Thus, an effective method should be made to utilize such unceasingly produced waste in a better way. Coir fiber is selected due to its wide range of characteristics. The fabrication can be done by hand layup technique. This technique is utilized to manufacture three samples. First one is coir fiber based bio composite, and second is hair based bio composite and the third sample is a hybrid bio composite made from both hair and coir fiber. The bio composite will be verified under mechanical properties such as tensile strength, compressive strength, flexural strength, impact strength and hardness. Mechanical trials conducted previously have disclosed that coir based bio composite is good in compression, flexural and impact strengths. The Hair based composite also has shown higher tensile strength and higher break load. The three composites possess the same hardness because these fibers constitute the matrix phase which is formed by epoxy resin. Analysis of hybrid composite shows that coir and hair composite constitute mutual properties. Therefore it is a better agreement to include hair fiber in the composite to reduce the overall cost of the composite, as the cost of coir is excess.

Keywords — Coir fiber, Hand lay-up, Human Hair, Hybrid, Mechanical Testing.

I. INTRODUCTION

In the development of modern technology, Fiber Reinforced Polymer (FRP) composites play a vital role in day to day life due to its low cost, processing advantage of lower density and possessing good mechanical

behavior over traditional reinforcement materials. [1-3]. Since from the time of human evolution humans have been using materials to fulfill their needs and comforts and it has been updated into new from time to time, since, it is a need to keep it par with the developing technology which holds many challenging requirements. In order to cope up with the rising challenges, the materials are expected to have several unique features. Primarily, the materials should possess complex performance efficiency and reliability. Secondly, the materials should contain less weight as possible. Thirdly, the material must be a combination of many properties, thus it can remain neutral without limited by any particular application. The above discussed requirements can be fulfilled only by the composite material and the replacement of synthetic fiber by natural fibers can avoid environmental degradation, so it is a boon to the nature too. Commonly plants and animals are the major sources of natural fibers but plant based (cellulose) composites are widely accessible for research work compared to animal fibers. Renewable natural fibers such as oil palm, flax, and pineapple leaf can be used to acquire high performance polymer materials. The renewable natural fiber as reinforcement for polymer is a sustainable choice to the environment [4-7]. But this research work is based on animal fiber based composite because coir, one among other animal fibers possesses major extensive properties both mechanically and physically. And also the Human hair is prominently used in this research to devise a new effective method that can be used in fabrication. The coir and human hair serve better use because the usage of fillers in this material is restricted. Filler materials are generally used in composite materials to increase the possessions of the material. But in most of the cases they tend to reduce the volume fraction of the resin which constitutes the matrix phase and it also reduces the mechanical properties of the material. Therefore fillers are highly restricted and this work mainly concentrates on identifying the mechanical components of coir and human hair fiber based composites which can be used in the replacement of metals in certain high performance materials.

II. MATERIALS

The raw materials included in the fabrication are Epoxy resin LY 554, Human hair Fiber, Coconut coir fiber, Hardener, and Mansion Wax. Human hair Fiber, Coconut coir fiber must be alkali-treated in 2% of NaOH solution from 10 min to 30 min to remove any oily material and hemi cellulose, and then must be dehydrated in sun light.

2.1 Coir Fiber

The coir fibers are first battered with 2% of detergent solution for one hour and washed with distilled dihydrogen monoxide and then it is sanctioned to dry in an air oven at 700c. Then these dried fibers are to be treated with sodium hydroxide solution. The NAOH commixed solution should be kept in the oven for the second time at 780c for 3 hours. Subsequently the treated fibers must be cautiously washed with dilute acid in order to abstract the alkali particles and then let it for final dehydration.



Fig.1: Coir Fiber

2.2 Human Hair Fiber

Human hairs constitute several components and the compositions are as follows. It constitutes proteins of 65-95% by weight, 32% dihydrogen monoxide and the rest is occupied by lipid pigments and other compounds. Keratin is the main occupant of human hair is a type of protein that is virtually 80% responsible for the formation of hair [8]. Structural analysis of hair shows that, it consists of three different layers such as cuticle, cortex and medulla. The surface properties of hair depend on the cuticle which forms the outermost layer by cross linked cystine [9].



Fig.2: Human Hair Fiber

The medulla contains highly concentrated lipid and less cystine and it is in the form of cylinder which forms the innermost hair thread. Utilization of hair as a reinforcement material is an incipient endeavor as it evolves an incipient method to utilize the material which is available in immensely colossal quantities. It can be used as a reinforcement material because it can resist stretching and compression [10]. Investigation on the mechanical properties of fiber composites can be done and it can be concluded that hybrid composites exhibit high vigor.

2.3 Resin and Hardener

The matrix phase binds the sundry layers of the fibers and it is constituted by epoxy resin, to amend the remedying rate 1 part of hardener is integrated to 10 components of resin. The commercial grade of resin used is Araldite LY554 and hardener used is amino hydrocarbon.



Fig.3: Resin and Hardener

III. FABRICATION PROCEDURE

The fabrication procedure is done utilizing the hand layup technique. For the fabrication of coir fiber, the following procedures are handled. First the coir fibers should be cleaned exhaustively and dried in shade. At the commencement of fabrication, the mould from the coir must be cleaned and kept dust free. Then a layer of Poly Vinyl Alcohol must be applied on the mould surface, so that it can facilely abstract the laminate after fabrication.

After that the epoxy resins (Araldite LY554) and hardener (amino hydrocarbon) should be commixed together in a proportion of 10:1. Then the resin should be applied in the mould utilizing a brush and the coir threads are laid on it horizontally. Caution about overlapping of fibers must be taken, as it can lead to the variation of thickness of the culminated composite. The roller can be acclimated to set the coir fibers firmly over the antecedent layer of resin and shuns air bubbles between.

Table.1: Orientation of fiber in composites

Sample A	Coir-horizontal	Coir - vertical	Coir-horizontal
Sample B	Hair-horizontal	Hair-vertical	Hair-horizontal
Sample C	Coir-horizontal	Hair vertical	Coir-horizontal

Then a double coating of resin must be given to the coir layer with the avail of a brush. Once more the same amount of coir fibers should be laid over the resin layer, in a vertical direction. This can be done to increment the overall vigor of the composite because transmutation in orientation has the competency to sentinel the material from the propagation of applied forces. The laminate must be then sanctioned to alleviate for duration of one hour. A force must be given on the surface of the composite to evade it from the formation of air bubbles. Conclusively it's consequential to ascertain that the resin has alleviated and after that it must be punctiliously abstracted from the mould and cut into required dimensions. The same procedure must be followed for all the samples. Three samples should be fabricated with the same procedure having fibers in different orientation as shown in Table-1.

IV. TESTING OF COMPOSITES

4.1 Tensile Test

Tensile test is one of the most widely used tests by the researchers to resolve the tensile properties. Tensile test must be done according to the format of the American Society for Testing and Materials (ASTM) specified test specimens. In the present examination, the tensile testing machine is Associated Scientific Engg. Works, FIE group of India which is provided with gear rotation speed of 1.25, 1.5 & 2.5 mm /min and it can be tested for a maximum load of 5 tons. Tests can be repeated on specimens achieved from three samples which are made with Coir, Hair and a hybrid of Coir-Hair. Tensile force is applied at the cessations by clamping the specimen in the UTM. The tensile breaking load consequent to each sample is attained. And the variation of tensile stress with strain can be plotted.



Fig.4: Tensile testing machine used in the present investigation

4.2 Compressive Test

For the tensile test a standard piece of laminate must be cut predicated on ASTM standard. The test is done in a FIE group of India, at room conditions. Tests are reiterated on specimens obtained from three samples made with coir, hair and a hybrid of coir-hair. Compressive force is applied at the terminuses by clamping the specimen in the UTM. The compressive breaking load consequent to each sample is attained. And the disparity of compressive stress with strain can be plotted.

4.3 Flexural Test

For the flexural test a standard piece of laminate must be cut predicated on ASTM standard. The test is done in a FIE group of India, at room conditions. Tests are reiterated on specimens obtained from three samples made with coir, hair and a hybrid of coir-hair. Flexural force is applied at the terminuses by clamping the specimen in the UTM. The flexural breaking load corresponding to each sample is obtained and the disparity of flexural stress with strain can be plotted.

4.4 Impact Test

Impact test gives extreme energy to the material. And this impact test can be done in a Charpy Impact Machine of ASTM standard. The samples for this test must be cut according to the standard dimensions. The specimen relents to the heavy blow obtained by the hammer and the blow which it fails to withstand gives the impact energy. Tests must be reiterated on specimens obtained from the three samples that are made with Coir, Hair and a hybrid of Coir-Hair.

4.5 Hardness Test

The Hardness Test estimates the indentation rigidity of polymer predicated materials. The test is done as per ASTM standard. The specimen must be indented utilizing a hardened steel indenter with certain force and geometry.

V. RESULT AND DISCUSSION

5.1 Tensile Properties

The fabricated sample must be tested as per the ASTM standard. The composites such as hair, coir and Coir-hair

hold varied tensile strength and that are shown in figure 6. The tensile strength of the coir, Hair, and Hybrid composite fiber varies from 16 MPa to 19 MPa.

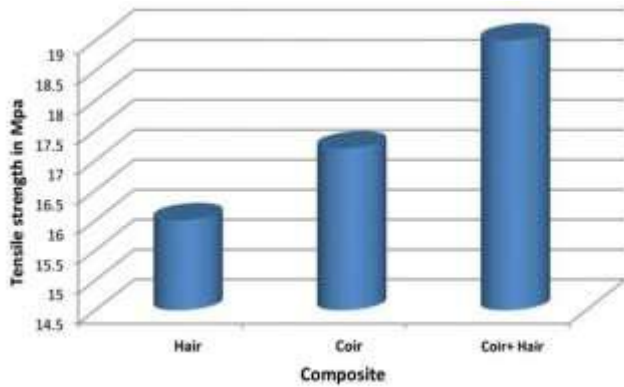


Fig.5: Tensile Properties

These outcomes clearly indicate the gradual increase of tensile strength for hair fiber more than the hybrid fiber. Comparable remarks are reported by Noorunisa Khanam et al. [11]. From this fig, it is conspicuous that the hybrid composite holds better tensile properties. This is because, the tensile vigor depends on the cross section area of the specimen and the modulus depends on the elongation percentage of the specimen. So these two parameters are liberated from each other and the elongation percentage is superior only for the hybrid composite. Consequently it's clear that the hybrid composite can endure more tensile load than the other two composites afore failure.

5.2 Compressive Properties

The Compressive Test can be done as per the ASTM: D695 standard and the variation in compressive strength of the composites which are alkali treated are shown in figure 7.

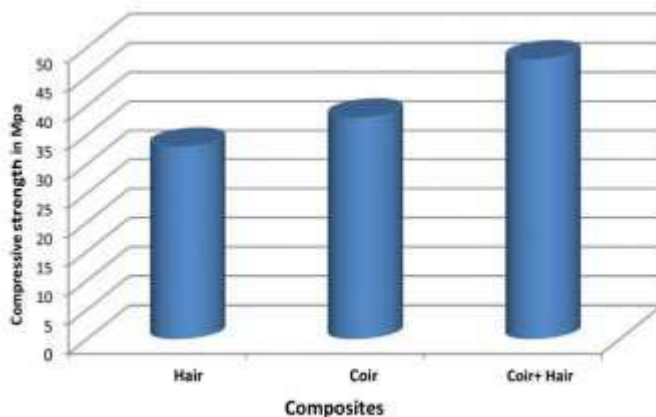


Fig.6: Compressive Properties

The composite materials must be tested and the compressive strength must be calculated. Three specimens of different fiber volume fractions and average compressive strength must be tested and reported. The compressive strength increases in the hybrid composite and the compressive strength of the Hair, Coir and Hybrid

composite fiber varies from 33 MPa to 48 MPa. The result of this test display that, the hybrid composite has superior properties compared to all the other parameters calculated.

5.3 Flexural Properties

Flexural test can also be called as bend test, and this test must be done with the appropriate fixture as per the ASTM-D 790 (0.125" x 0.5" x 5.0"). This test must be steered in the macrocosmic testing machine in a compression mode. First the sample must be placed on the bending fixture and the compressive load must be given under concrete conditions. During this function a curve will be engendered till the failure of the sample. The varied flexural strength of the three composites such as hair based, coir based, Coir-hair based samples are shown in figures 8. The flexural strength of the Hybrid composite fiber is 56 MPa. From these results, it is conspicuous that the hybrid composite holds better flexural properties.

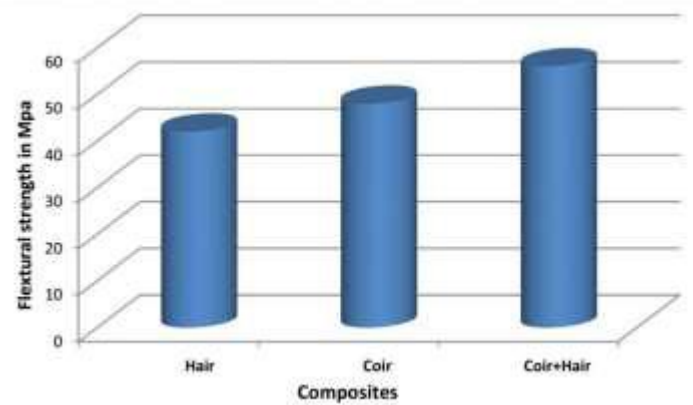


Fig.6: Compressive Properties

A. Impact Properties

To conduct the impact test, Charpy impact machine must be utilized. The result of the impact test is shown in fig .The impact vigor must be calculated from the energy engrossed by the specimen when exposed to a heftily ponderous blow. Resin toughness determines the impact vigor, rather than the fiber stiffness. The stacking system of the fibers plays a paramount role and integrates to the impact properties of the laminate because, the crack propagation is fortified by the alteration in the fiber placement thus incrementing the impact vigor of the specimen.

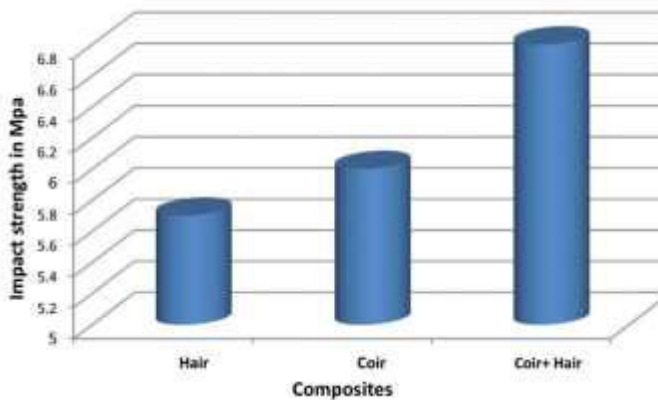


Fig 6: Compressive Properties

The maximum impact strength of the composites varies from 5.7 MPa to 6.8 MPa. Alkali treated coir fibers and Hair fibers show improved impact strength. This result is par with the findings of Varada Rajulu et al[12] and Ramachandra reddy et al [13] who have carried out research on characterization of bamboo composites. The results of this test display that the hybrid composites enhance good impact compared to the other composites.

B. Hardness

The hardness test must be conceded in a Shore Durometer. The samplings must be cut into dimensions as per the ASTM standard. The Results of this test are charted in Table-2 and the rigidity of the Hair based, Coir based and Hybrid composite varies from 624 to 683. The result of this test displays that, the hybrid composite has superior properties compared to all the other parameters calculated.

Table.2: Hardness Properties

Sample	Location 1	Location 2	Average
Coir	420	510	465
Hair	550	472	511
Cor+Hair	624	742	683

VI. CONCLUSION

The present investigation of mechanical properties of human hair, Coir, Hybrid (Human Hair + Coir) fiber reinforced epoxy resin composite leads to the following Conclusion. The value of tensile strength is increased from 16 to 19 MPa and the compressive strength of the Hair based, Coir based, and Hybrid based fiber varies from 33 MPa to 48 MPa. The flexural strength of the Hybrid composite fiber is 56 MPa and the maximum impact strength of the composites varies from 5.7 MPa to 6.8 MPa.

- i. The natural fiber/epoxy approach has been made use of in order to make cost effective composite.
- ii. In the present the work human hair fiber reinforced epoxy resin composites have been successfully fabricate by simple hand lay process.

- iii. It has been noticed that mechanical properties composites such as tensile strength, compressive strength, flexible strength, Impact Strength and hardness of the composite of found out varies specimen by varying fiber.
- iv. Hybrid composite of Hair-Coir composites accommodate good properties according to the capacity of the individual composite opted for.
- v. Human hair holds better mechanical properties compared to other composites but when Human hair is comprised with Coconut coir fiber the composite material gets better mechanical properties.

Thus it's vitally obvious that Eco – friendly Human hair and coconut coir influence superior mechanical properties.

REFERENCES

- [1] Feughelman, M. (2002) "Natural Fibres", Journal of Applied Polymer Science, Vol.83, pp. 489 –507.
- [2] Wang, W., Cai, Z., & Yu, J. (2008), "Study on the chemical modification process of jute fiber", Journal of Engineered Fibers and Fabrics, Vol. 3, No. 2, pp.1-11.
- [3] Taj S., Munawar, M.A. & Khan, S.U. (2007), Review: Natural fiber-reinforced polymer composites" Proc Pakistan Acad Sci , Vol 44, No.2 , pp. 129–144.
- [4] N.Abilash et al, "Environmental Benefits of Ecofriendly Natural Fiber Reinforced Polymeric Composite Materials", International Journal of Application or Innovation in Engineering & Management (IJAEM), Volume 2, Issue 1,pp 2319 – 4847.
- [5] C. W. Nguong et al, (2013) "A Review on Natural Fibre Reinforced Polymer Composites", World academy of Science, Engineering and Technology International Journal of Chemical, Materials Science and Engineering Vol:7 No:1.
- [6] Girisha.C et al, (2012), "Tensile Properties of Natural Fiber-Reinforced Epoxy-Hybrid Composites", International Journal of Modern Engineering Research (IJMER), Vol.2, Issue.2, Mar-Apr 2012 pp-471-474.
- [7] G. U. Raju et al, (2012), "Mechanical and physical characterization of agricultural waste reinforced polymer composites", J. Mater. Environ. Sci. 3 (5) (2012) 907-916.
- [8] Kaplin I. J., Schwan A. and Zahn H. 1982. Effects of cosmetic treatments on the ultrastructure of hair. Cosmet. Toiletries, Vol. 97, No. 8, pp. 22-26.
- [9] Wilkinson J. B. and Moore R. J. 1990. Cosmetología de Harry. Ediciones Díaz de Santos. pp. 1039-1043.

- [10] Velasco M. V. R., Dias T. C. D. S., Freitas A. Z. D., Júnior N. D. V., Pinto Kaneko, T. M. and Baby A. R.
- [11] P.Noorunisa Khanam, M.Mohan Reddy, K.Raghu, and S.Venkat Naidu, Tensile, Flexural and Compressive properties of Sisal/Silk hybrid composites, *Journal of Reinforced Plastics and Composites*, 26 (2010) 1065-1069.
- [12] H.Raghavendra Rao, A.Varada Rajulu, G.Ramachandra Reddy, and K.Hemachandra Reddy, Flexural and compressive properties of Glass /Bamboo fiber reinforced epoxy hybrid composites, *Journal of Reinforced Plastics and Composites*, 29 (2011) 1446-1450.
- [13] V.Naga Prasad naidu. and G. Ramachandra reddy, Compressive & Impact properties of sisal/glass fiber reinforced hybrid composites, *Journal of Fiber and Textile Research*, 4 (2011) 11-14.
- [14] A.Varada Rajulu, G. Babu Rao, L. Ganga Devi, D. Sidda Ramaiah, K. Shubhaprada, K.Shrikant Bhat, R. Shylashree, Mechanical properties of short natural fiber hildegardia populifolia-reinforced styrenated polyester composites, *Journal of Reinforced Plastics Composites*, 24 (2005) 423-428.
- [15] Mohd zuhri mohamed yusoff, Mohd sapuan salit, Napsiahismail & Riza wirawan, Mechanical Properties of Short Random Oil Palm Fiber Reinforced Epoxy Composites, *Composite Science Technology*, 39 (2010) 87–92.
- [16] Mansour Rokbi, Hocine Osmani, Abdellatif Imad , Noureddine Benseddiq , Effect of Chemical treatment on Flexure Properties of Natural Fiber-reinforced Polyester Composite, *Composite Science Technology*, 10 (2011) 2092– 2097.
- [17] V. Naga prasad naidu, M.Ashok kumar, G.Ramachandra reddy, K.V.P.Chakradhar, Tensile & flexural properties of sisal/glass fibre reinforced hybrid composite, *Journal of Macromolecular science*, 22 (2011) 19- 22
- [18] K.John, S. Venkata Naidu, Sisal fiber/glass fiber hybrid composites: the impact and compressive properties, *Journal of Reinforced Plastics Composites*, 23 (2004) 1253 –1258.

Effective Implementation of Agile Software Development with a Framework, Metric Tool, and in Association with Cloud and Lean Kanban

V. Esther Jyothi¹, K. Nageswara Rao²

¹Ph.D Research Scholar, Department of CSE, Rayalaseema University, Kurnool, Andhra Pradesh, India

²Research Guide and Principal, PSCMR College of Engineering and Technology, Vijayawada, India

Abstract— *Delivering software in traditional ways is challenged by agile software development to provide a different approach for developing a product. Agile methods aim at fast, light and efficient than any other vigorous method to develop and support customers business without being chaotic. A Collaborative and Innovative Framework presented suggests the solutions for the levelheaded difficulties in Agile that leads to a software product that proves in practice to be of much higher quality. Also an object oriented software metric tool “Metric Analyzer” is proposed that detects and eliminates code smells in the code base by refactoring.*

Keywords— *Agile, Cloud Computing, Lean Kanban, Metrics, Refactoring.*

I. INTRODUCTION

Agility is increasingly becoming the driving force in many organizations. Agile development - once a predominantly team-based practice, is grabbing the attention of the business. Software professionals are getting more knowledgeable about agile development and are now scaling it more broadly within their organizations. It's not just knowledgeable; the agile community is applying what they know about the methodologies more broadly in the workplace based on the success they have seen within single teams[1]. Agile momentum has taken off and its successes are being embraced at the enterprise level. Agile helps organizations complete projects faster and more people are recognizing that agile development is beneficial to business. It is proved that implementing agile on the whole delivers what organizations hope for.

My hypothesis is that the advantages of adopting an agile software development approach lies in the considerable raise in software quality. Amazingly there are two kinds of benefits for the customers who try agile. The first one is Quality and the second benefit is lower defect rates. Agile methods are a rising movement in the software

field. This realistic, people oriented method to software development demands software practitioners. Several adopters experienced enrichments in competence, superiority, work inspiration, and consumer satisfaction. User involvement is given high priority in the working style of agile, drawing user's right in to the heart the development process [11]. While transferring to agile methodology from the traditional pattern it produced the benefits above expectations which replicated in the decrease in fault rate as well as producing high quality software.

This research paper is the result of an immense research work on the effective implementation of agile software development. It summarizes my research work for Doctor of Philosophy and is organized as follows: Section II explains the collaborative and innovative framework for agile software development; Section III presents the way of detecting the code smells in the code base of a java project by using our tool called “MetricAnalyzer”; Section IV focuses on the impact of cloud computing during various phases of agile software development that affect the efficiency of software delivery in time and on budget and explains how agile software development is accelerated using cloud; Section V discusses the approaches that can be considered while implementing iterative agile in coordination with lean kanban method and issues to produce defect free product.

II. FRAMEWORK

A collaborative and innovative framework (Fig. 1) is a hybrid approach in which XP engineering practices are implemented in the scrum sprint. Sprints are iterative cycles where the functionality is developed or enhanced to produce new increments [13]. Each Sprint includes the traditional phases of software development: requirements, analysis, design, evolution and delivery phases[5].

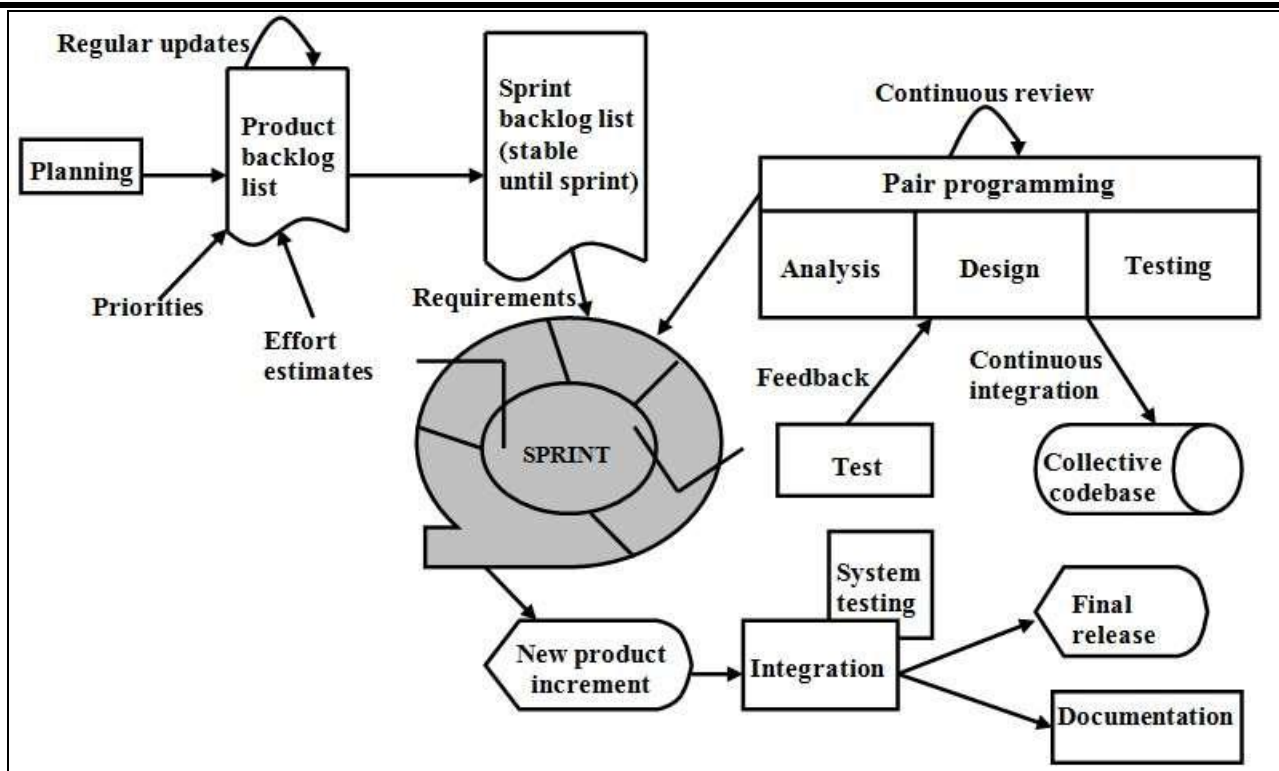


Fig. 1: Collaborative and Innovative Framework

These scrum phases are implemented using extreme programming methodology. The functional tests created by the customer are run at the end of each iteration.

Here the key characteristics of XP are included such as refactoring - restructuring the system by removing duplication, improving communication, simplifying and adding flexibility without changing its functionality, pair programming – two people write the code at one computer which is great for complex and critical logic, collective code ownership – code belongs to the project not to any individual engineer, continuous integration – a new piece of code is integrated into the code-base as soon as it is ready [9]. Thus the system is integrated and built many times a day.

All tests are run and passed for the changes in the code to be accepted. Extra testing and checking of the performance of the system before the system can be released to the customer. At this stage, new changes may still be found and the decision has to be made if they are included in the current release [3]. The postponed ideas and suggestions should be documented for later implementation. Communication and coordination between project members should be enabled at all times. Any resistance against XP practices from project members, management or customers may be enough to fail the process. Ultimately better results can be obtained by tailoring some of the scrum principles such as the daily scrum meeting to keep track of the progress of the scrum

team continuously and they also serve as planning meetings. Developing software on time and within budget is not good enough if the product developed is full of defects and customers today are demanding higher quality software than ever before [10] [12]. Now-a-days the software market is mature enough and users want to be assured of quality. Due to time-to-market pressures or cost considerations, the developer may limit the software quality assurance function and not choose to conduct independent reviews.

III. METRIC ANALYZER

In Agile software development, refactoring helps to improve software quality. The proposed object oriented software metric tool “MetricAnalyzer” showed us great results after refactoring the code compared to the original code base of different projects. This tool was very much useful in eliminating code smells from the code and maintains threshold values of the considered object oriented metrics [6].

The following are few screenshots of the “MetricAnalyzer” tool for the chosen six metrics TNOA (Total Number of Attributes) (Fig.2), WMPC (Weighted Methods per Class), MIT (Max Inheritance Tree) (Fig.3), NOCP (Number of classes Per Package), CCIM (Cyclomatic Complexity) (Fig.4), SIZE (Total Lines of Code). The red highlighter shows that the value exceeded the metric threshold value.



Fig. 2: Screen shot for SIZE metric in the “MetricAnalyzer” tool



Fig. 3: Screen shot for MIT metric in the “MetricAnalyzer” tool



Fig. 4: Screen shot for CCIM metric in the “MetricAnalyzer” tool

Since object oriented technology exploits objects and not algorithms as its elemental building blocks, the approach to software metrics for object oriented programs must be different from the standard metrics set. Some metrics, such as lines of code and cyclomatic complexity, have become accepted as "standard" for traditional functional/ procedural programs, but for object-oriented, there are many proposed object oriented metrics in the literature. Object-oriented design and development is becoming very popular in today's software development environment. It entails not only a special approach to design and implementation; it requires different software metrics.

Software refactoring is a technique to enhance the maintainability of software, improve reusability and understandability of the software. "MetricAnalyzer" applies the Object Oriented metrics on the code base and these metric values are then interpreted. Then various refactoring techniques were used to improve the code design and along with that we also studied the impact of refactoring on the software quality through various metrics. The red highlighter showed the values which exceeded the metric threshold value and this made us to refactor those parts of the code base and improve the quality of software.

IV. AGILE AND CLOUD

Even though the release cycles are speedier with agile software development there can be delays with respect to the insufficient availability of underlying platforms. But when agile using the cloud can overcome the delays and greatly enhance the speed of continuous integration and release cycles because of the large number of resources availability in the cloud [8]. Effective implementation of agile practices is much more achievable with the collaboration of cloud.

Below are the benefits and opportunities to maximize the agility of the software development process and practices with the help of cloud computing:

Reduces the lead time – Agile development teams are limited to one physical server. But when cloud instances are used, practically an unlimited number of servers are available for development teams. This leads to the reduction of lead time since they need not to wait for physical server to become free to continue their work.

Speed up release cycles – Even though agile methodology is used for software development, there can be delays with respect to the availability of underlying platforms. Having a large number of resources available in the cloud, the agile development team can overcome

the delays and greatly enhance the speed of continuous integration and release cycles.

Accelerates efficiency and effectiveness – Even though the agile software development team performs several activities in parallel and also in serial, the parallel activities are delayed due to lack of sufficient services. Cloud computing can push it towards parallel activity by providing the required services which accelerates efficient and effective agile software development.

Encourages innovation – Cloud encourages the development teams to innovate and experiment new strategies because of the wide range of available services. We can provision platform as a service environments for all stages such as development, testing, staging and production. This will make sure; they have all the base services, such as databases, application servers, artifact deployers, service handlers and API managers setup in a consistent manner and ready to go. When the developer is done developing the application or service, the artifact can be moved to the next environment for testing, and all that is required is to point to the testing environment and test the application by the QA team (Mc Breen, 2003). This is development governance with cloud computing.

Project creation, repository creation, build plans, triggering builds upon commits and deploying artifacts onto the servers upon successful builds can all be automated with a cloud based integrated setup [2]. In other words, continuous integration just got simpler. By incorporating the cloud into the agile development process, customer feedback becomes easier to obtain, because the application is being tested in a cloud-based environment.

V. LEAN KANBAN

As the years are been passed by, the software development teams have been taken transition from waterfall team to a well tuned and simple agile team. And now in the recent days agile teams are incorporating kanban principles to maintain continuous improvement. For this the team's mindset has to be changed in same aspects during the development process [4]. One such important factor is that the team should not just deliver code but should deliver tested and completed product. So, this type of transitions plays major role in the increased productivity. The lean way of development methodology started out to justify the agile way of development methodology but now it has come up in its own way. For the effective work distribution among the agile and kanban teams to work in coordination, the workflow should follow the sorter analogy (Fig. 5) for process.

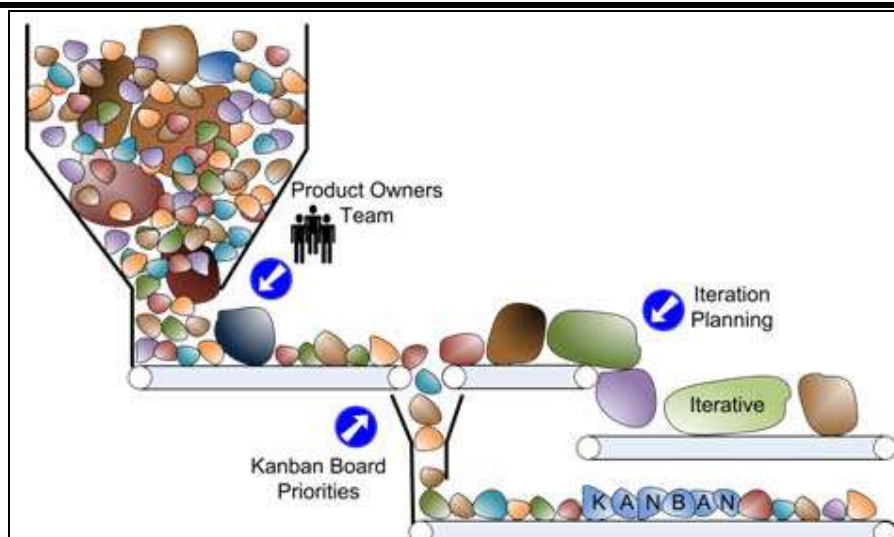


Fig. 5: The sorter analogy for the workflow process

Irrespective of the method of agility the teams / organizations follow the transition from agile to integrate agile & kanban teams can take place by incorporating the following approaches:

1. The concept of limiting work in progress (WIP) and the importance of flow through the system are to be the key factors to be taken care of while the product is under development.
2. The product owner team has to marshal all incoming work and help maintain a regular schedule of meetings to breakout user stories with the help of development team.
3. The standing meetings have to be conducted once in a week for story planning and estimation where in the development team should also be involved with product owner so that the teams will work in synchronization.
4. The kanban board can be used by the kanban teams instead of agile story boards which maintain the work items. Each work item corresponds to the user story.
5. As the daily standup meetings and iterative planning meetings are the necessary activities to be followed by the iterative agile teams, the kanban teams should also schedule 15 minutes for daily standup meeting.
6. Usually the iterative agile development teams are responsible for large-scale projects but the kanban teams can be effective while working for small –scale project along with bugs fixing.

Mc Breen defines agile quality assurance as the development of software that can respond to change, as the customer requires it to change. Beck defines agile software quality interims of efficiency, timeliness, cost effective, ease of use, maintainability, integrity,

robustness, extendibility and reusability. Some of the key factors that can influence quality assurance activities are as follows.

1. The turnaround time of bug fixes can be reduced by the early identification of defects.
2. Better functionality test cases should be formulated.
3. To ensure that standard processes are in place and traceability is maintained, QA is to be tasked perfectly and effectively [7].
4. Doing it right the first time keeps the maintenance cost low and learns how to make the most of the testing process.
5. Reduce the time of regression testing by proper implementation & maintenance of traceability matrix.
6. Effective test automation suits can be used for better and faster regression testing.

One of the key findings of agile software development is that the quality assurance activities should become a part from the kick off of the development activities itself. To make the agile more efficient the whole agile team should be responsible for quality. Every role in the team should involve in testing activities to produce defect free product [14].

VI CONCLUSION

Agile momentum continues strongly and widely across different organizations and the most widely used agile methodology is scrum undoubtedly. Keeping aside the misconceptions related to agile, organizations can succeed at the enterprise level. The proposed framework ensures transparency in communication and creates an environment of collective accountability and continuous progress. And our object oriented software metric tool

Metric Analyzer proposed has showed us great results after refactoring the code compared to the original code base of different projects.

ACKNOWLEDGEMENTS

The author Esther Jyothi Veerapaneni want to thank Dr. D. Punyaseshudu, Director, Research Studies, Rayalaseema University for his valuable suggestions during the research work and also specially thank the research guide Dr. K. Nageswara Rao for his continuous assessment and contribution throughout the research.

REFERENCES

- [1] Moran, Alan (2015). Managing Agile: Strategy, Implementation, Organisation and People. Springer Verlag. ISBN 978-3-319-16262-1.
- [2] Bowen, Janine Anthony (2011). Cloud Computing: Issues in Data Privacy/Security and Commercial Considerations. Computer and Internet Lawyer Trade Journal, 28 (8), 8.
- [3] Coram, M., and Bohner, S. (2005), The Impact of Agile Methods on Software Project Management, In Proceedings of the 12th IEEE International Conference and Workshops on the Engineering of Computer-Based Systems (ECBS), April 2005, pp. 363-370.
- [4] Veerapaneni Esther Jyothi, K. Nageswara Rao (2012) Effective Implementation of Agile Practices, International Journal on Computer Science and Engineering, Vol. 4 No. 01 Page No. 87
- [5] Veerapaneni Esther Jyothi, K. Nageswara Rao (2010) Effective implementation of agile practices – A collaborative and innovative framework, CiiT International Journal of Software Engineering and Technology, September 2010
- [6] Veerapaneni Esther Jyothi, Kaitepalli Srikanth, K. Nageswara Rao (2012) Effective Implementation of Agile Practices – Object Oriented Metrics Tool To improve Software Quality, International Journal of Software Engineering & Applications, Vol.3, No.4, July 2012.
- [7] Salem, A. M. (2010), A Model for Enhancing Requirements Traceability and Analysis. International Journal of Advanced Computer Science and Applications - IJACSA, 1(5), 14-21.
- [8] Veerapaneni Esther Jyothi, K. Nageswara Rao (2014) Effective implementation of agile practices – In Collaboration with Cloud Computing, International Journal of Current Engineering and Technology, Vol.4, No.3 (June 2014).
- [9] "Extreme Programming Core Practices." Extreme Programming Core Practices. N.p., n.d. Web. 17 Nov. 2013. <<http://c2.com/cgi/wiki?ExtremeProgrammingCorePractices>>.

- [10] "SCRUM Guide." Scrum Guide. N.p., n.d. Web. 13 Nov. 2013. <https://www.scrum.org/Portals/0/Documents/Scrum%20Guides/Scrum_Guide.pdf>.
- [11] McHugh, Martin; McCaffery, Fergal; Coady, Garret (2014-11-04). Mitasiunas, Antanas; Rout, Terry; O'Connor, Rory V.; et al., eds. "An Agile Implementation within a Medical Device Software Organisation". *Software Process Improvement and Capability Determination*. Communications in Computer and Information Science. Springer International Publishing. **477**: 190–201. Doi: 10.1007/978-3-319-13036-1_17. ISBN 978-3-319-13035-4.
- [12] Deemer, Pete, et al. "The scrum primer." Scrum Primer is an in-depth introduction to the theory and practice of Scrum, albeit primarily from a software development perspective, available at: <http://assets.scrumtraininginstitute.com/downloads/1/scrumprimer121.pdf> 1285931497 (2010).
- [13] "Prezi Presentation: Why Scrum@ IT RM by Christian Popp." *YouTube*. YouTube, n.d. Web. 10 Nov. 2014.
- [14] <http://www.stickyminds.com/interview/agile-mindset-and-agile-trends-2015-interview-jeff-nielsen>

AUTHORS PROFILE



Mrs. Veerapaneni Esther Jyothi is a Microsoft Certified Professional and Solution Developer, currently doing research work in the area of software engineering. She is working as an Assistant Professor in the department of Computer Applications, Velagapudi Siddhartha Engineering College, Vijayawada, Andhra Pradesh, India. She has published papers in various reputed international journals.



Dr. K. Nageswara Rao is a Principal of Potti Sriramulu Chalavadi Mallikharjuna Rao College of Engineering and Technology, Vijayawada, Andhra Pradesh, India. He has an excellent academic and research experience. He has contributed various research papers in the journals, conferences of International/national. His area of interest includes Artificial Intelligence, Software Engineering, Robotics, and Data mining.

Self-Compacting Concrete - Robustness of SCC

Nalini Thakre, Dipak Mangrulkar, Mahesh Janbandhu, Jaya Saxena

Department of Civil Engineering, S.B. Jain College Of Engineering Technology and Management , Nagpur, Maharashtra, India

Abstract— *Self-compacting concrete (SCC) is an innovative concrete that does not require vibration for placing and compaction. It is able to flow under its own weight, completely filling formwork and achieving full compaction, even in the presence of congested reinforcement. In the sense of SCC the robustness can be defined as the property that resist the changes of SCC like segregation during and placement (dynamic stability) and post placement (static stability). In a broader and more practical sense robustness as the ability of a given mixture to maintain its fresh properties and uniformity during processing, casting.*

Keywords— *Self-compacting concrete, consolidation, Slump flow, saturated surface dry, Robustness of SCC.*

I. INTRODUCTION

Self-compacting concrete (SCC) is an innovative concrete that does not require vibration for placing and compaction. It is able to flow under its own weight, completely filling formwork and achieving full compaction, even in the presence of congested reinforcement. For SCC it is generally necessary to use super plasticizers in order to obtain high mobility. If large amount of powdered material or viscosity modifying admixtures are added then it also helps to eliminate the segregation. So SCC is designed to meet some specific application. This can be achieved by its some rheological properties which is Robustness of SCC. Self-consolidating concrete is a highly flow-able type of concrete that spreads into the form without the need of mechanical vibration. Self-compacting concrete is a non-segregating concrete that is placed by means of its own weight. The importance of self-compacting concrete is that maintains all concrete's durability and characteristics, meeting expected performance requirements. In certain instances the addition of super plasticizers and viscosity modifier are added to the mix, reducing bleeding and segregation. Concrete that segregates loses strength and results in honeycombed areas next to the formwork. A well designed SCC mix does not segregate, has high deformability and excellent stability characteristics

Benefits of Self Compacting Concrete:-

1. SCC can be placed at faster rate with no type of vibrating equipments.

2. Improved and more uniform architectural surface finish can be achieved.
3. Ease in filling in restricted sections and hard-to-reach areas.
4. Improved consolidation around reinforcement and good bond with reinforcement.
5. It saves time and labor cost.
6. Shorter construction periods which results in cost savings.
7. Increased jobsite safety by eliminating the need for compaction.
8. Minimizes the movements of ready mixed truck and pumps during placement.
9. Reduction in noise pollution and makes healthy nature at site.

Self-Compacting Concrete Uses

Self-compacting concrete has been used in bridges and even on pre-cast sections. One of the most remarkable projects built using self-compacting concrete is the Akashi-Kaikyo Suspension Bridge. In this project, the SCC was mixed on-site and pumped through a piping system to the specified point, located 200 meters away. On this particular project, the construction time was reduced from 2.5 years to 2 years. This type of concrete is ideal to be used in the following applications:

- Drilled shafts
- Columns
- Earth retaining systems
- Areas with high concentration of rebar and pipes/conduits

Self-Compacting Concrete Benefits:-

Using self-compacting concrete produce several benefits and advantages over regular concrete. Some of those benefits are:

- Improved constructability
- Labor reduction.
- Bond to reinforcing steel.
- Improved structural Integrity.
- Accelerates project schedules.
- Reduces skilled labor.
- Flows into complex forms.
- Reduces equipment wear.
- Minimizes voids on highly reinforced areas.
- Produces superior surface finishes.

- Superior strength and durability.
- Allows for easier pumping procedure.
- Fast placement without vibration or mechanical consolidation.
- Lowering noise levels produced by mechanical vibrators. Produces a uniform surface.
- Allows for innovative architectural features.
- It is recommended for deep sections or long-span applications.
- Produces a wider variety of placement techniques.

Robustness of SCC- effects of ingredients on Rheology:-

A lack of robustness can be manifested in several ways that affects workability and the other assigned properties of SCC, i.e., flow ability, passing ability, and stability. Following is a review of the effects of ingredients on the rheological properties that affect robustness. The effects of entrapped air, silica fume, limestone, and moisture on the rheological properties. It has been shown that the air content increases the slump flow, reduces the plastic viscosity.

Robustness of SCC- effects of ingredients on segregation:-

Aggregate segregation, which is also referred to as sedimentation, is controlled by the viscosity and yield stress of the mixture, the binder density, aggregate size, aggregate density, as well as the content of fines. This implies that the stability of SCC (of low yield stress) can be enhanced by increasing both the viscosity and density of the matrix and by decreasing the maximum size and density of the aggregate. Higher w:c ratio and/or SP:c ratio increase the susceptibility to segregation and vice-versa, lower w:c ratio and SP:c ratio increase stability and therefore robustness. The tendency of the aggregate to segregate depends on the properties of both the aggregate and the homogeneous matrix. Large aggregate size and high density decreases stability and vice-versa. However, within common ranges of SCC mixtures and densities of aggregate. Compared with ordinary concrete, the segregation resistance of self-consolidating concrete (SCC) are more sensitive to small variations of mix proportions such as dosage of super-plasticizer, and the size, volume, and gradation, as well as moisture content of the fine and coarse aggregates. To design a SCC mixture, which is robust against small variations in raw materials, it is critical to understand the mechanism of how mix proportions affect robustness. In this paper, modified segregation probe was used to study the effects of various mixture properties on static stability robustness of SCC. It was found that a static segregation rate equation is helpful to explain how paste rheology and aggregate properties affect robustness. Mixture properties,

such as higher paste volume, lower super-plasticizer % by weight of cement, lower slump flow, smaller aggregate size, better gradation, and higher aggregate packing density may improve robustness. Among the aggregate properties, smaller aggregate size and better gradation seem to have more significant effects than higher aggregate packing density.

Robustness of SCC - Effect of Aggregate Moisture Content

The natural moisture content of aggregate affects the mixing water content in two ways:

1. If the moisture content of the aggregate is higher than saturated surface dry (SSD), then the amount of (free) mixing water in the mixture is reduced.
2. If the natural moisture content of the aggregate is lower than SSD, then the amount of mixing water is increased.

A strong influence on slump flow was observed by Sakai et al_ when the amount of water was changed by ± 5 kg/m². These effects were reduced when a viscosity agent was added to these mixtures. From slump flow test performed by the Japanese scientist Sakai et al it is observed that slump flow will increase by 100 mm if aggregate moisture content is increased by 1%.

Thus it can be concluded that the slump flow value tends to prominently decrease with an increase in natural moisture content of fine aggregate for mixtures with 0.35 w:c ratio as opposed to 0.5 w:c ratio.

The quality control manual for the National Precast Concrete Association (NPCA) states that surface moisture content shall be physically tested once a day prior to the first SCC batch, even when moisture probes are in use. If inline moisture meters are not used, both the Precast/Prestressed Concrete Institute and NPCA require that the moisture be manually measured at the beginning of each batching operation and every four hours of continuous batching or at any time a change in moisture content becomes apparent. A very robust mixture should be developed for production facilities that do not use inline moisture meters.

Robustness of SCC - Effect of mixing equipments

SCC is more sensitive from the point of view of designed target and mixing technique. Due to high cement content SCC requires more time in mixing than the ordinary concrete. Generally concrete is mixed with two mixers:

1. Tilting or forced pan mixers
2. Non-tilting or pug mill type mixers.

II. TEST METHODS

Self compacting concrete is distinct by its certain properties like filling ability, passing ability, robustness and resistance to segregation. Many different methods are available for characterize the property of SCC but there is no only single method that will give all the property of SCC. The following tables show the different limits stated by researchers:

Sr. no.	Property	Range
1.	Slump flow diameter	500-700 mm
2.	T50cm	2-5 sec
3.	V-funnel	6-12 sec

Slump flow test:-

The slump flow test is used to assess the horizontal free flow of SCC in the absence of any obstruction. When the slump cone is lifted filled with the concrete the concrete flows. The average diameter of the concrete circle is a measure for the filling ability of the concrete. It measures the time taken in seconds from the instant the cone is lifted to the instant when horizontal flow reaches diameter of 500 mm.



Fig.1: Slump Flow

V-funnel test:-

This test is measured to measure the flow ability of the fresh concrete. In this test the funnel is filled about 12 liters of concrete and the time taken for it to flow through the apparatus is measured. If the concrete shows the segregation, the flow time will increase significantly.



Fig.2: V-funnel test

L-box test:-

The passing ability is determined using the L- box test. The vertical section of the L-Box is filled with concrete, and then the gate lifted to let the concrete flow into the horizontal section. The height of the concrete at the end of the horizontal section is expressed as a proportion of that remaining in the vertical section (H_2/H_1). This is an indication of passing ability.



Fig.3: L-box test

4C – Rheometer test:-

The 4C-Rheometer is a system for automatic determination of the yield stress and plastic viscosity of Self-Compacting Concrete (SCC). The system is a PC automated slump flow test where the flow curve (spread vs. time) is determined using digital image analysis. The flow curve is subsequently compared to a database of simulated flow curves to give the yield stress and plastic viscosity.



Fig.4: Rheometer test

III. CONCLUSION

From the study of the paper we can conclude that the Self Compacting Concrete is the concrete of 20th century. The robustness is the most important property of SCC that makes it distinct and makes it possible to achieve its characteristics properties of consolidation.

REFERENCES

- [1] H. Okamura, "Self Compacting High Performance Concrete – Ferguson Lecture for 1996," Concrete International, Vol. 19, No. 7, 1997, pp. 50 – 54.
- [2] K. Ozawa, K. Maekawa, and H. Okamura, "Development of the High Performance Concrete,"

- Proceedings of JSI, Vol. 11, No. 1, 1989, pp. 699 – 704.
- [3] H. Okamura and M. Ouchi, “Applications of Self-Compacting Concrete in Japan,” Proceedings of the 3rd International RILEM Symposium on Self-Compacting Concrete, O. Wallevik and I. Nielsson, Ed., RILEM Publications, 2003, pp. 3 – 5.
- [4] Rooney, M., Bartos, P.M.J., ‘Development of the settlement column segregation test for fresh selfcompacting concrete (SCC)’, to appear in the second international symposium on SCC, Tokyo, Japan (2001).
- [5] Brite-EuRam programme: BE96-3801/BRPR-CT96-0366, ‘Rational production and improved working environment through using self-compacting concrete’.
- [6] Henderson N A, Baldwin N J R, McKibbins L D, Winsor D S, & Shanghavi H B, ‘Concrete technology for foundation applications’, CIRIA Report C569: 2002 © EFNARC 2002

A Framework for the analysis of 3-D Novel flange Microstrip Patch Antenna Design employing Flexible Teflon Substrate

Avneet Kaur¹, Ekambir Sidhu²

¹Department of Electronics and Communication Engineering, Punjabi University, Patiala, India

²Associate Professor, Department of Electronics and Communication Engineering, Punjabi University Patiala, India

Abstract—This paper summarises a novel microstrip patch antenna design over flexible Teflon substrate having dielectric constant $\epsilon_r= 2.1$. The proposed antenna exploits a King shaped slot (0.05mm thick) on the radiating patch along with microstrip feed line and reduced ground plane on the other side of the substrate. The radiating element of the flexible flanged antenna design has a King-shaped slot and a finite ground plane to accomplish an excellent impedance matching for maximum power transfer. The proposed antenna has an operating bandwidth of 550.7MHz (3.1244GHz-3.675GHz) with resonant frequency at 3.42GHz and has also an operating bandwidth of 369.1MHz (8.3507GHz-8.7198GHz) with resonant frequency at 8.3609GHz. This flexible flanged microstrip patch antenna design covers various applications including Radio astronomy/ Radiolocation (military&civil)/ UWB/PMSE/FSS Earth stations applications (3.3GHz-3.6GHz), Radio-determination/ Space-research/Fixed applications (8.4GHz-8.5GHz), activesensors (satellite)/ Radiolocation (civil&military)/ Aeronautical-navigation applications (8.5-8.55GHz). The proposed antenna operates for acceptable voltage standing wave ratio (VSWR) less than two. The characteristics of the proposed antenna fabricated on a flexible Teflon with different bending angles have been successfully measured. The antenna has been designed in CST Microwave Studio 2014. The proposed antenna has been fabricated and tested using E5071C Network analyser and anechoic chamber. It has been observed that the simulated results legitimately match with the experimental results.

Keywords—Flexible antenna, King shaped patch, reduced ground surface, Teflon.

I. INTRODUCTION

The microstrip antenna was first designed and analyzed in 1950's. It came in use later in 70's after the development of printed circuit boards (PCB) [1]. After then it became very popular among the data oriented individuals. The

microstrip patch antennas are widely popular in mobile phone market, military systems, medical appliances and in more fields. It is easy to design and fabricate owing to its 2D physical geometry [2-3]. They are booming in commercial sectors as they are low in cost, low profile, light in weight, small in size and have high competence [4]. But as we are well aware of the fact that the technology is ubiquitously getting advanced mostly on a daily basis, so there is a need of high efficiency in all communication fields. Conventional antennas have limitations in hostile military environment or biomedical sectors [5]. For today's modern electronic world, the Flexible antennas are becoming highly popular. Flexible materials can be molded in any shaped for better results for example in mobile phones, cars, robots, human body, buildings and many more. The competence of flexible systems mostly depends on the features of the integrated antenna [6-8].

Presently there has been an increase in the demand of transportable wireless communication devices and it is essential to be dual/multi band compatible to use in different areas or countries. The antennas constructed on the waveguide orifices with a crenellated flange have an extensive series of applications [9]. The boundary conditions require a relationship between the tangential electromagnetic fields, which leads to an integral equation. The need of satellite based portable communication devices are increasing bizarrely, specifically in areas like portable satellite station, vehicle tracking, aeronautical navigation, weather forecasting etc. Plentiful sorts of patch antennas have been ascertained and inspected by several investigators due to their exceptional properties. The Microstrip patch antennas utilize the monopole configuration such as annual ring, triangle, ring, elliptical, circular disc, hexagonal and pentagonal antennas, the dipole configuration like bow-tie antennas [10]. In satellite Communications circularly polarized radiation patterns are required using an either a rectangular or circular patch[11].

In this paper, a dual band slotted antenna has been designed on a rectangular shaped flexible Teflon substrate. The geometry of the antenna has been discussed in section II, followed by theoretical observations and results in section III and experimental results in section IV. Finally, section V illustrates the conclusion.

II. GEOMETRY OF THE ANTENNA

The novel design of flexible flanged microstrip patch antenna has been designed and simulated using the CST (Computer Simulation Technology) Microwave Studio 2014. The proposed antenna is constructed on flexible Teflon of thickness 2mm with relative permittivity of $\epsilon_r = 2.1$. The proposed antenna geometry is determined by inclining two rectangular flange vertically at 90 degrees with the radiating patch of dimension 50mm each. The dual-band microstrip patch antenna has a radiating patch with king shaped slot and reduced ground of thickness 0.05mm. The radiating patch, lossless feedline and ground plane are made up of copper material of thickness 0.05mm. The fig.1(a) shows the side view of the substrate. The fig. 1(b) portrays the top view of the King shaped slot on the radiating patch. The bottom view of the proposed antenna with reduced ground structure is shown in fig. 3(b) The dimensions of the radiating patch, substrate, reduced ground and the feed line have been listed in Table I. Microstrip-type antennas need a ground plane on the opposite side of the substrate for electromagnetic waves to travel along the feed line.

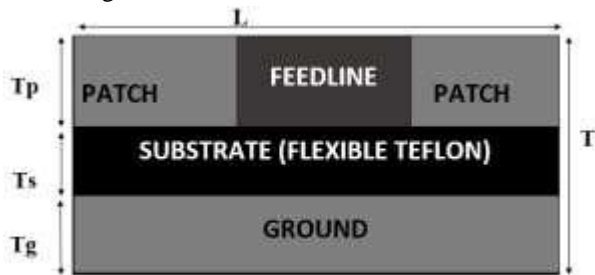


Fig.1(a): Side view of the proposed antenna design

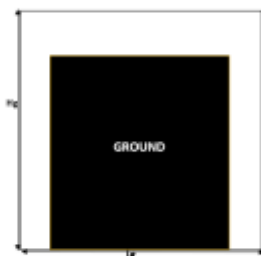


Fig. 1(b): Bottom view of the proposed antenna

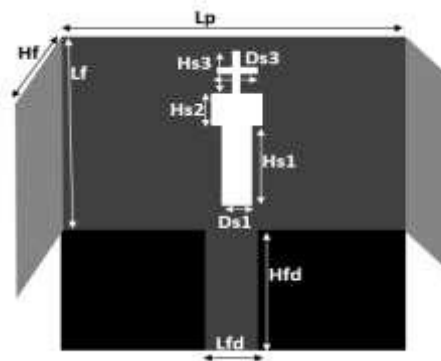


Fig.1 (c): Top view of the proposed antenna design

Table.I: Antenna Dimensions

Antenna Dimensions	Description	Value (mm)
L	Length of substrate	50
H	Height of substrate	50
T	Total thickness of antenna	2.05
Tp	Thickness of patch	0.05
Ts	Thickness of substrate	2
Tg	Thickness of ground	0.05
Hg	Height of ground	20
Lg	Length of ground	50
Lp	Length of patch	76
Hs1	Height of stride 1	3.3
Hs2	Height of stride 2	1.6
Hs3	Height of stride 3	2
Ds1	Distance to stride 1	2
Ds2	Distance to stride 2	2
Ds3	Distance to stride 3	4
Df	Distance to feedline	47.1
Ls	Length of slot	6
Hs	Height of slot	40
Lfd	Length of feedline	5.8
Hfd	Height of feedline	20
Lf	Length of flange	25
Hf	Height of flange	50

III. SIMULATED RESULTS

The proposed 3-D flexible patch antenna has been simulated and designed using CST(Computer Simulation technology) Microwave Studio 2014. A thorough parametric study of the designed antenna has been carried out in terms of return loss, impedance bandwidth, gain, directivity, VSWR and antenna impedance.

The proposed dual-band antenna has impedance bandwidth of 0.5507 GHz with operating frequency range of 3.1244GHz-3.6751GHz at resonating frequency 3.42GHz. It also has a resonant frequency at 8.42GHz with

impedance bandwidth of 0.3691GHz and operating frequency range of 8.3507GHz – 8.7198GHz as shown in figure 2(a). The return loss (S_{11}) plot of the antenna design

at 3.42GHz is observed to be -54.542792dB and at resonant frequency 8.36GHz is observed to be -47.587292.

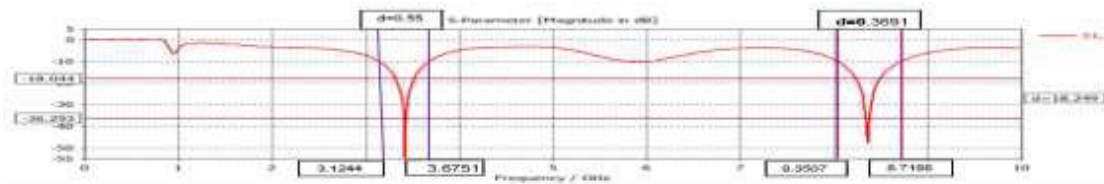


Fig. 2(a): Return loss (S_{11}) plot of the proposed antenna design

The far-field 3D directivity plot has been depicted in fig. 2(c) and 2(d). The maximum directivity of antenna obtained at resonant frequency 3.42GHz is measure to be 6.095dBi and 6.118dBi at resonant frequency 8.36GHz. In fig. 2(e) and fig. (2f), it has been shown that the proposed antenna design has gain of 6.252dB and 6.149dB at resonant frequency 3.42GHz and 8.36GHz, respectively.

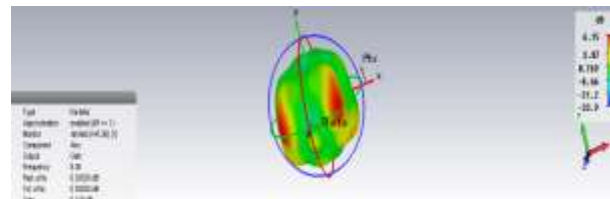


Fig 2(f): Gain of proposed antenna at 8.36 GHz

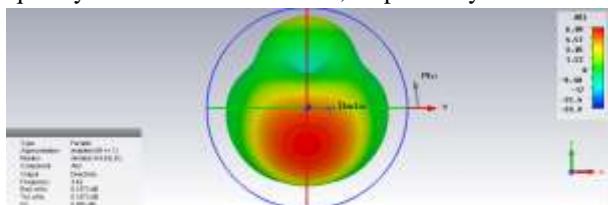


Fig. 2(c): Directivity of proposed antenna at 3.42GHz

The half power beam width (HPBW) of Flanged microstrip patch antenna with resonant frequencies at 3.42 GHz and 8.36 GHz has been observed to be 60.0 degree and 55.4 degrees, respectively as shown in figure 2(g) and figure 2(h).

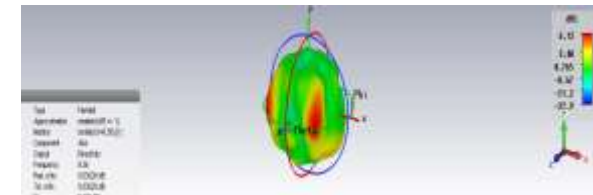


Fig. 2(d): Directivity of proposed antenna at 8.36GHz.

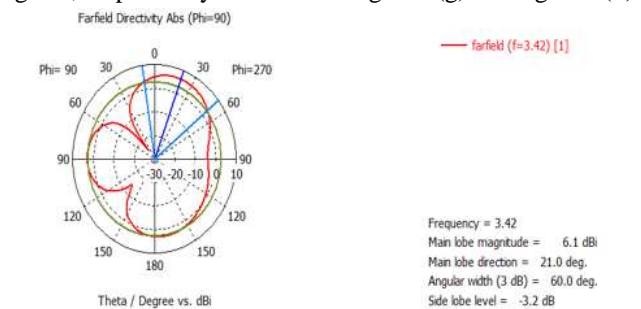


Fig. 2(g): HPBW plot of proposed antenna at 3.42GHz

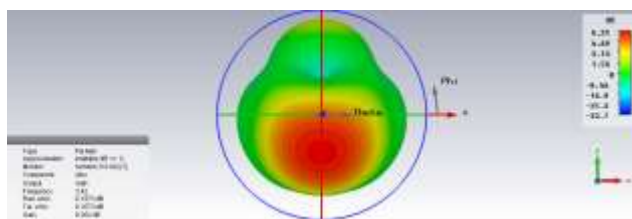


Fig 2(e): Gain of proposed antenna at 3.42 GHz

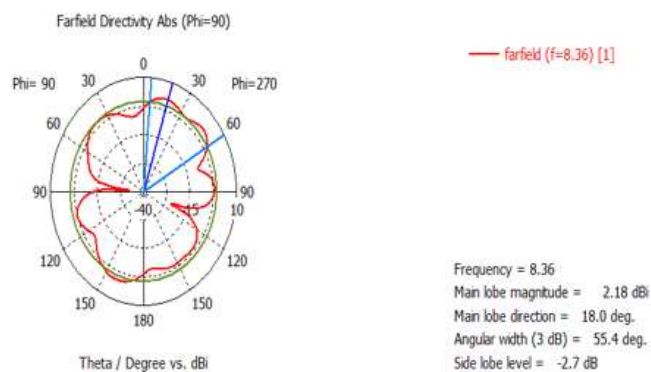


Fig. 2(h): HPBW of proposed antenna at 8.36GHz

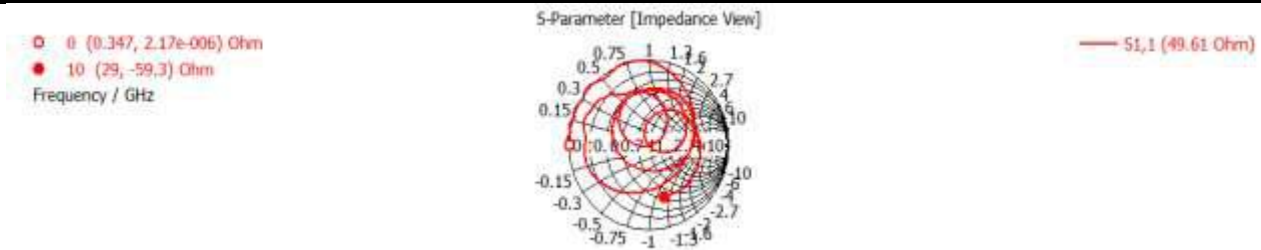


Fig. 2(i): VSWR plot of proposed antenna design

The reduced ground improved the return loss and also enhanced the bandwidth. The coaxial probe feeding is agreed at a specific site of the point where input impedance is approximately 50 Ω . Fig. 2(i) demonstrates the impedance of the proposed microstrip patch antenna which is calculated to be 49.3 Ω . It has been observed that for both the resonant frequencies the VSWR value lies below the maximum acceptable value of 2 as shown in fig.2(j) and 2(k).

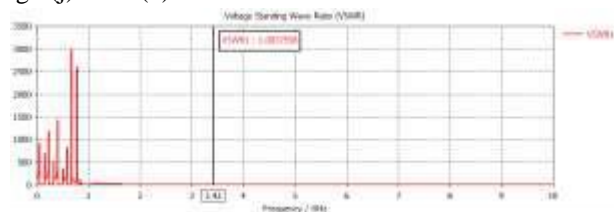


Fig. 2(j): VSWR plot of proposed antenna at 3.42 GHz

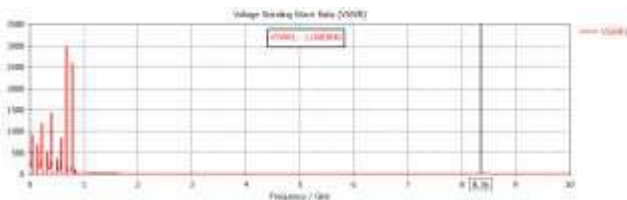


Fig. 2(k): VSWR plot of proposed antenna at 8.36 GHz

IV. CONCLUSION

The proposed flexible microstrip patch antenna has been designed and simulated using the CST (Computer Simulation Technology) Microwave Studio 2014. The proposed flexible flanged antenna has substrate thickness 1.05mm with dielectric constant 2.1 has been used. From the above discussion it has been concluded that the dual-band flanged microstrip patch antenna has operating frequency range from 3.1244GHz -3.6751GHz at resonating frequency 3.42GHz and operating frequency range of 8.3507GHz – 8.7198GHz at resonating frequency at 8.36Ghz. In the proposed antenna the reduced ground has been used in order to increase the return loss and enhance the impedance bandwidth. The resonant frequency of the proposed dual-band flexible antenna design has been simulated to be 3.42GHz with return loss of -54.542792dB and operating resonating frequency at 8.36Ghz with return loss of -47.587292. The directivity measured at resonating

frequency 3.42Ghz and at 8.36Ghz has been observed to be 6.095dB and 6.159dB, respectively. The Gain at resonating frequency 3.42Ghz and 8.36Ghz is observed to be 6.252dBi and 6.149dBi, respectively. This flexible flanged microstrip patch antenna design covers various applications including Radio astronomy/ Radiolocation (military & civil)/ UWB/ PMSE/ FSS Earth stations applications (3.3GHz-3.6GHz), Radio-determination/Space-research/Fixed applications (8.4GHz-8.5GHz), active sensors (satellite)/ Radiolocation (civil & military)/ Aeronautical-navigation applications (8.5-8.55GHz).

ACKNOWLEDGMENT

We would like to thank Prof. Ekambir Sidhu, Assistant professor, Department of Electronics and Communication Engineering, Punjabi University, Patiala for his supervision and assistance in completing this research work. We would also like to thank our parents and friends for their moral and motivational support.

REFERENCES

- [1] B. D. Patel, Tanisha Narang1, Shubhangi Jain, "Microstrip Patch Antenna- A Historical Perspective of the Development," Conference on Advances in Communication and Control Systems 2013 (CAC2S 2013)
- [2] Indrasen Singh, Dr. V.S. Tripathi, "Micro strip Patch Antenna and its Applications: a Survey," International Journal of Circuit Theory and Applications, Vol 2 (5), ISSN:2229-6093, SEPT-OCT 2011
- [3] Wei-Hua Zong*, Xiang-Yang Wei, "A Wideband Slot Antenna for Moblie Phone Applications,"
- [4] Pavan Kumar Sharma, Veerendra Singh Jadaun, "Multi-Band Rectangular Microstrip Patch Antenna with Defected Ground Structure and a Metallic Stripm" International Journal of Technological Exploration and Learning (IJTEL) Volume 1 Issue 1, ISSN: 2319-2135, August 2012.
- [5] Stephy john, Manoj k c, "Microstrip Patch Antennas for Uwb Applications: A Review," IOSR Journal of Electronics and Communication

- Engineering (IOSR-JECE), Volume 9, Issue 2, PP 34-37, Mar - Apr. 2014.
- [6] Jobin Kurian, Upama Rajan M.N, Shinoj K. Sukumaran, “*Flexible Microstrip Patch Antenna using Rubber Substrate for WBAN Applications,*” International Conference on Contemporary Computing and Informatics (IC3I), 2014.
- [7] C. Balanis, Antenna Theory Analysis and Design. New York: Wiley Interscience, 2005.
- [8] Rameez Shamalik, Sushama Shelke, “*Design and Simulation of Flexible Antenna for ISM band,*” International Journal of Engineering Research and Applications (IJERA), ISSN: 2248-9622, Vol. 2, Issue 3, pp.2168-2170, 2012.
- [9] Hirohide Serizawa and Kohei Hongo, “*Radiation From a Flanged Rectangular Waveguide,*” IEEE TRANSACTIONS ON ANTENNAS AND PROPAGATION, VOL. 53, NO. 12, DECEMBER 2005.
- [10] A. Zvyagintsev, A. Ivanov, “*RADIATION PATTERN CALCULATION OF FLANGED REFLECTOR ANTENNAS,*” 12th International Conference on Mathematical Methods in Electromagnetic Theory June 29 – July 02, 2008, Odesa, Ukraine.
- [11] T. Durga Prasad, K. V. Satya Kumar, MD Khwaja Muinuddin, Chisti B.Kanthamma, V.SantoshKumar, “*Comparisons of Circular and Rectangular Microstrip Patch Antennas,*” International Journal of Communication Engineering Applications-IJCEA, Vol 02, Issue 04; July 2011, ISSN: 2230-8520; e-ISSN-2230-8539.

Design and analysis of composite Leaf Spring for light Weight Vehicle

D. Lydia Mahanthi¹, C. Venkata Siva Murali²

¹PG. student, Mechanical Department, Sri Padmavathi Mahila Visvavidyalayam, Tirupati, India

²Assistant Professor, Mechanical Department, Sri Padmavathi Mahila Visvavidyalayam, Tirupati, India

Abstract— In recent year automobile industries are mostly concentrating on weight reduction and in improving the riding quality. To reduce vehicle weight, three techniques have been studied rationalizing the body structure, utilizing light weight materials for parts and decreasing the size of the vehicles. In this approach by introducing composite materials into automobile industries, which is having low cost, high strength to weight ratio and excellent corrosive resistance can fulfill the requirement. The suspension leaf spring is one of the potential entities for weight reduction in automobiles as it results in large unstrung mass. The introduction of fiber reinforced plastics (FRP) is used to reduce the weight of the product without any reduction on load carrying capacity and spring rate. As the materials high strain energy storage capacity and high strength-to-weight ratio compared to steel, multi-leaf springs are being replaced by mono-leaf FRP spring. FRP springs also have excellent fatigue resistance and durability.

Keywords— leaf spring, composites, CATIA, ANSYS, suspension system.

I. INTRODUCTION

A suspension system is one having springs and other devices that insulate the chassis of a vehicle from shocks transmitted through the wheels.

The main components of the suspension system are:

- Struts
- Shock absorbers
- Springs
- Tires

The automobile chassis is mounted by the axles, not directly but through some form of springs. This is done to isolate the vehicle body from the road shocks which may be in the form of bounce, pitch, roll or sway. These tendencies give rise to an uncomfortable ride and also cause additional stress in the automobile frame and body. All the part performs the function of isolating the automobile from the road shocks are collectively called a suspension system. It

also includes the spring device and various mountings. A suspension system consists of a spring and a damper. The energy of road shock causes the spring to oscillate. These oscillations are restricted to a reasonable level by the damper, which is more commonly called a shock absorber. A spring is defined as an elastic body, whose function is to distort when loaded and to recover its original shape when the load is removed. The different types of springs are:

1. Helical springs
2. Conical and volute springs
3. Torsion and spiral springs
4. Leaf springs
5. Disc or Belleville springs
6. Special purpose spring

II. LEAF SPRING

The leaf spring is main element of the suspension system. It can control for the wheels during acceleration, braking and turning, general movement caused by the road undulations. Leaf springs are designed in two methods: multi-leaf and mono leaf. The multi-leaf spring is made of several steel plates of different lengths stacked together. During normal operation, the spring compresses to absorb road shock. The leaf spring bends and slide on each other allowing suspension movement. An example of a mono-leaf spring is the tapered leaf spring. The leaf is thick in the middle and tapers towards the two ends. Many of these leaf springs are made of composite material, while others are made of steel. In most cases leaf springs are used in pairs mounted longitudinally (front and back). However, there is an increasing number of vehicle manufacturers using single transverse (side to side) mounted leaf spring.

Three types of leaf springs are:

1. Laminated or Multi-leaf springs.
2. Single or Mono-leaf springs.
3. Tapered leaf springs.

The third type of leaf spring is the combination of the above two. The multi-leaf springs are commonly used in the

automobile suspension system at the rear side and are still in use for commercial vehicles suspension system. It consists of a number of steel strips or leaves placed on the top of each other and then clamped together. The type of application and load carried determines the length and number of leaves. The top leaf is called as the main leaf and the ends of the leaf are rolled to form the eye of the spring. This is for attachment to the vehicle chassis or body. The spring eye allows movement about the shackle and pin at the rear.

III. DIFFERENT TYPES OF EYES USED IN LEAF SPRING



Fig.1: Standard eye



Fig.2: Reverse eye

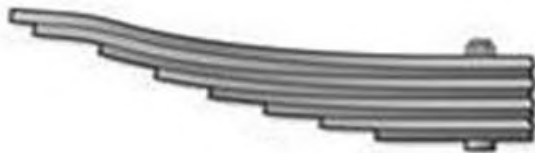


Fig.3: No eye



Fig.4: Berlin eye

IV. COMPOSITES

A composite is usually made up of at least two materials out of which one is the binding material, also called matrix and the other is the reinforcement material (fiber Kevlar and whiskers) . The advantage of composite materials over conventional materials stem largely from their higher

specific strength, stiffness, strong load carrying capacity and fatigue characteristics, which enables structural design to be more versatile.

Reinforcement provides strength and rigidity, helping to support structural load. The matrix or binder (organic or inorganic) maintains the position and orientation of the reinforcement. The reinforcement may be platelets, particles or fibers and are usually added to improve mechanical properties such as stiffness, strength and toughness of the matrix material.

V. PROPERTIES OF THE MATERIAL

Table.1: Properties of (65Si7) EN47 Steel leaf spring

Sr. No.	Parameter	Value
1	Young’s Modulus E(MPa)	2.1*10 ⁵
2	Poisson’s Ratio	0.266
3	Tensile Strength Ultimate(MPa)	1272
4	Tensile Yield Strength(MPa)	1158
5	Density(Kg/mm ³)	7.86*10 ⁻⁶

Table.2: Properties of E-Glass/ Epoxy composite leaf spring

Sr. No.	Parameter	Value
1	Tensile Strength (MPa)	900
2	Compressive Strength (MPa)	450
3	Poisson’s Ratio	0.217
4	Density (Kg/m ³)	2.16*10 ⁵
5	Flexural modulus (E) (MPa)	40000

Table.3: Properties of S-glass/ Epoxy composite leaf spring

Sr. No.	Parameter	Value
1	Tensile Strength(MPa)	4585
2	Poisson’s Ratio	0.22
3	Density (Kg/m ³)	2480
4	Young’s Modulus (E) (MPa)	86900

Table.4: Properties of KEVLAR composite leaf spring

Sr. No.	Parameter	Value
1	Tensile Strength(MPa)	3000
2	Poisson’s Ratio	0.360
3	Density(Kg/m ³)	1.44*10 ³
4	Young’s Modulus (E) (MPa)	112000

VI. DESIGN AND MODELING

Design:

Table.5: Design parameters

Parameter	Value
Length of master leaf spring	1200mm
Free Camber	200mm
Thickness	6mm
Width	50mm

Dimensions of the master leaf spring

- Number of graduated leaves = 6
 - Ineffective length = 200 mm
 - Length of second leaf = 1150 mm
 - Length of third leaf = 1000 mm
 - Length of fourth leaf = 700 mm
 - Length of fifth leaf = 580 mm
 - Length of sixth leaf = 430 mm
 - Length of seventh leaf = 300 mm
- This leaf spring is used in Ambassador Car. Material used for steel leaf spring is 55 Si 2 Mn90 steel.

Design data:

- Length of master leaf spring ($2L_1$) = 1200mm
- Free camber (y) = 200mm
- Thickness (t) = 6mm
- Width (b) = 50mm
- Radius of curvature (R) = $(L_1)^2 / 2y$
 $= (600)^2 / 2 * 200$
 $R = 900$ mm

Modeling using CATIA:

CATIA is the world’s leading CAD/CAM/CAE software. This software gives you a broad range of integrated solutions. CATIA is the digital product definition, simulation and manufacturing tool of choice for leading manufactures and have been for more than 20 years. Its capabilities have been shaped around the needs of leading edge companies across the aerospace, defense and automotive, industrial equipment, energy and consumer goods industry sectors.

CATIA (Computer Aided Three-Dimensional Interactive Application) started as an in-house development in 1977 by French aircraft manufacturer Avions Marcel Dassault, at that time customer of the CAD/CAM CAD software to develop Dassault's Mirage fighter jet.

CATIA provides a wide range of applications for tooling design, for both generic tooling and mold & die. A rich catalog of industry-standard components is provided to automate tooling definition. Specific tools are also provided to address the needs of mold tool injection designers.

Modeling:



Fig.5: leaf spring modeling

VII. PROCEDURE

- First create the key point 100 at origin, i.e. x, y, z = (0, 0, 0).
- Create another key point 200 at some arbitrary distance in Z-direction, say x, y, z = (0, 0, 200).
- Join the above two key points 100 and 200 to get the reference axis.
- By using data from mathematical analysis Create the key point1 with a distance of radius of curvature R1 in vertically down-ward direction, i.e. x, y, z = (0, -R1, 0).
- Similarly key points 2 and 3 correspond to R2, i.e. x, y, z = (0, -R2, 0) and key points 4 and 5 corresponds to R3, i.e. x, y, z = (0, -R3, 0).
- Key point 20 corresponds to R11. i.e. x, y, z = (0, -R11, 0).
- Join the pair of key points sequentially as follows Key points 1 and 2, 2 and 3, 3 and 4...and 19 and 20.
- Then line1 formed by the key points 1 and 2, line2 formed by the key points 2 and 3 and line10 formed by the key points 19 and 20.
- Extrude the above lines with respect to reference axis stated in step3 as follows:
 - Extrude line1 with an angle Φ_1 , will get area 1
 - Extrude line2 with an angle Φ_2 , will get area2,.....and
 - Extrude line10 with an angle Φ_{10} , will get area10.
- Extruding all the lines, the semi area of the spring without eye will form on XY- plane with significant degeneracy.
- To avoid degeneracy, extend the right side line of smallest area i.e. area 10 to some extent such that it cross the top most area i.e. area1.Now divide area by line. For this, select the areas left to extended line1 and divide with that line. Similarly, extend the right side

line of second smallest area i.e. area9 to some extent such that it cross the top most area i.e. areal. Again divide area by line. For this select the areas left to extended line2 and divide with that line.

- The above process is to be done up to extension of line of area9 and divide area by extension line9.
- Now perfect half area of leaf spring without eye will form.
- Eye construction:
Extend the right side line of top most area i.e. areal1 to the length equal to the radius of eye. Delete lines only, so that key point of that line will remain. Shift the origin to that key point. Create another key point say some key point300 in Z-direction. Join the above two key points to get reference axis to rotate the right line of area1. Extrude the line with respect to reference axis to an angle 275° to 280° . Delete all reference lines. So, half area of leaf spring with eye is formed.
- To get the full area of the leaf spring. Shift the origin to the top left most area key point i.e. key point1. Reflect the entire area with respect to YZ – plane.
- To get the solid model of the leaf spring, extrude the area by Z-offset to a length equal to the width of the leaf spring.
- To make a cylindrical hole at centre of the leaf spring to provide bolting for all the leaves, so that all the leaves are in perfect alignment: Create centre key point of the leaf spring on the top view i.e. XY-plane, by using key points between key points' command. Shift the origin to that key point. Choose the proper work plane by using work plane Create a cylinder along Z-axis in vertically downward direction. Subtract the cylinder from the solid leaf spring. So that leaf spring with hole to provide bolt will obtain. The models are presented in the below figures.

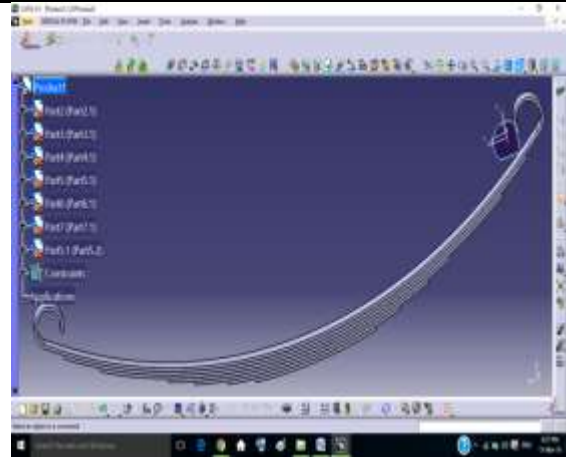


Fig.6: leaf spring

VIII. ANALYSIS OF THE LEAF SPRING

ANSYS finite element analysis (FEA) is a computer based numerical technique for calculating the strength and behavior of engineering structures. It can be used to calculate deflection, stress, vibration, buckling behavior and many other phenomena. It can be used to analyze either small or large-scale deflection under loading or applied displacement. It can analyze elastic deformation, or permanently bent out of shape plastic deformation. The computer is required because of the astronomical number of calculations needed to analyze a large structure. The power and low cost of modern computers has made Finite Element Analysis available to many disciplines and companies.

Methodology:

- Finite element model is prepared on CAD geometry.
- Hyper mesh software used to create mesh.
- Hexahedral mesh done on leaf spring geometry.
- Then deck is prepared
- Deck preparation steps –
 - 1) Apply material properties.
 - 2) Apply boundary conditions.
 - 3) Apply load.
 - 4) Export deck as *.inp file.

IX. MESHING

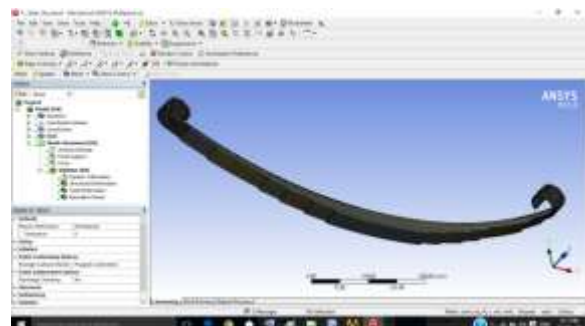


Fig.7: meshing

X. RESULTS

Analytical design and calculations of the composite leaf spring are shown according to their varying loads. In this project we are applying loads from 1000N to 4000N. Each load is applied to the composite materials which are tested. In each load the composite materials which we applied is shown with total deformation and equivalent stresses of the each composite material.

The results of the each material with the load of 1000N are shown with the total deformation and equivalent stresses in the below table.

Table.6: Details for load 1000N

Sr. No.	Material	Total Deformation, (mm)	Equivalent stresses (MPa)
1	AL Si 6150 Steel	0.88264	65.804
2	Ti 6A14V Alloy	1.7218	65.732
3	65 Si7 EN47	0.86242	66.065
4	Carbon Epoxy	1.0231	66.023
5	EN47 Steel	0.90604	66.227
6	Kevlar	1.6101	66.493
7	S-Glass Fiber	2.0871	66.502
8	E Glass Epoxy	5.3349	66.528

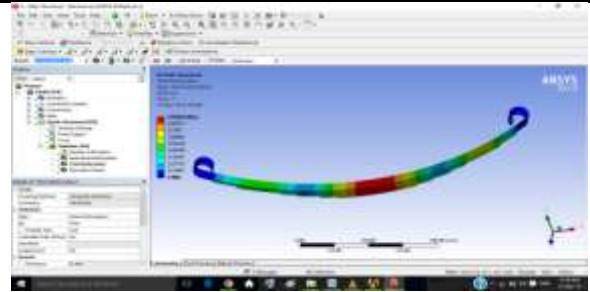


Fig.10: Total deformation of EN47 steel



Fig.11: Equivalent stress for EN47 steel

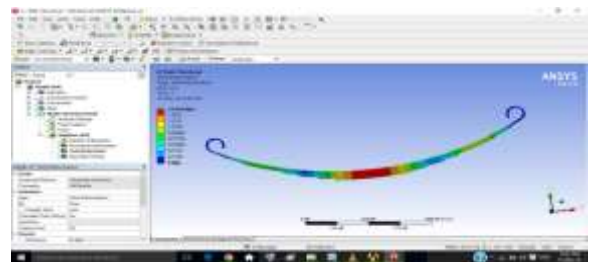


Fig.12: Total deformation of Kevlar



Fig.13: Equivalent stress for Kevlar

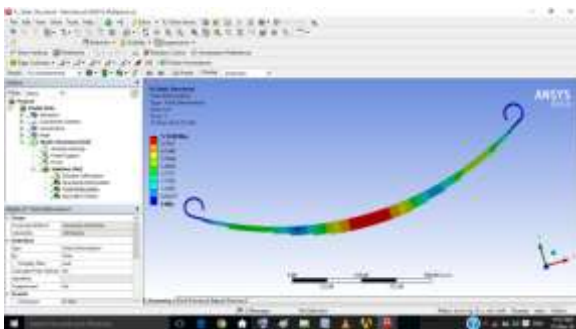


Fig.8: Total deformation of E-glass epoxy

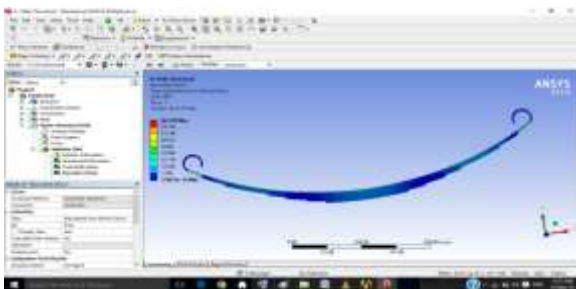


Fig.9: Equivalent stress for E-glass epoxy

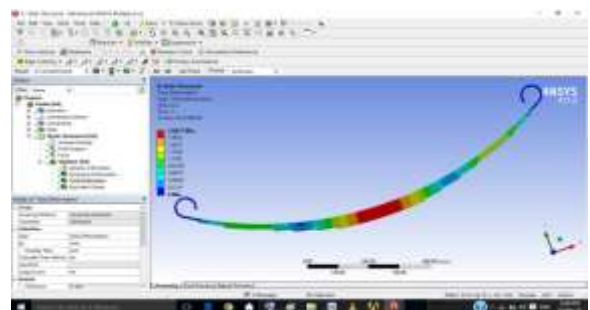


Fig.14: Total deformation of S-glass

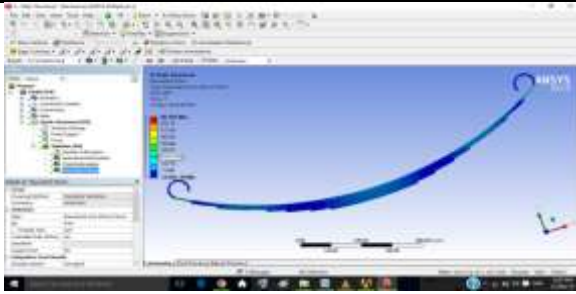


Fig.15: Equivalent stress for S-glass

XI. CONCLUSION

As automobile world demands research of reducing weight and increasing strength of products, composite material should be up to the mark of satisfying these demands. As leaf spring contributes considerable amount of weight to the vehicle and needs to be strong enough, we introducing Kevlar material which is least in weight and bears more load with less deformation when compared to other materials.

The results of static analysis of both steel and composite leaf springs like EN47, KEVLAR, S-Glass Epoxy & E-Glass Epoxy are discussed in this chapter. Thus by comparing the above results we can say that Kevlar material is better than conventional steel, E-Glass/Epoxy, S-Glass Epoxy and the other composite materials. The total deformation and the Equivalent stresses for the Kevlar are shown in the table below.

Table.7: Total Deformation and Equivalent Stresses at Variable Load Conditions

S. No	Load, (N)	Total Deformation,(mm)	Equivalent Stresses, (MPa)
1	1000	1.6101	66.49
2	2000	3.2202	132.99
3	3000	4.8302	199.48
4	4000	6.4403	265.97

REFERENCES

[1] M.Venkateshan , D.Helmen Devraj, “design and analysis of leaf spring in light vehicles”, IJMER 2249-6645 Vol.2, Issue.1,pp.213-218, Jan-Feb 2012.
 [2] R.S.Khurmi and J.K.Gupta Machine Design chapter 23.
 [3] U. S. Ramakant & K. Sowjanya, “Design and analysis of automotive multi leaf springs using composite material”, IJMPERD 2249-6890 Vol. 3, Issue 1,pp.155-162, March 2013.

[4] Rajendran.I Vijayarangan S.,“Design and Analysis of a Composite Leaf Spring”Journal of Institute of Engineers, India ,vol.-8,2-2002
 [5] Dakshraj Kothari,Rajendra Prasad Sahu and Rajesh Satankar Comparison of Performance of Two Leaf Spring Steels Used For Light Passenger Vehicle, VSRD-MAP 2249-8303 Volume2 (1), 9-16, 2012.
 [6] Mr. V. Lakshmi Narayana, “Design and Analysis Of Mono Composite Leaf Spring For Suspension in Automobiles” IJERT 2278-0181, Vol. 1 Issue 6, August – 2012.
 [7] Shishay Amare Gebremeskel, “Design, Simulation, and Prototyping of Single Composite Leaf Spring for Light Weight Vehicle”, Global Journals Inc. (USA) 2249-4596, Volume 12 Issue 7, 21-30, 2012.
 [8] Manas Patnaik, NarendraYadav, “Study of a Parabolic Leaf Spring by Finite Element Method & Design of Experiments”, IJMER 2249- 6645, Vol.2, 1920-1922, July-Aug 2012.
 [9] Kumar Krishan, Aggarwal M.L, “Computer Aided FEA Comparison of mono steel and mono GRP leaf spring”, IJAERS 2249–8974, vol. 1 issue 2, pp. 155-158, jan- march 2012.
 [10]Mr. V. K. Aher *, Mr. P. M. Sonawane , Static And Fatigue Analysis Of Multi Leaf Spring Used In The Suspension System Of LCV, (IJERA) 2248-9622 Vol. 2, Issue 4, pp.1786-1791, July-August 2012.
 [11]B. Raghu Kumar, R.VijayaPrakash and N. Ramesh, Static analysis of mono leaf spring with different composite materials” JMER , 2141- 2383, Vol. 5(2), pp.32-37, February 2013.
 [12]Y. N. V. Santhosh Kumar & M. Vimal Teja,Design and Analysis of Composite Leaf Spring International Journal of Mechanical and Industrial Engineering (IJMIE), ISSN No. 2231 –6477, Vol-2, Issue-1,pp. 97-100, 2012.
 [13]Deshmukh.et.al, Design and analysis of fibber reinforced polymer (FRP) leaf spring-A review, International journal of engineering technology and science, Vol.2(4), pp 289-291, 2011.
 [14]Pankaj Saini, Ashish Goel, Dushyant Kumar, Design and analysis of composite leaf spring for light vehicles, International journal of innovative research in science, engineering and technology, ISSI N0:2319-8753, Vol. 2, Issue 5, May 2013.

Automatic Solar Powered Fan for Regulation of Temperatures in a Green House

Harrison K. Tarus

Department of Mechanical and Production Engineering, University of Eldoret, Kenya

Abstract— Green houses are designed to support growth of crops under a variety of regulated environmental conditions such as temperature, humidity, light etc. Temperature being among them should be maintained at levels suitable for growth of a specific crop. Given that it may be costly to regulate the temperatures using electricity, energy cost can be reduced by use of automatic solar system because it is renewable. During the day the glass traps solar energy. The energy heats up the air which is then stored by the rock pebbles. During the night when the temperatures are low in the green house, the valve on the delivery duct is opened to allow warm air into the green house while at daytime temperatures is regulated by use of an automatic fan. The fan runs once the set temperature is reached and cools the greenhouse up to a certain point. The set point will be in accordance to the crop requirements. The design is cost effective, uses readily available materials and simple to construct which makes it ideal for small scale farmers.

Keywords— Green house, temperature, solar, fan.

I. INTRODUCTION

Green houses play a crucial role in the agriculture sector especially in the production of vegetables and horticultural products. Higher yields are realized in crops grown under regulated climatic conditions as in the case of green houses [1]. However, these temperatures may rise or fall to extreme levels affecting normal growth of plants. The majority of crops that are grown in greenhouses are usually warm-season species which are adaptable to temperatures in the range of 17–27 °C, with approximate limits of lower and upper values of 10 and 35°C [2]. According to Hugang Li, H.G. and Wang, [3] reduction of air temperature inside the greenhouse or the regulation of temperature close to the ambient temperature during summer is necessary for successful crop production. In the growth of tomatoes for example, flowering is affected when the night temperatures fall below 13°C and during the day when temperatures rise beyond 32°C, scorching and development of immature fruits is experienced.

Therefore, it is important to device a way of regulating the inside temperature to a level that is optimum for maximum crop yields during the day and night. It

sometimes proves expensive to maintain the temperature at required levels through use of methods like conventional energy to drive electric fans used in circulating air [4]. However with the use of an automatic solar system expenses are greatly reduced in terms of power and convenience is guaranteed [5]. During the day solar energy is tapped and stored. It is released at night into the green house when temperatures fall below a certain level warming the green house. During the day when temperatures rise beyond a certain level the fan automatically runs cooling the green house. By construction of a solar regulation system that is cost effective and reliable, problems associated with overheating and excess cold in the green house will be averted and ensure there is uniform distribution of temperatures inside the green house for maximum production.

Many different kinds of equipment are available for this conversion of solar energy. Flat plate collectors have been in service for a long time without any significant changes in their design and operational principles. Presently most thermal storage devices use sensible heat storage and a good technology is developed for the design of such systems.[6] However, above 100°C, the storage tank must be able to contain water at its vapor pressure and the storage tank cost rises sharply for temperatures above this point. Organic oils molten salts and liquid metals do not exhibit the same pressure problems but their use is limited because of their handling, containment, storage capacities and cost. Between liquid materials, water appears to be the most convenient because it is inexpensive and has a high specific heat. The difficulties and limitations relative to liquids can be avoided by using solid materials for storing thermal energy as sensible heat. But larger amounts of solids are needed than using water, due to the fact that solids, in general, exhibit a lower storing capacity than water. The cost of the storage media per unit energy stored is, however, still acceptable for rocks [7]. .

II. MATERIALS AND METHODS

Materials for greenhouse model were: Polythene, Metal rods, Arduino board, Solar panel, Fan, Battery, thermometer

A gable type greenhouse measuring 1m × 1m × 0.8m was constructed from metal. A polythene material was then fixed on the metal frames to cover the structure.

A centrifugal fan was used in the greenhouse to regulate the temperatures during the day. The fan is solar operated and automatically controlled by an Arduino board. When the temperatures go beyond a certain point the fan runs and cools the greenhouse up to the set point depending on the plant requirement. The fan also distributes heat during the night when the temperatures fall below the optimum.

A thermometer was used to measure the temperature of the greenhouse during the day and night and the response of the solar regulation system at different temperatures was then determined.

III. DESIGN AND OPERATION

3.1 Design

The circuit for solar powered fan was developed as shown in figure 1.

A program code for solar powered fan was developed to assist in controlling the temperatures automatically by either closing or opening regulator as well as giving a signal in form of a colored light.

Programming code:

```
bytefanPin = 3;
bytesensorPin = A1;
```

```
byteblueLED = 0;
byteredLED = 1;
byteCurrentTemp = 0;
void setup()
{ pinMode(fanPin, OUTPUT);
  pinMode(sensorPin, INPUT);
  analogReference(INTERNAL);
  pinMode(blueLED, OUTPUT);
  pinMode(redLED, OUTPUT);
}
void loop()
{ CurrentTemp = analogRead(sensorPin) / 10;
  if (CurrentTemp >= 30) {
    digitalWrite(fanPin, HIGH);
    digitalWrite(redLED, HIGH);
    digitalWrite(blueLED, LOW);
  } else if (CurrentTemp <= 13) {
    digitalWrite(fanPin, HIGH);
    digitalWrite(1, LOW);
    digitalWrite(0, HIGH);
  }
  else {
    digitalWrite(blueLED, LOW);
    digitalWrite(redLED, LOW);
    digitalWrite(fanPin, LOW);
  }
  delay(100);}

```

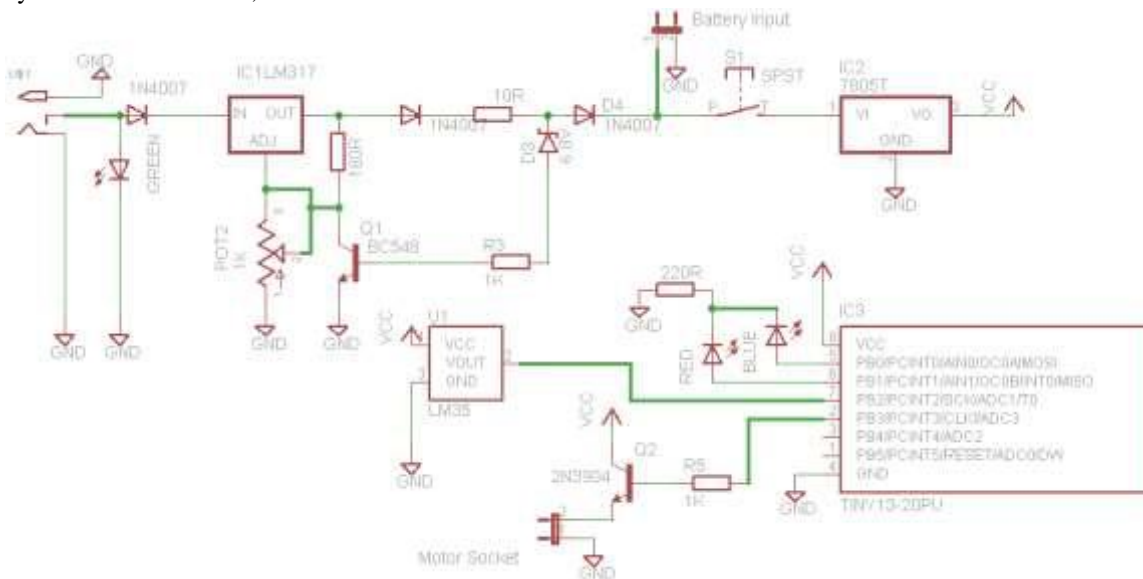


Fig.1: Schematic diagram of the automatic solar powered fan

3.2 Fan operation

The fan runs when there is power supply and once the set temperatures are obtained. When the temperature goes beyond 30°C the fan runs with a red indicator on. When the temperature cools and falls below 13°C the fan runs with a blue indicator on. Plates 1, 2 and 3 shows the various components of automatic solar powered fan, tests done on low as well as high temperatures. Therefore

when temperature exceeds 30°C inside the green house and the fan turns on, there is a reduction of temperature which falls within the recommended range. When temperature inside the greenhouse also tends to lower ranges of less than 13°C, the fan is also turned on and subsequently the warm air trapped in pebbles or any other source can be circulated to the entire area of greenhouse. The highest and lowest temperatures for operating the fan

can be adjusted depending on crop temperature requirements. The air flow in the fan is <500 cubic feet per metres and also depends on the size of greenhouse.



Plate 1: Photo of components of the automatic solar powered fan

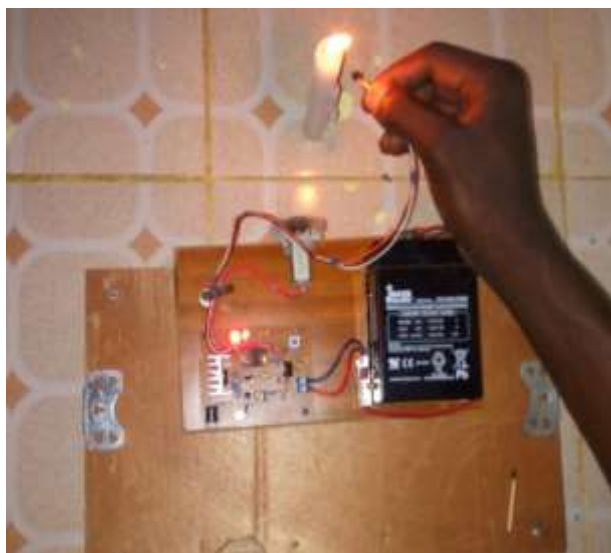


Plate 2: Testing the response of the solar powered fan at elevated temperatures



Plate 3: Testing the response of the solar powered fan at low temperature

IV. CONCLUSION

The automatic operation of fan at high and low temperatures inside the greenhouse assists in maintaining the required range of temperatures required in crop production. The design of solar powered fan is simple in construction and can be easily used.

ACKNOWLEDGEMENTS

I Sincerely appreciate my colleagues at University of Eldoret, Department of Mechanical and Production Engineering for their full while working on this project.

REFERENCES

- [1] P.P. Reddy, “ Sustainable Crop Protection under Protected Cultivation”, Springer, Singapore 2015 DOI 10.1007/978-981-287-952-3_2
- [2] W. Baudoin, R. Nono-Womdim, N. Lutaladio, A. Hodder, “Good Agricultural Practices for greenhouse vegetable crops”, FAO Plant Production and protection paper 217, Rome 2013.
- [3] Hugang Li, H.G. and Wang, S.X. “Technology and Studies for Greenhouse Cooling”. World Journal of Engineering and Technology 2015, Vol.3, 73-77. <http://dx.doi.org/10.4236/wjet.2015.33B012>
- [4] J. Kramer, “Greenhouse Heating.” Association of Education and Research Greenhouse Curators, AERGC Newsletter 2013, 25(1): 4-7,
- [5] B. Bellows, “Solar Greenhouses”, National Sustainable Agriculture Information Service, 2008 <https://attra.ncat.org>
- [6] S. P. Sukhatme, “Solar Energy”, Principles of Thermal Collection and Storage, Tata McGraw-Hill 1991
- [7] J.W. Bartok, “Energy Conservation for Commercial Greenhouses”, NRAES-3, 2001 Revision. Ithaca, New York. Natural Resource, Agriculture and Engineering Service

Implementation of CMOS Low Dropout Voltage Regulator with Frequency divider for Improved Stability

Kamlesh Sharma¹, Gajendra Sujediya², Abdul Naim Khan^{3*}

^{1,2}Department of ECE, Rajasthan Institute of Engineering & Technology, Jaipur, India

³Department of ECE, Jaipur National University, Jaipur, India

Abstract— A Amplifier is a gadget that is use to intensify the flag quality. The outline of superior and stable low drop-out voltage controllers is a test these days with diminishing gadget sizes and expanding power densities. The proposed circuit is recreated utilizing Cadence ORCAD Capture in 180nm CMOS innovation parameters with the supply voltage of 1.8V. It works at low request supply voltages and gives adequate yield stack current even with negligible utilization of info current. Proposed LDO engineering enhanced the transient reaction. The proposed configuration enhances soundness and gives superior as far as PSRR and slew rate, which are critical performing parameters for a LDO.

Keywords-MOS, LOWDROPOUT, MOSFET, ORCAD, PSRR.

I. INTRODUCTION

Compact Devices Such as mobile, Laptop, Calculator, etc. have become so popular and so has become the need of keeping them charged for longer times. Controllers have become an important part of power management system with the growing demand of portable battery operated products. LDO's work at low power inputs and low load current. Low power consumption makes them ideal for use in portable low energy requirement circuits. A Device cannot perform without energy and needs a stable and powerful supply voltage.

Complementary Metal Oxide Semiconductor (CMOS) is the semiconductor innovation utilized as a part of the transistors that are fabricated into the majority of today's PC microchips. Semiconductors are made of silicon and germanium, materials which "somehow" lead power, yet very little more. [1] LDOs (Low dropout controllers) are a straightforward reasonable approach to direct a yield voltage that will be fueled from a higher voltage input. They are anything but difficult to outline with and utilize. For a large portion of the applications, the parameters in a LDO (Low dropout controllers) datasheet are generally straightforward. In spite of the fact that, alternate applications require the architect to concentrate the

datasheet all the more nearly to check regardless of whether the LDO is appropriate for the particular circuit conditions. [2]

II. LOW DROPUT VOLTAGE REGULATOR

A low dropout or LDO controller is a DC straight voltage controller which has an exceptionally minor data yield differential voltage. The principle modules are a force FET and a differential intensifier (blunder speaker). One info of the differential intensifier shows a rate of the yield, as firm by the resistor proportion of R1 and R2. The second data to the differential enhancer is from a steady voltage reference (band hole reference). If the yield voltage increases too high close to the reference voltage, the drive to the power FET changes to keep a reliable yield voltage.

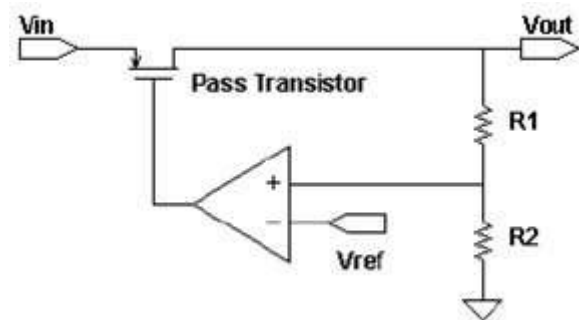


Fig. 2.1: LDO Voltage Regulators

2.1 Feedback Network:

The information framework makes the yield voltage to be differentiated and the voltage reference. This voltage is made by a voltage divider is given as:

$$V_{out} = V_{ref} \left(1 + \frac{R_1}{R_2}\right) \dots\dots (2.1)$$

2.2 General Architecture of LDO:

As a given particular estimation of CL is 1uF and for great burden current (200mA) size of pass transistor is substantial so aftereffect of which door capacitor of pass transistor is likewise huge in the scope of couple of hundred of pF [28]. This estimation of entryway capacitor

of pass transistor is vast contrast with the yield capacitor of blunder intensifier.

$$\left[\frac{W}{L}\right]_{PASS} = 2 \frac{I_{MAX}}{\mu C_{ox} V_{DSsat}^2} \dots\dots\dots (2.2)$$

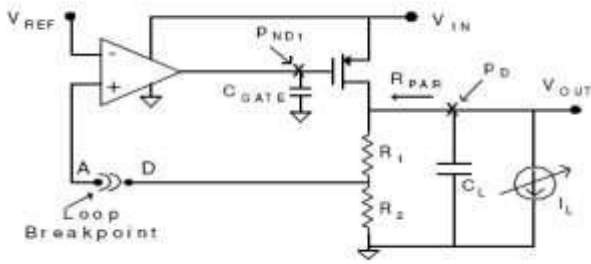


Fig.2.2: Typical LDO Open Loop Representations

Because of these gauges of capacitors the average LDO open circle reaction can be approximated by a second request exchange capacity given as:

$$H(S) = \frac{A_o}{\left(1 + \frac{s}{P_D}\right)\left(1 + \frac{s}{P_{ND1}}\right)} \dots\dots\dots (2.3)$$

This exchange capacity has two posts that are straight identified with the shafts marked in Fig. 3.2 and can be start at the yield of framework (P_D) and at the entryway of pass transistor (P_{ND1}).

$$P_D \approx \frac{1}{2\pi R_{PAR} C_L} \dots\dots\dots (2.4)$$

$$P_{ND1} \approx \frac{1}{2\pi R_A (C_{GATE} + R_{PAR} g_{mp} C_{GD} + C_{GD})} \dots\dots\dots (2.5)$$

These shafts take after the deviations the pass component encounters when a change in burden current is experienced on the grounds that the yield resistance of the LDO (R_{PAR}) is given by:

$$R_{PDR} = r_{DS} || R_1 + R_2 || R_L \dots\dots\dots (2.6)$$

The yield impedance (R_{PAR}) screens varieties in burden in light of the fact that both R_L and r_{DS} are elements of the heap current. The channel to-source impedance r_{DS} of the PMOS pass component has a reliance on burden current that is given by (2.7)

$$r_{DS} = \frac{1}{\lambda I_{DS}} \dots\dots\dots (2.7)$$

2.3 Output Noise:

The yield commotion voltage is generally educated as the RMS yield clamor voltage over a predetermined recurrence band (10Hz to 100 kHz) under the circumstances of a characterized yield voltage, a swell free information voltage and consistent burden current.

2.4 Load Regulation:

Load regulation is the capacity of the controller to keep up the fancied yield voltage with any adjustments in burden current. Load regulation can be measured by changing the heap current and measuring the adjustments in yield voltage.

$$\text{Load Regulation} \Xi \frac{\Delta V_o}{\Delta I_o} \dots\dots\dots (2.8)$$

2.5 Line Regulation:

Line regulation is the capacity of the circuit to support the predefined yield voltage with no impacts from deviations in info voltage. Line regulation can be measured by giving the supply voltage a short heartbeat and demonstrating the power of the circuit to this heartbeat. Line regulation can likewise be communicated as:

$$\text{Line Regulation} \Xi \frac{\Delta V_o}{\Delta V_i} \dots\dots\dots (2..9)$$

III. LDO EXPERIMENTAL CIRCUIT'S

3.1 LDO with Frequency driver and without current steering circuit:

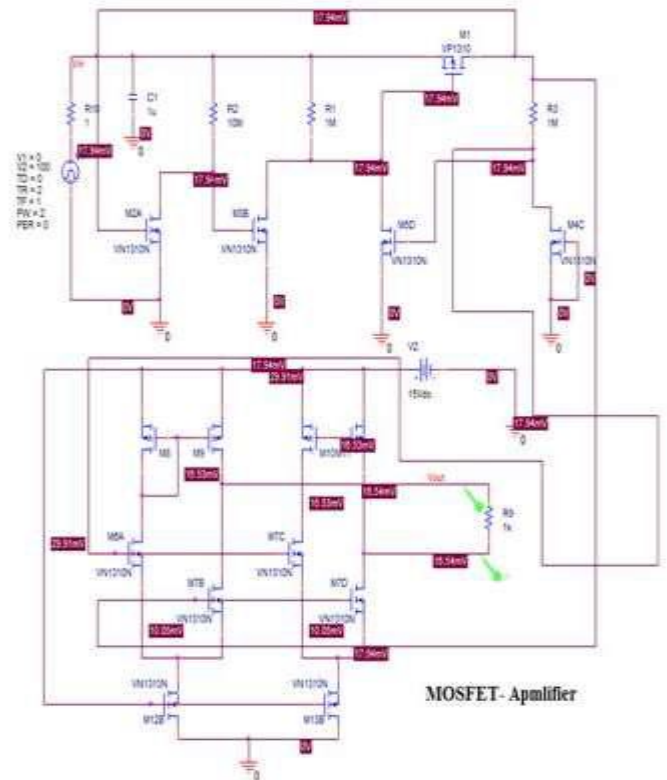


Fig. 3.1: Reference LDO with Frequency driver and without current steering circuit

3.1.1 Circuit Implementation:

Failure voltage is the input to output voltage difference at which the LDO is no longer able to regulate against further decreases in the input voltage. In the dropout region, the pass element acts like a resistor with a value equal to the drain to source on resistance. The competence of an LDO is determined by the ground current and input output voltages. Load regulation is the amount of the LDO's ability to sustain the definite output voltage under changing capacity situations. The line transient response is the output voltage difference for an

input voltage stage change. It is a function of the gain bandwidth of the LDO's control loop, and the size and slew rate of the input voltage change. PSRR is not defined by a single value because it is frequency dependent. An LDO consists of a reference voltage, error amplifier, and a power-pass element, such as MOSFET or bipolar transistor. The error amplifier provides DC gain to regulate the output voltage. The AC gain of the error amplifier in large part determines the PSRR. A typical LDO can have as much as 80dB of PSRR at 10 Hz, but the PSRR can fall to as little as 20dB a few tens of kilohertz.

3.2 LDO with current steering without amplifier:

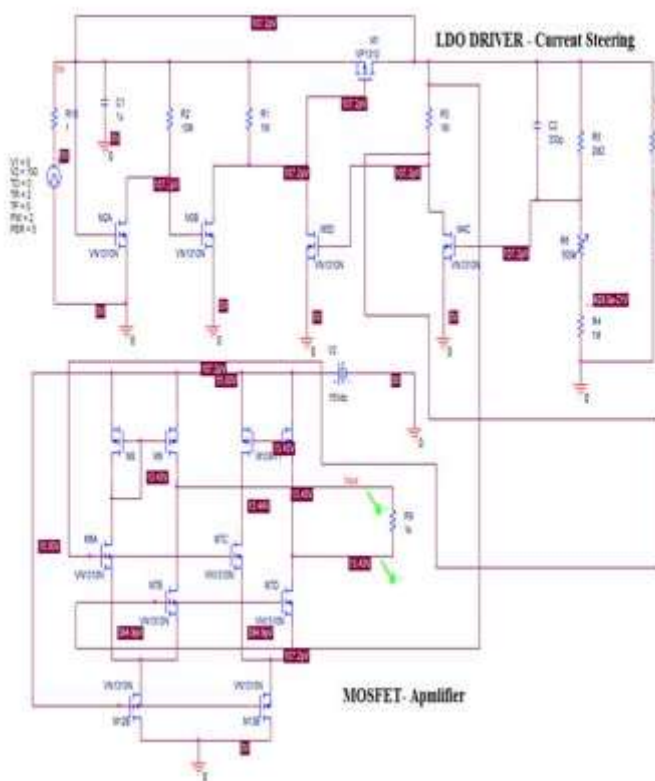


Fig.3.2: Reference LDO with current steering without amplifier

3.2.1 Circuit Implementation:

In this implementation we have designed a LDO with current steering without amplifier. Input pulse is varying from 0V to 100V and it gives a stable output at higher range. And also gives a gain of high order and we also calculate the output voltage at multipoint but there is disadvantage that it gives the low output voltage order of mV. And also gives high dropout voltage. Values of output voltage, gain and Transient time is calculated at multipoint as changing the position of voltage probe. Low-dropout regulators (LDOs) are deceptively simple devices that provide critical functions such as isolating a load from a dirty source or creating a low-noise source to power sensitive circuitry.

In this work we have presented a LDO Circuit, Low Drop-Out Voltage Regulator which is intended to work over a wide range of input voltage, typically the system has been tested over the 10V and the system responded well with a constant output of 1.57V, with few minute spikes after the input voltage ranges crosses the 750V mark and makes the output reach to the 1.61V.

Voltage regulators are useful for the digital circuits as the digital components are intended and designed in such a way that they consume less input power and are able to work at very low power voltages, as it is the necessity of the modern day gadgets as well.

The Circuit designed here comprises of several sections which are responsible for achieving the constant low dropped out voltage. The designed circuit comprises of the Startup Circuit, Current Steering Circuit, Current Frequency Driver, CMOS Inverter Circuit, CMOS Amplifier Circuit and MOSFET Driver Circuit. All the modules developed in this work are the combination of several n and p MOSFETs.

III. SIMULATIONS AND RESULTS

This chapter will discuss the result of the implemented project and tools & technology which is used.

4.1 Results of LDO with Frequency driver and without current steering circuit:

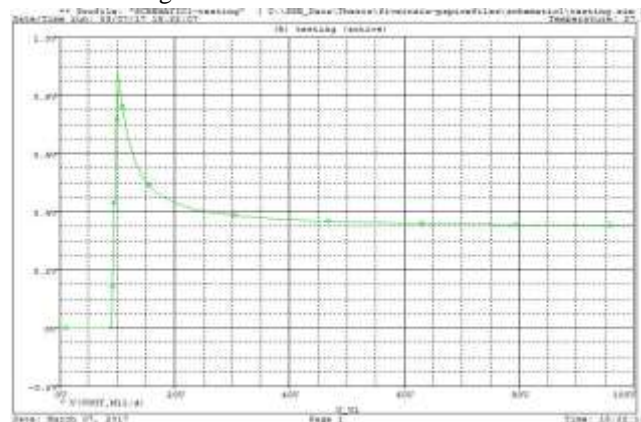


Fig. 4.1 Simulated Output Voltage

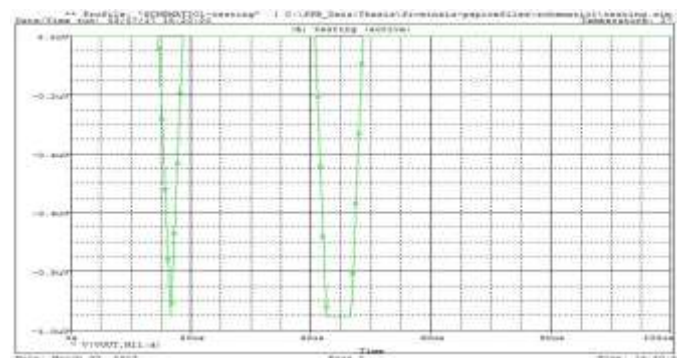


Fig. 4.2 Simulated Transient response

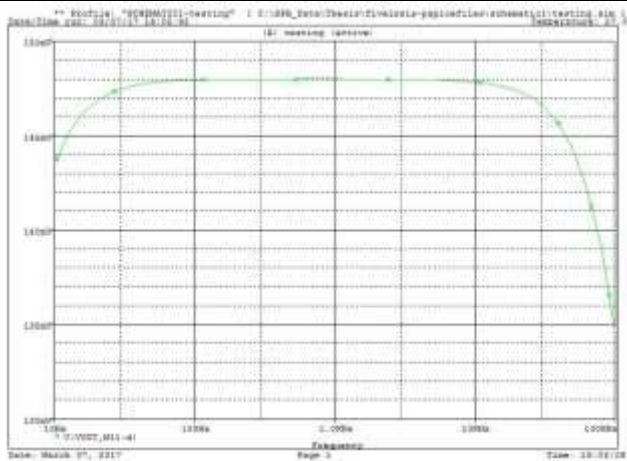


Fig: 4.3 Simulated_gain



Fig: 4.6 Simulated_gain

4.2 Results of LDO with current steering without amplifier:

4.2.1 R8 Across:

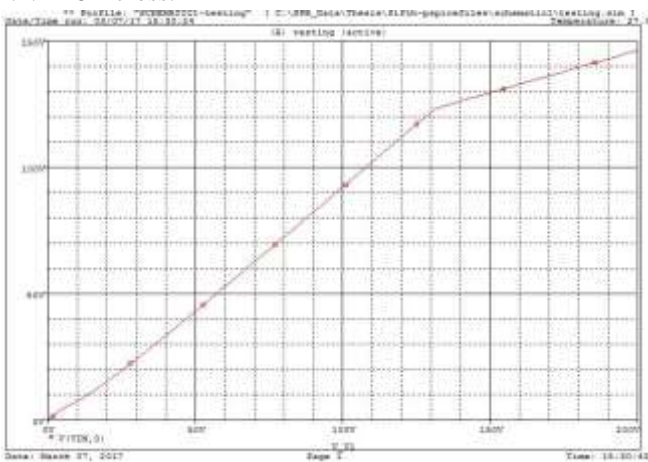


Fig: 4.4 Simulated_Output_Voltage

4.2.2 Vout Across:

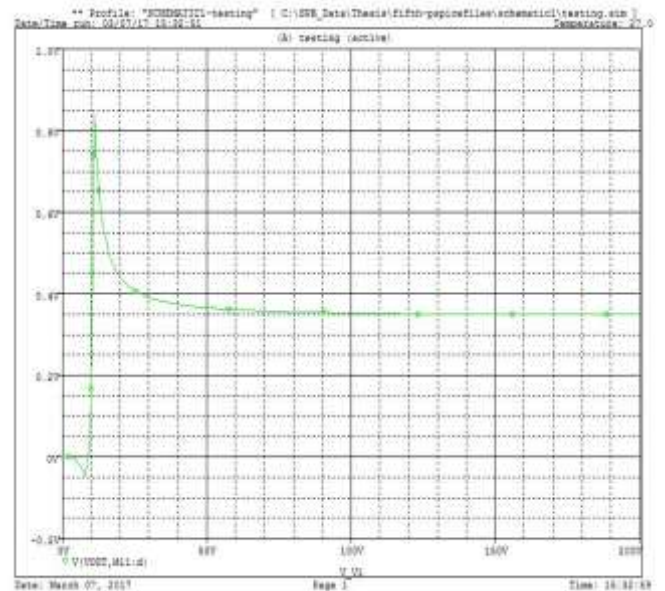


Fig: 4.7 Simulated_Output_Voltage

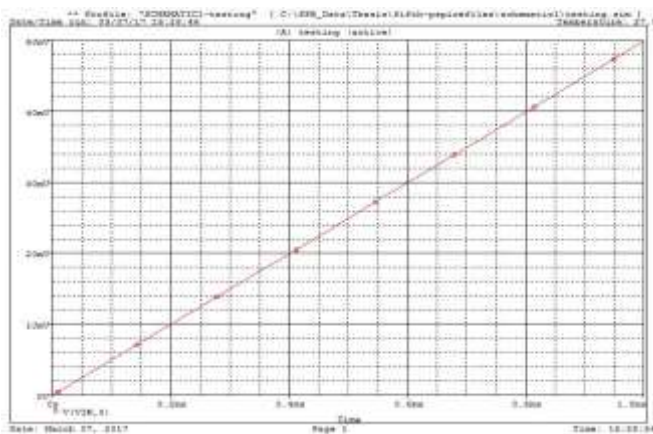


Fig: 4.5 Simulated_Transient_response

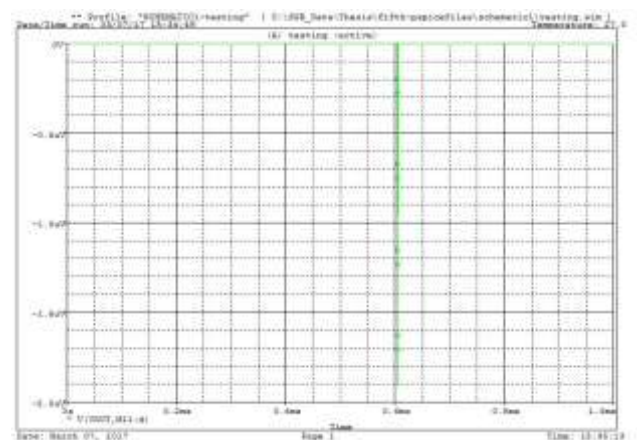


Fig: 4.8 Simulated_Transient_response

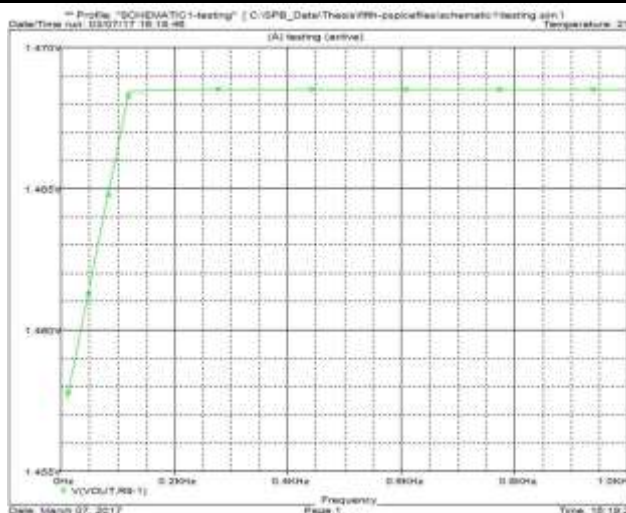


Fig: 4.9 Simulated_gain

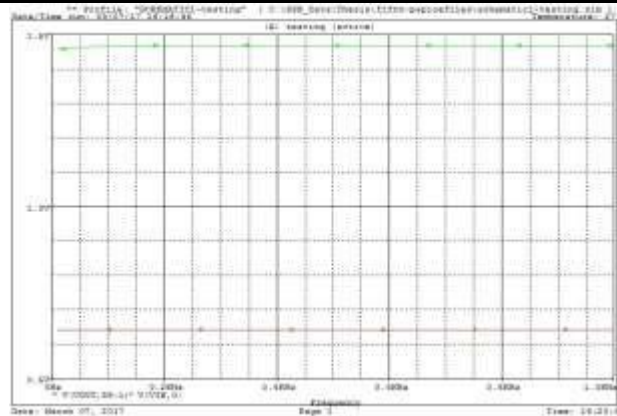


Fig: 4.12 simulated_gain

4.2.3 Both Across (R8 and Vout):

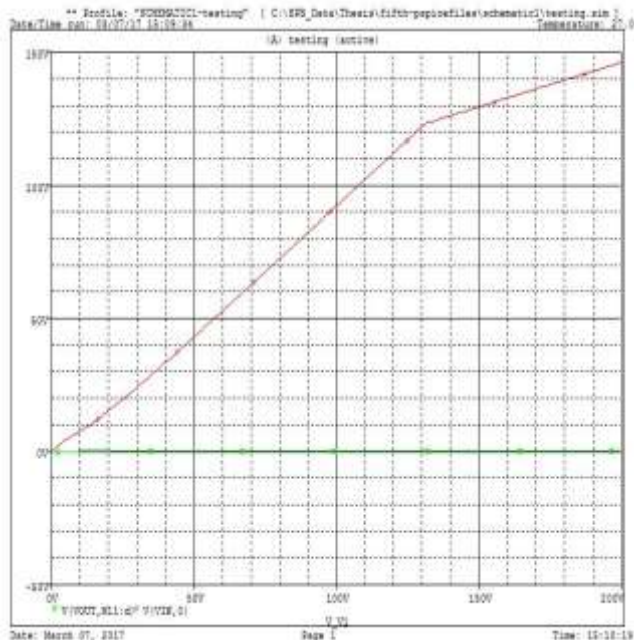


Fig: 4.10 Simulated_Output_Voltage

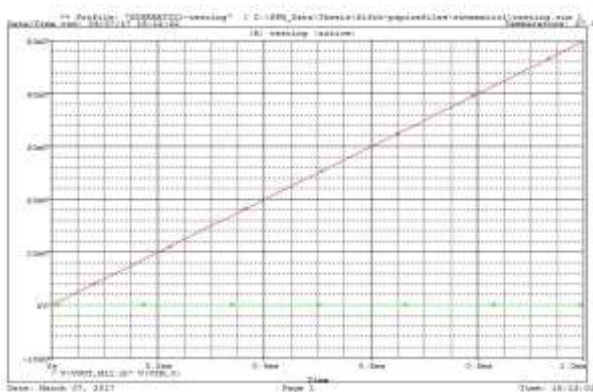


Fig: 4.11 Simulated_Transient_response

Table.4.1: Comparison of proposed circuit with the LDOs available in literature

Parameters	Design 1	Design 2	Base Paper	Paper 1	Paper 2	Paper 3
Vin	10 – 500V	10 – 500V	3V- 5.5 V	2.0V	N/A	N/A
Vout	~1.6 V	~1.6 V	~1.8	~1.8	~1.8	0.9V
Iout(Max)	0.97 mA	1.27 mA	1.25 mA	N.A.	N.A.	100 mA
Iout(Min)	0.47 mA	1.14 mA	N.M	N.A.	N.A.	6mA
Line Regulation Voltage	18.29 mV	17.24 mV	2.7 mV	N.A.	2mV	N.A.
Load Voltage	17.49 mV	18.34 mV	0.3 mV	N.A.	34mV	N.A.
PSRR	54db @10 kHz	57db @10 kHz	44dB @ 10kHz	N.A.	>45 dB	N.A.
Dropout voltage	8.27 V	8.09 V	1.2 V	N.A.	N.A.	N.A.
Settling Time	12ns	12ns	2us	<5us	N.A.	5.45 5ns
Delta vout	81mV	78mV	56 mV	<70 mV	54mV	90Mv

IV. CONCLUSION

Low Drop Out voltage regulators are the regulators which can generate the output from the very low voltage or from the input voltage equivalent to the range of the output voltage, however the ideal cases are not applicable to the practical solutions. In this work we have suggested a LDO circuit which comprises of various circuits like current steering, CMOS inverter, CMOS amplifier, current frequency driver and circuits like startup circuit. This LDO design will prove to be of great utility. Furthermore, the circuit can deliver higher addition than the reference circuit. The configuration additionally succeeds low space as the resistors and capacitor are kept away from.

REFERENCES

- [1] Amit P. Patel and Gabriel A. Rincón-Mora, "High Power-Supply-Rejection (PSR) Current-Mode Low-Dropout (LDO) Regulator," *IEEE Transactions on Circuits and Systems—II: Express Briefs*, Vol. 57, No. 11, November 2010.
- [2] Hung-Chih Lin, Hsiang-Han Wu, and Tsin-Yuan Chang, "An Active-Frequency Compensation Scheme for CMOS Low-Dropout Regulators with Transient-Response Improvement," *IEEE Transactions on Circuits and Systems—II: Express Briefs*, Vol. 55, No. 9, September 2008.
- [3] Socheat Heng and Cong-Kha Pham, "A Low-Power High-PSRR Low-Dropout Regulator with Bulk-Gate Controlled Circuit," *IEEE Transactions on Circuits and Systems—II: Express Briefs*, Vol. 57, No. 4, April 2010.
- [4] Li-Ke Wang, Jinguang Jiang, Shanshan Li, Xu Gong and Qingyun Li, "A High Stability Low Drop-out Regulator With Fast Transient Response," *IEEE 978-1-4244-5849-3/10/\$26.00 ©2010*.
- [5] Robert J. Milliken, Jose Silva-Martínez, and Edgar Sánchez-Sinencio, "Full On-Chip CMOS Low-Dropout Voltage Regulator," *IEEE Transactions on Circuits and Systems—I: Regular Papers*, Vol. 54, No. 9, September 2007.
- [6] Sreehari Rao Patri, and K. S. R. Krishna Prasad, "Self Compensating ON Chip LDO Voltage Regulator in 180nm," *World Academy of Science, Engineering and Technology* 44 2008.
- [7] Peter Hazucha, Tanay Karnik, Bradley A. Bloechel, Colleen Parsons, David Finan, and Shekhar Borkar, "Area-Efficient Linear Regulator With Ultra-Fast Load Regulation," *IEEE Journal of Solid-State Circuits*, Vol. 40, No. 4, April 2005.
- [8] David C. W. Ng, David K. K. Kwong, and Ngai Wong, "A Sub-1 V, 26 W, Low-Output-Impedance CMOS Bandgap Reference With a Low Dropout or Source Follower Mode," *IEEE Transactions on Very Large Scale Integration (VLSI) Systems*, Vol. 19, No. 7, July 2011.
- [9] Chenchang Zhan, and Wing-Hung Ki, "Output-Capacitor-Free Adaptively Biased Low-Dropout Regulator for System-on-Chips," *IEEE Transactions on Circuits and Systems—I: Regular Papers*, Vol. 57, No. 5, May 2010.
- [10] Abdul Naim Khan and Sandeep Kumar Toshniwal, "Multi-level CMOS LDO-Voltage Circuit with Differential Current Circuit Steering and Regulated Voltage," *IOSR Journal of VLSI and Signal Processing*, Volume 5, Issue 5, Ver. I, PP 40-46, Oct 2015.
- [11] Edward N. Y. Ho and Philip K. T. Mok, "A Capacitor-Less CMOS Active Feedback Low-Dropout Regulator with Slew-Rate Enhancement for Portable On-Chip Application," *IEEE Transactions on Circuits and Systems—II: Express Briefs*, Vol. 57, No. 2, February 2010.

Develop a model to map client's people development requirements and the delivery of the service to achieve effective results

S. K. Devanarayana, G. H. J. Lanel

Department of Mathematics, University of Sri Jayewardenepura, Sri Lanka

Abstract— *The People development requirements are individual skills and competencies required to improve performances of the entire organization or the company. Many competitive companies are concerned in fulfilling their internal employees' development requirements..*

It is very important to gather the exact requirements of the client and understand the skills that they are lacking because of the time and resources spent to fulfill the business needs and the mismatch between what is delivered and what was actually needed. This project attempts to develop a suitable model using graph theory concepts to map clients' people development requirements and how to cater an effective service for clients which will meet their requirements.

A questionnaire that contains fourteen question statements was designed to gather information from the participants and the questions are based on measuring confidence, knowledge, leadership and management, time management, communication skills, problem solving and decision making. The graph is drawn considering the interrelations between questions and according to participants' responses. Areas of improvements and strengths identified accordingly.

After analyzing all the graphs from the participants using graph theoretical concepts it concludes that their areas of improvement are broadly different from each other. By having a proper overall understanding about the areas of improvement of the participants will enhance the effectiveness through customized way of delivery.

Keywords— *Customized delivery, Effective service, Organizational benefits, People development requirements, Training effectiveness*

I. INTRODUCTION

Any organization, may it be profit oriented or nonprofit oriented, strives for success with the aim of being the market leader in the respective industry. Due to the highly competitiveness and the turbulence of the present day society, organizations, today, more than ever before, need to obtain and utilize human resources in it in an effective and efficient manner. Thus, they regularly focus on

keeping their human resources up-to date, where a special attention is paid by the management and the administration for all the core functions of human resource management (HRM). In the present day different organizational, social and economically related areas, this has become a main focal point, which is predicted to be highly influential to the achievement of the organizational goals and therefore organizations successful in the market.

As long as HRM is considered, Training and development could be considered as one of the main key responsibilities, which plays an important role in the effectiveness of organizations and to the experiences of people in work. Implications for productivity, health and safety at work and personal development are generally occupied by Training and Development and, as per today, even the employee laws state that all organizations employing people need to train and develop their staff as a compulsory requirement. Thus, many organizations are aware of this requirement and invest effort and other resources in training and development in larger scales. In here, training investment can take the form of several ways. One most popular training method could be employing specialist training and development staff and paying salaries to staff undergoing training and development department. However, outsourcing the training functions to another organization that is specialized in delivering training and development programs is also now so popular among organizations nowadays. In any of these forms the training program should be effective and it must meet the objectives of the employees of the organization.

This study, therefore, attempts to develop a mathematical model to identify the strengths and areas of improvement of the employees which will probably lead to a customized and effective training program of any organization.

1.1 Background of the Study

Due to intensified globalization, Organizations, today, are facing increased competition and this has been drastically

fastened by the changes in technology, political and economic environments and thus, prompting organizations to train their employees could be identified as one of the best methods to make them ready to adjust to the increases above and thus enhance their overall performance. Here, it is significant to not neglect the current evidence on growth of knowledge in the business corporate world throughout the last decade. This growth has not only been brought about by advancements in technology nor a combination of factors of production but enhanced efforts towards development of organizational human resources. It is therefore, every organization's responsibility to get the job performance of the employees improved. Thus, Implementation of training and development is one of the main steps that most companies need to achieve, regardless of the scale of operation it may own.

According to what has been talked in the previous discussion, employees are a crucial resource and, it is more crucial to optimize the contribution of employees to the company aims and goals as a means of sustaining effective performance. This therefore calls for management and administration of any organization to ensure a sufficient supply of staff that is technically and socially competent and capable of career development into specialist departments or management positions. This creates the basic question as to why Human Resource is this much important, and this question has been answered by a number of researchers over the past. As per them, human resources are the intellectual property of the firm, and, thus, employees prove to be a good source of gaining competitive advantage which is highly sustainable. In this case, training and development is considered to be the only way of developing organizational intellectual property through building employees competencies. In order to reach the organizational goals established, organizations have to obtain and utilize human resources effectively. Organizations, therefore, need to design its human resource management in ways that fit into the organization's structure as it will make the organizations realize ultimate success.

1.2 Problem Statement

On the other hand, human capital can be identified as the most important resource an organization can have as it has a direct and an observable impact on the organization's success. According to researchers, the modern workplace is a highly turbulent environment which calls for employees and managers of all levels to regularly improve and achieve objectives. This fact, in turn, requires that the organization continually invest in the enhancement of the human capital. Improving personal and group managing skills, shaping and implementing the ethics and norms that characterize the

organization's culture and which set it apart, managing and leading changes, and many more are included in this task of training employees in a precise manner.

Training and Development generally requires huge amounts of time and resources, but there is often a clear mismatch between what is delivered by the training program and what was actually required by the employees. However, conducting an effective training program will provide both the individual employees and company a satisfaction of a potential progress and, also more benefits that will make the cost and time a worthwhile investment.

1.3 Social Styles Characteristics

Characteristics of four social styles are listed below.

Analytical

- 1 Focuses on tasks more than people
- 2 Thoughtful, careful fact-oriented and precise
- 3 Good at objective evaluation and problem-solving
- 4 Likes organization and structure
- 5 Avoids group work, preferring to work alone
- 6 Cautious in decision-making

Amiable

- 1 Friendly and relates well to others
- 2 Good at listening and teamwork
- 3 Dislikes of conflict and risk-taking
- 4 Seeks security and like organized workplaces
- 5 Slow decision-making
- 6 Prefers to be told what to do than to lead
- 7 Fears change and uncertainty

Expressive

- 1 Creative
- 2 Outgoing and enthusiastic
- 3 Spontaneous and fun-loving
- 4 Interacts well with others at work
- 5 Good at persuading and motivating
- 6 Fears being ignored or rejected
- 7 Like to be acknowledged
- 8 Dislikes routine and complexity

Driver

- 1 Competitive and needs to win
- 2 Seeks control and being in charge
- 3 Fast-acting
- 4 Plans carefully
- 5 Results-oriented
- 6 Task-focused
- 7 Dislikes inefficiency and indecision

II. OBJECTIVES OF THE STUDY

The main objective of the study is to increase effectiveness of the training program by customizing the way of delivery and the specific objectives of the study is

to develop a mathematical model to identify employee's strengths and weakness individually.

III. METHODOLOGY

The social styles questionnaires with having fourteen statements were used to obtain information.

First objective is to show how the questionnaire can be represented as an undirected graph. For each question in the questionnaire associate a vertice and four vertices for the social styles which are Analytical, Amiable, Expressive and Driver.

That is,

If $\{Q_i\}$, $i = 1,2,3...14$ is the set of questions and we have a set of vertices $\{V_i\}$ $i=1,2,3...14$ where question Q_i corresponds to vertice V_i .

An edge will represent the link between response and its associated social style. Each question can have multiple responses and all the responses will be connected to its associated social style. All the fourteen questions responses will be connected to main four vertices which are Analytical, Amiable, Expressive and Driver.

After modeling the graph, betweenness centrality was calculated for each four vertices which represent the social styles.

Betweenness Centrality

For a given node v , calculate the number of shortest paths between nodes s and t that pass through v , and divide by all shortest paths between nodes s and t .

The betweenness centrality $C_b(V)$ of a node V is computed as follows:

$$C_b(V) = \sum_{i \neq n \neq j} (\sigma_{st}(V) / \sigma_{st})$$

IV. RESULTS AND DISCUSSION

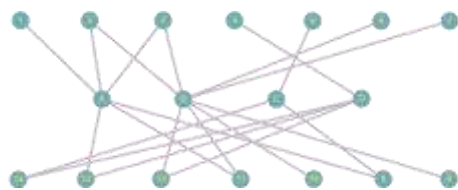


Fig. 1: Graph model for respondent 01

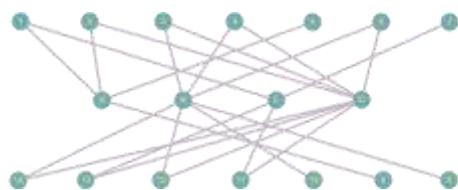


Fig. 2: Graph model for respondent 02

These two graph shows how the respondents selected the characteristics for the fourteen statements of the questionnaire.

Calculation of betweenness centrality for vertices A,B,C and D for respondent 01

$$\begin{aligned} C_b(A) &= (\sigma_{1,2}(b) / \sigma_{1,2}) + (\sigma_{1,3}(b) / \sigma_{1,3}) + (\sigma_{1,13}(b) / \sigma_{1,13}) \\ &+ (\sigma_{1,11}(b) / \sigma_{1,11}) + (\sigma_{1,9}(b) / \sigma_{1,9}) + (\sigma_{2,3}(b) / \sigma_{2,3}) \\ &+ (\sigma_{2,13}(b) / \sigma_{2,13}) + (\sigma_{2,11}(b) / \sigma_{2,11}) + (\sigma_{2,9}(b) / \sigma_{2,9}) \\ &+ (\sigma_{3,13}(b) / \sigma_{3,13}) + (\sigma_{3,11}(b) / \sigma_{3,11}) + (\sigma_{3,9}(b) / \sigma_{3,9}) \\ &+ (\sigma_{13,11}(b) / \sigma_{13,11}) + (\sigma_{13,9}(b) / \sigma_{13,9}) + (\sigma_{11,9}(b) / \sigma_{11,9}) \\ &= (1/1) + (1/1) + (1/1) + (1/1) + (1/1) + (1/1) + (1/1) + (1/1) \\ &+ (1/2) + (1/1) + (1/1) + (1/1) + (1/2) + (1/1) + (1/1) + (1/1) + (1/1) \\ &= 14 \end{aligned}$$

$$\begin{aligned} C_b(B) &= (\sigma_{2,3}(b) / \sigma_{2,3}) + (\sigma_{2,6}(b) / \sigma_{2,6}) + (\sigma_{2,7}(b) / \sigma_{2,7}) \\ &+ (\sigma_{2,12}(b) / \sigma_{2,12}) + (\sigma_{2,11}(b) / \sigma_{2,11}) + (\sigma_{2,10}(b) / \sigma_{2,10}) \\ &+ (\sigma_{2,8}(b) / \sigma_{2,8}) + (\sigma_{3,6}(b) / \sigma_{3,6}) + (\sigma_{3,7}(b) / \sigma_{3,7}) \\ &+ (\sigma_{3,12}(b) / \sigma_{3,12}) + (\sigma_{3,11}(b) / \sigma_{3,11}) + (\sigma_{3,10}(b) / \sigma_{3,10}) \\ &+ (\sigma_{3,8}(b) / \sigma_{3,8}) + (\sigma_{6,7}(b) / \sigma_{6,7}) + (\sigma_{6,12}(b) / \sigma_{6,12}) \\ &+ (\sigma_{6,11}(b) / \sigma_{6,11}) + (\sigma_{6,10}(b) / \sigma_{6,10}) + (\sigma_{6,8}(b) / \sigma_{6,8}) \\ &+ (\sigma_{7,12}(b) / \sigma_{7,12}) + (\sigma_{7,11}(b) / \sigma_{7,11}) + (\sigma_{7,10}(b) / \sigma_{7,10}) \\ &+ (\sigma_{7,8}(b) / \sigma_{7,8}) + (\sigma_{12,11}(b) / \sigma_{12,11}) + (\sigma_{12,10}(b) / \sigma_{12,10}) \\ &+ (\sigma_{12,8}(b) / \sigma_{12,8}) + (\sigma_{11,10}(b) / \sigma_{11,10}) + (\sigma_{11,8}(b) / \sigma_{11,8}) \\ &+ (\sigma_{10,8}(b) / \sigma_{10,8}) \\ &= (1/1) + (1/1) + (1/1) + (1/1) + (1/1) + (1/1) + (1/1) + (1/1) \\ &+ (1/1) + (1/1) + (1/1) + (1/1) + (1/2) + (1/1) + (1/1) + (1/1) \\ &+ (1/1) + (1/1) + (1/1) + (1/1) + (1/1) + (1/1) + (1/1) + (1/1) \\ &+ (1/1) + (1/1) + (1/1) + (1/1) + (1/1) + (1/1) \\ &= 28.5 \end{aligned}$$

$$\begin{aligned} C_b(C) &= (\sigma_{5,14}(b) / \sigma_{5,14}) + (\sigma_{5,9}(b) / \sigma_{5,9}) + (\sigma_{14,9}(b) / \sigma_{14,9}) \\ &+ (\sigma_{4,19}(b) / \sigma_{4,19}) \\ &= (1/1) + (1/1) + (1/1) \\ &= 3 \end{aligned}$$

$$\begin{aligned} C_b(D) &= (\sigma_{4,14}(b) / \sigma_{4,14}) + (\sigma_{4,13}(b) / \sigma_{4,13}) + (\sigma_{4,12}(b) / \sigma_{4,12}) \\ &+ (\sigma_{14,13}(b) / \sigma_{14,13}) + (\sigma_{14,12}(b) / \sigma_{14,12}) + (\sigma_{13,12}(b) / \sigma_{13,12}) \\ &= (1/1) + (1/1) + (1/1) + (1/1) + (1/1) + (1/1) \\ &= 6 \end{aligned}$$

Same calculations are carried for other respondents as per their answers and the node that has the highest number for the betweenness centrality is identified. Corresponding social style for the identified node is concluded as the respondents' social style. Characteristics of other social styles can be identified as weaknesses of the respondent.

	Social style with the highest value for betweenness centrality
Respondent 01	Amiable
Respondent 02	Driver
Respondent 03	Expressive, Driver
Respondent 04	Amiable
Respondent 05	Amiable

V. CONCLUSION

After identifying the highest betweenness centrality node which reflects the amount of control that node exerts over the interactions of other nodes in the network we can decide the most relevant social style of the respondent. This study was carried off with five respondents and results obtained from graphs conclude that each one of them have whole different social styles. Although this is carried out with lesser number of respondents and still their styles differ significantly indicates that people's areas of strengths and areas of developments are varying broadly.

ACKNOWLEDGEMENTS

I would like to express my deep sense of gratitude to my supervisor for the guidance, understanding, patience and most of all for making it possible for me to have a presentable thesis project.

Last but not least, I would like to thank my mother for her love and support. In particular, the patience and understanding shown by my mother and other family members during the time of this course, is greatly appreciated.

REFERENCES

- [1] Aidah Nassazi, 2013. *Effects of training on employee performance*. Business economics and tourism.
- [2] Berens, L.V. , 2001. *Understanding yourself and others. An introduction to interaction styles*. Telos Publications.
- [3] Chris Amisano, 2010. "Relationship between training and employee performance", eHowcontributer.
- [4] Kajitani, Y. and T. Aruyama 1976 ."*Functional expression of centrality in a graph - an application to the assessment of communication networks*", Electronics and communication in Japan 59-A.
- [5] Garrison, W. L. 1977."*A set of measures of centrality based on betweenness*". Sociometry 40(35)

An Improved AES Cryptosystem Based Genetic Method on S-Box, With, 256 Key Sizes and 14-Rounds

Ashutosh Pandey¹, Umesh kumar Lilhore²

¹M.Tech Scholar, Dept. of CSE, NIIST Bhopal, India

²NIIST Bhopal, A.P Dept. of CSE, NIIST Bhopal, India

Abstract— Cryptography methods are widely use in digital communication for secure data transaction. Cryptography methods have two categories symmetric and asymmetric. Both types of encrypting have their own importance and limitations. In Symmetric key based encryption same key is use for encryption and decryption process. One of the most popular and widely used symmetric encryption methods is (AES) Advance encryption standard, which attracts researchers to develop more efficient AES cryptosystem. In this research work we are presenting an improved AES encryption method “IAES”. Proposed IAES method uses a modified S-Box by employing Genetic algorithm (GA) with key size of 256 bit. In proposed method IAES, GA will be used in the S-box to perform various pipelined operations such as substitution, shifting of rows, mixing of column and to perform Add Round Key in the AES rounds. In this work proposed IAES and existing AES method both are implemented over MATLAB simulator and various comparison parameters such as encryption time, speed and decryption time and speed are calculated. The high level of system integration along with high speed and high throughput makes the proposed IAES based cryptosystem a perfect choice for a spread of application.

Keywords— Cryptography, Symmetric, AES, S-box, S-box, Genetic Algorithm.

I. INTRODUCTION

In today’s scenario people shares data and information to each other by using of network due to this more amount of information are so much private but some are less private due to this the attacker or the hackers are taking advantage and they are attempting to steal the information to overcome various used since 2001 since it provides high level of security and can be implementation easily [1,6]. With the introduction and revolution in communications, one more change that affected security is the introduction of

distributed systems which requires carrying of data between terminal user and a set of computers.



Figure 1.1: Cryptography

Network security measures are needed to protect data during their transmission. The mechanisms used to meet the requirements like authentication and confidentiality are observed to be quite complex. Cryptography is the science of information and communication security. Security mechanisms usually involve more than a particular algorithm or protocol for encryption & decryption purpose and as well as for generation of sub keys to be mapped to plain text to generate cipher text. It means that participants be in possession of some secret information (Key), which can be used for protecting data from unauthorized users [5].

II. AES ENCRYPTION

The Advanced Encryption Standard, in the following referenced as AES, is the winner of the contest, held in 1997 by the US Government, after the Data Encryption Standard was found too weak because of its small key size and the technological advancements in processor power. The Rijndael, whose name is based on the names of its two Belgian inventors, Joan Daemen and Vincent Rijmen, is a Block cipher, which means that it works on fixed-length group of bits, which are called blocks. It takes an input block of a size, usually 128, and produces a corresponding output block of the same size. The transformation requires a

second input, which is the secret key. It is important to know that the secret key can be of any size (depending on the cipher used) and that AES uses three different key sizes: 128, 192 and 256 bits. While AES supports only block sizes of 128 bits and key sizes of 128, 192 and 256 bits, the original Rijndael supports key and block sizes in any multiple of 32, with a minimum of 128 and a maximum of 256 bits.

2.1 AES APPLICATION-AES have following applications [22].

- A) Design of hardware and software-In various designing of H/w and S/w AES used.
- B) Design of processor-Variou processor are based on AES method
- C) In basic encryption and decryption process-Variou data security use AES encryption.
- D) Application archive and compression tools Like Rar and WinZip
- E) File encryption and disk or partition Encryption
- F) Security for communications in LAN IEEE 802.11i-2004, or 802.11i wireless networks
- G) Provides confidentiality and authentication For IPsec protocol
- H) SPN substitution -permutation networks uses the stages and rounds in AES.

III. GENETIC ALGORITHM-

A genetic algorithm is a randomized search that has proven to be reliable and powerful optimization technique which follows the principle of natural selection. It can be applied to both texts and images. Genetic algorithm is secure, since it does not utilize the natural numbers directly. The results obtained for generating keys using genetic algorithm should be good in terms of coefficient of autocorrelation [2].

The basic genetic algorithm operators are discussed as follows-

- **Selection-** It is the process of choosing the chromosomes from the initial population generated by function based on fitness value.
- **Crossover-** This operator combines the chromosome of one generation with another to reproduce a new set of values. Single point crossover, two point crossover and uniform crossover are the three types of crossover operators in GA.
- **Mutation-** This provides a genetic diversity of a chromosome in one generation. The chromosomes are flipped and a new chromosome is generated for a new generation.

IV. PROBLEM STATEMENT-

Cryptography methods are widely use in digital communication for secure data transaction. Cryptography methods have two categories symmetric and asymmetric. Both types of encrypting have their own importance and limitations. In Symmetric key based encryption same key is use for encryption and decryption process. One of the most popular and widely used symmetric encryption methods is (AES) Advance encryption standard, which attracts researchers to develop more efficient AES cryptosystem. In this research work we are presenting an improved AES encryption method "IAES".

The key challenges in AES algorithm are-

1. **High encryption time-** Existing AES have high encryption time.
2. **High the decryption time-** Existing AES have high decryption time.
3. **Slow Encryption Speed-** Existing AES have low encryption speed.
4. **Slow Decryption Speed-** Existing AES have low decryption time.
5. **Avalanche Effect-** Existing AES have poor avalanche effect.

V. PROPOSED IAES METHOD-

Proposed IAES method uses a modified S-Box and P- Box by employing Genetic algorithm (GA) with key size of 256 bit. In this proposed method IAES, GA will be used in the S-box to perform various operations such as substitution, shifting of rows, mixing of column and to perform Add Round Key in the AES rounds.

An enhanced AES implemented using evolutionary approach is expected to improve the performance of the AES which are mentioned above. AES is a symmetrical block cipher which uses Substitution box (S-box) and Permutation box (S-box) for the process of encryption and decryption. Substitution box (S-box) is a keystone of AES symmetric cryptosystem.

5.1 WORKING OF PROPOSED IAES (ENCRYPTION)-

Following steps are used in IAES-

Step 1-(divide plain text message in to equal size blocks) plaintext A in to A1 To An

Step 2-A (the 128-bit data path) consisting of 16 bytes A0, A1... A15 is arranged in a four-by-four byte matrix.

Step 3 The key bytes are arranged into a matrix with four rows and four (256-bit key).

Apply GA_Key();

Step 3.1 Key Generation Using GA-The process of generating the key from the Genetic Population has the following steps

3.1.1 In the first step a binary population is generated. Each cell is generated using the pseudo random number generator of the programming language. The number generated is one if the PRNG generates a number greater than 50 else it is 0. Each chromosome contains 25 such cells and the number of chromosomes in the experiment was taken as 1000.

3.1.2 Now for each chromosome we repeat the following process-

- a) Divide the chromosome into 5 groups. Calculate the number of ones in each group. If the number of one's is greater than 2 then the new array will have 1 as its cell otherwise 0.
- b) The above step converts the population of chromosomes having 25 cells as one having 5 cells.
- c) Now we have a 5X 1000 array with us. The array is then read vertically 25 cells at the time. The first column followed by the second and so on.
- d) The above step gives us an array of 25 X 200 which serves as the population now. This is followed by crossover and mutation operators being applied to the sample.
- e) Now each cell is multiplied by $2^{(12-i)}$ where 'i' is the cell number. This generates a sample of 200 numbers.
- f) Each number is then converted into an integer. The process is repeated 5 times.
- g) The coefficient of auto correlation is then calculated. If the result is favorable then the population is accepted else the whole process is repeated.

Step 4-Use of Modify Byte Substitution layer S-box-

The first layer in each round is the Byte Substitution layer. The Byte Substitution layer can be viewed as a row of 16 parallel S-Boxes, each with 8 input and output bits.

In the layer, each state byte A_i is replaced, i.e., substituted, by another byte B_i : $S(A_i) = B_i$

4.1-The first step of S-BOX generation is finding the multiplicative inverse this requires using the irreducible polynomial $p(x)$ defined by-

$P(x) = x^8 + x^4 + x^3 + x + 1$, And inverse of a polynomial $a(x)$ is calculated by $A(x) \text{ pow } -1 = b(x) \text{ mod } p(x)$

4.2- Affine Transform- Affine transformation of a single column.

4.3- Diffusion Layer- The Diffusion layer consists of two sub layers, the Shift Rows transformation and the Mix Column transformation.

4.4- Shift Rows Sub layer- The Shift Rows transformation cyclically shifts the second row of the state matrix by three bytes to the right, the third row by two bytes to the right and the fourth row by one byte to the right.

Step 5-MixColumn Sublayer-This step is a linear transformation which mixes each column of the state matrix. S represents the one complete column of the matrix B .

Step 6-Key Addition Layer-

The two inputs to the Key Addition layer are the current 16-byte state matrix and a subkey which also consists of 16 bytes (128 bits). The two inputs are combined through a bitwise XOR operation.

Step 7- Key Expansion-The Improve AES algorithm takes the Cipher Key, K , and performs a Key Expansion routine to generate a key schedule.

7.1 The Key Expansion generates a total of $N_b(N_r + 1)$ words: the algorithm requires an initial set of N_b words, and each of the N_r rounds requires N_b words of key data.

The resulting key schedule consists of a linear array of 4-byte words, denoted $[w_i]$ with i in the range $0 \leq i < N_b(N_r + 1)$

Step 8- Decryption process – Reverse of encryption process.

VI. EXPERIMENTAL SETUP & RESULT ANALYSIS

In this research proposed and existing methods are implemented over MATLAB simulator fig 6.1. Following results are calculated-

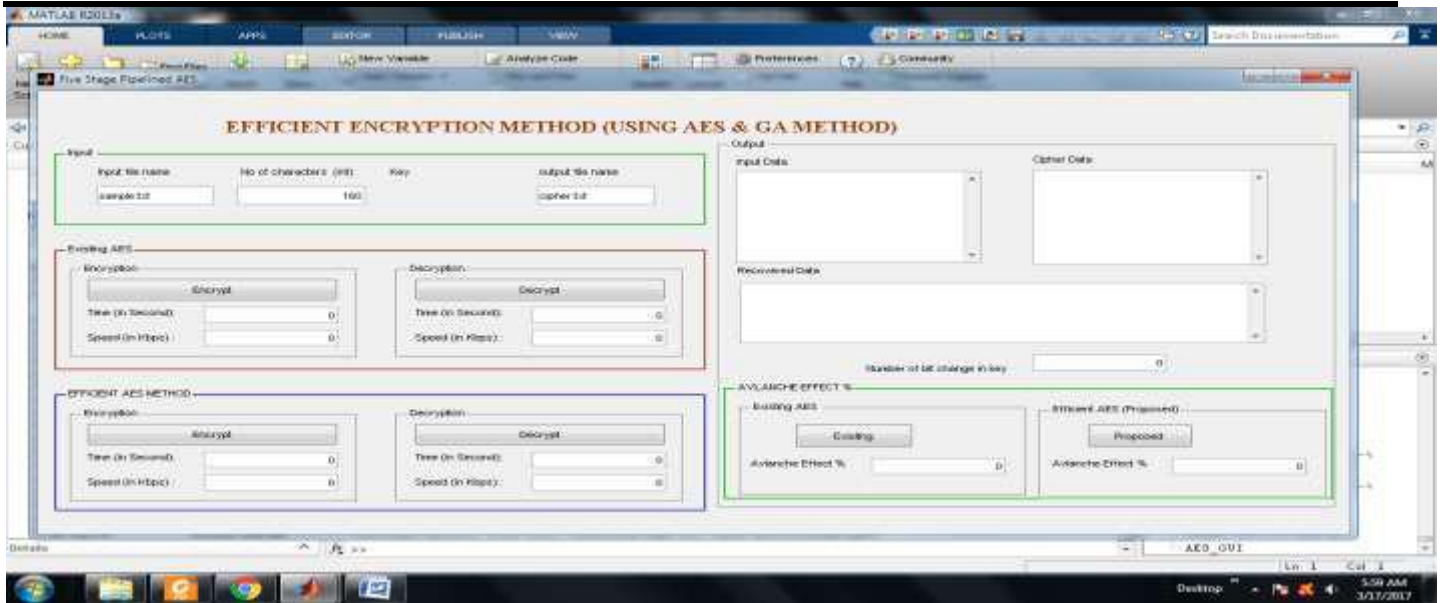


Fig.6: Simulation Screen

6.1 Encryption time for AES Vs Proposed IAES-Time
 that is require to convert a plain text to cipher text.

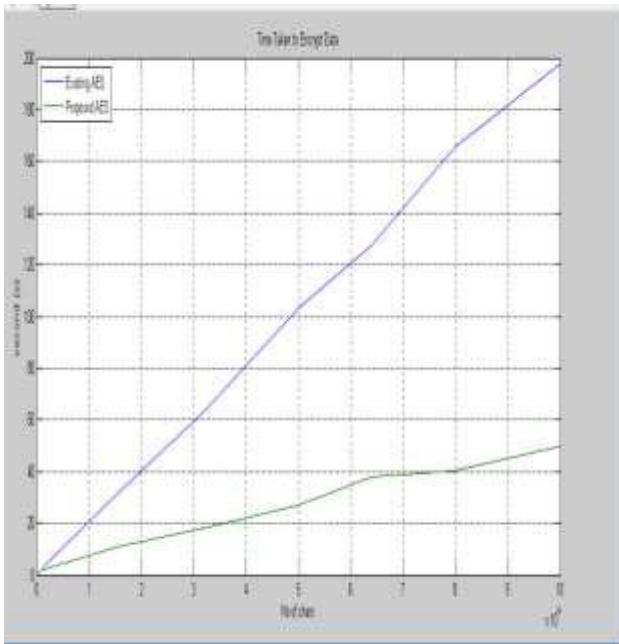


Fig.6.1: Encryption time for AES Vs Proposed IAES

6.2 Decryption time for AES Vs Proposed IAES - Time
 that is requiring converting a cipher text to plain text.

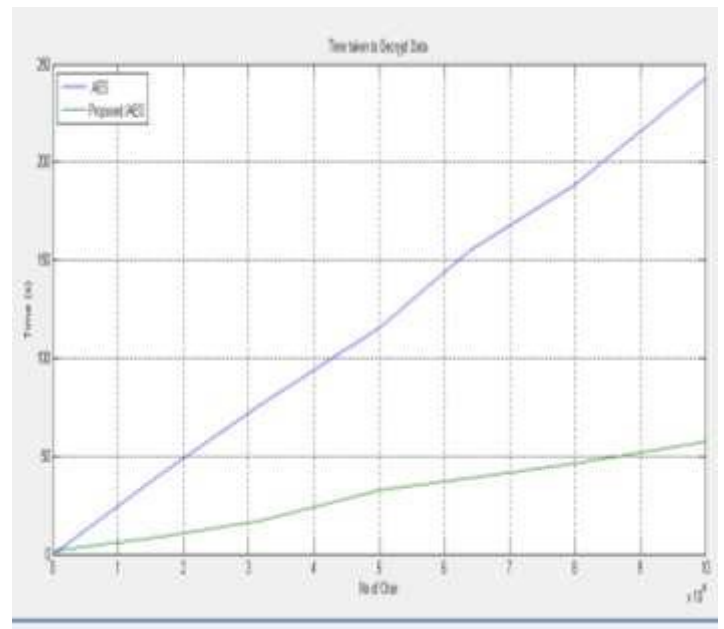


Fig.6.2: Decryption time for AES Vs Proposed IAES

6.3 Encryption speed AES Vs Proposed IAES- Processor
 speed/Time that is requires converting a plain text to cipher text.

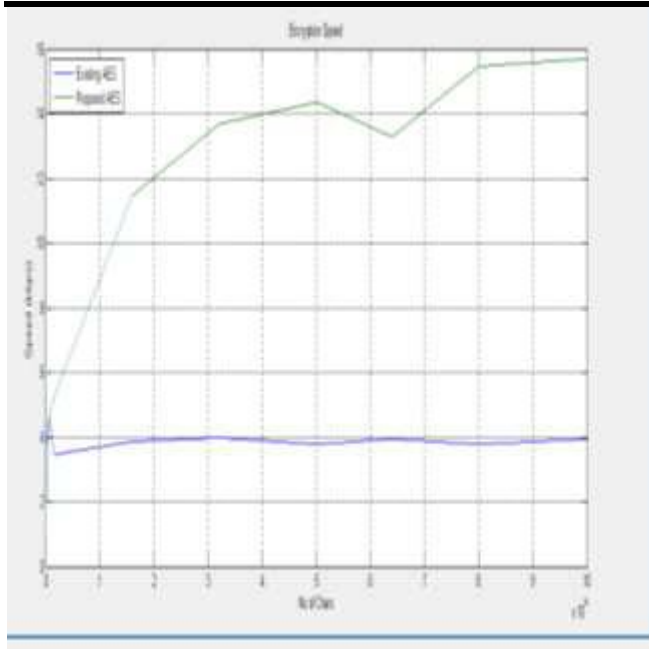


Fig.6.3: Encryption speed for AES Vs Proposed IAES

6.4 Avalanche Effect %- When changing some bit in plaintext and then watching the avalanche change in the outcome of the bits in the cipher text

Table.6.4: Avalanche Effect %

No of bit change	Avalanche Effect %	
	Existing AES	Proposed IAES
1	78	81
2	72	79
4	68	77

6.5 OVERALL COMPARISON RESULT-

An overall comparative analysis for the existing and proposed technique is presented in this section in terms of different relevant parameters-

Table.6.5: Overall comparisons of Existing and Proposed Technique

Sr. No	Simulation Parameter	Existing AES 256	Proposed IAES 256	Well Performance
1	Encryption Time	High	Low	Proposed Technique
2	Encryption Speed	Low	High	Proposed Technique
3	Decryption Time	High	Low	Proposed Technique
4	Decryption Speed	Low	High	Proposed Technique
5	Avalanche Effect	Medium	High	Proposed Technique

VII. CONCLUSIONS & FUTURE WORKS-

The AES encryption is widely used and most popular encryption standard. This is also used in various applications such as processors, hard disk partitioning and secure data transmission. In this work an efficient AES encryption method (IAES) is described. Proposed IAES method uses a modified S-Box by employing Genetic algorithm (GA) with key size of 256 bit. In this proposed method IAES, GA is used in the S-box to perform various operations such as substitution, shifting of rows, mixing of column and to perform Add Round Key in the AES rounds. Results comparisons between AES and proposed IAES clearly show that, due to some effective design considerations the proposed IAES, performance is outstanding over existing AES.

In future we will apply this mechanism in real time implementation instead of just a simulation. IAES method can be implements with more multi stage processors to achieved high throughput.

REFERENCES

- [1] Nishtha Mathura, Rajesh Bansode, “AES Based Text Encryption Using 12 Rounds with Dynamic Key Selection”, 7th International Conference on Communication, Computing and Virtualization, Science Direct, 2016, PP 1036 -1043
- [2] K.kalaiselv, and Anand kumar,” Enhanced AES Cryptosystem by using Genetic Algorithm and Neural Network in S-box”, CNN Conference IEEE 978-1-5090-1936-6/16 2016, PP 216-222
- [3] S.Rehman, S.Q. Hussain, W.Gul and Israr,” Characterization of Advanced Encryption Standard (AES) Algorithm for Textual and Image data ”, International Journal Of Engineering And Computer Science ISSN: 2319-7242 Volume 5 Issue 10 Oct. 2016, Page No. 18346-18349
- [4] D.Lohit Kumar, Dr. A.R.Reddy, Dr.S.A.K.Jilani "An Efficient Modified Advanced Encryption Standard (MAES) adapted for image cryptosystems". IJCSNS International Journal of Computer Science and Network Security, 2010. Vol.10 No.2 (226-232)
- [5] Amish Kumar, Namita Tiwari, “AES Security Enhancement by Using Double S-Box”, (IJCSIT) International Journal of Computer Science and Information Technologies, Vol. 3 ,3980-3984, ISSN-0975-9646, 2012.
- [6] Kunal Lala, Ajay Kumar, Amit Kumar, “Enhanced Throughput AES Encryption” International Journal

- of Electronics and Computer Science Engineering 2132, ISSN- 2277-2012.
- [7] Abhilasha CP, Nataraj KR Engel, A. Uhl, A survey on JPEG 2000 encryption. *Multimedia Systems*, 2009.15(4): p. 243-270.
- [8] Umalaxmi Sawant¹, Prof. Kishor Wane M.K. Khan, Modified AES Using Chaotic Key Generator for Satellite Imagery Encryption, in *Emerging Intelligent Computing Technology and Applications, Proceedings*, D.S. Huang, et al., Editors. 2009. p.1014-1024
- [9] Ankit K.Dandekar, Sagar Pradhan, Sagar Ghormade "Making AES Stronger: AES with Key Dependent S-Box". *IJCSNS International Journal of Computer Science and Network Security*, Septamber 2008. VOL.8(NO.9): p. pp 388-398
- [10] Pankaj Kamboj, and W Wan, "Research and Realization based on hybrid encryption algorithm of improved AES and ECC," in *IEEE International Conference on Audio Language and Image Processing (ICALIP2010)*, pp. 396-400, Nov. 2010
- [11] S.Suguna, Dr.V.Dhanakoti, R. Manjupriya and V kumar, "Efficient Implementation of AES ," in *International Journal of Advanced Research in Computer Science and Software Engineering* , Vol. 3, Issue 7, July 2013, pp.290-295.
- [12] D Jayasinghe, J Fernando, R Herath and R Ragel, "Remote Cache Timing Attack on Advanced Encryption Standard and Countermeasure," in *IEEE International Conference on Information and Automation for Sustainability (ICIAFs)*, pp. 177-182, Dec. 2010.
- [13] R Pahal and V kumar, "Efficient Implementation of AES ," in *International Journal of Advanced Research in Computer Science and Software Engineering* , Vol. 3, Issue 7, July 2013, pp.290-295.
- [14] C JunLi, Q Dinghu, Y Haifeng, Z Hao and M Nie, "Email encryption system based on hybrid AES and ECC," in *IET International Communication Conference on Wireless Mobile and Computing (CCWMC2011)*, pp. 347 - 350, Nov. 2011
- [15] V Patil, Prof.Dr.Uttam.L.Bombale ,P Dixit, "Implementation of AES algorithm on ARM processor for wireless network, " in *International Journal of Advanced Research in Computer and Communication Engineering* , Vol. 2, Issue 8, August 2013, pp.3204-3209.
- [16] H. Tange and B. Andersen, "Attacks and Countermeasures on AES and ECC," in *IEEE International Symposium on Wireless Personal Multimedia Communications (WPMC)*, pp. 1-5, Jun. 2013.

Parametric Instability in Mathieu Equation for Interaction P-S Waves

Hector Torres-Silva¹, Enrique Fuentes Heinrich²

¹Universidad de Tarapacá, EIEE, Arica, Chile

²Profesor Titular retirado, Universidad de Tarapacá, EIEE, Arica, Chile

Abstract— We propose an experimental study of parametric resonance between P-waves and S-waves, which can be used to describe various nonlinear phenomena qualitatively and to obtain bifurcation diagrams quantitatively. It is based on an electronic circuit and is easy to design. We show that it is a good simulation of parametric phenomena, and our results are in good agreement with theoretical predictions. In particular, it may be used to study the influence of pump P waves on the instability's threshold and amplitude of S waves.

Keywords—Mathieu equation, S -P waves, parametric resonance, damping .

I. INTRODUCTION

The difference in speed of travel of P-waves and S-wave is vital to transmit energy of seismic wave. The P wave is a *longitudinal* wave or a *compression* wave. Force is applied in the direction that the wave is travelling. Ground or earth is pretty incompressible, so the energy is transferred pretty quickly. In S wave, the medium is displaced in a *transverse* (up and down - compared to the line of travel) way, and the medium must *shear* or "move away" from the material right next to it to cause the shear and transmit the wave [1, 2].

On the other hand, parametric amplifiers and oscillators have been widely studied in electronics and optics. For instance, parametric amplification has been used to achieve low-noise amplification in electronic systems. This parametric instability is called the Faraday instability. Recently, Pritchett and Kim proposed a simple system to observe Faraday instabilities [3]. We propose here an alternative way to study parametric instabilities by doing an analog experiment that models the Mathieu equation [4].

A study can be made on the torsional-lateral motions of non-linear symmetrical structures subjected to lateral ground motion. The torsional and lateral response of a single mass symmetrical system subjected to sinusoidal ground motion can be investigated where non-linear coupling exists between the lateral and rotational motions like S waves. For sinusoidal lateral response, the

torsional motion equation can be cast in the form of a Mathieu equation. The likelihood of induced torsional response can be studied in terms of unstable regions in the parametric amplitude-frequency parameter space. The implication of this type of non-linear torsional-lateral coupling to the responses of real symmetrical structures subjected to actual earthquake ground motion can be simulated with an electronic model.

Our proposed simulation is easy to understand conceptually and has several advantages, including fast data acquisition. It also allows students to explore the behavior of a driven oscillator and to understand the concepts of supercritical and subcritical bifurcations in earthquake phenomena.

The experiments involve two control parameters: the forcing amplitude P and the forcing pulsation ω_e .

Here, for wave P we make $\omega_e = 2\text{rad/s}$. Varying these two parameters allows us to study the threshold of the instability for different driving frequencies and to explore the Mathieu extension of the bifurcation. We also study the nonlinear dependence of the oscillation amplitude on P .

II. PARAMETRIC RESONANCE

A system is subjected to a parametric forcing if one of its parameters is temporally modulated producing parametric instability which occurs when a tank containing a liquid is vertically vibrated: one then observes standing waves on the free surface. [5]. This parametric instability is called the Faraday instability. The physical situation is more complex because of the great number of degrees of freedom in the system leading to the generation of complex patterns on the surface. The study of parametric surface waves has led to a large number of theoretical and experimental studies [6]. In the simple case of an incompressible, irrotational, and inviscid fluid, Benjamin and Ursell [7], showed that, in the linear approximation, each mode $\xi_{\mathbf{k}}$ (of wave vector \mathbf{k}) of the surface deformation is governed by a Mathieu equation.

$$\frac{d^2\xi_k}{dt^2} + \lambda \frac{d\xi_k}{dt} + \omega_0^2(1 + F \cos(\omega_e t))\xi_k = 0 \quad (1)$$

which can be extended to rotational motion

$$\frac{d^2\xi_0}{dt^2} + \lambda \frac{d\xi_0}{dt} + \omega_0^2(1 + P \cos(\omega_e t))\xi_0 = 0 \quad (2)$$

Where ξ_0 is transversal This system leads to a canonical example of a parametric instability [5], ω_e is the external forcing pulsation, and P is directly related to the amplitude of the vibration acceleration relative to the acceleration of gravity produced by P- waves. The presence of a small viscous dissipation can be taken into account by including a phenomenological damping term λ .

In the undamped case $\lambda = 0$, when $P \rightarrow 0$, the parametric resonance occurs when $\omega_e / \omega_0 = 2/n$, where n is an integer. The most unstable oscillation corresponds to $n = 1$, that is, $\omega_e / \omega_0 = 2$, [8]. In the following, we are interested only in this last case.

With $\lambda = 0$ and $\omega_0^2 P = \varepsilon$ Mathieu equation (2) is

$$\frac{d^2\xi_0}{dt^2} + (\omega_0^2 + \varepsilon \cos(2t))\xi_0 = 0, \quad \omega_0^2 > 0 \quad (3)$$

which is reversible, A typical question is: for which values of ω_0 and ε in $(\omega_0^2, \varepsilon)$ -parameter space is the trivial solution $\xi_0 = 0, d\xi_0 / dt = 0$ stable?

We find that periodic solutions exist for $n = 1$ if: $\omega_0^2 = 1 \pm \varepsilon / 2 + O(\varepsilon^2)$. In the case $n = 2$, periodic solutions exist if: $\omega_0^2 = 4 - \varepsilon^2 / 48 + O(\varepsilon^4)$, and $\omega_0^2 = 4 + \varepsilon^2 5 / 48 + O(\varepsilon^4)$.

The corresponding instability domains are called Floquet tongues, instability tongues or resonance tongues, see fig. 1.

On considering higher values of n , we have to calculate to a higher order of ε . At $n = 1$ the boundary curves are intersecting at positive angles at $\varepsilon = 0$, at $n = 2$ ($\omega_0^2 = 4$) they are tangent; the order of tangency increases as $n - 1$ (contact of order n), making instability domains more and more narrow with increasing resonance number n .

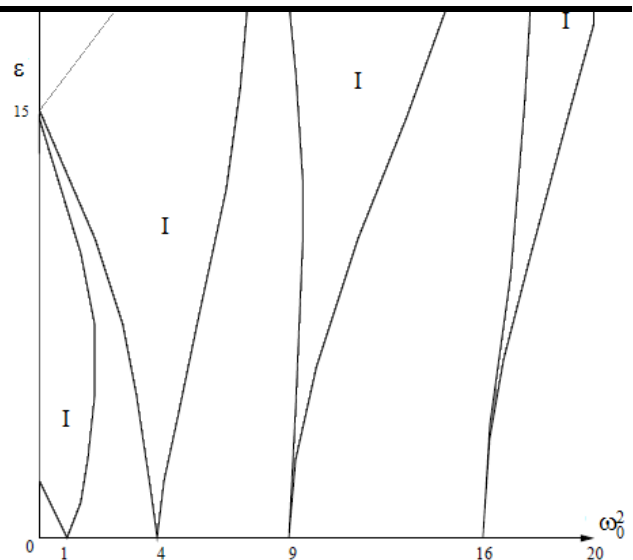


Fig.1: Floquet tongues of the Mathieu eq. (3); the instability domains are marked with I.

III. THE MATHIEU EQUATION WITH VISCOUS DAMPING

In real seismic applications there is always the presence of damping. We shall consider the effect of its simplest form, small viscous damping. Eq. (3) is extended by adding a linear damping term λ :

$$\frac{d^2\xi_0}{dt^2} + \lambda \frac{d\xi_0}{dt} + \omega_0^2(1 + P \cos(2t))\xi_0 = 0, \quad \lambda > 0 \quad (4)$$

We assume that the damping coefficient is small, $\lambda = \varepsilon \kappa_0$, and we put $\omega_0^2 = n^2 - \varepsilon \beta$ to apply the Poincare-Lindstedt method [9].

We find periodic solutions in the case $n = 1$ if:

$$\omega_0^2 = 1 \pm \sqrt{\varepsilon^2 / 4 - \lambda^2} \quad (5)$$

Relation (5) corresponds with the curve of periodic solutions, which in $(\omega_0^2, \varepsilon)$ -parameter space separates stable and unstable solutions. We observe the following phenomena.

If $0 < \lambda < \varepsilon / 2$, we have an instability domain which by damping has been lifted from the

ω_0^2 -axis; also the width has shrunk. If $\lambda > \varepsilon / 2$ the instability domain has vanished. For an illustration see fig. 2.

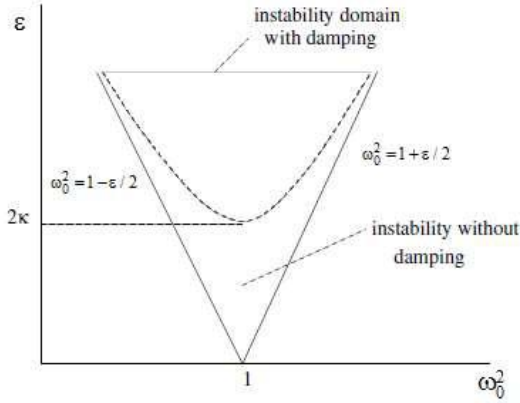


Fig.2: Reduced schematic instability with the damping presence.

Repeating the calculations for $n > 2$, we find no instability domains at all; damping of $O(\epsilon)$ stabilizes the system for ϵ small. To find an instability domain we have to decrease the damping, for instance if $n = 2$ we have to take $\lambda = \epsilon^2 \kappa_0$ (Figure 3).

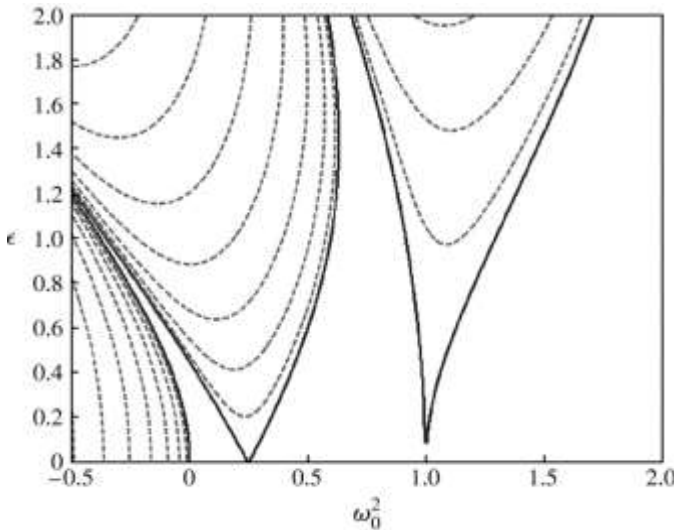


Fig.3: (ω_0^2, ϵ) space for different values of damping

IV. AN OSCILLATORY ELECTRIC CIRCUIT

Previous simulation can be verified experimentally through the following approach which can be used for a depth investigation of seismic S waves which can be attenuated or amplified. This proposed circuit and its dynamics can be approximately modeled with the Mathieu equation (4).

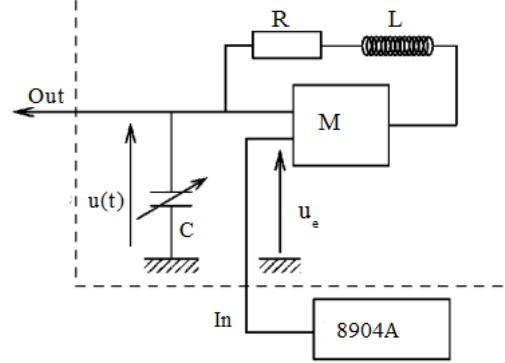


Fig.4: Electronic analog of the Mathieu equation.

We will propose an analog model of the parametric instability with an scaled frequency such that $\omega_e / \omega_0 = 2$. In fact, the Mathieu equation, Eq. (4) above, leads to the amplitude in Eq. (5), which is analogous to the one derived in the Faraday problem in the limit of small viscosity. Our electronic device is shown in Fig 4. M is an AD633 multiplier; its output voltage, $u_0(t)$ is proportional to the product of the two input voltages, $u_1(t) \times u_2(t)$. C is a capacitor with a voltage-dependent capacity made with variable capacitance diodes (varicaps) BB909A. As mentioned in Ref. [10], these diodes introduce some nonlinearities in contrast to the circuit proposed in Ref. [11,12] where no nonlinear component is present. To avoid electromagnetic perturbations, the electronic oscillator can be enclosed in a metallic container which serves as a Faraday cage.

The electronic system is forced by a periodic voltage $u_e(t) = u_0 \cos(\omega_e t)$, $\omega_e / \omega_0 = 2$. We can use Kirchhoff's voltage law and the property of the multiplier to find that the charge q of the capacitance C is governed by (see Fig. 4). The circuit LC have a time varying resistance R

$$L \frac{d^2q}{dt^2} + R \frac{dq}{dt} + \frac{q}{C} (1 + k u_0 \cos(2t)) = 0 \quad (6)$$

where k is the gain of the multiplier ($k=1/10V$) in our case. The capacitance C depends on the charge q , but the use of a pair of oppositely polarized varicaps leads to the symmetry $q \rightarrow -q$ of the function $C(q)$. Hence, we can write

$$C = C_0 \quad (7)$$

$$\frac{d^2q}{dt^2} + \lambda_e \frac{dq}{dt} + \omega_0^2 (1 + P_e \cos(2t)) q = 0 \quad (8)$$

with $\lambda_e = R/L$, $\omega_0^2 = 1/LC_0$, $\omega_0^2 P_0 = \omega_0^2 k u_0 = \epsilon_e$.

$$\frac{d^2q}{dt^2} + \lambda_e \frac{dq}{dt} + (\omega_0^2 + \epsilon_e \cos(2t))q = 0 \quad (9)$$

Equation (9) is identical to expression for seismic waves and we can expect experimental results for the charge amplitude similar to those described for the P and S waves.

We propose a 1-H inductance, and measured the resonance frequency of the RLC circuit to be $\omega_0 = 2\pi \times 6.812\text{kHz}$ so that $C_0 \approx 546\text{pF}$. For $\omega_e = 2\omega_0$, the threshold is simply determined by the relation $P = \lambda = R / (2L\omega_0)$. Thus, the global resistance of the circuit is $R = 555\Omega$, and the quality factor of the RLC circuit is $QP = L\omega_0 / R \approx 77$. As mentioned below, we are interested in the evolution of the voltage $u \approx q / C_0$, the analog of the amplitude ξ_0 . We thus can utilize a digital synthesizer like HP8904A or equivalent and a signal analyzer HP35670A or equivalent to calculate, via a real-time averaged fast Fourier transform, the voltage amplitude $|A|$, defined by

$$u(t) = Ae^{i\omega_e t/2} + cc \quad (10)$$

After interfacing the experimental setup using LABVIEW or equivalent, we can directly record the control parameters u_0 with $\omega_e = 2\omega_0$, and the voltage amplitude $|A|$. Thus we can study the interaction of P-S waves [13], especially when the P-S interaction occurs in the metamaterial region.

V. CONCLUSION

We have proposed an experimental study of parametric resonance between P-waves and S-waves, which can be used to describe various nonlinear phenomena qualitatively and to obtain bifurcation diagrams quantitatively. It is based on an electronic circuit and is easy to design. We have shown that it is a good simulation of parametric phenomena, and our results can be in good agreement with theoretical predictions. In particular, it may be used to study the influence of pump P waves on the instability's threshold and amplitude of S waves.

REFERENCES

- [1] H. Torres-Silva and J. Lopez-Bonilla . "Early Prediction and detection of Strong Earthquakes through Chiral Radiation Waves", Journal of Vectorial Relativity, 6, 2, 1-11, 2011.
- [2] H. Torres-Silva , D. Torres Cabezas D , "Chiral Seismic Attenuation with Acoustic Metamaterials " Journal of Electromagnetic Analysis and Applications, Vol.5, No.1, 2013
- [3] T. Pritchett and J. K. Kim, "A low-cost apparatus for the production of surface wave patterns in a vertically oscillating fluid," Am. J. Phys. **66**, 830–833, 1998.
- [4] D. G. Luchinsky, P. V. E. McClintock, and M. I. Dykman, "Analogue studies of non-linear systems," Rep. Prog. Phys. **61**, 889–997, 1998.
- [5] K. Kumar, "Linear theory of Faraday instability in viscous liquids," Proc. R. Soc. London, Ser. A **452**, 1113–1126 ~1996.
- [6] M. Faraday, "On the forms and states assumed by fluids in contact with vibrating elastic surfaces," Philos. Trans. R. Soc. London **52**, 319–340, 1831.
- [7] T. B. Benjamin and F. Ursell, "The stability of the plane free surface of a liquid in vertical periodic motion," Proc. R. Soc. London, Ser. A **225**, 505–515, 1954
- [8] L. Landau and E. Lifschitz, *Mechanics* ~Pergamon, London, 1960, Sec. 27.
- [9] F. Verhulst, *Methods and applications of singular perturbations*, Springer (2005). F. Verhulst ., *Nonlinear differential equations and dynamical systems*, Springer-Verlag, New York, 1996.
- [10] L. Falk, "Student experiments on parametric resonance," Am. J. Phys. **47**, 325–328 ,1979.
- [11] F. X. Bally and P. Boisse', "Un modele electronique simple et exact de l'oscillateur parametrique," Bulletin de l'Union des Physiciens 747, 1267–1276 ,1992.
- [12] Hector Torres-Silva, Diego Torres Cabezas, A Seismic Channel Model: The San Ramon Fault. International Journal of Advanced Engineering Research and Science (IJAERS), [Vol-3, Issue-11, Nov- 2016].
- [13] Hector Torres-Silva, "Una Revisión sobre los metamateriales", Dyna New Technologies, Accepted: 1/Mar/2017 - DOI: <http://dx.doi.org/10.6036/NT8331>.
- [14] Hector Torres-Silva, "Metamaterial: Present and Future" , Accepted in Dyna, 2017.

Impact Analysis of Soybean in Supply of Edible Oil in India

Prem Narayan

ICAR-National Institute of Agricultural Economics and Policy Research (NIAP), D.P.S. Marg, Pusa, New Delhi – 110 012, India

Correspondence to Author: prem.ncap@gmail.com

Abstract —Soybean plays an important role in providing a nutritionally balanced diet. It is the principal source of edible oil and protein in human diets. The edible oil industry is one of the most important sectors of agriculture in India. India is a leading player in the industry, with the World's largest importer from Indonesia and Malaysia and third largest consumer. India is the fourth largest Soybean producing country in the world after US 118.68 MT Brazil 102 MT, followed by Argentina 57 MT, China 12.5 MT and India 12.30 MT during 2015-16. India is the largest consumer and importer of edible oils the global level. Basically a total oilseed area occupied 28.051 million hectares which contributed production 32.75MT during 2013-14. Soybean play an important role, its area 11.16 million hectares 42 percent was contributed production 12.30 million tons production and 41 percent share of total oilseed crops during TE 2015. However, the annual compound growth rate of Soybean area 14%, production 15.5% and yield 1.34%, while in total oilseed area 1.33% production 3.31% and yield 1.96% recorded during 4.5 decades (1970-71 to 2014-15), However the Soybean is leading crop first rank in oilseeds share, while it was start cultivation 1970s decades. It is emerged fastest growth in Indian an oilseed crop and cheap sources of edible oil next to palm oil in India in terms of volumes, crude edible oil contributes about 89% and refined oil contributes about 11% of the total import during 2014-15. The share edible oil of the 89% of imported crude edible oil, palm oil, soybean oil and sunflower oil contributes about 54%, 21% and 11%, respectively. The demand for edible oils in India has shown a steady growth at a CAGR of 6.50 % over the period from 2012-13 to 2016-17. The current per capita consumption edible oil in India (at 15.91 Kg/year for 2015-16) was lower than global averages (25 kg/year).

Keywords — Soybean, edible oil industry, demand-supply, area, production and yield.

I. INTRODUCTION

The Soybean *Glycine max* (L.) the 'miracle bean', which has a dual character as oilseeds and pulses but basically legume and comes under oilseed crop. The western world provided a massive push to its growth during the 1960. The crop, in fact, has revolutionized the agricultural economy of

the USA, with its immense potential a food crop, feed and numerous industrial products. At present, the USA, Brazil, Argentina, China and India are the major soybean producing countries, which contributed 90 percent share of total production soybean in the world. The USA now has over 35 percent, followed 30 percent Brazil and 17 percent in Argentina of the total soybean area in the world (USDA DATA). Soybean has come to be recognized as one of the premier agricultural crops today for various reasons. Soybean, with over 40 percent protein and 20 percent oil, has now been recognized all over the world as a potential supplementary source of edible oil and nutritious food. The protein of soybean is called complete protein, because it supplies sufficient amounts of the kinds of amino acids required by the body for repair of tissues.

Its food value in heart disease and diabetes is well known. It is significant that Chinese infants using soybean milk in place of cow's milk are practically free from rickets. Soybean is a rich source of edible oil containing no cholesterol and almost none of the saturated fat. Soybean oil surpasses all other oils because it is an ideal food for heart patients and those who wish to avoid heart disease. It also contains a large amount of lecithin and a fair amount of fat-soluble vitamins. Lecithin is an important constituent of all organs of the human body and especially of the nervous tissue, the heart and liver.

Soybean is, therefore, a good food. Besides its nutritive quality, functional properties of soy protein have opened avenues for producing new products and improving the quality of existing standard food products. A chain of soy based industries has emerged in the USA. Oil is extracted for human consumption and industrial uses like bio-diesel in the US and Brazil, and defatted soy meal is converted into various protein rich food and poultry feed products. In industry, soybean is used in the manufacture of edible lard, margarine, vegetable ghee, milk, pastries, as well as the manufacture of paints, varnishes, adhesives, etc. Soybean protein concentrates, protein isolate and textured protein has found their way into multifarious commercial food industries. Being a versatile crop with innumerable possibilities, soybean can support many agro-based industries.

Soybean was looked upon not merely as a means to supply food for humans and animals, but also at the same time to serve as a means for improving the soil fertility through their ability to fix atmospheric nitrogen. As a legume, it is an ideal component of a sound sustainable agricultural development. It is in the perspective of all these advantages of soybeans and its adaptability and productivity across tropical, subtropical and temperate environments that significant strides have been made in its innovation. In fact, the expansion of soybean crop the boosting edible oil processing industry, seed industry and edible oil industry, which generates lot employment in the agriculture sector in India. The present study is an attempt to examine these issues. The specific objectives of the study are:

1. Analysis Scenario of Soybean development, performance and ACGR of India.
2. Share of area and production share in global in terms of its productivity.
3. To analysis the domestic growth, share of soybean area, production and yield.
4. To analyse demand, supply and trade of soybean oil and other edible oil soybean meal.
5. Analysis of global production, export, import and consumption of edible oil.
6. Strategy for improving productivity Soybean in India.

II. RESEARCH METHODOLOGY

For the purpose of this study, secondary time series data regarding area, production and productivity of Soybean crops 1970-71 to 2014-15 decade analysis and impact of before and after launching Technology Mission On Oilseeds during 1986-87 to 2014-15. The annual compound growth rate and instability were analyzed all oilseed crops, however the state wise area, production, yielding changing pattern analyses after launching TMO 1986-87 to 2013-14 as per the data available. The demand-supply, availability for consumption of edible oil and import ACGR were also analyzed. The availability of input constraints and MSP of various oilseeds were also analyzed.

i. The Annual compound growth rate model for area, production and yield were estimated using the following model.

$$Y = ab^t$$

Where,

Y = area / production/ yield of oilseed crops

a = intercept

b = regression coefficient of Y on time t

ACGR in (%) = $\text{antilog}(B - 1) * 100$

ii. The instability was measured for different periods by estimating the co-efficient of variation of area, production and productivity as follows:

$$CV = \frac{SD}{Mean} * 100 \quad \text{Where,}$$

C.V. = Co-efficient of variation,

S.D. = Standard Deviation

III. RESULT AND DISCUSSION

3.1 Analysis Scenario of Soybean development, performance and ACGR of India.

3.1.1 Analysis Scenario of Soybean in India:

India has been struggling hard to bridge the oil and protein gap, fresh attempts were initiated in the 1960s to explore the possibility of developing soybean as a commercial crop in the country. It was indicated that production of soybeans would increase farm income and provides a cheap sources of supply of high quality protein and edible oil suitable for human consumption. Many forces have been operating in motivating India to be an active participant in the soybean development race since the beginning of the 1970s. The Soybean in India had increased from about 32 thousand hectares in 1971-72 to about 10911 thousand hectares at the AGCR 14 % and production increased from 14 to 10374 thousand tons in the AGCR 15.50 % during the 1971-72 to 2014-15.

At global scenario the India ranked 4th in area 11.15 million hectares, producing 12.38 million tons, while the 68th rank in productivity 1110 kg per hectare during TE 2014. The soybean productivity was very low 438 kg/ha during 1970, it was doubled within 5 year 978 kg/ha during 1975-76 and the highest productivity recorded 1353 kg/ha during 2012-13, after that it was down fall 951 kg/hectare during 2014-15 and decreased about 30 percent. The annual compound growth rate of yield of soybean 1.35 percent, while total food grain growth rate 2.26 percent and total oilseeds 2.00 percent during the 4.5 decade period 1970 to 2015-15 much lower as compared to other soybean producing countries of World (see fig1).

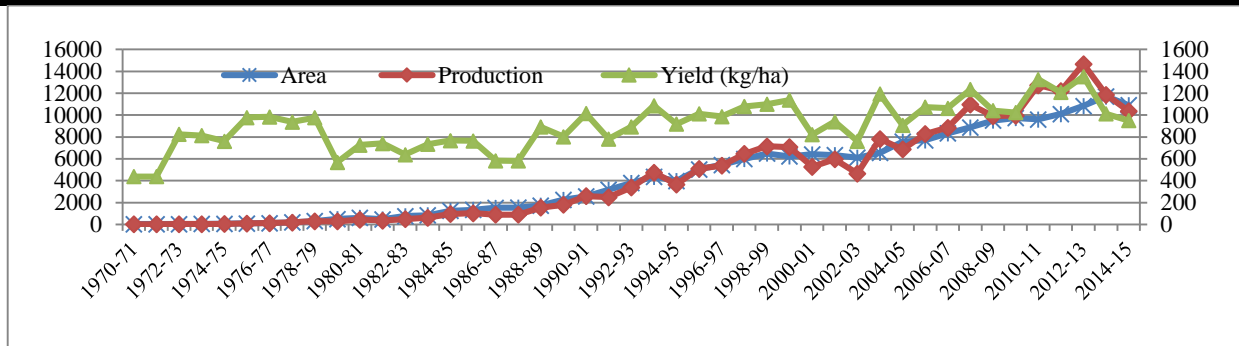


Fig.1: Area, production and yield of Soybean

Data Source: Agricoop.nic.in

3.1.2 Soybean AGCR and coefficient of variation:

The Soybean was recorded highest annual compound growth rate were accelerated 45.49 % in production followed 37.38 % in area and 5.89 percent in yield during the period 1970s with highest coefficient of variation 107 % in production and 96 % in area, this showed area and production highly fluctuated during same period during the next 1980s decade the Soybean was recorded were accelerated growth rate 17.22 %, in area and 17.95 % in production , however the yield very low 0.62 , this means the production growth has been due to area the same pattern

and no impact of Technology, while earlier decade yield growth recorded 5.89 percent during 1986-87the Technology mission on oilseeds has been launched for self-sufficiency in oilseeds but the effect of TMO was not sustain in long period. The growth rate of area and production decelerated from 10.28 and 13.10 during 1990s to 7.91 and 7.42 during the current decade 2010s but CV percent showed stability in area 7.63%, production 12.57 and yield 15.55 showed positive sign of Stability in soybean crop in India (see table 1).

Table.1:ACGR and coefficient of variation of Soybean

Particular		1970-71 to 1979-80	1980-81 to 1989-90	1990-91 to 1999-00	2000-01 to 2009-10	2010-11 to 2014-15*
Decadal ACGR	A	37.38	17.22	10.28	5.73	7.91
	P	45.49	17.95	13.10	8.93	7.42
	Y	5.89	0.62	2.56	3.03	3.38
Decadal CV %	A	106.47	45.42	28.46	17.58	7.63
	P	96.00	52.48	36.26	27.15	12.57
	Y	28.17	13.49	10.98	14.97	15.55

Data source: agricoop.nic.in

3.2 Share of area and production share in global in terms of its productivity

3.2.1 Global production of soybean:

India is the fifth largest producer of soybean (*Glycine max*) in the world after US 118.68 MT Brazil 102 MT, followed by Argentina 57 MT, China 12.5 MT and India 12.30 MT during 2015-16 as per (USDA Data). Soybean play important role in the oilseed sector occupies an important position in the agricultural economy of the country. Oilseeds are among the major crops that are grown in the country apart from cereals. In terms of acreage, production and economic value, these crops are second after food grains. The soybean is grown as a

commercial crop in more than 40 countries as the major oilseed crops.

In the **United States of America**, soybean is the dominant oil seed, and account of 90 percent of the nation’s oil seed production (USDA Data). That is an agricultural commodity class that also includes canola/rapeseed, sunflower, and flax seeds, as all of these are produced in vegetable oils. The US accounts for 35.31 percent of the world’s soybean production. At 42 percent market share, it’s also the largest exporter of raw soybeans according to Commodity Basis. There are around 34.4 million hectare area occupied for soybeans in the US. Kentucky, Minnesota, Ohio, Pennsylvania, and Wisconsin are the states with the largest soybean plantations

in average size. Meanwhile, Illinois, Iowa, Indiana, Minnesota, and Nebraska were the states producing the largest soybean yield more than 3000 kg/ha. Unlike other soybean producing countries, prices in the US are more significantly determined by increased bio-diesel demand, where the soy oil is used to fuel combustion engines.

Brazil is the second largest producer of soybeans worldwide, accounts for 28.37 percent of the global production of the crop. The country has over 33.80 million hectares of land available and used for farming soybean during 2016, soybean production has been on a steady rise production 102 million tons and yield more than 3000 kg/ hectare. Soybeans grown in Brazil have higher protein levels than those grown in many other parts of the world, and thereby fetch higher prices in international markets, according to Commodity Basis.

Argentina is the third largest producer of Soybean was occupied area 19.45 million hectares and contributed production 57 million tons during 2016. Buenos Aires, Cordoba, and Santa Fe are the states where soybeans are grown in largest quantity according to Commodity Basis. The country accounts for 16.83 percent of the world's soybean production. Though Argentina exports only 7 percent of global raw soybean exports, it's the biggest exporter of soybean oil and meal.

China accounts for 4 percent of soybean production in the world, according to Commodity Basis. Much of the country's Soybeans are grown in the northern Heilongjiang Province, near the Russian border. According to the province's

Agriculture Commission, there are over 7.10 million hectares used as soybean and contributed production 12.50 million tons. Still, China has to import 86 million tons of soybeans to meet the domestic demand 100.80 million tons. China accounts for 60 percent of worldwide soybean imports, making it the largest importer of soybeans, followed by the collective members of the European Union. The prices in the world market for soybean are dictated by China's demand. The other important countries like Paraguay, Canada, Ukraine and Bolivia under the list of top ten, according to the USDA data (see table 2).

Among the top ten countries the United States of America showed the highest productivity 3532 kg/ ha followed by Canada 2856 kg/ha, Brazil 2818 kg/ha and Argentina 2539 kg per ha, however the India was lowest 1110 kg/ha while area share 10 percent and production share 4.50 percent of total World. The main reason of low productivity Non-availability of effective packages for management of biotic and abiotic stresses. Soybean plants have broad leaf and legume, which attracted more pest and diseases in a rainy season. Sometimes crop losses occurred more than 60 percent due to biotic and abiotic stresses. The crop is mainly grown under rain-fed conditions and is depends to the vagaries of monsoon. Sometimes on the stage of maturity, dry spell hits the crop losses. The Seed Replacement Rate (SRR) was very low 12 percent at the present resulted the farmers used 82 present domestic seed, which causes of low productivity.

Table.2: Soybean area, production and yield in major countries during 2016:

Sr. No.	Country	Area in million ha.	Production in million tons	Yield kg/ha
1	Brazil	33.80	1,02.00	3018
2	US	33.60	1,18.68	3532
3	Argentina	19.45	57.00	2931
4	India	11.40	9.70	851
5	China	7.100	12.50	1761
6	Paraguay	3.460	9.17	2650
7	Canada	2.200	6.00	2727
8	Russian Federation	2.150	3.00	1395
9	Ukraine	1.840	4.00	2174
10	Bolivia	1.250	3.12	2500

<https://www.usda.gov/wps/portal/usda/usdahome>

3.3 To analysis the domestic growth, share of soybean area, production and yield

3.3.1 Domestic scenarios of Soybean:

The soybean productivity was very low 438 kg/ha during 1970, it was doubled within 5 year 978 kg/ha during 1975-76 and the highest productivity recorded 1353kg/ha during 2012-13. The annual compound growth rate of productivity of soybean 1.35 percent, while total food grain growth rate

2.26 percent and total oilseeds 2.00 percent during 4.5 decade period 1970 to 2015-15 much lower as compared to other countries of World. In India soybean productivity was very low and needs for adoption of improved technologies, highlighting a combination of high-yielding varieties/ hybrids, balanced and integrated crop nutrition, efficient crop management, protective irrigation, integrated pest management and selective farm mechanization. The post-

harvest technology like processing, marketing and proper storage facilities should be assured.

3.3.2 Domestic share of soybean crop in oilseeds:

During 1951–2014, the area, production and yield of annual oilseeds in India showed AGCR was recorded 1.57%, 3.01% and 1.42% respectively. Major gain in soybean in area as well as production came from third earlier TE 1989 to first position presently and the area increased from 7.92 % to 40.43 %,

production increased 7.95 % to 4.144 % and the second position rape-seed mustard area increased from 21.71% to 23.45% and production 24% to 25 % showed stable during the period TE 1989 to TE 2014. The groundnut position was first in area 36.84% to decrease 19.22 % as well as production decrease from 51 % to 22.86 % earlier during TE 1989 to TE 2014. The castor increased both area and production jumped forth position during TE 1989 to TE 2014 followed by sesame and sunflower.

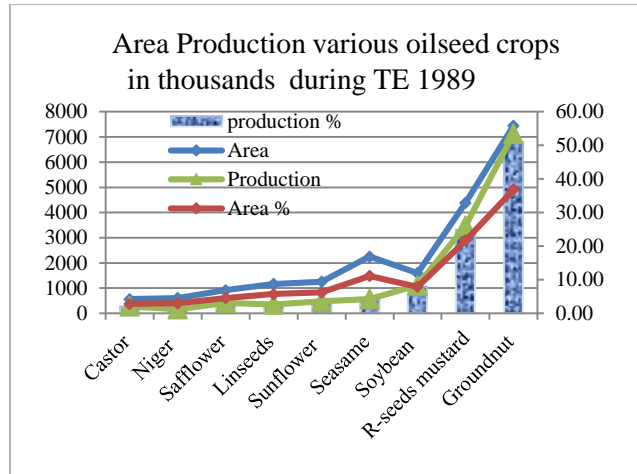


Fig.2: Area Production during TE 1989

It has been seen large regional variation in area, production and productivity changes during the last two and half decades. The changing scenario of oilseeds crops due the demand, supply and profitability of the meticulous crops. Only a few states like Haryana, Madhya Pradesh, Maharashtra, Rajasthan and West Bengal increased their oilseeds production both through area expansion and productivity improvement. A

state like Gujarat increased oilseeds production mainly due to productivity improvement. In a state like Punjab, oilseeds production declined mainly in response to a sharp decline in the area, whereas in Orissa area and productivity declined sharply leading to large declines in oilseeds production (see figs. 2 and 3).

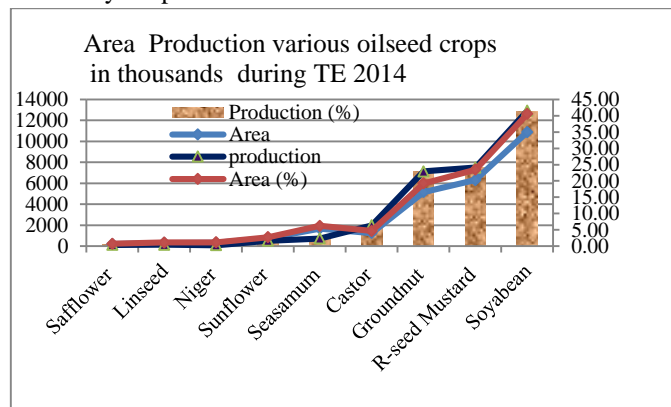


Fig.3: Area Production during TE 2014

Data source: http://eands.dacnet.nic.in/PDF/Agricultural_Statistics_At_Glance-2015.pdf

3.3.3 State wise Area, Production of soybean:

New varieties of soybeans were introduced in India during the 1960s. The crop was promoted initially with the expectation that it would meet the demand for pulses in the country. Soybeans were seen as a miracle crop and were expected to repeat the success story achieved in the United States. In India soybean cultivation has been started early 1970s with the 30

thousand hectares area contributed 14 thousand tons production and average yield 440 kg/ha., which increased to 11861 thousand hectares contributed 14666 thousand million tons and increased productivity 1353 kg/hectare during the period 1970-71 to 2012-13 there are tremendous changes in area, production and yield.

Madhya Pradesh is the major producing state in area 84 per cent and contributed production 83 %, followed by Rajasthan area 5.0 % and production 6.7 % and Maharashtra 4.5 % and production 3.0 % during TE 2089. The current scenario quietly changed during TE 2016 Madhya Pradesh is the major producing state in the area share decreased from 84 to 62 % and contributed production decreased from 83 to 54% second emerging state Maharashtra soybean are increased from 4.5 to 32 % and production 3.0 to 30%, followed by Rajasthan area increased 5.0 to 10 % and production 6.7% and Maharashtra 4.5% and production 3.0 to 9 percent during TE 2016.

3.3.4 Changing scenario of soybean during decades:

The Chhattisgarh reported highest increased in area 23 to 106 thousand hectares which was 359 percent, followed by Karnataka 62 to 256 thousand hectares, which was 312 percent followed and lowest increased in Madhya Pradesh 30 percent in the area. In case of production of soybean in

Uttarakhand 3 to 20 thousand, which was 506 percent, followed Andhra Pradesh 63 to 316 thousand tons, which was 401 percent, followed by Chhattisgarh 20 to 100 thousand tons, which increased about 398 percent and the lowest in Gujarat, while Maharashtra and Rajasthan emerging states for increasing area 121 and 74 production 108 and 87 respectively. The soybean area shifted to Maharashtra and Rajasthan. As per the all India scenario of soybean area was increased from 6744 to 10911 thousand hectares, about 62 percent and production was from 6450 to 12300 thousand tons during decades TE 2004 to TE 2014 (see table 3).

In case of productivity was recorded from 573 to 1548 kg/ ha about 170 percent in Uttarakhand followed by and Madhya Pradesh leading state for soybean was recorded from 859 to 1159 kg/ ha about 35 percent during decades TE 2004 to TE 2014, while the All India productivity of Soybean was recorded from 956 to 1127 kg/ ha about 18 percent increased during the same period decades TE 2004 to TE 2014.

Table.3: States area production during decades:

Sr. No	State	Area		Change %	Production		Change %
		TE 2004	TE 2014		TE 2004	TE 2014	
1	M. P.	4296	5578	30	3691	6465	75
2	Maharashtra	1649	3640	121	1896	3937	108
3	Rajasthan	529	923	74	605	1133	87
4	A. P.	103	243	135	63	316	401
5	Karnataka	62	256	312	90	212	136
6	Chhattisgarh	23	106	359	20	100	398
7	Gujarat	27	57	109	40	45	13
8	U.P.	19	52	179	12	24	106
9	Nagaland	18	25	40	19	31	63
10	Uttarakhand	6	13	125	3	20	506
11	Others	11	18	60	12	17	45
	All India	6744	10911	62	6450	12300	91

Data source: agricoop.nic.in

3.3.5 State wise analysis decadal AGCR of soybean:

The Soybean was recorded the highest ACGR in area 33.97%, production 52.87% in Maharashtra, followed by area 25.41 %, production 29.57%, followed by Karnataka 20.39%, in area, 24.38% in production and the leading Madhya Pradesh recorded area 14.60% and production 21.13% during the period 1986-87 to 1995-96, however All India ACGR was recorded growth rate in area 15.90% and production 22.49% during same period. The growth rate of soybean quietly changed during 1996- 97 to 2005-06, the Nagaland emerging

state recoded the highest ACGR were accelerated in, area 20.17 %, production 25.52 %, followed by Gujarat area 18.94%, production 17.39%, followed by Himachal Pradesh area 4.88%, production 18.60% and the leading Madhya Pradesh recorded decelerated growth rate in area -0.24 and production -1.34 %, however All India was recorded growth rate in area 2.93% and production 2.22% during same period. The AGCR of soybean quietly low recorded during 2006-07 to 2013-14, the Karnataka was recorded 8.19% in area, 16.62% production, followed by Maharashtra 3.80% in area,

7.47% production and Madhya Pradesh recorded 3.92% in area, 3.21% in production, however the All India was recorded growth rate 4.32% in area and 5.35% in production during same period. In case of Soybean yield AGCR was the highest recorded in Maharashtra 14.11, followed by Himachal Pradesh 9.66% and Nagaland 8.68% during the period 1986-87 to 95-96.

The state wise analysis of decadal growth rate of soybean revealed that the high growth rate observed in the area 15.90%, production 22.49% during the period 1986-87 to 1995-96 due to the impact of launching Technology Mission on Oilseeds during 1986-87 after that the next decades soybean AGCR was slow down area 2.93%, production 2.22% during 1996-97 decades and further again slow down during 2006-07 to 2013-14 (see table 4).

Table.4: Analysis decadal state wise growth rate of soybean:

S.No.	States	1986-87 to 1995-96			1996- 97 to 2005-06			2006-07 to 2013-14		
		Area	Production	Yield	Area	Production	Yield	Area	Production	Yield
1	Maharashtra	33.97	52.87	14.11	12.65	11.00	-1.47	3.80	7.47	3.54
2	Rajasthan	25.41	29.57	3.32	2.48	2.74	0.26	7.13	6.19	-0.88
3	Nagaland	17.23	27.41	8.68	20.17	25.52	4.45	-1.05	-0.58	0.47
4	Karnataka	20.39	24.38	3.31	10.18	4.31	-5.33	8.19	16.62	7.79
5	Madhya Pradesh	14.60	21.13	5.70	-0.24	-1.34	-1.11	3.92	3.21	-0.68
6	Himachal Pradesh	5.65	15.86	9.66	4.88	18.60	13.07	0.01	5.40	5.39
7	Gujarat	-0.05	7.26	7.31	18.94	17.39	-1.30	-3.26	6.03	9.61
8	All India	15.90	22.49	5.69	2.93	2.22	-0.68	4.32	5.35	0.98

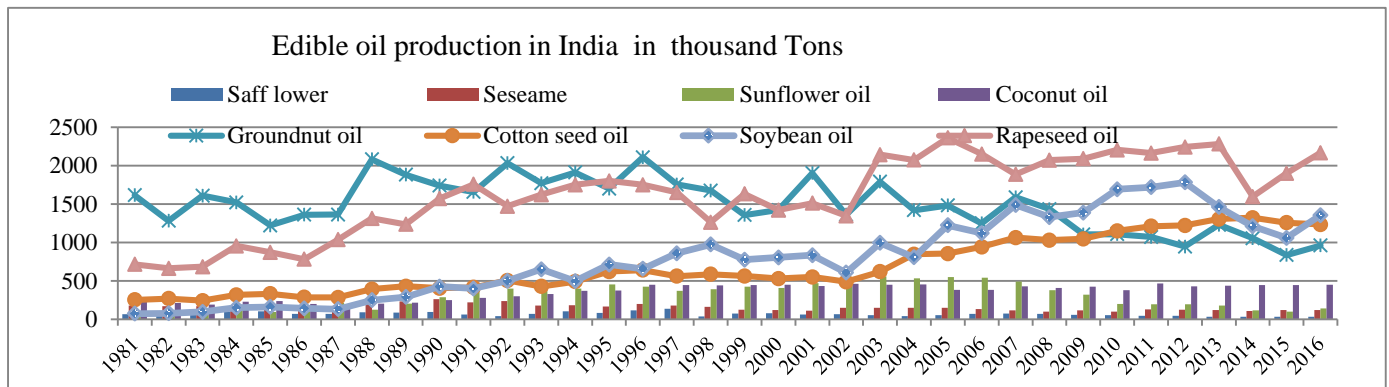
Data Source: agricoop.nic.in

3.4 To analyse demand, supply and trade of soybean oil and other edible oil soybean meal

In the agricultural economy of India, edible industry plays an important role next only to food grains in terms of area, production and value. The diverse agro-ecological conditions in the country are favourable for growing all the nine annual oilseeds, which include major edible oilseeds, viz. Groundnut, Rapeseed–Mustard, Soybean, Cottonseed, Coconut oil, Sunflower, Sesame, Safflower and Niger. Apart from annual

3.4.1 Soybean oil and other oil production in India:

oilseeds plantation crops, including in particular coconut and oil palm are cultivated in the country. In addition, substantial quantity of vegetable oils is also obtained from rice bran and cotton seed. The highest domestic of edible oils were produced by groundnut 1615 followed by rapeseeds 714 thousand tons and cottonseed oil 251 and total edible production 3183 thousand tons in India during 1981.



Source: USDA Dataset

Fig.4: Major edible oil production in India

The groundnut oil leading number one rank produced 2108 thousand tons, followed by rapeseeds oil 1750 thousand tons and Soybean oil and cottonseed oil almost same 657 thousand tons up to 1996. The rapeseeds and groundnut oil both downfalls from 1996 to 2002 due to abnormal weather condition and drought during 2002. The edible oil scenario has been changed and rapeseeds oil production surged from 1345 thousand tons to 2360 thousand tons in 2005 and the groundnut continued downfall 2108 thousand tons during to 1996 to 835 thousand tons up to 2015. The soybean oil continued increasing from 602 thousand tons during 2002 to 1780 thousand tons during 2012. The cotton seed oil 251 thousand tons production was showed highly stable from 1981 to increase 1320 thousand tons during 2014 (see fig 4).

3.4.2 Annual compound growth rate edible oil in India:

The high ACGR and coefficient of variation were recorded in soybean edible oil 15.22% and 68.80%, followed by sunflower oil 11.04 % and 53.93 coconut oil and total edible oil recorded 4.12%, 24.94 respectively during period 1980 - 2000. The highest instability was recorded in soybean edible oil resulted that more fluctuation in production of soybean crops followed by sunflower. During the second period 2001 to 2006, the AGCR 6.16% of cotton seed oil followed by 4.08% in Soybean oil and the negative growth rate also observed highest in sunflower oil -11% followed by safflower - 4.66 percent. The highest CV recorded 52.19 in Sunflower, which the production down falls drastically. The high ACGR were recorded in soybean edible oil 8.61 %, followed by 5.06% of cotton oil and total edible oil 2.25%, however the highest CV recorded 112.14% of sunflower oil 11.04 % and 74.87% in safflower and 37 % in soybean oil during period 1981 – 2016 (see table 4).

Table.4: Annual compound growth rate and Coefficient of variation:

Particular	1981 to 2000		2001 to 2016		1981 to 2016	
	AGCR (%)	CV (%)	AGCR (%)	CV (%)	AGCR (%)	CV (%)
Safflower oil	-0.39	28.45	-4.66	29.09	-2.45	74.87
Sesame oil	-0.61	20.57	-1.36	13.47	-1.67	34.32
Groundnut oil	0.81	16.08	-4.16	23.82	-1.32	33.46
Rapeseed oil	5.03	31.11	1.13	14.51	2.96	24.77
Coconut oil	5.23	33.50	0.17	6.60	2.58	22.67
Cotton seed oil	5.12	30.30	6.16	26.79	5.06	28.03
Sunflower oil	11.04	52.93	-11.40	52.19	1.71	112.14
Soybean oil	15.22	68.80	4.08	27.14	8.61	37.82
Total edible Oil	4.12	24.94	0.41	9.22	2.25	20.64

Source: USDA Dataset

3.4.3 Analysis of demand supply gap of edible oil in India:

The vegetable oil consumption depends both income and price-elasticity. The per capita consumption of vegetable oils has increased from around 3 kg/year in 1950 to 16 kg/year during 2016. Increase in per capita income pushes the demand for oil significantly. A similar effect is exercised by the price factor as well. In contrast to the pre-WTO period, the real price of vegetable oils had sharply declined in the subsequent period, which enabled consumers to access large quantities that were made possible through liberal imports. There have been dramatic changes in the edible oil consumption of the country during the last 35 years. India changed from net importer 23 percent of total consumption status in the 1981 to increase 36.14 during 1987 which was downfall 8.26 percent 1988 and lowest import of edible oil 1.49 percent share of total share of availability, which was again reversed 24.75 percent next five years 1997 and due the drought during 2001 edible import was raised 52.79 percent when the country had to spend huge foreign exchange to meet the domestic needs of

edible oils. However, as per capita consumption of edible oils has risen significantly.

The total demand in the country has risen at a very high rate and has created a big gap between domestic production 6663 thousand tons, total consumption 21709 thousand tons and edible imports increased by 70.86 percent during 2016. Demand of edible oil is mainly driven by an increase in per capita consumption of edible oil, rising income levels and improvement of living standards. However, the Indian edible oil market continues to be represented as current per capita consumption level of India (at 16 Kg/year for 2015-16) is much lower than global averages (25 kg/year). Further, domestic consumption of edible oil is expected to increase with enhancement in income level and population (see Fig. 5). The domestic consumption of edible oils has increased substantially and has touched the level of 18.90 million tonnes in 2011-12 and is likely to increase further 22.89 million tonnes during 2016. The total import edible oil likely to be estimated for 2015 16.2 million tons higher 17%

previous year 2015, however crude edible oil 10 million tons, soybean oil 4.00 million tons, sunflower 1.8 million tons and rape-seed mustard 0.4 million . The vegetable oil import at 6.27 million tons worth Rs 27,990 crore during November 2015 and March 2016. For the full oil year, as mentioned

earlier, import is estimated to be 16 million tons, worth Rs 75,000 crore. Prices are likely to remain firm through this year on reducing supply from the world's top two producers, Indonesia and Malaysia, due to adverse climatic conditions.

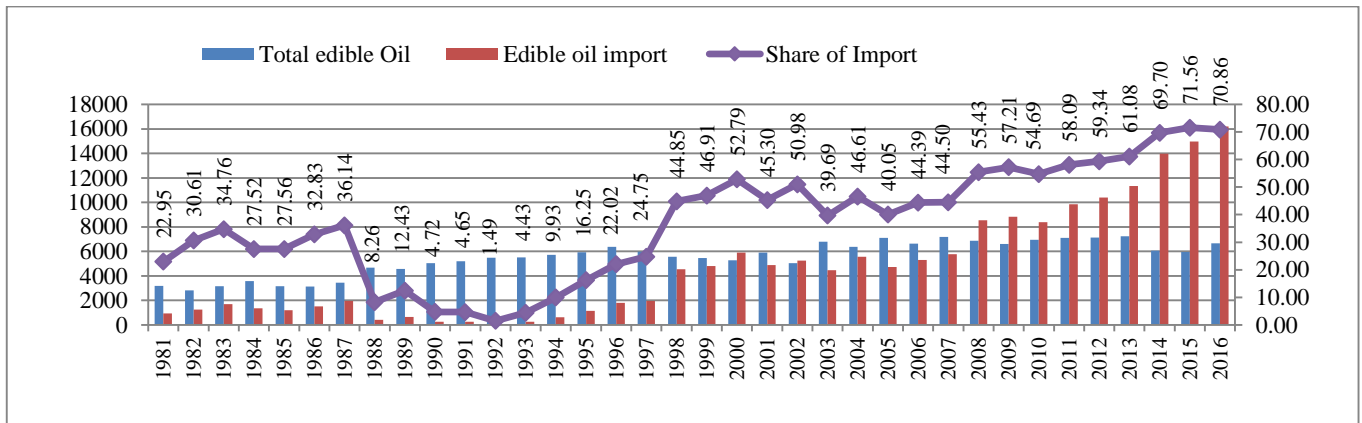


Figure 5. Domestic edible production, Import and its percent share:

Source: USDA Dataset

3.5 Analysis of global production, export, import and consumption of edible oil

3.5.1 Imports of edible oil in India:

The India is the number one edible importer in the world, the total import increased from 5767 to 16200 thousand tonnes during 2007 to 2016 and ACGR were recorded 10.50 percent, however the domestic production edible oil in India creasing -1.73 percent during the same period. The Import continued increasing due to the domestic edible oil production growth rate decreasing pattern. The highest AGCR of import of edible oil were recorded at 57 % in rapeseed mustard oil

followed by sunflower oil 39 % and 20 % of soybean during period 2007 to 2016. The highest share of import of edible oil 62 percent palm oil followed by 25 percent of soybean oil and sunflower 11 percent. In case of the highest import of volume edible oil, the palm oil ranked first increased from 5013 to 10000 thousand tons almost double during the decade 2007 to 2016. The import of Soybean oil increasing very fast from 733 to 4000 thousand tons more 5 times followed by Sunflower 18 to 1800 thousand tonnes just 100 times increased during the same period 2007 to 2016 (see Table 5).

Table.5: Import of edible oil, percent share and ACGR during the decade in India

Market Year	2007	2008	2009	2010	2011	2012	2013	2014	2015	2016	AGCR
Palm oil	5013	6867	6603	6661	7473	8364	7820	9256	8735	10000	6.37
Share (%)	87	80	75	79	76	80	69	66	58	62	--
Soybean oil	733	1060	1598	945	1174	1086	1830	2799	4360	4000	19.85
Share (%)	13	12	18	11	12	10	16	20	29	25	--
Sunflower oil	18	583	611	776	1114	939	1528	1531	1532	1800	39.28
Share (%)	0	7	7	9	11	9	13	11	10	11	--
Rape seeds	0	42	18	5	98	8	160	383	350	400	57.05
Share (%)	0	0	0	0	1	0	1	3	2	2	--
Total Edible oil import	5764	8552	8830	8387	9859	10397	11338	13969	14977	16200	10.50

Source: USDA Dataset

3.5.2 Share of edible oil export and import top 5 Country:

Presently, India number one in edible oil importing country 22 percent, followed by 13 percent in European Union, china 11 and US 5.40 percent of the total import of the World during 2016 as per the USDA data. In case of edible oil

exporting county , the Indinasia is number one 38.83 percent , followed by Malaysia 25.93 per cent , followed by Urgentina 8.42 percent total export of the World during 2016 (see table 6).

Table.6: Top 5 Exporting , Importing country of edible oil in thousand tons:

Exporting countries	Quantity	Share (%)	Importing countries	Quantity	Share (%)
Indonesia	28400	38.83	India	16330	22.21
Malaysia	18965	25.93	European Union	9570	13.02
Urgentiana	6160	8.42	China	8205	11.16
Ukraine	5160	7.05	United States	3973	5.40
Russian Federation	2302	3.15	Pakistan	3580	4.87

3.5.3 Import of Refined and Crude Oil:

In terms of volumes, crude edible oil contributes about 82% and refined oil contributes about 18% of the total import during 2015-16. The share edible oil of the 82% of imported crude edible oil, palm oil, soybean oil and sunflower oil

contributes about 54%, 21% and 11%, respectively. India is importing edible oil from Indonesia, Malaysia, Argentina and Ukraine, contributing about 36%, 23%, 17% and 13%, respectively, of total imports of edible oil (see table 7).

Table.7: Import of Refined and Crude Oil Ratio in 2015-16:

Oil Year (November - October)	Refined Oils	share (%)	Crude Oils	share (%)	Total
2011-12	1,577	16%	8,404	84%	9,981
2012-13	2,223	21%	8,162	79%	10,385
2013-14	1,576	14%	10,042	86%	11,618
2014-15	1,659	12%	12,762	88%	14,421
2015-16	2,623	18%	11,948	82%	14,571

Source: Solvent extractors Association of India

3.5.4 Export of total oil meals and Soymeal's from India:

The total oil meal and soya meal's export downfall due to the severe drought from 3096 and 2573 thousand tons respectively, during 2001 to decrease 1973 and 1510 respectively, during 2002, which dramatically increased 6607 thousand tons of total oil meal and 5285 thousand tons of

soya meal were exported during 2007. The export of total oil meal 452 thousand tons and Soya meal 150 thousand tons during 2015 drastically down fall as compared to 2007. The share of Soya meal ranged 83 to 80 percent during 2001 to 2012 and further drastically from 80 to 33 during 2012 to 2016 as per USDA data (see fig. 6).

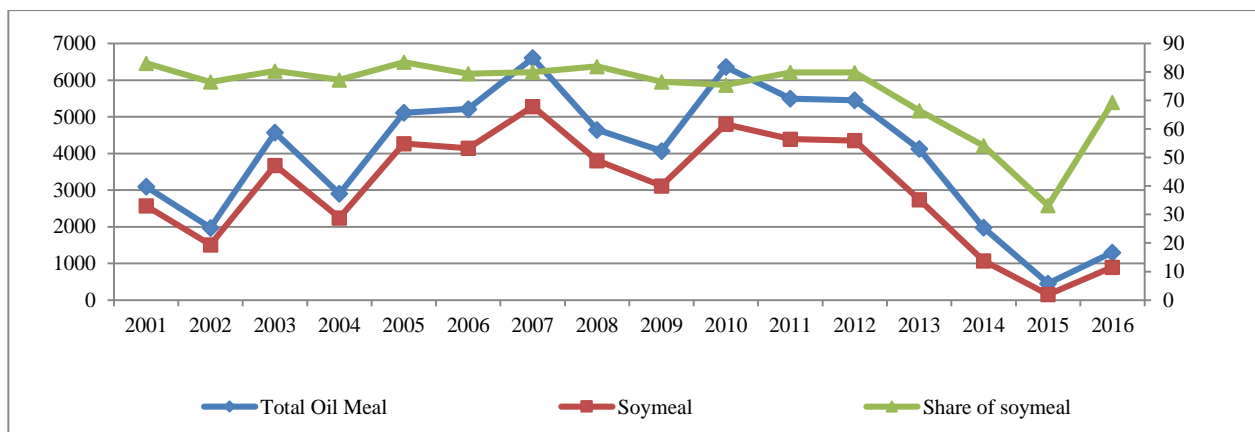


Fig.6: Export of Oil meals and Soymeals

Source: USDA Dataset

3.5.5 The Global production of Edible Oil :

The total global production of edible oils were increased from 161.66 million tons during 2012-13 to 186.95 million tons during 2016-17 with annual compound growth rate 3.27 percent during the same period, however the Indonesia was recorded the top producer ranged from 32.72 to 39.98 million tons during 2012/13 to 2016/17 with the AGCR 4.58 percent followed by China 23.05 to 26.59 percent and AGCR 3.17 percent and the third Malaysia also important country in edible oil production

ranged 21.70 million oil to 22.50 million tons but the AGCR was showed 0.51 percent . The Argentina is emerging edible oil production 7.45 million tons to 9.98 million tons with highest growth 8.30 percent during 2012-13 to 2016-17, however the Total World edible production recorded 161.66 to 186.95 million tons at the AGCR 3.27 percent. The India only country was showed downfall production 7.95 to 6.69 million tons with the highest negative AGCR -5.27 percent during 2012-13 to 2016-17 (see table 8).

Table.8: Global Production of Edible oil in million tons:

Production	2012/13	2013/14	2014/15	2015/16	2016/17	ACGR (%)
Indonesia	32.72	35.02	37.78	36.71	39.98	4.58
China	23.05	24.31	25.04	26.30	26.59	3.71
Malaysia	21.70	22.63	22.29	20.01	22.50	-0.51
European Union	16.15	18.30	18.00	18.42	17.85	2.09
United States	10.23	10.42	10.94	11.20	11.62	3.32
Argentina	7.45	7.84	8.98	9.70	9.98	8.30
Brazil	7.55	7.97	8.57	8.41	8.52	3.00
India	7.95	7.28	7.14	5.98	6.69	-5.27
Other	42.83	45.36	45.59	46.48	49.91	3.36
Total World	161.66	171.85	177.18	177.24	186.95	3.27

Source: USDA Datas

3.5.6 Global Imports of Edible oil in million tons:

The total global imports of edible oils were increased from 65.49 million tons during 2012-13 to 74.67 million tons during 2016-17 with annual compound growth rate 3.22 percent during the same period, however the India was recorded the top importer ranged from 1.72 to 11.73 million tons during 2012-13 to 2016-17 with the AGCR 11.53 percent, followed by Bangladesh 1.44 to 2.07 percent and AGCR 10.21 ranged million oil to 3.38

million tons with AGCR was showed 8.19 percent. The China was reducing the edible oil import 10.84 million tons to 8.18 million tons with highest decelerated growth rate -0.91 percent during 2012-13 to 2016/17, while China was the top importer during 2012/13. The total World edible import recorded 65.49 to 74.67 million tons at the percent, followed by Pakistan 2.30 edible oil import AGCR 3.22 percent during 2012-13 to 2016/17 (see table 9).

Table.9: Global Imports of Edible oil in million tons

Imports	2012/13	2013/14	2014/15	2015/16	2016/17	ACGR (%)
India	10.72	11.5	14.14	15.11	16.14	11.53
European Union	9.95	9.98	9.88	9.91	9.89	-0.19
China	10.84	9.1	8.63	7.81	8.18	-6.91
United States	3.80	4.02	4.23	4.54	4.59	5.12
Pakistan	2.30	2.84	2.98	2.89	3.38	8.19
Egypt	1.92	2.08	2.25	2.24	2.25	3.99
Bangladesh	1.44	1.68	1.79	2.15	2.07	10.21
Turkey	1.35	1.46	1.53	1.41	1.63	3.48
Other	20.23	22.12	22.81	22.58	23.91	3.61
Total	65.49	67.24	71.05	71.02	74.67	3.22

Source: USDA Dataset

3.5.7 Global Export of Edible oil in million tons:

The total global export of edible oils were increased from 68.45 million tons during 2012-13 to 78.46

million tons during 2016/17 with annual compound growth rate 3.25 percent during the same period , however the Indonesia was recorded the top exporter

ranged from 22.64 to 28.10 million tons during 2012/13 to 2016/17 with the AGCR 5.02 percent, followed by Malaysia 19.99 to 18.97 million but the AGCR -1.54 percent followed Argentina 4.69 to 6.31 edible oil with AGCR was showed 9.81 percent during the same period . The Russia federation was

increasing the edible oil export 1.35 million tons to 2.23 million tons with highest accelerated growth 13.24 percent followed by Ukraine 3.32 million tons to 5.27 million tons and AGCR 10.76 percent during 2012-13 to 2016/17 (see table 10).

Table.10. Global Export of Edible oil in million tons:

Exports	2012/13	2013/14	2014/15	2015/16	2016/17	ACGR (%)
Indonesia	22.64	23.94	28.51	25.35	28.10	5.02
Malaysia	19.99	18.75	18.84	17.83	18.97	-1.54
Argentina	4.69	4.55	5.73	6.41	6.31	9.81
Ukraine	3.32	4.36	4.12	4.81	5.27	10.76
Canada	2.63	2.45	2.54	2.92	3.31	6.56
Russia Federation	1.35	2.46	2.23	2.23	2.64	13.24
European Union	2.43	2.31	2.48	2.48	2.35	0.04
Other	11.41	11.43	12.11	11.57	11.51	0.30
Total	68.45	70.24	76.56	73.6	78.46	3.25

Source: USDA Dataset

3.5.8 Global Consumption of Edible oil:

The total global consumption of edible oils were increased from 159.24 million tons during 2012-13 to 184.95 million tons during 2016/17 with annual compound growth rate 3.73 percent during the same period, however the China was recorded the top consumer ranged from 31.66 to 35.66 million tons during 2012/13 to 2016/17 with the AGCR 2.97 percent followed by European Union 24.56 to 25.90 million tons as per AGCR 1.36 percent and the third India also important country in edible oil consumption ranged 17.79 to 24.94 million tons to 22.50 million tons with

the highest AGCR was showed 6.51 percent and the same trend followed by Pakistan, which edible oil consumption growth rate 7.86. The Argentina is emerging edible oil consumption, which recoded 7.45 million tons to 9.98 million tons with highest growth 8.30 percent during 2012-13 to 2016/17, however the total World edible consumption recorded 161.66 to 186.95 million tons at the AGCR 3.27 percent. The India only country was showed downfall consumption 7.95 to 6.69 million tons with the highest negative AGCR -5.27 percent during 2012-13 to 2016/17 (see table 11).

Table 11. Global Consumption of Edible oil in million tons

Domestic Consumption	2012/13	2013/14	2014/15	2015/16	2016/17	ACGR(%)
China	31.66	32.77	33.61	34.62	35.66	2.97
European Union	24.56	25.17	25.75	25.90	25.90	1.36
India	17.79	18.66	20.05	21.08	22.94	6.51
United States	13.06	13.49	13.68	14.54	14.99	3.57
Indonesia	10.08	11.05	9.9	11.98	12.06	4.49
Brazil	6.74	6.97	7.43	7.39	7.54	2.87
Malaysia	4.03	4.4	4.59	4.72	4.9	4.72
Pakistan	3.37	3.72	4.11	4.2	4.63	7.86
Argentina	2.93	3.42	3.21	3.5	3.72	5.13
Russia	3.07	3.16	3.24	3.37	3.51	3.38
Other	30.89	32.5	33.94	34.45	35.96	3.69
Total	159.24	166.82	171.66	178.34	184.95	3.73

Source: USDA Dataset

3.6 Strategy for improving productivity Soybean in India

- In most other parts of the world, GM varieties of soybeans are replacing non-GM varieties and providing cost advantages, at least in the immediate term. India has not yet allowed the cultivation of GM varieties of soybeans.
- India should adopt GM varieties of soybean as other country of the world adopting new technologies, otherwise it will lose the domestic as well as the export market to other major soybean producing countries such as Brazil, Argentina and the United States.
- It seems that the niche India enjoys in the export of non-GM soya products to the European Union is small compared with the loss of the domestic and international markets to soya products from GM varieties being grown in other countries. The domestic market demand for edible oil is increasing at a very high rate.
- To provide an effective package and practices for management of biotic and abiotic stresses. Soybean plant broad leaf and legume, which attracted more pest and diseases in a rainy season. Sometimes crop losses occurred more than 60 percent due to biotic and abiotic stresses.
- The crop is mainly grown under rain-fed conditions and is depends to the vagaries of monsoon. Sometimes on the stage of maturity, dry spell hits the crop losses. To increase the Seed Replacement Rate (SRR) was very low 12 percent at the present resulted the farmers used 82 percent domestic seed, which causes of low productivity.
- Limited scope for mechanization and inadequacies in implements used for soybean cultivation, especially for marginal and small farmers.
- Lack of promotion for the utilization of soybean domestically for food and feeds uses in India. Soybean meal mostly for export purposes, which depend on the Exim policies of governments. Soybean meal should be used for as a value added product which create, the more utility to costumers.
- Improvement of marketing and infrastructural facilities soybean in non-conventional area as compared to potential soybean growing regions. The farmers fully depend of processing industry and exporter to sell their produce. The soybean grower's unorganized sector, which selling their produce to organized sector governed by SOPA.
- Lack of forecasting system for aspects like weather, disease and pest outbreaks and market prices. These problems may be a technological transformation in economical, educational as well as infrastructural ones.

IV. CONCLUSION

India is the fifth largest producer of soybean (*Glycine max*) in the world after US 118.68 MT Brazil 102 MT, followed by Argentina 57 MT, China 12.5 MT and India 12.30 MT during 2015-16 as per (USDA Data). Soybean play important role in the oilseed sector occupies an important position in the agricultural economy of the country. The Soybean *Glycine max* (L.) the 'miracle bean', which has a dual character as oilseed and pulse but basically legume and comes under oilseed crop. The western world provided a massive push to its growth during the 1960. The Soybean was recorded highest annual compound growth rate were accelerated 45.49 % in production followed 37.38 % in area and 5.89 percent in yield during the period 1970s with highest coefficient of variation 107 % in production and 96 % in area, this showed area and production highly fluctuated during same period during the next 1980s decade the Soybean was recorded were accelerated growth rate 17.22 %, in area and 17.95 % in production, however the yield very low 0.62 , this means the production growth has been due to area the same pattern and no impact of Technology, while earlier decade yield growth recorded 5.89 %.

The soybean productivity was very low 438 kg/ha during 1970, it was doubled during 5 year 978 kg/ha during 1975-76 and the highest productivity recorded 1353 kg/ha during 2012-13. The annual compound growth rate of productivity of soybean 1.35 percent, while total food grain growth rate 2.26 percent and total oilseeds 2.00 percent during 4.5 decade period 1970 to 2015-15 much lower as compared to other countries of the World.

In India, Madhya Pradesh is the major producing state in area 84 per cent and contributed production 83%, followed by Rajasthan area 5.0% and production 6.7% and Maharashtra 4.5% and production 3.0% during TE 2089. The current scenario of soybean absolutely changed during TE 2016 Madhya Pradesh is the major producing state in the area share decreased from 84 to 62% and contributed production decreased from 83 to 54 percent second emerging state Maharashtra soybean area increased from 4.5 to 32 % and production 3.0 to 30% followed by Rajasthan area increased 5.0 to 10% and production 6.7% and Maharashtra 4.5% and production 3.0 to 9 percent during TE 2016. The Soybean was recorded the highest ACGR accelerated in the area 33.97%, production 52.87% in Maharashtra followed by area 25.41%, production 29.57%, followed by Karnataka area 20.39%, production 24.38% and the leading Madhya Pradesh recorded area 14.60% and production 21.13% during the period 1986-87 to 1995-96, however All India was recorded growth rate in area 15.90% and production 22.49% during same period.

The edible oil scenario has been changed and rapeseeds oil production surged from 1345 thousand tons to 2360 thousand tons in 2005 and the groundnut continued downfall 2108 thousand tons during to 1996 to 835 thousand tons up to 2015. The soybean oil continued

increasing from 602 thousand tons during 2002 to 1780 thousand tons during 2012. The cotton seeds oil 251 thousand tons production was showed highly stable from 1981 to increased 1320 thousand tons during 2014.

The vegetable oil consumption is depend both income and price-elasticity. The per capita consumption of vegetable oils has increased from around 3 kg/year in 1950 to 16 kg/year during 2016. There have been dramatic changes in the edible oil consumption of the country during the last 35 years. India changed from net importer 23 percent of total consumption status in the 1981 to increase 36.14 during 1987 which was downfall 8.26 percent 1988 and lowest import of edible oil 1.49 percent share of total share of availability.

The total demand in the country has risen at a very high rate and has created a big gap between domestic production 6663 thousand tons, total consumption 21709 thousand tons and edible imports increased by 70.86 percent during 2016. Demand of edible oil is mainly driven by an increase in per capita consumption of edible oil, rising income levels and improvement of living standards. The Import continued increasing due to the domestic edible oil production growth rate decreasing pattern. The highest AGCR of import of edible oil were recorded in 57 % in rapeseed mustard oil followed by sunflower oil 39 % and 20 % in soybean and the total edible oil 10.50 % during period 2007 to 2016.

The Indonesia was recorded the top producer ranged from 32.72 to 39.98 million tons during 2012/13 to 2016/17 with the AGCR 4.58 percent followed by China 23.05 to 26.59 percent and AGCR 3.17 percent and the third Malaysia also important country in edible oi production ranged 21.70 million oil to 22.50 million tons but the AGCR was showed 0.51 percent. The Argentina is emerging edible oil production, which recoded 7.45 million tons to 9.98 million tons with highest growth 8.30 percent during 2012-13 to 2016/17.

The total global export of edible oils were increased from 68.45 million tons during 2012-13 to 78.46 million tons during 2016/17 with annual compound growth rate 3.25 percent during the same period , however the Indonesia was recorded the top exporter ranged from 22.64 to 28.10 million tons during 2012/13 to 2016/17 with the AGCR 5.02 percent followed by Malaysia 19.99 to 18.97 million but the AGCR -1.54 percent followed Argentina 4.69 to 6.31 edible oil with AGCR was showed 9.81 percent during the same period . The Russia federation was increasing the edible oil export 1.35 million tons to 2.23 million tons with highest accelerated growth 13.24 percent followed by Ukraine 3.32 million tons to 5.27 million tons and AGCR 10.76 percent during 2012-13 to 2016/17.

A critical review of the relative prices and incomes from oilseed crops compared with those of their major competing crops has revealed some interesting features. It can be said that the oilseed crops were relatively non-remunerative compared to their competing crops like rice, wheat and

sugar cane due the low productivity. A comprehensive policy to promote oilseed crops should also contain components aimed at making the relative profitability from oilseed cultivation more attractive. The marketing support provided for oilseed crops is inadequate and is available only for the selected oilseed crops in a limited area. A systematic approach for providing adequate market support for oilseed producers will go a long way in ensuring higher production of oilseed crops. A weak and inefficient marketing system coupled with unfavourable and unstable import policy has adversely affected the oilseed producers and processors alike.

The government reduced the import duty all the edible oil like crude palm oil 70 to 7.5% , refined palm oil 80 to 15 % , Soybean oil 40 to 20% and sunflower oil 75 to 20 per during period 2007 to 2014 to control domestic prices edible oil in India . The Import continued increasing due to the domestic edible oil production growth rate decreasing pattern. The highest AGCR of import of edible oil were recorded in 57 % in rapeseed mustard oil followed by sunflower oil 39 % and 20 % in soybean and the total edible oil 10.50 % during period 2007 to 2016.

The sequential and persistent policy of reduction in import tariffs for both crude and refined edible oils has led to a surge in imports of relatively cheaper edible oils like palm oil. The sudden shift from a protected oilseed economy and the exposure to a highly competitive international edible oil market have hurt the interests of domestic oilseed growers rather than motivating them towards adoption of more efficient production and competitive strategies. The producers in the major edible oil exporting countries work under an inherently different set of economic conditions and social endowments which are alien to our domestic oilseed cultivators to be implemented to enhance productivity of oilseeds.

In policy improvement its current (12th) Five-Year Plan (Indian fiscal year 2012/13 to 2016/17), the National Mission on Oilseeds and Oil Palm (NMOOP) is targeting vegetable oil production to reach 9.51 MMT, a 35 percent increase over the previous Five-Year Plan's average (7.06 MT). This was initiated in response to India's growing reliance on imported palm oil from South East Asia. NMOOP claims that India can achieve greater levels of independence in vegetable oils if it can boost production in various oilseeds, oil palm, and tree borne oilseeds (TBOs).

REFERENCES

- [1] Hegde, D. M., Can India achieve self-reliance in vegetable oils? In National Symposium on Vegetable Oils Scenario: Approaches to Meet the Growing Demands, 29-31 January 2009, pp.1-15.
- [2] Narasinga Rao, B. S., Nutrient requirement and safe dietary intake for Indians. *NFI Bull.*, 2010, 31, 1-8.
- [3] Various issues of Agricultural Statistics at a glance 2013, 2014 and 15 for secondary data , Published by

- Ministry of Agriculture and farmers welfare , Krishi Bhavan, New Delhi -110001 .<http://www.agricoop.nic.in>
- [4] http://www.fao.org/fileadmin/templates/est/COMM_MARKETS_MONITORING/Oilcrops/Documents/Food_outlook_oilseeds/Food_Outlook_June_2016_oilseeds.pdf
- [5] http://www.iari.res.in/files/Edible_Oilseeds_Supply_and_Demand_Scenario_in_India.pdf
- [6] Hegde, D. M., 2012. Carrying capacity of Indian agriculture: oilseeds, CURRENT SCIENCE, VOL. 102, NO. 6, 25 MARCH 2012, Page No. 867 – 873.
- [7] R.R. Burman¹, S.K. Dubey, Girish K. Jha, Gajab Singh and M.K. Sharma, 2012. Analysis of Production Gap, Marketing and Processing Status and Associated Constraints for Major Oilseeds in the States of Rajasthan and Gujarat *Journal of Community Mobilization and Sustainable Development* Vol. 7(2), page 198-209, July-December, 2012.
- [8] Ramesh Chand 2007, Agro-industries characterization and appraisal: Soybeans in India.
- [9] <http://www.fao.org/docrep/016/ap300e/ap300e.pdf>
- [10] Mruthyunjaya, Kumar, S.; M.T. Rajashekherappa; L.M. Pandey; S.V. Ramanarao and P. Narayan. 2005. Efficiency in Indian edible oilseed sector: Analysis and implications; *Agricultural Economics Research Review*, 18: 153-166.
- [11] Kumar, A.; S.S. Rathore; O.P. Premi and L. Thomas. 2008. Crop management research strategies for oilseeds crops in India. In: Hedge, D.M. (Ed.) *Vegetable Oils Scenario: Approaches to Meet the Growing Demands*, Indian Society of Oilseeds Research Hyderabad.
- [12] Report on Oilseeds : World Markets and trade <https://apps.fas.usda.gov/psdonline/circulars/oilseeds.pdf>

A Study on Various Security Aspects in Cloud Policy Oriented Architecture

Sonia¹, Kirti Bhatia²

¹Department of CSE, M.Tech. (student) Sat Kabir Institute of Technology and Management, Bahadurgarh, India

²HOD, Department of CSE, Sat Kabir Institute of Technology and Management, Bahadurgarh, India

Abstract— Security is the major requirement for data environment. A cloud system provides the data repository and services in public domain so that it suffers from various security specific threats. The presented work is here defined to analyze the policy driven architecture for cloud system as well as identify the associated criticalities. The work also cover the process stage of this security driven architecture so that the interconnection model can be explored. The system is also defined the secure system integration under the service aspect specification. The work is defined as an improvement to the security system architecture under policy driven specifications.

Keywords— Policy Driven, Secure, Architecture, Cloud System, File System.

I. INTRODUCTION

A cloud environment actually provides the integration to the virtual aspects in the cloud system with specification of data distribution, service distribution and platform distribution. These shared systems improve the system capabilities so that the better utilization of available system resources will be done. These kind of systems are available in public domain with private constraints. The constraints are defined in terms of various rules defined to provide system level access and service level integration so that the system improvement and the aspect analysis can be obtained. The shared system is here defined under the environmental constraints. The resource distribution and service specifications are provided at different levels of distribution so that the robust and improved integrity system will be obtained. Here figure1 is showing the interconnection model for cloud system. The model is showing the physical characteristics driven architecture. The cloud system is here defined as the global cloud environment. The interconnection system is here defined with specification of interconnection devices. These devices include the switch inclusion and routers. The switches where provided the low level platform switching if the client is not capable to handle the cloud system content. The platform level independence is provided the switches. The routers are defined to integrate the global environment with client system. This global environment

is defined to provide the distribution localized information storage among available multiple clouds. The selection of this storage cloud depends on multiple parameters such as client localization, load, scheduling mechanism etc.

As the cloud system is configured, it is defined by multiple number of cloud servers integrated in a global environment. Each of the server is defined with relative constraints such as accessibility, security restriction, resource availability vector, connectivity domain, restricted access constraints etc. These cloud servers are the physical entities defined with the memory, processing system and the device integration.

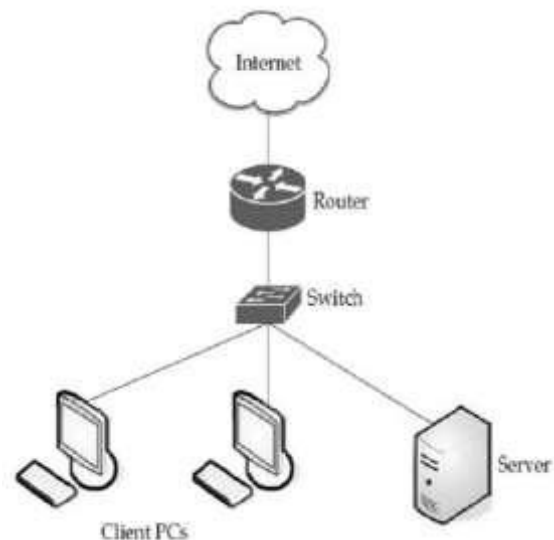


Fig.1: Cloud Service Interaction System

The physical parameters of the cloud system are not available to the client environment but some of the intermediate layer can access these characteristics to device the cloud server performance and reliability vector.

The cloud system is further divided in multiple virtual machines so that the maximum utilization of cloud server capabilities will be done. The virtual machines are divided to achieve the work load over the cloud system. This work load distribution is achieved in terms of number of requests processed by the system, service load, security requirements, location of server etc. The

processing architecture of cloud system is shown in figure 2.

The figure is showing the data driven, storage driven secure system architecture. The main model is divided in two sub blocks. The first block is here defined to achieve the storage level and data level security and the second block is defined to process the user level data access and security.

A) Layer I

The first layer of this model is described as the high security or data model that defines the physical constraints related to the system. These constraints includes the cluster generation at the server end and the data formation based under the specification of location driven clustering, data driven clustering and user specific clustering. This clustering process is performed on the inner most layer of the cloud system. Once the storage system is configured, the next work is to provide the interaction between this data system and the cloud servers. The data blocker is defined between the data architectural view and the cloud servers to provide the effective system allocation. This allocation process is here defined under the constraints and the configuration management. The cloud server performance, requirement and the security constraints are here identified by the broker to allocate the clusters to the cloud server. A cloud server can allocate one or more clusters based on the specification and the relative constraints.

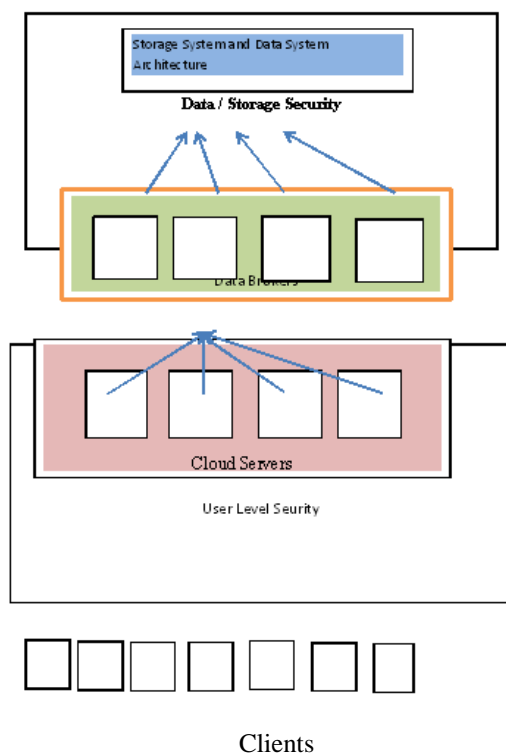


Fig.2: Data Access Architecture

B) Layer II

This layer is defined as the second stage model applied between the cloud server system and the client integration. This integration process is defined with specification of multiple clients. Each client is defined in two main categories called public user or the licensed users. The public users are the free users and of low priority whereas the licensed users are the application specific or service specific users. Once the multiple requests are applied on server with specification of requirement constraints. The intermediate model accept these request and perform the request analysis. The analysis is performed on the request parameters and security requirements. Based on this analysis, the allocation to the particular cloud server is done.

In this paper, a security driven policy architecture is defined in which the data and the services are available to the cloud system. The paper has explored the cloud system data model and the process integration under policy driven architecture. In this section, the cloud system architecture is presented as the global view as well as detailed data view. The section has divided the data modeling on cloud system in two main stages. In first stage, the physical characteristic the storage space allocation to cloud servers is described and in second layer, the client driven mapping is done. In section II, some of the work defined by earlier researchers is described. In section III, the policy driven model along with characteristics exploration is described. In section IV, the conclusion obtained from the work is presented.

II. EXISTING WORK

Lot of work is already presented by different cloud servers to explore the cloud system architecture under different constraints. These architecture and relative improvements are suggested by many researchers. In this section, some of the contribution of earlier researchers is discussed. Ching-Nung Yang[1] has presented a data driven architecture in hadoop environment. The defined system is able to improve the service driven architecture in hadoop system along with the storage policy specification. Author also presented the key based secure system to explore the system resources and the authentication to the system. The system modeling is here done to achieve the symmetric, bivariate information processing in distributed environment. Author explored the service policies and defined a service driven mechanism to improve the cloud service distribution in public environment with private constraints integration. J. McDermott [2] presented an application effective cloud environment for military application. Author defined a work on infrastructure driven analysis so that the processing in virtual environment will be done. Author defined the secure system layer specification for authentication to the system. Author presented a kernel

driven mechanism to perform the systematic security checks for users in cloud system environment. Jonathan A.P. Marpaung [3] presented a work in hadoop environment to define a security architecture for cloud system. Author defined a cloud system based analytical study on the secure environment and its future mapping with key driven constraint. Auhtor defined the work on the service integration under security constraints so that the scaled system development will be obtained.

Piotr K. Tysowski [4] presented a work on scalable Hadoop environment with specification of application level constraints. Author defined a Hadoop environment so that policy driven constraints are described. Author defined the specification of key management scheme so that the secure application constraints are described. Author defined a coordination over the server and the system users so that the information tracking will done in secure way. Chang-Ji WANG [5] defined a work on encryption driven processing for cipher text generation and processing under cryptographic algorithmic approach. Author defined a grained data processing with shared decentralized system to achieve the access control so that the policy driven architecture will be formed. Author provided the size specification and data sharing capabilities in secure system so that the storage and structural aspects of cloud system are described and improved. Author defined the hadoop based storage system with integrated key exchange mechanism using Diffie Hellman Approach. Dexian Chang [6] provided a work on relationship analysis in virtual cloud environment with specification of user domain. Author defined a trust mechanism with migration constraints so that the reliable system composition will be obtained. Author defined the inter domain communication in virtual environment so that the server level integration for the cloud system will be improved.

M.Venkatesh [7] has provided a secure data storage system under public auditability so that the system integration and feature extraction with data support system will be obtained. Author defined the secure remote communication with specification of data utilization aspects. Author defined a RSA inclusive security system to achieve the public information auditing so that the security over the system will be improved. Author defined the time domain specific constraints so that the improved system integration will be achieved. Author provided the work under secure system constraints so that the derivation to the work will be done under multiple information constraints and provides the system improved under critical information aspects. Sahil Madaan[8] has provided a secure system for hadoop system environment. Author improved the root oriented security in cloud system in distributed policy driven environment. Author analyze the cloud system under identity analysis so that

the secure system behavior will be achieved. Author integrated the third party in the system for improving the system robustness and security. Tamal Kanti Chakraborty [9] has provided the cloud system integration and security under resolvment of various associated issues. Author provided a long term solution for cryptographic and authenticated problems. Author provided the secure way for information collection and problem rectification so that the domain specific communication over the system will be performed.

Vasyl Ustimenko [10] provided a work on cloud system aspect formation and homomorphic encryption process applied with muti variate key specification. Author improved the system by integrating the quantum cryptography. Christian Schridde[11]presented an infrastructure driven process model for secure cloud system composition under data integration and data modeling with constraint specification. The trust vector is here performed to improve the system integration in security domain. Yingjie Xia[12] has provided a work on ECC based secure system to improve the communication constraints under protocol specification. Author defined the policy driven communication with security specification.

III. SECURITY INCLUSIVE POLICY DRIVEN CLOUD MODEL

In this section, the cloud security distribution environment is defined to provide the effective service distribution. In this section, the policy model aspects and the functioning are described in detail. The section includes the effective constraint specification with rule specification under associated constraints. As a policy driven architecture is defined, the model includes the integrated with some integrated security constraints. These policy specification are defined in figure 3. The figure shows that the complete model is divided in four main phases to setup different process constraints.

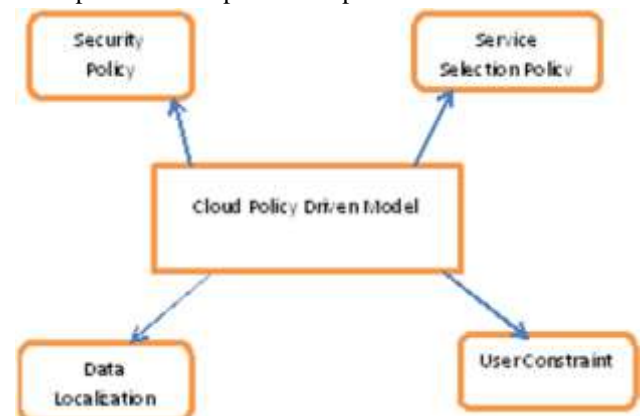


Fig.3: Policies Under Scheduling Consideration

A) Security Policy

The security is the foremost constraint and requirement for cloud system model. This policy model is defined at different level to identify the type of security required in the system. These all security constraints or types include data driven security, user level security, communication level security. The security constraints are applied between two stages of the cloud system model. It can be applied between the hardware and the cloud server to achieve the data driven security at low level. In second security model, the security integration is defined as the middle layer between the clients and the cloud server. In this layer, the cloud system authentication, communication level security and data driven security can be applied. This security policy is defined to achieve the secure communication. The policy is able to provide the separation of available services based on the secure component availability and requirements.

B) Service Selection Policy

This policy rule basically defines as the middle layer architecture provides the effective service selection. This service selection is based on multiple parameters. These parameters include the availability of cloud service, reliability vector, response time etc. The service driven policy analysis is here performed to provide the analysis between the requirements and availability. This parameter specifications here defined under multiple constraints and parameters. These all associated constraints are shown in figure 4.

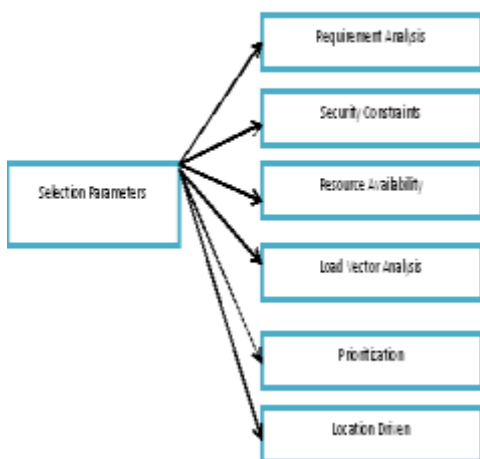


Fig.4 : Service Selection Policy

C) Data Localization Policy

The localization policy actually defines the availability of the requested information on the particular cloud server as well as the way of availing the information on service request. The localization policy defines the process applied on specialized server under the integration of data

base server and services. The localization is here defined three main parameters called transparency vector, scalability and access robustness. The process driven mechanism is here defined to achieve the data modeling so that the attribute specification analysis on the request is done. Based on the request feature analysis, the physical location of the data or request elements can be obtained. The utilization server specification along with domain specification is done under the location boundation and the user specification. The user constraints are defined as the selection process under the security and the requirement constraints. The location driven parameter are shown in figure 5.

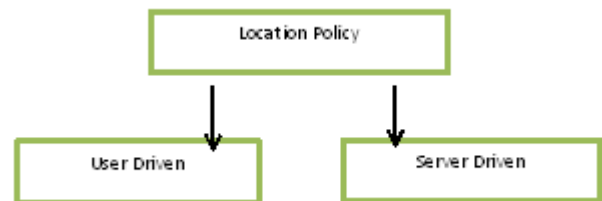


Fig.5: Location Driven Policy

The requirement constraints are here defined under adaptive feature constraints and load vectors. These vectors include the adaptive information assignment to various cloud system with specification of requirement and availability constraints.

D) User Policy The user is the actual element in the process policy model that actually perform the information request on cloud server. The request performed by a user is processed by middle layer architecture and processed on cloud server to extract the information. This stage includes the server driven processing, constraints satisfaction, security constraint specification. The process processing modeling is here defined to identify the service driven architecture. The user specification and constraints consider in this model are shown in figure 6

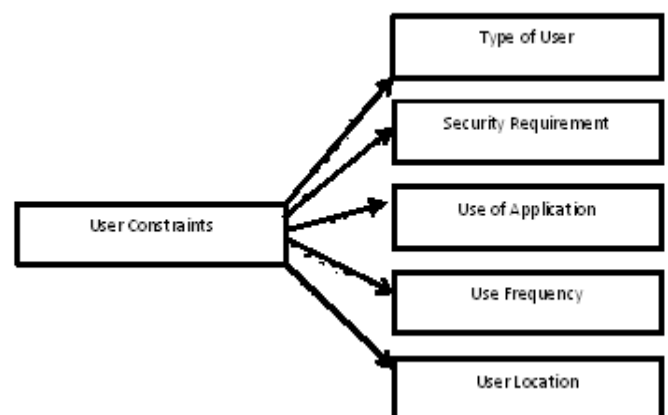


Fig.6: User Constraints

Once these all constraints are processed, the intermediate layer identify the appropriate cloud system that can fulfill the request of user.

IV. CONCLUSION

In this paper, the complete cloud system model is described under the security and policy driven mechanism. This model is here defined with four main stages and policies. These policies include user level policy, data localization policy, security policy and service selection policy. Based on these all constraints and stages the user request can be processed on cloud system and the service availability in secure way can be obtained.

REFERENCES

- [1] Vikki Tang, "A Framework for Reducing Instruction Scheduling Overhead in Dynamic Compilers".
- [2] Lichen Weng, "Scheduling Optimization in Multicore Multithreaded MicroDistributed Clouds through Dynamic Modeling", CF'13, May 14–16, 2013, Ischia, Italy. ACM 978-1-4503-2053-5
- [3] Hsiang-Yun Cheng, "An Analytical Model to Exploit Memory Task Scheduling", INTERACT-14, March 13, 2010, Pittsburgh, PA, USA ACM 978-1-60558-921-3/10/03
- [4] Vishakha Gupta, "Kinship: Efficient Resource Management for Performance and Functionally Asymmetric Platforms", CF'13, May 14–16, 2013, Ischia, Italy. ACM 978-1-4503-2053-5
- [5] Morris A. Jette, "Performance Characteristics of Gang Scheduling in Multiprogrammed Environments", 1997 ACM 0-89791-985-8/97/0011
- [6] Minyoung Kim, "Design Space Exploration of Real-time Multi-media MPSoCs with Heterogeneous Scheduling Policies", CODES+ISSS'06, October 22–25, 2006, Seoul, Korea. ACM 1-59593-370-0/06/0010
- [7] Jonathan A. Winter, "Scalable Thread Scheduling and Global Power Management for Heterogeneous Many-Core Architectures", PACT'10, September 11–15, 2010, Vienna, Austria. ACM 978-1-4503-0178-7/10/09
- [8] Rony Ghattas, "Energy Management for Commodity Short-Bit-Width Microcontrollers", CASES'05, September 24–27, 2005, San Francisco, California, USA. ACM 1-59593-149-X/05/0009
- [9] Andrei Terechko, "Cluster Assignment of Global Values for Clustered VLIW Distributed Clouds", CASES'03, Oct. 30 – Nov. 1, 2003, San Jose, California, USA. ACM 1-58113-676-5/03/0010
- [10] Andrew Riffel, "Mio: Fast Multipass Partitioning via Priority-Based Instruction Scheduling".
- [11] Hiroshi Sasaki, "Energy-Efficient Dynamic Instruction Scheduling Logic through Instruction Grouping", ISLPED'06, October 4–6, 2006, Tegernsee, Germany. ACM 1-59593-462-6/06/0010
- [12] Flavius Gruian, "Hard Real-Time Scheduling for Low-Energy Using Stochastic Data and DVS Distributed Clouds", ISLPED'01, August 6-7, 2001, Huntington Beach, California, USA. ACM 1-58113-371-5/01/0008
- [13] Martin Schoeberl, "Architecture for Object-Oriented Programming Languages", JTRES '07 September 26-28, 2007 Vienna, Austria ACM 978-59593-813-8/07/09
- [14] Jared Stark, "On Pipelining Dynamic Instruction Scheduling Logic", 0-7695-0924-X/2000© 2000 IEEE.

Secure and Efficient Data Transmission for Cluster Based Wireless Sensor Network Using Cryptography

Sangamsh J. kalyane, Dr.Nagaraj B. Patil

Assistant professor, Dept. of Computer Science and Engineering BKIT, Bhalki Karnataka, India
Associate &HOD CSE Dept Govt Engineering College, Raichur, India

Abstract— *Wireless Sensor Networks (WSN) plays vital role in research field. Due to its rapidly increasing application in monitoring various kinds of environment by sensing physical phenomenon. Clustering is an efficient and effective method to enhance performance of the WSNs system. In this project work, we study a secure transmission of data for cluster-based WSNs (CWSNs), where the clusters are formed dynamically and randomly. We propose two Secure and Efficient data Transmission (SET) protocols for CWSNs, called SET-IBS and SET-IBOOS, by using the Identity-Based digital Signature (IBS) scheme and the Identity-Based Online/Offline digital Signature (IBOOS) scheme, respectively. The cluster routing protocol LEACH (Low-Energy Adaptive Clustering Hierarchy) is considered and improved. In SET-IBS, security relies on the hardness of the Diffie-Hellman problem in the pairing area. SET-IBOOS additionally decreases the computational operating cost for protocol security, which is critical for WSNs, while its defense depends on the stability of the problem of discrete logarithm. We propose a clustering routing protocol named Enhanced LEACH, which extends LEACH protocol by balancing the energy consumption in the network. The simulation results show that Enhanced LEACH outperforms LEACH in terms of network system lifetime and reduce the energy consumption.*

Keywords—CWSN, LEACH, SET-IBS, SET-IBOOS.

I. INTRODUCTION

Secure and efficient data transmission is a critical issue for cluster-based wireless Sensor Networks (WSNs).

In Cluster-based WSNs authentication of users is a very Important issue .So, by authenticating the sent user and the destination user , we can achieve the security and efficiency of data over CWSNs. To provide security of data and authentication of user we proposed a technique where we are implementing two concepts for performing those operations.

The first one is identity based signature (IBS) for verification of user generated by the verifier and second one is a key is xor operated with the data and get the cipher and then binary level technique for encryption and decryption of the original message.

The binary level technique converts the plain text into binary form and then splits the data into blocks and assign values to it based on identification mark (IM) technique which depends upon the length of the binary digits, then these are divided into two level, 1st level is 2 bit and 2nd level is 4 bit . Then at the receiver user the Cipher text will be decrypted by using the reverse technique and the destination user will get the original message. By providing those techniques we can improve efficiency, security overhead and energy consumption.

A wireless sensor network is a group of specialized transducers with a communication infrastructure that uses radio to monitor and record physical or environmental conditions and also used in the variety of application such as military sensing and tracking, environmental monitoring, disaster management etc.

The individual nodes are capable of sensing their environments, processing the information locally, and sending data to one or more collection points in a WSN. Secure data transmission is one of the most important issues for WSNs.

At the same time, many WSNs are deployed in rough, disregarded, and often adversarial physical environments for certain applications, such as military domains and sensing tasks with trustless surroundings. Secure data transmission is especially necessary and is demanded in many such practical WSNs.

Their own dynamic attributes for soldiers in their deployed regions or echelons, which could be frequently changed. To refer to this DTN architecture where multiple authorities issue and manage their own attribute keys independently as a

decentralized DTN. Sensor technology, low-power electronics, and low-power radio frequency (RF) design have enabled the development of small, relatively inexpensive and low power sensors, called *micro sensors* that can be connected via a wireless network.

These wireless micro sensor networks represent a new paradigm for extracting data from the environment and enabling the reliable monitoring of a variety of environments for applications that include surveillance, machine failure diagnosis, and chemical/biological detection.

An important challenge in the design of these networks is that two key resources communication and width and energy—are significantly more limited than in a tethered network environment. These constraints require innovative design techniques to use the available bandwidth and energy efficiently.

In order to design good protocols for wireless micro sensor networks, it is important to understand the parameters that are relevant to the sensor applications. While there are many ways in which the properties of a sensor network protocol can be evaluated, we use the following metrics.

A. Ease of Deployment

Sensor networks may contain hundreds or thousands of nodes, and they may need to be deployed in remote or dangerous environments, allowing users to extract information in ways that would not have been possible otherwise. This requires that nodes be able to communicate with each other even in the absence of an established network infrastructure and predefined node locations.

B. System Lifetime

These networks should function for as long as possible. It may be inconvenient or impossible to recharge node batteries. Therefore, all aspects of the node, from the hardware to the protocols, must be designed to be extremely energy efficient.

C. Latency

Data from sensor networks are typically time sensitive, so it is important to receive the data in a timely manner.

D. Quality

The notion of —quality‖ in a micro sensor network is very different than in traditional wireless data networks. For sensor networks, the end user does not require all the data in the network because 1) the data from neighboring nodes are highly correlated; making the data redundant and 2) the end user cares about a higher-level description of events occurring in the environment being monitored.

The quality of the network is, therefore, based on the quality of the aggregate data set, so protocols should be designed to optimize for the unique, application- specific quality of a

sensor network. This paper builds on the work described by giving a detailed description and analysis of low energy adaptive clustering hierarchy (leach), an application-specific protocol architecture for wireless micro sensor networks. Leach employs the following techniques to achieve the design goals stated: 1) randomized, adaptive, self-configuring cluster formation;

2) localized control for data transfers;

3) low energy media access control (MAC); and

4) application specific data processing , such as data aggregation or compression. Simulation results show that leach is able to achieve the desired properties of sensor networks.

II. RELATED WORK

Proposed creation of a Secured Cluster-based architecture for a Dynamic Wireless Sensor Network that applies two topology management procedures: node-move-in and node-move-out. The planned security protocol incorporate one round Zero Knowledge Proof and AES algorithm to relate for node authentication, wherever only authenticated nodes will be acknowledged through node-move-in operation. In addition they explained that, it needs $O(h+q)$ rounds for a node to connect into a network securely, where h is the height of the dynamic cluster-based wireless sensor network and q is the number of adjacent nodes of a joining node. After the $O(h+q)$ attempts to join the network, the node is considered as insecure and is eventually discarded from joining the network as in [1]. Hichem Sedjelmaci *et al* proposed an intrusion detection framework for a cluster-based WSN (CWSN) that intend to merge the advantage of anomaly and signature detection which are high discovery rate and low false positive, correspondingly. Wireless sensor networks (WSNs) have a enormous potential to be used in vital circumstances like armed forces and commercial applications. On the other hand, these applications are mostly frequently to be deployed in hostile surroundings, where nodes and communication are smart targets to intruders. This makes WSNs susceptible to arrange of possible attacks. Because of their characteristics, conservative security methods are not appropriate. So here the authors have proposed an intrusion detection framework for a cluster-based WSN (CWSN) that aims to merge the advantage of signature detection and anomaly which are high detection rate and low false positive, correspondingly as in [2]. Maan Younis Abdullah *et al* inspected the problem of security addition to cluster based communication protocols for homogeneous wireless sensor networks containing sensor nodes with very limited resources, and proposed a security

resolution where clusters are created periodically and dynamically. Their explanation depicts re-keying function protocol for wireless sensor networks security.

They have projected the local administrative functions as master function, derivation function and rekeying function is imprinted with sensor node. A security and performance study proved that it is very proficient in communication, storage, computation and this technique is very successful in defending against a lot of complicated attacks [3] Tingyao Jiang *et.al* presented a new dynamic intrusion detection method for cluster-based wireless sensor networks(CWSN). The nodes in a wireless sensor network are assembled into clusters depending on the particular relationships with a cluster head (CH) in every cluster. The projected scheme initially makes use of a clustering algorithm to construct a model of standard traffic behavior, and then uses this model of standard traffic to detect anomalous traffic patterns. Along with the diverse network conditions of clusters, this method might also dynamically set different detection factors for different clusters to accomplish a more proper detection algorithm.

The performance study showed that the projected intrusion detection method can progress the detection accuracy and decrease the false positive rate, and is extremely efficient of the energy preservation as in [4]. Nikolaos A. Pantazis *et.al* presented a classification of energy efficient routing protocols and expanded the classification initially done by Al-Kariki to better describe which issues/operations in each protocol illustrate/enhance the energy efficiency issues. The distributed behavior and dynamic topology of Wireless Sensor Networks (WSNs) brings in many unusual requirements in routing protocols that should be fulfilled. The main important aspect of a routing protocol, so as to be efficient for WSNs, is the energy usage and the extension of the network's life span.

During the past few years, a lot of energy efficient routing protocols have been projected for WSNs. The authors here presented the four types of schemes of energy efficient routing protocols: Network Structure, Communication Model, Topology Based and Reliable Routing. The routing protocols which belong to the first type can be additionally classified as hierarchical or flat. The routing protocols belonging to the second type can be additionally classified as Query-based or Coherent and non-coherent based or Negotiation-based. The routing protocols belonging to the third type can be additionally classified as Location-based or Mobile Agent-based.

The routing protocols belonging to the fourth type can be additionally classified as QoS-based or Multipath based.

Lastly, a systematic review on energy efficient routing protocols for WSNs is provided as in [5]. Key management methods, except many of them were planned for flat wireless sensor networks, which are not suitable for cluster-based wireless sensor networks (like LEACH). Here Kun Zhang *et.al* investigated adding security to cluster based routing protocols for wireless sensor networks which consist of sensor nodes with very inadequate resources, and have proposed a security solution for LEACH which is a protocol in which the clusters are created periodically and dynamically. The solution proposed by authors makes use of enhanced Random Pair-wise Keys (RPK) method, an optimized security method that depends on symmetric key methods and is a lightweight and conserves the heart of the original LEACH protocol.

Simulations demonstrate that security of RLEACH has been enhanced, with reduction in energy utilization and very less operating cost as in [6]. In Wireless Sensor Networks (WSNs), a crucial security necessity is authentication to evade attacks against secure Communication, and to diminish DoS attacks utilize the limited resources of sensor nodes. Resource restraint of sensor nodes are major difficulty in applying strong public key cryptographic based mechanisms in WSNs.

To deal with the problem of authentication in WSNs, Yasmin, R *et.al* have proposed secure and efficient framework for authenticated broadcast/multicast by sensor nodes and for outside user authentication, which uses identity based cryptography and online/offline signature schemes. The most important objectives of this framework are to allow all sensor nodes in the network, initially, to broadcast and/or multicast an authenticated message rapidly; secondly, to confirm the broadcast/multicast message sender and the message contents; and lastly, to confirm the authenticity of an outside user.

The projected framework is also evaluated by means of the most secure and efficient identity-based signature (IBS) schemes as in [7]. A secure routing for cluster-based sensor networks is where clusters are formed periodically and dynamically. Together with the investigation of ID-based cryptography for security in WSNs, Huang Lu *et.al* proposed a new secure routing protocol with ID-based signature scheme for cluster-based WSNs within which the security is dependent on the hardness of the Diffie-Hellman problem in the random oracle model. Here the deficiency in the secure routing protocols with symmetric key pairing is pointed out by authors. Because of the communication operating cost for security, authors provide simulation investigation results in

details to demonstrate how various parameters act among energy efficiency and security as in [8].

A process by which data is collected and sent from sensor nodes to the base station is known as data aggregation. It is completed via some sensor nodes called aggregators. A key role is played by security in data aggregation procedure to make sure confidentiality and privacy of aggregated data., In [9] Nguyen Xuan Quy et.al proposed a data aggregation method for cluster-based WSN that improves the security against attackers. This method was based on accelerated homomorphism public key encryption which presents continuous suppression of and supports hop-to-hop verification. The logical investigation and association demonstrate that this approach has both lower computational and better security performance as compared to other approaches as in [10]. In this paper, we do not assume any prior knowledge about the data indeed in many applications; raw data may not be easily categorized into different types. To transmit the collected data to a remote location is also considered Expensive because the total collected data may be in a very large quantity. To facilitate data query. The operation of LEACH is divided into rounds. Each round begins with a setup phase when the clusters are organized, followed by a Steady-state phase when data are transferred from the nodes to the cluster head and on to the Base Station (BS).

The LEACH network has two phases: 1) set-up phase

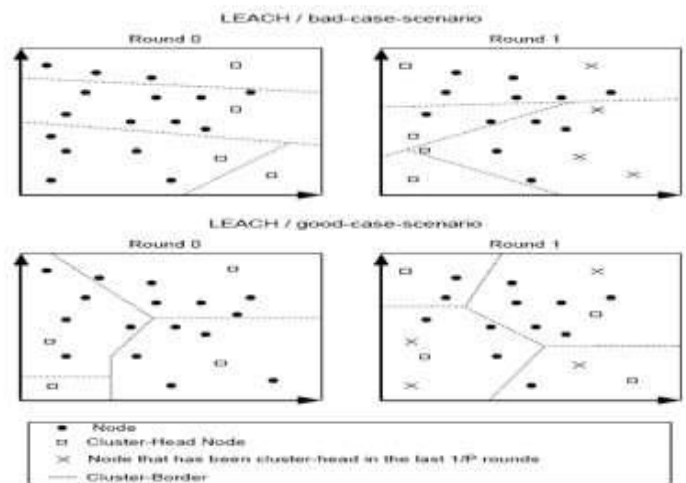
$$T(n) = \begin{cases} \frac{p}{1-p(r \bmod \frac{1}{p})} & n \in G \\ 0 & \text{otherwise} \end{cases}$$

The selected CH informs about its selections as CH among the group. Non cluster-head nodes decide their cluster for current round by choosing the CH that requires minimum communication energy, based on the received signal strength of the advertisement from each CH. After the selection each non-CH informs the CH by transmitting a join request message (Join-REQ) back to the CH. Then the CH node sets up and broadcast a TDMA schedule to all member non-CH nodes.

2) Steady state phase: The Steady State Phase is broken into many frames, in which nodes can send their data to the CH at most once per time slot. CH sends the aggregated data to BS in single hop manner. The LEACH provides better results compared to earlier existing protocols e.g. direct communication protocol, minimum- transmission-energy protocol and static Clustering protocol in Wireless Sensor Network. The available redundant information is subsequently cancelled during aggregation process performed by CH.

Then the CH will broadcast an advertisement message to inform all others that it is the new cluster-head. The nodes send the join-request message containing their IDs by using CSMA (carrier sensing multiple access) to join a cluster. The node joins that cluster from which they received strongest strength signal. After that, each CH knows its own cluster members information. Based on the message, the CH creates TDMA schedule table and broadcasts it to the cluster members. So all the member nodes know their idle slots, and then the steady-state phase begins.

The cluster based protocols (like LEACH) which are the data transmission protocols for WSNs, are susceptible to many security attacks. In general, the attacks to Cluster Heads in CWSNs can produce serious damage to the network, since security attacks. data aggregation and data transmission rely on the CHs primarily. If an invader manages to act as if it's a CH or negotiate the CH, it can incite attacks such as selective forwarding attacks and sinkhole, thus upsetting the network. Alternatively an attacker may mean to insert false sensing data into the WSN, like pretending as a leaf node transferring false information to the CHs. However, LEACH like protocols are extra tough against insider attacks rather than other types of protocols in WSNs. Since CHs are rotating from nodes to nodes in the network by rounds making it harder for types of protocols in WSNs.



Example of LEACH Network

The goal of the proposed secure data transmission for CWSNs is to guarantee a secure and efficient data transmission between leaf nodes and CHs, as well as transmission between CHs and the BS.

Meanwhile, most of existing secure transmission protocols for CWSNs in the literature, however, apply the symmetric key management for security, which suffers from the orphan

node problem that is introduced, In this paper, we aim to solve this orphan node problem by using the ID-based crypto-system that guarantees security requirements, and propose SET-IBS by using the IBS scheme. Furthermore, SET-IBOOS is proposed to reduce the computational overhead in SET-IBS with the IBOOS scheme. The propose two novel Secure and Efficient data Transmission (SET) protocols for CWSNs, called SET-IBS and SET-IBOOS, by using the IBS scheme and the IBOOS scheme, respectively. We first present SET-IBS in this section. The proposed SET-IBS has a protocol initialization prior to the network deployment and operates in rounds during communication, which consists of a Setup phase and a Steady-state phase in each round. We introduce the protocol initialization; describe the key management of the protocol by using the IBS scheme, and the protocol operations afterwards. After the protocol initialization, SET-IBS operates in rounds during communication. Each round consists of a setup phase and a steady-state phase. We suppose that, all sensor nodes know the starting and ending time of each round, because of the time synchronization.

The operation of SET-IBS is divided by rounds as shown in Figure, which is similar to other LEACH-like protocols. Each round includes a setup phase for constructing clusters from CHs, and a steady-state phase for transmitting data from sensor nodes to the BS.

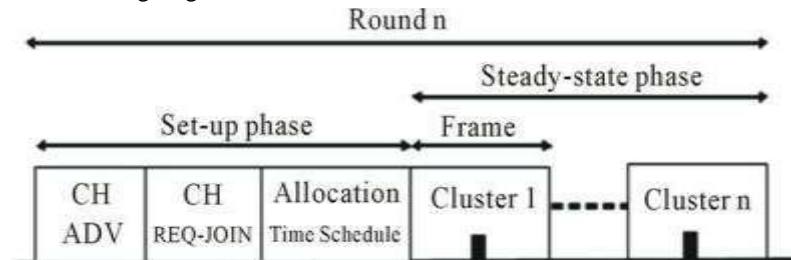
In each round, the timeline is divided into consecutive time slots by the TDMA (time Division multiple access) control. Sensor nodes transmit the sensed data to the CHs in each frame of the steady state phase. For fair energy consumption, nodes are randomly selected as CHs in each round, and other non-CH sensor nodes join clusters using one-hop transmission, depending on the highest received signal strength of CHs. In order to elect CHs in a new round, each sensor node determines a random number and compares it with a threshold.

If the value is less than the threshold, the sensor node becomes a CH for the current round. In this way, the new CHs are self-elected based by the sensor nodes themselves only on their local decisions, therefore, SETIBS functions without data transmission with each other in the CH rotations.

The steady-state phase consists of the latter two Steps. In the setup phase, the time-stamp T_s and node IDs are used for the signature generation. Whereas, in the Steady-state phase, the time-stamp t_i is used for the signature generation securing the inner cluster communications, and T_s is used for the signature generation securing the CHs-to-BS data transmission. The proposed SET-IBOOS operates similarly

to that of SETIBS. SET-IBOOS works in rounds during communication, and the self-elected CHs are decided based on their local decisions, thus it functions without data transmission in the CH rotations.

For the IBOOS key management in SET-IBOOS, the offline signatures are generated by the CHs, which are used for the online signing at the leaf nodes



LEACH Protocol operation

- 1) *Setup –Phase:* In cluster each node creates a random number with the probability p , each node has the random probability (p) at the each round, and the next round it will creates another probability. Each node generates a random probability (p) at the beginning of a new round and computes the threshold value ($T(n)$) with the use of equation (1). If $r=1$ (i.e. the first round), let $EMAX$ of all nodes be 1. In case of $P < P_T$, the node is selected as a cluster head. A selected cluster head broadcasts an advertisement message over neighbor nodes. The neighbor nodes collect advertised message during a given time interval and then send a “join REQ” message to the nearest cluster head. The cluster head receives the “join-REQ” message and builds a cluster member list schedule. The member node receives and save the message for data transfer
- 2) *Pre-State phase:* The main idea of this phase is to calculate the cluster Workload (which include aggregates the sensed data from cluster members and send the aggregated data to the base station) in one frame, then try to elect cluster member node that can handle the aggregation processes through all frames in the round. If not exist such a node, try to elect cluster member nodes that can handle the aggregation processes for each one frame in the round and the cluster head will handle the aggregation process for frames that there are no aggregator nodes for them.
- 3) *Steady State Phase:* In Steady State phase, the operation is divided into frames, in each frame; cluster member nodes send their data to the aggregation node N Aggregator according to their time slots. The aggregation node must keep its receiver on to receive

all the data from the nodes in the cluster. When all the data has been received, the aggregation node sends it to the base station after performs data aggregation. Cluster head maintains the received information of member nodes. The member nodes will have all the data in the form of TDMA table sent by sink node.

III. OBJECTIVE OF THE WORK

The wireless sensor network providing security and efficient of data is the critical problems. Secure and Efficient data transmission protocols for WSNs are vulnerable to a number of security active and passive attacks. Mostly, attacks to CHs in CWSNs could result in serious damage to the network because data transmission and data aggregation depend on the CHs(Cluster Head) node for Wireless Sensor Network.[2] The attacker manages to compromise or pretend to be a CH, it can provoke attacks such as sinkhole and selective forwarding attacks, hence disrupting the Sensor N/W.[3] The Existing System Sense the wireless sensor nodes to monitor physical or environmental conditions, and processing. The information data locally and sending to one or more collection points in a Wireless Sensor Network.

Limitations of Existing System:

- Adding security to LEACH-like protocols is challenging, because they dynamically, randomly and periodically rearrange the network's clusters and data links. Node-to-node trust relationships and common key distributions are inadequate for LEACH-like protocols.
- Apply the symmetric key management for security, which suffers from a so-called orphan node problem. This problem occurs when a node does not share a pair wise key with others in its preloaded key ring.
- In order to mitigate the storage cost of symmetric keys, the key ring in a node is not sufficient for it to share pair wise symmetric keys with all of the nodes in a network

There are two Secure and Efficient data Transmission (SET) protocols for CWSNs known as IBS and IBOOS.

The main idea using both IBS and IBOOS protocol is to authenticate the encrypted data which is sensed by sensor and apply the digital signatures to data which is encrypted which are efficient in communication and it signifies the security. Secret keys and pairing parameters are distributed in all

sensor nodes by the base station which overcomes the key escrow problem Secure communication in IBS protocol is relies on the identity based cryptography is efficient in communication and saves energy. IBOOS protocol is proposed which is used to minimize the computational complexity for security. Both IBS and IBOOS protocol solve the orphan node problem with respect to symmetric key management in secure data transmission. In Proposed System Security and efficient transmission of data is necessary and demanded in many practical wireless sensor networks.

Advantages of Proposed System:

- Less computation and communication.
- High security.

IV. WORK CARRIED OUT SO FAR

Secure and efficient data transmission is a critical issue for cluster-based wireless Sensor Networks (WSNs).

In Cluster-based WSNs authentication of users is a very Important issue .So, by authenticating the sent user and the destination user , we can achieve the security and efficiency of data over CWSNs. To provide security of data and authentication of user we proposed a technique where we are implementing two concepts for performing those operations. The first one is identity based signature (IBS) for verification of user generated by the verifier and second done is a key is xor operated with the data and get the cipher and then binary level technique for encryption and decryption of the original message. The binary level technique converts the plain text into binary form and then splits the data into blocks and assign values to it based on identification mark (IM) technique which depends upon the length of the binary digits, then these are divided into two level, 1st level is 2 bit and 2nd level is 4 bit .

Then at the receiver user the Cipher text will be decrypted by using the reverse technique and the destination user will get the original message. By providing those techniques we can improve efficiency, security overhead and energy consumption.

V. RESULTS AND DISCUSSIONS

Signature generated by Client

First sender is going to calculate a public key based on the P,Q values given by the user and those values are again used to generate the private key which is XOR with Hash function and generates the signature which will be send to the server for authentication..



Server Authentication

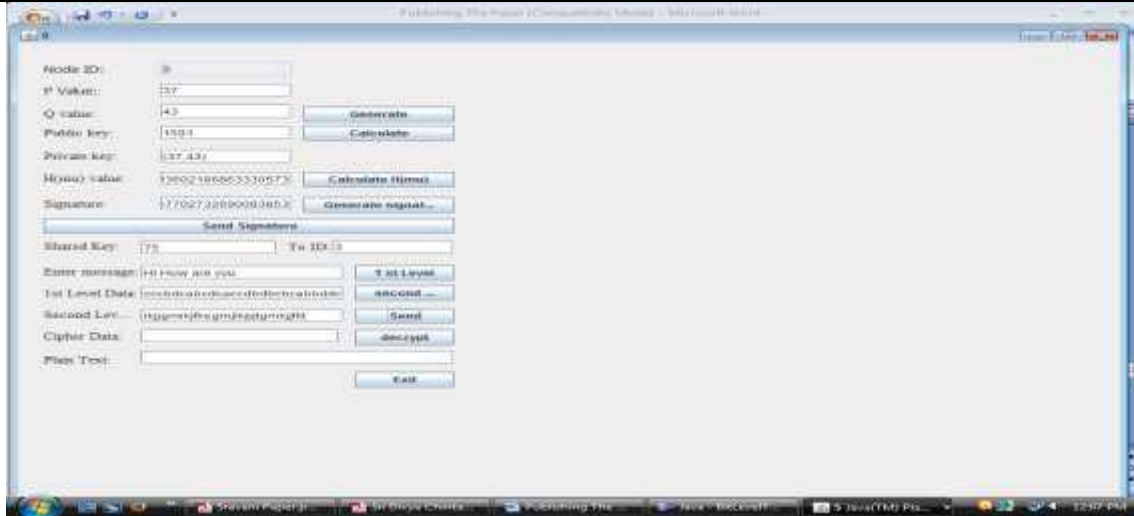
After receiving the signature the server authenticated the user and sends a shared key to all the clients who has send the signature to enhance further communication.



Transferring the Message

After receiving the shared key sent by the server, the user will enter the id of receiving user and then enters the message which will be encrypted using encryption techniques and message send to the particular user. Here we are using 2 level of encryption techniques, Here we have 4 distinct blocks, according to the order they are 01, 00, 10, 11. So we put according to key generation technique 01=a, 00=b, 10=c, 11=d that is 1st level identification marks. For the generation of 2nd level identification marks, again the

two bit representation of a ,b, c & d is aa, ab, ac, ad, bb, bc, bd,cc, cd, dd, ba, ca, da,cb, db, dc. Now we put aa=e, ab=f, ac=g, ad=h, bb=i, bc=j,bd=k, cc=l, cd=m, dd=n, ba=o, ca=p,da=q, cb=r, db=s,dc=t. As level of generation of identification marks for each block and length of decomposed block are chosen at run time as randomly, for it key is differed from each encryption to another. Not only that we are taken decomposed blocks in its sequence appearing for generating the identification marks for each block.

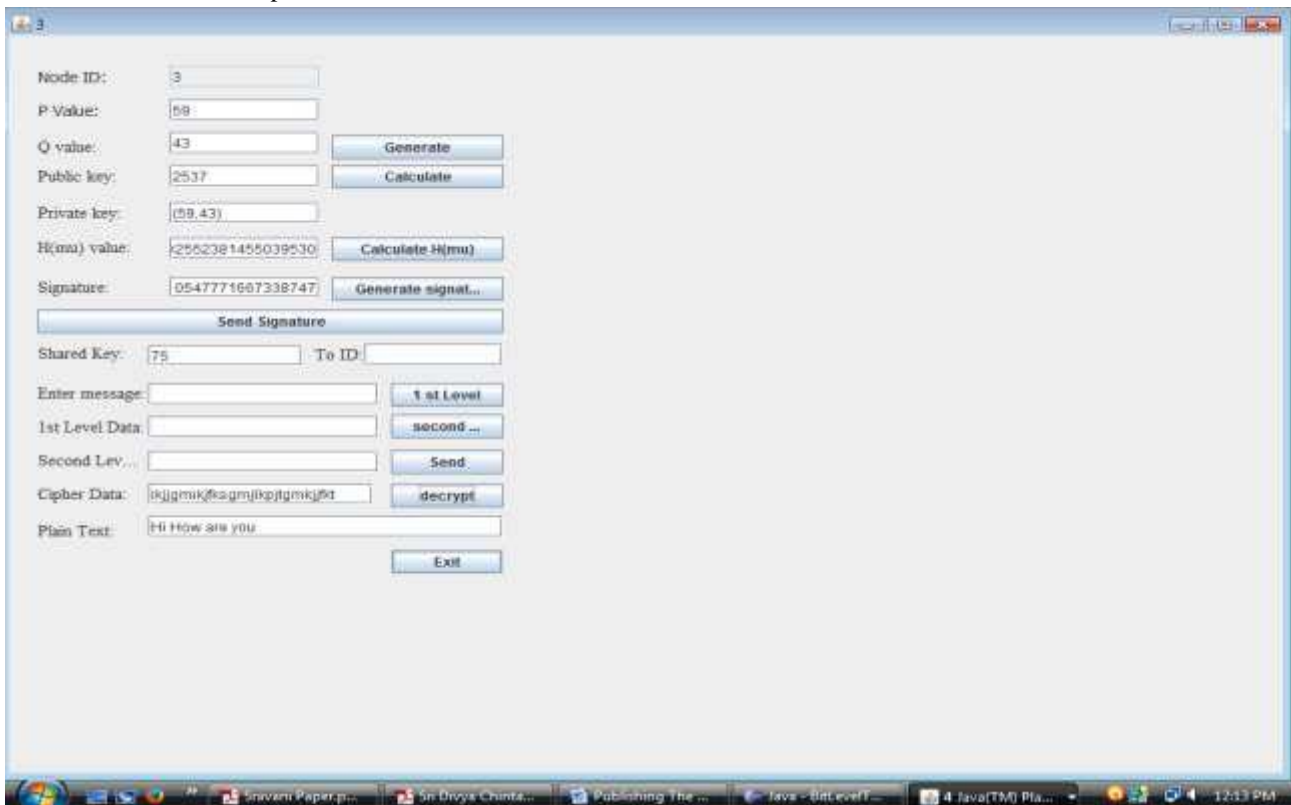


Receiving the message

The receiver will decrypt the message by decryption method and will get the actual message sent by the sender. Collecting all distinct blocks, identification marks for each block is assigned. This identification mark is same as First level of identification mark. From the beginning of the encrypted text, unchanged block (ML) is collected, length of which is defined in to the key.

Then every identification marks is replaced into identification marks. In that process we find two different

Identification marks against each distinct block .Now we repeat finding identification marks up to D level in inverse Manner. Repeat the same procedure to identification marks up to Dang will get the data back .Replace the all Identification marks into its binary form with the help of key. Now we collected the entire bit-stream-blocks are merge together. After this merging, UB is attached at last of the recently generated decrypted bit of stream.



VI CONCLUSIONS

In these the concepts of user authentication, Identity Based Signature, Encryption and Decryption, were proposed. By proposing those concepts more security and efficiency will be added to the given system.

Now a days the data transferring plays an important part in our daily life but the transfer of data must be secure. So to send the data in secure manner we has to follow some techniques. Such as authenticating the user with the verifier, and for the communication key generation algorithm is used. In this we are using another technique for the key is xor operated with the data and get the cipher and then binary level technique is used for encryption and decryption. By providing those technique we provide more security and efficiency for transferring data

REFERENCES

- [1] S. Sharma and S. K. Jena, "A survey on secure hierarchical routing protocols in wireless sensor networks," in Proc. ICCCS, 2011.
- [2] Heinzelman W. B., Chandrakasan A. P., Balakrishnan H., "An applicationspecific protocol architecture for wireless microsensor networks," IEEE Trans on Wireless Communications, Vol. 1, No. 4, 2002, pp. 660-670, doi: 10.1109/TWC.2002.804190.
- [3] X. H. Wu, S. Wang, "Performance comparison of LEACH and LEACHC protocols by NS2," Proceedings of 9th International Symposium on Distributed Computing and Applications to Business, Engineering and Science. Hong Kong, China, pp. 254-258, 2010
- [4] P.T.V.Bhuvanawari and V.Vaidehi "Enhancement techniques incorporated in LEACH- a survey"Department of Electronics Engineering, Madras Institute Technology, Anna University Chennai, India, 2009
- [5] Wu Xinhua and Huang Li "Research and Improvement of the LEACH Protocol to Reduce the Marginalization of Cluster Head"Journal of Wuhan University of Technology Vol. 35, No. 1, Feb. 2011, pp. 79-82, doi:10.3963/j.issn.1006-2823.2011.01.019 (in Chinese).

Tourist Guide Information System using Google Map and GPS

Honey Soe, Myint Myint Sein

University of Computer Studies Yangon

Abstract— With the evolution of technology, the tourists can be effectively guided by the aid of Location Based Service of their smart phone. Solo travelling is popular in today's touring industries and therefore mobile tourist guided system can efficiently support to solo traveler. By applying the combination of Location Based Service of the mobile phone and Google Map services, this tourist guide information system is developed. The purpose of this system is to provide user's current location, the detailed information of the nearest places and the routes to reach their interesting nearest place. This smarter tour guide system use mobile phones' GPS for the current location access and also use Google Maps for efficient guidance to users. The tour guide system provides real-time and location-sensitive tourist information of the Yangon region.

Keywords — Location Based Service, tourist guide system, Google Map, Haversine Formula.

I. INTRODUCTION

With the large of globalization, tourism also widely increases in nowadays. The technology in tourism also increase and the tourist can find the tourism information on blogs, forums and websites and etc. However, the mobile tourist guided systems are more conveniently supported to user by their real time and location sensitive information. Due to this fact, this system is proposed as the tourist guide information system for the mobile smart phone. The goal of this system is to provide the personalized access to tourism information at anytime from anywhere in Yangon City. In this system, the user can easily check their current location by the use of the Location Based Service of the mobile phone. Users can also get the find the detailed information of the nearest places from them. Users can also easily be guided to their interesting nearest places by the Google Map service.

The local information of Yangon city is stored in online server database. The distance between the user's current place and nearest place is calculated with 'Haversine' Formula. By using the web version of Google map instead of Google Map API, this system can be used in every mobile phone even if it doesn't have the Google play services. Since the system use the online server database, the database can easily be updated at anytime

and anywhere. The complexity will be reduced since the user interesting places within the user desired distance range can be easily viewed at the same time on the simple Graphical User Interface. This paper is organized as follows: the related works are described in section 2. The section 3 is about the background theory of the system. In section 4, the design of this system is described. The section 5 is the conclusion of this paper.

II. RELATED WORKS

The research about the tourist guide system [1] "Tourist Guide using GPS" is developed for the Mumbai city. In this research, the system can provide information of Buses to guide the tourists in their trip. PS is used to fetch the user current location and display the result in map based interface. "Tour-Guide: Providing Location-Based Tourist Information on Mobile Phones" by Xiaoyu Shi[2] expressed the tour guide system designed for iPhone. Since it is specialized for the iPhone, it uses Xcode (version 3.0) in the MAC OS environment. In that system, the users can get tourism guidance information they need anytime and anywhere. It can be used by both on-line and off-line phases. In off-line phases, it displays the list of all tourist cities and the user's current location and the nearby attractions are displayed on map in on-line case. Alexander and Krill[3] research the tourist guide system that support the tourist during the trip and is not aimed to provide the real time information.

There are two stages in the system, (1) plan preparation before trip and (2) tourist support during trip. The first stage use internet connection and the second stage can process on offline mode. Uses third party services (e.g.- Wikipedia) to obtain attractions when the user select the target region, and pre downloaded them and store in device memory. On the trip, the android app can support the user by displaying that predownloaded information. In the research of Sawsan Alshattawi [4], it presented the tour guide system that contains two steps; the first step is discovering the location and the interesting points on the website before the real visit. After that, the application is built and installed in the mobile phone and can be used during the trip. The website is online mode and the application is offline mode. To use the website, the user must register and sign up the account.

Location Based Services (LBS) are information services accessible with mobile devices through the mobile network and utilizing the ability to make use of the location of the mobile device. Almost all LBSs are based on four components: Service and Content Provider, Mobile Device, Positioning Systems, and Communication Network. These components are presented on figure. The main advantage of LBS for users is that they don't need to enter location information manually but it is automatically collected [5-10]. Location Mainly, four components are considered for the Location Based Service (See Figure. 1).



Fig.1: Components of the Location Based Service

III. LOCATION INFORMATION

GPS Receiver determines its position using a process called trilateration. Assume that GPS-like signals are being transmitted from radio towers in FRESNO, LOS ANGELES, and LAS VEGAS. Assume that you can decode the signals so that you know how far away you are from each transmission tower (R1, R2, R3). Use this known distance as the radius for drawing a circle around each tower.

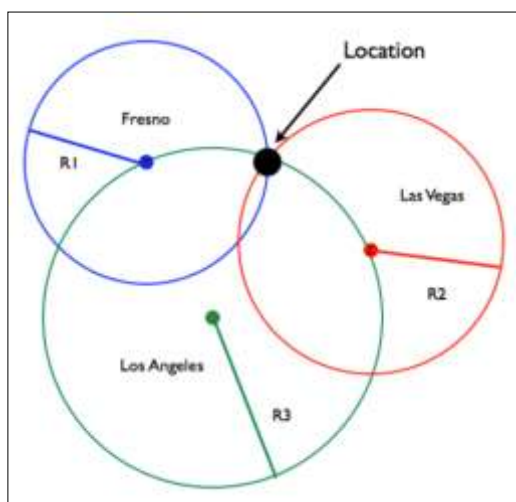


Fig.2: Trilateration Method

If you only have the signals from LAS VEGAS and LOS ANGELES, then you could be at one of the intersection points for those two circles. But if you can add the

satellite from FRESNO, then you can figure out where you are exactly because there is only one intersection points for all three circles. The GPS receiver on the Earth is located at the intersection of those spheres. The 'Trilateration Method' is illustrated in Figure 2.

The Haversine formula is an equation important in navigation, giving great-circle distances between two points on a sphere from their longitudes and latitudes. The Haversine Formula is

$$d_{Lon} = lon2 - lon1$$

$$d_{Lat} = lat2 - lat1$$

$$a = (\sin(d_{lat}/2))^2 + \cos(lat1) * \cos(lat2) * \sin(d_{lon}/2)^2$$

$$c = 2 * \text{atan2}(\text{sqrt}(a), \text{sqrt}(1-a))$$

$$d = R * c$$

Where,

R is the radius of the Earth.

lat1 is the latitude of the location1.

lat2 is the latitude of the location2.

lon1 is the longitude of the location1.

lon2 is the longitude of the location2.

d is the distance between place1 and location2.

IV. PROPOSED SYSTEM

In outline, the system has the following steps.

1. Initialize the system, check whether network enabled and GPS enabled.
2. Retrieve the current location.
3. Input the category and distance range.
4. Retrieve the relevant data.
5. Calculate the distance between the location items and the current location.
6. Output the relevant location items.
7. Input the place to view details on the map.
8. Output the details of the place and show the location on map.

The proposed system develops an application system that provides the tour guided information of famous places in Yangon City. Generally, the user can search the tour guides information by means of categories (Pagodas, Museums, Hotels, etc...) and distance ranges (1mile, 2miles, 3miles, etc...). The system is composed of three components: a mobile device (front-end), server devices (middle-tier) and database (back-end). The system architecture is shown in Figure 3. The front end layer interacts with the user and gets the user's current location by the GPS and shows it on Google Map. The distances between the user's current location and the location of the places in the mobile phone's DB are calculated at the middle layer. The details of a place (Latitude, Longitudes, image, etc...) are stored in the mobile server repository of back end layer. Based on the user selected categories;

the data are abstracted to the mobile phone's DB of middle layer.

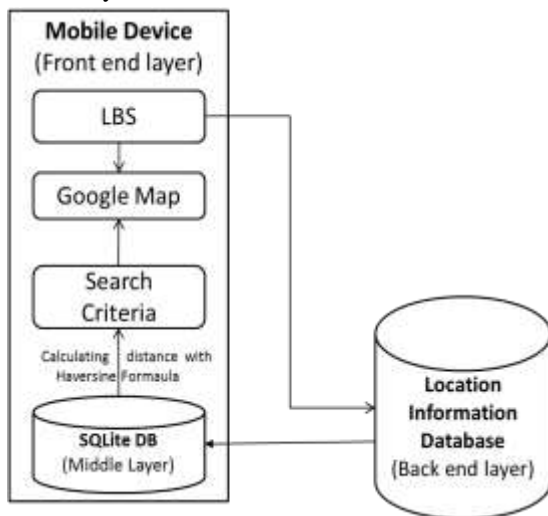


Fig.3: The system architecture

Creating Database

To store the location data of the system, the type of spatial database is used. Spatial database is used to store and query data that represents geometric objects such as points, lines and polygons. Some spatial databases handle more complex structures such as 3D objects, topological coverage, linear networks, and TINs. In this system, the database contains the two tables named 'Category' and 'Near'. 'Category' table contains the three attributes namely 'ID', 'cat' and 'type'. The 'Category' table is designed in Table 1. In 'Near' table, there are eight attributes; 'ID', 'name', 'lon', 'lat', 'des', 'detaildes', 'cat', 'image' and 'cat' is the primary key. The design of 'Near' table is shown in Table 2.

Table.1: 'Near' Table

ID
Cat
Type

Table 2. 'Category' Table

ID
Name
Lon
Lat
Des
Detaildes
Cat
Image

Available Services of the system

The available services of the system are shown in Table 3.

Table.3: Available Services of the system

No.	Available Services
1	Pagoda
2	Churches
3	Mosque
4	Hinduism
5	Musician
6	Historical Buildings
7	Chinese Restaurant
8	Myanmar Restaurant
9	Indian Restaurant
10	European Restaurant
11	Airport
12	Railway Station
13	Depot
14	School
15	University
16	Shopping Mall
17	Market
18	Embassy
19	Banks

Upon the user desired distance range, the system will find the nearest famous place. By applying the Haversine formula, the distance between Shwe Dagon Pagoda and Sule Pagoda is 2.875004819709077 km, the distance between Hledan Center and Sule Pagoda is 6.453772614821444 km and the distance Shwe Dagon Pagoda and Hledan Center is 3.6059009151724584 km each (see Table 4).

Table.4: Calculation using Haversine Formula

Place 1	Place 2	dLon	dLat	a	c	Distance (km)
Shwedagon Pagoda (96.1465332, 16.7984419)	Sule Pagoda (96.156641, 16.7744656)	-	1.76414	5.0909	4.5126	2.8750048 19709077
Hledan Center (96.1283111, 16.8257796)	Sule Pagoda (96.156641, 16.7744656)	-	4.94450	2.5653	0.0010	6.4537726 14821444
Shwedagon Pagoda (96.1465332, 16.7984419)	Hledan Center (96.1283111, 16.8257796)	4.771328	-	8.0085	5.6598	3.6059009 15172458 4

V. EXPERIMENTS AND RESULTS

Before the system initialize, the user may check whether the internet access enabled and GPS enabled. When the system initialized, it fetch the current location of the user by the GPS of the mobile phone. Figure 4 show the GUI of the system.



Fig.4: The illustration of developed GUI

In developed application, the current location is also available by using the button of " My Location" .See in figure 5. To find the nearest interesting place, the system is customized by the user.Figures 6 shows the category and distance range that can be inputted by user.

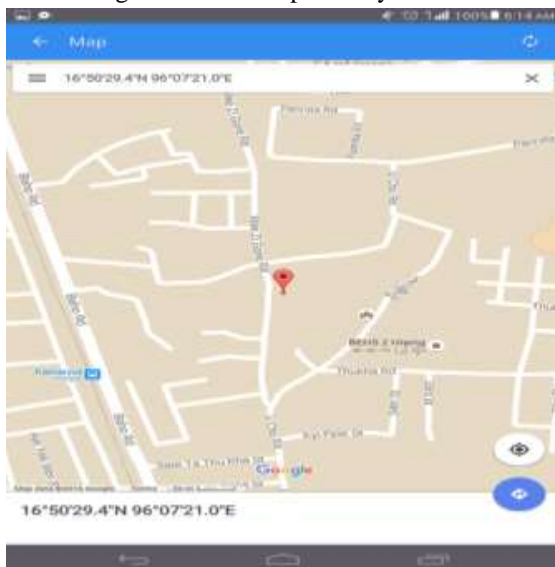


Fig.5: The current location of user' on the Google Map



Fig.6: The category and distance range of the system.

Retrieving all the nearest location items

After calculating distance range by the 'Haversine Theory' the user interesting nearest places can be shown,Figure 7 shows the screenshot of the system showing the user's desired nearest famous places.



Fig.7: User's desired nearest famous places



Fig.8: The detail of selected famous place

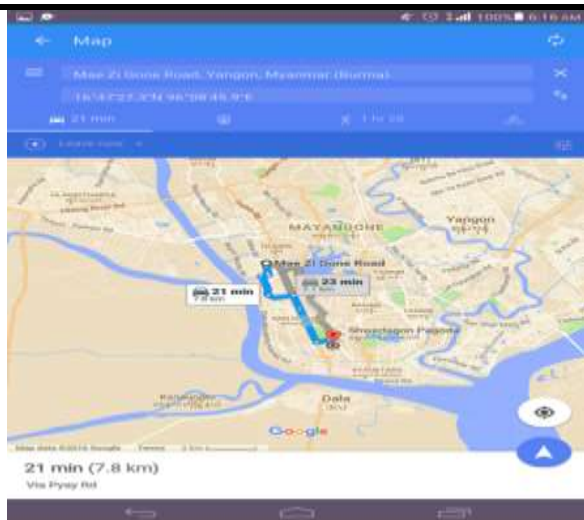


Fig.9: Location of current and desired famous place

If the user select one item from them, the detailed information of that place is giving as an output. Figure 8 shows the screenshot of the detailed information of the user selected place. After viewing the detailed information, the user can get the route from the current location to there. Figure 9 shows the screenshots of the route from the user current place to the interesting nearest place on Google Map.

VI. CONCLUSIONS

The mobile application for location based tourist information tools is developed in this research. This system use the Location Based System including the GPS feature of smart phone and the Google Map to efficiently assist the tourist. By this mobile tourist guide information system, the tourist can conveniently visit in Yangon City. This system is firstly intended to develop tour guide mobile application for Yangon City. After that, it can be updated to be used for the whole Myanmar Country.

REFERENCES

- [1] Prashant Beldar, Prashant Bansode, Rajendra Mane and Swapnil Gaikwad, "Traveler Guide using GPS", International Journal of Computer Science and Mobile Computing, Vol. 3, Issue. 2, February 2014, pg.406 – 409
- [2] Xiaoyu Shi, Ting Sun, Yanming Shen, Keqiu Li and Wenyu Qu, "Tour-Guide: Providing Location-Based Tourist Information on Mobile Phones", 2010 10th IEEE International Conference on Computer and Information Technology (CIT 2010) pp. 2347-2400.
- [3] Alexander Troshkov and Kirill Kulakov Petrozavodsk (State University Petrozavodsk, Russia), "TourMe: Tourist Application for Mobile Platforms", The Proceeding of the 4th conference of Fruct Association, pp.208-211.

- [4] Sawsan Alshattawi (Yarmouk University, Irbid, Jordan), "Building Mobile Tourist Guide Applications using Different Development Mobile Platforms", International Journal of Advanced Science and Technology , vol 54, May 2013.
- [5] Su Nandar Aung and Myint Myint Sein, "Modify Compact R-tree Dynamic Index Structure for Myanmar GIS Database ", in Proceedings of the 12th International Conference on Computer Applications (ICCA2014), Yangon, Myanmar, pp. 201-204, February 2014.
- [6] Yutaka Ohsawa, Htoo Htoo, Naw Jacklin Nyunt and Myint Myint Sein, "Generalized Bichromatic Homogeneous Vicinity Query Algorithm in Road Network Distance", June 2015.
- [7] Su Nandar Aung and Myint Myint Sein, "Geotextual Index Structure for Approximate Keyword Search within Given Range on Spatial Database ", in Proceedings of 7th International Conference on Science, Technology, Engineering and Management (ICSTEM,2015), Singapore, pp.49-54, January 2015.
- [8] Su Nandar Aung and Myint Myint Sein, "K-Nearest Neighbours Approximate Keyword Search for Spatial Database", in Proceedings of 9th International Conference on Technological Advances in Electrical, Electronics and Computer Engineering (ICTAEECE), Bangkok, Thailand, pp. 65-68, 7th February 2015.
- [9] Su Nandar Aung and Myint Myint Sein, " K-Nearest Neighbors Approximate Keyword Search for Spatial Database", in International Journal of Advances in Electronics and Computer Science (IJA ECS), ISSN:2393-2835, Volumn-2, Issue-4, April-2015.
- [10] Su Nandar Aung and Myint Myint Sein, "Efficient Combined Index Structure for K-Nearest Neighbors Keyword Search on Spatial Database ", in Proceedings of the 13th International Conference on Computer Applications (ICCA2015), Yangon, Myanmar, pp. 324-328, February 2015.

Optimizing the Size of A Multi-Layered Patch Antenna for K-Band Applications

M.hamdaoui^{1,2}, J.Foshi², A. Roukhe¹

¹Team Treatments Optronics Information Faculty of Science, Meknes, Morocco

²Team Electronics, Instrumentation and Measurement Physics Faculty of Science and Technology, Errachidia, Morocco

Abstract—In this work, the size of the antenna has been optimized by introducing an air-filled cavity into the lower substrate of the antenna with two layers. Analysis and modeling were performed using the HFSS (High Frequency Structure Simulator) simulator based on the finite element method. The simulation results obtained for the reflection coefficient, bandwidth, and gain were compared with those published. This comparison showed a good satisfaction

Keywords— Multilayer patch antenna, K band, air-filled cavity, S11, gain, bandwidth, HFSS.

I. INTRODUCTION

Microstrip antennas play a very important role in the development of wireless communication technologies. Indeed, these patch antennas, despite their relatively narrow bandwidth[1], are among the devices that most respond to the miniaturization requirements imposed by new telecommunication devices. Compatible with Monolithic Microwave Integrated Circuit (MMIC) designs, such as Cell phones[2], [3]

The simplest typical structure of a patch antenna consists of a radiating element printed on a dielectric substrate disposed on a ground plane[4].

At present, satellite communication in the K-band is of major interest for the development of telecommunication systems such as satellite television channels [5], because this band has a large number of unused bandwidth [2]

One of the effective techniques for the miniaturization of this type of antenna is the use of a dielectric substrate having a high dielectric constant [6]. Indeed, the ceramic materials provide adequate dielectric permittivity; in addition they possess very useful physical properties [7] [8]. Several works have been published to increase the bandwidth[9], [10], but they have a relatively large antenna size[11] however we find other works that proposed a miniaturized size but with A very narrow bandwidth[12].

This work presents a miniaturized antenna with a wider bandwidth by using a second layer of the dielectric substrate while introducing an air-filled cavity into the lower substrate of the microstrip antenna.

II. PRESENTATION OF THE MICROSTRIP ANTENNA

fig. 1 shows the diagram of a microstrip antenna formed by a radiating structure (patch), two dielectric substrates of the same electrical permittivity separated by a rectangular probe and a ground plane.

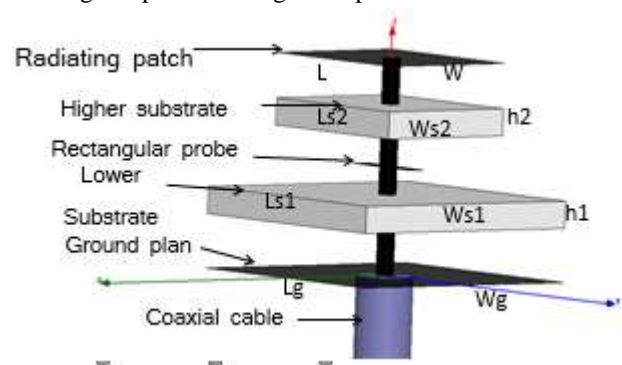


Fig.1: Structure of the studied antenna.

The microstrip antenna is fed by a coaxial cable to ensure the excitation of the probe in order to have an almost omnidirectional radiation pattern. The introduction of a second dielectric substrate increases the performance of the microstrip antenna, namely the bandwidth and the gain [7]

III. RESULTS AND DISCUSSIONS

a. Without air-filled cavity

Using the following parameters: $L = 10\text{mm}$, $W = 8\text{mm}$, $h1 = 1.5\text{mm}$ and $\epsilon_r = 9.8$ given by[2], and after a certain number of simulations with the HFSS software concerning the physical parameters of the microstrip antenna, The appropriate values are described in the following table

Table.1: Physical Parameters of the Microstrip Antenna

paramètre	description	Valeur (mm)
L	Length of the patch	8
W	Width of the patch	10
Lg	Length of the ground plane	14
Wg	Width of the ground plane	14
Ls1	Length of the first layer	14
Ws1	Width of the first layer	14
h1	Thickness of the first layer	1.5

Ls2	Length of the second layer	8
Ws2	Length of the second layer	10
h2	Thickness of the second layer	1.5

In fig. 2, the simulation result obtained for the reflection coefficient is presented. This curve shows that the microstrip antenna resonates at a frequency of 20 GHz antenna with a coefficient of reflection equal to -32.5 dB and a bandwidth of 0.2 GHz. The results obtained are unsatisfactory in particular the bandwidth which is relatively narrow compared with the results given in references [2],[13].

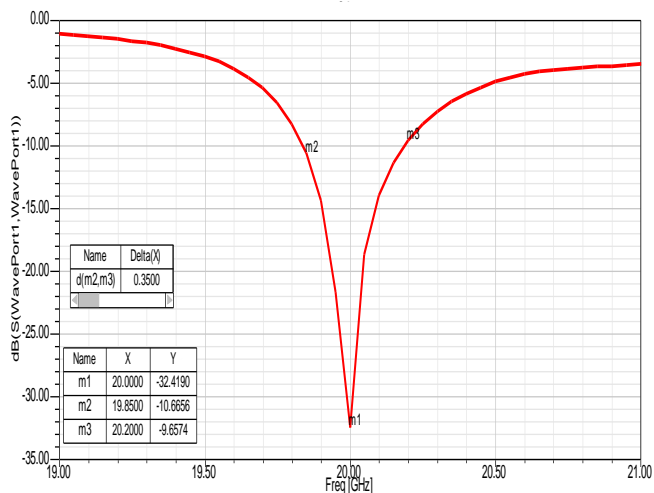


Fig.2: Reflection coefficient as a function of the frequency of the antenna without air-filled cavity for $L=8$ mm, $W=10$ mm and $\epsilon_r=9.8$ [2]

b. Insertion of an air-filled cavity

To remedy this problem due to the excitation of the surface waves and the bad adaptation between the coaxial cable and the patch [14], we chose to introduce an air-filled cavity at the lower substrate [15] (Figure 3), which will reduce the effect of the dielectric permittivity on the bandwidth and increase considerably the gain of the antenna.

The dimensions of the air-filled cavity with (3x3x1.5mm³) are obtained, after a certain number of tests, equal to those of the radial connector SMA.

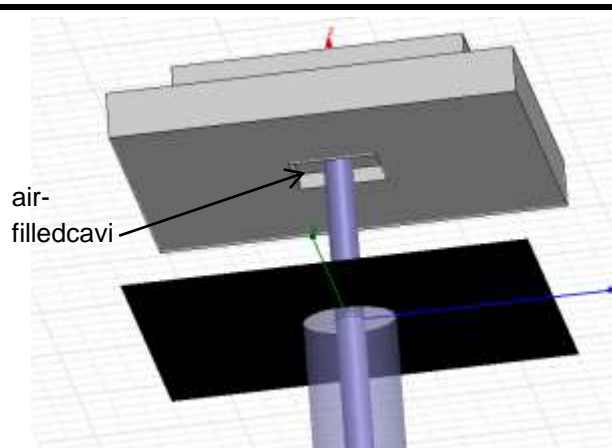


Fig.3: antenna in two layers after the insertion of an air-filled cavity in the lower substrate

Figs. 4a and 4b illustrate the distribution of the surface current at the patch of the antenna without air-filled cavity (Fig. a) and with air-filled cavity (Fig. b). These graphs show that the density of the current is greater in the second configuration at the center of the patch, which allows a greater radiation

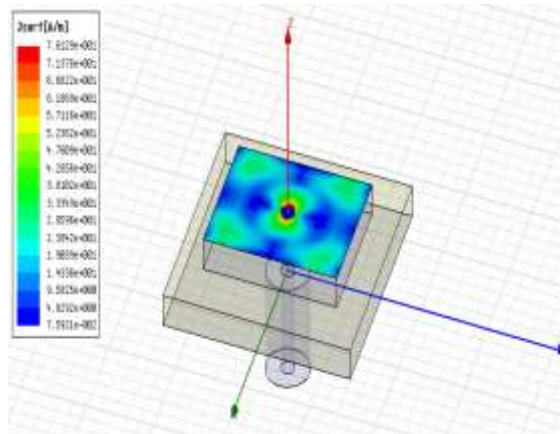


Fig. 4a : without air-filled cavity

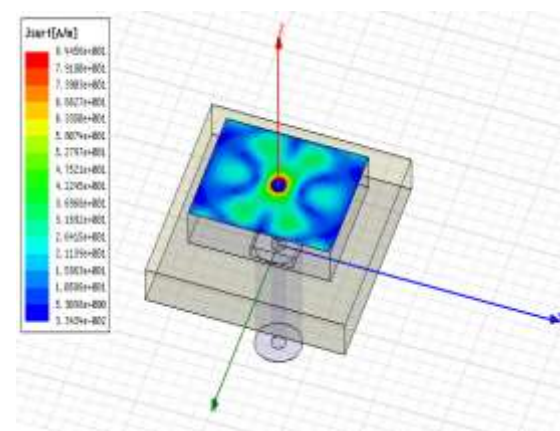


Fig. 4b : with air-filled cavity

Fig.4: Illustrates the distribution of the surface current at the patch of the antenna without cavity FIG. A and with cavity Fig. B for $L = 8$ mm, $W = 10$ mm and $\epsilon_r = 9.8$

Figs. 5 and 6 show the results obtained of the reflection coefficient S_{11} of the microstrip antenna in the K band for the two configurations of the antenna.

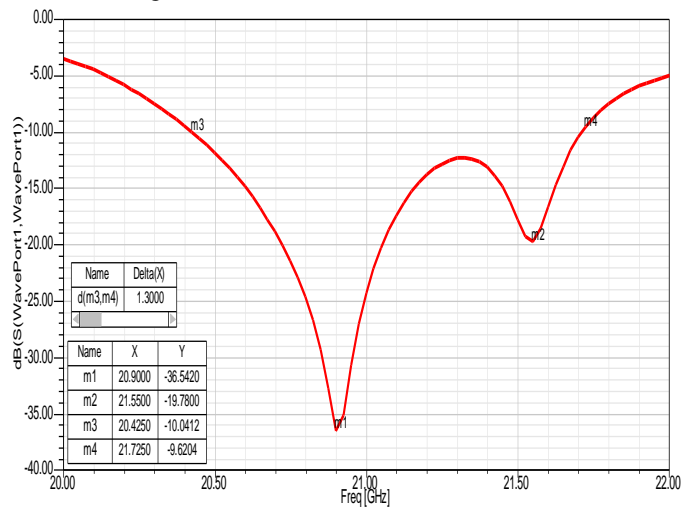


Fig.5: Reflection coefficient as a function of the frequency of the antenna with air-filled cavity for $L=8$ mm, $W=10$ mm and $\epsilon_r=9.8$

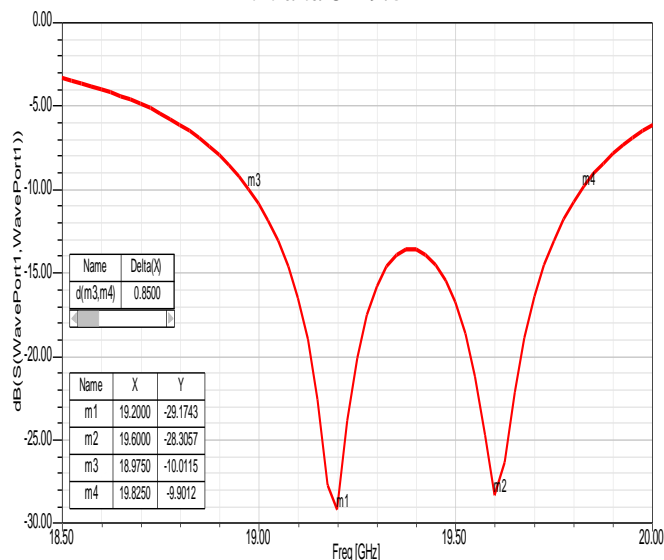


Fig.6: Reflection coefficient as a function of the frequency of the antenna with air-filled cavity for $L=8$ mm, $W=8$ mm and $\epsilon_r=11$

Figs. 7 and 8 show the gains of the microstrip antenna for $L = 8$ mm, $W = 10$ mm, $\epsilon_r = 9.8$ and for $L = 8$ mm, $W = 8$ mm, $\epsilon_r = 9.8$ respectively.

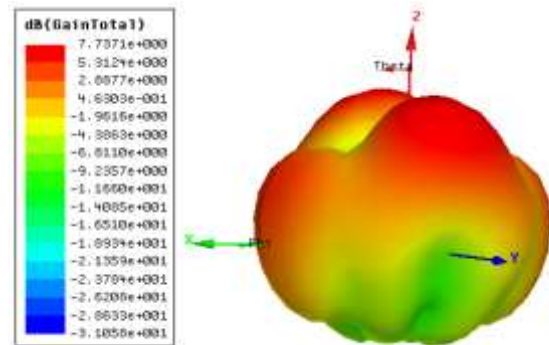


Fig.7: Gain of the microstrip antenna, for $L=8$ mm, $W=10$ mm $\epsilon_r=9.8$

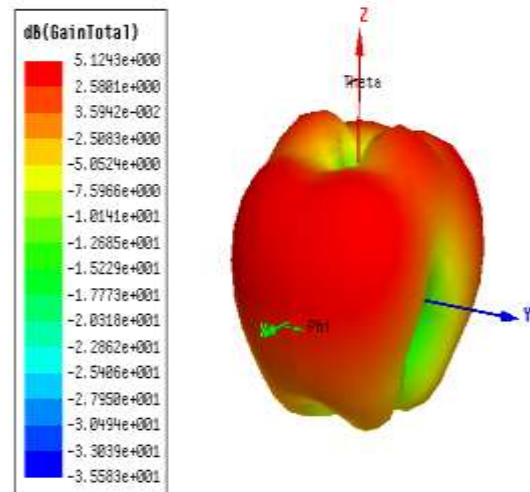


Fig.8: Gain of the microstrip antenna, for $L=8$ mm, $W=8$ mm $\epsilon_r=11.0$

Table 2 summarizes the results obtained from the simulation and those published for different dimensions of the microstrip antenna.

Table.2: Comparison between the published results of the characteristics of the antenna and those obtained

Physical Parameters	References	Resonant Frequency (GHz)	S_{11} (dB)	Bandwidth (MHz)	Gain Max(dB)
$L \times W = 8 \times 10 \text{mm}^2$ $\epsilon_r=9.8$	[2]	fr1=20.13	-26.00	830	3.50
		fr2=20.53	-29.00		
	Our work	fr1=20.85	-36.60	1300	7.73
		fr2=21.55	-19.80		
$L \times W = 8 \times 8 \text{mm}^2$ $\epsilon_r=11.0$	[13]	19.75	-18.75	250	2.80
	Our work	19.6	-28.30	900	5.12

The results obtained show that the resonant frequencies are included in the K band, as well as a clear improvement in the reflection coefficient, the bandwidth and the maximum gain.

II. CONCLUSION

In this paper, research has been presented on the miniaturization of the dimensions of the microstrip antenna, operating in the K band while improving these characteristics, namely the reflection coefficient S_{11} , bandwidth and gain. This improvement is due to the use of a second layer of the substrate and to the introduction of a cavity filled with air at the level of the lower substrate. The comparison of the results obtained with those published showed a great satisfaction, which will make it possible to encourage more the use of this type of antennas in the field of wireless telecommunications.

REFERENCES

- [1] Yahya S. H. Khraisat "Comparison between Rectangular and Triangular Patch Antennas Arrays" *applied Physics Research* Vol. 4, No. 2; 2012
- [2] M. HabibUllah "A Compact Wideband Antenna on Dielectric Material Substrate for K Band » *ELECTRONICS AND ELECTRICAL ENGINEERING* ISSN 1392 – 1215. No.7(123) 2012
- [3] M.hamdaouiJ.Foshi A. Roukhe "Expanding the Bandwidth of Rectangular Microstrip Antenna by Inserting a Slot" *International Journal of Advanced Engineering, Management and Science (IJAEMS)* ISSN : 2454-1311 ,Vol-2, Issue-8, Aug- 2016
- [4] J.-C. Iriarte, I. Ederria, and R. Gonzalo, "Design and characterisation of a high efficiency ceramic ebg patch antenna," *IET Microwave Antennas Propagation*, Vol. 4, No. 8, 2010, pp. 1056-1062.
- [5] M. Habib ULLAH, M. T. ISLAM, J. S. MANDEEP, N. MISRAN "Design and Analysis of A Multi Band Electrically Small Antenna" *PRZEGLĄD ELEKTROTECHNICZNY*, ISSN 0033-2097, R. 89 NR 1a/2013
- [6] Kula J.S., Psychoudakis D., Liao W.-J., Chen C.-C., Volakis J. L., Halloran J. W., Patch-antenna miniaturization using recently available ceramic substrates, *IEEE Antennas and Propagation Magazine*, 48 (2006), No. 6, 13-20.
- [7] Azim R., Islam M. T., Misran N., Mobashsher A. T., "Compact UWB planar antenna for broadband applications", *Informacije MIDEM*, vol 41, No.1, pp. 37-40,2011
- [8] Kai Xu Wang, Li Gao, HauWah Lai , Kwok Kan So, Hang Wong, QuanXue, Xiu Yin Zhang, "Multilayer Wide-Band Patch Antenna Using Lprobe and Structure", *High Speed Intelligent Communication Forum (HSIC)*, 4th International , 10-11 May 2012
- [9] SoufianLakrit Hassan Ammor « Conception et Simulation d'Antenne Rectangulaire Multicouches Pour Les Systèmes de Communication ULB » *MediterraneanTelecommunication Journal* Vol. 4, N° 2, October 2014
- [10] M. Samsuzzaman, M. T. Islam, "Dual band X shape Microstrip Patch Antenna for Satellite Applications" *The 4th International Conference on Electrical Engineering and Informatics (ICEEI 2013) Procedia Technology* 11(2013) 1223 – 1228
- [11] Theodore K. Anthony "Wafer Level Antenna Design at 20 GHz" *Army Research Laboratory Adelphi, MD 20783-1197 ARL-TR-4425* April 2008
- [12] A. S. Elmezughi, W. S. T. Rowe and R. B. Waterhouse, "Further investigations into edge-fed cavity backed patches", *Proc. IEEE. Ant. & Prop. Symp.,Honolulu, HI*, pp. 920 – 923, June 2007.
- [13] W. S. T. Rowe and R. B. Waterhouse, "Investigation of edge-fed cavity backed patches", *Proc. IEEE. Ant. & Prop. Symp.,Albuquerque, NM*, pp. 3967 – 3970, July 2006.

Analysis of High Temperature Monitoring Using Fiber Bragg Grating Sensor

Shruthi S.V¹, S. Sundaravadivelu²

Department of ECE, SSN College of Engineering, Chennai, India

Abstract— Measuring the temperature in high temperature industrial application is an important factor and a challenging part where sensors need to withstand high temperature without destruction. Temperature measurement and monitoring in the industries are necessary to ensure correct and accurate operation of the equipment. In these high temperature application conventional electronic sensors like thermocouple, bimetal switches etc cannot withstand high temperature, malfunction due to overheating and also easily pick up Electromagnetic Interference (EMI). In this paper these conventional sensors are replaced by Fiber Bragg Grating (FBG) sensors which is based on the principle of measurement of reflected Bragg's wavelength and the corresponding shift in the wavelength for the temperature sensed. Advantages of FBG sensors for temperature measurement is that its light weight, small size, flexibility, non interfering, low loss, long range sensing(remote sensing), multiplexing capabilities, withstands high temperature. In this paper the simulation of 2D and 3D model is done using the Comsol software and also the experiment is performed for FBG temperature sensors to depict the shift in Bragg's wavelength that can be used in high temperature monitoring in oil wells, high temperature optical sensing in gas turbines, widely used in nuclear reactors which has elevated temperature and high levels of electromagnetic interference (EMI).

Keywords— electromagnetic interference, Comsol software, Bragg's wavelength, Fiber Bragg grating sensor.

I. INTRODUCTION

Optical fiber based sensing technology have several inherent advantages that make them attractive for a wide range of industrial sensing applications. The conventional sensors like thermocouples, resistance temperature detectors, thermistors cannot be used in high temperature measurement owing to failure at high temperature, EMI coupling, and not appropriate to be used in high microwave fields[3]. The FBG sensors are typically small in size, passive, immune to EMI, resistant to harsh environments and have a capability to perform distributed sensing.

The Fiber Bragg Grating is optical fiber sensor that is created by photo inscribing the core of the silica fiber with the Ultra violet rays by the photomask method. There is a

periodic perturbations created in the core refractive index of the optical fiber created by exposure to intense UV radiation. The refractive index of the fiber is permanently altered according to the intensity of light it is exposed. The alteration in the refractive index depends on the photosensitivity of the fiber. The resulting periodic variation in the refractive index is called a fiber Bragg grating. The Fig. 1 shows the expanded view of FBG with the core of the fiber being inscribed and grating is produced with the period Λ .

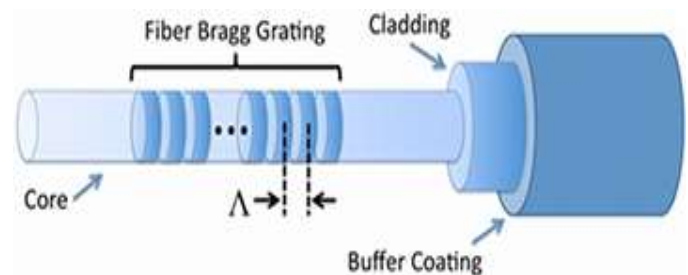


Fig.1 : An expanded view of Fiber Bragg Grating sensors.

The FBG sensors are made of germanium doped silica because of its high melting point 938.2 °C and 1600 °C respectively to withstand high temperature. The FBG reflects a particular wavelength called the Bragg's wavelength and transmits all other wavelength in a broadband source. This property of reflecting the Bragg's wavelength paves way for sensing applications using FBG. The reflected Bragg's wavelength is given as

$$\lambda_b = 2 \times n \times \Lambda \quad (1)$$

In the equation (1) λ_b indicates the Bragg's wavelength and n for refractive index and Λ is the grating period. The sensing function of an FBG originates from the sensitivity of both the refractive index of the optical fiber and the grating period within the fiber to externally applied mechanical or thermal perturbations. When an external physical parameter like temperature is applied to the FBG there is a shift in the reflected Bragg's wavelength[3]. Based on the shift the amount of variation in the temperature is obtained. In this way the temperature can be monitored and measured regularly in high temperature sensitive regions. The FBG can measure high temperature as 1000 degree Celsius due to the characteristics of the fiber

material[3]. The shift in the wavelength can be measured from the following equation:

$$\Delta\lambda_b = \lambda_b (1 + \xi) \Delta T \tag{2}$$

The equation (2) λ_b is the Bragg wavelength, ξ is the fiber thermo-optic coefficient, ΔT is temperature change and $\Delta\lambda_b$ is the change in the Bragg's wavelength.

1.1 Design of 2D and 3D models

A 2D model of a furnace in rectangle shape is modeled where the length is 0.6m and breadth 0.2m. The aluminum material is assigned to the model due to its high thermal conductivity. The temperature is assigned at one side of the model which is conducted throughout. The probe points are placed at three different places and the temperature is measured.

Similarly a 3D model is designed with the length 4m, breadth 1m and height 1m. The temperature is assigned to one face of the cube and the edge probes are used to measure the temperature.

1.2 Experiment To Determine Bragg's Wavelength Shift

In the model created using Comsol the temperature is measured using the probe points at different places. These probe points are replaced by the FBG sensors measuring the same temperature that was given in Comsol. If conventional sensors are used at that points it cannot withstand high temperature.

The Fig. 2 shows the block diagram of FBG temperature measurement. Broadband light source is given to the FBG using superluminescent light emitting diode(SLED). The light passes via the port 1 and 2 of circulator to the FBG pasted on the HOTPLATE. All the connections are made using the fiber pigtailed. The FBG reflects the Bragg's wavelength which is obtained at the IMON via port 3 of the circulator and then the IMON to the laptop using USB. The temperature of the hot plate is increased in steps and the corresponding shift in the wavelength is noted in IMON software in the laptop.

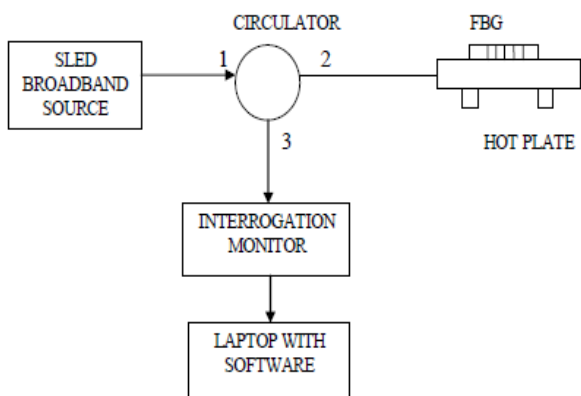


Fig. 2: Block diagram of FBG temperature measurement.

II. HIGH TEMPERATURE MONITORING

2.1 Simulation of 2D and 3D models

The Fig. 3 shows the 2D model for the temperature measurement. The temperature is given at one side of the model which traverses along based on the conductivity of the material. The blue line on the left side indicates the temperature assigned. The Fig. 4 shows the time dependent study is done for the model and the heat is transferred along the model which is shown in different shades.

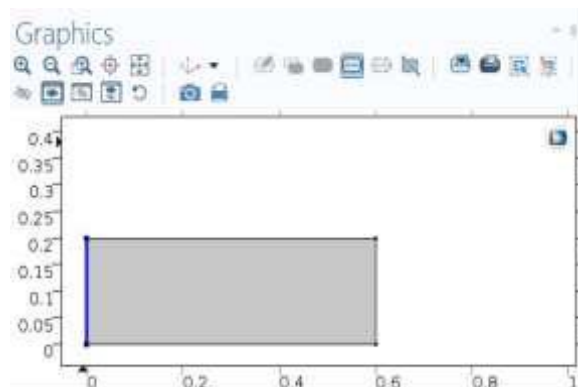


Fig. 3: The 2D model designed using Comsol

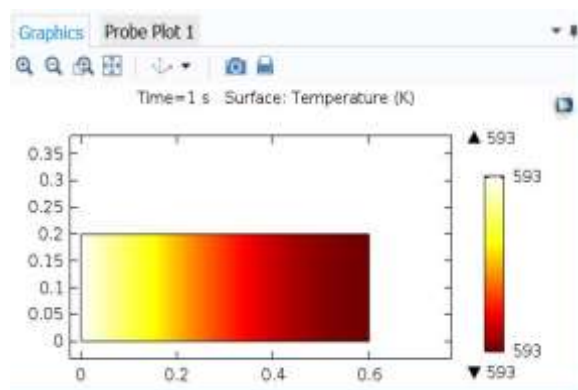


Fig. 4 : The heat transfer along the model

The Fig. 5 shows the 3D model for the temperature measurement where the aluminum is assigned to the entire block and the temperature is assigned to one face of the block which is indicated with blue shade. The Fig. 6 shows the heat transfer in 3D model when a time dependent study is performed in Comsol.

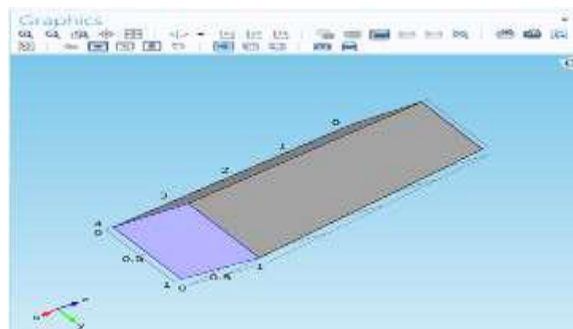


Fig. 5: The 3D model using Comsol

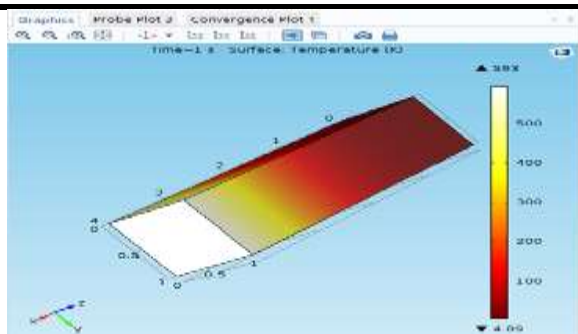


Fig. 6: The heat transfer in the 3D model

2.2 Sensor Location And Temperature Monitoring Waveform For 2D Model

The sensors are placed at three different places to measure the heat transfer. The figures at the top of Fig. 7 shows that the domain probe points placed at the three different places in the model. The probe points are used to measure the temperature at different instants. The bottom part of the figure depicts the respective waveforms or temperature measured for the probe points in the figure. Different temperature values like 300 °C or 573.15 K, 500 °C or 773.15 K is given and measured.

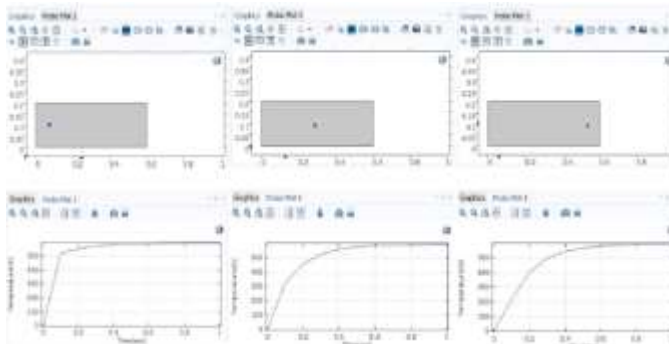


Fig. 7: Domain probe points placement and respective temperature (573.15 K) measured waveforms

The Fig. 8 shows the all the three waveforms of the probe points plotted in the same the same plot. The plots here are temperature (K) versus Time (sec). The blue, green and red lines indicates the waveforms of first, second and third probe points respectively. The difference in the waveforms for same temperature throughout is due to distance from the source of temperature to the probe points. These probe points are replaced by the FBG sensors rather than the conventional sensors.

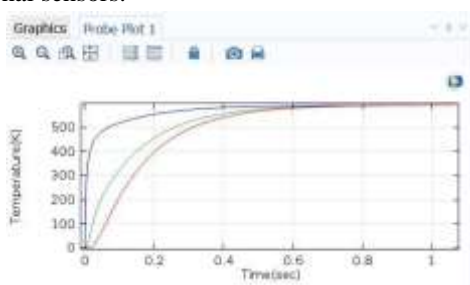


Fig. 8: Waveform for all the three probe points

2.3 Sensor Location And Temperature Monitoring Waveform For 3Dmodel

The Fig. 9 shows the domain boundary probe points to measure the temperature given at the one face of the model. The probe is kept at the boundary of the sides of the 3D model designed.

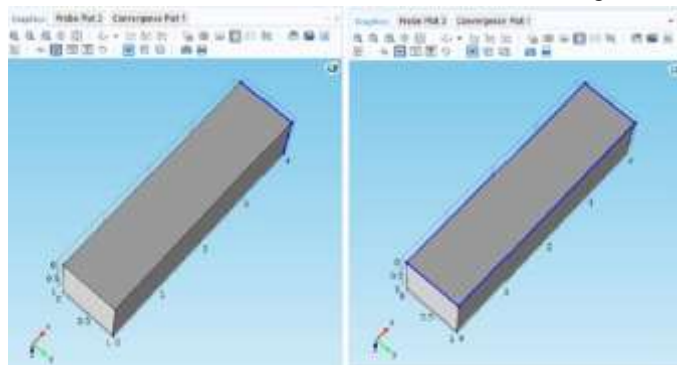


Fig. 9: The domain boundary edge probe points assignment

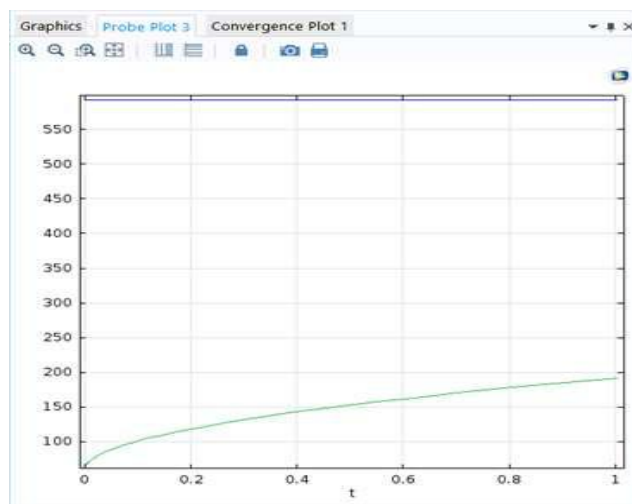


Fig. 10: Plot for temperature (573 K) measurement

The Fig. 10 shows the time dependent study made for the 3D model and also the waveforms for temperature measured using the boundary domain probe points. The temperature of 573 (K) is given and plots are obtained. The first picture gives the heat transfer in the 3D model where it gradually reaches the end. The waveforms are temperature (K) versus time (sec). The two plotted line indicates the measured values at the instant of the boundary probes. As the heat traverses through the model gradually, the waveforms obtained is also different based on the placement of the probes. The probes at the edge face measure less due to low heat reached at the end.

III. EXPERIMENTAL SETUP

The Fig. 11 depicts the practical experimental setup performed at IIT MADRAS of the FBG sensor to measure the temperature which is given as the perturbation to the

FBG. The temperature to FBG placed on the ceramic hotplate is measured by increasing in steps.



Fig. 11: Experimental setup for temperature monitoring

3.1 Experimental Results

When the experiment is performed as shown in the Fig. 11, there is an external perturbation i.e. the temperature to the FBG given by the ceramic hotplate over which the FBG is placed. The range of the hotplate is 40-500 °C. The temperature is increased in the hotplate in steps and readings are taken. The wavelength shift in the Bragg's wavelength is noted in the IMON evaluation software in the laptop.

The initial reflected Bragg's wavelength is 1551.54 nm. The Fig. 12 shows the example of reflected wavelength for temperature of 340 °C that is obtained in the IMON software and there is a shift noted in the wavelength which is 1555.0 nm.



Fig. 12: Example waveform for 340 °C in IMON software

These values i.e. the readings obtained for the different wavelength shift due to temperature change in the IMON software is tabulated in the excel sheet. For each temperature increase the readings are tabulated. The tabulation includes the wavelength shift and the power in pixel. Then these counts are converted into power in watts using MATLAB and the plot for power (watts) versus wavelength (nm).

The Fig. 13 shows the waveform for the initial reflected Bragg's wavelength when no temperature is given to the FBG and it is at 1551.43 nm. Only the input broadband light source is present in the fiber.

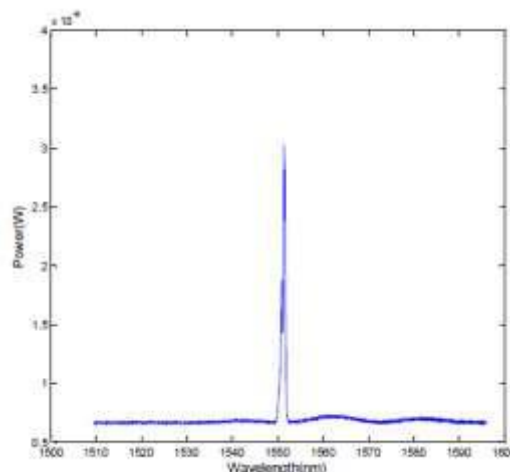


Fig. 13 : The reflected FBG spectrum .

The Fig. 14 depicts the wavelength shift plotted for 43.5°C from initial 0°C and its shifted to 1551.60 nm. The plot is done for power (watts) versus wavelength (nm).

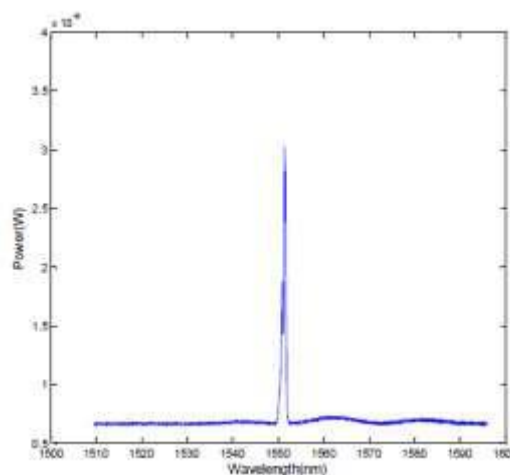


Fig. 14: The wavelength shift at 43.5°C

Similarly Fig. 15 depicts the wavelength shift for 500°C and it is 1557.0 nm. Now from initial reflected Bragg's wavelength 1551.43 nm has shifted to 1557.0 nm

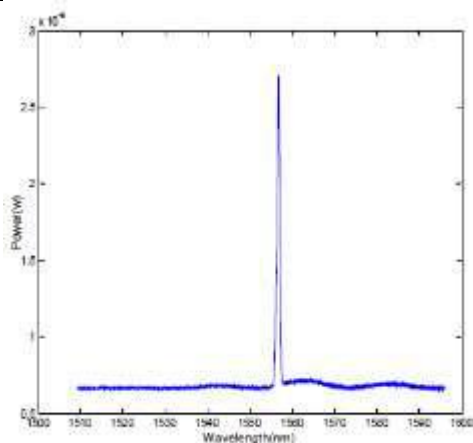


Fig. 15. The wavelength shift at 500°C

The Table I shows the tabulated values for different temperature raised in steps and the respective wavelength shift of the reflected spectrum that is noted in the IMON evaluation software and the readings are also plotted in MATLAB, which is shown in Fig. 15.

TABLE I. Tabulation For Temperature And Wavelength

Temperatur e(°C)	Wavelengt h(nm)	Temperatur e(°C)	Wavelengt h(nm)
0	1551.43	320	1555.0
108.8	1552.40	370	1555.54
151.2	1552.81	420	1556.06
212.1	1553.50	460	1556.00
270.5	1554.36	500	1557.00

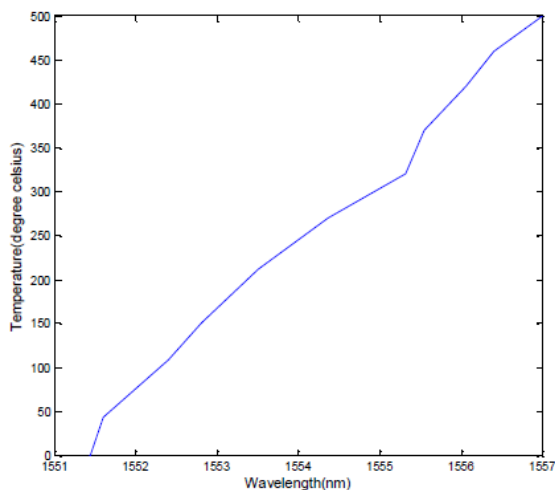


Fig. 15: Plot for temperature (°C) versus wavelength (nm)

From the Fig. 15, it can be inferred that the wavelength shifts linearly with the temperature as it is increased. The temperature is increased in steps to obtain the variations and increase in the reflected Bragg’s wavelength. The stability of FBG to high temperature can also be analyzed.

IV. CONCLUSION

A temperature sensor based on Fiber Bragg gratings is analyzed both theoretically via simulations and experimentally. The response of the grating to changes in temperature is very linear and this makes the FBG a rugged device for sensing applications. Here the experiment is performed to measure temperature is up to 500°C using the FBG. If the conventional sensors like resistance temperature detectors ,bimetal switches and thermistors are used, it will malfunction at 150°C[1] causing instability in the measurement of the temperature at high sensitive areas where temperature needs to be monitored regularly. The fragile nature and its small size with stable characteristics have helped to sense temperature in sensitive region. These FBG’s can replace conventional sensors in remote applications like oil wells, nuclear reactors, boilers etc...withstanding high temperature range.

REFERENCES

- [1] Grzegorz Fusiek, Pawel Niewczas, James R. McDonald, “Design of a highly accurate optical sensor system for pressure and temperature monitoring in oil wells”, IEEE Sensors Journal, Vol. 12, No. 1, January 2009.
- [2] Stephen J. Mihailov , “ Fiber Bragg Grating Sensors for Harsh Environments” , Sensors 2012, 12, 1898-1918.
- [3] Ogério M. Cazo, Carmem L.Barbosa, HaroldoT. Hattori,Renato C.Rabelo,Osni Lisbôa, Jorge L. S. Ferreira, “Fiber Bragg Grating Temperature Sensor ” , Sensors 2009, 9, 8377-8381.
- [4] Yun-jiang Rao, David J. Webb, David A. Jackson, Lin Zhang, and I. Bennion, “In-Fiber Bragg-Grating Temperature Sensor System for Medical Applications”, Journal Of Lightwave Technology, Vol. 15, No. 5, May 1997.
- [5] David Barrera, Vittoria Finazzi, Joel Villatoro, “Packaged Optical Sensors Based on Regenerated Fiber Bragg Gratings for High Temperature Applications” , IEEE Sensors Journal, Vol. 12, No. 1, January 2012.
- [6] S. Gingras, C. Hudon, C. Guddemi, paper titled as ‘Rotor Temperature Monitoring Using Fiber Bragg Grating Sensors’ Sensors 2011, 12, 1880- 1886

Strain Measurement Using Fiber Bragg Granting Sensor for Crack Detection

K. Vinnarasi¹, Dr. S. Sundaravadivelu²

Dept. of ECE, SSN College of Engineering, Chennai, India

Abstract—In this paper the wavelength shift due to strain is measured by using Fiber Bragg Grating sensors. Structural health monitoring is the emerging field where it involves monitoring of several physical parameters. Strain measurement is one of the most external parameter to be measured in various sensing applications. The conventional strain sensors used to measure strain has many disadvantages in terms of low stability, not immune to Electromagnetic Interference (EMI) and other external factors. The Fiber Bragg Grating Sensors has replaced the sensor like strain gauge in various remote applications. The work is centered on fiber optic Bragg grating (FBG) sensors, to detect strains with the wavelength shift that is observed due to the physical perturbation. This kind of strain analysis can be used to monitor strain in complex structures and in remote applications.

Keywords— *Fiber Bragg grating sensor strain measurement, structural health monitoring, Comsol software.*

I. INTRODUCTION

Fiber-optic communication industries have significantly reduced optical component prices and improved quality.[1]FBG sensors introduce a great number of advantages. They allow to obtain absolute measures obtained analyzing the Bragg wavelength shift induced by the measured parameters. The production costs are very low, making this family of sensors competitive also in the comparisons of the electrical strain gauges.

Fiber Bragg grating strain sensors does not break at any case of cracks. Using Comsol software a 2-D and 3-D model for crack detection was designed. Strain is developed by the pressure wave produced due to crack. So the concrete material is to be used for simulation process. This paper uses a FBG sensor that works based on shift in Bragg wavelength due to strain. Instead of sensing strain is to be sensed.

1.1 DESIGN

To create the 2D model using COMSOL. To measure the strain using probe points for detecting the crack in concrete. In real time applications the probe points are replaced by the fiber Bragg grating (FBG) sensors. The whole block was

assigned the concrete material, which are in the Comsol material library.

1.2 EXPERIMENTAL SETUP TO DETERMINE BRAGG WAVELENGTH SHIFT

The connection of experimental procedure for strain measurement using SLED broad band light source, IMON, circulator and laptop with software. The broadband light that is sent to the FBG reflects a particular wavelength called the Bragg's wavelength. This reflected wavelength reaches the IMON via the third port of the circulator. Then the reflected wavelength is noted in the IMON evaluation software. Now when the voltage is given to the PZT is increased in step which in turn produces the corresponding strain due to the stretching of PZT test bed. The strain produced is sensed by the FBG sensor. Due to the physical perturbation produced due to strain in the FBG, the wavelength that was reflected shifts accordingly. The shifted wavelength can be measured and based on which the strain produced can be measured.

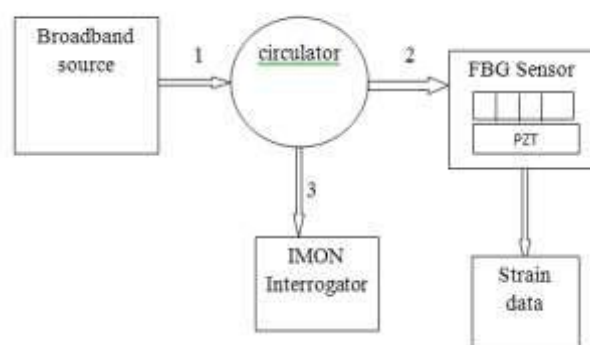


Fig. 1: Experimental setup for determination of Bragg wavelength shift.

II. CRACK DETECTION

2.1 SIMULATION-2D MODEL

Specifications for simulation using Comsol software:

- The Input (pressure) waveform shown in Fig. 5 was taken.
- The simulation done at time dependent study.
- Sensors location shown in Fig. 3 and 4 shown the strain creation.

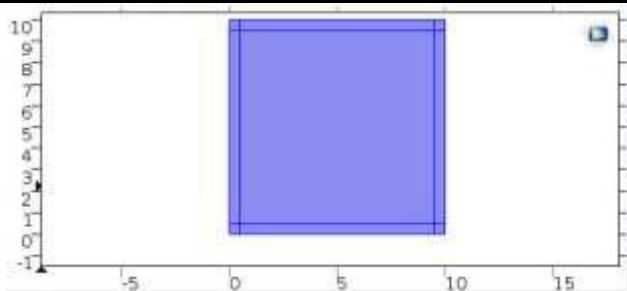


Fig.2: 2D model - concrete material assigned.

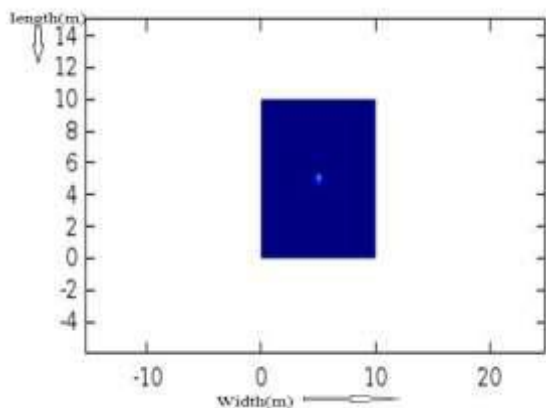


Fig. 3: Strain creation of single point source

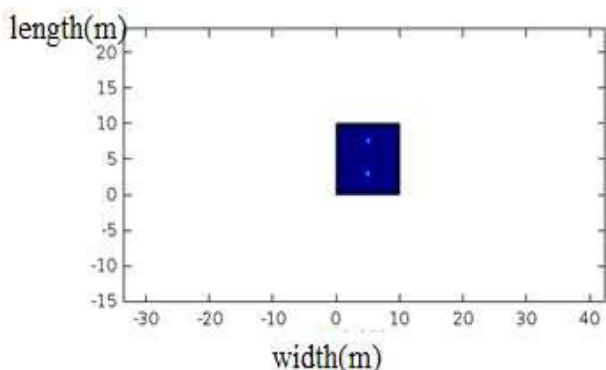


Fig. 4: Source at different point.

2.2 INPUT WAVEFORM

The crack detection occurs due to the creation of strain . The pressure waveforms nature is a sudden rise and then an exponential decay. In this simulation part we have used the input pulse given below.



Fig. 5: 2D Input (pressure) waveform

Mathematical representation of
 Input wave form= $A t * e^{-B t} * \sin(2\pi * f) t$

2.1.1 Strain plot for single point load

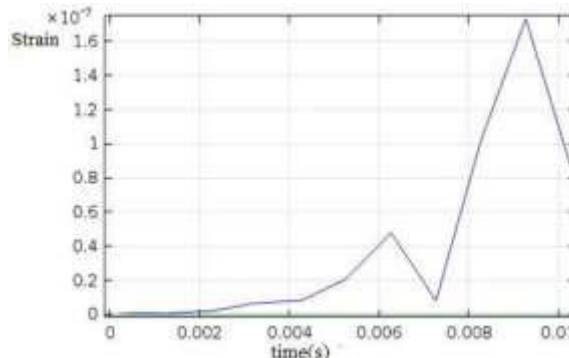


Fig.6: Strain plot for single point load using edge point probe.

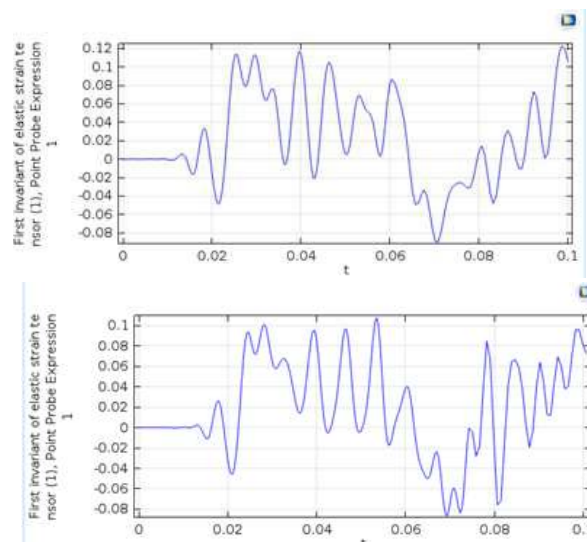
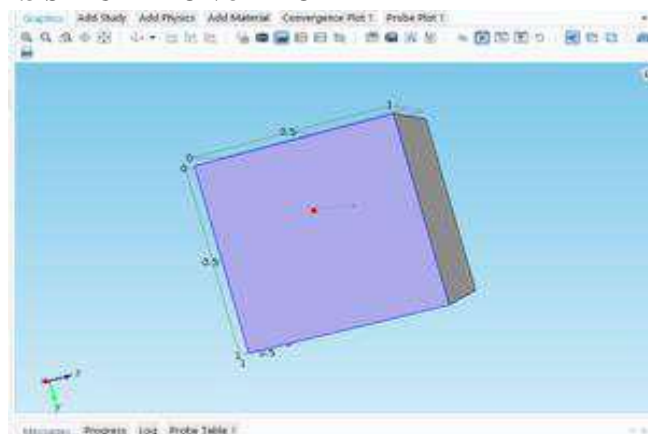


Fig. 7: Strain plot for different point load using edge point probe.

2.3 SIMULATION-3D MODEL



The fig. 8 shows the simple model for 3D using Comsol. Concrete material is to be assigned for the full block. It shows all the three dimension view with different dimensions for length, width, and height.

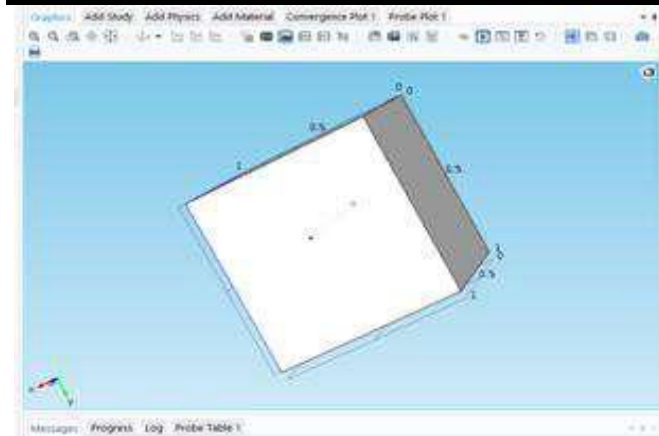


Fig. 8: Different Point load

The fig.9 and 4B shows the different point loads at the different directions X, Y,Z and the probes are fixed the edges using edge point probes.

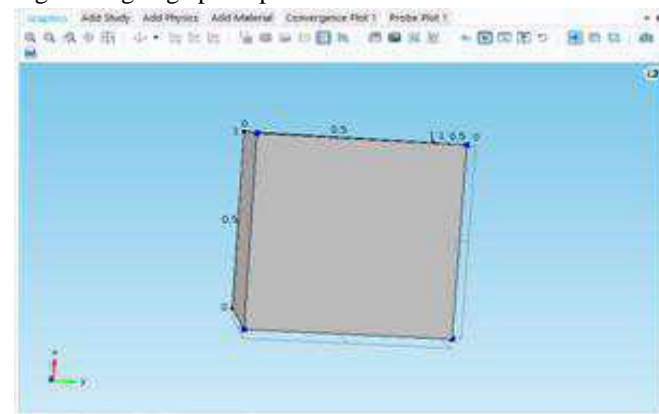


Fig. 9: Placed Edge point probe

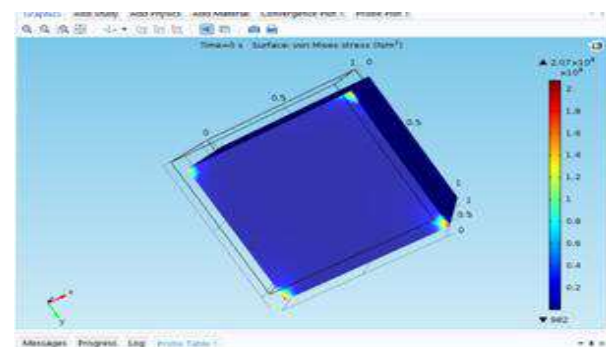


Fig. 10: strain creation-3Dmodel

This fig.10 shows the time dependent study for strain created, using 3D model..

2.4 STRAIN PLOT FOR DIFFERENT POINT LOAD FOR 3D MODEL

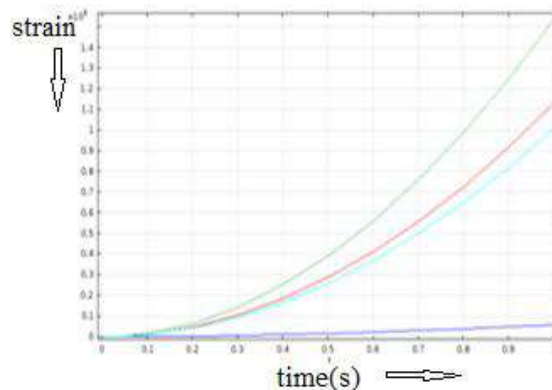


Fig.11: Strain plot for 3Dmodel.

The output waveform is produced. The value of the strain decreased at the particular point using the probe points. So only the real time applications the probe points are replaced by the Fiber Bragg Grating (FBG) sensors.

III. EXPERIMENTAL SETUP

As per the fig. 12 shows the connection of experimental procedure for strain measurement using SLED broad band light source, IMON, circulator and laptop with software.



Fig. 12 : Experimental setup at IIT, Madras

For this experimental setup, the wavelength will shift in accordance to the strain done at IIT, Madras. The voltage value is varied in the steps of 3volts up to 30 volts. This variation in the voltage creates a strain which is in linear with the voltage applied to the PZT stretcher. Now when the voltage is given to the PZT is increased in step which in turn produces the corresponding strain due to the stretching of PZT test bed. The strain produced is sensed by the FBG sensor



Fig. 13: Bragg wavelength at zero strain in IMON evaluation software.

The fig. 13 shows the waveform obtained for the FBG reflected spectrum obtained from the FBG sensor which is noticed in the IMON evaluation software.

F.BRAGG WAVELENGTH AND POWER

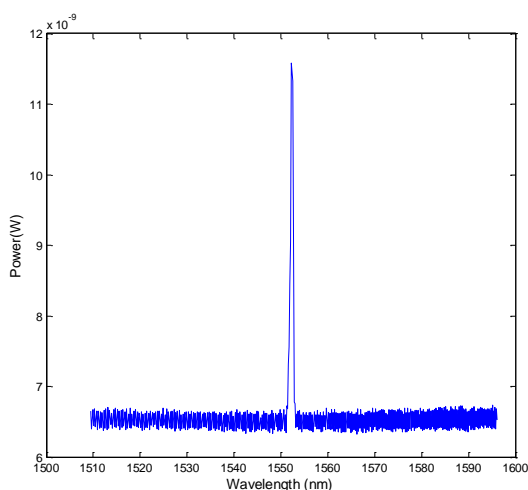


Fig. 14: FBG reflected spectrum without strain:

This fig. 14 shows the reflected spectrum without strain. The values are taken from IMON (Interrogator Monitor). It is interfaced using the Ethernet cables with the laptop with software. The concern pixel, wavelength values are saved in excel data sheet. Then each values are converted using MATLAB.

The fig: 5.13 shows the FBG reflected spectrum for the strain value of 0.348. The wavelength of the strain shifted from 1550nm in to 1552.3nm. the difference between the values of the 0 to 0.348 $\mu\epsilon$ is 2.3 $\mu\epsilon$.

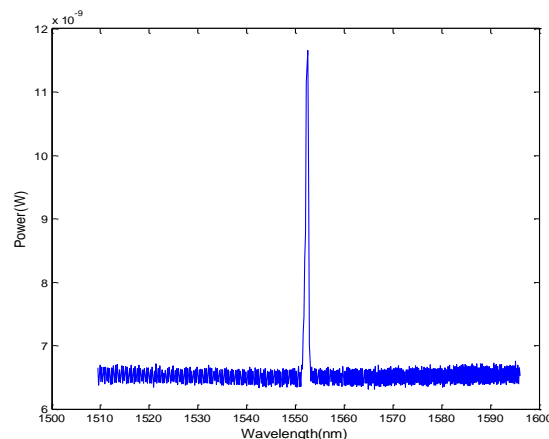


Fig.15: FBG reflected spectrum for 0.348 $\mu\epsilon$

The fig. 15 shows the FBG reflected spectrum for the strain value of 1.392 $\mu\epsilon$. The wavelength of the strain shifted from 1552.3 in to 1552.35nm. The difference between the values of the 0.348 $\mu\epsilon$ to 1.392 $\mu\epsilon$ is 0.05 $\mu\epsilon$.

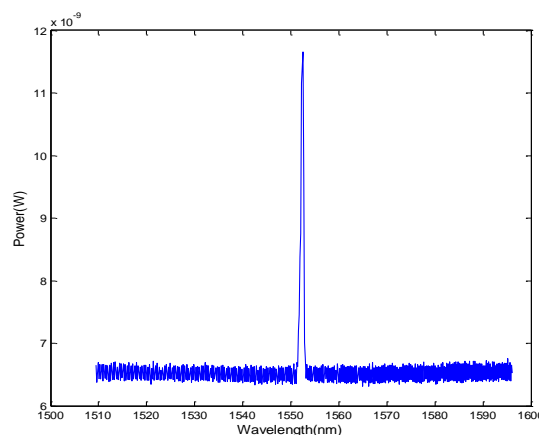


Fig.16: FBG reflected spectrum for 1.392 $\mu\epsilon$

The fig. 16 shows the FBG reflected spectrum for the strain value of 2.436. The wavelength of the strain shifted from 1552.35nm to 1552.50nm. The shift difference between the values of 1.392 $\mu\epsilon$ to 2.436 $\mu\epsilon$ is 0.15 $\mu\epsilon$.

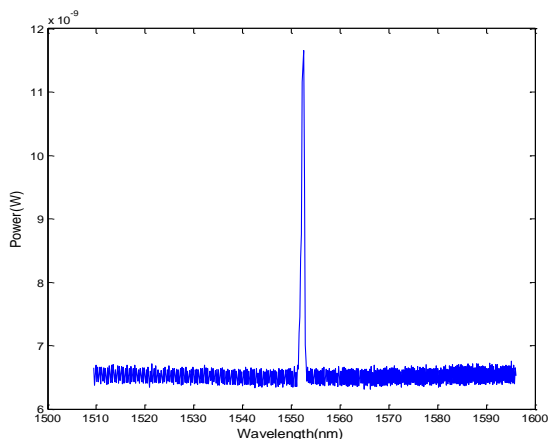


Fig.17.:FBG Reflected spectrum for maximum strain

The fig. 17 shows the FBG reflected spectrum for the strain value of 2.436. The wavelength of the strain shifted from 1552.35nm to 1552.50nm. The shift difference between the values of 1.392 $\mu\epsilon$ to 2.436 $\mu\epsilon$ is 0.15 $\mu\epsilon$.

Table I. Tabulation Of Strain Vs Wavelength

S.NO	STRAIN VALUES ($\mu\epsilon$)	WAVELENGTH(nm)
1.	0.348	1552.0
2.	1.392	1552.30
3.	2.436	1552.46
4.	3.48	1552.50
5.	1.5	1552.60

The tabulation shows the plot of strain versus wavelength. The values are obtained from IMON. The power versus wavelength values are taken and then the values are converted in to strain. From this conversion the minimum value of zero and maximum value of wavelength shift has to be calculated.

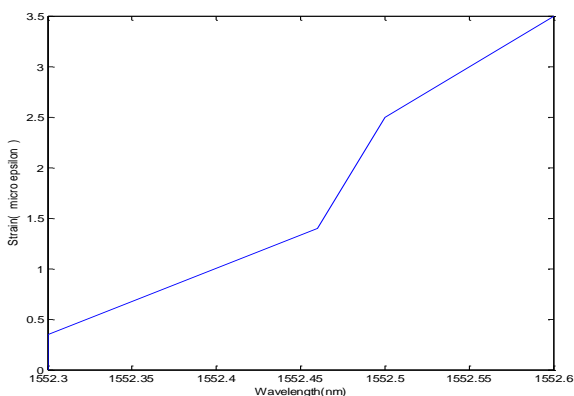


Fig. 18: Bragg wavelength at maximum strain

To plot the graph using the values of strain and wavelength (nm). The wavelength shift for the strain values varies very

minute. So the Fiber Bragg Grating sensors are stable at maximum strain compare to the probe points and other conventional sensors.

IV. CONCLUSION

Bragg wavelength shift for zero strain and maximum strain was observed. From this result it is clear that we can fix the threshold strain level for safety of avoid the crack in buildings. I have measured the wavelength shift for different strain values increased in steps using FBG sensor. The shift in the wavelength from 1552.00nm to 1552.60nm for the corresponding strain values from 0.348 $\mu\epsilon$ to 1.5 $\mu\epsilon$. From the graph it can be inferred that the wavelength shift varies proportionally to that of the strain.

REFERENCES

- [1] Abdelfateh Kerrouche, J. Leighton, W. J. O. Boyle, Y. M. Gebremichael, TongSun, K.T.V. Grattan, and B.Talijsten, "Strain Measurement on a Rail Bridge Loaded to Failure Using a Fiber Bragg Grating-Based Distributed Sensor System," IEEE Sensors Journal, VOL. 8, NO. 12, DECEMBER 2008.
- [2] Fan Yang, Dawei He, Tao Wang, Yongsheng Wang, "The Real-Time Safety Monitoring of Railway Condition by FBG Sensor," IEEE Sensors Journal Vol. 15, No.6; pp. 3390 – 3394 June 2015.
- [3] G. Pereira, L. Mikkelsen and M. McGugan, "Crack Growth Monitoring by Embedded Optical Fiber Bragg Grating Sensors Fiber Reinforced Plastic Crack Growing Detection," IEEE Transactions on Dielectrics and Electrical Insulation Vol. 21, No.1; February 2014.
- [4] Li Zhiquan, Wu Zhaoxia and Yan Dongmei, "Bridge Structure Monitoring System Based on Practical FBG" IEEE Sensors Journal, VOL. 14, NO. 8, AUGUST 2014.
- [5] M. Iodice, V. Striano, G. Cappuccino, A. Palumbo and G. Cocorullo, "Fiber Bragg grating sensors based system for strain measurements," optical Fiber Technology, Vol. 9, No. 2, pp. 57–79, 2003.

A Novel Study of Semiconductor Material as a Substrate Layer for Microstrip Patch Antenna

Praveen Kumar E¹, Sundaravadivelu S²

¹Department of ECE, SSN College of Engineering, Chennai, India

²Professor, Department of ECE, SSN College of Engineering, Chennai, India

Abstract— This paper describes about the solarcell antenna which is an integrated device used for trans-receiving the RF signal and generates DC voltage simultaneously. Solarcell Antenna consists of Microstrip patch antenna and Solarcells, during integration various parameters of antenna such as substrate (dielectric materials used), shape of the patch, dimensions of feed are to be obtained for desired frequency range. Different shapes of patches, dielectric materials are taken into account and compared with the results in which Microstrip Patch model suits the best for 2.4GHz frequency. We have integrated Solarcells and Microstrip patch antenna using CST Microwave studio software so that it can act as stand-alone system in remote places for various applications such as disaster alert system, moving vehicles, remote sensing, and meteorological surveillance.

Keywords— Solarcell antenna, Microstrip patch antenna, Solarcells..

I. INTRODUCTION

Electrical energy is used as a source requirement for the use and operation of wireless communication. Applications like environmental monitoring system, remote sensing and disaster alert system, needs a net-independent power supply which is preferably reliable by use of renewable energy i.e., photovoltaic cell, an advanced technology distinguished by reliability, longevity and eco-friendliness [1]. Besides that antennas requires to receive or transmit electromagnetic waves. Solar cell generator or photovoltaic cells and antenna are individual devices. Integrating them into a single system produces more compactness by reducing the space, cost and also acts as stand-alone system which has higher radiation energy. Even one solar cell can be used for the conversion of solar radiation to produce electrical energy. The electrically conductive contacts of the solarcell are simultaneously used as an antenna for transmission or reception of electromagnetic waves [2]. In this, solar cell is sandwiched between the platforms of radiating patch and ground plane.

II. USAGE OF PHOTOVOLTAIC CELLS IN MICROSTRIP PATCH ANTENNA DESIGNS

2.1 Equivalent circuit of Microstrip Patch and Solarcell Antenna

In order to provide higher gain and efficiency, the substrate material used in Microstrip patch antenna should be lossless as possible. Numerous measurements have shown, in that RF point of view the solarcell and Microstrip patch antenna are nearly to be equal. The equivalent circuit comparison of Microstrip patch antenna and Solarcell are represented in the figure 1.

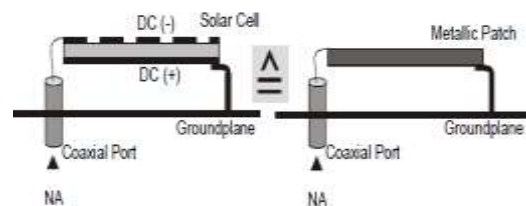


Fig. 1: Equivalent circuit of Microstrip patch antenna and Solarcell

To know whether the dielectric layer (insulator) of Microstrip patch antenna can be replaced by solarcells (semi-conductor) detailed study is done. The electromagnetic interference and back-off current from solarcells into feed of the antenna can be avoided by common ground [3], [4]. Insulation layer is added between solarcells and patch such that the above mentioned problems can be neglected [5], [6].

2.2 Design for Microstrip patch antenna

2.2.1 Rectangular Patch Antenna: The 2-D view of Rectangular Microstrip patch antenna is shown in the figure 2. To determine the width (W) and length (L) of the Rectangular Microstrip patch antenna [7], [8], we can directly substitute the resonant frequency (f_r), height of the substrate (h), and substrate dielectric constant (ϵ_r) values into the equation (1). The width (W) of the Rectangular Microstrip patch antenna is obtained.

$$W = \frac{C}{2f_r \sqrt{\frac{\epsilon_r + 1}{2}}} \quad (1)$$

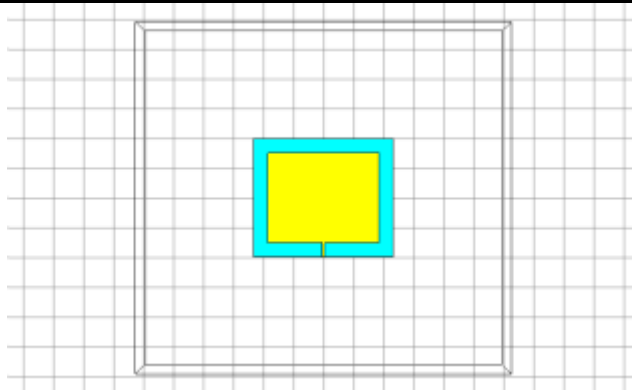


Fig. 2: 2-D view of Rectangular Microstrip patch antenna

Length (L) of Rectangular Microstrip patch antenna can be found by substituting the width (W), resonant frequency (f_r), height of the substrate (h), substrate dielectric constant (ϵ_r) values into the equation (2) to get effective dielectric constant (ϵ_{eff}) which is determined as:

$$\epsilon_{eff} = \frac{\epsilon_r + 1}{2} + \frac{\epsilon_r - 1}{2} \left[1 + 12 \frac{h}{W} \right]^{-2} \quad (2)$$

and equation (3) gives effective length (L_{eff}),

$$L_{eff} = \frac{C}{2f_r \sqrt{\epsilon_{eff}}} \quad (3)$$

Further substituting in equation (4) we get the extended length (ΔL).

$$\Delta L = 0.412h \frac{(\epsilon_{reff} + 0.3) \left(\frac{W}{h} + 0.264 \right)}{(\epsilon_{reff} - 0.3) \left(\frac{W}{h} + 0.8 \right)} \quad (4)$$

Henceforth, the actual length of the Rectangular Microstrip patch antenna is

$$L = L_{eff} - 2\Delta L \quad (5)$$

Further optimization is done in dimensions of patch to produce better performance.

2.2.2 Circular Patch Antenna: The 2-D view of Circular Microstrip patch antenna is represented in the figure 3. The area (a) of Circular Microstrip patch antenna is obtained by substituting the resonant frequency (f_r), height of the substrate (h), and substrate dielectric constant (ϵ_r) values into equation (6),

$$a = \frac{f}{\left\{ 1 + \frac{2h}{\pi \epsilon_r f} \left[\ln \left(\frac{\pi f}{2h} \right) + 1.7726 \right] \right\}^{\frac{1}{2}}} \quad (6)$$

Effective Area (a_e) can be determined using equation (7)

$$a_e = a \left\{ 1 + \frac{2h}{\pi \epsilon_r a} \left[\ln \left(\frac{\pi a}{2h} \right) + 1.7726 \right] \right\}^{\frac{1}{2}} \quad (7)$$

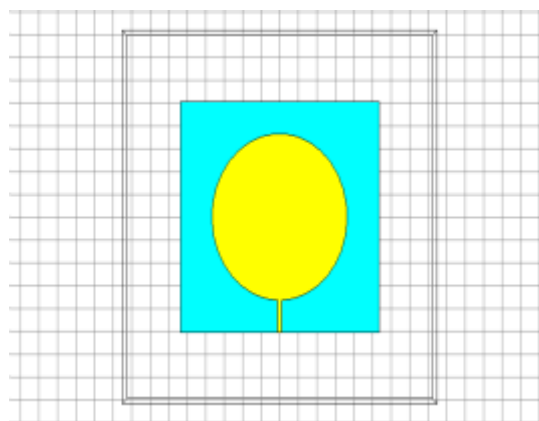


Fig. 3: 2-D view of Circular Microstrip patch antenna

Substituting effective area (a_e) value in equation (8), we get the area of the circle which is further more optimized in

$$f_r = 1.8412 \times \frac{C}{2\pi a_e \sqrt{\epsilon_r}} \quad (8)$$

dimensions of the patch to yield high performance characteristics of the antenna [6].

2.2.3 Square Patch Antenna: The area (a) of the square patch is determined by considering rectangular microstrip patch antenna width (square - all sides are equal, rectangle-opposite sides are equal so $W=a$). Substituting the known resonant frequency (f_r), substrate dielectric constant (ϵ_r), height of the substrate (h) into equation (1) to get the area of Square Microstrip patch antenna which is further more optimized for its dimensions to get better antenna performance[7], [8]. The 2-dimensional view of the Square Microstrip patch antenna is represented in the fig. 4.

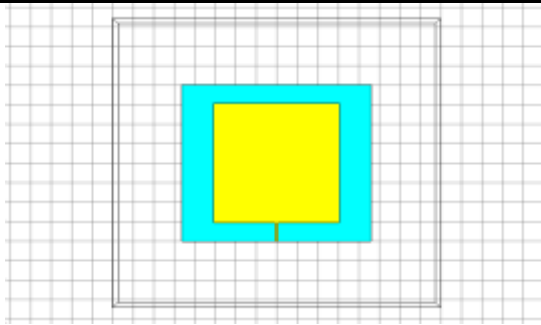


Fig. 4: 2-dimensional view of Square Microstrip patch antenna

III. SUBSTARTE SPECIFICATION

Multilayered substrate is considered to perform both RF and DC production simultaneously. A solarcells or Photovoltaic cells of 55x85mm dimension, which consists of 8 cells in serial combination in order to produce 6V [3], [4]. To avoid the electric conductivity between patch of antenna and solarcell insulating material should be used. In order to attain high optical transparency such that solarcell efficiency is increased by transparent insulating material called as PMMA (Poly Methyl Methacrylate).

IV. SOLARCELL MICROSRIIP PATCH ANTENNA

First, three different shapes of patch antenna such as square, circle and rectangle is considered. Next, Microstrip patch antenna is simulated for these different patches using a standard substrate FR-4 and observed their characteristics. Later by changing the substrate material to PMMA antenna parameters are analyzed. The table 1 shows the detailed design specification consideration of Rectangular Microstrip patch antenna.

Table.1: Design specification of Rectangular patch

Parameters	Specification
Substrate material	PMMA
Dielectric constant	2.8-4
Substrate thickness	1.6mm
Patch thickness	0.035mm
Ground material	copper
Width of Patch	37mm
Length of Patch	30.11mm
Feed width	1.45mm
Feed length	-22.71mm

The table 2 shows the detailed design specification of Circular Microstrip patch antenna. The table 3 shows the detailed design specification of Square Microstrip patch antenna. From the comparison table, it is clear that rectangular patch antenna showed S11(dB)-17.48, directivity(dBi)-5.31, gain(dB)-4.78, bandwidth(%) -8.71 during PMMA as substrate material. Circular and square

patch antenna showed lower performance. Table 4 illustrates the comparison between different patch.

Table 2: Design specification of Circular patch

Parameters	Specification
Substrate material	PMMA
Dielectric constant	2.8-4
Substrate thickness	1.5mm
Patch thickness	0.035mm
Ground material	copper
Area of Patch	36.5mm
Length of Patch	30.11mm
Feed width	1.45mm
Feed length	-18mm

Circular and square patch antenna showed lower performance. Table 4 illustrates the comparison details of different patch.

Table.3: Design specification of square patch

Parameters	Specification
Substrate material	PMMA
Dielectric constant	2.8-4
Substrate thickness	1.6mm
Patch thickness	0.035mm
Ground material	copper
Area of Patch	37mm
Feed width	1.45mm
Feed length	-22.71mm

From the comparison table results, S11 parameters for different patches are plotted and represented using figure 5. Rectangular Microstrip patch Solarcell antenna is designed by integrating Rectangular Microstrip patch antenna by adding solarcells.

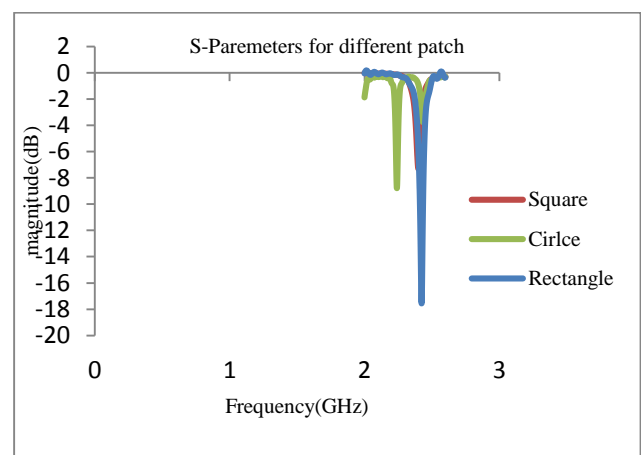


Fig. 5: S11 parameters for different patche

Table.4: Comparison table of different patch

Patch Shapes	S11 (dB)	Directivity (dBi)	Gain (dB)	Bandwidth
Rectangular	-17.48	5.31	4.78	8.71
Circular	-8.78	4.43	3.81	1.77
Square	-7.28	3.95	3.5	2.15

V. RESULTS AND DISCUSSION

Microstrip patch antenna for various shapes of patch and substrate material is compared and from the comparison it is concluded that Rectangular Microstrip patch antenna has higher performance. The 2-D view of Rectangular Microstrip patch Solarcell antenna is represented in the figure 6. Design specification of Rectangular Microstrip patch solarcell antenna is shown in the table 5. S11 parameters plot of Rectangular Microstrip patch solarcell antenna is shown in the figure 7. Obtained results from the design of Rectangular Microstrip patch solarcell antenna is tabulated in table 6. Block diagram of Rectangular Microstrip patch Solarcell antenna is represented in the figure 8. The designed Rectangular Microstrip patch Solarcell Antenna produces 6V.

Table.5: Design specification of Rectangular microstrip patch solarcell antenna

Parameter	Specification
Substrate Material(layer1)	Solarcell (55x85mm)
Substrate Material(layer2)	PMMA
Dielectric constant(layer 1)	4.3
Dielectric constant(layer 2)	2.8-4
Substrate Thickness(layer1)	2.3mm
Substrate Thickness(layer2)	1.6mm
Patch thickness	0.035mm
Ground material	copper
Width of patch	37.80mm
Length of the patch	28.80mm
Feed width	0.7mm
Feed length	-7.5mm

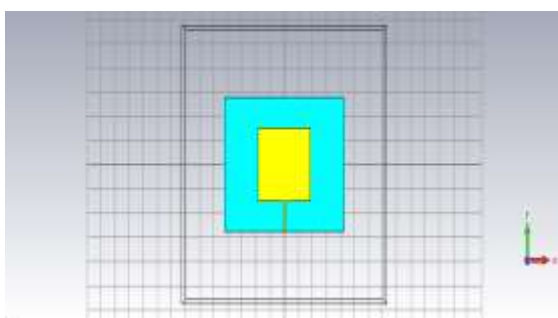


Fig. 6: 2-D view of Rectangular Microstrip patch Solarcell Antenna

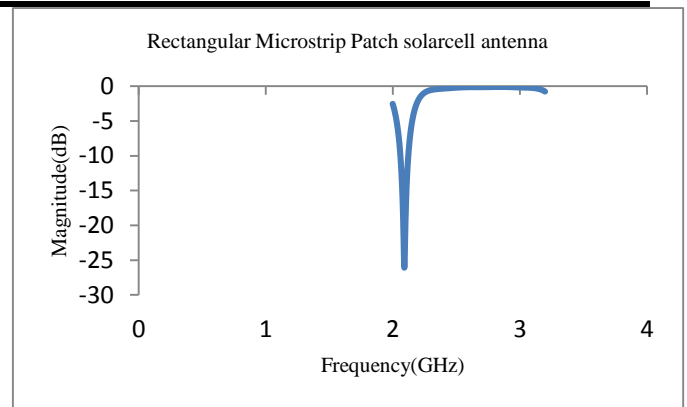


Fig. 7: S11 parameters of Rectangular Microstrip patch Solarcell Antenna

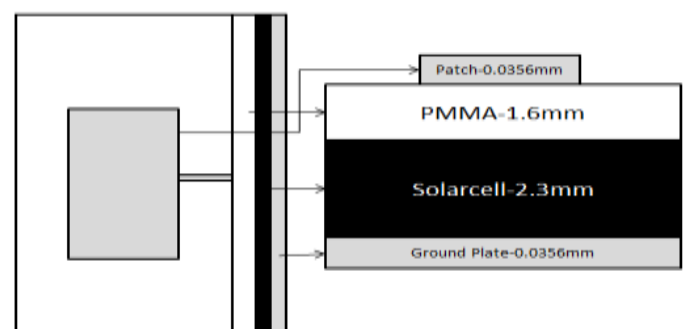


Fig. 8: Block diagram of Rectangular Microstrip patch Solarcell Antenna

Table.6: Results of Rectangular Microstrip patch Solarcell antenna

Patch Shapes	Rectangular
S11(dB)	-25.67
Directivity(dBi)	7.09
Gain(dB)	6.45
Bandwidth	6.531

VI. CONCLUSION

Different shapes of microstrip patch such as circular, rectangle and square are realized using substrate material as PMMA are compared and its performance is analysed. By comparing the different patches, Rectangular patch antenna shows the better performance such as high directivity, gain and bandwidth. So, Rectangular patch antenna is considered for designing solarcell antenna. Shift in frequency, high gain and directivity are inferred from the proposed antenna, if solarcell is used along with PMMA as substrate materials. The scope of remote communication is increasing more and more, so it is insufficient to feed electricity through grid for remote access. In such places, solarcell antenna will be more compact as well as can act as stand-alone system without any maintenance. The scope of Solarcell antenna increased day by day. Energy of solarcell can be increased by forming array based on serial combination of solarcells. Optically transparent patch

antenna can be designed to avoid malfunctioning of solar cells. Two or more patch can be added together to form array for MIMO communication and IOT (Internet of Things) Technology.

REFERENCES

- [1] Caso, R. Garroppo, S. Giordano, "Antennas and photovoltaic panels: Toward a green Internet of Things," IEEE 2nd World Forum on Internet of Things (WF-IoT), Milan, pp. 128-131, 2015.
- [2] T. R. Lockett, A. Martinez, D. Boyd, "Advancements of the Lightweight Integrated Solar Array and Transceiver (LISA-T) Small Spacecraft System," IEEE 42nd Photovoltaic Specialist Conference (PVSC), New Orleans, LA, 2015, pp. 1-6, 2015.
- [3] A. S. Kumar and S. Sundaravadivelu, "An Efficient Design of Solar Cell Antenna for Mobile and Vehicular Applications," IEEE Global Humanitarian Technology Conference, Seattle, WA, pp. 36-39, 2011.
- [4] T. Shahvirdi and R. Baktur, "A study on the effect of space solar cells on the antennas integrated on top of their cover glass," IEEE Antennas and Propagation Society International Symposium (APSURSI), Memphis, TN, pp. 215-216, 2014.
- [5] Y. Tawk, J. Costantine and C. G. Christodoulou, "An inverted-F antenna integrated with solar cells for energy harvesting," 9th European Conference on Antennas and Propagation (EuCAP), Lisbon, pp. 1-2, 2015.
- [6] Y. Tawk, J. Erickson, F. Ayoub, O. Lavrova and C. G. Christodoulou, "The integration of solar cells with PIFA for energy harvesting," IEEE Antennas and Propagation Society International Symposium (APSURSI), Memphis, TN, pp. 1351-1352, 2014.
- [7] R. Fotedar, P. Garia, R. Saini, A. Vidyarthi and R. Gowri, "Performance Analysis of Microstrip Antennas Using Different Shapes of Patch at 2.4 GHz," 2015 Second International Conference on Advances in Computing and Communication Engineering, Dehradun, 2015, pp. 374-377.
- [8] Constantine A. Balanis, *Antenna Theory Analysis and Design*, 3rd ed. Published by John Wiley & Sons, Inc., Hoboken, New Jersey.

High Frequency Gas Tungsten Arc Welding Process for Dressing of Weldment

Cibi Anthony J, K T Thilagam

Department of Metallurgical Engineering, Government College of Engineering, Salem, India

Abstract— The present investigation aims to apply High frequency GTAW variants to apply for the purpose of dressing of weldments. Numerous studies has reviled that the different dressing techniques has improved the life for weldments by modifying the weld bead geometry. It is found that the cracks occur at the weld joints where the stress concentration of the weld geometries is very high. GTAW Dressing reduce the severity of the stress concentration at the weld, remove imperfections, and/or introduce local compressive stresses at the weld can be used for improvement of the fatigue life. This paper compares the variants of GTAW process used for Dressing process in a mild steel fillet welded plate and evaluates the weld bead geometry, microstructure and its surface hardness.

Keywords— High Frequency, Dressing, Bead geometry, Toe radius, Surface toughness.

I. INTRODUCTION

Tungsten inert gas (TIG) welding is an arc welding process that produces coalescence of metals by heating them with an arc between a non-consumable electrode and the base metal. GTAW process is generally preferred because it produces a very high quality welds. The prpose of this investigation is to optimise the dressing technique usig variants of GTAW process. Implying dressing to a weld highlighted the fact that fatigue cracks that initiate very readily at the weld toe, virtually eliminating a crack initiation period and giving a fatigue life which is spent largely in crack propagation. The presence of these flaws, together with the stress concentration arising from the abrupt increase in section thickness at the weld joint, explained the relatively poor fatigue strengths of fillet welds. The flaws were not produced in TIG welding. This was thought to be due to the stable nature of the process. The above finding prompted the use of TIG simply to refine weld toes already deposited and confirmed the value of TIG dressing as an improvement techniques.

II. OBJECTIVE

The objective of the project is to perform High frequency Gas Tungsten Arc Welding process in the dressing application of fillet welded plate. Initially the Carbon plate is

to be welded by GMAW welding process using ER-70s6 filler wire. Then dressing will done on the welded plate by conventional GTAW dressing, conventional GTAW dressing with High frequency, pulsed GTAW dressing and pulsed GTAW dressing with high frequency. Then sample specimens will be prepared for micro, macro structure analysis and micro hardness. Results will be obtained and conclusion will be arrived.

III. CHEMICAL COMPOSITION OF BASE METAL

ASME SA516 Grade 60 carbon steel plate	
Composition	Percentage %
C	0.18
Si	0.4
Mn	0.95/1.50
P	0.015
S	0.008
Al	0.02 (Min)
Cr	0.3
Fe	Remaining

IV. CHEMICAL COMPOSITION OF FILLER WIRE

ER 70S-6	
Elements	Content
Carbon	0.06-0.15%
Manganese	1.4-1.85%
Phosphorous	0.025%
Sulphur	0.035%
Silicon	0.80-1.15%

V. GMAW WELDING

The heat is produced by an electric arc between the continuously fed metal electrode and the base metal. Both the base metal and the filler are melt. The weld area is protected by inert shield gases. As per AWS5.1 standard ER70S-6 wire was selected to weld the carbon steels plates. The plates were arranged in the automatic GMAW machine. The weld was performed in 2G position. Initial connections were given and 100% argon gas cylinder was connected and shielding gas flow was ensured. The electrode spool was fixed and the feed rate was set in the GMAW machine. The

plates supported in the fixture of the GMAW machine. The electrode tip was cleaned and the process was started

WELDING PARAMETERS FOR GMAW WELDING.

PARAMETERS	VALUE
ELECTRODE WIRE	ER70S6
WIRE DIAMETER	1.2mm
SHIELDING GAS	ARGON
GAS FLOW RATE	20 lpm
WIRE FEED RATE	7.5 mm/min
TRAVEL SPEED	300 mm/min
STARTING CURRENT	128 amps
STARTING VOLTAGE	25 volts
WELDING CURRENT	208-215 amps
WELDING VOLTAGE	25 volts
NO OF PASSES	3

VI. GTAW DRESSING

A standard TIG welding machine is used. Argon is normally used as shielding gas. Additions of helium is beneficial since this gives a larger pool of melted metal due to a higher heat input.

6.1) WELD PREPARATIONS

TIG dressing is sensitive to most types of common weld contaminants such as mill scale, rust, oil and paint. The weld and adjacent plate should be thoroughly de-slugged and wire brushed. If necessary light grinding should be used to obtain a clean surface insufficient cleaning tends to result in the formation of gas pores that can have a strongly detrimental effect on fatigue performance. The problem of porosity is particularly important in TIG dressed aluminium welds.

6.2) TUNGSTEN ELECTRODE FOR TIG DRESSING

The shape of the arc depends on the shape and condition of the electrode tip. If the tip is contaminated or rounded by wear (oxidation) the arc becomes concentrated, so that the remelted zone narrows with an unfavourable effect on the bead shape. It is also difficult to start the arc and keep it stable. These problems can be avoided by regrinding the tip or replacing the electrode.

6.3) SHIELDING GAS

If the gas flow rate is low or strong draughts disturb the gas shield the arc becomes unstable and defects such as surface pores are formed, or the electrode and bead oxidize. An adequate gas supply rate depends on many factors, including gas cup size, welding conditions and welding location (presence of draughts). An optimum flow rate should therefore be determined by trial dressing.

6.4) POSITION OF TIG TORCH AND DRESSING ZONE

For an optimum result the remelted zone has to be positioned carefully with respect to the original weld toe. Normally the best result is obtained when the arc centre is located a small distance away from the weld toe

6.5) WELDING CURRENT

Due to the Constant-Current (CC) process nature of GTAW, current is the main parameter determine the arc characteristic and the heat input, while other welding parameter is adjusted according to current change. Current is the measure of amount of electron flow per second, and related to amount of heat input. In direct-current process of electrode negative GTAW process, electron is flow from tungsten electrode to the workpiece. Higher current meaning more electron is flow through tungsten electrode and hit on the workpiece, in result of higher heat generated to melt the base metal. While voltage is potential different between tungsten electrode and workpiece, which direct related to the arc length. In Interpulse technique GTAW, there are main current , background current, and interpulse or delta current.

6.5.1) Main Current

Main current is the fundamental current or maximum weld current for GTAW. It can use alone in straight arc mode, or as peak current in pulse arc mode.

6.5.2) Background Current

Background current is the low current in pulse arc mode, use to maintain the arc during pulsing at low frequency of less than 50 Hertz. The greater the different between main current and background current, the greater pulse effect will be notice.

6.5.3) Delta Current

Delta current also known as interpulse current. This current runs on a 50% duty cycle with the Main current and/or background current at very high frequency of 20kHertz. This is the pulsing current generate magnetic force to constrict the arc, hence a stiff narrow arc

Delta straight arc unlike normal pulse arc, the waveform is taking shape of saw-tooth rather than square wave. This give a very special character to current waveform to behave differently when delta current is higher or lower than main current. The delta waveform has three sections. The rise in current time , fall in current time and the agitation current (flat wave).

The penetration weld or build up weld depends on whether the main current is higher that the delta current or lower than the delta current. In either case it is the speed at which the rise and fall times occur which influences the way in which the magnetic field works.

In the case where the main current is higher than the delta current, the waveform looks like the picture at left, thus the rise time is relatively slow compared with the fall time . This means that the magnetic field increases slowly, thus the

arc is slowly constricted. This gives a gentle decrease in the arc width until the time of is complete. Then the fall in current happens fairly quickly, reducing the magnetic field and allowing the arc to get wider.

This cycle can be seen as slow compression of arc and a quick release to the original arc width. The agitation section acts as a small increase then decrease in current. This works a bit like the slow pulse and where the surface tension of the pool is agitated allowing the material is to "stirred" gently. This helps reduce the energy required for the next cycle to take place.

If delta current is higher than main current, a build-up configuration which exact opposite waveform is effectively occur as shown at right Figure. The rise time is relatively fast compared with the fall time. This means that the magnetic field increases quickly, thus the arc is quickly constricted and allowed to return to its normal state slowly. Thus this is good for build-up welds and filling small gaps inside materials.

6.5.4) AVERAGE CURRENT CALCULATION

As there are 3 different current involve in GTCAW, the calculation of the average current become more complicated by the fact that the high frequency modulation of the current generate a saw-tooth waveform. For the analysis here, it is thought that it is sufficient to simplify the calculations by assuming that all the waveforms take the form of a square wave, though a better interpretation should take duty cycle of 54% of delta current. If this is assumed to occur with a square waveform, the average current of either weld is simply the mean of these values. When delta current is superimposed at high frequency between main current and background current,

When delta current is superimposed at high frequency between main current without pulse current. The average current can be simplify to mean of the main and delta current.

VII. ARC MODE FOR INTERPULSE WELDING

These 3 different current when integrate together, having it's on unique character waveform that contribute to different application of welding, and greatly reduce heat input as compare to main current alone.

7.1) STRAIGHT ARC

Straight arc is the most basic arc mode, and available in all GTAW welding machine. In straight arc, there is only main current. The arc character is spread wide, a lot of heat is dissipated and wasted in the outer flare.

7.2) DELTA STRAIGHT ARC

Delta straight arc is mode of arc when delta current is pulsing with main current. The arc is constricted by magnetic force, hence the heat is focus and less wasted heat on the outer flare. This allow heat to perform at lower heat input than straight arc required. As explain previously, delta straight arc can alter to activate penetration weld or build-up weld depend on whether delta current is higher or lower than main current.

7.3) PULSE ARC

In the pulsed-current mode, the welding current rapidly alternates between two levels at low frequency up to 50 Hertz. The higher current state is known as the pulse current, while the lower current level is called the background current. During the period of pulse current, the weld area is heated and fusion occurs. Upon dropping to the background current, the weld area is allowed to cool and solidify. Pulsed-current GTAW has a number of advantages, including lower heat input and consequently a reduction in distortion and warpage in thin workpieces.

In addition, it allows for greater control of the weld pool, and can increase weld penetration, welding speed, and quality. A similar method, manual programmed GTAW, allows the operator to program a specific rate and magnitude of current variations, making it useful for specialized applications

7.4) DELTA PULSE ARC

Delta pulse arc is combination of both delta arc and pulse arc, where the delta magnetic current is modulate at 20 kHz between both main current and background current.

As there are main current, background current and delta current present in the wave form, the delta current can be set at lower, in between, or higher than main and background current. These setting allow the arc mode being manipulate to meet certain application.

VIII. SPECIMEN PREPARATION

The specimen was prepared by cutting the GMAW welded specimen to 15 mm from the centre. The specimen was deburred by grinding wheel and was done surface milling. In the surface milling operation the thickness was reduced to 10 mm. This made the specimen surface smooth and free from visible cracks. Then the specimen was polished using emery and disc polishing wheel. This makes the workpiece mirror like surface. The polished surface is then etched in 15ml nital for a few seconds and washed with the water. Then the specimen is observed in macroscopic image viewer under proper illumination.

IX. RESULTS AND DISCUSSION

9.1) WELDING PARAMETERS

Sl. No.	Processes	Welding Parameters					Heat Input, kJ/mm
		Welding Current, A	Arc Voltage, V	Welding Speed, mm/min	High Frequency current, A	High Frequency, Hz	
1	GMAW-Undressed	222	30	300	-	-	1.332
2	GTAW	150	16.8	129.47	-	-	1.167
3	GTAW + HF	120	16.4	129.47	50	20000	1.204
4	P-GTAW	110-140	15.7	96.32	-	-	1.055
5	P-GTAW + HF	130-150	16.8	90.4	100	20000	1.449

9.2) MACRO-PHOTOGRAPH OF WELD JOINT



Fig.1: Typical macrograph of Undressed weldment

The macro structure of undressed weldment reveals the base metal, weld metal and HAZ zones. It is clearly seen that the weld toe is highly stress concentrated due to its sharp toe angle. It is seen that the weld toe angle is higher any fracture would eventually start at the weld toe surface.

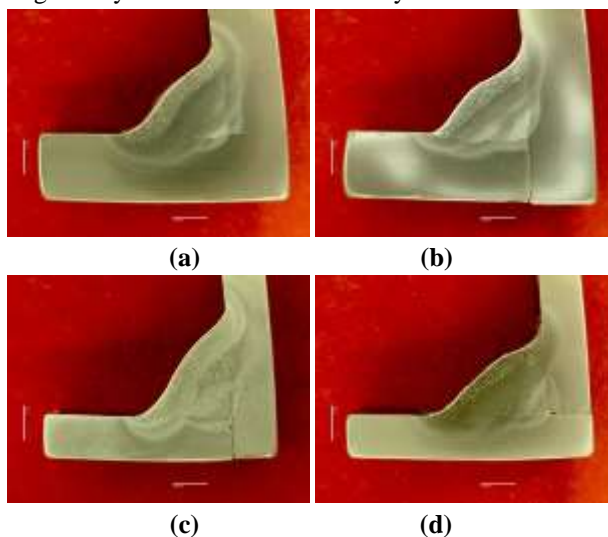
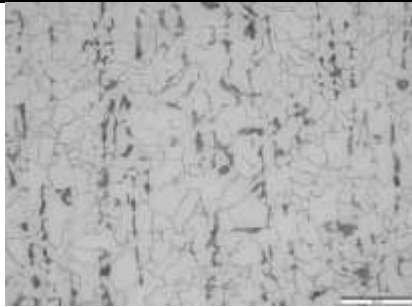


Fig.2: Typical Macrograph of dressed weldment (a) GTAW, (b) GTAW + HF, (c) P-GTAW and (d) P-GTAW + HF

The above macro graphs shows the dressed weldment which shows the remelted weld toe this reduces the stress concentration at the weld toe and improves the fatigue life. There is a reheat region which occurred due to dressing and the heat affected zone is further increased considerably the dressing reduces the throat length and the weld area this reduces the internal tensile residual stress developed during welding.

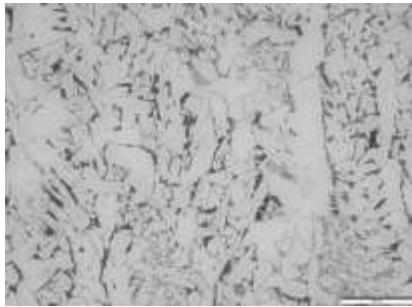
9.3.1) MICRO STRUCTRE OF GMAW WELDED SPECIMEN

9.3) METALLOGRAPHY



500X

Fig.3: Microstructure of base metal



500X

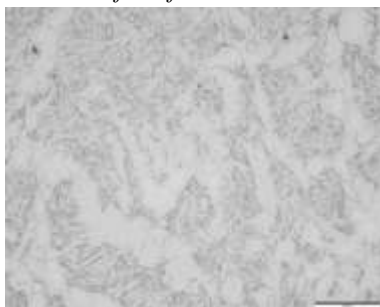
Fig.4: Microstructure of as-welded GMA weld deposit

9.3.2) MICROSTRUCTURE OF CONVENTIONAL GTAW DRESSED



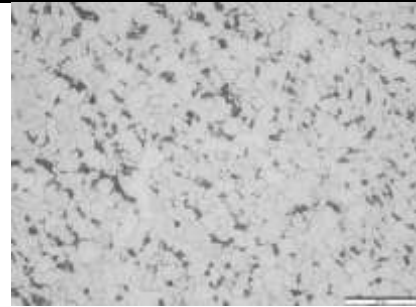
500X

Fig.5: Microstructure of as-welded HAZ near to top surface of the fusion line



500X

Fig.6: Microstructure of dressed weld deposit by conventional GTAW



(b) 500X

Fig.7: Microstructure of re-heat refined zone in weld deposit due to conventional GTAW dressing

9.3.3) MICROSTRUCTURE OF CONVENTIONAL GTAW WITH HF DRESSED



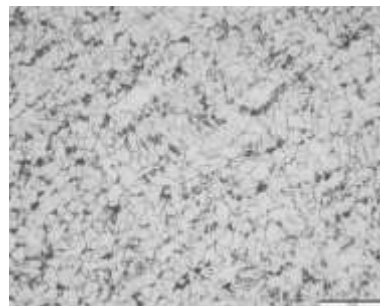
500X

Fig.8: Microstructure of undressed GMA weld deposit



500X

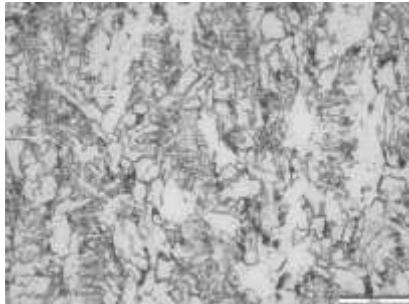
Fig.9: Microstructure of dressed weld deposit by conventional GTAW + HF



500X

Fig.10: Microstructure of re-heat refined zone in weld deposit due to GTAW + HF dressing

9.3.4) MICROSTRUCTURE OF PULSED GTAW DRESSED



500X

Fig.11: Microstructure of undressed GMA weld deposit



500X

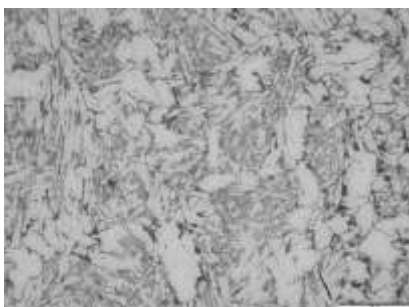
Fig.12: Microstructure of dressed weld deposit by P-GTAW



500X

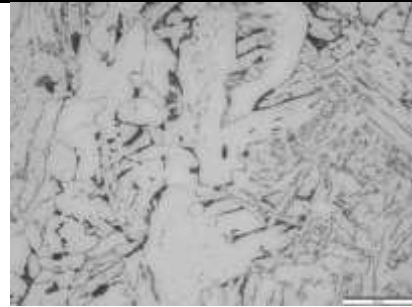
Fig.13: Microstructure of re-heat refined zone in weld

9.3.5) MICROSTRUCTURE OF P-GTAW WITH HF DRESSED



500X

Fig.14: Microstructure of undressed GMA weld deposit



500X

Fig.15: Microstructure of dressed weld deposit by P-GTAW + HF



500X

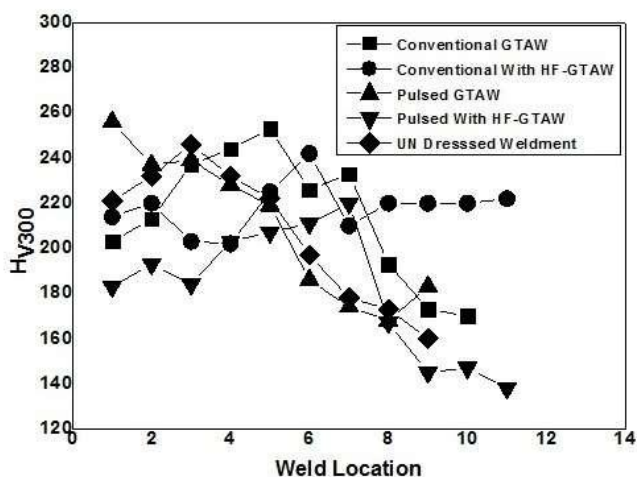
Fig.16: Microstructure of re-heat refined zone in weld deposit due to P-GTAW + HF dressing

The reduction in the weld flaws and inclusion in combination with the increase in the weld toe radius is assumed to create the beneficial behaviour of the GTAW dressed specimen compared to as welded specimen.

The microstructure of the carbon steel depends upon the carbon content, temperature, and cooling rates. Austenite is formed above the transition temperature and will transfer back to ferrite and pearlite when cooled down. Carbon causes cementite to form.

The microstructure study revealed that the structure is distributed with ferrite and pearlite. The grains of the Reheat region is finer than the deposited metal. Hence the toughness of the surface is improved. In contrast in pulsed GTAW dressing process due to sudden cooling and heating the grains become finer hence hardness has improved suppressing the toughness.

X. MICROHARDNESS



The micro hardness was done using the Vickers hardness test machine. The hardness was examined from the top surface of the weld bead and throughout its throat length. It was found the surface hardness decreased because of the dressing process. In contrast in pulsed GTAW dressing the hardness of the surface has been increased considerably. Through the result it is noted that the hardness of the conventional GTAW dressed specimen and conventional GTAW with High frequency dressed specimen have the most desired hardness profile.

XI. CONCLUSION

The dressing technique was applied on the fillet welded carbon steel plate using various arcs such as conventional tungsten arc, conventional tungsten arc with high frequency, pulsed tungsten arc, pulsed tungsten arc with high frequency. The initial fillet weld was welded by automatic metal inert gas welding.

- 1) The typical macro graph revealed that the dressed surface is smooth and uniform throughout the cross section. The sharp comers at the weld toe has been eliminated the weld bead angle has been decreased due to dressing process. The reduction in the weld area indicates reduction of tensile residual stress. The macro image further revels in improvement of symmetric of the weld bead.
- 2) The typical microstructure of the dressed specimen was studied under the magnification of 200x and 500x. The microstructure was examined at the top surface of the dressed zone, re heat affected zone, weld metal deposited region and base metal. The microstructure revels that the base metal and the weld metal are of same composition of ferrite and pearlite. The formation of acicular ferrite implies that toughness has been improved in the surface of the metal.

- 3) The micro hardness test was conducted on the prepared specimen. The resulted were displayed in the form of graph hardness vs distance. Expect pulsed GTAW dressing all the other dressing process the surface hardness was reduced by the dressing process. The conventional gas tungsten arc dressing process showed considerable uniformity in the hardness throughout the thickness.

REFERENCES

- [1] Madoxx S.J. 'Fatigue strength of welded structures', Abington Publishing, 1991
- [2] Effect of TIG-dressing on fatigue strength and weld toe geometry of butt welded connections in high strength steel- S H J Van Es- VM publications 250-2008.
- [3] Dahle, T. 'Design fatigue strength of TIG-dressed welded joints in high-strength steels subjected to spectrum loading', *International Journal of Fatigue*, Vol. 20, No. 9, pp. 677-681, 1998.
- [4] Gurney, T.R. 'Fatigue of welded structures', Cambridge University Press, 1979.
- [5] Pijpers, R.J.M. 'Fatigue strength of welded connections made of very high strength cast and rolled steels', Dissertation, M2I, 2011.
- [6] Sonsino, C.M. and Fricke, W. 'Fatigue assessment of welded joints by local approaches- 'second edition', Woodhead publishing limited, 2006.
- [7] Gudehus, H. Zenner, H. 'Leitfaden fur Betriebsfestigkeitsrechnung', Verlag Stahleisen GmbH, 1999.
- [8] C.M. Branco ^{a,*}, S.J. Maddox ^b, V. Infante ^a, E.C. Gomes ^a Fatigue performance of tungsten inert gas (TIG) and plasma welds in thin sections. *International Journal of Fatigue* 21 (1999) 587-601.

A Slotted-sense Streaming MAC for Real-time Multimedia Data Transmission in Industrial Wireless Sensor Networks

Md Abul Kalam Azad¹, Amina Khatun¹, Md Abdur Rahman²

¹Department of Computer Science & Engineering, Jahangirnagar University, Dhaka, Bangladesh

²Department of Mathematics, Jahangirnagar University, Dhaka, Bangladesh

Abstract—To attain a flawless real-time data transfer over a communication channel of Industrial Wireless Sensor Networks (IWSNs) is a difficult issue. The reason is that data transmission reliability degrades remarkably due to the dynamically changing network topology. Although TDMA-based protocols are widely used for real-time data transmission in IWSNs, they are not suitable for dynamically changing network topology. Therefore, we analyze the communication behavior of real-time multimedia data transmission and try to find out some performance enhancing factors. Then, we propose a slotted-sense scheduling scheme in which a big time slot is shared among the nodes at same tree-level. A sharable slot not only assures the time constraint but also improves the reliability of multimedia data greatly. Moreover, the block data transmission technique with an adaptive acknowledgement is proposed to optimize the size of a sharable slot. Finally, the experimental results show that our approach outperforms other standard MAC protocols for real-time multimedia data transmission in IWSNs.

Keywords— Industrial, NACK, Re-transmit, SS-MAC, Streaming.

I. INTRODUCTION

Instead of paying the required attention to the underlying Medium Access Control (MAC) protocols, most of the contemporary research works tried to improve the routing protocols for increasing the data transmission efficiency of Wireless Sensor Networks (WSNs) [1]. In practice, a poorly designed MAC protocol often creates a bottleneck problem in data packet transmission, and hence a network sometimes does not work efficiently as expected. Such a shortcoming seriously affects the transmission of real-time multimedia data, which requires more channel bandwidth, more energy and incurs a higher delay than that of scalar data transmission [2].

Interference is a common phenomenon in industry. Therefore, WSNs intended to industrial sectors should address the interference from industrial applications. Due to its real-time nature of data acquisition, Time Division

Multiple Access (TDMA) is frequently used in industry. However, TDMA-based protocols have to encounter at least two complex issues for industrial applications. *Firstly*, they require a frequent time synchronization among the deployed nodes in WSNs. We know that the frequency of time synchronization depends on the skew rate and slew rate of a local clock, as well as, the size of a time slot. For a fixed skew rate and slew rate, a protocol along with smaller time slot requires frequent time synchronization than that of larger time slot. *Secondly*, a particular node requires a hard and fast rule for allocating the precise number of time slots. Moreover, introducing a new node to a WSN or removing an existing node from a WSN requires a fresh slot allocation for the whole network, which seriously affects data transmission efficiency [3]. In industry, these weaknesses of TDMA-based MAC protocols adversely affect the data transmission efficiency of WSNs.

To address the above weaknesses, some of the contemporary Carrier Sense Multiple Access (CSMA)-based MACs, IEEE-802.11 [4], SMAC [5], and their variants DMAC [6], TMAC [7], RMAC [8], and MMSPEED [9] attempt to increase the data transmission efficiency and to reduce the time delay of multimedia data packets in WSNs. However, these MAC protocols cannot provide any specific tool for assuring the time constraint of data packets. Moreover, some of them do not consider the data transmission reliability, while others do not consider the time constraint of data transmission. MMSPEED [9] considers both aspects by allowing multipath data transmission. However, its multipath data transmission significantly increases the collisions among data packets, and increases the energy consumption as well for industrial WSNs.

The Distributed Coordination Function (DCF) of IEEE 802.11 standard is modified for enhancing the real-time data transmission in wireless networks [10-12]. The findings of [10] are that the throughput increases with an increase in the number of backoff stages, and that the average number of transmission per packet decreases with

an increase in the size of the initial backoff window. The works [11-12], based on the contention design of [10], propose to optimize the retry limit for reducing the delay of multimedia data transmission using IEEE 802.11 DCF. However, these works are intended for AdHoc wireless networks where the fairness requires a different type of resource allocations among users than that of WSNs.

In this paper, we propose a reliable MAC protocol for multimedia data streaming termed as Slotted-sense Streaming MAC (SS-MAC), which exploits the transmission characteristics of multimedia data in WSNs. Instead of using either CSMA or TDMA-based slot scheduling, we use a hybrid slot scheduling in which a big slot is shared among the nodes at same tree level so that the nodes can share the big slot using CSMA. The time constraint is preserved by the size of big slots whereas the robustness of data delivery is achieved by switching to alternate parents through the contention process within a big slot. At any time, only the nodes of two adjacent tree levels are active in which the nodes at high tree level are the sender and the nodes at low tree level are the receiver of multimedia data packets. If a node with multimedia data wins over a channel, it sends all fragmented packets to a direct parent node or an alternate parent node in a reliable and timely manner. When a node finishes data packet transmission, it will be informed with a Negative ACKnowledgement (NACK) message about the corrupted or lost data packets if there is any. Consequently, the sender re-transmits the corrupted data packets in a burst for the maximum allowed number of times, which is adaptively determined. Therefore, SS-MAC is able to overcome the difficulties of dynamically changing wireless channel, and hence outperforms other MAC protocols in data transmission, as well as, energy consumption efficiency.

The paper is organized as follows: Section 2 deals with some related works. Section 3 describes the motivation and problem statements underpinning the expectations from SS-MAC. The step by step design of the protocol is discussed in section 4. Section 5 discusses some experimental results followed by some concluding remarks in section 6.

II. RELATED WORKS

In IEEE 802.11 [4], a familiar communication protocol for wireless networks, a sender exchanges Request-to-Send (RTS) and Clear-to-Send (CTS) control messages with a receiver to reserve a communication channel only for the first fragment of a data packet and the corresponding ACKnowledgement (ACK). The first fragment and its ACK reserve the channel for the second fragment of a data packet and its ACK, and so on. However, when the sender transmits a fragment of a data

packet, it releases the channel and monitors the channel for an ACK of previously transmitted data fragment. Relinquishing the medium in such a way requires an extra contention time and hence, a data packet suffers from high delay. If an ACK of any data fragment is lost, the sender must leave the transmission process in an incomplete stage, and re-contend for the channel to transmit the remaining fragments.

A duty cycle version of IEEE 802.11, SMAC [5] fragments a long message into many small pieces in order to transmit them in burst. Only one pair of RTS and CTS control packet reserves the channel for transmitting all of the data fragments. The sender waits for an ACK for each transmitted fragment. In case of a failure, it extends the reserved transmission time for this fragment, and then retransmits the current fragment immediately. The logic behind of sending an ACK for each fragment is to avoid the hidden terminal problem at receiver premises. This causes an extra delay for a large data packet in real-time multimedia transmission. As the integrity of a data packet must be maintained, the successful reception of an isolated data fragment is meaningless to a multimedia data application. Therefore, an ACK for each individual data fragment wastes the precious time and bandwidth of a communication channel.

In DMAC [6], a staggered wakeup schedule is designed for streaming of data packets from the sources to a sink. Instead of implementing the RTS and CTS handshaking for reducing the control overhead, the protocol keeps the basic active cycle with a Receive + ACK period followed by a Transmit + ACK period in a data transmission slot. If an ACK is not found, the corresponding data packet is sent in the next active transmission slot within the maximum of three retransmission attempts. For transmitting multiple data packets, the nodes on the multi-hop path need to increase the duty cycle adaptively. The protocol does not propose the streaming of multimedia data fragments and does not provide the influence of data streaming on network performance.

On the other hand, each node in TMAC [7] transmits its queued packets in a burst at the start of a frame. This adaptive duty cycle MAC determines some activation events, and then an inactive period after which a node can go to sleep for the remaining cycle time. The protocol reduces idle listening by transmitting all messages in bursts of variable length, and sleeping between two bursts. Though the protocol effectively addresses the data forwarding pattern of small packets, it fails to consider the transmission of large multimedia data packets in which the fragmentation is mandatory for channel efficiency. Moreover, the assumed error free channel for data transmission is very unrealistic in any industrial WSNs applications.

Toward designing a reliable MAC, RMAC [8] adopts both the explicit and the implicit ACK for reliability assurance. Every intermediate node skips backoff period and immediately transmits a successfully received packet to the next forwarding node. By overhearing the data transmission of next forwarding node, each node considers its transmission as successful, which is treated as an implicit ACK. As there requires no transmission beyond a sink, an explicit ACK is required for the immediate neighbors (1-hop away) of a sink. The process indeed reduces the delay time of data streaming; however, if the next hop node requires an extended amount of time to get the channel for data transmission, the implicit technique incurs even more delay than other techniques. Moreover, the protocol suffers from the poorly designed retransmission attempts, which allows only one increment in retransmission attempts for any types of error from a communication channel.

MMSPEED [9], a cross layer approach, adopts the reliability and real-time Quality-of-Service (QoS) over multipath data transmission. The protocol differentiates various services by mapping the data packets to different priority queues. That it sends multiple copies of same data packet over multiple paths enhances the real-time constraints and reliability of data transmission. However, this way of packet delivery gives high packet collisions and consequently, it incurs more retransmission attempts and delay in industrial WSNs. The protocol does not consider the energy consumption efficiency and fragmentation of data packets. Moreover, a node of this protocol requires multicasting support as well as a large amount of memory to remember multiple paths. Therefore, this protocol is not suitable for the real-time multimedia data transmission in WSNs.

Last but not least, it is worth mentioning to discuss about *SMAC with Block Acknowledgement* [13] – we termed it as BA-MAC - an important work on the fragmentation of data packets. It introduces the Block Acknowledgement (BA) concept from IEEE 802-11e standard [14] in SMAC. The protocol improves the packet delivery efficiency and reduces end-to-end delay by fragmenting a large data packet. However, it is not free from data forwarding interruption problem as off SMAC. Additionally, some key deficiencies such as formation of variable logical groups, duplicate packet discarding and impractical arrival time of packets *etc.*, are observed in the protocol operation.

III. BACKGROUND

3.1 Motivation and Problem Statements

In industry, the vibration rate of the generated signal by various appliances is in the range of 40 KHz [15]. If we want to build a safety monitoring system for appliances,

the sensed signals from sensor nodes are required to be sent to a sink. The received signals are required to be analyzed to know whether a safety measure is required or not. To get a functional system, the sensed signal is required to follow the “Nyquist-Shannon” sampling rate [16], which states that the sampling frequency should be at least twice of the highest frequency of sensed signal (input signal) to reproduce the monitoring phenomenon at a sink node as follow:

$$F_s \geq 2B \quad (1)$$

In (1), F_s stands for the sampling frequency of sensed signal and B stands for the highest frequency of the sensed signals at a sensor node. Therefore, the minimum required bandwidth (data rate) by a node should be 320 Kbyte/sec, where 4 byte single precision FPA-IEEE 754 [17] coding is used for floating point integer representation as follow:

$$\begin{aligned} BW_{node} &= 80 \text{ KHz} \times 4 \text{ Bytes} \\ &= 320 \text{ KByte/sec} \end{aligned} \quad (2)$$

The above analysis shows that the amount of data to be transmitted for a simple vibration signal requires a high channel bandwidth. Therefore, any multimedia data such as still images, audios and videos require much more bandwidth than that of scalar data. The bandwidth calculation in (2) is for a noise-free channel. In practice, a noise-free wireless channel in industrial applications does not exist. In a noisy channel, more retransmissions are taking place due to the corrupted or lost data packets. Therefore, a high volume of data is required to be transmitted through an industrial WSN for such applications. Compression may be an effective tool for reducing the volume of transmitted data.

A 10:1 compression level results in a little distortion in transmitted multimedia data. This level of compression is able to reduce the data rate of WSNs to 30 packets/sec in which each packet contains of 8738 bits. However, transmission of such a large data packet through a noisy industrial channel is very inefficient. For the channel efficiency and minimum delay, small data packets are required to be transmitted through a noisy channel. Therefore, a data fragmentation technique is required so that a packet loss reduces the channel occupation. In this paper, we propose a MAC protocol that is able to transmit a large data packet reliably in a fragmented form at hop-by-hop basis instead of end-to-end basis [18] without any loss of simplicity.

3.2 Network Model

A WSN consists of one data collection and control server (referred to as simply *node* or *sink node*), and a number of sensor devices (referred to as simply *node* or *sensor node*) that includes at least one sensor module for thermal, gas, oxygen, smoke, or flame sensing. Each sensor node

generates a multimedia data packet from sensed data, fragments them accordingly, and sends them to a sink node within a specified time bound defined by an industrial application.

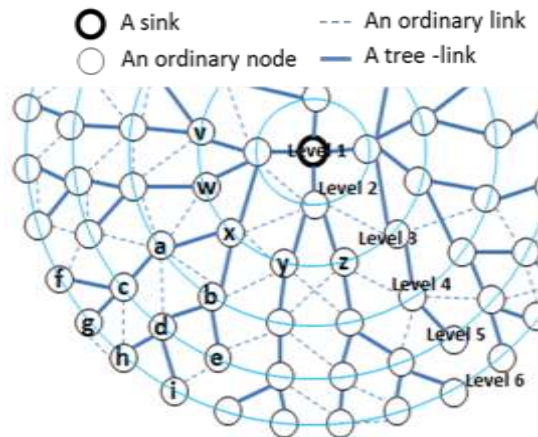


Fig. 1: A network model

Sensor nodes form a tree originating from a sink node, and each sensor node has a parent and may have multiple children. A node is said to be a *tree-node* if it belongs to a tree. Otherwise, it is an *orphan-node*. Two nodes that can directly and mutually communicate with each other are said to have a *link* or an *ordinary link*. Especially, a link between a node and its parent is called a *tree-link*.

Fig. 1 shows a network model of a tree originating from a sink node where the tree has a tree level (depth) of six. The solid lines and the dashed lines indicate *tree-links* and *links*, respectively.

3.3 Notations and Definitions

We use some notations as follows:

TABLE I: Notations

-	$level(i)$: The level of node i
-	$N(i)$: A set of neighbors of node i
-	$N-1(i), N=(i), N+1(i)$: A set of neighbors of node i at i 's level-1, i 's level, i 's level+1, respectively. Then, $N(i) = N-1(i) \cup N=(i) \cup N+1(i)$
-	$C(i)$: A set of children of node i
-	$D(i)$: A set of descendants of node i
-	$D[i] = D(i) \cup \{i\}$
-	$P(i)$: The parent of node i
-	$CN(i)$: A set of the nodes with which a node i competes to acquire a channel.
-	$CN[i] = CN(i) \cup \{i\}$
-	H : The depth of a tree

For the convenience of description, we define some terminologies as follows:

A link (a, b) is defined to be *bidirectionally reliable* (B -reliable) iff a directional link from a to b , and a

directional link from b to a are both reliable. If a tree is constructed along with B -reliable links, the tree is said to be a *B-reliable tree*.

A *sharable slot* (SS) is a time span in which all nodes at the same tree level share to receive data packets from their children and transmit their data packets to their respective parents using CSMA. $SS(i)$ is used to denote a sharable slot allocated to level i and divided into two parts, $SS^{Rx}(i)$ and $SS^{Tx}(i)$ where the nodes at level i use to receive data packets from their children and to transmit data packets to their parents, respectively.

Definition 1: A superframe (SF) is given by the sum of the transmission portions of all the sharable slots allocated to different levels of a tree as follows:

$$SF = \sum_{i=2}^H SS^{Tx}(i) \quad (3)$$

where $SS^{Tx}(i)$ and $SS^{Tx}(j)$ when slot i and slot j do not overlap.

An application states the SF as the maximum time that a sink can wait to acquire data packets from all participating nodes. For any loss of generality, we use big-slot as a slot when it is used in our SS-MAC protocol.

IV. FORMULATION OF PROPOSED PROTOCOL

Most of the MAC protocols show some limitations for their apathetic role in categorizing the impaired received packets. Impairment in the received packet can be occurred for a variety of reasons such as noise burst, collisions by multiple senders at the receiver premises, collision between different destined packets for the overlapped collision domains. Moreover, packet may be lost altogether due to multipath fading and congestion at a choke point in the forwarding path of data packet transmission. Most of the protocols generally address all of these problems by packet re-transmission *i.e.*, re-sending the lost or corrupted packet with doubling the size of a contention window [4].

Doubling the contention window has a serious consequences on the time delay and hence, on the data delivery efficiency of WSNs. In case of congestion and hidden terminal problems, increasing contention window allows the competing nodes an additional time span to choose its mutually exclusive slot to avoid collisions. However, the two common problems in successful data packet reception: *data collision* and *data loss*. These should be handled differently. Using the same solutions for both will produce unnecessary delay and thereby, waste costly bandwidth of wireless channel. We, therefore, need to analyze the topological structure and operational behavior of WSNs to design an effective data transmission protocol for multimedia applications.

4.1 Collision behavior of a sensor network

Collision that seems to be a usual phenomenon in WSNs should be carefully addressed by any MAC protocols. In a contention based tree protocol, there are some specific locations of a tree in which the probability of collisions might be high compared to other regions. We all know that collisions are receiver oriented. Therefore, if the receiver nodes can be kept at mutually exclusive collision domains, then data packets are safe from collision. On the other hand, the intermediate node acting as a relay in the sensor network paradigm may expose to collision when either its parent or children simultaneously try to transmit data packets.

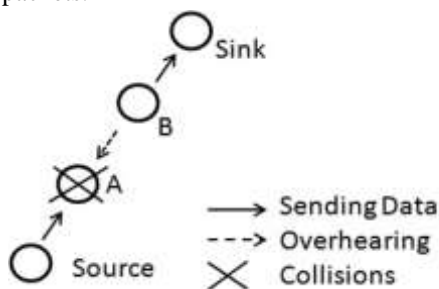


Fig. 2: Collision at node-A due to simultaneous neighbor transmissions

In Fig. 2, node B is transmitting to the Sink, and node A is overhearing the transmission phenomenon. At the same time, if the a source unaware of the transmission of B tries to transmit, a collision happens at node A. Multiple children can also make a collision to their receiving parent node at the branching point of a subtree as shown in Fig. 3.

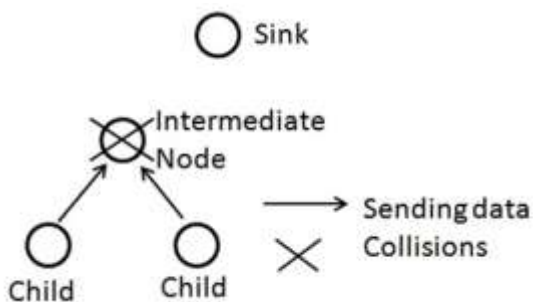


Fig. 3: Collision for simultaneous activation from the data transmission of children

Nodes in the parallel paths within the overlapping collision domain of each other may interfere when their data sending scheduling time coincides as in Fig. 4. It is interesting to note that the collision probability is more severe near the sink node rather than source nodes as all of the routes converge to a common sink.

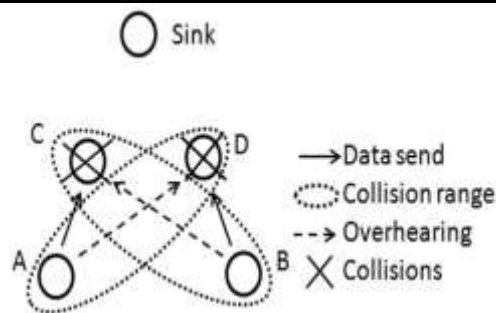


Fig. 4: Collisions for the overlapping interference domain

4.2 Overhearing behavior of sensor network

All of the immediate neighbors of both the sender and receiver should keep silent after they hear the RTS and CTS packet for the first time until the current transmission is over [5]. Sketching the process in Fig. 5, it can be concluded that within five successive nodes along the path, only one node can transmit its data to its neighbor toward the sink. The remaining three nodes can go to sleep to conserve energy by setting their appropriate wake up timer. However, the farthest node from sink in this group has some flexibility *i.e.*, it can receive packet from its children if necessary. So, the immediate neighbor nodes of sender and receiver should not take part in any transmitting and receiving actions.

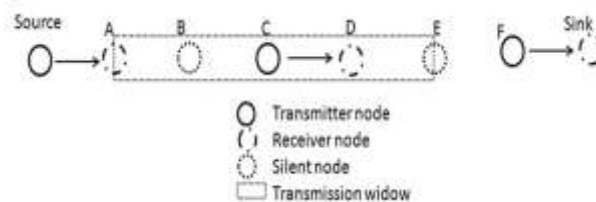


Fig. 5: Showing 4-Hop blocking by a transmitting node

In Fig. 5, node C is transmitting to node D while other nodes adjacent to them along the path have nothing to do. So, node B and node F can easily go to sleep for the time duration of a packet transmission. But node A can receive packets if the source has any for reducing the packet delay of the overall transmission process.

4.3 Determining ACK and re-transmission attempts

In order to guarantee the reception of all fragments at a receiver, the appropriate type of ACK is necessary for the real time multimedia applications. As the single fragment of a multimedia packet is meaningless, they all need to be transmitted to the next forwarding node along the path almost simultaneously. Thus introducing an ACK at every fragment produces high transmission delay, which may be the cause of failing the mission altogether. As the data packet transmission in a WSN is generally unidirectional - from all data sources to a sink - the modified Negative ACK (NACK) is more plausible than positive ACK. In

other words, when a data fragment of a burst is corrupted, the receiver will notify the sender about the corrupted fragment after the completion of current burst.

To adaptively combating the volatile behavior of a lossy channel, the Bite Error Rate (BER), e_{ber} of a transmission channel is directly calculated from the Signal to Noise Ratio (SNR) sensed at a receiver. At the end of the burst, the receiver informs the sender about the fragment loss, and retransmission attempts (*ReTX*). *ReTX* is calculated as in (4) at the receiver end and piggybacked on the NACK.

$$ReTX = ReTX_{max} - \left\lceil \log_{10} \left(\frac{1}{e_{ber}} \right) \right\rceil \quad (4)$$

where, $ReTX_{max}$ is the threshold

The second term in the right side of (4) decreases with an increase of the BER value of the corresponding channel and therefore, the number of adaptive re-transmission attempts, *ReTX* will increase, and *vice versa*. $ReTX_{max}$ may be a tuning parameter depending on the characteristics of a channel. Thus an initial $ReTX_{max}$ value can be set empirically and then, optimized through experiment. After taking the maximum number of attempts, the packet is considered to be undeliverable and discarded from the system.

4.4 Data Forwarding in SS-MAC

From the above analysis, we conclude that in a carefully planned MAC protocol for multimedia applications, per hop data delivery plays a crucial role in the overall success of a system. Influenced by the idea of message passing [5] designed for handling unorthodox size packet in scalar sensor network, we propose SS-MAC protocol for multimedia applications with an adaptive re-transmission technique.

In our work, the large multimedia packet is broken down into several small sized fragments, and transmitted them in burst as in Fig. 6. The channel is allocated by *RTS+CTS* contention method only at the first slot of data transmission. Afterwards, sender will stream the remaining fragments in a nonintermittent way.

Input: multimedia packet (P) and fragment size (s)

1. Start of sending process
2. Divide P of size s into n fragments
3. Augment n and ID in each fragment
4. *for* $\leftarrow 1$ to RTS_{max}
 - a. Send *RTS*
 - b. If it hears nothing, *continue*
 - c. If it hears a *CTS* packet
 - i. Stream all the fragmented packets with necessary interval; and *break*

end for

5. *If* it gets a *NACK* within a timeout interval after last packet
 - a. Retransmit the fragments specified by *NACK*

else

- b. Change state accordingly

end if

6. End of sending process

Fig. 6: Block sending process within a big-slot

After sending the final fragment, a receiver will acknowledge the sender about the failure of any fragments as in Fig. 7. For successful transmission, sender will wait for an *ACK* and start sending the next multimedia packet when *ACK* timer expires. In case of failure, sender will retransmit the missing data fragments for a number of times specified by the receiver depending on the condition of a channel. The following algorithm clearly states the process.

Input: Fragments (f), and total number (n) of fragments

1. Start of receiving process
2. *If* it senses a *RTS* packet
 - a. Send a *CTS* packet to the sender
 - b. Wait for the timeout interval
 - c. If nothing happens, *Exit*

end if
3. Buffer all transmitted data fragments
4. Inspect the checksum
5. *If* n fragments have received correctly
 - a. Reconfigure this node as the future sender of the packet
 - b. Change state accordingly, and *Exit*

else

 - c. Construct an *NACK* packet with ID of corrupted fragments and *ReTX*, and do following:
 - i. Send the *NACK* packet to the sender
 - ii. Receive the retransmitted copies
 - iii. Fuse the corrected copies in order
 - iv. Reconfigure this node as

the future sender of the packet
 V. Go to the sending state, and Exit
 end if
 6. End of receiving process

Fig. 7: Block receiving process within a big-slot

V. SIMULATION EXPERIMENTS

5.1 Simulation Environment

In order to evaluate the performance of SS-MAC, a set of simulation experiments have been performed using NS-2.34 simulator using random waypoint model. We compare our proposed SS-MAC with IEEE 802.11-based MAC, SMAC and BA-MAC for various simulation scenarios. The simulation parameters and values are given in Table II. The simulation for each scenario was performed five times, and then the average value for each metric was calculated.

TABLE II: Simulation parameters

Parameter	Value
Simulator	NS-2.34
Mobility model	Random waypoint
Traffic	CBR
Transmission range	20m
Number of nodes (MAX)	50
Terrain size ($a \times a$)	$a = 100m$
Maximum speeds	5, 10, 15 m/s
Pause time	30s
Number of sessions	15
Simulation time	600 seconds
Packet size	512 bytes
Packet transmission rate	4 packets/s
Channel Bit Rate	1 Mbit/s
Slot time, T	20 μs
Retransmit Limit, $ReTX$	2 ~ 4 (Adaptive)
Buffer Size	40 Packets
BER	$10^{-2} \sim 10^{-4}$
Transmit Power	28 mW

To compare SS-MAC with other MAC protocols, we use some metrics such as energy consumption, packet delivery ratio and end-to-end delay for multihop WSNs.

Packet delivery ratio (PDR): It indicates the ratio of the total number of data packets received at destinations to the total number of data packets generated during simulation.

$$PDR = \frac{\sum_{i \in S} nPacketsReceived(i.d)}{\sum_{i \in S} nPacketsSent(i.s)} \quad (5)$$

where S is a set of sessions created during the simulation, and $nPacketsReceived(i.d)$ and $nPacketsSent(i.s)$ are the number of packets received at a destination d and sent from a source s for the session i , respectively.

End-to-End Delay (E2ED): The average time taken to deliver a data packet from its source to its destination is as follows:

$$E2ED = \frac{1}{R} \sum_{i=1 \dots n} \sum_{j=1 \dots k_i} (r(p_{ij}) - t(p_{ij})) \quad (6)$$

where R is the total number of packets received by all destinations, p_{ij} is the sequence of j^{th} packets received at node i , and $r(p_{ij})$ and $t(p_{ij})$ is the receiving and transmitting time of p_{ij} , respectively.

According to [20], the CC2420 radio consumes 23 mA current in a receiving or listening mode, 8.5 mA current when transmitting at -25 dBm, 21 μA current in an idle mode, and 1 μA current in a sleep mode. Therefore, due to measure the energy consumption of a sensor mote, we count the amount of time that each node has to spend in a particular mode: *sleep*, *idle*, *receiving* or *transmitting*. Then, energy consumption of a node is calculated by multiplying the cumulative time stayed at each mode and power consumed to operate the radio in that mode, considering a battery of 3 volts. In this way, energy consumption is measured indirectly because the direct measurement of current imposes an additional burden on the low-powered sensor motes.

5.2 Simulation Results

To maximize data transmission efficiency over an error prone wireless channel, the optimum size of a data packet should be around of 152 byte for any terrestrial communication [19]. Since the size of a multimedia packet is large, we divided a multimedia data packet into a number of data fragments (usually 125 byte), and add the necessary PHY and MAC headers for increasing transmission efficiency.

The simulation results of our propose SS-MAC along with the other three standard MAC protocols are shown in in this section. In Fig. 8, packet delivery ratio (PDR) is simulated of a sensor node at different levels (depths) in a tree network. It is shown that the PDR for SS-MAC is higher than other three MACs, especially far better than 802.11-based MAC and SMAC protocols. The reason for lower PDR in 802.11-based MAC and SMAC is that they are intended for small scale data packet, as well as, for single hop data transmission. When it comes to the question of multimedia and multihop data transmission, those two protocols show lower PDR than others due to their less adaptable nature toward the changing of channel conditions.

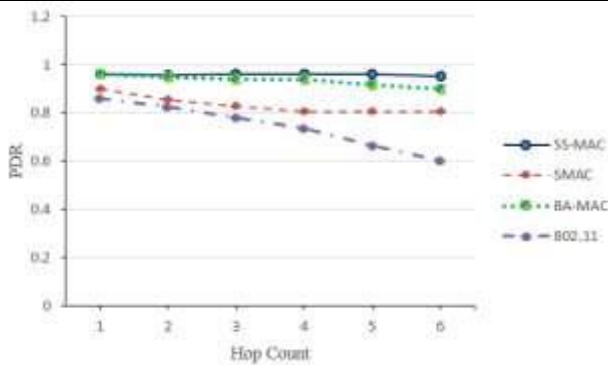


Fig. 8: Packet delivery ratio at different depths of a tree

BA-MAC, on the other hand, shows a better PDR than those two protocols. However, its packet-wise ACK makes its PDR lower than the proposed blockwise ACK-based SS-MAC protocol.

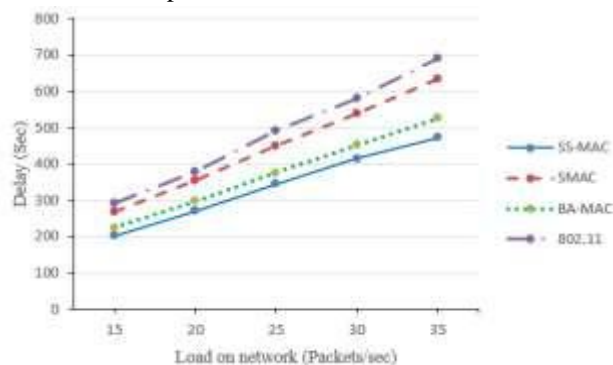


Fig. 9: End-to-end delay for various load levels

Fig. 9 depicts the end-to-end delay for data packets when the network load is varied. As of the figure, SMAC and 802.11 rise more sharply than SS-MAC, and BA-MAC rises marginally compared to SS-MAC. Though the delay reduction technique used in our proposed MAC seems to be insignificant compared to BA-MAC for single hop data transmission, this small delay reduction gives a significant improvement in multihop data transmission. The interesting outcome is that both 802.11 and SMAC fail to achieve the real-time constraints quickly as the load increases. However, our proposed MAC is less sensitive to network load and can easily support multimedia data transmission in WSNs.

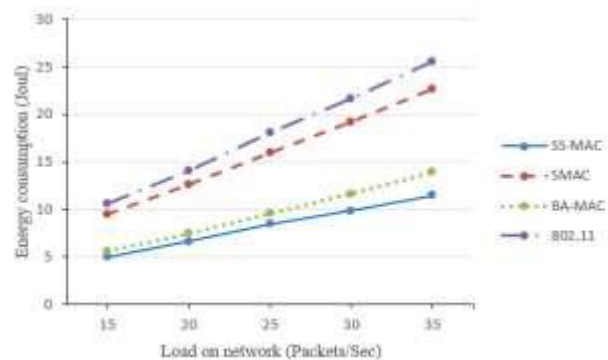


Fig. 10: Energy consumption under different loads

Due to space constraint, we do not provide the detail calculations of energy consumption efficiency. Our proposed SS-MAC is inherently energy efficient for its dynamic slot allocation ability, data aggregation and filtering. Moreover, we are able to reduce a sufficient amount of energy consumption by reducing the control overhead. Fig. 10 shows that our proposed protocol outperforms the other two standard MAC protocols, while it marginally outperforms BA-MAC. In summary, we can say that the proposed SS-MAC shows the better performance than other three standard protocols in every aspects.

VI. CONCLUSION

In this paper, we have developed SS-MAC protocol capable of reducing the transmission delay for real-time multimedia data in industrial WSNs. For such type of applications, we discovered some suitable parameters through analyzing the contention characteristics of wireless nodes with a due consideration on existing MAC protocols. Moreover, our modified formula for adaptive retransmission of multimedia data packets gives an improved data transmission rate. In simulation results, SS-MAC shows the superior performance over the 802.11-based MAC, SMAC and BA-MAC in improving data transmission efficiency as well as in reducing delay and energy consumption. Therefore, we conclude that SS-MAC can be an efficient MAC protocol for the real-time multimedia data transmission in industrial WSNs.

REFERENCES

- [1] L. Shi, A. Fapojuwo, N. Viberg, W. Hoople, and N. Chan, "The Effectiveness of QoS Constrained AODV Routing for Voice Support in Multi-Hop IEEE 802.11 Mobile Ad Hoc Networks," in IEEE Wireless Communications and Networking Conference (WCNC-2009), pp. 1-6, Hungary, 2009.
- [2] I. F. Akyildiz, T. Melodia, and K.R. Chowdury, "Wireless Multimedia Networks: A survey," IEEE Wireless Communications, vol. 14, no. 6, pp. 32-39, 2007.
- [3] P. Suriyachai, U. Roedig, and A. Scott, "A Survey of Protocols for Mission-Critical Applications in Wireless Sensor Networks," IEEE Communications Survey and Tutorials, vol.14, no. 2, pp. 240-264, 2012.
- [4] LAN MAN Standards Committee of the IEEE Computer Society, Wireless LAN medium access control (MAC) and physical layer (PHY) specification, IEEE, New York, NY, USA, IEEE Std 802.11-1999 edition, 1999.
- [5] W. Ye, J. Heidemann, and D. Estrin, "Medium access control with coordinated adaptive sleeping for

- wireless sensor networks,” IEEE/ACM Trans. Netw., vol. 12, pp. 493-506. June 2004.
- [6] G. Lu, B. Krishnamachari, and C. S. Raghavendra, “An adaptive energy efficient and low-latency MAC for data gathering in wireless sensor networks,” in 18th Int. Parallel and Distributed Processing Symp., pp. 224-231, Santa Fe, NM, USA, 2004.
- [7] T. V. Dam and K. Langendoen, “An Adaptive Energy-Efficient MAC Protocol for Wireless Sensor Networks,” in 1st ACM Conf. Embedded Networked Sensor Systems, pp. 171-180, Los Angeles, CA, USA, 2003.
- [8] R. Biswas, V. Jain, C. Ghosh, and D. P. Agrawal, “On-Demand Reliable Medium Access in Sensor Networks,” in 7th IEEE Int. Symp. on a World of Wireless, Mobile and Multimedia Networks, WoWMoM’06, pp. 251-257, Buffalo, NY, USA, 2006.
- [9] E. Felemban, C. -G. Lee, and E. Ekici, “MMSPEED: Multipath Multi-SPEED Protocol for QoS Guarantee of Reliability and Timeliness in Wireless Sensor Networks,” IEEE Trans. Mobile Comput., vol. 5, pp.738-754, June 2006.
- [10] G. Bianchi, “Performance Analysis of the IEEE 802.11 Distributed Coordination Function,” IEEE Journal on Selected Areas in Communications, Vol. 18, no. 3. March 2000.
- [11] P. Chatzimisios, A. C. Boucouvalas, and V. Vitas, “IEEE 802.11 Packet Delay – A Finite Retry Limit Analysis,” IEEE Global Telecommunications Conference, GLOBECOM’03, vol. 2, pp. 950-954, San Francisco, USA, 2003.
- [12] B. J. Oh and C. W. Chen “Analysis of Retry Limit for Supporting VoIP in IEEE 802.11 EDCA WLANs,” in 16th International Conference on Computer Communications and Networks, ICCCN’2007, pp. 464-469, Hawaii, USA, 2007.
- [13] Y. -T. Park, P. Sthapit, D. -H. Lee, Y. -S. Choi, and J. -Y. Pyun, “Data Fragmentation Scheme with Block ACK in Wireless Sensor Networks,” in 5th FTRA International Conference on Multimedia and Ubiquitous Engineering, pp. 79-83, Crete, Greece, June 2011.
- [14] LAN MAN Standards Committee of the IEEE Computer Society, Wireless LAN Medium Access Control (MAC) and Physical Layer (PHY) specifications. IEEE Std 802.11e-2005 edition, 2005.
- [15] J. Molina, J. M. Mora-Merchan, J. Barbancho, and C. Leon, “Multimedia Data Processing and Delivery in Wireless Sensor Networks,” Wireless Sensor Networks: Application-Centric Design, Open Access, Chapter 23, December 2010.
- [16] The Nyquist–Shannon Sampling Theorem, http://ptolemy.eecs.berkeley.edu/eecs20/week13/nyquist_Shannon.html
- [17] H. Yokoo, “Overflow/underflow-free floating-point number representations with self-delimiting variable-length exponent field,” in 10th Symposium on Computer Arithmetic, pp. 110-117, Grenoble, France, 1991.
- [18] L. Parziale, D. T. Britt, C. Davis, J. Forrester, W. Liu, C. Matthews, and N. Rosselot, “TCP/IP Tutorial on Technical Overview,” International Technical Support Organization, 8th Edition, IBM. December 2006.
- [19] M. C. Vuran and I. F. Akyildiz, “Cross-layer Packet Size Optimization for Wireless Terrestrial, Underwater, and Underground Sensor Networks,” in 27th Conference on Computer Communications, INFOCOM 2008, pp. 226-230, Phoenix, Arizona, USA, 2008.
- [20] CC2420 Datasheet, TI. Available online: <http://www.ti.com/lit/ds/swrs041b/swrs041b.pdf> (accessed on 28 September 2013).

Hybrid Model Based on User Tags and Textual Passwords and Pearsonian Type III Mixture Model

Pavan Gujjar Panduranga Rao¹, Dr.P.Srinivasa Rao², Dr. G. Lavanya Devi³

¹Research Scholar, Department of Computer Science and System Engineering, Andhra University College of Engineering (A), Vishakhapatnam, Andhra University, India

^{2,3}Professor, Department of Computer Science and System Engineering, Andhra University College of Engineering(A), Andhra University, Vishakhapatnam, Andhra Pradesh, India

Abstract— The latest advancements in Science and Technology, have witnessed radical changes in the banking system. Today most of the banks adopt the net banking facility and most of the users are also addicted to this system. Accordingly, most of the transactions are now online based and much emphasis is therefore needed to ensure the security of authenticating a person and validating the transaction. Many models are therefore proposed in the literature. Most of these are an alphanumeric based password schemes or biometric schemes or graphical password based schemes. Each of these models is proposed by underlying an advantage. The alphanumeric passwords are proposed, with the assumption that generating the password is easy and the generated password is unique, the biometric password schemes are proposed with the assumption that tampering a biometric is next to impossible. Graphical passwords are proposed with an option to the user so that he can select an image of his choice and then select some points which is called a click pattern, which is unique to every user.

Keywords— Graphical Password Authentication, Pearsonian Type III Mixture Model, Statistics, Probabilistic model, MIR Flickr.

I. INTRODUCTION- PEARSONIAN TYPE III MIXTURE MODEL

In the earlier research work, we developed and analyzed a model for segmentation based on the mixture Pearsonian Type I Distribution with K-means algorithm. These models are useful when the pixel intensities of the feature

vector in the image regions are left skewed. But in some image the pixel intensities of the image regions may not be left skewed. They may have long upper tail with a right skewed nature. To segment these types of images, it is needed to consider that the pixel intensities of the image regions follow a right skewed distribution. Hence, in this research article we develop and analyze image segmentation method based on mixture of Pearsonian Type III Distribution. The Pearsonian Type III Distribution is capable of portraying right skewed and long upper tail distributions. Here, it is assumed that the pixel intensities of each image region follow Type III Pearsonian Distribution and the pixel intensities in the whole image is characterized by a finite mixture of Pearsonian Type III Model.

II. PEARSONIAN TYPE III MIXTURE DISTRIBUTION

In any image analysis, the entire image is considered as a union of several image regions. In each image region the image data is quantified by pixel intensities. The pixel intensity $z = f(x, y)$ for a given point (pixel) (x, y) is a random variable, because of the fact that the brightness measured at a point in the image is influenced by various random factors like vision, lighting, moisture, environmental conditions etc. To model the pixel intensities of the animal and human image regions, it is assumed that the pixel intensities of the region follow a Pearsonian Type III Distribution (PTIHD). The probability density function of the pixel intensity is

$$f_i(z | a_i, q_i) = \frac{(q_i a_i)^{(q_i a_i + 1)}}{e^{q_i a_i} a_i \Gamma(q_i a_i + 1)} e^{-q_i z} \left(1 + \frac{z}{a_i}\right)^{a_i q_i}, -a_i \leq z_s < \infty, -\infty \leq q_i < \infty \quad (\text{Equation-1})$$

Where Γ is a Gamma Function

For different values of the parameters the various shapes of probability curves associated with Pearsonian Type III Distribution are shown in Figure-1.

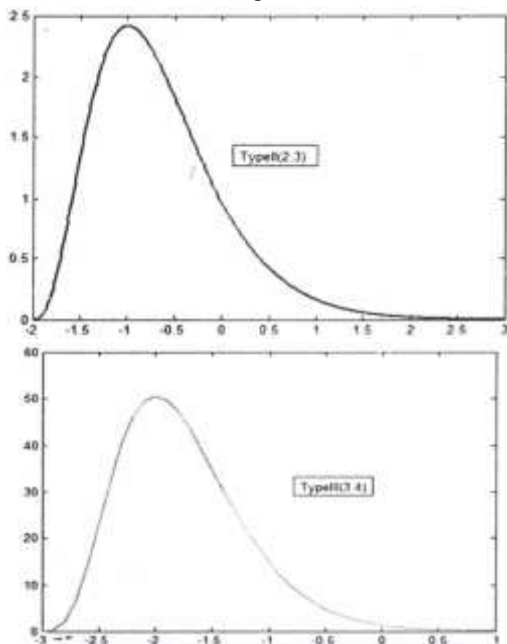


Fig.1: Frequency Curves of Pearsonian Type III Distribution

The entire animal and human image is a collection of regions which are characterized by Pearsonian Type III Distribution. Here, it is assumed that the pixel intensities of the whole image follow a K-component mixture of Pearsonian Type III Distribution and its probability density function is of the form:

$$p(z) = \sum_{i=1}^K \alpha_i f_i(z | a_i, q_i)$$

Where, K is number of regions, $0 \leq \alpha_i \leq 1$ are weights such that $\sum \alpha_i = 1$ and is $f_i(z | a_i, q_i)$ as given in equation (1) α_i is the weight associated with i^{th} region in the whole image.

In general the pixel intensities in the image regions are statistically correlated and these correlations can be reduced by spatial sampling (Lei T. and Sewehand W. (1992)) or spatial averaging (Kelly P.A. et al (1998)). After reduction of correlation, the pixels are considered to be uncorrelated and independent. The mean pixel

intensity of the whole image is $E(Z) = \sum_{i=1}^K \alpha_i \mu_i$

III. INDENTATIONS AND EQUATIONS

In this section, it is derived estimates of the model parameters using Expectation Maximization (EM) algorithm. The likelihood function of the observations given by

Z_1, Z_2, \dots, Z_N drawn from an image with probability density function is given in equation – 1.

$$L(\theta) = \prod_{s=1}^N p(Z_s, \theta^{(1)})$$

That is $L(\theta) = \prod_{s=1}^N \left(\sum_{i=1}^K \alpha_i f_i(Z_s, \theta) \right)$

This implies

$$L(\theta) = \sum_{s=1}^N \log \left(\sum_{i=1}^K \alpha_i f_i(Z_s, \theta) \right)$$

$\alpha_i, i=1, 2, \dots, K$ is the set of parameters

$$\log L(\theta) = \sum_{s=1}^N \log \left[\sum_{i=1}^K \frac{\alpha_i (q_i a_i)}{e^{q_i a_i} \Gamma(q_i a_i + 1)} e^{-q_i z_s} \left[1 + \frac{z_s}{a_i} \right]^{q_i a_i} \right]$$

(Equation-2)

The beginning step of the Expectation Maximization algorithm requires the initialization of two parameters

$(\alpha_i, q_i; i=1, 2, \dots, k)$ and component weights

$(\alpha_i; i=1, 2, \dots, K)$ from the observed values. The idea of EM algorithm is to iteratively calculate Maximum likelihood estimates of unknown parameters

$$\theta = (\alpha_i, q_i, \alpha_i; i=1, 2, \dots, K)$$

E-STEP :

In the expectation (E) step, the expectation value of $\log L(\theta)$ with respect to the initial parameter vector $\theta^{(0)}$

$$Q(\theta; \theta^{(0)}) = E_{\theta^{(0)}} [\log L(\theta) / \bar{z}]$$

Given the initial parameters $\theta^{(0)}$, one can compute the density of pixel intensity z_s as

$$p(z_s, \theta^{(1)}) = \sum_{i=1}^K \alpha_i^{(1)} f_i(z_s, \theta^{(1)}), L(\theta) = \prod_{s=1}^N p(z_s, \theta^{(1)})$$

This implies $\log L(\theta) = \sum_{i=1}^K \log \left[\sum_{i=1}^K \alpha_i f_i(z_s, \theta^{(1)}) \right]$

(Equation-3)

The conditional probability of any observation z_s , belongs to any region K is

$$t_k(z_s, \theta^{(1)}) = \left[\frac{\alpha_k^{(1)} f_k(z_s, \theta^{(1)})}{p(z_s, \theta^{(1)})} \right] = \left[\frac{\alpha_k^{(1)} f_k(z_s, \theta^{(1)})}{\sum_{i=1}^K \alpha_i^{(1)} f_i(z_s, \theta^{(1)})} \right]$$

The conditional of the log likelihood function of the sample is

$$Q(\theta; \theta^{(0)}) = E_{\theta^{(0)}} [\log L(\theta) / \bar{z}]$$

Following the heuristic arguments of Jeff A. Bilmes (1997) we have

$$Q(\theta; \theta^{(1)}) = \sum_{i=1}^K \sum_{s=1}^N (t_i(z_s, \theta^{(1)})) (\log f_i(z_s, \theta^{(1)}) + \log \alpha_i^{(1)})$$

(Equation-4)

But we have

$$f_i(z/a_i, q_i) = \frac{(q_i, a_i)^{(q_i a_i + 1)}}{e^{q_i a_i} a_i \Gamma(q_i, a_i + 1)} \left[1 + \frac{z_s}{a_i} \right]^{q_i a_i}$$

and

$$Q(\theta; \theta^{(1)}) = \sum_{i=1}^K \sum_{s=1}^N (t_i(z_s, \theta^{(1)})) (\log f_i(z_s, \theta^{(1)}) + \log \alpha_i^{(1)})$$

M-STEP:

$$\frac{\partial}{\partial \alpha_i} \left[\sum_{i=1}^K \sum_{s=1}^N (t_i(z_s, \theta^{(1)})) \log \left[\frac{(q_i, a_i)^{(q_i a_i + 1)}}{e^{q_i a_i} a_i \Gamma(q_i, a_i + 1)} \left[1 + \frac{z_s}{a_i} \right]^{q_i a_i} + \log \alpha_i \right] \right] + \lambda \left[1 - \sum_{i=1}^K \alpha_i \right] = 0$$

This implies

Summing both sides over all observations, we get $\lambda = N$

$$\hat{\alpha}_i = \frac{1}{N} \sum_{s=1}^N t_i(z_s, \theta^{(1)})$$

Therefore

The updated equation of for α_i $(l+1)^{th}$ iteration is

$$\alpha_i^{(l+1)} = \frac{1}{N} \sum_{s=1}^N t_i(z_s, \theta^{(1)})$$

$$= \frac{1}{N} \sum_{s=1}^N \left[\frac{\alpha_i^{(l)} f_i(z_s, \theta^{(1)})}{\sum_{i=1}^K \alpha_i^{(l)} f_i(z_s, \theta^{(1)})} \right]$$

(Equation-6)

For updating the parameter $\alpha_i ; i=1,2,\dots,k$ we consider the derivative of $Q(\theta; \theta^{(1)})$ with respect to α_i and equate it to zero.

We have $Q(\theta; \theta^{(1)}) = E[\log L(\theta^{(1)})]$

Therefore $\frac{\partial}{\partial \alpha_i} Q(\theta; \theta^{(1)}) = 0$

implies $E[(\log L(\theta^{(1)}))] = 0$

For obtaining the estimation of the model parameters one has to maximize $Q(\theta; \theta^{(1)})$ such that $\sum_{i=1}^K \alpha_i = 1$. This can be solved by applying the standard solution method for constrained maximum by constructing the first order Lagrange type function,

$$s = \left[E(\log L(\theta^{(1)})) + \lambda \left[1 - \sum_{i=1}^K \alpha_i \right] \right]$$

(Equation-5)

Where, is λ Lagrange multipliers combining the constraint with the log likelihood function to be maximized

Hence, $\frac{\partial S}{\partial \alpha_i} = 0$

This implies

$$\frac{\partial}{\partial \alpha_i} \left[\sum_{i=1}^K \sum_{s=1}^N (t_i(z_s, \theta^{(1)})(\log f_i(z_s, \theta^{(1)}) + \log \alpha_i^{(l)}) \right] = 0$$

$$\frac{\partial}{\partial \alpha_i} \left[\sum_{i=1}^K \sum_{s=1}^N \left[(t_i(z_s, \theta^{(1)})) \log \left[\frac{(q_i, a_i)^{(q_i a_i + 1)}}{e^{q_i a_i} a_i \Gamma(q_i, a_i + 1)} \left[1 + \frac{z_s}{a_i} \right]^{q_i a_i} + \log \alpha_i^{(l)} \right] \right] = 0$$

$$\frac{\partial}{\partial \alpha_i} \sum_{i=1}^K \sum_{s=1}^N \left[(q_i a_i + 1) \log(q_i a_i) - \log a_i - q_i a_i - \log(\Gamma(q_i a_i + 1)) - q_i z_s + q_i a_i \log \left[1 + \frac{z_s}{a_i} \right] \right] t_i(z_s, \theta^{(1)}) = 0$$

$$\sum_{s=1}^N \left[(q_i) \log(q_i a_i) + \frac{(q_i a_i + 1)}{q_i a_i} q_i - q_i + q_i \left[\log \left[1 + \frac{z_s}{a_i} \right] - \frac{z_s}{a_i + z_s} \right] - q_i \Gamma(q_i a_i + 1) t_i(z_s, \theta^{(1)}) \right] = 0$$

$$\sum_{s=1}^N \left[\left[q_i \log \left[q_i a_i \left[\frac{a_i + z_s}{a_i} \right] \right] \right] + \frac{1}{a_i} - \frac{a_i z_s}{a_i + z_s} \right] - q_i \Gamma(q_i a_i + 1) t_i(z_s, \theta^{(1)}) = 0$$

$$\sum_{s=1}^N \left[\frac{a_i z_s}{a_i + z_s} + q_i \Gamma(q_i a_i + 1) - q_i \log(q_i (a_i + z_s)) \right] t_i(z_s, \theta^{(1)}) = \frac{1}{a_i} \sum_{s=1}^N t_i(z_s, \theta^{(1)})$$

$$a_i = \frac{\sum_{s=1}^N t_i(z_s, \theta^{(1)})}{\left[\frac{a_i z_s}{a_i + z_s} + q_i \Gamma(q_i a_i + 1) - q_i \log(q_i (a_i + z_s)) \right] t_i(z_s, \theta^{(1)})}$$

The updated equation of a_i at $(l+1)^{th}$ iteration is

$$a_i^{(l+1)} = \frac{\sum_{s=1}^N t_i(z_s, \theta^{(l)})}{\left[\frac{q_i^{(l)} z_s}{a_i^{(l)} + z_s} + q_i^{(l)} \Gamma(q_i^{(l)} a_i^{(l)} + 1) - q_i^{(l)} \log(q_i^{(l)} a_i^{(l)} (a_i + z_s)) \right] t_i(z_s, \theta^{(l)})}$$

Where $t_i(z_s, \theta^{(1)}) = \frac{\alpha_i^{(1)} f_i(z_s, \theta^{(1)})}{\sum_{i=1}^K \alpha_i^{(1)} f_i(z_s, \theta^{(1)})}$

For updating the parameter $q_i, i=1,2,\dots,K$ we consider the derivative of Q

With respect to q_i and equate it to zero

We have $Q(\theta; \theta^{(l)}) = E[\log L(\theta; \theta^{(l)})]$

Therefore $\frac{\partial}{\partial q_i} Q(\theta; \theta^{(l)}) = 0$ implies $E \left[\frac{\partial \log L(\theta; \theta^{(l)})}{\partial q_i} \right] = 0$

$$\frac{\partial}{\partial q_i} \left[\sum_{i=1}^K \sum_{s=1}^N (t_i(z_s, \theta^{(1)})(\log f_i(z_s, \theta^{(1)}) + \log \alpha_i^{(l)}) \right] = 0$$

$$\frac{\partial}{\partial q_i} \sum_{i=1}^K \sum_{s=1}^N \left[(q_i a_i + 1) \log(q_i a_i) - \log a_i - q_i a_i - \log(\Gamma(q_i a_i + 1)) - q_i z_s + q_i a_i \log \left[1 + \frac{z_s}{a_i} \right] \right] t_i(z_s, \theta^{(1)}) = 0$$

$$\begin{aligned} & \frac{\partial}{\partial q_i} \sum_{i=1}^K \sum_{s=1}^N \left[(q_i a_i + 1) \log(q_i a_i) - \log a_i - q_i a_i - \log(\Gamma(q_i a_i + 1)) - q_i z_s + q_i a_i \log \left[1 + \frac{z_s}{a_i} \right] \right] t_i(z_s, \theta^{(1)}) = 0 \\ & \sum_{s=1}^N \left[\alpha_i \log(q_i a_i) + \frac{(q_i a_i + 1) a_i}{q_i a_i} - q_i - z_s + a_i \log \left[1 + \frac{z_s}{a_i} \right] - \frac{\int_0^l z_s^{q_i a_i} a_i e^{-z_s} \log z_s dz_s}{\int_0^l z_s^{q_i a_i} a_i e^{-z_s} dz_s} \right] t_i(z_s, \theta^{(1)}) = 0 \\ & \sum_{s=1}^N \left[\alpha_i \log(q_i a_i) + \frac{(q_i a_i + 1)}{q_i a_i} - (q_i - z_s) + a_i \log \left[1 + \frac{z_s}{a_i} \right] - \frac{\int_0^l z_s^{q_i a_i} a_i e^{-z_s} \log z_s dz_s}{\int_0^l z_s^{q_i a_i} a_i e^{-z_s} dz_s} \right] t_i(z_s, \theta^{(1)}) = 0 \\ & \sum_{s=1}^N \left[a_i \log \left[q_i a_i \left[\frac{z_s + a_i}{a_i} \right] \right] - (a_i + z_s) + \frac{(q_i a_i + 1)}{q_i} - \frac{a_i \Gamma(q_i a_i + 1) \psi_0(q_i a_i + 1)}{\psi_0(q_i a_i + 1)} \right] t_i(z_s, \theta^{(1)}) = 0 \\ & \sum_{s=1}^N \left[a_i \log \left(q_i a_i \left(\frac{z_s + a_i}{a_i} \right) \right) - (a_i + z_s) + \frac{(q_i a_i + 1)}{q_i} - a_i \Gamma(q_i a_i + 1) \right] t_i(z_s, \theta^{(1)}) = 0 \\ & q_i = \frac{\sum_{s=1}^N \left[a_i \Gamma(q_i a_i + 1) + (a_i + z_s) - a_i \log \left(q_i a_i \left(\frac{z_s + a_i}{a_i} \right) \right) \right]}{a_i \sum_{s=1}^N t_i(z_s, \theta^{(1)})} - 1 \quad \text{(Equation-7)} \end{aligned}$$

The updated equation of $q_{il(l+1)}^{th}$ iteration is

$$q_i^{(l+1)} = \frac{\sum_{s=1}^N \left[a_i^l \Gamma(q_i^{(l)} a_i^{(l)} + 1) + (a_i^{(l)} + z_s) - a_i^{(l)} \log \left(q_i^{(l)} a_i^{(l)} \left(\frac{z_s + a_i^{(l)}}{a_i^{(l)}} \right) \right) \right]}{a_i^{(l)} \sum_{s=1}^N t_i(z_s, \theta^{(1)})} - 1 \quad \text{(Equation-8)}$$

Where $t_i(z_s, \theta^{(1)}) = \frac{\alpha_i^{(l+1)} f_i(z_s, \theta^{(1)})}{\sum_{i=1}^K \alpha_i^{(l+1)} f_i(z_s, \theta^{(1)})}$

IV. K-MEANS CLUSTERING ALGORITHM

The K-means algorithm is one of the simplest clustering technique for which the objective is to find the partition of the data which minimizes the squared error or the sum of squared distances between all points and their respective cluster centers (Rose H. Turi, (2001)). K-means algorithm uses an iterative procedure that minimizes the sum of distances from each object to its cluster centroid, over all clusters. This evaluational procedure consists of the following steps.

1. Randomly choose K data points from the whole

data set as initial clusters. These data points represent initial cluster centroids.

2. Calculate Euclidean distance of each data point from each cluster center and assign the data points to its nearest cluster center.
3. Calculate new cluster center so that squared error distance of each cluster should be minimum.
4. Repeat step II and III until clustering centers do not change.
5. Stop the process.

In the above algorithm, the cluster centers are only updated once all points have been allocated to their

closed cluster center. The advantage of K-Means algorithm is that it is a very simple method, and it is based on intuition about the nature of a cluster, which is that the within cluster error should be as small as possible. The disadvantage of this method is that the number of clusters must be supplied as a parameter, leading to the user having to decide what the best number of clusters for the image is (Rose H. Turi, (2001)). Success of K-means algorithm depends on the parameter K, number of clusters in image.

After determining the final value of K (number of regions), we obtain the initial estimates a_i , q_i , and α_i of for the i th region using the segmented region pixel intensities with Pearsonian Type III Distribution. The initial estimate a_i , $a_i=1/K$, where is taken as $i=1,2,\dots,K$. The parameters a_i and q_i are estimated by the method of moment's μ_1 as first moment μ_i and its three central moment's μ_2 , μ_3 and μ_4 .

V. CONCLUSION

The number of image regions is estimated by utilizing the image histogram. The model parameters are estimated by deriving the updated equations of EM algorithm. The initialization of the model parameters is done through K-means algorithm and moment method of estimation. The segmentation algorithm is developed through maximizing the component likelihood under Bayes framework applied in MIR Flickr .

ACKNOWLEDGEMENT

I Pavan Gujjar P, working as Professor and Head in Computer Engineering Department sincerely acknowledge thanks to St.John College of Engineering and Management (SJCEM), Palghar for Providing the infrastructure support in publishing this research article under ALDEL Educational and Research Consultancy Services.

REFERENCES

- [1] K.Srinivasa Rao, M.Seshashayee, Ch.Satyanarayana, P.Srinivasa Rao, (2012), "Performance of Hybrid Image Segmentation Based On New Symmetric Mixture Model and Hierarchical Clustering", *International Journal of Graphics and Image Processing*, vol 2, issue 3.
- [2] Kelly .P.A et al(1988), " Adaptive segmentation of speckled images using a hierarchical random field model". *IEEE Transactions Acoust. Speech. Signal Processing*, Vol.36, No.10, Pg.1628-1641.
- [3] Komanduri, S. & Hutchings, D.R. (2008), "Order and entropy in picture passwords", *Proceedings of graphics interface 2008*, Canadian Information Processing Society, Pg. No. 115.
- [4] Ku W. C. and Chang S. T., "Impersonation attack on a dynamic ID based remote user authentication using smartcards", *IEICE Transaction on Communication*, Vol.88– b, No.5, May 2005.
- [5] L. D. Paulson, "Taking a Graphical Approach to the Password," *Computer*, vol. 35, 2002, Pg. No.19.
- [6] L.Lamport, "Password authentication with insecure communication," *Communications of the ACM*, v.24 n.11, November 1981, Pg. No. 770-772.
- [7] *Learning and Cybernetics*, Vol. 6, Issue 12-15, '08, Pg 3283 – 3287
- [8] Lei T. and Udupa J. (2003) "Performance evaluation of finite normal mixture model-based image segmentation techniques," *IEEE Transactions on Image Processing*, vol. 12, no.10, Pg. 1153–1169.
- [9] Lerner, J. 2010. *The Litigation of Financial Innovations*. *Journal of Law and Economics*, 53(4), Pg. 807-831.
- [10] Li Gong, "A Security Risk of Depending on Synchronized clocks" in *ACM Operating Systems Review*, Vol 26, No. 1, Jan '92, Pg. 49-53.
- [11] Lie. T and Sewehand. W (1992), "Statistical approach to X -ray CT imaging and its Applications in image analysis", *IEEE Trans. Med. Imag.* Vol.11, No.1, Pg 53 -61.
- [12] M Sreelatha, M Shashi, M Anirudh, Md Sultan Ahamer, V Manoj Kumar, "International Journal of Network Security & Its Applications (IJNSA)", Vol.3, No.3, May 2011.
- [13] M. Burrows, M. Abadi, and R. Needham. "Logic of authentication", *ACM Transactions on Computer Systems*, Vol. 8(1), '90, Pg: 18-36.
- [14] M. Jordan and R. Jacobs (1994) "Hierarchical mixtures of experts and the EM algorithm", *Neural Computation*, 6: Pg. 181–214.
- [15] M. Naor and B. Pinkas, Efficient Oblivious Transfer Protocols, *Proceedings of 12th SIAM Symposium on Discrete Algorithms (SODA)*, January 7-9 2001, Washington DC, Pg. 448–457.
- [16] M.Frank, R.Biedert, E.Ma, I.Martinovic, and D.Song, (2013) "Touchalytics: On the applicability of touch screen input as a behavioral biometric for continuous authentication," *IEEE Trans. Information Forensics Security*, vol. 8, no. 1, Pg. 136–148.
- [17] M.Martinez-Diaz, J.Fierrez, and J.Galbally,(2013) "The DooDB graphical password database: Data analysis and benchmark results," *IEEE Access*, vol. 1, Pg. 596–605.
- [18] M.Seshashayee, K.Srinivasa Rao, Ch.Satyanarayana And P.Srinivasa Rao, (2011) "Image Segmentation Based on a Finite Generalized New Symmetric Mixture Model with K–Means", *International journal*

- of Computer Science Issues, Vol.8, No.3, Pg. 324-331.
- [19] M. Shahzad, A.X. Liu, and A. Samuel, "Secure unlocking of mobile touch screen devices by simple gestures: You can see it but you cannot do it," in *Proc. 19th Ann. Int. Conf. Mobile computer Networks*, 2013, Pg.39–50.
- [20] Marcos Martinez-Diaz, Julian Fierrez, and Javier Galbally, "The DooDB Graphical Password Database: Data Analysis and Benchmark Results", IEEE Access, September 2013.
- [21] Mclanchlan G. And Krishnan T (1997)., "The EM Algorithm and Extensions", John Wiley and Sons, New York -1997.
- [22] Mclanchlan G. and Peel D.(2000), "The EM Algorithm For Parameter Estimations", John Wileyand Sons, New York - 2000.
- [23] Michael Sherman, Gradeigh Clark, Yulong Yang, Shridatt Sugrim, Arttu Modig, Janne Lindqvist, Antti Oulasvirta, and Teemu Roos, 2014. "User-generated free-form gestures for authentication: security and memorability", In Proceedings of the 12th annual international conference on Mobile systems, applications, and services (MobiSys '14). ACM, New York, NY, USA, Pg. 176-189.
- [24] Michael Toomim, Travis Kriplean, Claus Portner, and " James Landay. 2011. Utility of Human-Computer Interactions: Toward a Science of Preference Measurement. In Proc. CHI'11: 29th Annual ACM Conference on Human Factors in Computing Systems. <http://doi.acm.org/10.1145/1978942.1979277>.
- [25] Min-Shiang Hwang and L. H. Li, "A new remote user authentication scheme using smart cards," IEEE Transactions on Consumer Electronics, vol. 46, no. 1, 2000, Pg. 28-30.
- [26] Misbahuddin M, Ahmed M.A, Rao A.A, Bindu C.S, Khan M.A.M, "A Novel Dynamic ID-Based Remote User Authentication Scheme", in the proceedings of Annual IEEE Indicon Conference, Delhi, 2006.

Enhancement of Natural Ventilation using Solar Chimney: A Numerical Investigation

Jitendra Kumar¹, Abhishek Raj², Hari Mohan Sharma³

¹M.Tech Scholar, Thermal Engineering, Apex Institute of Engineering & Technology, Jaipur, India

²M.Tech, Thermal Engineering, Apex Institute of Engineering & Technology, Jaipur, India

³ Assistant Professor, Mechanical Dept., Apex Institute of Engineering & Technology, Jaipur, India

Abstract— Rural areas have shortage of electricity, so natural ventilation becomes necessary. Ventilation through solar chimney harnesses solar energy as energy source and can be installed in rural buildings for improvement of air circulation. Rate of ventilation of a solar chimney for natural ventilation was investigated for both Horizontal type and Vertical type. Ventilation rate greatly depends on the temperature gradient of the room. The current work presents the comparative analysis of a room apartment with solar chimney of both types attached to them. In this study, a reduced scale Chimney of Horizontal and Vertical design is modelled through CFD to investigate the improvement of Natural Ventilation. Two different parameters have been considered for current study viz. Outlet Velocity and Temperature of Absorber plate.

Keywords— Solar Chimney, Natural Ventilation, Enhancement, Flow Velocity.

Nomenclature

L	Length of Duct (m)
W	Width of Duct (m)
H	Height of Duct (m)
m	Mass flow rate (kg/s)
T_{in}	Inlet Temperature (K)
T_{out}	Outlet Temperature (K)
V_{in}	Inlet Velocity (m/s)
V_{out}	Outlet Velocity(m/s)
R	Room
SC	Solar Chimney
$R-100$	Height of 100 mm in Room
$R-300$	Height of 300 mm in Room
$R-500$	Height of 500 mm in Room
$R-700$	Height of 700 mm in Room
$R-900$	Height of 900 mm in Room
$SC-100$	Height of 100 mm in Solar Chimney
$SC-300$	Height of 300 mm in Solar Chimney
$SC-500$	Height of 500 mm in Solar Chimney
$SC-700$	Height of 700 mm in Solar Chimney
$SC-900$	Height of 900 mm in Solar Chimney

I. INTRODUCTION

Most of the energy derived from the various system found on earth originate from sun. Sun emits massive amount of

electromagnetic radiation into space. The mean distance between Sun and Earth is 1.50×10^8 km. At surface of the sun the intensity of solar radiation is 6.33×10^7 W/m². It subtends an angle of only 32 minutes at the earth's surface. Solar radiation that reaches at surface of the earth is quite differs in both amount and character from the radiation at the top of atmosphere. Some amount of the radiation is reflected back into the atmosphere by clouds. Then the radiation entering the atmosphere is absorbed by molecules and dust particle present in air. U.V. rays are absorbed by oxygen (O₃) Ozone and some of the infrared energy is absorbed by water vapour and CO₂. Some of the radiations is scattered by dust particle molecule and droplet in clouds and atmosphere. Solar radiation that reaches the ground directly from sun without being absorbed or scattered is called Direct Radiation or Beam Radiation. Solar radiation obtained from sun after its direction has been hanged by reflection and scattering is diffuse radiation.

The total solar radiation energy received on horizontal surface of unit area on the ground in unit time. Position of Sun directly overhead is Zenith Position. Zenith angle is the angle between the beam from the sun and vertical. Solar altitude is the angle between the beam from sun and horizontal.

1.1 ROLE OF SOLAR ENERGY IN WIND FORMATION

The radiation continuously showered on earth by sun represents the most basic and inexhaustible source of all forms of energy- conventional and non-conventional, renewable and non-renewable the only exception is nuclear energy. The heat from sun causes continuous evaporation of water from oceans, lakes, rivers, plant and soil. The sun also heats up the air due to difference in nature of terrains, altitudes and distances from the sun, this heating is not uniform. The air acquires different temperature horizontally as well as vertically. This leads to wind- slow fast, providing wind energy. Wind also plays important role in solar chimney and is also considered as an important parameter in natural ventilation with solar

chimney. The wind flows over the earth surface is broadly classified as Global winds and Local Winds.

Global Winds- the forces which determines the global wind are in two form.

- i. Primary Force: These forces are developed because of differential heating of earth's surface at equator and polar region. There is net heat gain in tropical region due to solar radiation whereas in polar region there is net heat loss. This causes transportation of air from tropic region towards pole.

- ii. Secondly, the causes of wind is spinning of earth about its axis.

Coriolis force: Responsible for generation of wind current towards west. Between 30°N to 30°S heated air at equator rises and is replaced by cooler air coming from North to South. This flow of air pattern is Hadley circulation.

The western winds are found between 30°N to 70°S these winds form circulation transferring cool air southward and warm air northward.

This pattern is Rossby calculation.

1.2 SOLAR CHIMNEY

Solar chimney employs convective current to draw air out of a building. Ventilation effect in the structure can be created by drawing air into the house due to the creation of warm or hot zone with an exhaust outlet.

Sun rooms can be utilized to achieve this function. Air can be drawn into the living space by connecting the north side windows with the lower vents of living space and any side operable windows must be closed and thermal mass wall in the sunroom must be shaded.

The construction of narrow configuration of thermal chimney can be done by using heated black metal absorber inside a glazing that can withstand high temperatures and can be isolated. The chimney must terminate above the roof level. Thermal chimney effects be integrated into the house with open stairwells.

SOLAR CHIMNEY

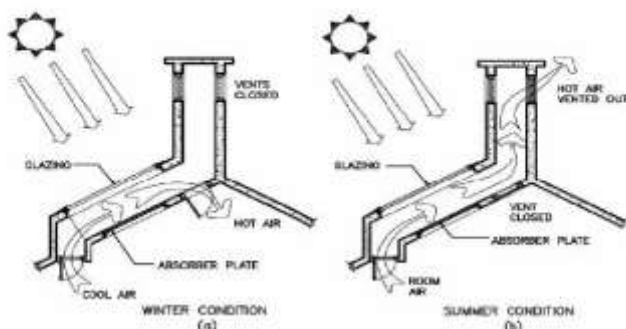


Fig.1.1 : Components of Solar Air Heater[6]

A solar chimney consists of a glazed solar collector inside which the air gets heated by the day solar energy, and with

a vertical shaft as chimney to enhance the ventilation and cooling of the building.

A solar chimney is an example of natural passive method, which harnesses solar energy to create buoyancy effect which helps in generating air flow inside air channel. Solar chimney system is extensively utilized in drying of crops, wood or grains heating and cooling applications. Lots of works and studies have been done in the area of solar chimney which is evident from literature which is discussed in Chapter 2. The heating can be supplied by use of a fan to direct the heated air into the building. Thus, Outside temperature is the key factor in the efficiency of the chimney. Primary studies on the solar chimneys prove that even cloudy days are capable of creating chilling effect by warming the air. Also, the local climate conditions should be considered to optimize the thermal comfort since solar chimney might need another type of heating/cooling systems.

Principle of the solar chimney contains three essential elements as follows:

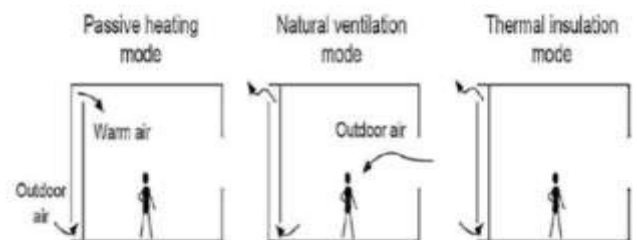


Fig.1.2 : Components of Solar Chimney

II. LITERATURE REVIEW

Wei *et al* [1] studied about the performance of ventilation when the solar chimney are connected in series and integrated with building. Both the physical and mathematical model were set up, and the effects of sizes on ventilation performance were analysed by RNG *k-ε* model and enhanced wall function method using a CFD software and concluded that performance of ventilation of solar chimney which are connected in consisting of an inclined section on roof and vertical section, the velocity decreased after the first increase with chimney channel width. The optimal ratio of length to width was found to be 12:1. The improvement of fluid flow as well as increase in flow rate can be achieved by decreasing the inclined angle of second floor chimney inlet. They found that the optimum angle of inclination was 4°. The ventilation rate is decreased inside the chimney increases with length ratio of the inclined section to vertical section. These are indicating that the vertical section height should be maximum to increase the flow rate inside the chimney as well as to optimize the chimney ventilation performance. The ventilation performance was enhanced with the increase of total chimney length.

Christine Walker et.al [2] examined on a building model of reduced scale in which air is used as working fluid for natural ventilation through buoyancy effect analysed and it is experimentally found using the scaled model for common natural ventilation building, which is connected to central atrium of open office floor plans. The parameters of the scaled building model's experiments thus were used as inputs into CFD (computational Fluid Dynamics) simulation model to compare predicted and measured airflow patterns, temperatures and velocity distribution in scale building model.

Shiv Lal et.al. [3] Studied about solar chimney performance which are used in Power generation in warm and steppe climate of Kota, Rajasthan. The study was based on Computational Fluid Dynamics (CFD) and mathematical formulas. The specific parameters energetic and exergetic efficiencies are calculated by CFD modelling. They concluded that the high rise chimney and a lot of collector area required for MW power generation and it is feasible solution for sustainable development. They observed that the velocity of air is 12.2m/s and the temperature of air is 42.4 °C at 1200h and recorded maximum solar radiation of 820W/m² at 1400h. They found that the temperature of absorber plate is 4°C to 6°C higher than the atmospheric temperature of air. At 1200h the high energy is calculated by 3.5% and it is reduced in morning and evening time. The exergy efficiency is also observed about low of 8%. The aim of this study was based on the power generation so the turbine is installed at the point where maximum velocity is obtained by the simulation software. The performance of the chimney was based on the parameters height of chimney, inlet temperature and solar radiations. The diameter of the opening of chimney is taken very low as 0.20 m and generated low velocity so it produced small power and it can be used as small power plant.

Mathur et al [4] conducted an experiment to investigate the increment in ventilation rate increased with the ratio of absorber height to gap between glass and absorber. They setup a small size solar chimney to conduct the experiment and their calculations are based on mathematical approach. The parameters are taken of nine different combination of air gap between glass and absorber plate and the height of the absorber. It was found that the highest rate of ventilation of 5.6 Air Changes per hour in the room of 27 m³ at solar radiation of 700 W/m² with the ratio between absorber height and air gap of 2.83 for a 1 m chimney height. So on the basis of experiment they finally concluded that in hot climatic conditions, when windows are kept closed /covered for preventing direct entry of solar heat, concept of solar chimney can be utilized by making minor modification to existing windows.

Rakesh Khanal et al. [5] performed an experiment with an inclined solar chimney model of passive wall with constant

heat flux on absorber plate. The performance of the design has been evaluated for the range of 100 W/m² to 500 W/m² of heat flux with a constant air gap of 10 cm and the inclination angle of the passive wall was varying between 0 to 6 degrees. They found that the angle of inclination is not provide an influenced effect on the distribution of temperature across the gap width and along the height of chimney. The experimental results show that the inclined passive wall solar chimney provide the sufficient ventilation for a room of 27m³ volume with absorber height of 70 cm and 10 cm air gap at an angle of 6° at an input heat flux of 500 W/m² based on ASHREA standard. The present design of inclined passive wall solar chimney has influenced improvement to achieve the maximum ventilation rate in comparison with other conventional chimney design.

Somaye Asadi et al [6] studied on a solar chimney to investigate the performance of solar chimney which are based on its layout in southern, west-southern and east southern part of the building. The performance of seven models are examined by simulated models which are performed on energy plus simulation software. These seven models are installed in different part of a seven story building. Their results are based on the only two parameters which are building layout and the materials of the walls and glasses. They found that the chimney which was installed in east southern part has maximum ventilation rate with compare to others and every solar chimney provides the necessary ventilation for space which are attached to it. The results was based on the 24 hours model and solar radiation through simulation.

De Carli et.al [7] context a numerical model able to perform the detailed simulation of the dynamic behaviour of water based surface embedded heating and cooling systems developed by authors is presented. To perform validation the test room was subjected to heating/cooling load profiles aimed to simulate different climatic conditions.

The conclusion made was when comfort conditions are achieved, the indoor parameters are close to each other and therefore small differences between the surface temperatures and air and operative temperatures are present. This explains why the calculations based on fixed or variable heat exchange coefficients do not differ in terms of calculated operative temperatures compared to the measured values.

III. NUMERICAL MODELLING

A reduced scale air model is developed for solar chimney model analysis. All major investigations are done using commercial CFD software ANSYS FLUENT. The reason behind the CFD application is the cost effective for analysis. In present study, Two designs viz. Horizontal and

Vertical Chimney have been fabricated to investigate the enhancement of Natural Ventilation.

3.1. COMPUTATIONAL MODEL

Ansys fluent software is selected for simulation of solar chimney model. The main reason is recent published research paper on solar chimney power plant[3]. Ansys Fluent is most widely accepted commercial software for natural ventilation or buoyancy driven modelling. Thickness of wooden walls is neglected in computational model due to virtual thickness option available in Ansys fluent software.

Simulations are carried out under unsteady state conditions as the ambient solar irradiance as well as the air temperature and air speed within the solar chimney model from experiments data recorded in test facility are found to be fairly proper for whole day, only morning data is have more error than afternoon data. These equations are converted into their integral forms and solved using the finite volume method. In addition, the evaluation of the gradients and derivatives are carried out using the least square cell-based evaluation method since the flow solution is solved on unstructured meshes.

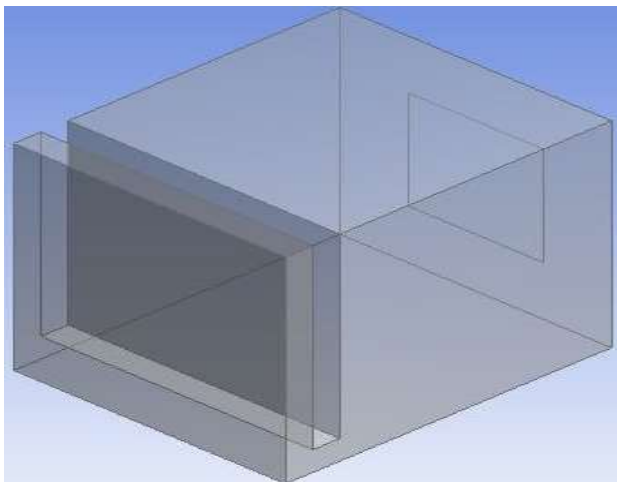


Fig.3.1 : CAD Geometry of Vertical Solar Chimney

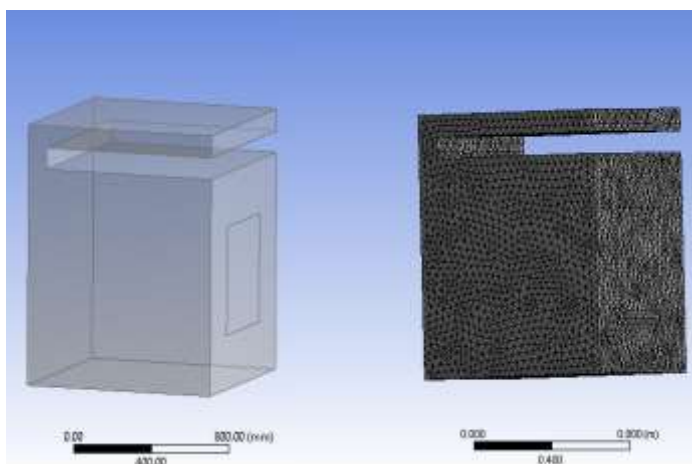


Fig.3.2 : CAD Geometry & Meshing of Horizontal Solar Chimney

3.2. SOLVER SETTING

The buoyancy of air is modelled using the Boussinesq approximation as the solar chimney stack effect is natural convection under small change in air temperature. The computational model considers density to be constant except for the buoyancy term in the momentum equation. From Equation 4-3, the gravitational acceleration is defined as 9.81m/s in the negative y-direction while the density is specified as 1.177Kg/m³ at an operating temperature of 27°C.

$$(\rho - \rho_0)g = -\rho_0 \cdot \beta(T - T_0) \cdot g$$

Where T = 300k

$$\rho_0 = 1.177 \text{ kgm}^{-2}$$

$$\beta = 3.1 \cdot 10^{-3} \text{ k}^{-1}$$

Equation of Boussinesq Model

In Solver, Inlet and Outlet was taken as Pressure Inlet and Outlet. Glass was taken as Semi Transparent Wall. Solar Load Calculator was used to specify the value of Solar Radiation at Absorber Plate.

IV. RESULTS AND DISCUSSION

In present study only vertical solar chimney is fabricated but in CFD simulation one special case is also designed for vertical solar chimney. In present section comparison is made between these two chimneys for one day full simulation basis for whole year. Figure 4.3 and figure 4.2 show line diagram of both designs used for CFD simulation.

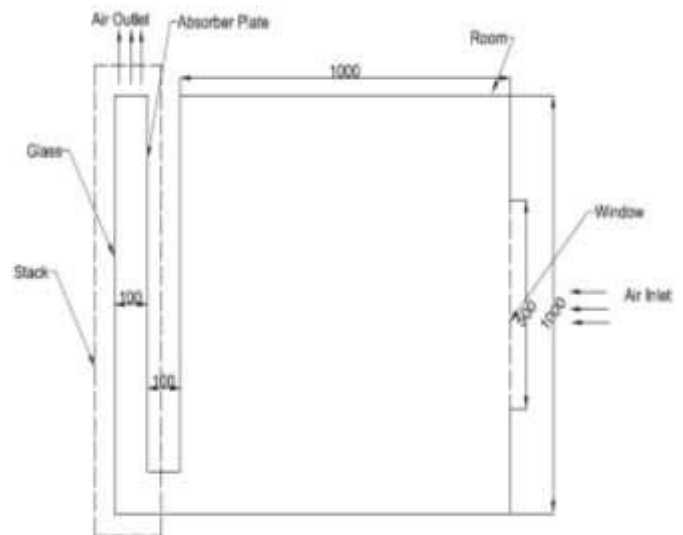


Fig.4.1: Line Diagram of Vertical Solar Chimney

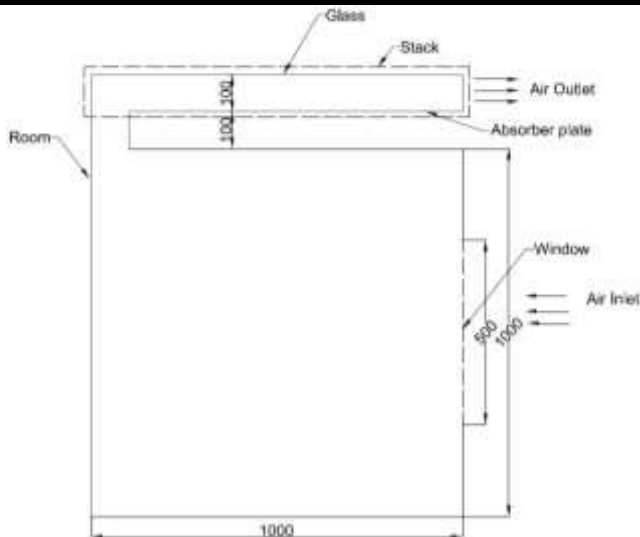


Fig.4.2: Line Diagram of Horizontal Solar Chimney

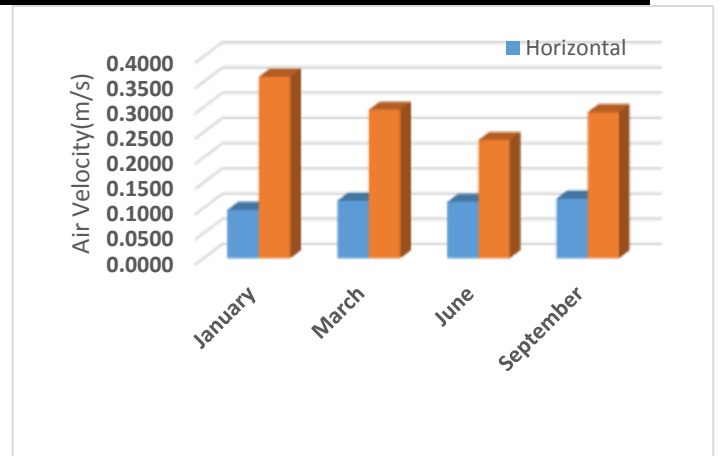


Fig.4.5: Design comparisons for solar chimney at SC-700 measuring location

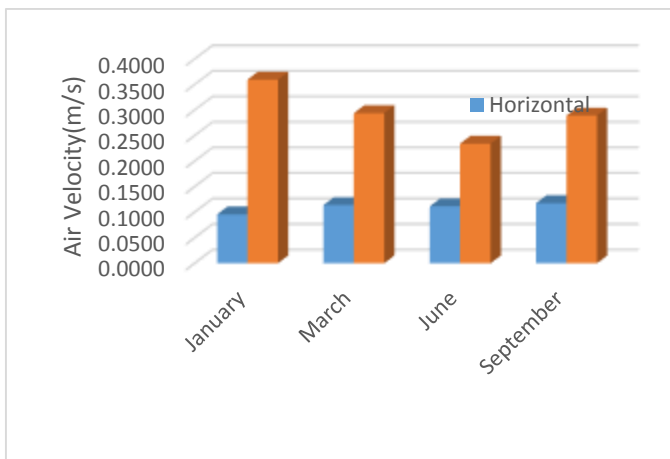


Fig.4.3: Design comparisons for solar chimney at R-500 measuring location

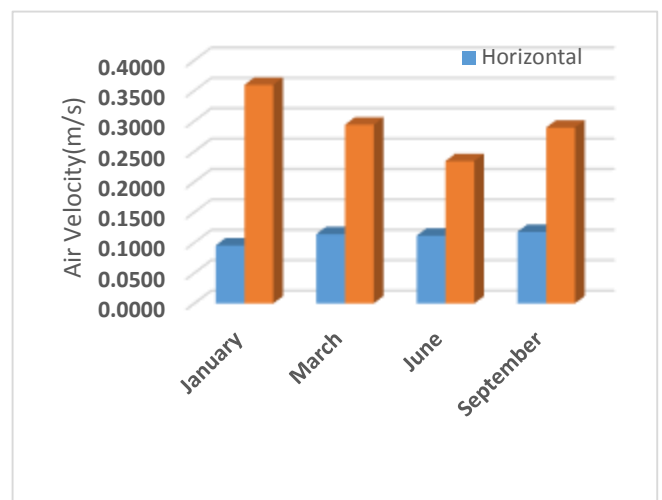


Fig.4.6: Design comparisons for solar chimney at SC-out measuring location

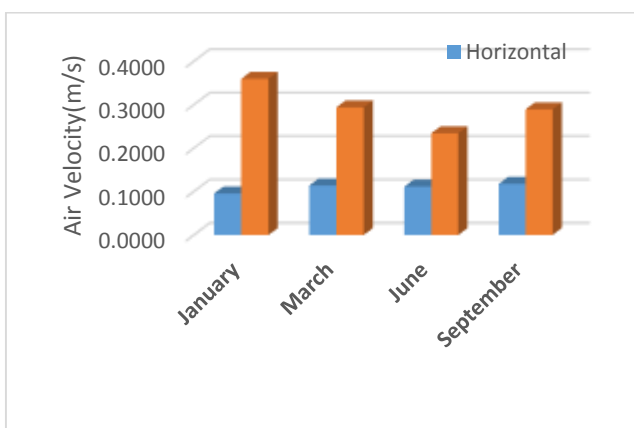


Fig.4.4: Design comparisons for solar chimney at SC-500 measuring location

Fig. 4.3 Show that effect of solar chimney position in horizontal and vertical direction, R-500 shows the mid-point of solar chimney, at this point, vertical direction air velocity is maximum.

Fig. 4.4, 4.5, 4.6 shows the effect of solar chimney position in horizontal and vertical direction with respect to chimney height, SC-500 and SC-700 are the points at 500 mm and 700mm height of solar chimney respectively. SC-Out is the point at the outlet of solar chimney.

V. CONCLUSION

In this study, a reduced scale Chimney of Horizontal and Vertical design is modelled through CFD to investigate the improvement of Natural Ventilation. Two different parameters have been considered for current study viz. Outlet Velocity and Temperature of Absorber plate. Comparison between Horizontal and Vertical designs has been done. Following Conclusions can be drawn:

- i) Both designs viz. Vertical and Horizontal have been compared and it was found that Vertical Chimney

- enhanced ventilation rate much better in comparison to Horizontal chimney as much as 275% enhancement.
- ii) It was found that Vertical Solar Chimney enhanced air flow stream velocity up to 22 times.

REFERENCES

- [1] Du Wei, Yang Qirong, Zhang Jincui, "A study of the ventilation performance of a series of connected solar chimneys integrated with building." *Renewable Energy*, vol- 36, page no.- 265- 271, 2011.
- [2] Christine Walker, Gang Tan, Leon Glicksman, "Reduced-scale building model and numerical investigations to buoyancy-driven natural ventilation.", *Energy and Buildings*, vol- 43, page no.- 2404-2413, 2011.
- [3] Shiv Lal, S.C. Kaushik, Ranjana Hans, "Experimental investigation and CFD simulation studies of a laboratory scale solar chimney for power generation", *Sustainable Energy technologies and Assessments*, vol.-13, page no.- 13-22, 2016.
- [4] Jyotirmay Mathur, N.K. Bansal, Sanjay Mathur, Meenakshi Jain, Anupma, "Experimental investigations on solar chimney for room ventilation", *Solar Energy*, vol.- 80, page no.-927-935, 2006.
- [5] Rakesh Khanal, Chengwana Lei, "An experimental investigation of an inclined passive wall solar chimney for natural ventilation", *Solar Energy*, vol.- 107, page no.- 461-474, 2014.
- [6] Somaye Asadi, Maryam Fakhari, Akram Mahdavi Parsa, "The effect of Solar Chimney Layout on Ventilation Rate in Buildings", *Energy and Buildings*, vol. - 123, page no. - 71-78, July 2016.
- [7] Michele De Carli, Massimiliano Scarpa, Roberta Tomasi, Angelo Zarrella, "A numerical model for the thermal balance of rooms equipped with radiant systems", *Building and Environment*, vol.-57, page no.- 126-144, 2012.

Breast Cancer Diagnostic System Based on MR images Using KPCA-Wavelet Transform and Support Vector Machine

Mustafa Zuhaer AL-Dabagh, Dr. Firas H. AL-Mukhtar

Department of Computer Science, Knowledge University, Erbil, Iraq.

Abstract—Automated detection and accurate classification of breast tumors using magnetic resonance image (MRI) are very important for medical analysis and diagnostic fields. Over the last ten years, numbers of methods have been proposed, but only few methods succeed in this field. This paper presents the design and the implementation of CAD system that has the ability to detect and classify the tumor of the breast in the MR images. To achieve this, k-mean clustering methods and morphological operators are applied to segment the tumor. The gray scale, Texture and symmetrical features as well as discrete wavelet transform (DWT) are used in feature extracted stage to obtain the features from MR images. Kernel principle components analysis (K-PCA) are also applied as a feature reduction technique and support vectors machine (SVM) are used as a classifier. Finally, the experiments results have confirmed the robustness and accuracy of proposed system

Keywords— *k-mean clustering, Morphological operators, gray scale, Texture, symmetrical, kernel principle components analysis and Support vectors machine.*

I. INTRODUCTION

After the evaluation of technology, the detection and classification of the tumor in magnetic resonance images (MRI) became very significant because it gives important information for each of medical diagnosis and surgical [1]. Nevertheless, detection and classification of tumor is a very hard task because of the size, the shape and the location of tumors is very different and any wrong diagnostic can lead to serious collateral damage [2]. MRI is considered as the most accurate technique used to study the tumors in soft tissues for two reasons. The first one, the MRI images gives many details about the tumor and, the second one is, there is no known side effects related to radiation exposure [3].

In recent years and after the fast evolution of computer technology, computers are used to support the medical decision systems and spread in various medical fields such as breast cancer, gastroenterology, Breast tumors etc.

There are many image processing techniques that have been proposed to detect and classify MRI Breast tumor. The complexity of the pathology of the human Breast and the high quality of the images are required in the diagnosis are remain an obstacle in front of any new method [4].

Different types of techniques have been modified for extracting the features from MR images. Some of these techniques are simple such as mean and variance of the gray level of the image but it is not enough to get a good recognition rate. Therefore, other gray-scale statistics techniques such as the gray-level co-occurrence matrices (GLCM) are applied [5] to solve the problem. GLCM is considered as one of the popular techniques used in this field and very popular in various other applications of texture analysis. GLCM depends on statistical methods for extracting number of textural features from the images [6]. Co-occurrence matrices can provide significant information about patterning of the texture, and it is applied to define the textural features from them [7].

The main problem of most diagnostic systems is how the systems can enhance the performance automatically with the increase of experience. For this reason, different types of machine learning methods were developed to solve these problems like random forests, artificial neural networks, decision tree and support vector machine (SVM). SVM is one of a popular classifier that depends on small sample learning and gives a good generalization capability. It is used in many of the real-time applications such as text mining, face recognition, and image processing, and these make SVMs considered as one of the most developed tools in the field of machine learning and data mining [8].

Various methods have been used for feature extraction and to reduce the data dimensionality such as Principal Components Analysis (PCA), Linear Discriminate Analysis (LDA), Independent Components Analysis (ICA) and Kernel Principal Components Analysis (k-PCA). Kernel-Principal Components Analysis (k-PCA) is considered as a dimensions reduction and feature extraction method which has been widely and effectively used in different types of applications [9-10].

This paper is organized as follows: Section II introduces the proposed system architecture. In Section III, experiments and results are discussed. Finally, conclusions are documented in Section IV.

II. PROPOSED SYSTEM ARCHITECTURE

In this proposed system, six stages will be used to detect and classify the tumor in MR image. In the first stage, preprocessing techniques (histogram equalization and median filter) will be applied to improve the images and to eliminate the noise. In the second stage, K-mean clustering and morphological operators will be used to segment the tumor. Features such as gray scale, texture, symmetrical and DWT features will be extracted from the images to use it in the training and the classification stages. K-PCA is applied in the reduction stage to reduce the size of data. Finally, SVM has been applied to determine the types of tumor (Malignant or Benign).

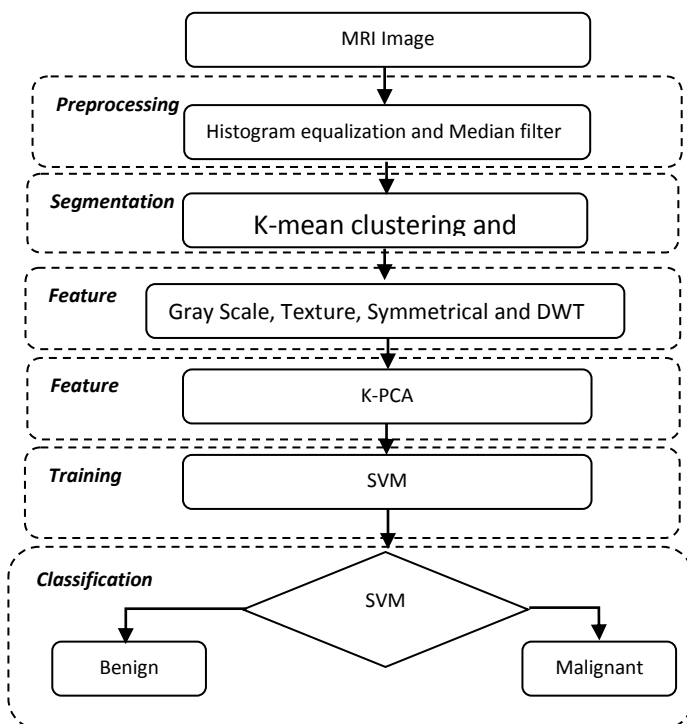


Fig.1: Six Stage of Proposed System

2.1 PRE-PROCESSING

In this stage, the input image is passed into two processing steps (Median filtering and histogram) before it enters to the next processing stage to enhance the quality of the input image as well as remove noise in the image. Median filtering and histogram equalization are used to make the image in the best quality and minimum noise.

2.1.1 Median filter

It is a nonlinear filter and it is applied to remove the noise of an image. It is work depends on window slide idea. The windows slide scans the whole image depending on its central pixel through scanning each part of the image.

Through this scan, the neighboring pixels are ordered depending on the intensity value of the pixel and then the median value is replaced with the central pixel value. The benefit of using a median filter is to remove certain kind of noise especially when some pixels of the image contain extreme values. In this way, new pixels value is not generated because the output pixel value is one of the neighboring pixels values. In the median filter, the edges are not affected during removing the noise and it is possible to use it more than one time [11].

2.1.2 Histogram Equalization

It is one of a popular image pre-processing techniques for adjustment the contrast of the image. During acquisition stage, the distribution of intensity in the image may be affected and this leads to a bad contrast and low quality of the image, therefore histogram equalization is employed to enhance the appearance of an image. The main idea of histogram equalization is based on creating a new gray scale from the old gray scale of the input image [12]. The equation used to calculate the histogram equalization is shown below:

$$k_0 = \text{round} \left(\frac{c_i(2^k-1)}{w.h} \right) \quad (6)$$

Where k_0 represents a gray level value of histogram equalization, c_i refers to the cumulative distribution of i^{th} gray scale from original image; round represents rounding to the nearest value, while w and h refer to the width and height of the image [13].

2.2 SEGMENTATION

This method is considered as the one of most important stage in the CAD system. It aims to partition the image into a number of segments to make the analysis of the image. In this stage, combinations of K-Means clustering and morphological operators along with basic image processing techniques are applied to implement this function. K-Means clustering aims to detect tumor and shows some abnormality while morphological operators with another basic image processing techniques aims to rectify this detection through separating the tumor cells from the normal cells. The steps of segmentation are as the follows:

2.2.1 Threshold Operation

It is one of widely known techniques. It is used to create a binary format from gray-scale images depending on a particular intensity level. The main idea of thresholding operation is to turning all the pixels that have value larger than intensity level to 1 and all pixels that have value less than the intensity level to 0. The operation of thresholding is described in the following equation:

$$g(x,y) = \begin{cases} 1 & \text{if } f(x,y) > T \\ 0 & \text{if } f(x,y) < T \end{cases} \quad (1)$$

Where $f(x,y)$ represents the image of x rows and y columns and T refers to the intensity level [14].

2.2.2 Watershed Transformation

It is one of the widely used techniques to collect pixels of an image that have similar intensity levels. It is considered as a region-based segmentation technique. The essential idea of this technique based on segregates the image to various intensity portions and then it starts to fill the deeper gradient and then fills the lighter gradient. In a gray scale image the tumor cells have high-intensity values comparing with other parts, therefore watershed segmentation is considered as one of the best tools to classify tumors and high-intensity tissues in MR image [15].

2.2.3 K-means Clustering

It is a high computational efficiency unsupervised method and it is a widely used in many applications. The letter "k" refers to the number of clusters used. Clustering process is grouping the data points that have similar features into the same cluster and the data points of dissimilar features into different clusters. To understand the K-means clustering method, let us consider that, $X = \{x_1, x_2, \dots, x_N\}$ is a set of data points and we want to separate into a number of clusters $C = \{c_1, c_2, \dots, c_k\}$. K-means method is aimed to compute the center of data, and then assign the data of the same features to a cluster center. K-means iterates this method until clustering all the data. The center of all clusters is calculated as displayed in the equation:

$$J = \sum_{n=1}^N \sum_{k=1}^K \|X_n - C_k\|^2 \quad (2)$$

Where $\|X_n - C_k\|^2$ refers to the distance between a data point X_n and the center of cluster C_k , while J represents the distance of n points from their respective cluster centers [16].

2.2.4 Morphological Operators

Morphological operations are used to reconstructing the structure or shape of an object. They can be employed for both pre-processing and post-processing operations, like obtaining a representation or description of the shape of objects or can be used for filtering, thinning or pruning. The main morphological operations are erosion, dilation, opening and closing. Opening and closing operations are applied in this stage. At first, Opening is applied by implementing erosion to remove unwanted pixels from the image and after that dilation is implemented to focus on the area of interest. Secondly, closing is applied by implementing dilation and then erosion to fill holes. The mathematical expressions of closing and opening are explained in equations 3 and 4:

$$\begin{aligned} A \circ B &= (A \ominus B) \oplus B \\ A \bullet B &= (A \oplus B) \ominus B \end{aligned} \quad (3)$$

After applying these techniques, the pixels which have high intensity value are grouped together into one cluster while other pixels grouped into other cluster. Figure 2. shows the output image from this stage [17].

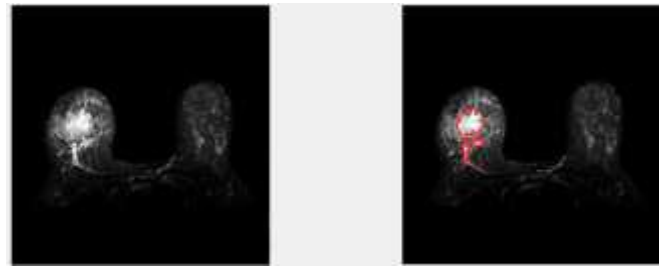


Fig.2: The output image of segmentation stage

2.3 Feature Extraction

It is considered as one of the main parts of the diagnostic system. It is applied to extract unique features from the input image to use it in the classification stage. It aims to reduce the amount of data that can be used to represent a large set of accurate data by computing the properties or features that can be used to recognize different samples. There are many methods available for feature extraction. In this stage, the gray scale, Texture and symmetrical features as well as discrete wavelet transform (DWT) method are applied to implement this function.

2.3.1 Discrete wavelet transform

Discrete wavelet transform is one of the efficient features extraction and decomposition techniques that is widely used in different applications. It is applied to convert the images to the frequency domain by using each of a low pass and a high pass filter. It is aimed to split the input image to the four sub-bands (LL, LH, HL, and HH). The mathematical expression of DWT is shown in an equation below [18]:

$$A. \varphi_{(i,j)}(x) = 2^{\frac{i}{2}} \varphi(2^{-i}x - l) \quad (4)$$

B. Where x refers to the variable, s and l represent the integers that scale and stretch the function φ to produce wavelets. Three stage of DWT are applied to extract features from input image.

2.3.2 Gray Scale features

In this step, five types of Gray Scale features are extracted. These features are included as: mean variance, standard deviation, skewness and kurtosis [19]. These are explained as follows:

- **Variance:** is defined as the difference in intensity of gray levels.

$$Variance = \frac{1}{N} \sum_{i=1}^N (|x_i - \mu|^2) \quad (5)$$

Where, x refers to the individual data point, μ represents the mean of data points and N indicates to the total number of data points

- **Standard Deviation:** defined as the measure of difference asset of data from its mean value.

$$SD = \sqrt{\text{Variance}} \quad (6)$$

- **Skewness:** is defined as the measure of the symmetries of gray level.

$$\text{Skewness} = \text{Variance}^{-3} \sum_{x=1}^m \sum_{y=1}^n (f(x, y) - \mu)^{-3} \quad (7)$$

- **Kurtosis:** is defined as the measure of the flatness of the histogram gray levels.

$$\text{Kurtosis} = (\text{Variance}^{-4}) \sum_{x=1}^m \sum_{y=1}^n (f(x, y) - \mu)^{-4} \quad (8)$$

2.3.3 Texture Features

They are the second kind of features that are used. In this stage, thirteen features are taken from co-occurrence matrices which are calculated for each input image. Some of these features are described below [18]:

-

$$\text{Entropy} = - \sum_{i=1}^n \sum_{j=1}^n p(i, j) \log(p(i, j)) \quad (9)$$

-

$$\text{Dissimilarity} = \sum_{i=1}^n \sum_{j=1}^n p(i, j) * |i - j| \quad (10)$$

-

$$\text{Inverse} = \sum_{i,j=1}^n \frac{p(i, j)}{(i - j)^2} \quad (11)$$

-

$$\text{Energy} = \sum_{i=1}^n \sum_{j=1}^n (p(i, j))^2 \quad (12)$$

-

$$\text{Contrast} = \sum_{i=1}^n \sum_{j=1}^n p(i, j) * (i - j)^2 \quad (13)$$

-

$$\text{IDM} = \sum_{i=1}^n \sum_{j=1}^n \frac{p(i, j)}{1 + (i - j)^2}$$

2.3.4 Symmetrical feature

$$\text{Exterior Symmetry} = \frac{\sum_{i=1}^n (m - M)^2}{n} \quad (15)$$

2.4 Feature Reduction

The feature reduction stage aims to minimize the size of features set to reduce the time required to do the mathematic operations, as well as to reduce the size of storage without affecting the efficiency of the system. For this reason, feature reduction stage is very impotent to any system. K-PCA is aimed to extract principal components by mapping a set of data in high-dimensional feature space to a low-dimensional feature space. By this way, kernel PCA reduces the complicated coefficient dependencies that otherwise might not be simply reduced in a linear subspace and this gives k-PCA preference over traditional PCA methods [20].

2.5 Training and Classification

This stage aims to classify the features that came from previous stage using SVM. SVM is a binary classifier that depends on supervised learning method. It is used to classify tumor to abnormal or normal. The accuracy of SVM classifier is based on the kernels function. There are different types of kernel functions that can be used with SVM classifier like linear, polynomial and radial basis function [21-22]. The corresponding equations of the widely used kernels functions are shown below:

- *Linear kernel*

$$f_k = f(x, x') \quad (16)$$

Where x and x' are represented as the sample vectors and f_k as the linear kernel.

- *Polynomial kernel*

$$k(x, x') = (1 + x \cdot x')^2 \quad (17)$$

Where x and x' represents the sample vectors, while $\|x - x'\|^2$ represents the Euclidean distance between these sample vectors.

- *RBF kernel*

$$k(x, x') = e^{-\|x - x'\|^2} \quad (18)$$

Where x and x' represents the sample vectors.

III. EXPERIMENTS AND RESULTS

The proposed CAD system is developed and simulated using MATLAB® 2016b environment. Graphic USER interface (GUI) is designed also to help any user to use the proposed system easily. Figure 2 is displays the GUI of proposed system. This GUI consists of inputs and outputs for the GUI. The inputs are the loaded image and segmentation pushbutton.

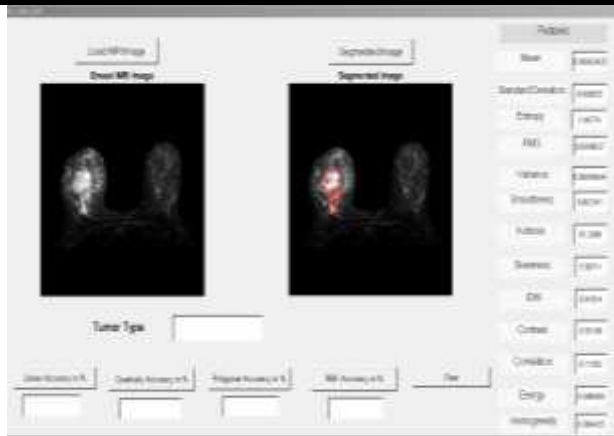


Fig.2: The GUI of the proposed system

The outputs are feature parameters, type of tumor and the performance of the kernel function of the SVM classifier (Linear, Quadratic, and polynomial and RBF kernels). Our database [23-24] consists of 38 cases, 15 of these cases are benign and 23 are malignant. These cases are employed to evaluate the performance of the system. Three other parameters (sensitivity, specificity, and accuracy) are also applied. The sensitivity parameter indicates the proportion of actual positives that are correctly identified, while Specificity parameter represents the proportion of negatives that are correctly identified; and Accuracy parameter, which is the proportion of both true positives and true negatives. The equations of these three parameters are shown in equations below [25]:

$$Sensitivity = \frac{TP}{(TP + FN)} * 100\% \quad (19)$$

$$Specificity = \frac{TN}{(TN + FP)} * 100\% \quad (20)$$

$$Accuracy = \frac{(TP + TN)}{(TP + TN + FP + FN)} * 100\% \quad (21)$$

True Positives (TP) refers to the correctly identified positive cases, True Negatives (TN) refers to the correctly identified negatives, False Positives (FP) represents the incorrectly identified positives and False Negatives (FN) refers to the incorrectly identified negatives. The performances of the four SVM kernels are shown in table I.

TABLE I. SVM KERNELS PERFORM

Se q.	Kernel Type	Sensitivity	Specificity	Accuracy
1.	Linaer	91.304%	84%	88.421%
2.	Quadratic	90.869%	88%	89.736%
3.	Polynomial	95.217%	93.333%	94.210%
4.	RBF	93.913%	92%	93.157%

IV. CONCLUSION

In this paper, CAD to segment and classify breast tumor is designed and implemented. The system consists of six stages (preprocessing, segmentation, features extraction, features reduction, training and classification). The segmentation of tumor is implemented using k-mean clustering and morphological Operators and it is successfully applied for most of the images of the database. The gray scale, Texture and symmetrical features as well as discrete wavelet transform (DWT) method are applied in feature extracted stage to obtain the features from MR images. The classification is implemented using SVM method with four kernel functions (Linear, Quadratic, polynomial and RBF). The system is tested using database consists of 34 cases, 9 of these cases are benign and 24 are malignant. Three parameters (sensitivity, specificity, and accuracy) are also applied to compute the performance of the system. From the observation of the results of these three parameters, it can be noticed that polynomial kernel give the best performance comparing with other SVM kernels.

REFERENCES

- [1] Xiao Xuan and Qingmin Liao, "Statistical Structure Analysis in MRI Brain Tumor Segmentation", Fourth International Conference on Image and Graphics, pp.421-426, 2007.
- [2] Hassan Khotanlou, Olivier Colliot, Jamal Atif, Isabelle Bloch, "3D brain tumor segmentation in MRI using fuzzy classification, symmetry analysis and spatially constrained deformable models", Fuzzy Sets and Systems, Volume 160, Issue 10, pp.1457-1473, 16 May 2009.
- [3] Prakash Tunga P, Vipula Singh, "Extraction and Description of Tumour Region from the Brain MRI Image using Segmentation Techniques", IEEE International Conference On Recent Trends In Electronics Information Communication Technology, pp.1571-1576, May 20-21, 2016.
- [4] Mahmoud Khaled Abd-Ellah, Ali Ismail Awad, Ashraf A. M. Khalaf, and Hesham F. A. Hamed, "Design and Implementation of a Computer-Aided Diagnosis System for Brain Tumor Classification", 2016 28th International Conference on Microelectronics (ICM), pp.73-76, 17-20 Dec. 2016.
- [5] A. Latif-Amet, A. Ertzn, and A. Eril, "An efficient method for texture defect detection: sub-band domain co-occurrence matrices," Image and Vision Computing, vol. 18, no. 67, pp. 543-553, 2000.
- [6] Anna N. Karahaliou, et. al. "Breast Cancer Diagnosis: Analyzing Texture of Tissue Surrounding Microcalcifications", IEEE Transactions on

- Information Technology in Biomedicine, vol. 12, no. 6, pp.731–738,2008.
- [7] Arnau Oliver et. al., “A Novel Breast Tissue Density Classification Methodology”, IEEE Trans. on Info. Tech. in Biomedicine, vol.12, no.1, pp55-65, 2008.
- [8] M. P. Arakeri and G. R. M. Reddy, “Computer-aided diagnosis system for tissue characterization of brain tumor on magnetic resonance images,” Signal, Image and Video Processing, vol. 9, no. 2, pp. 409–425, 2015.
- [9] Mathieu Fauvel ; Jocelyn Chanussot ; Jon Atli Benediktsson,” Kernel Principal Component Analysis for Feature Reduction in Hyperspectral Images Analysis”, Proceedings of the 7th Nordic Signal Processing Symposium - NORSIG , 7-9 June 2006.
- [10] Sidhu GS, Asgarian N, Greiner R and Brown MRG (2012) Kernel Principal Component Analysis for dimensionality reduction in fMRI-based diagnosis of ADHD. Front. Syst. Neurosci, Vol. 6, article 74, November, 2012.
- [11] Padmakant Dhage, M. R. Phegade and S. K. Shah, “Watershed segmentation brain tumor detection”, 2015 International Conference on Pervasive Computing (ICPC),pp.1-5, 16 April 2015.
- [12] Natarajan.P, Krishnan.N, ”MRI Brain Image Edge Detection with Windowing and Morphological Erosion”, IEEE International Conference on Computational Intelligence and computing Research, pp: 94-97, 2011.
- [13] W.Gonzalez, “Digital Image Processing”, 2nd ed. Prentice Hall, Year of Publication 2008.
- [14] P. Natarajan; N. Krishnan; Natasha Sandeep Kenkre; Shraiya Nancyand et.al.” Tumor detection using threshold operation in MRI brain images”, 2012 IEEE International Conference on Computational Intelligence and Computing Research, 18-20 Dec. 2012.
- [15] L. Vincent and P. Soille, “Watersheds in digital spaces: an efficient algorithm based on immersion simulations,” IEEE Trans. Pattern and Machine Intelligence. vol. 13, no. 6, pp. 583-598, August 1999.
- [16] Hengjin Tang; Tatsushi Matsubayashi and Hiroshi Sawada,” Blocked Time Step Algorithm for Accelerating k-means and Fuzzy c-Means”, 2015 IEEE International Conference on Systems, Man, and Cybernetics,pp.2561-2566, 9-12 Oct. 2015.
- [17] Muzni Sahar; Hanung Adi Nugroho, Tianur; Igi Ardiyanto and et.al.” Automated detection of breast cancer lesions using adaptive thresholding and morphological operation”, 2016 International Conference on Information Technology Systems and Innovation (ICITSI), 24-27 Oct. 2016.
- [18] M. Abo-Zahhad, R. R. Gharieb, S. M. Ahmed, and M. K. Abd Ellah, “Huffman image compression incorporating DPCM and DWT,” Journal of Signal and Information Processing, vol. 6, pp. 123–135, 2015.
- [19] Rasel Ahmmed and Md. Foisal Hossain,” Tumor detection in brain MRI image using template based K-means and Fuzzy C-means clustering algorithm”, 2016 International Conference on Computer Communication and Informatics (ICCCI), 7-9 Jan. 2016.
- [20] Syed Z. Rizvi ; Javad Mohammadpour ; Roland Tóth ; Nader Meskin,” A Kernel-Based PCA Approach to Model Reduction of Linear Parameter-Varying Systems”, IEEE Transactions on Control Systems Technology ,Vol. 24, Issue: 5, Sept. 2016 .
- [21] Abdul Qayyum and A. Basit,” Automatic breast segmentation and cancer detection via SVM in mammograms”, 2016 International Conference on Emerging Technologies (ICET), 18-19 Oct. 2016.
- [22] Y. Zhang and L. Wu, AN MR BRAIN IMAGES CLASSIFIER VIA PRINCIPAL COMPONENT ANALYSIS AND KERNEL SUPPORT VECTOR MACHINE, Progress In Electromagnetics Research, Vol. 130,pp. 369-388, 2012.
- [23] Lingle, W., Erickson, B. J., Zuley, M. L., Jarosz, R., Bonaccio, E., Filippini, J., ... Grusauskas, N. (2016). Radiology Data from The Cancer Genome Atlas Breast Invasive Carcinoma [TCGA-BRCA] collection.
- [24] Clark K, Vendt B, Smith K, Freymann J, Kirby J, Koppel P, Moore S, Phillips S, Maffitt D, Pringle M, Tarbox L, Prior F. The Cancer Imaging Archive (TCIA): Maintaining and Operating a Public Information Repository, Journal of Digital Imaging, Volume 26, Number 6, pp 1045-1057, December, 2013.
- [25] M. G. Sumithra and B. Deepa,” Performance analysis of various segmentation techniques for detection of brain abnormality”, 2016 IEEE Region 10 Conference (TENCON),pp.2056-2061, 22-25 Nov. 2016.

The impact of applying the Unified Banking Evaluation model (Camels) on enforcing the banking supervision of commercial banks (The case study of Bank Bemo Saudi French – BBSF)

Dr. Ghassan Farouk Ghandour

Lecturer, Department of Accounting and Information Technology, Faculty of Administrative and Financial Sciences, Cihan University, Sulaymaniyah-Iraq.

Abstract— This research discusses the impact of applying the Unified Banking Evaluation model (Camels) on enforcing the banking supervision and control processes. The research explained the nature and consistence of relationship between the evaluation system with its different dimensions and characteristics, and the banking supervision on site and off site; it also analyzed and evaluated the case study of BBSF (as the first private bank in the Syrian banking system). The evaluation results were combined with the other elements that are to be considered when assuming the tasks of banking supervision. Such a case study can be generalized to other banks.

Keywords— banking supervision, on- site supervision, off-site supervision.

I. INTRODUCTION

The safety of national economy and effectiveness of monetary policy of any country over the safety of the financial system and in particular the safety of banking sectors, as one of the main pillars of the financial system, as banks face challenges and great difficulties due to various reasons, some dating back to the internal and external environmental conditions, which may lead to kind of crises differ in their causes and levels according to the prevailing conditions, which prompted a lot of these banks to seek to improve its performance and the application of innovative methods for the detection of weaknesses and strengths, targeting a re-evaluation of the bank for its own sake and the launch of innovative capabilities inherent, here comes this study to learn about the importance of the banking supervision process and the tasks entrusted to the regulatory institutions in order to maintain the stability of the banking

system and efficiency to get to a safe banking sector maintains the rights of depositors, investors and ensure the proper implementation of the economic policy of the government and achieve their goals. From here it came the banking assessment known as the "CAMELS" of the system provides an analysis of the strengths and weaknesses in the performance of banking institutions so as to support the banking supervision system and achieves goals.

Research problem

In Syria, The banking system is suffering, the lack of a flexible legislative framework is able to intervene and compel the banks to comply with the procedures intended to be performed by the regulators, which will reflect on the performance of these banks and then on the goal of development and growth and the achievement of the elements of continuity, so the problem of the research revolves around the following question : How to benefit from the application of the "camel" model to support the effectiveness of supervision and off site and on site supervision carried out by the banking regulators system.

Research hypotheses

In light of the research problem and objectives can be formulated hypotheses in the following major premise:

The development and application of supervision systems supporting the operations off site and on site supervision by the regulatory authorities on the banking system, leading to the disclosure of the strengths and weaknesses in the performance of the device and draw attention to ways of processing that supports efficient and effective performance.

Research importance

The importance of this research by emphasizing the need for effective monitoring tools to assess the performance of the financial and banking institutions to identify institutions that need to be brought to the attention and the interest of its own, which will maximize the results of the application of the proposed model.

Research objectives

This research aims to build a support system for operations supervision on the banking sector, thus helping the regulatory authorities and departments of banks to know the conditions of those banks, and the difficulties and obstacles they face. Which allows taking control procedures and precautions before the occurrence of any problem by describing and measuring applications on the first private banks operating in Syria?

II. RESEARCH METHODOLOGY

This research effort is divided on two main sides:

First: Theoretical side, the formulation and analysis of the general framework for banking model assessment "Camels" as a system for evaluating the performance of the banking system units from a regulatory perspective.

Second: practical side depends on the collection and analysis of data on the subject of the problem in order to stand on ways to apply the valuation model to support inspection and use in the sectors of banking operations relying on a descriptive approach and deductive in scientific research.

Chapter One: Analysis of the concept of banking supervision And its objectives

Banking supervision is considered an integrated system practiced by the monetary authority (central bank) to licensed banks that engage in banking activities, and are closely linked to the nature of the functions assigned to those authorities.

1. The concept of banking supervision

the concept of banking supervision knew remarkable development moved it from traditional banking supervision phase which stands for banking supervision in a given period of time through the extrapolation of the financial statements of banks, whether through off –site supervision (Sayrafi, 2006: 291), or by on-site supervision, and ensure the safety of the accounting system of the bank and the extent of its commitment to the banking supervision systems, then moved the concept of banking supervision to the ongoing banking supervision stage to stand on the

developments in the financial situation of the bank changes, so as to detect deviations that get them through the point in time early , and due to the developments in the banking activities of bank and its risks, not the concept of banking supervision is limited when the previous stage but evolved to include risk control system risk supervision, which was Through the development of the tools of on-site supervision (Abdullah, 2003: 392), which contributes to adjust the current deterioration in the financial situation of the bank early.

Due to the continuous development of the banking supervision process, addressing a number of the concept of banking supervision and the researchers tried to determine the dimensions and the statement of significance, it has been identified as the banking supervision:

"Practical application of the reality of supervision in the banking industry, with the aim of comparing the bank's operations with laws set by the highest monetary authority, the central bank" (Jasim, 2000: 241).

As a banking supervision of researchers known as "set of procedures and methods undertaken by the monetary authority (central bank) to ensure the implementation of monetary policy, and assess the banking sector's performance and maintain the integrity of his work "(Ghannam, 2005: 57).

From the above researcher defines that the banking supervision: set of rules, procedures and methods taken by the monetary authorities, (central banks), in order to achieve monetary policy goals properly and maintain the integrity of the financial centers of the banks leading to the formation of a banking system efficient and able to transfer the impact of monetary policy to the real sector, which contributes to increased economic growth rates.

2. The objectives of banking supervision

the process of banking supervision on the banking sector's activities take with great interest by those in charge of monetary and banking policies in order to achieve the following objectives:

- Ensure the application of Bank policies and procedures issued by the central bank.
- Credit supervision and direction of quality and quantity in accordance with economic policy.
- Work to protect of public deposits in banks and protect of shareholders' equity.
- Maintaining the financial and banking system stability, by monitoring the practices of the banks as well as establishing rules and regulations for the management of liquidity in the banks / (Sesi, 2005: 9) and (Mazzawi, 2003: 175).

Chapter Two: Analysis of the elements of the unified banking system assessment “Camels “And its impact on banking supervision operations

This system is one of the most commonly used systems for the assessment and classification, who values on the basis of the performance of bank Bemo Saudi France in this research, so we will study its components in detail.

The purpose of the method of risk assessment, or the camels system, is specifically a unified comprehensive way to put the banking system. It's also helps in determining which banks Financial weaknesses, and operational and administrative a significant risk to their performance, and require special oversight to address the weaknesses risks. CAMELS system of monetary authorities to assess the overall strength and safety of the banking industry. CAMELS system requires comprehensive analysis of banking situations, can carry out this analysis only in the course of a comprehensive on-site supervision, as well as it can be observers during on-site supervision to understand the administration's ability to risk-averse, and its method of risk management . CAMELS system based on the method of risk which emphasizes six key elements rating:

Capital Adequacy, Asset Quality, Management, Earnings, Liquidity, Sensitivity

And show the application of CAMELS system on the banking system as follows (PMA, 2003: 15): allocates each bank a standardized assessment system to assess the six key elements based, which all provides a general framework for assessing administrative factors, financial, operational, the task for each bank is subject to monitor the monetary authorities. CAMELS system requires the allocation of digital classification of each bank, based on the six basic elements and identifies each element Digital (1 classification) to (5), as the Rating (1) be a better assessment, classification (5) to be the worst evaluation. And determines the classifications of the bank, based on evaluations of each essential element of (1) to (5), and are taken into account in giving this assessment of all the factors affecting the assessments essential elements in determining the standardized assessment, because the process of determining the common assessment is a personal and objective judgment of the inspector. Banks that classified (4) or (5) refers to the existence of serious problems require supervisory certain conduct, but banks that classified (3) They are generally has weaknesses that must be corrected within a certain period of time, otherwise may cause big problems in the solvency and liquidity, While banks that are classified Unified (1) or (2) in all aspects and with a well-established and able to cope with

the economic crisis management, and require only minimal regulatory supervision to ensure the continuity of performance (Al karasneh, 2006: 33).

1. Capital Adequacy

The capital adequacy Reflect the financial strength of the bank, and its ability to contain the risks inherent in its tracks and banking activities and control, which makes it imperative for the bank that has enough capital commensurate with the size of its assets and supports risks (Hammad, 2003: 194).

2. Asset quality

It means good controlling on credit concentrations so as to provide a minimum level of risk, which means that the management of the loan portfolio controlled effectively and the good result of the policies of Prudential in the granting of credit and the study of the client's ability to repay, and also means the administration retain sufficient reserves to cover loan losses.

The investments and loans (financing) the main components of a portfolio of assets in any bank that does use them to achieve the revenue and earnings, whether through his granting of loans (financing) to clients with him, or through his investments (purchase of securities, buy debt securities, stock purchase .. etc). The importance of the quality of assets being affect the solvency of the bank, both revenues and liquidity, and its capital, and then the asset quality reflects the quality of the financial situation of the bank, the size of the risks of the current non-payment and the future that might be exposed (Al-Ghandour, 2003: 188).

3. Management

Quality performance of any bank based in various areas of its activity on the management efficiency of all levels in terms of overall understanding of the risks inherent in the banking activities of the bank, and the rate of the good financial performance in all areas. And understanding and appropriate response to the economic environment variables, and a commitment to effective surveillance, and not to give priority to self-interest, and the response of management and the Board of shareholders with the procedures of monetary and banking authorities and recommendations.

4. Earnings

It means that the bank is characterized by sufficient income to meet reserve requirements and a reasonable distribution of profits to shareholders, and the face of unexpected losses, which means planning and strong control over income and expenditure items, also means reduced reliance on special items and non-traditional sources of income.

The importance of earnings element as the main factor that the bank can pursue its business and provide its services, as well as the profitability is a source of confidence for clients with the bank.

5. Liquidity

Liquidity means the bank's ability to provide the necessary to cover current and future needs of the destination of funds, as well as its ability to meet the obligations it all in a timely manner and without additional costs on the other. One of the main responsibilities of the administration is to retain sufficient liquid assets to meet their daily obligations and to maximize profitability and minimize risk. Taking into account that the administration maintained a high level of liquid assets take a few risks of low profits, on the contrary, the administration maintained a low level of liquid assets has a strong high-risk profits.

With reference to the liquidity management depends on the bank's ability to invest excess liquidity has optimally, in order to achieve his best returns in accordance with the acceptable level of risk, with an appropriate hedge for cash withdrawals to meet the customer's requirements.

Liquidity management and are subject to the bank to harmonize the management ability of the maturities of bank liabilities (sources of funds from deposits or pay obligations) and how to use sources of funds (in the form of financing and investment) when making decisions related to liquidity, in order to maintain an adequate level of liquidity.

6. Sensitivity to Market price

Reflecting the sensitivity of the elements of the market price of the degree of change in interest rates, foreign exchange rates, commodity prices, or the possible impact stock prices adversely in the bank's profits or capital. When assessing this element, consideration must be given to the ability of management to identify and market risk measurement and monitoring, and the size of the bank, and the nature and complexity of its activities, and the adequacy of its capital and profits in relation to the level of its exposure to market prices.

Chapter Three: The practical framework for the banking system for standardized assessment "Camels" (Case study - BBSF)

This chapter deals with an analytical study to learn about the application of the banking system assessment and its impact on the banking inspection and supervision systems in place a mechanism and that the application to a bank operating in Syria (BBSF).

Is BBSF first private banking institution has been operating in Syria, has been creation of the bank in 2003, and began

to engage in activity in 04/01/2004, taking the bank's expansion and proliferation and was able to take a strategic steps in all directions and has made progress and broad technology all areas of banking work and follow the latest global systems and methods applied and now has 35 branches and offices covering all Syrian provinces and has international relationships and network correspondents and wide in many countries of the world, its assets totaled more than 138 billion Syrian pounds, property rights more than 11 billion Syrian pounds as the volume of customer deposits totaled more than 118 billion Syrian pounds, the bank is one of the leading banking business in Syria's banks.

The study came to shed light on the position of the bank and stand on the banking evaluation system Camels applications and its impact mechanism on the development of banking supervision and inspections, as shown by the budgets and accounts of the bank for the period (2006-2014), enabling regulators to know the development of the bank, and take appropriate prudential regulatory measures to face any malfunction before it happens.

1. Capital Adequacy

The capital can be evaluated using the Bank's banking and financial ratios depending on the classification indicators prepared by EXAMINER ORIENTATION Foundation of America, which divides the capital as follows (Examiner Orientation, op.c4: 14):

Well Capitalized: capital ratio be good if the total capital based on the risk of 10% or more, leverage of 5% or more and the ratio.

Adequately Capitalized: be appropriate capital ratio if the total capital risk-based 8% or more, leverage 4% or more and the ratio.

Under Capitalized: capital ratio be weak if the total capital is less than 8% 4% leverage ratio and less.

Significantly Under Capitalized: be very weak capital if it is less than 6% leverage is less than 3% and the ratio.

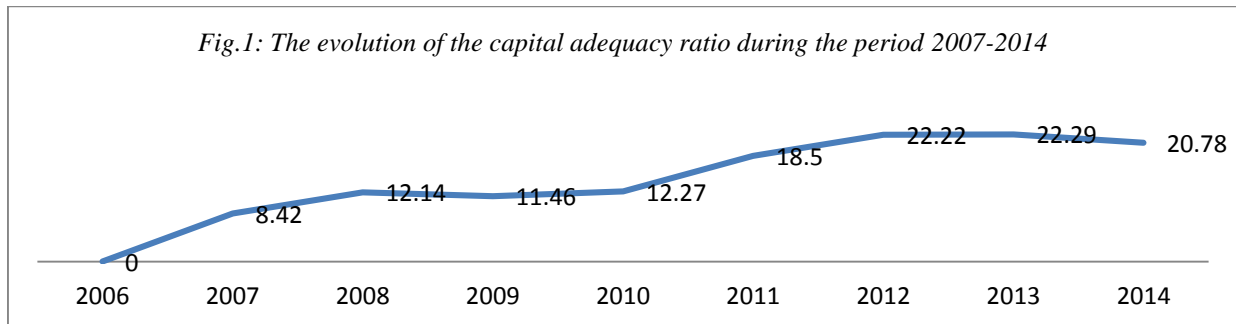
Critically Under Capitalized: capital ratio critically be if they leverage ratio of less than 2%. Among the most important indicators of capital at the bank:

First: the capital adequacy ratio:

It is a ratio of total regulatory capital to total assets and liabilities outside the risk-weighted balance, as this ratio measures the financial strength of the bank, reflecting its ability to withstand the shocks, so it must be on the bank owning the capital strong to support risky assets (Sheikh Mousa, 2007). It is worth noting that the decline in the capital adequacy ratio leads to increased vulnerability of the budget items to the risk, as the bank is committed to

maintaining well above the minimum capital adequacy requirements amounting rates (8%, according to the central bank instructions) and (8%, according to the decisions of the international Basel Committee) and (10%, according to the previous classification indicators that have been adopted in the analysis). The high capital adequacy ratio significantly higher for not strong indication as to that

sound impact on profitability in the light of the reliance on investments with high liquidity that yield a low return, so it is located on the banks departments creating a balance between the requirements of adequacy ratio and performance indicators, and reflecting this balance over banking management efficiency in the management of its assets and liabilities (Khja, 2010: 15).



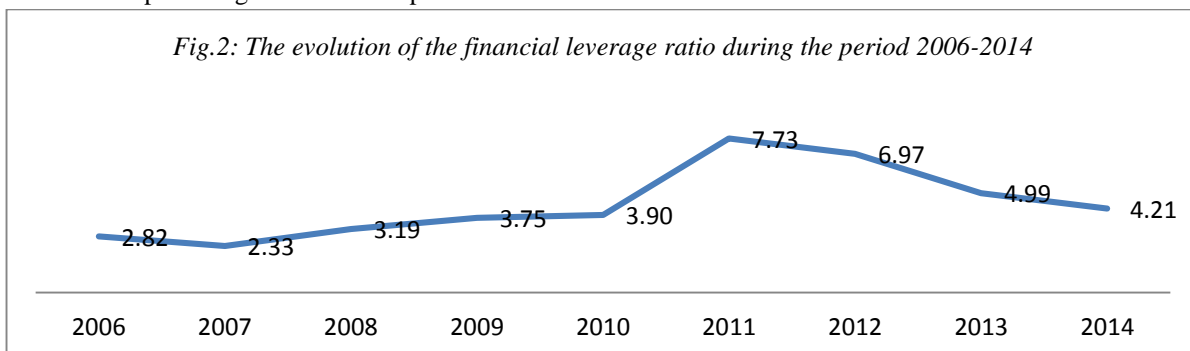
from Figure 1 the evolution of the results of the capital adequacy ratio of the Bank during the period from 2007 to 2014, the ratio rose from 8.42% in 2007 to 20.78% in 2014, reached the capital adequacy ratio per year on average during the period 2007 to 2014 the Bank 16.01 %. From the above we note that in spite of rising rates converged in the capital adequacy ratio on average during the period 2007 - 2014 at the bank, but it is the basis of indicators previous classification is a good bank's capital base any (Category 1) and it was due to the regulatory authorities in the Syria as follows:

1. Law No. 3 of 2010, which included raising the minimum capital of traditional private banks to 10 billion SP, and Islamic banks to 15 billion SP
2. As the monetary and supervisory authorities in Syria to raise the maximum percentage of ownership Arabs and

foreigners from 49% to 60%, but the share of legal persons from 49% to 60% figures provided that such increase is to cover the contributions of public institutions.

Second: the financial leverage ratio (capital and reserves / assets):

Also called the capital ratio, the ratio reflects the degree lever funding DEGREE OF FINANCIAL LEVERAGE in the bank, the ratio shows the extent of the bank's reliance on its own funds (capital and reserves) in financing assets, and then over the risk of others with money in his investments, where this ratio shows the level of margin of safety provided by the capital and reserves of the Bank, the larger the rate was greater if it means that a small percentage of capital, and that the Bank operates a small capital to fund a major expansion in lending and investment more than the bank's risk.



Leverage ratio increased at the bank during his stay in the Syrian banking market phase, from 2.82% in 2006 to 7.73% in 2011, then the ratio is back and fell to 4.21% in 2014 and at an average annual growth rate amounted to 4.43% during the entire study period (2006 to 2014), and thus is

considered the head of an appropriate bank's capital on the grounds that the leverage ratio of more than 4%, according to previous indications of any classification within the (Category 2).

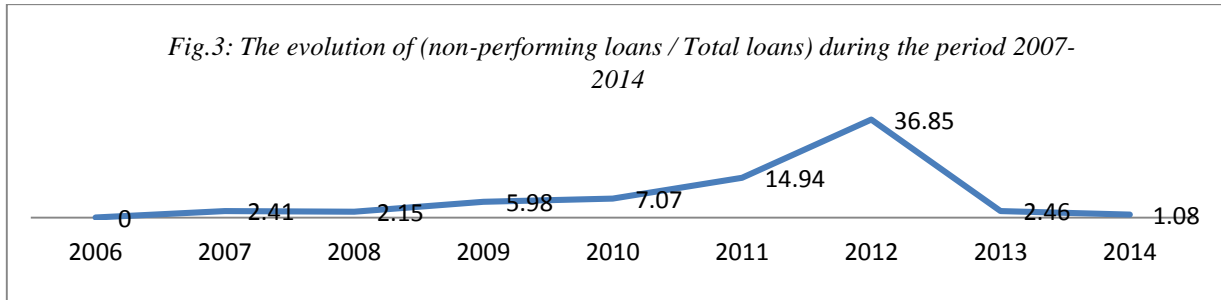
From the above clearly shows the ability of monetary and supervisory authorities in Syria to some extent during the study period (2006-2014) to raise capital and reserves relative to assets at the bank, and it came in line with the International Committee of the Basel requirements, which significantly contribute to the reduce the risks faced by the Bank as a result of reducing the bank's reliance on capital and reserves to finance its assets.

2. Asset quality

It came the most important asset quality evaluation of the Bank as the following indicators:

First: the rate of non-performing loans / Total loans:

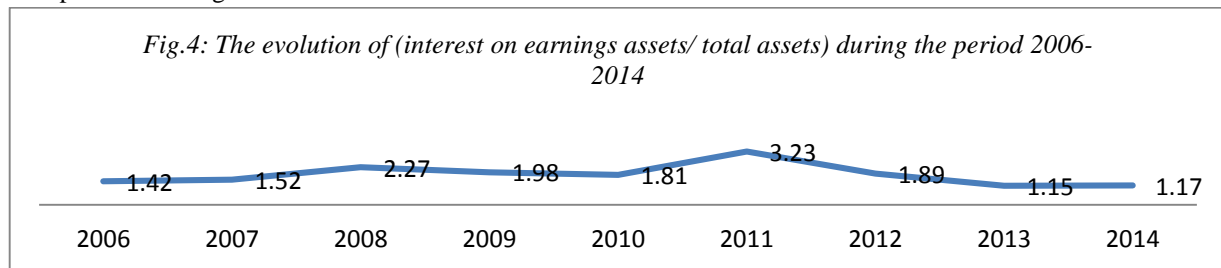
Refers to loans non-performing loans past due 90 days or more whole, the ratio reflects the efficiency of the existing credit policy within the banks in credit management and analysis, monitoring and follow-up and the safety of the credit portfolio of the bank, as this ratio reflects the follow-up to the financial situation of the bank's customers as the best, and the ratio of standard according to indicators according to rating assessment institution mentioned earlier, is ($\leq 10\%$).



Note from Figure 3 the results of non-performing loans to total loans at the bank, it had risen through the phase from 2007 to 2014 from 2.41% in 2007 to 36.85% in 2012, with the ratio was on average during the period 2007-2014 with the Bank 9.12 %, and this percentage is a good, and we can interpret the rise in non-performing loans to total loans at the bank during the period 2007 - 2014 to the crisis and the pressures experienced by Syria, and then reduced the volume of exports and the volume of production and increased imports and rising inflation.

From the above we note that despite the rise in non-performing loans to total loans on average during the period 2007 - 2014 at the Bank of the study sample, which amounted to 9.12%, but it is a satisfactory ratio of any part of (Category 2), where no more than 10% upper limit acceptable for this ratio.

Second: the rate of interest on earnings assets / total assets:



The rate of interest on earnings assets to total assets ratio showed a marked decline during this phase of the Bank, where he rose from 1.42% in 2006 to 3.23% in 2011 and then returned to the decline of up to 1.17% in 2014, to reach an average per year over the entire study period of about 1.83%.

3. Management

Management is so conscious activity aimed from which you can achieve maximum profits less expenses and maximize the profitability of the organization, as the bank

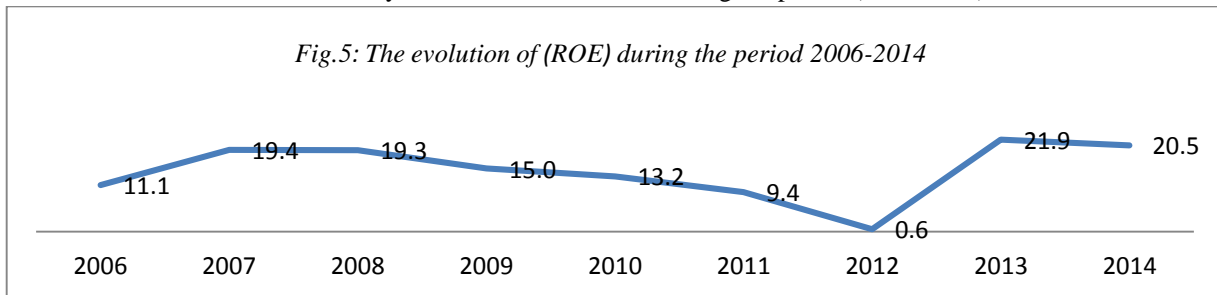
management is one of the key factors that are reflected on the quality of the performance of any bank in the various activities, as manifested efficient management in creating an effective balance between liquidity system, profitability and over capital adequacy and risk management in the context of (risk management). It is noted that the management are difficult to measure in quantitative terms as it inherently is measured qualitatively.

4. Earnings

First: the rate of return on equity (ROE)

Is a ratio of net income after tax to the total property rights, as this ratio measures the rate of return to shareholders, any net profit earned by shareholders from investing their money in the bank rate, and therefore reflects the return on their risks in the recruitment of their money in the bank, as

it demonstrates the ratio on the efficiency of the bank's management in the recruitment of shareholders' funds, and the ratio is the standard accepted ($\geq 15\%$). Figure 5 shows the evolution of the rate of return on equity at the bank during the period (2006-2014).



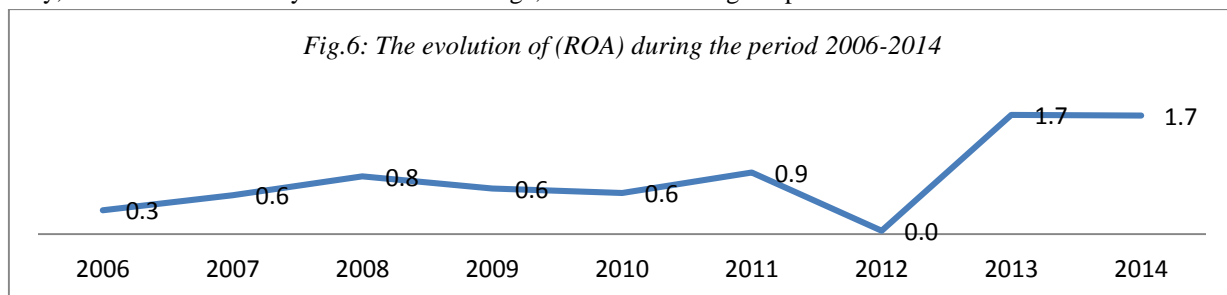
Increased rate of return on equity at the bank during the period (2006 - 2014), this percentage has raised an average of 11.1% in 2006 to 20.5% in 2014, to reach an average per year during the study period, 14.5%, and we can explain as follows:

This positive development in the rate of return on equity at the bank of the study sample during the years 2006-2014 due to several factors, including: the stability of the turnover of these banks, and an increase in the size of his own money, which led to stability in financial leverage, as

well as the employment of the bank about 40% of his own money in the bank.

Second: the rate of return on assets (ROA)

This ratio is a net income after tax to total assets, this ratio measures the net income resulting from the investment of the assets, as this ratio shows how efficiently the bank's management in the use of assets and management, and the ratio of standard accepted are ($\geq 1\%$). diagram No. 6 evolution of the rate of return on the assets of the Bank during the period 2006-2014.



Increased rate of return on the assets of the Bank during the period (2006 - 2014), where the average increased from 0.3% in 2006 to 1.7% in 2014, and this figure was on average during the years 2006 to 2014 about 0.8%, and we can explain as follows:

This positive development in the rate of return on assets in the bank study sample during the years 2006-2014 due to an increase in profit margins, and increased asset turnover rate at the bank, as a result of Bank to hire asset rather than owned, note that this is not acceptable, especially in stages

Founded as the first it will lead to a decrease in the volume of assets.

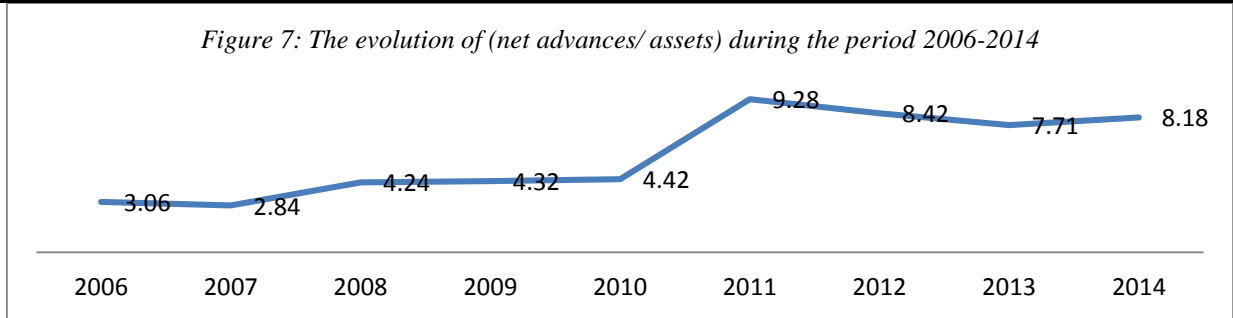
Based on the financial ratios related to profitability (ROA - ROE) it shows that the profit of the Bank is considered satisfactory and within the (Category 2) and did not exceed the average standard ratios accepted.

5. Liquidity

First: the rate of net advances / assets

This ratio is also called quick liquidity ratio, this ratio shows liquid assets for banks that are accused of doing utilizing it in the form of loans or investment size.

Figure 7: The evolution of (net advances/ assets) during the period 2006-2014



The rate of net advances to assets has seen increased significantly during the study period (2006-2014) and the rate of growth of average annual rate of about 5.83%, with the ratio rising from 3.06% in 2006 to 8.18% in 2014 at a rate of gain of approximately three times, and we can interpret this quick rise in the rate of ready money in the bank for several reasons:

□ Central Bank of Syria has committed working in the Syrian market, banks as well as the reserve requirements on deposits ratio, to retain sufficient cash liquidity so as to ensure the safety of its finances and its ability to meet its obligations when due, has stated in Resolution No. (588 / MN / 4) of the Monetary and credit Council that each bank

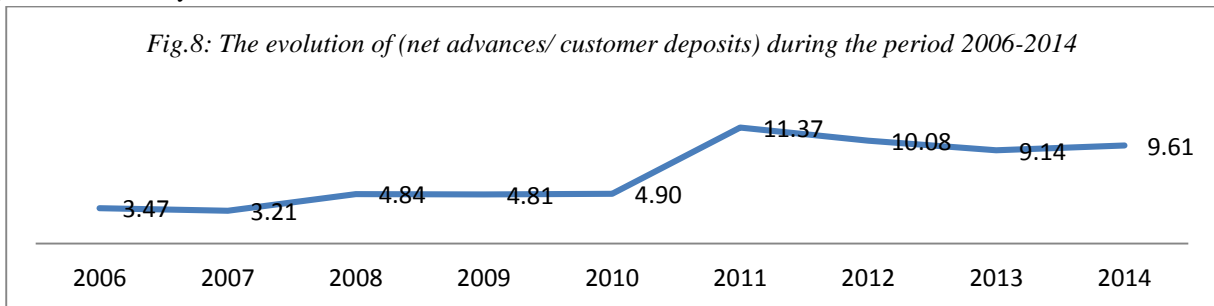
must be maintained in each working day by the whole currency liquidity of not less than 30% to be less liquidity in Syrian pounds percentage of 20%.

□ entering the bank to the Syrian banking market and having to dramatically funds ready (Syrian pound and foreign currency) is not utilizing it full form, but resorted to retain large portion of which count as credits at the central bank, as it was quick liquidity in the average rate of the Bank during the period (2006-2014) about 5.83%.

Second: the rate of net advances / customer deposits:

This ratio measures the ability of banks to respond deposits of net advances.

Fig.8: The evolution of (net advances/ customer deposits) during the period 2006-2014



The rate of net advances to customer deposits has seen increased significantly during the study period (2006-2014) and the rate of growth of average annual rate of about 6.83%, with the ratio rising from 3.47% in 2006 to 9.61% in 2014 at a rate of rise of about approximately three times, and we can the interpretation of this rise in this ratio at the bank to the following reasons:

□ increase in deposit growth rates increased significantly with the Bank during his stay in the Syrian banking market phase, with increased deposits of 56 billion SP in 2006 to more than 118 billion SP in 2014, an increase of more than doubled in the past (2006-2014) , due as a result of the bank to attract the large size of the funds in the local market is deposited.

□ Bank's commitment to standards, regulatory and prudential ratios, both legal reserve requirements and

liquidity ratios as a hedge to counter the high deposit-withdrawal possibilities.

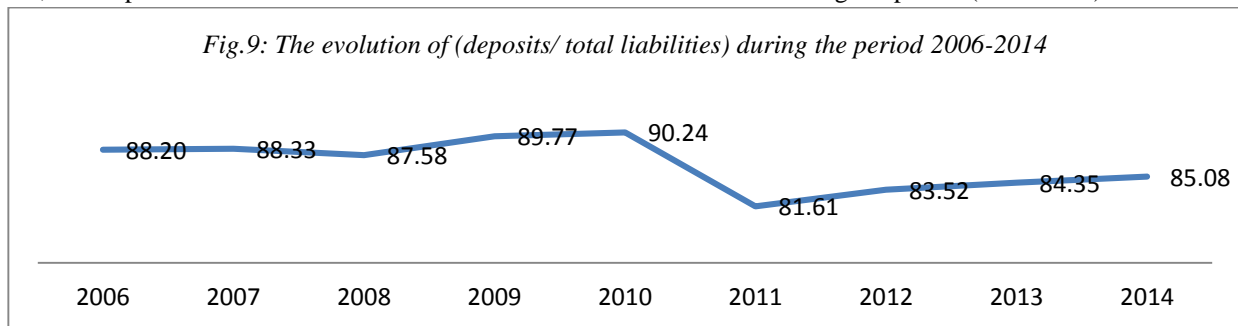
□ the failure of the bank's recruitment and deposits for fear of market risk, so the increased liquidity the Bank clearly. Financial ratios mentioned refers to the safety of the liquidity situation of the bank, where he has a high degree of liquidity, and that the volume of deposits is considered strong, and therefore can be given to the bank for this indicator (classification then 1), which shows that there is a clear improvement in the banking supervision at the Bank operation during this period and to ensure commitment to regulatory standards, both the rate of reserve requirements or legal liquidity ratios, which does not threaten the safety and exposure to liquidity risk in the future.

6. Sensitivity to Market price

Sensitive element reflects the degree of sensitivity of the bank (assets and liabilities) to changes in market prices (interest rates, exchange rates) that affect the financial position of the bank.

It should be noted that the sensitive element is difficult to measure due to the complexities associated with the study and the difficulty of doing his account of being not rely on key financial ratios such as other elements of the system CAMELS, but depends on the balance sheet and activities

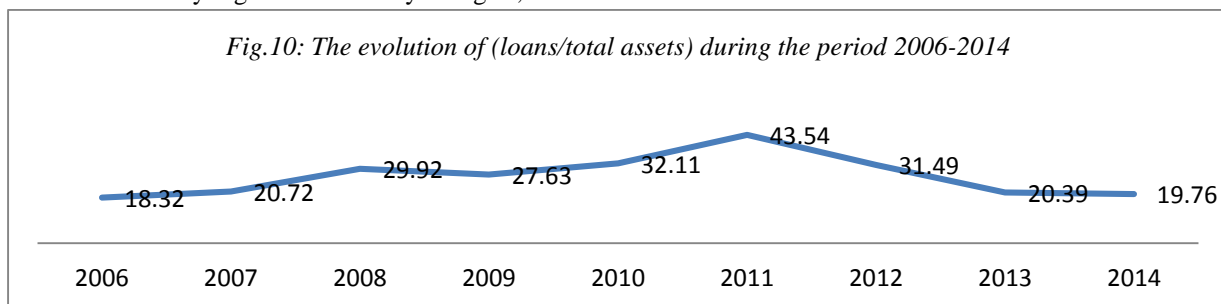
included in components, so the item needs to be elements of the observers have professional and efficient experience high, though, we briefly examine each of the loans and deposits to measure the degree of sensitivity to the Syrian banks against market risk, given that the loans and deposits of the assets and liabilities more sensitive to market prices and their volatility. The following diagram illustrates the No. 9 evolution of the rate of deposits to the Bank's liabilities during the period (2006-2014).



Deposit to total liabilities ratio has seen declined during the period (2006-2014), and the rate of growth of average annual rate of about 86.52%, since this ratio fell at the bank from 88.20% in 2006 to 85.08% in 2014, and despite the decline in this ratio the Bank has during the study period, but it is considered a very high rate Taken by allergies, and

then the rise in interest rates in the market have a major impact negatively on the bank's profits.

On the other hand Figure 10 illustrates the evolution of the rate of loans to assets of the Bank during the period (2006-2014).



Loans to total assets ratio increased significantly during the period (2006-2011), where the average rose from 18.32% in 2006 to 43.54% in 2011, and then resumed the decline clearly for up to 19.76% in 2014, and the rate of growth of average annual rate of about 27.10%, and therefore this change in the ratio of loans to total assets at the bank during this period makes it an impressive ratio Taken by Sensitivity, and therefore any change in interest rates could have an ambivalent impact on the bank's profits.

Based on previous financial ratios relating to sensitive to market risk shows the strong influence of the sensitivity of profits at the bank as a result of changes in interest rates during the study period.

III. CONCLUSIONS AND RECOMMENDATIONS

Conclusions:

1. Research has shown the importance of applying a supportive system for the operations of banking supervision being carried out by monetary and supervisory authorities, including confirming the validity of the hypothesis research, hence the importance of the system (camels) and the role they play in providing monetary and supervisory authorities with data and information that show the weaknesses and shortcomings as a gateway to find solutions radical banking problems and their causes.

2. CAMELS system help monetary authorities and regulatory system to identify dangerous weaknesses of the theoretical and practical banks would lead to direct attention and focus efforts towards it and then take the necessary steps to address the regulatory procedures, and thus achieve the objectives of depositors, investors and shareholders the service both as to ensure efficiency of the system banking and safety.
3. The reports help by the monetary authorities and regulators on the results of inspections and banking supervision as stated in this research to increase the effectiveness of reporting and directing their results in order to serve the goals of growth and keep pace with modern progress.
4. Emphasize the importance of integration and interdependence between supervision and inspection system currently in place (Traditional his image) and the banking system for standardized assessment camels so that he can keep up with the development witnessed by the banking industry under the age of technology and information systems.
5. Importance of integration and interdependence between the stages of the positive controls and field inspection and evaluation elements standardized camels, which contributes to the increased power and efficiency in the application of control and inspection of the banking operations.
6. CAMELS system works on a comprehensive analysis of the performance of Bank Bemo Saudi France and its activities and his works compared to other existing banks in the banking market, which contributes to the formulation Court plans inspection and implementation stages meticulously operations with a focus on the negative elements that need greater care and attention.

Recommendations:

1. There are complementary and interdependent relationship between the elements of the CAMELS system, and then be on the banks departments to choose the optimum combination of these elements that are compatible and integrate these elements with each other in order to ensure the achievement of strength and safety of banking for the bank at the domestic level, and help regulatory authorities to determine dangerous weaknesses in banks and take the necessary steps to address them so as to ensure

the efficiency of the banking system as a whole and safety control procedures.

2. CAMELS system for the purpose of supporting the efficiency and effectiveness of oversight and inspections by the banking supervision and inspection devices monetary authorities on the banking system.
3. The work included the final inspection report prepared by the Banking Supervision devices all around the positive and negative points that result from the application of the evaluation system and its impact on the results of inspections and audits.
4. The performance of the active role of oversight for the advancement of the banking and supervisory work requirements and raise its efficiency, requires the availability of highly qualified, which has the skill and experience in the field of banking supervision and human frameworks, as well as the availability of a high degree of coordination and cooperation among the various regulatory and supervisory, especially in the control of business with an international banking activity.
5. The need to do more attention by monetary authorities and regulators to develop the banking system assessment mechanisms to become inspection reports an effective tool for the control of the bank and achieve targets.

REFERENCES

- [1] Hammad, Tareq Abdel Aal: Risk Management, Al-Dar University, Cairo, 2003.
- [2] Khja, Jumana: the role of banking supervision in achieving the safety of the banking situation, Master Thesis, University of Damascus, 2010.
- [3] Sisi, Salah al-Din Hassan: the Basel Committee standards for capital adequacy, the General Authority for general banking book, Egypt, 2005.
- [4] Sheikh Mousa, Othman: banking safety, Dar-al moueen for publication, Sudan, 2007.
- [5] Sayrafi Mohamed Abdel Fattah: Banks management, Oman, the first edition, 2006.
- [6] Abdullah, Khalid Amin: Banking Operations, Dar Wael for Publishing and Distribution, Amman, 2003.
- [7] Aqeel Jassim Abdullah: money and banking, Oman, the second edition, 2000.
- [8] Ghannam, Reem: the role of the Central Bank in monitoring and evaluation of policies in government banks / application of the Industrial Bank of Syria /, Master Thesis, University of Damascus, 2004-2005.

- [9] Ghandour, Hafez Kamel: Effective update axes in the Arab Banks (postmodern thought), the Union of Arab Banks, Beirut, 2003.
- [10] Credit and Monetary Council resolutions, the Central Bank of Syria.
- [11] Al Karasneh, Ibrahim: Basic and contemporary frameworks in the oversight of banks' risk management, the Arab Monetary Fund, the Economic Policy Institute, Abu Dhabi, 2006.
- [12] Unpublished research about / use of evaluation Composite Commercial Banks' policy, PMA / Banking Supervision Department /, 2003.
- [13] Basel C0mmittee on Banking Supervision "International convergence of capital measuring and capital standards", Basel, july, 1988.
- [14] Ian H. Giddy, Who should be the Banking Supervision? Some General Considerations, IMF, March, 1997.
- [15] Examiner Orientation, op.c4.

Text Detection in Document Images: Highlight on using FAST algorithm

Geetika Mathur¹, Ms. Suneetha Rikhari²

¹Student, Department of E.C.E., College of Engineering and Technology, Mody University, Lakshmanagarh, Sikar, India

²Assistant Professor, Department of E.C.E., College of Engineering and Technology, Mody University, Lakshmanagarh, Sikar, India

Abstract—In recent years, text extraction from document images is one of the most widely studied topics in Image Analysis and Optical Character Recognition. These extractions of document images can be used for document analysis, content analysis, document retrieval and many more. Many complex text extracting processes Maximization Likelihood (ML), Edge point detection, Corner point detection etc. are used to extract text documents from images. In this article, the corner point approach was used. To extract document from images we used a very simple approach based on FAST algorithm. Firstly, we divided the image into blocks and their density in each block was checked. The denser blocks were labeled as text blocks and the less dense were the image region or noise. Then we check the connectivity of the blocks to group the blocks so that the text part can be isolated from the image. This method is very fast and versatile, it can be used to detect various languages, handwriting and even images with a lot of noise and blur. Even though it is a very simple program the precision of this method is closer or higher than 90%. In conclusion, this method helps in more accurate and less complex detection of text from document images.

Keywords—Corner point, FAST (Features from Accelerated Segment Test), OCR, multilingual documents, handwritten documents.

I. INTRODUCTION

In recent years, the trend to digitalize documents has emerged. With digitalization of the world the paper based documents need to be converted into digital to make them handier, searchable and for preserving of the documents. Optical Character recognition is used for this process. OCR can be described as Mechanical or electronic conversion of scanned images where images can be handwritten, typewritten or printed text [2]. For over a half century research in this area is ongoing and character recognition

rate in modern OCR is above 99% on a high-quality document and 90% on handwritten documents. For degraded documents and books the efficiency of OCR comes down to 80%. In recent times, many techniques have been used for text extraction in document images. Here we will use a very simple approach based on FAST point's algorithm. Firstly, we divide the document image into smaller non-overlapping blocks of a fixed size. We then check the density in each block using FAST corner detection technique. The denser blocks were labeled as text blocks and the less dense were the image region or noise region. Then we check the connectivity of the blocks to group the blocks so that the text part can be isolated from the image. We then build the text region and save it.

This method is very fast and versatile, it can be used to detect various languages, handwriting and even images with a lot of noise and blur. Even though it is a very simple program the precision of this method is closer or higher than 90%. In conclusion, this method helps in more accurate and less complex detection of text from document images.

II. OPTICAL CHARACTER RECOGNITION

The development of character recognition in last decade is remarkable and the method for character detection is vast. The advancements of Character Recognition are evident in Optical Character Recognition (OCR), Document Classification, Computer Vision, Data Mining, Shape Recognition, and Biometric Authentication [2]. Character recognition is the process to classify the input character per the predefined character class [1]. Character recognition has its application in identification of text in images. The text maybe a scanned document or a handwritten text.

A. Text from Images:

In recent years, the trend to digitalize documents has emerged. With digitalization of the world the paper based documents need to be converted into digital for more handy,

searchable and preserving of the documents. Optical Character recognition is used for this process. OCR can be described as Mechanical or electronic conversion of scanned images where images can be handwritten, typewritten or printed text [2]. For over a half century research in this area is ongoing and character recognition rate in modern OCR is above 99% on a high-quality document and 90% on handwritten documents. For degraded documents and books the efficiency of OCR comes down to 80%. In recent times, many organizations depend on OCR for better performance and more efficiency. OCR can be performed offline and/or online. Online recognition the OCR processor recognizes the character as they are given. In offline method, the processor may recognize both document as well as handwritten characters but recognition in offline mode highly depends on the quality of the scanned images.[10]

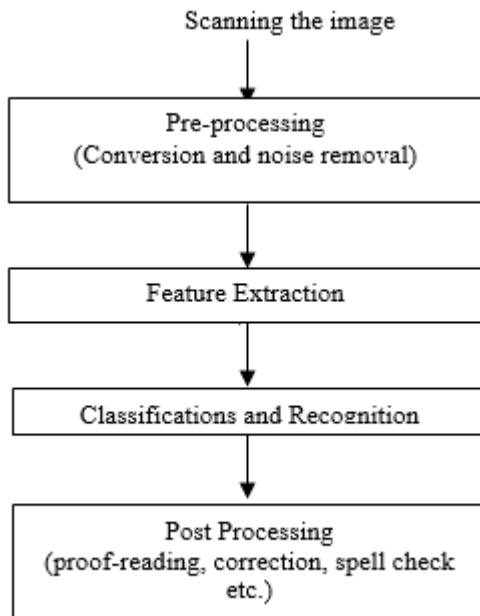


Fig.1: Stages for OCR

OCR consists of many phases such as Scanning of image, Pre-processing, Segmentation, Feature Extraction, Classifications and Recognition, Post Processing. The task of preprocessing relates to the removal of noise and variation in the image [3]. In scanning step the image is acquired. The quality of image depends highly on the scanner being used. In practical applications, the scanned images are not perfect there may be some noise due to some unnecessary details in the image which can cause a disruption in the detection of the characters in the image. Preprocessing involves removal of noise (applying filters

like Gaussian filter, Gabor filter etc.) and proper conversion of image like a colored image can be converted into gray scale or binary image for further processing of image. Feature extraction involves recognizing the feature required. Classifications and Recognition phase is the extraction phase of the process. After finishing the OCR process several postprocessing steps are necessary depending on the application, e.g. tagging the documents with meta-data (author, year, etc.) or proof-reading the documents for correcting OCR errors and spelling mistakes [4].

OCR is still in research and much advancement need to be made in this technology. The future scope of this is OCR in mobile devices, handwriting recognition, recognition of various languages except English (like Arabic, Devanagari, Telugu text), extraction and processing of images from video, processing and restoration of old documents and many more.

B. Document Images:

A document image contains various information such as texts, pictures and graphics [5]. These images are obtained by scanning handwritten documents, old documents, printed documents, journals etc. Many challenges are faces for recognizing scanned documents like low contrast, low resolution, color bleeding, complex background and unknown text color, size, position, orientation, layout etc. Even if the OCR system is of supreme quality the system can still not give proper output due to the problems discussed above. Generally, the process of OCR works best if the background of the image is clean and the image is free of any noise.[6]

C. Extraction from Document Images:

Many techniques have been used for text extraction in document images. In this article, we will use a very simple approach based on FAST point's algorithm. Firstly, we divide the document image into smaller non-overlapping blocks of a fixed size. We then check the density in each block using FAST corner detection technique. The denser blocks were labeled as text blocks and the less dense were the image region or noise region. Then we check the connectivity of the blocks to group the blocks so that the text part can be isolated from the image. We then build the text region and save it.

This method is very fast and versatile, it can be used to detect various languages, handwriting and even images with a lot of noise and blur. Even though it is a very simple program the precision of this method is closer or higher

than 90%. In conclusion, this method helps in more accurate and less complex detection of text from document images.

III. COMPONENTS OF AN OCR SYSTEM

A distinctive OCR system consists of various components for OCR systems. OCR consists of many phases such as Scanning of image, Pre-processing, Segmentation, Feature Extraction, Classifications and Recognition, Post Processing. The task of preprocessing relates to the removal of noise and variation in the image [3]. In scanning step the image is attained and the image is digitalized. The quality of image depends highly on the scanner being used. In practical applications, the scanned images are not perfect there may be some noise due to some unnecessary details in the image which can cause a disruption in the detection of the characters in the image. Preprocessing involves removal of noise (applying filters like Gaussian filter, Gabor filter etc.) and proper conversion of image like a colored image can be converted into gray scale or binary image for further processing of image. Feature extraction involves recognizing the feature required. Classifications and Recognition phase is the extraction phase of the process. After finishing the OCR process several postprocessing steps are necessary depending on the application, e.g. tagging the documents with secondary data like author, year, etc. or proof-reading the documents for correcting OCR errors and spelling mistakes [4].

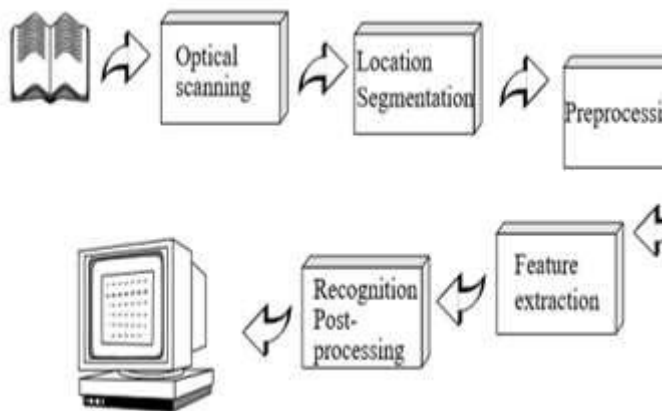


Fig.2: Components of an OCR system [7]

1. Optical Scanning:

In the scanning process the digital image of the document is captured. A scanner is used to scan the documents. The quality of the document depends highly on the scanner being used. So, a scanner with high speed and good color quality is necessary for proper processing of the image.

2. Location and segmentation:

This process locates the places where contents are present. The process that determines the constituents of an image is segmentation. It is essential to locate the regions of the document that have data printed and distinguish them from noise and pictures. For example, during automatic mail-sorting, the address is located and separated from other constituents of the envelope like stamps or logos, before recognition process.

Segmentation is the separation of characters or words from image which is performed on text. Most optical character recognition systems segment the words into isolated characters which are documented individually. This technique is easy to device, but problems occurs if the characters' touch or if characters are disjointed and consist of several parts. The main problems in segmentation may be divided into four groups:

1. Extraction of touching and disjointed characters.
2. Distinguishing noise from text. Dots and accents may be mistaken for noise, and vice versa.
3. Mistaking graphics or geometry for text. This leads to nontext being sent to recognition.
4. Mistaking text for graphics or geometry. In this case the text will not be passed to the recognition stage. This often happens if characters are connected to graphics [7].

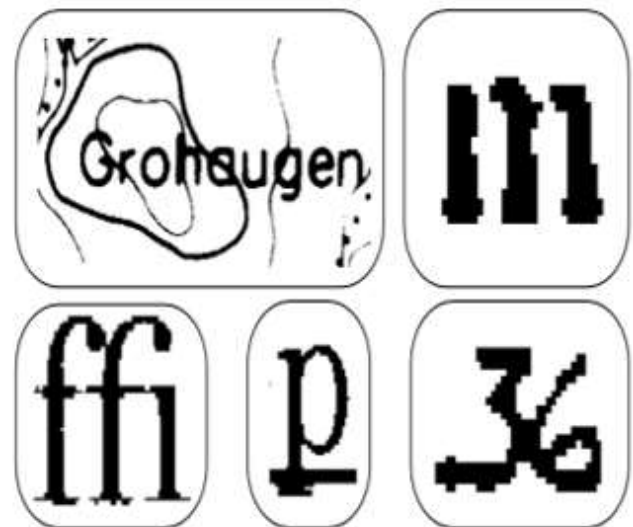


Fig.3: Example of Degraded symbols[7]

3. Pre-Processing:

The image is scanned and is converted into gray scale. The gray scale image maybe converted to binary image. This process is called Digitization of image (Binarization). In practical applications, a scanner is not perfect; the image

that is scanned may have some noise. This may be due to some redundant details present in the image. The denoised image is produced by applying some appropriate methods. This denoised image is saved for further processing [2]. Depending on the resolution on the scanner and the success of the applied technique for thresholding, the characters may not be perfectly scanned.

4. Feature extraction:

The pre-processed image serves as the input to this and each single character in the image is found out [2]. The image from the extraction stage is matched with all the preloaded characters in the system. Once the matching is completed, the template with the maximum correlated value is declared as the character present in the image. [1]

The objective of feature extraction is to detect the essential characteristics of the characters, and it is generally accepted that this is one of the most difficult problems of pattern recognition. The best way of describing a character is by the actual image. The techniques for extraction of such features are often divided into three main groups, where the features are found from:

- The distribution of the points.
- Transformations and series expansions.
- Structural analysis.[14]

5. Post Processing :

After feature extraction stage, there might be some unrecognized characters, those characters may get defined in the post-processing step. [2] Character grouping to make a meaningful text and error detection and correction is done in this step.

IV. PROPOSED WORK

In the proposed approach to extract document from images we used a very simple FAST algorithm. Firstly, we divided the image into blocks and their density in each block was checked. The denser blocks were labeled as text blocks and the less dense were the image region or noise. Then we check the connectivity of the blocks to group the blocks so that the text part can be isolated from the image. This method is very fast and versatile, it can be used to detect various languages, handwriting and even images with a lot of noise and blur. Even though it is a very simple program the precision of this method is closer or higher than 80%. In conclusion, this method helps in more accurate and less complex detection of text from document images.

The flowchart in figure 4 shows the steps involved in the proposed approach. The details of the steps are given below:

Step 1: The image is scanned and is converted into gray scale. The gray scale image maybe converted to binary image. This process is called Digitization of image (Binarization) The noise is due to the scanner. In the project we have used Gaussian filter .Gaussian filtering is used to blur images , remove noise and remove unwanted details in the image.[12][13]

$$G(x, y) = \frac{1}{2\pi\sigma^2} e^{-\frac{x^2+y^2}{2\sigma^2}}$$

Step 2: The corner points are determined by FAST algorithm[9]

Step 3: Divide the image in non-overlapping blocks and calculate the number of corner points.

Step 4: From the block find the block which has the maximum number of corner points (Nmax), define a threshold using the selected block, threshold used as $T=0.2*Nmax$. (20% of maximum value)

Step 5: Divide the blocks having more number of corners than the threshold belong to text regions, and blocks having less threshold belong to image or background region.

Step 6: After detecting text blocks from corner point, check for connectivity of these blocks (8-connected regions) to rebuild text regions. [15]

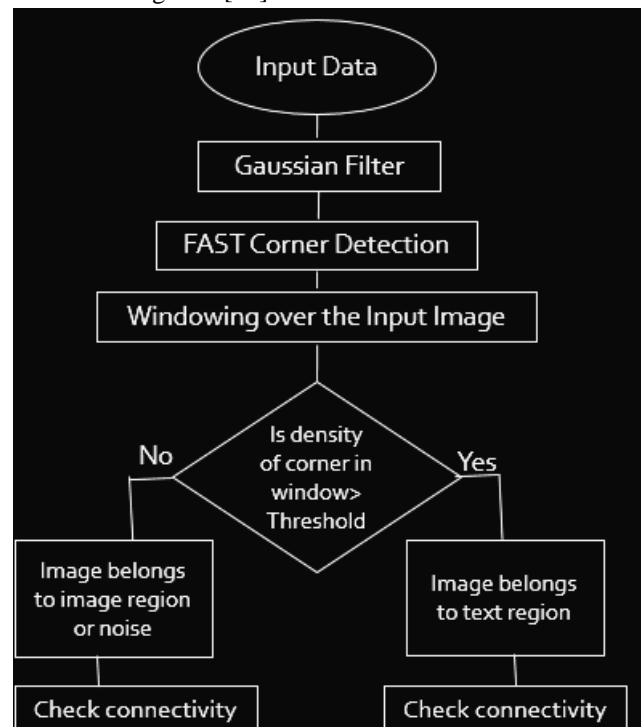


Fig.4: Flow chart for the algorithm[8]

V. EXPERIMENTAL RESULT

This is a simple method with precision and recall are over 90% and often with 95% on an average. However, this technique is not very effective for big size fonts as well as for some specific pictures for which corners are responding

too much. Despite of these problems it is fast (and can be parallelized) and less complex as compared to other OCR tools and could be further improved in the future. Finally, this method seems also to be very efficient in extracting more complex layouts such as paragraphs, and lines.

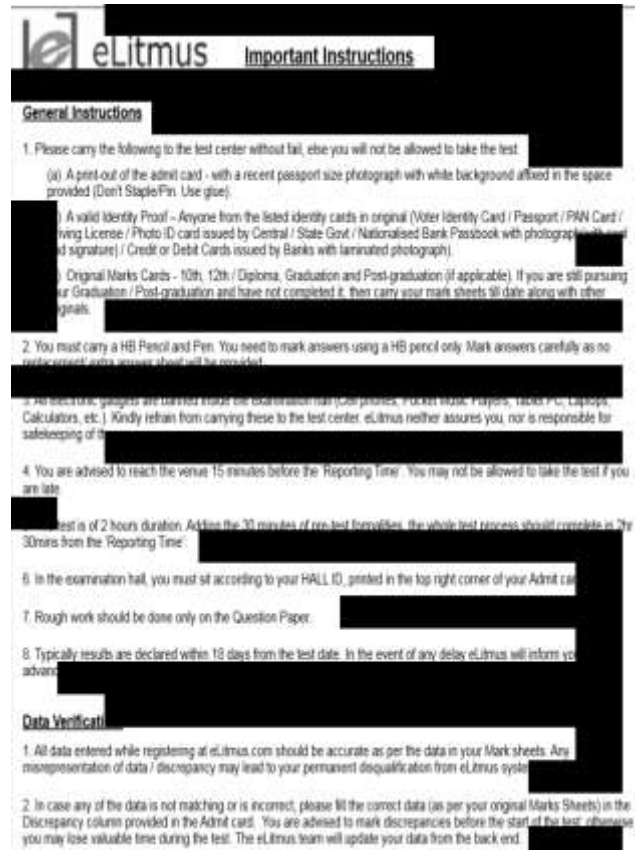
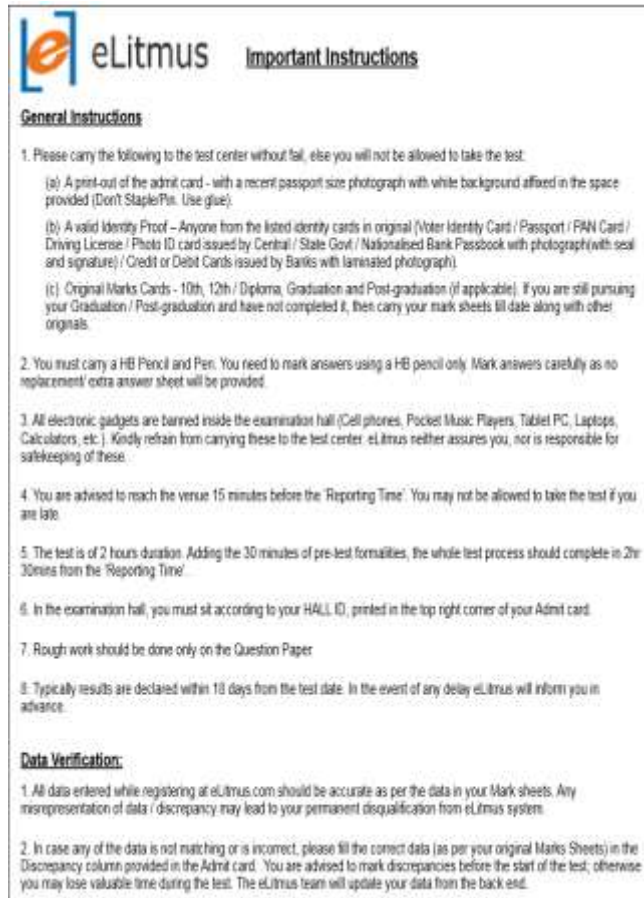


Fig.5: English document image (Original image, Detection of text image)

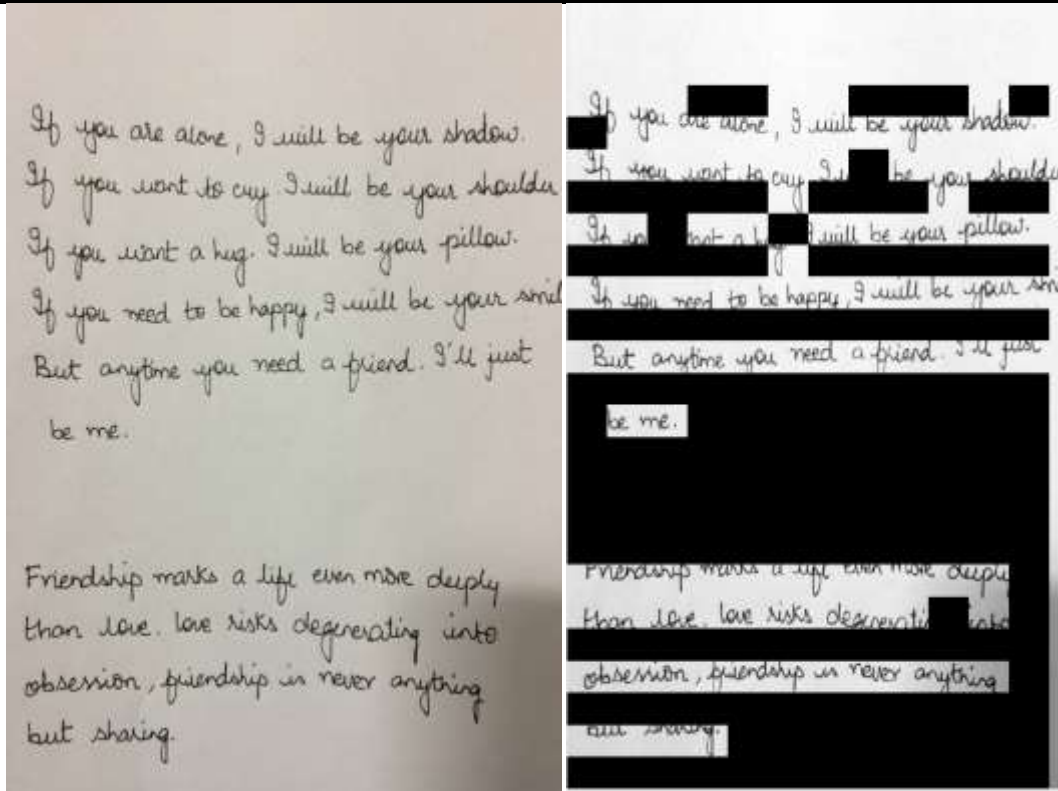


Fig.6: English handwritten image (Original image, Detection of text image)

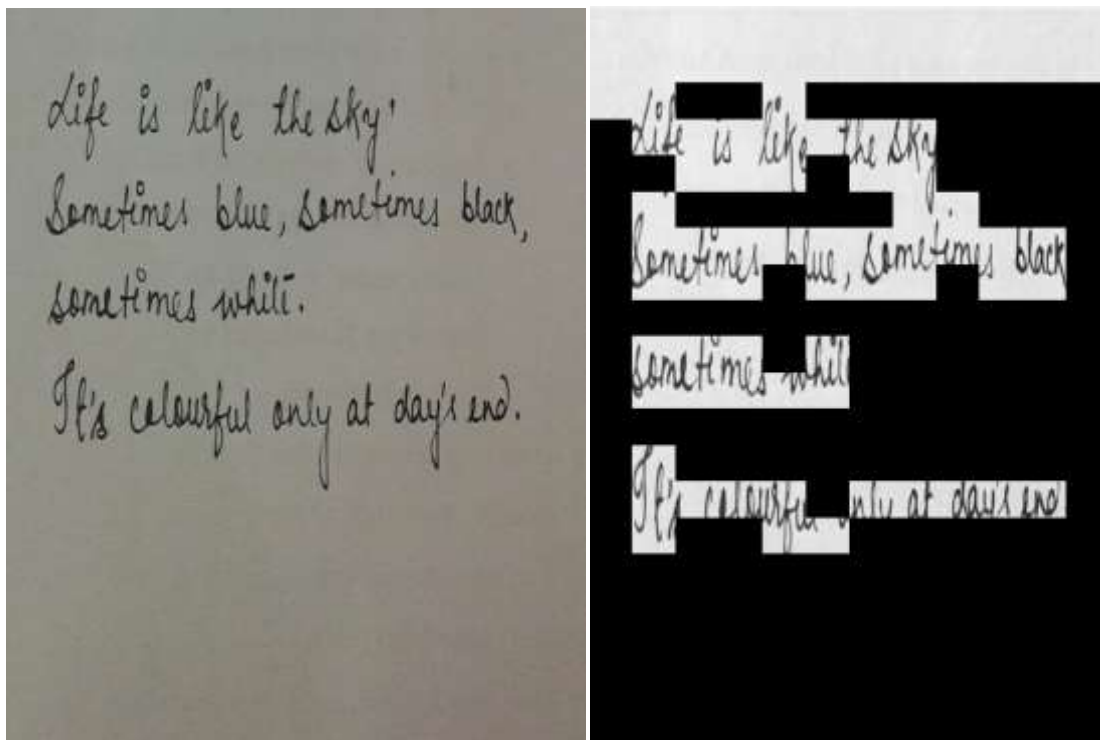


Fig.7: English handwritten image (Original image, Detection of text image)

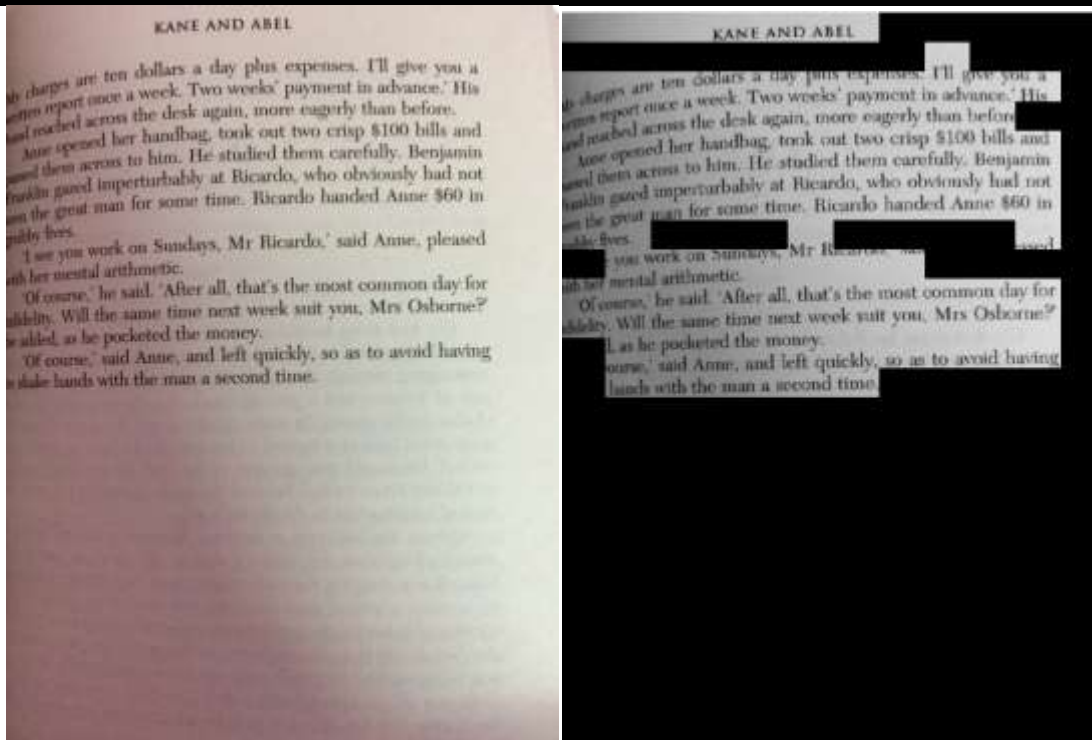


Fig.8: Skewed Document Image (Original image, Detection of text image)



Fig.9: Non- English text images-Arabic language (Original image, Detection of text image)

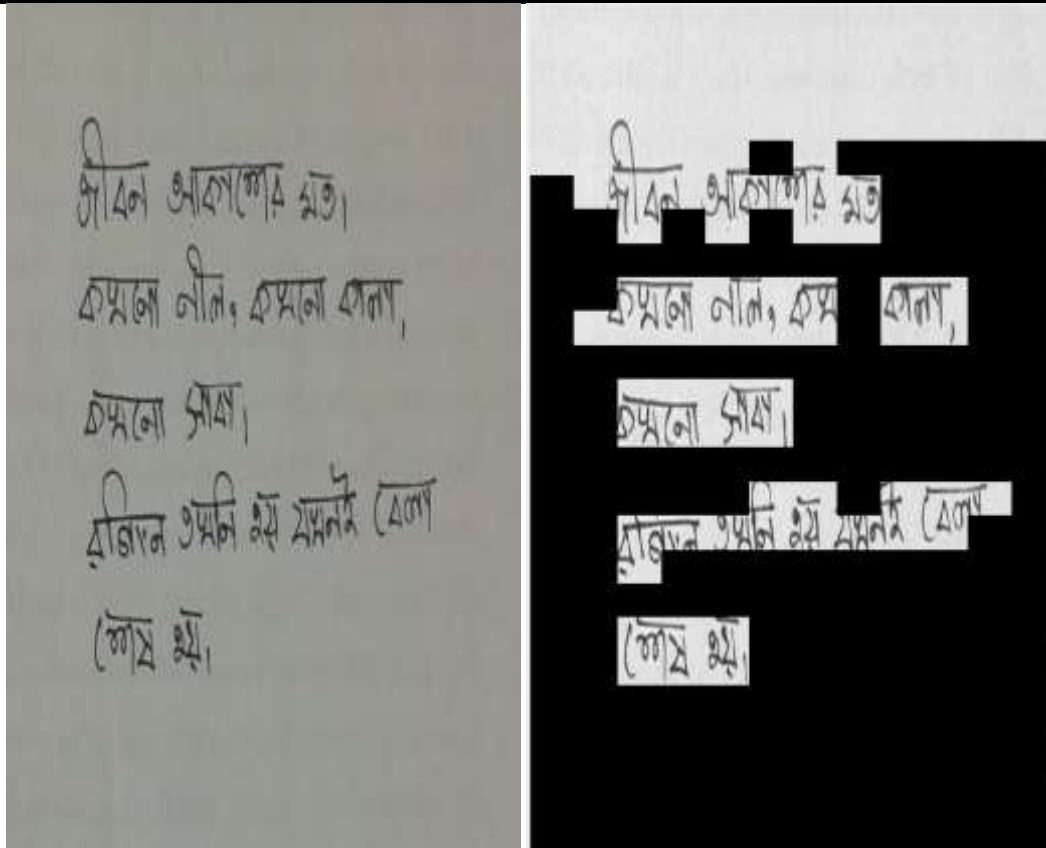


Fig.10: Non- English text images-Assamese language (Original image, Detection of text image)

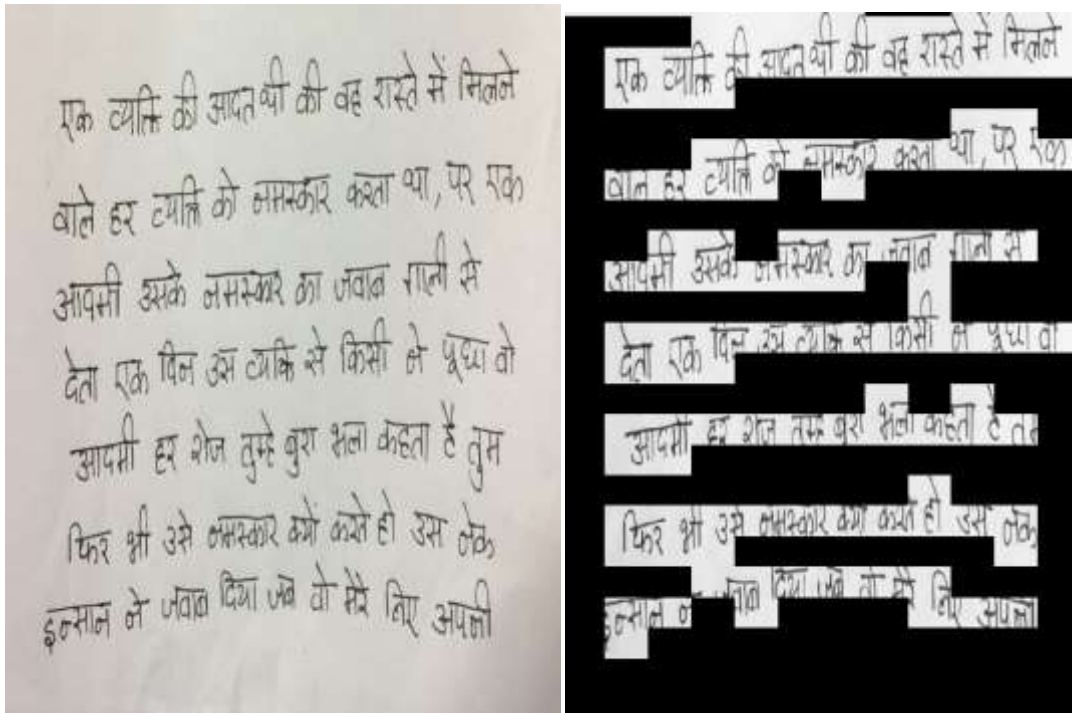


Fig.11: Non- English text images-Hindi language (Original image, Detection of text image)

VI. CONCLUSION AND FUTURE SCOPE

In this approach, we saw that via corner points on document images of any quality, orientation or handwritten, it could be very simple to obtain an accurate text extraction at low cost and without using a lot about parameters. To extract text from images we use a very simple approach based on FAST algorithm. Firstly, we divided the image into blocks and their density in each block was checked. The denser blocks were labeled as text blocks and the less dense were the image region or noise. Then we check the connectivity of the blocks to group the blocks so that the text part can be isolated from the image.

This method is very fast, less complex and versatile, it can be used to detect various languages, handwriting and even images with a lot of noise and blur. Even though it is a very simple program the precision of this method is closer or higher than 80%. Results show that with this simple method, precision is over 80% (most often around 85% in average). But, this technique fails for big fonts and for some specific pictures for which corners are responding too much. Despite of these problems it is fast (and can be parallelized) and less complex as compared to other OCR tools and could be further improved in the future. Finally, this method seems also to be very efficient in extracting more complex layouts such as paragraphs, and lines.

Future Scope:

Font Independent OCR:

Development of OCR considering the multiple font style needs to be developed in the future. The corner point approach is very much useful for the font independent OCR, because, for font or character size, it finds the block and the blocks are analyzed to recognize the character.

OCR for all Indian Languages:

Development of OCR for languages other than English needs to be researched on and developed in the future. The corner point approach is very much useful for the OCR of languages other than English, because, for font or character size, it finds the block and the blocks are analyzed to recognize the character. This further proves to be an efficient way to detect handwritten languages.

Cursive Characters OCR:

There is heavy demand for an OCR system which recognizes handwritten cursive scripts. This avoids keyboard typing and font coding for the image. This method helps in detecting handwritten characters with a precision of about 90%.

Language Converter through OCR:

Once we detect languages we can develop a converter to convert sentences from one language to another through a conversion and translation scheme.

Speech recognition from OCR:

Speech recognition is one of the most important application today. The recognized Printed or Handwritten OCR could be recorded and speech output could be generated. This would help the blind to send and receive information.

Speech to text converter through OCR:

Speech recognition is one of the most important application today. The recognized speech could be recorded and output of text could be generated.

REFERENCES

- [1] Suruchi G. Dedgaonkar, Anjali A. Chandavale, Ashok M. Sapkal, "Survey of Methods for Character Recognition", *International Journal of Engineering and Innovative Technology (IJEIT)*, Volume 1, Issue 5, May 2012, ISSN: 2277-3754.
- [2] Shalin A. Chopra, Amit A. Ghadge, Onkar A. Padwal, Karan S. Punjabi, Prof. Gandhali S. Gurjar, "Optical Character Recognition", *International Journal of Advanced Research in Computer and Communication Engineering*, Vol. 3, Issue 1, January 2014, pp. 4956-4958, ISSN (Online) : 2278-1021, ISSN (Print): 2319-5940.
- [3] Sarika Pansare, Dhanshree Joshi, "A Survey on Optical Character Recognition Techniques", *International Journal of Science and Research (IJSR)*, Volume 3 Issue 12, December 2014, pp. 1247-1249, ISSN (Online): 2319-7064.
- [4] Sukhpreet Singh, "Optical Character Recognition Techniques: A Survey", *Journal of Emerging Trends in Computing and Information Sciences*, Vol. 4, No. 6 June 2013, pp. 545-550, ISSN 2079-8407.
- [5] Deepika Ghai, Neelu Jain, "Text Extraction from Document Images- A Review", *International Journal of Computer Applications (0975 – 8887)*, Volume 84 – No 3, December 2013, pp. 40- 48.
- [6] Keechul Junga, Kwang In Kim, Anil K. Jain, "Text information extraction in images and video: a survey", *Pattern Recognition*, 37, pp. 977-997, 2004.
- [7] Line Eikvil, "Optical Character Recognition", Norsk Regnesentral, P.B. 114 Blindern, N-0314, December 1993.

- [8] Vikas Yadav, Nicolas Ragot," TEXT EXTRACTION IN DOCUMENT IMAGES: HIGHLIGHT ON USING CORNER POINTS", in *2016 12th IAPR Workshop on Document Analysis Systems*, pp. 281-286.
- [9] Viswanathan, Deepak Geetha. "Features from Accelerated Segment Test (FAST)." (2009), pp. 1-5.
- [10] Nauman Saleem, Hassam Muazzam, H.M.Tahir , Umar Farooq ,," AUTOMATIC LICENSE PLATE RECOGNITION USING EXTRACTED FEATURES" in *4th International Symposium on Computational and Business Intelligence*,September 5-7, 2016, Olten, Switzerland, pp. 221-225.
- [11] Mr. Rohit Verma, Dr. Jahid Ali," A Comparative Study of Various Types of Image Noise and Efficient Noise Removal Techniques", *International Journal of Advanced Research in Computer Science and Software Engineering*, Volume 3, Issue 10, October 2013, ISSN: 2277 128X,pp. 617-622.
- [12] Yao Wang," Image Filtering: Noise Removal, Sharpening, Deblurring", *EE 3414 Multimedia Communication Systems*, Polytechnic University, Brooklyn, NY11201.,
- [13] Ajay Kumar Boyat and Brijendra Kumar Joshi," A Review Paper: Noise Models In Digital Image Processing", *Signal & Image Processing : An International Journal (SIPIJ)* , Vol.6, No.2, April 2015, pp. 63- 75.
- [14] Q. Yuan, C. L. Tan," Text Extraction from Gray Scale Document Images Using Edge Information" , Washington, Sept. 10-13 (2001) , pp. 302-306.
- [15] http://www.imageprocessingplace.com/downloads_V3/root_downloads/tutorials/contour_tracing_Abeer_George_Ghuneim/connectivity.html

Analysis of Simply Supported Rectangular Kirchhoff Plates by the Finite Fourier Sine Transform Method

Mama B.O., Nwoji C.U., Ike C. C.*, Onah H.N.

Lecturer, Dept of Civil Engineering, University of Nigeria, Nsukka

Abstract—In this work, the boundary value problem of simply supported rectangular Kirchhoff plates subjected to applied transverse loads is solved by the method of finite Fourier sine transform. The finite Fourier sine transform method was adopted as the analytical research tool due to the Dirichlet boundary conditions of the plate problem. Application of the finite Fourier sine transform to the fourth order governing partial differential equation of the Kirchhoff plate problem and the associated boundary conditions simplified the problem to an algebraic problem in the transform domain. The solution is obtained in the plate domain by inversion. The problem was solved for general distributed load $p(x, y)$, point load applied at an arbitrary point on the plate, uniformly distributed patch load over the plate region $x_0 \leq x \leq x_1$, $y_0 \leq y \leq y_1$, and uniformly distributed load over the entire plate. The finite Fourier sine transform solutions obtained in each case were found to be identical solutions obtained with the Navier's double trigonometrical series method as presented in Timoshenko and Woinowsky-Krieger. The finite Fourier sine transform method was found to yield exact solutions to the classical thin plate flexure problem for simply supported edges.

Keywords— Finite Fourier sine transform method, Kirchhoff plate, Dirichlet boundary conditions, distributed transverse load, patch load, point load, Navier's double trigonometric series method.

I. INTRODUCTION

Plates are three dimensional structural members with extensive applications in civil, mechanical, aeronautical, naval and geotechnical engineering used to carry external loads by the development of bending resistance about the two axes of the plate [1, 2, 3].

The term plate theory denotes an approximate theory used to determine the stress fields and deformation field in elastic bodies one dimension of which (the plate thickness, h) is small compared with the other dimensions (the width and length of a rectangular plate supported at the edges or the diameter of a circular plate) [4]. The approximations consist of the introduction of certain simplifying assumptions into the governing kinematic, stress strain and equilibrium

equations of the mathematical theory of elasticity [3, 4, 5]. These simplifications yield results which do not differ significantly from those obtained from the exact equations for the range of definition of the problem. The simplifications used in various plate theories derive from the definition of a plate as a three dimensional structure with one small dimension; and also from the consequences of Bernoulli-Navier's hypothesis for beams when extended to plates.

In the classical Kirchhoff -Love's plate theory, the influence of transverse shear strains is assumed to be negligible, and a simultaneous consideration of kinematics, stress-strain law and the differential equation of equilibrium for an infinitesimal plate element results in a fourth order partial differential equation as the governing equation of equilibrium [7]. Consequently, the number of boundary conditions appurtenant to the support conditions appears to be in disagreement with the order of the governing partial differential equation [3, 8]. This limits the validity of the expressions for the shearing forces to the open region of the plate middle surface and introduces Kirchhoff's shearing forces for the boundary of the plate. Three actual boundary conditions at each edge of the plate have to be replaced by two approximate conditions transformed in the Kirchhoff sense [2, 4].

Despite the shortcomings of the classical Kirchhoff-Love plate theory, it is well documented that for the majority of engineering applications, the theory gives sufficiently accurate results. The limitations and imperfections of the classical Kirchhoff-Love plate theory have led to the development of other plate theories. Some of these are Reissner plate theory [9, 10]; Mindlin plate theory [11], Henky refined plate theory [12, 13], Shimpi refined plate theory [14], Higher Order Plate Deformation theory [2], Third Order plate theory [15], Leung's Plate theory and Osadebe plate model [16]. Modified plate theories have also been used in plate bending analysis [17].

The plate problem in general is a boundary value problem which is a system of differential equations to be satisfied in the plate domain and the associated boundary conditions to be satisfied at the plate boundaries [18]. The plate problem

has been solved successfully in the technical literature using two basic approaches – classical methods – Navier’s double trigonometric series and Levy’s single trigonometric series methods, and Numerical or Approximate Methods – Finite Difference Method [17], Finite Element Method, Boundary Integral Method, Variational Methods [20, 21] (Ritz Variational method [22], Galerkin Variational Method), Integral transform methods (Laplace transforms, Fourier transforms and Hankel transforms) [23] and Perturbation methods. In this work, the finite Fourier sine transform method is applied to solve the boundary value problem of simply supported rectangular Kirchhoff plates under given transverse loads.

II. METHODOLOGY

The finite transforms follow from the theory of Fourier series [24, 25]

The finite sine transform S_n of a function of $x, f(x)$ is defined as

$$S_n = S(f(x)) = \frac{2}{l} \int_0^l f(x) \sin \frac{n\pi x}{l} dx ; \quad (1)$$

$$m = 1, 2, 3 \dots, \quad n = 1, 2, 3 \dots$$

where $0 \leq x \leq l$, $S_n = S(f(x))$ is the finite Fourier sine transform of $f(x)$

with its inverse sine transform as

$$S^{-1}(S_n) = f(x) = \sum_{n=1}^{\infty} S_n \sin \frac{n\pi x}{l} \quad (2)$$

where S^{-1} is the inverse finite sine transform

The finite sine transform is commonly used with Dirichlet boundary conditions, that specify the value of $f(x)$ at the domain boundaries; $x = 0$, and $x = l$.

The Finite cosine transform C_n of a function of $x, f(x)$, normally used with Neuman boundary conditions that specify the value of $\frac{\partial f}{\partial x}$ at the domain boundaries, $x = 0$, and $x = l$ is defined as

$$C_n = C(f(x)) = \frac{2}{l} \int_0^l f(x) \cos \frac{n\pi x}{l} dx , \quad (3)$$

$$n = 1, 2, 3 \dots$$

The inverse cosine transform, denoted by C^{-1} , is defined by:

$$C^{-1}(C_n) = f(x) = \frac{C_0}{2} + \sum_{n=1}^{\infty} C_n \cos \frac{n\pi x}{l} \quad (4)$$

These transforms reduce a partial differential equation PDE to an ordinary differential equation ODE.

If $f(x, y)$ is a function of two independent variables x and y , defined in a given region $0 \leq x \leq a$, $0 \leq y \leq b$, its double finite Fourier sine transform $F_s(f(x, y))$ is defined by [26, 27]

$$F_s(f(x, y)) = F(m, n) = \int_0^a \int_0^b f(x, y) \sin \frac{m\pi x}{a} \sin \frac{n\pi y}{b} dx dy \quad \dots(5)$$

The inverse double finite Fourier sine transform is given by the double series:

$$F_s^{-1}(f(m, n)) = f(x, y) = \frac{4}{ab} \sum_m^{\infty} \sum_n^{\infty} F(m, n) \sin \left(\frac{m\pi x}{a} \right) \sin \frac{n\pi y}{b}, \quad m, n = 1, 2, 3 \quad \dots(6)$$

where $F_s^{-1}(f(m, n))$ is the inverse double finite Fourier sine transform of $(f(m, n))$

III. APPLICATION OF THE FINITE FOURIER SINE TRANSFORM METHOD

The governing partial differential equation to be solved is given by Kirchhoff plate equation:

$$\frac{\partial^4 w}{\partial x^4} + 2 \frac{\partial^4 w}{\partial x^2 \partial y^2} + \frac{\partial^4 w}{\partial y^4} = \frac{p(x, y)}{D} \quad (7)$$

where $p(x, y)$ is the transverse distributed load acting on the plate, D is the flexural rigidity of the plate material,

$$D = \frac{Eh^3}{12(1-\mu^2)}, E = \text{Young's modulus of elasticity, } h = \text{plate thickness, } \mu \text{ is the Poisson's ratio, and } w(x, y) \text{ is the transverse deflection of plate, } x \text{ and } y \text{ are the space variables in the plane of the plate, and } 0 \leq x \leq a, 0 \leq y \leq b.$$

The boundary conditions for simple supports at the plate edges: $x = 0, a$; $y = 0, b$ are $w = 0$ on $x = 0, a, y = 0, b$, $w_{xx} = 0$ on $x = 0, a$, $w_{yy} = 0$ on $y = 0, b$

where $w_{xx} = \frac{\partial^2 w}{\partial x^2}$, and $w_{yy} = \frac{\partial^2 w}{\partial y^2}$

Transverse Distributed load $p(x, y)$

For distributed transverse load $p(x, y)$, taking the finite Fourier Sine transforms of both sides of Equation (7), we have Equation (8)

$$\int_0^a \int_0^b \left(\frac{\partial^4 w}{\partial x^4} + 2 \frac{\partial^4 w}{\partial x^2 \partial y^2} + \frac{\partial^4 w}{\partial y^4} \right) \sin \alpha_m x \sin \beta_n y dx dy = \frac{1}{D} \int_0^a \int_0^b p(x, y) \sin \alpha_m x \sin \beta_n y dx dy \quad (8)$$

$$\text{where } \alpha_m = \frac{m\pi}{a}, \quad \beta_n = \frac{n\pi}{b}$$

Using the linearity property of the finite Fourier Sine transform, and noting the finite Fourier Sine transform of

$$\frac{\partial^4 w}{\partial x^4} \text{ given by Equation (9)}$$

$$\int_0^a \int_0^b \frac{\partial^4 w}{\partial x^4} \sin \alpha_m x \sin \beta_n y \, dx dy$$

$$= -\alpha_m \int_0^b [(-1)^m w_{xx}|_{x=a} - w_{xx}|_{x=0}] \sin \beta_n y \, dy$$

$$+ \alpha_m^4 \int_0^a \int_0^b w(x, y) \sin \alpha_m x \sin \beta_n y \, dx dy$$

$$= \alpha_m^4 w(m, n) \quad \dots(9)$$

since $w_{xx}|_{x=a} = w_{xx}|_{x=0} = 0$
 where

$$w(m, n) = \int_0^a \int_0^b w(x, y) \sin \alpha_m x \sin \beta_n y \, dx dy \quad (10)$$

$w(m, n)$ = finite Fourier Sine transform of the transverse deflection function $w(x, y)$, we have Equation (11):

$$\int_0^a \int_0^b (\alpha_m^4 + 2\alpha_m^2 \beta_n^2 + \beta_n^4) w(x, y) \sin \alpha_m x \sin \beta_n y \, dx dy$$

$$= \frac{1}{D} \int_0^a \int_0^b p(x, y) \sin \alpha_m x \sin \beta_n y \, dx dy \quad (11)$$

$$(\alpha_m^2 + \beta_n^2)^2 \int_0^a \int_0^b w(x, y) \sin \alpha_m x \sin \beta_n y \, dx dy$$

$$= \frac{1}{D} \int_0^a \int_0^b p(x, y) \sin \alpha_m x \sin \beta_n y \, dx dy \quad (12)$$

$$(\alpha_m^2 + \beta_n^2)^2 w_{mn} = \frac{P_{mn}}{D} \quad (13)$$

where p_{mn} is the finite Fourier Sine transform of the transverse distributed load

Hence,

$$w_{mn} = \frac{P_{mn}}{D(\alpha_m^2 + \beta_n^2)^2} \quad (14)$$

By inversion,

$$w(x, y) = \frac{4}{Dab} \sum_{m=1}^{\infty} \sum_{n=1}^{\infty} w_{mn} \sin \alpha_m x \sin \beta_n y \quad (15)$$

$$w(x, y) = \frac{4}{abD} \sum_{m=1}^{\infty} \sum_{n=1}^{\infty} \frac{P_{mn} \sin \alpha_m x \sin \beta_n y}{(\alpha_m^2 + \beta_n^2)^2} \quad (16)$$

$$= \frac{4}{abD} \sum_m \sum_n \frac{P_{mn} \sin \frac{m\pi x}{a} \sin \frac{n\pi y}{b}}{\left(\left(\frac{m\pi}{a} \right)^2 + \left(\frac{n\pi}{b} \right)^2 \right)^2} \quad (17)$$

$$= \frac{4}{\pi^4 abD} \sum_m \sum_n \frac{P_{mn} \sin \frac{m\pi x}{a} \sin \frac{n\pi y}{b}}{\left(\frac{m^2}{a^2} + \frac{n^2}{b^2} \right)^2} \quad (18)$$

This satisfies the boundary conditions

Case of concentrated load $p(x, y) = P_0$ at $x = \xi, y = \eta$ inside the plate domain

The load $p(x, y)$ is represented using Dirac delta functions as
 $p(x, y) = P_0 \delta(x - \xi) \delta(y - \eta)$ (19)

where P_0 is a constant and $\delta(x - \xi) \delta(y - \eta)$ are the Dirac delta functions, ξ and η are the coordinates of application of point load on the plate.

then, $0 \leq \xi \leq a; 0 \leq \eta \leq b$

$$\int_0^a \int_0^b \nabla^4 w(x, y) \sin \alpha_m x \sin \beta_n y \, dx dy$$

$$= \frac{1}{D} \int_0^a \int_0^b P_0 \delta(x - \xi) \delta(y - \eta) \sin \alpha_m x \sin \beta_n y \, dx dy \quad (20)$$

$$(\alpha_m^4 + 2\alpha_m^2 \beta_n^2 + \beta_n^4) w_{mn} = \frac{P_0}{D} \sin \frac{m\pi \xi}{a} \sin \frac{n\pi \eta}{b} \quad (21)$$

$$w_{mn} = \frac{\frac{P_0}{D} \sin \frac{m\pi \xi}{a} \sin \frac{n\pi \eta}{b}}{\left[\left(\frac{m\pi}{a} \right)^2 + \left(\frac{n\pi}{b} \right)^2 \right]^2} \quad (22)$$

$$= \frac{P_0}{D\pi^4} \frac{\sin \frac{m\pi \xi}{a} \sin \frac{n\pi \eta}{b}}{\left(\frac{m^2}{a^2} + \frac{n^2}{b^2} \right)^2} \quad (23)$$

By inversion,

$$w(x, y) = \frac{4}{ab} \sum_m \sum_n w_{mn} \sin \alpha_m x \sin \beta_n y, \quad (24)$$

$m, n = 1, 2, 3, 4 \dots$

$$= \frac{4}{ab} \sum_m \sum_n \frac{P_0}{D\pi^4} \frac{\sin \frac{m\pi \xi}{a} \sin \frac{n\pi \eta}{b} \sin \frac{m\pi x}{a} \sin \frac{n\pi y}{b}}{\left(\frac{m^2}{a^2} + \frac{n^2}{b^2} \right)^2} \quad \dots(25)$$

$$= \frac{4P_0}{Dab\pi^4} \sum_m \sum_n \frac{\sin \frac{m\pi\xi}{a} \sin \frac{n\pi\eta}{b} \sin \frac{m\pi x}{a} \sin \frac{n\pi y}{b}}{\left(\frac{m^2}{a^2} + \frac{n^2}{b^2}\right)^2} \dots(26)$$

$$w(x, y) = P_0 K(x, y, \xi, \eta) \quad (27)$$

K = Kernel or Green function. This, satisfies the boundary conditions.

The bending moments are found from the bending moment displacement relations.

For point load P at the centre of the plate, $x = \xi = a/2$, $y = \eta = b/2$ the deflection, and loading moment value become

$$w\left(x = \frac{a}{2}, y = \frac{b}{2}\right) = \frac{4P_0}{D\pi^4 ab} \sum_m \sum_n \frac{\sin^2 \frac{m\pi}{2} \sin^2 \frac{n\pi}{2}}{\left(\frac{m^2}{a^2} + \frac{n^2}{b^2}\right)^2} \dots(28)$$

$$m = 1, 3, 5 \dots \quad n = 1, 3, 5 \dots$$

$$M_{xx} = \frac{4P\alpha}{\pi^2} \sum_m \sum_n \frac{(-1)^{m+n-2} (m^2 \alpha^2 + 0.3n^2)}{(m^2 \alpha^2 + n^2)^2} \quad (29)$$

$$M_{yy} = \frac{4P\alpha}{\pi^2} \sum_m \sum_n \frac{(-1)^{m+n-2} (n^2 + 0.3m^2 \alpha^2)}{(m^2 \alpha^2 + n^2)^2} \quad (30)$$

Uniformly distributed patch load over the plate region

$$x_0 \leq x \leq x_1 \quad y_0 \leq y \leq y_1$$

The plate deflection due to a uniformly distributed patch load over the region $x_0 \leq x \leq x_1$, $y_0 \leq y \leq y_1$ is found by integration of the point load solution; as

$$w(x, y) = \frac{4}{Dab\pi^4} \sum_m \sum_n \int_{y_0}^{y_1} \int_{x_0}^{x_1} \frac{p(\xi, \eta) \sin \frac{m\pi\xi}{a} \sin \frac{n\pi\eta}{b} \sin \frac{m\pi x}{a} \sin \frac{n\pi y}{b} d\xi d\eta}{\left(\frac{m^2}{a^2} + \frac{n^2}{b^2}\right)^2} \dots(31)$$

$$= \frac{16P_0}{\pi^6 D} \sum_m \sum_n \frac{S_{mn} \sin \frac{m\pi x}{a} \sin \frac{n\pi y}{b}}{mn \left(\frac{m^2}{a^2} + \frac{n^2}{b^2}\right)^2} \quad (32)$$

$$S_{mn} = \sin \frac{m\pi\xi}{a} \sin \frac{m\pi u}{2a} \sin \frac{n\pi\eta}{b} \sin \frac{n\pi v}{2b} \quad (33)$$

where, $u = (x_0 - x_1)$, $v = (y_1 - y_0)$

From the bending moment displacement equations,

$$M_{xx} = \frac{16p_0}{\pi^4} \sum_m \sum_n \frac{S_{mn} \left(\frac{m^2}{a^2} + \mu \frac{n^2}{b^2}\right) \sin \frac{m\pi x}{a} \sin \frac{n\pi y}{b}}{mn \left(\frac{m^2}{a^2} + \frac{n^2}{b^2}\right)^2} \dots(34)$$

$$M_{yy} = \frac{16p_0}{\pi^4} \sum_m \sum_n \frac{S_{mn} \left(\frac{n^2}{b^2} + \mu \frac{m^2}{a^2}\right) \sin \frac{m\pi x}{a} \sin \frac{n\pi y}{b}}{mn \left(\frac{m^2}{a^2} + \frac{n^2}{b^2}\right)^2} \dots(35)$$

Uniformly Distributed load p_0 over the entire plate

The plate deflection for uniformly distributed load p_0 on the entire plate domain is found by integrating the point load solution over the entire plate are as:

$$w(x, y) = \frac{4}{Dab\pi^4} \sum_m \sum_n \int_0^b \int_0^a \frac{p_0 \sin \frac{m\pi\xi}{a} \sin \frac{n\pi\eta}{b} \sin \frac{m\pi x}{a} \sin \frac{n\pi y}{b} d\xi d\eta}{\left(\frac{m^2}{a^2} + \frac{n^2}{b^2}\right)^2} \quad (36)$$

$$= \frac{16p_0}{D\pi^6} \sum_m \sum_n \frac{\sin \left(\frac{m\pi x}{a}\right) \sin \left(\frac{n\pi y}{b}\right)}{mn \left(\frac{m^2}{a^2} + \frac{n^2}{b^2}\right)^2} \quad (37)$$

$$m = 1, 3, 5 \dots \quad n = 1, 3, 5 \dots$$

From the bending moment-displacement equations, the bending moment distributions become

$$M_{xx} = \frac{16p_0}{D\pi^4} \sum_m \sum_n \frac{\left(\frac{m^2}{a^2} + \mu \frac{n^2}{b^2}\right) \sin \frac{m\pi x}{a} \sin \frac{n\pi y}{b}}{mn \left(\frac{m^2}{a^2} + \frac{n^2}{b^2}\right)^2} \dots(38)$$

$$M_{yy} = \frac{16p_0}{D\pi^4} \sum_m \sum_n \frac{\left(\frac{n^2}{b^2} + \mu \frac{m^2}{a^2}\right) \sin \frac{m\pi x}{a} \sin \frac{n\pi y}{b}}{mn \left(\frac{m^2}{a^2} + \frac{n^2}{b^2}\right)^2} \dots(39)$$

$$m, n = 1, 3, 5, 7 \dots$$

IV. RESULTS AND DISCUSSIONS

The Finite Sine transform method has been applied to the boundary value problem of simply supported rectangular Kirchhoff plates under general distributed load $p(x, y)$, point

load P at (ξ, η) uniformly distributed patch load over a given area of the plate and uniformly distributed load over the entire plate. The deflection functions computed are shown in each case as Equations(18), (26), (32) and (37). The deflection functions were found to be identical with the Navier’s double trigonometric series solution for the deflection in each case. The double series of infinite terms obtained for the deflection $w(x, y)$ for point loads is a rapidly convergent series and the deflection at any point can be obtained with good accuracy by considering only the first few terms. For point load applied at the plate centre, the deflection was observed to be symmetrical about the plate axes of symmetry, and maximum deflection was found to occur at the plate centre. The series solutions obtained for both $w(x, y)$, M_x and M_y (for point load) were found to diverge at the point of application of the point load.

Variation of maximum deflection at the plate centre, with the plate aspect ratio are tabulated in Table 3

For the case of uniformly distributed load on the entire plate, the displacement was found to be identical to the corresponding Navier’s double trigonometric series solution. The deflection was found to be a double series of infinite terms, symmetrical about the two axes of symmetry of the plate. Bending moment functions found from the moment displacement relations were similarly found to be doubly symmetrical about the plate axes. Maximum values of deflection and bending moments for various b/a values were found to occur at the plate centre and are tabulated as shown in Table 1. The convergence characteristics of the series of w , M_{xx} , M_{yy} are shown in Table 2, which shows the deflections converge faster than the bending moments.

Table.1: Deflection and Bending Moment coefficients for Simply Supported Rectangular Kirchhoff Plates under uniformly distributed loads

b/a	$w_{\max} = F \frac{pa^4}{D}$ Timoshenko and Woinowsky-Krieger	Present study (deflection coefficient)	$M_{xx \max}$ Timoshenko and Woinowsky-Krieger	$M_{xx \max}$ Present study (moment coefficient)	$M_{yy \max}$ Timoshenko and Woinowsky-Krieger	$M_{yy \max}$ Present study
1.0	4.06×10^{-3}	4.062×10^{-3}	0.0479	0.047886	0.0479	0.047886
1.1	4.85×10^{-3}	4.85×10^{-3}	0.0554	0.0554	0.0493	0.0493
1.2	5.64×10^{-3}	5.64×10^{-3}	0.0627	0.0627	0.0501	0.0501
1.3	6.83×10^{-3}	6.83×10^{-3}	0.0694	0.0694	0.0503	0.0503
1.4	7.05×10^{-3}	7.05×10^{-3}	0.0755	0.0755	0.0502	0.0502
1.5	7.72×10^{-3}	7.724×10^{-3}	0.0812	0.08116	0.0498	0.049843
1.6	8.30×10^{-3}	8.30×10^{-3}	0.0862	0.0862	0.0492	0.0492
1.7	8.83×10^{-3}	8.83×10^{-3}	0.0908	0.0908	0.0486	0.0486
1.8	9.31×10^{-3}	9.31×10^{-3}	0.0948	0.0948	0.0479	0.0479
1.9	9.74×10^{-3}	9.74×10^{-3}	0.0985	0.0985	0.0471	0.0471
2	10.13×10^{-3}	10.12866×10^{-3}	0.1017	0.101683	0.0464	0.046350
3	12.23×10^{-3}	12.2328×10^{-3}	0.1189	0.118861	0.0406	0.0406266
4	12.82×10^{-3}	12.81865×10^{-3}	0.1235	0.12346	0.0384	0.038415
5	12.97×10^{-3}	12.97×10^{-3}	0.1246	0.124625	0.0375	0.03745
∞	13.02×10^{-3}	13.0208×10^{-3}	0.1250	0.1250	0.0375	0.0375

Table.2: Convergence study for Deflection and Bending moments at the center of simply supported square Kirchhoff plates under uniform load

No of terms	w_{\max} $\frac{pa^4}{D} \times 10^{-2}$	$M_{xx \max}$ $pa^2 \times 10^{-2}$	$M_{yy \max}$ $pa^2 \times 10^{-2}$
1	0.416	5.34	5.34
2	0.405	4.69	4.69
3	0.406	4.86	4.94
4	0.406	4.81	4.90
Exact	0.406	4.79	4.79

Table.3: Simply supported rectangular Kirchhoff plates under point load at the center

b/a	w_{max}	
	Timoshenko and Woinowsky-Krieger	Present study
1.0	0.01160	0.01160
1.2	0.01353	0.01353
1.4	0.01464	0.01464
1.6	0.01570	0.01570
1.8	0.01620	0.01620
2	0.01651	0.01651

V. CONCLUSIONS

The double finite Fourier sine transform method has been used to derive analytic flexural solutions of simply supported rectangular Kirchhoff plates under general distributed load, point load at ξ, η , uniform patch load and uniform load on the entire plate. The analysis is performed without any assumption of the displacement trial (shape) function which illustrates the advantage of the method. The method is an efficient and accurate analytical tool for Kirchhoff plate bending analysis and can be extended to other boundary value problems of plates such as buckling and vibration.

REFERENCES

- [1] Reddy, J.N. (1999): Theory and Analysis of Elastic Plates. Taylor and Francis London.
- [2] Chandrashekhara K. (2011) Theory of Plates. University Press (India) Limited Hyderabad.
- [3] Szilard, (2004): Theories and Applications of Plate Analysis Classical, Numerical and Engineering Methods. John Wiley and sons Inc.
- [4] Panc, V. (1975): Theories of Elastic Plates. Noordhoff International Publishing, Leyden, the Netherlands.
- [5] Ventsel and Krauthammer (2001) Thin Plates and Shells Theory, Analysis and Applications. Marcel Dekker Inc New York, USA.
- [6] Kapadiya H.N. and Patel A.D. (2015): Review of Bending Solutions of Thin Plates. International Journal of Scientific Research and Development (IJSRD) Vol. 3 Issue 03, 2015, ISSN 2321-0613, pp 1709-1712.
- [7] Osadebe N.N., Ike C.C., Onah H., Nwoji C.U. and Okafor F.O. (2016). Application of Galerkin-Vlasov Method to the Flexural Analysis of Simply Supported Rectangular Kirchhoff Plates under Uniform Loads. Nigerian Journal of Technology NIJOTECH Vol. 35, No 4, October, 2016 pp. 732-738.
- [8] Timoshenko S. and Woinowsky-Krieger S (1999) Theory of Plates and Shells. Mc Graw Hill Book Co. Singapore.
- [9] Reissner, E. (1945): The Effect of Transverse Shear Deformation on the Bending of Elastic Plates. Journal of Applied Mechanics, 12.
- [10] Reissner, E. (1947): On Bending of Elastic plates. Quart. Appl. Math; 5.
- [11] Mindlin, R.D (1951): Influence of Rotary Inertia and Shear on Flexural Motions of Isotropic Elastic Plates. J. Appl. Mech Vol 18 No 1, pp.31-38.
- [12] Hencky, H. (1913): Der Spannungszustand in rechteckigen Platten R. Oldenbourg, München u Berlin.
- [13] Hencky, H. (1947): Über die Berücksichtigung der Schubverzerrungen in ebenen Platten Ing Arch 16.
- [14] Shimpi, R.P. (2002): Refined Plate Theory and its Variants. AIAA Journal vol 40, No 1 January, 2002.
- [15] Reddy, J.N. (1984): A Simply Higher Order Theory for Laminated Composite Plates. ASME Journal of Applied Mechanics, Vol 51, pp. 745-752.
- [16] Osadebe, N.N. (1997): Differential Equations for Small Deflection Analysis of Thin Elastic Plates Possessing Extensible Middle Surface. University of Nigeria Virtual Library.
- [17] Suetake Y (2006) Plate Bending Analysis by using a Modified Plate Theory. CMES Vol.11 No.3, pp. 103-110, Tech Science Press.
- [18] Sebastian V.K. (1983): An Elastic Solution for Simply Supported Rectangular Plates. Nigerian Journal of Technology (NIJOTECH) Vol. 7, No.1 September, 1983, pp. 11-16.
- [19] Ezeh J.C. Ibearugbulam O.M. and Onyechere C.I. (2013): Pure Bending Analysis of thin Rectangular Flat Plates using Ordinary Finite Difference Method. International Journal of Emerging Technology and Advanced Engineering (IJETA), Volume 3, Issue 3, March 2013, www.ijetae.com, ISSN: 2250-2459.
- [20] Aginam C.H., Chidolue C.A. and Ezeagu C.A. (2012): Application of Direct Variational Method in the Analysis of Isotropic thin Rectangular Plates ARPN Journal of Engineering and Applied Sciences

- Vol. 7, No 9, September 2012. Asian Research Publishing Network (ARPN) ISSN 1819-6608.
- [21] Ibearugbulem O.M., Ettu L.O. and Ezeh J.C. (2013): Direct Integration and Work Principle as New Approach in Bending Analysis of Isotropic Rectangular Plates. *The International Journal of Engineering and Science (IJES)* Volume 2, Issue 3, 2013 pp 28-36, ISSN 2319-1813.
- [22] Balasubramanian Ashwin (2011): Plate Analysis with Different Geometries and Arbitrary Boundary Conditions. MSc Thesis: Mechanical Engineering Faculty of Graduate School, the University of Texas at Arlington, December, 2011.
- [23] Zhong Yang, Zhao Xue-Feng, and Liu Hang (2014): Vibration of plate on foundation with four edges free by finite cosine integral transform method. *Latin American Journal of Solids and Structures*, Vol 11, No 5, Rio de Janeiro, October, 2014.
- [24] Lokenath D. and Bhatta D. (2007): *Integral Transforms and their Applications*, Second Edition. Chapman and Hall/ CRC Taylor and Francis Group LLC New York.
- [25] Brown D. (2002): *Integral Transforms and their Applications*, Third Edition. Texts in Applied Mathematics 41, Springer.
- [26] Antimorov M.Ya, Kalyshkin A. and Vaillanconot Remi (1993): *Applied Integral Transforms* Centre des Recherches Mathematiques, Universite de Montreal Volume 2 CRM Monograph Series. American Mathematical Society Providence, Rhode Island USA.
- [27] Andrews L.C. and Shivamoggi B.K. (1999): *Integral Transforms for Engineers*. University of Central Florida, SPIE Optical Engineering Press, A publication of SPIE, The International Society for Optical Engineering, Bellingham, Washington USA.

Flexural - Torsional Buckling Analysis of Thin Walled Columns Using the Fourier series Method

Onah, H. N.¹, Ike, C.C.^{2*}, Nwoji, C.U.³

^{1,3}Dept of Civil Engineering, University of Nigeria, Nsukka

²Dept of Civil Engineering, Enugu State University of Science & Technology, Enugu

Abstract— In this work, the governing differential equations of elastic column buckling represented by a system of three coupled differential equations in the three unknown displacement functions, $v(x)$, $w(x)$ and $\theta(x)$ are solved using the method of Fourier series. The column was pinned at both ends $x = 0$, $x = l$. The unknown displacements were assumed to be a Fourier sine series of infinite terms, which was found to satisfy apriori the pinned conditions at the ends and substituted into the governing equations. The governing equations were found to reduce to a system of algebraic eigenvalue – eigenvector problem. The buckling equation was found to be a cubic polynomial for the general asymmetric sectioned column. The buckling modes were found as flexural torsional buckling modes. For columns with monosymmetric sections, it was found that the buckling mode could be flexural or flexural – torsional depending on the root of the cubic polynomial buckling equation which is the smallest. For columns with bisymmetric sections, it was found that the buckling modes are uncoupled and bisymmetric columns could fail by pure flexural buckling about the axes of symmetry or pure torsional buckling. The findings are in excellent agreement with Timoshenko’s solutions.

Keywords—Monosymmetric columns, bisymmetric columns, flexural torsional buckling mode, algebraic-eigen vector problem.

$$E(I_{yy}I_{zz} - I_{yz}^2) \frac{d^4 v}{dx^4} - I_{yy}N_x \frac{d^2 v}{dx^2} + I_{yz}N_x \frac{d^2 w}{dx^2} + [I_{yy}M_{ly} + I_{yz}M_{lz} - N_x(e_z I_{yy} + e_y I_{yz})] \frac{d^2 \theta}{dx^2} + (I_{yy}V_z + I_{yz}V_y) \frac{d\theta}{dx} = q_y I_{yy} - q_z I_{yz} \quad (2.1)$$

$$E(I_{yy}I_{zz} - I_{yz}^2) \frac{d^4 w}{dx^4} - I_{zz}N_y \frac{d^2 w}{dx^2} + I_{yz}N_x \frac{d^2 v}{dx^2} + [-I_{zz}M_{lz} - I_{yz}M_{ly} + N_x(e_y I_{zz} + e_z I_{yz})] \frac{d^2 \theta}{dx^2} - (I_{zz}V_y - I_{yz}V_z) \frac{d\theta}{dx} = q_z I_{zz} - q_y I_{yz} \quad (2.2)$$

$$EC_w \frac{d^4 \theta}{dx^4} - \left(GJ + \frac{I_E N_x}{A} + C_z M_{lz} + C_y M_{ly} + \frac{H_w W_w}{C_w} \right) \frac{d^2 \theta}{dx^2} +$$

I. INTRODUCTION/LITERATURE REVIEW

Euler’s [1] work on column flexural buckling presented the first analytical method of determining the buckling strengths of slender columns. St Venant [2] later worked on uniform torsion and presented the first reliable work on the twisting response of structures to torsion. Flexural torsional buckling was studied by Michell [3] and also by Prandtl [4] who considered the lateral buckling of beams of narrow rectangular cross sections.

Prandtl and Michell’s work were extended by Timoshenko [5] to include the effects of warping torsion in T section beams. The works of Wagner [6], Vlasov[7], Timoshenko [8] and Timoshenko [9] led to the development of a general theory of flexural torsional buckling. Other researchers who have studied flexural torsional buckling of structures include Nwakali[10], Timoshenko and Gere [11], Alsayed[12],Trahair[13], Zlatko[14] and Al-Sheikh [15].

II. THEORETICAL FRAMEWORK

The generalized elastic column buckling problem formulated in terms of the displaced configuration is represented by the following set of three linear differential equations obtained when the non linear terms are neglected [16][13].

$$(M_{ly} - e_z N_x) \frac{d^2 v}{dx^2} - (M_{lz} - e_y N_x) \frac{d^2 w}{dx^2} + V_z \frac{dv}{dx} - V_y \frac{dw}{dx} - \left(C_z V_y + C_y V_z + \frac{H_w V_w}{C_w} \right) \frac{d\theta}{dx} = t(x) \quad (2.3)$$

where M_{lz}, M_{ly} = moments caused by transverse loads only.

$I_E = I_{yy} + I_{zz} + (e_y^2 + e_z^2)A$ = polar moment of inertia about the shear centre.

$$H_y = \iint_A z(y^2 + z^2) dA \quad I_{yy} = \int_A z^2 dA$$

$$H_z = \iint_A y(y^2 + z^2) dA \quad I_{zz} = \int_A y^2 dA$$

$$H_w = \iint_A 2(w_0 - w)(y^2 + z^2) dA \quad I_{yz} = \int_A yz dA$$

$$C_y = \frac{I_{zz} H_y - I_{yz} H_z}{I_{yy} I_{zz} - I_{yz}^2} = 2e_z$$

$$C_z = \frac{I_{yy} H_z - I_{yz} H_y}{I_{yy} I_{zz} - I_{yz}^2} = 2e_y$$

J = St Venant torsional stiffness of the section

E = Young's modulus of elasticity

G = shear modulus

I_{yy}, I_{zz} = moments of inertia

C_w = warping constant

I_{yz} = product of inertia

e_y, e_z = coordinates of the shear center

V_y, V_z = shear forces

q_y, q_z = transverse loads

N_x = axial load

$v(x), w(x)$ are transverse displacements

θ_x = twist rotational displacement

x = longitudinal axial coordinate, yz is the plane of the cross section

A = area of the cross section of the column.

The governing equilibrium equations for the generalized column buckling problem is represented by the system of three simultaneous differential equations in the three unknown displacements $v(x)$, $w(x)$ and $\theta(x)$. For columns with prismatic cross-sections, the elasticity properties (GJ and E) as well as the inertial and geometrical properties are constant; but the load coefficients (M_{ly} , M_{lz} , V_y , V_z , W_w , V_w) are variables depending on the axial longitudinal coordinate (x). The system of governing differential equations thus have variable coefficients, rendering them difficult to solve mathematically.

However, simplifications of the system of governing differential equations can be obtained by using special characteristics of different types of column problems. A simplification of the governing equilibrium equations can be obtained if the yz coordinates are principal coordinates. Then $I_{yz} = 0$, and the governing differential equations become [16][13]

$$EI_{zz} \frac{d^4 v}{dx^4} - N_x \frac{d^2 v}{dx^2} + (M_{ly} - N_x e_z) \frac{d^2 \theta}{dx^2} + V_{zy} \frac{d\theta}{dx} = q_y \quad (2.4)$$

$$EI_{yy} \frac{d^4 w}{dx^4} - N_x \frac{d^2 w}{dx^2} + (-M_{lz} + N_x e_y) \frac{d^2 \theta}{dx^2} - V_y \frac{d\theta}{dx} = q_z \quad (2.5)$$

$$EC_w \frac{d^4 w}{dx^4} - \left(GJ + \frac{I_E N_x}{A} + C_z M_{lz} + C_y M_{ly} + \frac{H_w W_w}{C_w} \right) \frac{d^2 \theta}{dx^2} + (M_{ly} - e_z N_x) \frac{d^2 v}{dx^2}$$

$$-(M_{Iz} - e_y N_x) \frac{d^2 w}{dx^2} + V_z \frac{dv}{dx} - V_y \frac{dw}{dx} - \left(C_z V_y + C_y V_z + \frac{H_w V_w}{C_w} \right) \frac{d\theta}{dx} = t(x) \quad (2.6)$$

If the member is free of transverse loads q_y, q_z become zero; and the transverse moments are constant, then the shear forces V_y, V_z are also zero. For member (columns) subjected only to axial compressive load N_x acting through the centroid of the section, the moments due to the transverse loads vanish, the applied torque vanishes; and if the load is applied such that the bimoment vanishes, the system of differential equations become [15][16]

$$EI_{zz} \frac{d^4 v}{dx^4} + N_x \frac{d^2 v}{dx^2} + N_x e_z \frac{d^2 \theta}{dx^2} = 0 \quad (2.7)$$

$$EI_{yy} \frac{d^4 w}{dx^4} + N_x \frac{d^2 w}{dx^2} - N_x e_y \frac{d^2 \theta}{dx^2} = 0 \quad (2.8)$$

$$EC_w \frac{d^4 \theta}{dx^4} - \left(GJ - \frac{I_E N_x}{A} \right) \frac{d^2 \theta}{dx^2} + N_x e_z \frac{d^2 v}{dx^2} - N_x e_y \frac{d^2 w}{dx^2} = 0 \quad (2.9)$$

The system of differential Equations (2.7), (2.8) and (2.9) represent the governing equilibrium equations for a particular case of the generalized elastic column buckling problem presented by Equations (2.1), (2.2) and (2.3) when $I_{yz} = 0, q_y = q_z = 0, V_y = \theta_z = 0, M_{Iy} = M_{Iz} = 0, W_w = 0$.

III. APPLICATION OF THE FOURIER SERIES METHOD

We seek to apply the Fourier series method to solve the system of differential Equations (2.7), (2.8) and (2.9) representing the governing-equilibrium equations for the elastic column buckling problem for the case when the ends at $x = 0, x = l$ are on pinned supports.

For pinned ends at $x = 0, x = l$, the relevant boundary conditions are

$$\begin{aligned} v(x=0) &= 0 & v''(x=0) &= 0 \\ w(x=0) &= 0 & w''(x=0) &= 0 \\ \theta(x=0) &= 0 & \theta''(x=0) &= 0 \\ v(x=l) &= 0 & v''(x=l) &= 0 \\ w(x=l) &= w''(x=l) &= 0 \\ \theta(x=l) &= \theta''(x=l) &= 0 \end{aligned} \quad (3.1)$$

Suitable Fourier series representations of the three unknown displacement functions that satisfy a priori the above boundary conditions are given by

$$\begin{aligned} v(x) &= \sum_{m=1}^{\infty} v_m \sin \frac{m\pi x}{l} \\ w(x) &= \sum_{m=1}^{\infty} w_m \sin \frac{m\pi x}{l} \\ \theta(x) &= \sum_{m=1}^{\infty} \theta_m \sin \frac{m\pi x}{l} \end{aligned} \quad (3.2)$$

where v_m, w_m and θ_m are infinite number of unknown coefficients of the Fourier sine series representations of the unknown displacement functions $v(x), w(x)$ and $\theta(x)$ that we seek to determine. If Equation (3.2) represent solutions of the governing Equations (2.7), (2.8) and (2.9), then

$$EI_{zz} \frac{d^4}{dx^4} \left(\sum_{m=1}^{\infty} v_m \sin \frac{m\pi x}{l} \right) + N_x \frac{d^2}{dx^2} \left(\sum_{m=1}^{\infty} v_m \sin \frac{m\pi x}{l} \right) + N_x e_z \frac{d^2}{dx^2} \left(\sum_{m=1}^{\infty} \theta_m \sin \frac{m\pi x}{l} \right) = 0 \quad (3.3)$$

$$EI_{yy} \frac{d^4}{dx^4} \left(\sum_{m=1}^{\infty} w_m \sin \frac{m\pi x}{l} \right) + N_x \frac{d^2}{dx^2} \left(\sum_{m=1}^{\infty} w_m \sin \frac{m\pi x}{l} \right) - N_x e_y \frac{d^2}{dx^2} \left(\sum_{m=1}^{\infty} \theta_m \sin \frac{m\pi x}{l} \right) = 0 \quad (3.4)$$

$$\begin{aligned} EC_w \frac{d^4}{dx^4} \left(\sum_{m=1}^{\infty} \theta_m \sin \frac{m\pi x}{l} \right) - \left(GJ - \frac{I_E N_x}{A} \right) \frac{d^2}{dx^2} \left(\sum_{m=1}^{\infty} \theta_m \sin \frac{m\pi x}{l} \right) \\ + N_x e_z \frac{d^2}{dx^2} \left(\sum_{m=1}^{\infty} v_m \sin \frac{m\pi x}{l} \right) - N_x e_y \frac{d^2}{dx^2} \left(\sum_{m=1}^{\infty} w_m \sin \frac{m\pi x}{l} \right) \end{aligned} \quad (3.5)$$

$$EI_{zz} \sum_{m=1}^{\infty} \left(\frac{m\pi}{l}\right)^4 v_m \sin \frac{m\pi x}{l} - N_x \sum_{m=1}^{\infty} \left(\frac{m\pi}{l}\right)^2 v_m \sin \frac{m\pi x}{l} - N_x e_z \sum_{m=1}^{\infty} \left(\frac{m\pi}{l}\right)^2 v_m \sin \frac{m\pi x}{l} = 0 \quad (3.6)$$

$$EI_{yy} \sum_{m=1}^{\infty} \left(\frac{m\pi}{l}\right)^4 w_m \sin \frac{m\pi x}{l} - N_x \sum_{m=1}^{\infty} \left(\frac{m\pi}{l}\right)^2 w_m \sin \frac{m\pi x}{l} + N_x e_y \sum_{m=1}^{\infty} \left(\frac{m\pi}{l}\right)^2 \theta_m \sin \frac{m\pi x}{l} = 0 \quad (3.7)$$

$$EC_w \sum_{m=1}^{\infty} \left(\frac{m\pi}{l}\right)^4 \theta_m \sin \frac{m\pi x}{l} + \left(GJ - \frac{I_E N_x}{A}\right) \sum_{m=1}^{\infty} \left(\frac{m\pi}{l}\right)^2 \theta_m \sin \frac{m\pi x}{l} - N_x e_z \sum_{m=1}^{\infty} \left(\frac{m\pi}{l}\right)^2 v_m \sin \frac{m\pi x}{l} + N_x e_y \sum_{m=1}^{\infty} \left(\frac{m\pi}{l}\right)^2 w_m \sin \frac{m\pi x}{l} = 0 \quad (3.8)$$

Simplifying,

$$\sum_{m=1}^{\infty} \left\{ \left(EI_{zz} \left(\frac{m\pi}{l}\right)^2 - N_x \right) v_m \sin \frac{m\pi x}{l} - N_x e_z \theta_m \sin \frac{m\pi x}{l} \right\} = 0 \quad (3.9)$$

$$\sum_{m=1}^{\infty} \left\{ \left(EI_{yy} \left(\frac{m\pi}{l}\right)^2 - N_x \right) w_m \sin \frac{m\pi x}{l} + N_x e_y \theta_m \sin \frac{m\pi x}{l} \right\} = 0 \quad (3.10)$$

$$\sum_{m=1}^{\infty} \left\{ \left(EI_w \left(\frac{m\pi}{l}\right)^2 + \left(GJ - \frac{I_E N_x}{A} \right) \right) \theta_m \sin \frac{m\pi x}{l} - N_x e_z v_m \sin \frac{m\pi x}{l} + N_x e_y w_m \sin \frac{m\pi x}{l} \right\} = 0 \quad (3.11)$$

In matrix format, we have

$$\sum_{m=1}^{\infty} \begin{pmatrix} \left(EI_{zz} \left(\frac{m\pi}{l}\right)^2 - N_x \right) & 0 & -N_x e_z \\ 0 & \left(EI_{yy} \left(\frac{m\pi}{l}\right)^2 - N_x \right) & N_x e_y \\ -N_x e_z & N_x e_y & \left(EC_w \left(\frac{m\pi}{l}\right)^2 + \left(GJ - \frac{I_E N_x}{A} \right) \right) \end{pmatrix} \times \begin{pmatrix} v_m \\ w_m \\ \theta_m \end{pmatrix} \sin \frac{m\pi x}{l} = \begin{pmatrix} 0 \\ 0 \\ 0 \end{pmatrix} \quad (3.12)$$

The stability problem represented by the system of differential equations is now reduced to an algebraic eigenvector eigenvalue problem given by the homogeneous Equation (3.12). For non-trivial solutions, the characteristic buckling equation is the determinantal Equation (3.13)

$$\begin{vmatrix} \left(EI_{zz} \left(\frac{m\pi}{l}\right)^2 - N_x \right) & 0 & -N_x e_z \\ 0 & \left(EI_{yy} \left(\frac{m\pi}{l}\right)^2 - N_x \right) & N_x e_y \\ -N_x e_z & N_x e_y & \left(EC_w \left(\frac{m\pi}{l}\right)^2 + GJ - \frac{I_E N_x}{A} \right) \end{vmatrix} = 0 \quad (3.13)$$

Let

$$P_{zz} = EI_{zz} \left(\frac{m\pi}{l}\right)^2$$

$$P_{yy} = EI_{yy} \left(\frac{m\pi}{l}\right)^2$$

$$P_{\phi} = \frac{A}{I_E} \left(EC_w \left(\frac{m\pi}{l} \right)^2 + GJ \right)$$

$$\therefore EC_w \left(\frac{m\pi}{l} \right)^2 + GJ = \frac{P_{\phi} I_E}{A}$$

Hence we have

$$\begin{vmatrix} (P_{zz} - N_x) & 0 & -N_x e_z \\ 0 & (P_{yy} - N_x) & N_x e_y \\ -N_x e_z & N_x e_y & \left(\frac{P_{\phi} I_E}{A} - \frac{I_E N_x}{A} \right) \end{vmatrix} = 0 \quad (3.14)$$

By expansion of the determinant, we have

$$(P_{zz} - N_x) \begin{vmatrix} (P_{yy} - N_x) & N_x e_y \\ N_x e_y & \frac{I_E}{A} (P_{\phi} - N_x) \end{vmatrix} - N_x e_z \begin{vmatrix} 0 & (P_{yy} - N_x) \\ -N_x e_z & N_x e_y \end{vmatrix} = 0 \quad (3.15)$$

$$(P_{zz} - N_x) \left[(P_{yy} - N_x)(P_{\phi} - N_x) \frac{I_E}{A} - (N_x e_y)^2 \right] - N_x e_z (0 + N_x e_z (P_{yy} - N_x)) = 0 \quad (3.16)$$

$$(P_{zz} - N_x)(P_{yy} - N_x)(P_{\phi} - N_x) \frac{I_E}{A} - (N_x e_y)^2 (P_{zz} - N_x) - (N_x e_z)^2 (P_{yy} - N_x) = 0 \quad (3.17)$$

$$(P_{zz} - N_x)(P_{yy} - N_x)(P_{\phi} - N_x) - N_x^2 e_y^2 \frac{A}{I_E} (P_{zz} - N_x) - N_x^2 e_z^2 \frac{A}{I_E} (P_{yy} - N_x) = 0 \quad (3.18)$$

But

$$r_0^2 = e_y^2 + e_z^2 + \left(\frac{I_{xx} + I_{yy}}{A} \right)$$

$$I_E = I_{xx} + I_{yy} + (e_x^2 + e_z^2)A$$

$$\frac{I_E}{A} = \frac{I_{xx} + I_{yy}}{A} + e_y^2 + e_z^2 = r_0^2$$

Hence,

$$(P_{zz} - N_x)(P_{yy} - N_x)(P_{\phi} - N_x) - N_x^2 \frac{e_y^2}{r_0^2} (P_{zz} - N_x) - N_x^2 \frac{e_z^2}{r_0^2} (P_{yy} - N_x) = 0 \quad (3.19)$$

$$(P_{zz} - N_x)(P_{yy} - N_x)(P_{\phi} - N_x) - N_x^2 \frac{e_y^2}{r_0^2} (P_{zz} - N_x) - \frac{N_x^2 e_z^2}{r_0^2} (P_{yy} - N_x) = 0 \quad (3.20)$$

This is the characteristic equation for determining the buckling load of a column with an asymmetric cross-section. The buckling equation is a third order polynomial in N_x . Thus, it can be solved using the methods for solving polynomials to obtain the three roots P_{cr1} , P_{cr2}

and P_{cr3} . The smallest of the three critical buckling loads will govern the buckling behaviour of the column.

However, if the zz axis is the axis of symmetry of the cross-section, $e_y = 0$, and the characteristic buckling equation simplifies to become

$$(P_{zz} - N_x)(P_{yy} - N_x)(P_{\phi} - N_x) - N_x^2 \frac{e_z^2}{r_0^2} (P_{yy} - N_x) = 0 \quad \dots(3.21)$$

or,

$$(P_{yy} - N_x) \left[(P_{zz} - N_x)(P_{\phi} - N_x) - \frac{N_x^2 e_z^2}{r_0^2} \right] = 0 \quad \dots(3.22)$$

Hence, in this case (monosymmetric cross-section), the column can buckle in two possible buckling modes namely pure flexural buckling in the yy – axis, and flexural torsional buckling, otherwise. If P_{yy} is the smallest of the three roots, of Equation (3.22) the monosymmetric section column will buckle in pure Eulerian flexure, otherwise flexural torsional buckling failure will take place.

If the column has two axis of symmetry then $e_y = 0$, $e_z = 0$ and the characteristic buckling equation simplifies to

$$(P_{zz} - N_x)(P_{yy} - N_x)(P_{\phi} - N_x) = 0 \quad (3.23)$$

We find that for bisymmetric columns, the buckling equations become uncoupled and the three roots become P_{zz} , P_{yy} and P_{ϕ} . For bisymmetric columns, the column can buckle in pure Eulerian flexure in the yy or zz axes, or pure torsional buckling mode. The smallest of the three roots governs the buckling mode. Critical values of each buckling mode is obtained in each case when $m = 1$.

IV. DISCUSSIONS AND CONCLUSIONS

The system of governing differential equations of buckling of an elastic column with thin walled sections have been solved for pinned pinned columns using the Fourier series method. In general, the equations were found to be reduced to a system of algebraic eigenvalue eigenvector problem. For the general use of asymmetric columns, the characteristic buckling equation was found to be identical with the Timoshenko's solution for the same problem. The buckling equation for asymmetric columns was found as Equation (3.20). The equation is a cubic polynomial in N_x as the unknown. The solution will yield three values for N_x called the three critical loads as P_{cr1} , P_{cr2} and P_{cr3} . All the buckling modes in this case are flexural – torsional buckling modes. The critical buckling load, which is the lowest of the three loads P_{cr1} , P_{cr2} and P_{cr3} will always be smaller than the Euler critical flexural buckling loads P_{Ezz} , P_{Eyy} and the pure torsional buckling load P_{ϕ} . For columns with asymmetric sections the buckling mode always include all three displacements $v(x)$, $w(x)$ and $\theta(x)$; hence it is a flexural – torsional buckling mode.

For columns with monosymmetric cross-sections, one of the governing differential equations will become uncoupled. This results in two possible modes of buckling failure – pure flexural buckling failure in the yy axes (for columns symmetrical about the zz axes) and flexural torsional buckling. The characteristic buckling equation was found as Equation (3.22). For columns with two axes of symmetry, the governing differential equations of equilibrium become uncoupled. The characteristic buckling equation was found as Equation (3.23). The

buckling equations are uncoupled and the three roots indicate the bisymmetric column can buckle in pure Eulerian flexure in the axes of symmetry or pure torsional buckling mode.

REFERENCES

- [1] Euler, I. (1759): Sur la force des colonnes. Memoires de l'academie des sciences de Berlin 1757 Vol 13, pp. 252 – 282 In Opera Omnia set 2 Vol 17 (1982) pp 89 – 118.
- [2] St Venant, A.J.C.B (1855): Memoire sur la Torsion des Prismes Mem. Divers Savants 14 pp. 233 – 560.
- [3] Michell A.G.M. (1899): Elastic Stability of Long Beams under Transverse Forces. Philos Mag. 48 (5th Series) pp. 298 – 309.
- [4] Prandtl, L. (1899): Kipperscheinungen Dissertation des Universitat Munchen.
- [5] Timoshenko, S.P. (1905): On the stability in pure bending of a T-beam. Bull. Pol. Inst. St Petersburg p4 – 5.
- [6] Wagner, H. (1936): Torsion and Buckling of Open Sections. T.M. No. 807, US National Advisory Committee for Aeronautics.
- [7] Vlasov, V.Z. (1961): Thin Walled Elastic Beams English Translation. National Science Foundation, Washington DC, London, Oldbourne Press.
- [8] Timoshenko, S.P. (1936): Theory of Elastic Stability. McGraw Hill, New York.
- [9] Timoshenko, S.P. (1945): Theory of bending, torsion and buckling of thin walled members of open cross-section. Journal Franklin Institute pp. 559 – 609.
- [10] Nwakali, J.A. (1990): The Collapse Behaviour of Double Layer Space Trusses Incorporating Eccentrically Loaded Tee – Section Members. PhD Thesis Dept of Civil Engineering University of Surrey, November, 1990.
- [11] Timoshenko, S.P. and Gere, J.M. (1961): Theory of Elastic Stability. McGraw Hill Koga Kusha Ltd, New York.
- [12] Alsayed, S.H. (1987): Inelastic Behaviour of Single Angle Columns. PhD Thesis The University of Arizona, University Microfilms International <http://hdl.handle.net/10150/184041>.
- [13] Trahair, N.S. (1993): Flexural – Torsional Buckling of Structures. CRC Press Ann Arbor.
- [14] Zlatko, T.Z. (2012): Stress and Strain Deflection of an Open Profile Thin Walled Beam at Constrained Torsion by Boundary Element Method. Journal of Theoretical and Applied Mechanics, Sofia, 2012 Vol. 42, No, pp. 43 – 54.

- [15] Al – Sheikh A.M.S. (1985): Behaviour of Thin-Walled Structures under Combined Loads. PhD Thesis Loughborough University of Technology, May 1985.
- [16] Torsion in Structural Design.
<http://people.virginia.edu/ttb/torsion.pdf>.